INTERNATIONAL DOCTORAL
SCHOOL OF THE USC

Alejandro
Rivera Pousa

PhD Thesis

Multiscale simulation of ionic liquid mixtures with inorganic salts and cosolvents of electrochemical and photonic interest in liquid and gel phases (hybrid ionogel)

Santiago de Compostela, 2024

Doctoral Programme in Materials Science

ESCOLA DE DOUTORAMENTO
INTERNACIONAL DA USC

TESIS DOCTORAL

MULTISCALE SIMULATION OF IONIC LIQUID MIXTURES WITH INORGANIC SALTS AND COSOLVENTS OF ELECTROCHEMICAL AND PHOTONIC INTEREST IN LIQUID AND GEL PHASES (HYBRID IONOGEL)

Autor

Alejandro Rivera Pousa

Codirector: Luis Miguel Varela Cabo

Codirectora: Trinidad Méndez Morales

Tutor/a: Luis Miguel Varela Cabo

PROGRAMA DE DOCTORADO EN CIENCIA DE MATERIALES

SANTIAGO DE COMPOSTELA

Resumo

Esta tese pretende aumentar o coñecemento sobre as propiedades relevantes das mesturas de líquidos iónicos (LIs) con outros cosolventes moleculares de interese. A intención é contribuír aos esforzos actuais de investigación para desenvolver novos tipos de electrólitos con características melloradas para baterías e outros dispositivos electroquímicos. Os LIs son un tipo de material composto puramente por ións, cuxa propiedade máis característica é o seu baixo punto de fusión. Tradicionalmente, unha sal iónica é considerada LI se está en estado líquido por debaixo de 100 °C. Crese que esta característica é causada pola diferencia de xeometrías entre os compoñentes iónicos do LI, o que dificulta enerxeticamente a formación da usual rede cristalina iónica. A importancia dos LIs ven das interesantes propiedades que posúen, como unha moi baixa presión de vapor, grandes ventás electroquímicas e térmicas, boa condutividade ou as súas capacidades de disolución. Por este motivo, os LIs son un tipo de material avanzado con aplicacións en diversos campos, actuando coma lubricantes, catalizadores, disolventes ou coma electrólitos en dispositivos electroquímicos. Ademais das propiedades xenéricas mencionadas, a inmensa cantidade de posibles LIs que poden ser creados ao seleccionar de maneira coidadosa o anión e catión fai posible practicamente garantir que existe un LI coas características desexadas para unha tarefa específica.

Nesta tese, estábamos interesados sobre todo na aplicación dos LIs relacionada con baterías e outros dispositivos electroquímicos. Dada a súa grande ventá electroquímica, os LIs poden soportar maiores voltaxes que los electrólitos tradicionais. A baixa presión de vapor fai que sexan máis seguros de manexar e menos perigosos en caso de filtracións, mentres que son bos condutores iónicos. Por tanto, os LIs son candidatos ideais para ser usados como electrólitos en baterías. Sen embargo, para explotar ao máximo as propiedades dos LIs, usualmente son combinados con outros cosolventes de interese. Por outro lado, recentemente incrementouse a busca de electrólitos con propiedades mecánicas propias dun sólido, xa que solucionarían problemas comúns como a grande volatilidade ou o difícil manexo que presentan os electrólitos tradicionais. Un dos camiños que se seguen é a disolución dunha sal metálica en matrices poliméricas, obtendo así un medio condutor. Estes materiais, chamados electrólitos sólidos poliméricos, sofren unha condutividade menor ca dos electrólitos líquidos. Para solucionalo, engádense LIs a estes compostos para flexibilizar a matriz polimérica, incrementando a condutividade do medio. Estes materiais coñécense como electrólitos sólidos poliméricos ternarios (TSPEs polas súas siglas en inglés). Os TSPEs son unha subclase dentro dun amplo abanico de materiais iónicos coñecidos como ionoxeis híbridos. Estes materiais inclúen mesturas de LIs con diferentes aditivos que inmobilizan o sistema, coma polímeros ou nanotubos de carbono. Nesta tese centrámonos no estudo deste tipo de materiais para incrementar o coñecemento sobre as súas propiedades, e para contribuír ao desenvolvemento eventual de baterías de nova xeración.

Nos dispositivos electroquímicos hai dous compoñentes principais, eléctrodo e electrólito. Tradicionalmente, a investigación nesta área de coñecemento estaba dividida, estudando as características de cada compoñente por separado. Sen embargo, recentemente recalcouse a inmensa importancia das interaccións entre eléctrodo e electrólito. O contacto entre estes compoñentes fai que unha dobre capa eléctrica sexa formada. Ao mesmo tempo, unha rexión coñecida como a interfase sólido electrólito aparece, onde teñen lugar reaccións químicas. Estas interaccións son responsables dos mecanismos clave que gobernan o comportamento das baterías, polo que o seu coñecemento detallado é de gran importancia. Por esta razón, nos estudos contidos nesta

USC DE SANTIAGO

tese, analizamos as implicacións de incluír interfases sólidas nos nosos sistemas baseados en LIs, dende o impacto na nanoestrutura ata os mecanismos de transferencia de carga entre eles ou os cambios nas propiedades electrónicas do eléctrodo.

Para levar a cabo os estudos desta tese empregamos ferramentas computacionais. Desta maneira, usando simulacións moleculares, puidemos acceder dunha maneira máis directa ás características microscópicas do sistema. No noso caso, dúas metodoloxías foron empregadas para desenvolver os estudos detallados nesta tese: dinámica molecular (MD) e teoría do funcional da densidade (DFT). En MD, seguimos a evolución temporal dun sistema de partículas integrando as ecuacións de movemento de Newton. Esta técnica posúe resolución atómica, e as escalas típicas de tamaño e tempo están nas decenas de nanómetros e nanosegundos respectivamente. As forzas entre átomos foron modeladas aplicando campos de forza, que teñen en conta interaccións intramoleculares (como enlaces ou ángulos) e interaccións entre moléculas (coma os termos enerxéticos coulómbicos e dispersivos). Aplicáronse varias restricións ás simulacións para obter un sistema no estado desexado, coma seleccionar a temperatura ou a presión. Nesta tese, os estudos de MD computáronse usando GROMACS, un paquete de simulación de código aberto. O campo de forzas seleccionado foi OPLS-AA, que está especificamente optimizado para o seu uso en simulacións de líquidos.

Para considerar de forma explícita os graos de liberdade electrónicos nas nosas simulacións tivemos que optar por métodos máis precisos coma DFT. En DFT, as ecuacións de Kohn-Sham (que son derivables da ecuación de Schrödinger independente do tempo) resólvense de maneira iterativa, obtendo o estado de mínima enerxía do sistema. Deste xeito, a densidade electrónica do sistema é recuperada, o que nos permite obter información das propiedades electrónicas do sistema. Debido á natureza deste cálculo, os sistemas a considerar deben ser subnanométricos (sobre uns 100 átomos). Nos estudos detallados nesta tese usamos os paquetes de software VASP e Quantum Espresso co funcional de intercambio e correlación PBE-GGA.

Empezamos o desenvolvemento desta tese cun estudo xeral por MD das propiedades da mestura dun LI, [EA][NO_3], con amoníaco (NH_3). Este traballo (Capítulo 4), levado a cabo en colaboración con colegas da Universidade de Cambridge, era un punto de partida adecuado para a liña de investigación, xa que o sistema a estudar non fora explorado de maneira computacional previamente. Ademais, o amoníaco é un cosolvente con moitas aplicacións, tales como o almacenamento enerxético, polo que era unha sustancia interesante que considerar. Por outro lado, a cabeza polar do catión $[EA]^+$ ten unha composición química moi similar á das moléculas de NH_3, o que pode influenciar a nanoestruturación do sistema. É un feito coñecido que considerar a polarización electrónica das moléculas (omitido pola meirande parte dos campos de forza tradicionais) ten un gran impacto na dinámica dos sistemas. Neste traballo queriamos descubrir as implicacións que tería esta consideración para a estrutura. En oposición ao modelo tradicional de 4 puntas do NH_3, consideramos un novo modelo 6 puntas con 2 átomos virtuais (que conteñen carga, pero non masa) e unha reestruturación das cargas atómicas parciais, resultando nunha parametrización que reflicte de maneira máis realista os momentos multipolares (ata o cuadrupolo) do amoníaco. Este modelo desenvolveuse co software CamCASP. O estudo estrutural do sistema revelou que o modelo de 6 puntas leva a un posicioamento máis estrito das diferentes moléculas nas capas de solvatación, aínda que as posicións sexan similares. Deste xeito, nas proximidades das moléculas de NH_3, as cabezas polares do catión $[EA]^+$ colócanse enriba do átomo de nitróxeno, mentres que os anións $[NO_3]^-$ encóntranse preto dos átomos de hidróxeno. Ao mesmo tempo, as moléculas de $[NO_3]^-$ e NH_3 compiten polas mesmas posicións ao redor

da cabeza polar do catión $[EA]^+$. O estudo estendeuse para considerar a inclusión de interfases sólidas no sistema. Deste xeito, dúas láminas de grafeno monoatómicas colocáronse en extremos opostos do noso sistema de simulación (a uns 8 nm de distancia) e o electrólito colocouse no medio. Estas paredes foron cargadas con densidades de carga de signo oposto, modificando a estrutura do sistema. Os ións de LI foron atraídos pola superficie cargada con signo oposto, mentres que as moléculas de NH_3 competían con elas polas posicións cerca da interfase. Unha clara estruturación estaba presente na parede cargada positivamente, dando lugar á formación dunha rede cadrada.

Despois deste estudo inicial, continuamos a nosa liña de investigación con estudos que trataban de maneira máis directa co material clave nesta tese: os ionoxeis híbridos (Capítulos 5 e 6). Estes estudos por MD xurdiron dunha fecunda colaboración con colegas da Universidade de Münster e do Instituto Helmholtz, que posúen un extenso coñecemento e experiencia con simulacións de mesturas poliméricas. Comezamos no Capítulo 5 cun traballo onde caracterizamos as propiedades bulk dunha mestura ternaria LI/polímero/sal de litio. O óxido de polietileno (PEO) é un dos polímeros máis coñecidos e estudados, polo que o seleccionamos para os nosos estudos. O LI foi escollido posteriormente despois de realizar un estudo de solubilidade, que desvelou que [EA][ACE] era o candidato óptimo, xa que non tiñan lugar separacións de fase ou formación de clústeres, e o comportamento era próximo ao de cadeas ideais. O anión do LI foi tamén empregado para a sal de litio. Co sistema seleccionado, xurdiu unha dificultade inicial. Obter configuracións iniciais para sistemas deste tipo é moi importante debido á dinámica tan lenta do sistema. Unha configuración inicial realista reduciría en grande medida o tempo necesario para obter un sistema ben estabilizado, do cal poidamos empezar a extraer resultados e analizar as propiedades desexadas. Para isto, desenvolvemos unha ferramenta de software que se encarga da colocación de moléculas grandes na caixa de simulación tendo en conta as condicións de contorno periódicas. Tendo superado esta dificultade inicial, o estudo mostrou resultados interesantes. Unha gran interacción Li^+-$[ACE]^-$ levou á formación de complexos tetraédricos moi fortemente ligados que conformaban entidades cinéticas estables (con dous modos de coordinación diferentes, mono e bidentado) durante todo o tempo de simulación. Estes complexos eran tan estables que non se detectou adsorción preferente do catión litio na cadea polimérica. Este resultado contrasta con outros reportados na literatura para mesturas con LIs diferentes. Coma o polímero non modificou as propiedades da mestura binaria LI-sal de litio, estaba en efecto actuando coma unha matriz de soporte, conservando as propiedades da mestura líquida mentres que ofrecía algunhas vantaxes mecánicas.

No Capítulo 6 continuamos refinando os nosos estudos nesta liña de investigación incorporando ao sistema un par de láminas de grafeno que actuaban como eléctrodos, de modo que o sistema imitase a estrutura típica da interfase eléctrodo-electrólito das baterías. Practicamente ningún estudo computacional de TSPEs na presenza de interfases fora realizado previamente a este traballo, converténdoo nun estudo pioneiro neste campo de investigación. A composición do TSPE foi modificada para permitir aos catións de litio interactuar dunha maneira máis relevante coas cadeas poliméricas, xa que estas foran previamente reportadas como facilitadoras de novos modos de transporte iónico que poden contribuír á condución iónica. Para conseguilo precísase un anión con carga máis deslocalizada, que non forma complexos tan ligados coma os observados no estudo anterior. Desta maneira, escollemos o anión $[TFSI]^-$ tanto para a sal de litio coma para o LI. O PEO seguiu sendo o noso polímero de estudo, e escollemos dous candidatos para a posición de catión do LI, $[PYR_{14}]^+$ e $[EMIM]^+$, para determinar se a escolla de catión é relevante para as propiedades do sistema. Do mesmo modo que no anterior estudo,

USC UNIVERSIDADE DE SANTIAGO DE COMPOSTELA

tivemos que considerar detidamente algúns problemas antes de comezar coa simulación. Neste caso a dificultade ven da lenta dinámica dos TSPEs. A inclusión de interfases de grafeno no sistema restrinxe aínda máis o movemento das partículas. Ademais, as simulacións que inclúen eléctrodo e electrólito empregan sistemas moito maiores que aquelas en condicións bulk (isto é necesario para recuperar as condicións bulk na zona intermedia entre eléctrodos). Isto significa que os tempos de simulación son inmensamente largos. Tomáronse algunhas medidas, coma o escalado de cargas para mellorar a dinámica do sistema, ou a simulación a maior temperatura (423 K) co mesmo propósito. Aínda así, os cálculos duraron de 2 a 3 meses no noso clúster de simulación, para tempos de simulación de 500 ns - unha orde de magnitude máis grande que os tempos típicos.

Neste traballo centrámonos en entender a composición das proximidades ao redor do catión Li^+, xa que este é o portador de carga principal nas baterías de ión litio. A través do cálculo de funcións de distribución radial e números de coordinación puidemos determinar que o catión Li^+ coordina fortemente cos átomos de osíxeno presentes no sistema, tanto dos anións $[TFSI]^-$ como das cadeas de PEO. Puidemos corroborar deste xeito que a selección de anión permitiu ás moléculas de Li^+ interactuar coa cadea polimérica. Isto era especialmente certo nas proximidades da interfase, onde a fracción de catións de litio coordinados con PEO aumentaba. Un resultado moi interesante xa que o comportamento oposto fora reportado previamente para estudos de TSPEs similares, pero na presenza de interfases de litio metal. A razón detrás deste desacordo pode ser o comportamento hidrofóbico do PEO, o que aumentaría a súa interacción co eléctrodo de grafeno. De feito, unha análise de capas revelou que os polímeros colocábanse preferentemente na capa máis próxima á interfase. Aplicar cargas de distinto signo aos eléctrodos modificou esta estrutura, empuxando aos ións del LI cara a superficie de carga inversa. Sen embargo, os catións de litio solo conseguían chegar ao eléctrodo negativo no sistema que consideraba $[PYR_{14}]^+$, indicando que a escolla do catión do LI posúe unha relevancia potencialmente crítica para o correcto funcionamento de dispositivos electroquímicos. Tamén analizamos a orientación que as diferentes especies adoptaban. As cadeas de PEO colocábanse de forma paralela ao plano do eléctrodo, de forma que un correcto contacto eléctrodo-electrólito debería estar asegurado.

Ademais de comprender a nanoestrutura xeral que se forma na interfase eléctrodo-electrólito, é crítico entender as interaccións que están presentes, xa que estas gobernan o comportamento dos dispositivos electroquímicos. Debido á natureza electrónica de estas interaccións, os estudos por MD non son suficientes para o seu estudo. Para superar esta barreira, cambiamos a escala de simulación e levamos a cabo os estudos diferentes baseados en DFT (Capítulos 7 e 8). Como na DFT se consideran explicitamente os graos de liberdade electrónicos, esta técnica está especialmente capacitada para os propósitos dos nosos estudos. Sen embargo, debido ao escalado de tamaño da DFT, tivemos que restrinxirnos a estudar sistemas moito máis reducidos. De feito, unha única cadea de polímero xa conten un número de átomos similar ao máximo soportado para que os cálculos acaben nun tempo razoable. Por este motivo, tivemos que optar por non considerar de maneira explícita as cadeas poliméricas nestes estudos. O propósito da matriz polimérica no electrólito debería ser proporcionar soporte mecánico e facilitar a mobilidade do catión Li^+ para que cheguen aos eléctrodos. Sen embargo, non debería ter un rol relevante nas interaccións electrónicas que suceden na interfase, polo que a nosa aproximación é razoable. Desta maneira, os estudos a seguir solo considerarán a mestura binaria LI/sal, así como ao eléctrodo.

No estudo descrito no Capítulo 7, queriamos analizar a transferencia de carga electrónica

que sucede na interfase eléctrodo-electrólito entre un ión metálico e a superficie do eléctrodo. Para este propósito, levamos a cabo unha serie de cálculos DFT (usando o paquete de software VASP) nos que un átomo metálico é aproximado progresivamente cara o eléctrodo. Para ter posibles comparativas, consideramos dous metais diferentes, litio e potasio. Ao mesmo tempo, consideramos dous modelos de eléctrodo: unha única lámina de grafeno á que o ión metálico aproximábase perpendicularmente, e un eléctrodo formado por unha tripla capa de grafeno, en cuxo caso o ión metálico seguía un camiño perpendicular ao plano borde. Este último eléctrodo permitía a intercalación dos catións metálicos. Os sistemas completáronse coa presenza dun LI (neste caso, [BMIM][BF_4]) que é parte do electrólito e supervisa a transferencia. Fixándonos nos perfís enerxéticos, puidemos observar que ambos metais absorbíanse na interfase do electrodo dunha capa con grandes barreiras enerxéticas, cuxo máximo sucede na distancia na que LI e catión metálico están dispostos no mesmo plano (paralelo á interfase). A súa vez, aparecía un mínimo de enerxía máis cerca do eléctrodo. Sen embargo, nesta posición de equilibrio, a transferencia de carga co eléctrodo non era suficiente como para considerar que un complexo MC_6 fora formado, para ningún dos catións metálicos. Por outro lado, no segundo conxunto de simulacións, cando o metal chegaba a súa posición de equilibrio intercalado dentro das tres capas de grafeno, unha transferencia de carga relevante foi detectada. Así, puidemos afirmar que os complexos metálicos MC_{12} estábanse a formar. Desta maneira, concluímos que a intercalación era necesaria para obter a transferencia de carga desexada.

No último traballo contido nesta tese, detallado no Capítulo 8, ampliamos este tipo de estudos para considerar de maneira sistemática máis átomos metálicos na presenza dunha interfase e un LI. Estabamos interesados nos efectos que a presencia do electrólito induciría nas propiedades electrónicas do eléctrodo. O mesmo LI que no traballo previo, [BMIM][BF_4], foi empregado, e seleccionamos varios átomos metálicos, ampliando o noso estudo para incluír a meirande parte dos catións metálicos presentes en baterías na actualidade (ceLi, Na, Ca, Al y Mg). Neste estudo, a superficie do eléctrodo foi modelada coma unha simple lámina de grafeno. Neste caso, non aplicamos ningunha restrición á distancia entre as diferentes especies, senón que unha relaxación iónica completa tivo lugar, computada vía DFT usando o paquete de software Quantum Espresso. Primeiro analizamos a redistribución de carga que sucedía ao transferir o metal carga ao eléctrodo de grafeno. As diferenzas entre distintos metais estaban asociadas as súas enerxías de ionización. Curiosamente, o Mg non transferiu unha gran cantidade de carga. De feito, de maneira consistente con esta ausencia de transferencia, a disposición estrutural do sistema é diferente neste caso, xa que o Mg colocábase máis lonxe da superficie do eléctrodo comparado coa posición do metal nos demais sistemas estudados. A estrutura de bandas electrónica dos sistemas desprazouse, pero a estrutura propia do grafeno aínda era visible, e tan so no sistema con Ca (o que transfería a maior cantidade de carga) era modificada notablemente a estrutura. Puidemos mostrar que a cantidade de desprazamento era directamente proporcional á carga transferida. A densidade de estados revelou novos niveis moleculares próximos ao cono de Dirac. Unha análise final centrada nas propiedades ópticas do sistema mostrou o comportamento anisotrópico do mesmo.

Para finalizar esta tese, no Capítulo 9, as conclusións xerais, así coma algunhas perspectivas de futuro son discutidas. Ademais, unha lista das diferentes publicacións incluídas nesta tese está incluída no texto. Tamén aparecen listas das figuras e táboas. Finalmente, hai apéndices coas versións de impresión das publicacións, así coma as súas informacións de soporte asociadas e datos relevantes sobre as publicacións (incluíndo a autorización da revista para a reprodución dos contidos).

USC DE COMPOSTELA

Resumen

Esta tesis pretende aumentar el conocimiento sobre las propiedades relevantes de las mezclas de líquidos iónicos (LIs) con otros cosolventes moleculares de interés. La intención es contribuir a los esfuerzos actuales de investigación para desarrollar nuevos tipos de electrolitos con características mejoradas para baterías y otros dispositivos electroquímicos. Los LIs son un tipo de material compuesto puramente por iones, cuya propiedad más característica es su bajo punto de fusión. Tradicionalmente, una sal iónica es considerada LI si está en estado líquido por debajo de 100 °C. Esta característica se cree que es causada por la diferencia de geometrías entre los componentes iónicos del LI, lo que dificulta energéticamente la formación de la usual red cristalina iónica. La importancia de los LIs proviene de las interesantes propiedades que exhiben, como una muy baja presión de vapor, grandes ventanas electroquímicas y térmicas, buena conductividad o sus capacidades de disolución. Por ello, los LIs son un tipo de material avanzado con aplicaciones en diversos campos, actuando como lubricantes, catalizadores, disolventes o como electrolitos en dispositivos electroquímicos. Además de las propiedades genéricas mencionadas, la inmensa cantidad de posibles LIs que pueden ser creados al seleccionar cuidadosamente el anión y catión hace posible prácticamente garantizar que existe un LI con las características deseadas para una tarea específica.

En esta tesis, estábamos interesados sobre todo en la aplicación de los LIs relacionada con baterías y otros dispositivos electroquímicos. Dada su gran ventana electroquímica, los LIs pueden soportar mayores voltajes que los electrolitos tradicionales. La baja presión de vapor hace que sean más seguros de manejar y menos peligrosos en caso de filtraciones, mientras que son buenos conductores iónicos. Por tanto, los LIs son candidatos ideales para ser usados como electrolitos en baterías. Sin embargo, para explotar al máximo las propiedades de los LIs, usualmente se combinan con otros cosolventes de interés. Por otro lado, recientemente se ha incrementado la búsqueda de electrolitos con propiedades mecánicas propias de un sólido, ya que solventarían problemas comunes como la gran volatilidad o el difícil manejo que presentan los electrolitos tradicionales. Uno de los caminos que se siguen es la disolución de una sal metálica en matrices poliméricas, obteniendo así un medio conductor. Estos materiales, llamados electrolitos sólidos poliméricos, sufren de una conductividad menor que la de los electrolitos líquidos. Para solventarlo, LIs se añaden a estos compuestos para flexibilizar la matriz polimérica, incrementando la conductividad del medio. Estos materiales se conocen como electrolitos sólidos poliméricos ternarios (TSPEs por sus siglas en inglés). Los TSPEs son una subclase dentro de un amplio abanico de materiales iónicos conocidos como ionogeles híbridos. Estos materiales incluyen mezclas de LIs con diferentes aditivos que inmovilizan el sistema, como polímeros o nanotubos de carbono. En esta tesis nos centramos en el estudio de este tipo de materiales para incrementar el conocimiento sobre sus propiedades, y para contribuir al desarrollo eventual de baterías de nueva generación.

En los dispositivos electroquímicos hay dos componentes principales, electrodo y electrolito. Tradicionalmente, la investigación en esta área de conocimiento estaba dividida, estudiando las características de cada componente por separado. Sin embargo, recientemente se ha recalcado la inmensa importancia de las interacciones entre electrodo y electrolito. El contacto entre estos componentes hace que una doble capa eléctrica se forme. A la vez, una región conocida como la interfase sólido electrolito aparece, donde tienen lugar reacciones químicas. Estas interacciones son responsables de los mecanismos clave que gobiernan el comportamiento de las

baterías, por lo que su conocimiento detallado es de gran importancia. Por esta razón, en los estudios contenidos en esta tesis, hemos analizado las implicaciones de incluir interfases sólidas en nuestros sistemas basados en LIs, desde el impacto en la nanoestructura hasta los mecanismos de transferencia de carga entre ellos o los cambios en las propiedades electrónicas del electrodo.

Para llevar a cabo los estudios de esta tesis hemos empleado herramientas computacionales. De esta manera, usando simulaciones moleculares, pudimos acceder de una manera más directa a las características microscópicas del sistema. En nuestro caso, dos metodologías se usaron para desarrollar los estudios detallados en esta tesis: dinámica molecular (MD) y teoría del funcional de la densidad (DFT). En MD, seguimos la evolución temporal de un sistema de partículas integrando las ecuaciones de movimiento de Newton. Esta técnica posee resolución atómica, y las escalas típicas de tamaño y tiempo están en las decenas de nanómetros y nanosegundos respectivamente. Las fuerzas entre átomos fueron modelizadas aplicando campos de fuerza, que tienen en cuenta interacciones intramoleculares (como enlaces o ángulos) e interacciones entre moléculas (como los términos energéticos coulómbicos y dispersivos). Se aplicaron varias restricciones a las simulaciones para obtener el sistema en el estado deseado, como seleccionar la temperatura o la presión. En esta tesis, los estudios de MD se computaron usando GROMACS, un paquete de simulación de código abierto. El campo de fuerzas seleccionado fue OPLS-AA, que está específicamente optimizado para su uso en simulaciones de líquidos.

Para considerar de forma explícita los grados de libertad electrónicos en nuestras simulaciones tuvimos que optar por métodos más precisos como la DFT. En DFT, las ecuaciones de Kohn-Sham (que se derivan de la ecuación de Schrödinger independiente del tiempo) se resuelven de manera iterativa, obteniendo el estado de mínima energía del sistema. De esta manera, la densidad electrónica del sistema es recuperada, lo que nos permite obtener información de las propiedades electrónicas del sistema. Debido a la naturaleza de este cálculo, los sistemas a considerar han de ser subnanométricos (sobre unos 100 átomos). En los estudios detallados en esta tesis hemos usado los paquetes de software VASP y Quantum Espresso con el funcional de intercambio y correlación PBE-GGA.

Empezamos el desarrollo de esta tesis con un estudio general por MD de las propiedades de la mezcla de un LI, [EA][NO_3], con amoníaco (NH_3). Este trabajo (Capítulo 4), llevado a cabo en colaboración con colegas de la Universidad de Cambridge, era un punto de partida adecuado para la línea de investigación, ya que el sistema a estudiar no había sido explorado de manera computacional previamente. Además, el amoníaco es un cosolvente con muchas aplicaciones, tales como el almacenamiento energético, por lo que era una sustancia interesante que considerar. Por otro lado, la cabeza polar del catión $[EA]^+$ tiene una composición química muy similar a la de las moléculas de NH_3, lo que puede influenciar la nanoestructuración del sistema. Es un hecho conocido que considerar la polarización electrónica de las moléculas (omitido por la mayoría de los campos de fuerza tradicionales) tiene un gran impacto en la dinámica de los sistemas. En este trabajo queríamos descubrir las implicaciones que acarrearía esta consideración para la estructura. En oposición al modelo tradicional de 4 puntas del NH_3, consideramos un nuevo modelo 6 puntas con 2 átomos virtuales (que contienen carga, pero no masa) y una reestructuración de las cargas atómicas parciales, resultando en una parametrización que refleja de manera más realista los momentos multipolares (hasta el cuadrupolo) del amoníaco. Este modelo se desarrolló con el software CamCASP. El estudio estructural del sistema reveló que el modelo de 6 puntas lleva a un posicionamiento más estricto de las diferentes moléculas en las capas de solvatación, aunque las posiciones son similares. De esta manera, en la cercanía de las

moléculas de NH_3, las cabezas polares del catión $[EA]^+$ se colocan encima del átomo de nitrógeno, mientras que los aniones $[NO_3]^-$ se encuentran cerca de los átomos de hidrógeno. A la vez, las moléculas de $[NO_3]^-$ y NH_3 compiten por las mismas posiciones alrededor de la cabeza polar del catión $[EA]^+$. El estudio se extendió para considerar la inclusión de interfases sólidas en el sistema. De esta manera, dos láminas de grafeno monoatómicas se colocaron en extremos opuestos de nuestro sistema de simulación (a unos 8 nm de distancia) y el electrolito se colocó en medio. Estas paredes se cargaron con densidades de cargas de signo opuesto, modificando la estructura del sistema. Los iones del LI fueron atraídos por la superficie cargada con signo opuesto, mientras que las moléculas de NH_3 competían con ellas por las posiciones cerca de la interfase. Una clara estructuración era presente en la pared cargada positivamente, dando lugar a la formación de una red cuadrada.

Después de este estudio inicial, continuamos nuestra línea de investigación con estudios que trataban de manera más directa con el material clave en esta tesis: los ionogeles híbridos (Capítulos 5 y 6). Estos estudios por MD surgieron de una fructífera colaboración con colegas de la Universidad de Münster y del Instituto Helmholtz, que poseen un extenso conocimiento y experiencia con simulaciones de mezclas poliméricas. Empezamos en el Capítulo 5 con un trabajo donde caracterizamos las propiedades bulk de una mezcla ternaria LI/polímero/sal de litio. El óxido de polietileno (PEO) es uno de los polímeros más conocidos y estudiados, y lo seleccionamos para nuestros estudios. El LI fue elegido posteriormente después de realizar un estudio de solubilidad, que desveló que [EA][ACE] era el candidato óptimo, ya que no tenían lugar separaciones de fase o formaciones de clústeres, y el comportamiento era cercano al de cadenas ideales. El anión del LI fue también empleado para la sal de litio. Con el sistema seleccionado, surgió una dificultad inicial. Obtener configuraciones iniciales para sistemas de este tipo es muy importante debido a la dinámica tan lenta del sistema. Una configuración inicial realista reduciría en gran medida el tiempo necesario para obtener un sistema bien estabilizado, del cual podemos empezar a extraer resultados y analizar las propiedades deseadas. Para ello, desarrollamos una herramienta de software que se encarga de la colocación de moléculas grandes en la caja de simulación teniendo en cuenta las condiciones de contorno periódicas. Habiendo superado esta dificultad inicial, el estudio arrojó resultados interesantes. Una gran interacción Li^+-$[ACE]^-$ llevó a la formación de complejos tetraédricos muy fuertemente ligados que conformaban entidades cinéticas estables (con dos modos de coordinación diferentes, mono y bidentado) durante todo el tiempo de simulación. Estos complejos eran tan estables que no se detectó adsorción preferencial del catión litio en la cadena polimérica. Este resultado contrasta con otros reportados en la literatura para mezclas con LIs diferentes. Como el polímero no modificó las propiedades de la mezcla binaria LI-sal de litio, estaba en efecto actuando como una matriz de soporte, conservando las propiedades de la mezcla líquida mientras que ofrecía algunas ventajas mecánicas.

En el Capítulo 6 continuamos refinando nuestros estudios en esta línea de investigación incorporando al sistema un par de láminas de grafeno que actuaban como electrodos, de modo que el sistema imitase la estructura típica de la interfase electrodo-electrolito de las baterías. Prácticamente ningún estudio computacional de TSPEs en la presencia de interfases se había realizado previamente a este trabajo, convirtiéndolo en un estudio pionero en este campo de investigación. La composición del TSPE fue modificada para permitir a los cationes de litio interactuar de una manera más relevante con las cadenas poliméricas, ya que estas habían sido previamente reportadas como facilitadoras de nuevos modos de transporte iónico que pueden contribuir a la conducción iónica. Para conseguirlo se necesita un anión con carga más desloca-

lizada, que no forma complejos tan ligados como los observados en el estudio anterior. De esta manera, escogimos el anión $[TFSI]^-$ tanto para la sal de litio como para el LI. PEO siguió siendo nuestro polímero de estudio, y escogimos dos candidatos para la posición de catión del LI, $[PYR_{14}]^+$ y $[EMIM]^+$, para determinar si la elección de catión es relevante para las propiedades del sistema. Del mismo modo que en el anterior estudio, tuvimos que considerar detenidamente algunos problemas antes de comenzar con la simulación. En este caso la dificultad viene de la lenta dinámica de los TSPEs. La inclusión de interfases de grafeno en el sistema restringe aún más el movimiento de las partículas. Además, las simulaciones que incluyen electrodo y electrolito emplean sistemas mucho mayores que aquellas en condiciones bulk (esto es necesario para recuperar las condiciones bulk en la zona intermedia entre electrodos). Esto significa que los tiempos de simulación son inmensamente largos. Se tomaron algunas medidas, como el escalado de cargas para mejorar la dinámica del sistema, o la simulación a mayor temperatura (423 K) con el mismo propósito. Aun así, los cálculos duraron de 2 a 3 meses en nuestro clúster de simulación, para tiempos de simulación de 500 ns - un orden de magnitud más que los tiempos típicos.

En este trabajo nos centramos en entender la composición de los alrededores del catión Li^+, ya que éste es el portador de carga principal en las baterías de ion litio. A través del cálculo de funciones de distribución radial y números de coordinación pudimos determinar que el Li^+ coordina fuertemente con los átomos de oxígeno presentes en el sistema, tanto de los aniones $[TFSI]^-$ como de las cadenas de PEO. Pudimos corroborar de esta manera que la selección de anión permitió a las moléculas de Li^+ interactuar con la cadena polimérica. Eso era especialmente cierto en las proximidades de la interfase, donde la fracción de cationes de litio coordinados con PEO aumentaba. Un resultado muy interesante ya que el comportamiento opuesto había sido reportado previamente para estudios de TSPEs similares, pero en la presencia de interfases de litio metal. La razón detrás de este desacuerdo puede ser el comportamiento hidrofóbico del PEO, lo que aumentaría su interacción con el electrodo de grafeno. De hecho, un análisis de capas reveló que los polímeros se colocaban preferencialmente en la capa más cercana a la interfase. Aplicar cargas de distinto signo a los electrodos modificó esta estructura, empujando a los iones del LI hacia la superficie de carga inversa. Sin embargo, los cationes de litio solo conseguían llegar al electrodo negativo en el sistema que consideraba $[PYR_{14}]^+$, indicando que la elección del catión del LI posee relevancia potencialmente crítica para el correcto funcionamiento de dispositivos electroquímicos. También analizamos la orientación que las diferentes especies adoptaban. Las cadenas de PEO se colocaban de manera paralela al plano del electrodo, de forma que un correcto contacto electrodo-electrolito debería estar asegurado.

Además de comprender la nanoestructura general que se forma en la interfase electrodo-electrolito, es crítico entender las interacciones que están presentes, ya que gobiernan el comportamiento de los dispositivos electroquímicos. Debido a la naturaleza electrónica de estas interacciones, los estudios por MD no son suficientes para su estudio. Para superar esta barrera, cambiamos la escala de simulación y llevamos a cabo dos estudios diferentes basados en DFT (Capítulos 7 y 8). Como en la DFT se consideran explícitamente los grados de libertad electrónicos, está especialmente capacitada para los propósitos de nuestros estudios. Sin embargo, debido al escalado de tamaño de la DFT, tuvimos que restringirnos a estudiar sistemas mucho más reducidos. De hecho, una única cadena de polímero ya contiene un número de átomos similar al máximo soportado para que los cálculos acaben en un tiempo razonable. Por este motivo, tuvimos que optar por no considerar de manera explícita las cadenas poliméricas en estos estudios. El propósito de la matriz polimérica en el electrolito debería ser el proveer soporte mecánico y

facilitar la movilidad del catión Li^+ para que lleguen a los electrodos. Sin embargo, no debería tener un rol relevante en las interacciones electrónicas que suceden en la interfase, por lo que nuestra aproximación es razonable. De esta manera, los estudios a seguir sólo considerarán la mezcla binaria LI/sal, así como al electrodo.

En el estudio descrito en el Capítulo 7, queríamos analizar la transferencia de carga electrónica que sucede en la interfase electrodo-electrolito entre un ion metálico y la superficie del electrodo. Para este propósito, llevamos a cabo una serie de cálculos DFT (usando el paquete de software VASP) en los que un átomo metálico es acercado progresivamente hacia el electrodo. Para tener posibles comparativas, consideramos dos metales diferente, litio y potasio. A la vez, consideramos dos modelos de electrodo: una única lámina de grafeno a la que el ion metálico se aproximaba perpendicularmente, y un electrodo formado por una triple capa de grafeno, en cuyo caso el ion metálico seguía un camino perpendicular al plano borde. Este último electrodo permitía la intercalación de los cationes metálicos. Los sistemas se completaron con la presencia de un LI (en este caso, $[BMIM][BF_4]$) que es parte del electrolito y supervisa la transferencia. Fijándonos en los perfiles energéticos, pudimos observar que ambos metales se absorbían en la interfase del electrodo de una capa con grandes barreras energéticas, cuyo máximo sucede en la distancia en la que LI y catión metálico se disponen en el mismo plano (paralelo a la interfase). A su vez, aparecía un mínimo de energía más cerca del electrodo. Sin embargo, en esta posición de equilibrio, la transferencia de carga con el electrodo no era suficiente como para considerar que un complejo MC_6 se había formado, para ninguno de los cationes metálicos. Por otro lado, en el segundo conjunto de simulaciones, cuando el metal llegaba a su posición de equilibrio intercalado dentro de las tres capas de grafeno, una transferencia de carga relevante fue detectada. Así, pudimos afirmar que los complejos metálicos MC_{12} se estaban formado. De esta manera, concluimos que la intercalación era necesaria para obtener la transferencia de carga deseada.

En el último trabajo contenido en esta tesis, detallado en el Capítulo 8, ampliamos este tipo de estudios para considerar de manera sistemática más átomos metálicos en la presencia de una interfase y un LI. Estábamos interesados en los efectos que la presencia del electrolito induciría en las propiedades electrónicas del electrodo. El mismo LI que en el trabajo previo, $[BMIM][BF_4]$, fue usado, y seleccionamos varios átomos metálicos, ampliando nuestro estudio para incluir la mayoría de los cationes metálicos presentes en baterías en la actualidad (ceLi, Na, Ca, Al y Mg). En este estudio, la superficie del electrodo fue modelizada como una simple lámina de grafeno. En este caso, no aplicamos ninguna restricción a la distancia entre las diferentes especies, sino que una relajación iónica completa tuvo lugar, computada vía DFT usando el paquete de software Quantum Espresso. Primero analizamos la redistribución de carga que sucedía al transferir el metal carga al electrodo de grafeno. Las diferencias entre distintos metales estaban asociadas a sus energías de ionización. Curiosamente, el Mg no transfirió una gran cantidad de carga. De hecho, de manera consistente con esta ausencia de transferencia, la disposición estructural del sistema es diferente en este caso, ya que el Mg se coloca más lejos de la superficie del electrodo comparado con la posición del metal en los demás sistemas estudiados. La estructura de bandas electrónica de los sistemas se desplazó, pero la estructura propia del grafeno aún era visible, y tan solo en el sistema con Ca (el que transfería la mayor cantidad de carga) se modificaba sustancialmente la estructura. Pudimos mostrar que la cantidad de desplazamiento era directamente proporcional a la carga transferida. La densidad de estados reveló nuevos niveles moleculares cercanos al cono de Dirac. Un análisis final centrado en las propiedades ópticas del sistema mostro el comportamiento anisotrópico del mismo.

USC DE COMPOSTELA

Para finalizar esta tesis, en el Capítulo 9, las conclusiones generales, así como algunas perspectivas de futuro son discutidas. Además, una lista de las diferentes publicaciones incluidas en esta tesis está incluida en el texto. También aparecen listas de las figuras y tablas. Finalmente, hay apéndices con las versiones de impresión de las publicaciones, así como sus informaciones de soporte asociadas y datos relevantes sore las publicaciones (incluyendo la autorización de la revista para la reproducción de los contenidos).

USC
UNIVERSIDADE DE SANTIAGO DE COMPOSTELA

Summary

This thesis aims to improve the knowledge of the relevant properties of mixtures of ionic liquids (ILs) with other molecular cosolvents of interest, with the purpose of contributing to the current research efforts to develop new types of electrolytes with improved capabilities for batteries and other electrochemical devices. ILs are a kind of material composed solely by ions, whose most defining characteristic is the low melting temperature that they exhibit. Traditionally, an ionic salt is considered an IL if it is liquid below 100 °C. This feature is believed to stem from the difference in geometries of the ionic components of ILs, which energetically hinders the formation of the usual ionic solid lattice. The relevance of ILs comes from the shared general properties that they exhibit, such as very low vapor pressure, large electrochemical and thermal stability, high conductivity or their solvation capabilities. Because of these features, ILs constitute an advanced kind of material with application in diverse fields, acting as lubricants, catalytic compounds, solvents or as electrolytes in electrochemical devices. In addition to these general properties, the vast amount of possible ILs that can be created by carefully selecting the anions and cations makes it possible to almost guarantee that an IL with the desired characteristics for a specific task exists.

In this thesis, we were mainly interested in the application of ILs to batteries and other electrochemical devices. Because of their large electrochemical window, ILs can withstand larger voltages than traditional electrolytes. The low vapor pressure makes them safer to handle, and less harmful if leakages were to happen, while they are good ionic conductors. Hence, they seem ideal candidates to be used as electrolytes in batteries. Notwithstanding, in order to fully exploit the properties of ILs, they are usually employed in mixtures with other cosolvents of relevant interest. On the other hand, in recent times, electrolytes with solid-like mechanical properties are sought after, as they would solve common electrolyte problems such as their high volatility or difficult handling. An approach that has been taken is to dissolve a metal salt in polymeric matrices, obtaining a conducting medium. These materials, named solid polymer electrolytes (SPEs) suffer from lower conductivity than the usual liquid electrolytes. ILs are added to these mixtures so that they plasticize the polymer matrix, increasing the conductivity of the medium. These materials are known as ternary solid polymer electrolytes, or TSPEs. TSPEs are a subclass of a broader kind of ionic materials known as hybrid ionogels. These materials include mixtures of ILs with different additives that immobilize the system, such as polymers or carbon nanotubes. In this thesis, we focused on the study of such materials, in order to improve the knowledge about their properties, and to further contribute in the eventual developing of next generation batteries.

In electrochemical devices, there are two main components, electrode and electrolyte. Traditionally, research in this area of knowledge was split, focusing on one of the components in particular and studying its characteristics. However, it has been recently brought to attention the immense importance of the electrode-electrolyte interactions. The contact between them causes an electric double layer to be formed. At the same time, a region known as the solid electrolyte interphase appears as chemical reactions take place. These interactions are responsible for the core mechanisms that rule battery behavior, so their detailed understanding is of utmost importance. For this reason, in the studies contained in this thesis, we analyzed the implications of the inclusion of solid interfaces in our IL-based system, from their impact in the nanostructure to the mechanisms of charge transfer between them or the changes in the surface electronic properties.

In order to perform the studies of this thesis, computational tools were employed. This way, through the use of molecular simulations, we accessed in a more direct manner the microscopic features of the systems. In our case, two methodologies were used to develop the studies detailed throughout this thesis, molecular dynamics (MD) and density functional theories (DFT). In MD, we follow the time evolution of a system of particles by integrating Newton's equations of motion. This technique has atomic resolution, and the typical scales of size and time are around the tens of nanometers and nanoseconds. The forces between atoms were modeled through the application of force fields, which take into account intramolecular interactions such as bonds or angles and interactions between molecules such as coulombic or dispersive energy terms. Several restrictions were applied to the simulation in order to set the system to a desired state, such as selecting the temperature or pressure conditions. In this thesis, MD simulations were performed using GROMACS, an open source simulation suite. The selected force field was OPLS-AA, which is specifically optimized to be used in simulations of liquids.

In order to explicitly consider the electronic degrees of freedom in our simulation, we had to opt for more precise methods such as DFT. In DFT, the Kohn-Sham equations (derived from the time-independent Schrödinger equation) are iteratively solved, obtaining the minimal energy ground state of the system. This way, the electronic density of the system is recovered, which enables us to obtain insights into electronic properties of the systems. Due to the nature of the calculation, smaller subnanometric systems must be considered (around 100 total atoms). In the studies detailed in this thesis, we used the software packages VASP and Quantum Espresso with the PBE GGA exchange correlation functional.

We started the development of the thesis with a general MD study of the properties of a mixture of an IL, [EA][NO_3], with ammonia (NH_3). This work (Chapter 4), performed in collaboration with colleagues from the University of Cambridge, was a fitting starting point to the research line, as the system of study had not been computationally explored beforehand. Moreover, ammonia is a cosolvent with many applications, such as energy storage, so it was an interesting species to consider. In fact, the polar head of the $[EA]^+$ cation has a chemical composition very similar to that of NH_3 molecules, which might influence the nanostructure of the system. It is a well-known fact that considering the electronic polarization of molecules (which is omitted by most traditional force fields) has large impact on the dynamics of the systems. In this work, we wanted to uncover the implications that this consideration would carry for structural purposes. In opposition to the traditional 4-site model of NH_3, we considered a new a 6-site model with two virtual atoms (carrying charge but not mass) and a restructuring of the partial atomic charges, resulting in a parametrization that depicts more realistically the multipole moments (up to the quadrupole) of ammonia. This model was developed with the software package CamCASP. The structural study revealed that the 6-site model leads to more strict positioning of the different molecules in the solvation shells, but the positioning is not significantly changed. This way, in the vicinity of NH_3 molecules the polar head of ammonia $[EA]^+$ polar heads are placed on top of the nitrogen molecules, while $[NO_3]^-$ anions are located near the hydrogen atoms. At the same time, $[NO_3]^-$ and NH_3 molecules compete for the same positions around the $[EA]^+$ polar head. The study was then extended to consider the inclusion of solid interfaces to the system. This way, two graphene interfaces were placed in the opposite extremes of our simulation system (around 8 nm apart) and the electrolyte was placed in between. This resulted in a layering of the system, with NH_3 molecules preferentially adsorbed at the interfaces. Then, these neutral interfaces were charged with opposite charge densities, modifying the structural picture. The IL ions were attracted to the surface charged with the opposite sign, while NH_3

USC DE COMPOSTELA

competed with them for the position near the interface. A clear structuring was present near the positively charged wall, with a square lattice being formed.

After this initial study, we followed our investigation with studies that dealt more directly with the core material of this thesis: hybrid ionogels (Chapters 5 and 6). These MD studies arose from a fruitful collaboration with colleagues from the University of Münster and the Helmholtz Institute, which had an extensive knowledge and experience with simulations of polymeric mixtures. We start in Chapter 5 with a work where we characterized the bulk properties of a ternary IL/polymer/Li^+ salt mixture. Polyethylene oxide (PEO) is currently one of the most researched polymer compounds, and we selected it as the polymer reference for our studies. The IL was subsequently chosen after having carried out a solubility study, which deemed [EA][ACE] as the optimal candidate, as no phase separation or clustering was observed, as well as showing behaviors close to ideal chains. The anion of the lithium salt was selected to match that of the IL. With the system selected, we had to face an initial difficulty. Obtaining initial configurations for these solid-like systems is really important because of the slow dynamics of the systems. A realistic initial configuration would greatly reduce the time needed to obtain a well stabilized system, from which we can start extracting data and analyzing the desired properties. For this purpose, we developed a software tool that deals with the placement of long molecules in the simulation box in a well mixed manner, unlike other available packing softwares that do not take into account the periodic boundary conditions of the simulation box. Having overcome this initial difficulty, the actual study unveiled some interesting results. A large Li^+-$[ACE]^-$ interaction lead to the formation of strongly bound tetrahedral complexes that form stable kinetic entities (with two different coordination modes, mono and bidentate) throughout the simulation time. These complexes were so stable that no preferential adsorption of Li^+ on the polymer backbone was detected. This result is different from what other studies on the literature observed for mixtures using different ILs. As the polymer did not disturb the properties of the binary IL-salt mixture, it was indeed acting as a supporting matrix, preserving the properties from the liquid mixture while offering some mechanical advantages.

In Chapter 6 we continued to refine our studies on this research line by incorporating to the system a pair of graphene interfaces that acted as electrodes, so that our system mimicked the typical structure of the electrolyte-electrode interface of batteries. Almost no computational studies of TSPEs in the presence of interfaces were conducted prior to this work, making it a pioneering study in this research field. The composition of the TSPE was modified in order to allow Li^+ cations to interact more meaningfully with the polymer chains, which had been previously reported to open more Li^+ transport mechanisms that can contribute to the ionic conduction. In order to achieve this, an anion with more delocalized partial charges is needed, which do not form the strong compounds observed in the previous work. This way, we selected $[TFSI]^-$ anion for both the lithium salt and the IL. PEO was kept as the polymer of study, and we chose two candidates for the IL cation position, $[PYR_{14}]^+$ and $[EMIM]^+$, so as to determine if the cation choice is relevant for the properties of the system. As with the previous study, we had to carefully consider some issues before even starting the actual simulation. In this case, the difficulty comes from the slow dynamics of TSPEs. The inclusion of the graphene interfaces in the system restricts even further the motion of the particles in the system. In addition, simulations with electrolyte between electrodes tend to use systems much larger than those of bulk simulations (needed to recover bulk properties in the intermediate zone between the two electrodes). This means that the simulation times needed for this type of simulations are abnormally large. Some measures were taken, such as scaling the charges to enhance the dynamics of the

USC COMPOSTELA

system, or simulating at a higher temperature (423 K) with the same purpose. Even then, the calculations took around 2 to 3 months in our simulation clusters, for simulated times of 500 ns - an order of magnitude above typical times.

In this work, we placed our focus on understanding what the composition of the Li^+ surroundings is, as the Li^+ cation is the main charge carrier in Li-ion batteries. Through the calculation of radial distribution functions and coordination numbers we could determine that Li^+ coordinates strongly with the oxygen atoms present in the system, both from $[TFSI]^-$ anions and PEO chains. We could corroborate, therefore, that this selection of anion allowed Li^+ to interact with the polymer backbone. This was specially true in the regions close to the interface, where the fraction of Li^+ cations coordinated with PEO increased. Interestingly, the opposite behavior was previously detected in the literature for studies of similar TSPEs but using Li metal surfaces as electrodes. The reason for the disagreement could be caused by the hydrophobic behavior of PEO, which would enhance its interaction with the graphene electrode. Indeed, a layer analysis revealed that polymers were placed preferentially at the layer closest to the interface. Applying opposing charges to the electrodes modified the structure, pushing the IL ions towards the inversely charged surface. However, Li^+ ions could only reach the negative electrode in the system with $[PYR_{14}]^+$ present, indicating that the choice of IL cation is of relevance and critical to the correct functioning of electrochemical devices. We further studied the structure by analyzing the orientation that the different species adopted. PEO chains placed themselves parallel to the electrode plane, a fact that should ensure a proper electrode-electrolyte contact.

On top of understanding the general nanostructure that is formed at the electrode-electrolyte interface, it is of critical importance to understand the interactions that are present, as they rule the behavior of the electrochemical devices. As the nature of these interactions is electronic, MD studies fell short for their study. To overcome this issue, we changed the scale of simulation and performed two different studies based on DFT (Chapters 7 and 8). As DFT considers the electronic degrees of freedom explicitly, it is specially suited for the purpose of these studies. However, due to the system size scaling of DFT, we had to restrict ourselves to much smaller systems. In fact, a single polymer chain already has a number of atoms that is close to the maximum, so that the calculations finish in a reasonable amount of time. For this reason, we had to compromise and not consider in an explicit way the polymer chains in the following studies. The purpose of the polymer matrix inside the electrolyte should be to provide mechanical support and to facilitate Li^+ ion mobility, so that the cations reach the electrodes. On the other hand, it should not take a relevant role on the electronic interactions that take place at the interface, rendering our approach reasonable. This way, the following studies will only consider the binary IL/salt mixture as well as the electrode.

In the study described in Chapter 7, we wanted to analyze the electron charge transfer that takes place in the electrode-electrolyte interface between a metal ion and the electrode surface. For this purpose, we computed a series of DFT calculations (performed with the software package VASP) in which a metal atom gets progressively displaced towards the electrode. In order to provide some comparison means, two different metals were considered, lithium and potassium. At the same time, two electrode models were considered: a single graphene sheet which was approached perpendicularly by the metal ions, and a trilayer graphene electrode, in which case the metal ion followed a path perpendicular to the edge plane. This latter electrode allowed for intercalation of the metal ions. The systems are completed by the presence of an IL (in this case, $[BMIM][BF_4]$) which is part of the electrolyte and oversees the transfer. Looking at the

energetic profiles, we could observe that both ion metals were absorbed at the single layer interface with high energetic barriers, whose maximum happens at the distance where IL and metal ion lay in the same plane (parallel to the interface). Then, an energy minimum closer to the interface is achieved. However, at this equilibrium position, the charge transfer with the electrode was not found to be large enough to consider that a MC_6 complex was indeed formed for either metal ion. On the other hand, in the second set of simulations, when the metal arrives to its equilibrium position intercalated inside the trilayer graphene electrode, a significant charge transfer is detected. Therefore, we could state that metal complexes MC_{12} were indeed being formed. This way, we concluded that intercalation was necessary in order to obtain the desired charge transfer.

In the last work contained in this thesis, detailed in Chapter 8, we further broadened this type of study to systematically consider more metal atoms at the presence of an interface and an IL. We were interested on the effects that the presence of the electrolyte would induce in the electronic properties of the electrode material. The same IL as in the previous work, [BMIM][BF_4], was used, and we selected several metal atoms, broadening our studies to include most salt cation species present in batteries (Li, Na, Ca, Al and Mg). In this study, the electrode surface was modeled using a single sheet of graphene. In this case, no restriction on the distance of the different species was in place, and a complete ionic relaxation of the system was computed via DFT using the Quantum Espresso software package. We first analyzed the charge redistribution that took place as the metal atom transfers charge to the graphene electrode. Differences between metals were associated with the different ionization energies of each species. Interestingly, Mg did not transfer a substantial amount of charge. Indeed, consistent with the absence of charge transfer, the structural disposition of the system is different in this case, as Mg is placed further away from the electrode surface compared to the metal atom position in the other studied systems. The electronic band structure of the systems was downshifted, but the underlying graphene band structure was still visible, with just the Ca system (that transferred the greatest charge) modifying substantially its structure. The degree of shifting was shown to be directly proportional to the amount of charge transferred. The density of states revealed that new molecular levels are present close to the Dirac cone. A final analysis focused on the optical properties of the system showed the anisotropic behavior of the system.

To finalize this thesis, the general conclusions, as well as some future perspectives are discussed in Chapter 9. Furthermore, a list of the different publication discussed on this thesis is included throughout the text. Lists of figures and tables are also incorporated. Finally there are appendices with the post-print version of the publications as well as their associated supporting information and the relevant publication data (including the journal authorization for the reproduction of contents).

USC
UNIVERSIDADE DE SANTIAGO DE COMPOSTELA

“Ya lo saben...
si parpadean, se lo van a perder.”
Gonzalo Serrano

USC
UNIVERSIDADE
DE SANTIAGO
DE COMPOSTELA

Agradecimientos

En esta tesis está contenido el trabajo realizado en los últimos cinco años. Para conseguirlo, he gozado del apoyo de mucha gente, sin el que no habría sido posible llegar a completar este estudio. Por este motivo, quiero agradecer en estas líneas a todas esas personas, y especialmente:

- A mi familia, en especial a mis padres y a mi hermano, que siempre me han ofrecido su atención y apoyo incondicional.
- A María, por aceptarme como soy y estar a mi lado todos estos años. Ahora, compartimos la vida aún más unidos, y afrontaremos juntos los retos que nos deparará el futuro.
- A mi nueva familia política, que inmediatamente me ha acogido en sus vidas como a uno más.
- A Luis Miguel, mi codirector de tesis, por acogerme en el grupo de investigación y darme su apoyo, siempre buscando lo mejor para mí, como hace con todos sus discípulos. No me cabe duda de que el grupo de investigación que lidera siempre será otro hogar para mí.
- A Trini, mi otra codirectora de tesis, que a pesar de incorporarse a mediados del desarrollo de la misma, mostró una cercanía, amistad y paciencia conmigo que han facilitado en enorme medida el trabajo realizado estos años.
- A Hadrián, sin cuyos consejos y ayudas no habría sido posible realizar este trabajo. Para mí, es mi tercer codirector en espíritu.
- A Txema y Víctor, la vieja guardia, por las conversaciones y discusiones que hicieron del despacho un sitio ameno en el que querer trabajar cada día.
- A Raúl, Martín y Pablo, las nuevas generaciones, con las que compartí grandes momentos y que estoy seguro de que tienen un futuro brillante por delante.
- A todos los demás familiares, amigos y conocidos, que en un momento u otro me ofrecieron su apoyo.

Además, el desarrollo de la tesis no habría sido posible sin contar con la financiación y recursos suministrados por las siguientes entidades: Al Ministerio de Educación por la financiación a través de la beca para formación de profesorado universitario (FPU) que me fue concedida. Al Ministerio de Economía y Competitividad por la financiación a través de los proyectos MAT2017-89239-C2-1P y MAT2017-89239-C2-2P. Al Ministerio de Ciencia e Innovación por la financiación a través del proyecto PID2021-126148NA-I00. A la Xunta de Galicia por la financiación a través de los proyectos ED431D 2017/06, ED431E 2018/08, GRC ED431C 2016/001 y GRC ED431C 2020/10. A la Unión Europea, por la financiación a través de los fondos FEDER. Al centro de supercomputación de Galicia (CESGA) por los recursos computacionales que fueron utilizados para ciertas secciones de los estudios realizados.

USC
UNIVERSIDADE DE SANTIAGO DE COMPOSTELA

Index

List of publications included in this thesis **xxiv**

I Introduction and Methods **1**

1 Introduction **2**
1.1 Motivation and purpose 2
1.2 Objectives 3
1.3 Ionic liquids 4

2 Methods **8**
2.1 Molecular dynamics 8
2.2 Density functional theory 15

II Results **19**

3 Summary of the Results **20**

4 The interaction of ammonia with the protic ionic liquid ethylammonium nitrate: a simulation study **28**
4.1 Introduction 28
4.2 Simulation Details 30
4.3 Results and Discussion 31
4.4 Conclusions 40

5 Computational Study of the Structure of Ternary Ionic Liquid/salt/polymer Electrolytes based on Protic Ionic Liquids **41**
5.1 Introduction 41
5.2 Simulation Details 42
5.3 Results and Discussion 45
5.4 Summary and Conclusion 55

6 Ternary solid polymer electrolytes at the electrochemical interface: a computational study **57**
6.1 Introduction 57
6.2 Simulation details 60
6.3 Results and discussion 62

USC UNIVERSIDADE DE SANTIAGO DE COMPOSTELA

6.4 Conclusions 77

7 Density functional theory of alkali metals at the IL/graphene electrochemical interface 79
7.1 Introduction 79
7.2 Computational details 83
7.3 Results 84
7.4 Conclusions 90
7.5 Data Availability Statement 91

8 Ionic liquid/metal salt mixtures at the graphene interface: a density functional theory approach 92
8.1 Introduction 92
8.2 Simulations details 94
8.3 Results and Discussion 95
8.4 Conclusions 108

III Conclusions 110

9 Conclusions and Future Perspectives 111
9.1 Conclusions 111
9.2 Future Perspectives 112

List of Figures 113

List of Tables 117

IV Appendix 118

A Post-Print Version of the Publications 119
A.1 The interaction of ammonia with the protic ionic liquid ethylammonium nitrate: A simulation study 120
A.2 Computational study of the structure of ternary ionic liquid/salt/polymer electrolytes based on protic ionic liquids 128
A.3 Ternary solid polymer electrolytes at the electrochemical interface: a computational study 137
A.4 Density functional theory of alkali metals at the IL/graphene electrochemical interface 153
A.5 Ionic liquid/metal salt mixtures at the graphene interface: A density functional theory approach 164

B Supplementary Information 175
B.1 Supplementary information for: The interaction of ammonia with the protic ionic liquid ethylammonium nitrate: A simulation study 176
B.2 Supplementary information for: Computational study of the structure of ternary ionic liquid/salt/polymer electrolytes based on protic ionic liquids 181

B.3 Supplementary information for: Ternary solid polymer electrolytes at the electrochemical interface: a computational study . . . 185
B.4 Supplementary information for: Ionic liquid/metal salt mixtures at the graphene interface: A density functional theory approach . . . 192

C Information of the publications **200**
C.1 The interaction of ammonia with the protic ionic liquid ethylammonium nitrate: A simulation study . . . 201
C.2 Computational study of the structure of ternary ionic liquid/salt/polymer electrolytes based on protic ionic liquids . . . 202
C.3 Ternary solid polymer electrolytes at the electrochemical interface: a computational study . . . 203
C.4 Density functional theory of alkali metals at the IL/graphene electrochemical interface . . . 204
C.5 Ionic liquid/metal salt mixtures at the graphene interface: A density functional theory approach . . . 205

Bibliography **206**

USC UNIVERSIDADE DE SANTIAGO DE COMPOSTELA

List of publications included in this thesis

- **The interaction of ammonia with the protic ionic liquid ethylammonium nitrate: A simulation study,** Alejandro Rivera-Pousa, José M. Otero-Mato, Alberto Coronas, Anthony J. Stone, Ruth M. Lynden-Bell, Trinidad Mendez-Morales, Luis M. Varela, *Journal of Molecular Liquids,* **320**, 114437 (2020). **Journal information:** Impact factor in 2020: 6.165. Cathegory: Physics, Atomic, Molecular & Chemical. Ranking inside cathegory: 04/37 (Q1).

- **Computational study of the structure of ternary ionic liquid/salt/polymer electrolytes based on protic ionic liquids,** José M. Otero-Mato, Alejandro Rivera-Pousa, Hadrián Montes-Campos, Oscar Cabeza, A. Heuer, D. Diddens, Luis M. Varela, *Journal of Molecular Liquids,* **333**, 115883 (2021). **Journal information:** Impact factor in 2021: 6.633. Cathegory: Physics, Atomic, Molecular & Chemical. Ranking inside cathegory: 06/36 (Q1).

- **Ternary Solid Polymer Electrolytes at the Electrochemical Interface: A Computational Study,** Alejandro Rivera-Pousa, José Manuel Otero-Mato, Hadrián Montes-Campos, Trinidad Méndez-Morales, Diddo Diddens, Andreas Heuer, Luis Miguel Varela, *Macromolecules,* **57**(9), 3921-3936 (2024). **Journal information:** Impact factor: 5.1. Cathegory: Polymer science. Ranking inside cathegory: 12/94 (Q1). Data obtained from the year 2023 due to lack of data availability for 2024.

- **Density functional theory of alkali metals at the IL/graphene electrochemical interface,** Hadrián Montes-Campos, Alejandro Rivera-Pousa, Trinidad Méndez-Morales, *The Journal of Chemical Physics,* **156**(1), 014706 (2022). **Journal information:** Impact factor in 2022: 4.4. Cathegory: Physics, Atomic, Molecular & Chemical. Ranking inside cathegory: 08/35 (Q1).

- **Ionic liquid/metal salt mixtures at the graphene interface: A density functional theory approach,** Alejandro Rivera-Pousa, José M. Otero-Mato, Carlos Damián Rodríguez-Fernández, Kazem Zhour, Hadrián Montes-Campos, Trinidad Méndez-Morales, Luis M. Varela, *Journal of Molecular Liquids,* **392**, 123460 (2023). **Journal information:** Impact factor in 2023: 5.3. Cathegory: Physics, Atomic, Molecular & Chemical. Ranking inside cathegory: 06/40 (Q1).

USC
UNIVERSIDADE DE SANTIAGO DE COMPOSTELA

Part I

Introduction and Methods

USC
UNIVERSIDADE
DE SANTIAGO
DE COMPOSTELA

1- Introduction

1.1 Motivation and purpose

The world we live in is in constant and rapid evolution. Every year, new technologies are designed all around the globe, as technicians and scientists develop new devices needed for the most specific purposes. Most of this progress is often based in some manner on electrical instruments, which demand some power source to operate. Traditionally, machinery was physically attached to fixed electric current source points. However, as more and more of these inventions become portable to meet the present day human demands, batteries have risen as the most convenient way to carry this power around. At the same time, the global population is growing every year.[1] Consequently, the amount of people with access to 21st century technologies is steadily increasing,[2;3] specially as underdeveloped countries begin to adopt the latest advances in machinery. This means that the global energy demand is accordingly rising as well.[4]

The current trend in the world industry is a progressive decarbonization and a transition to "greener" technologies. One of the most notable examples is the rise of the production of electric vehicles.[5] As a counterpart to the classical combustion powered means of transport, electric cars function without emitting any greenhouse gases, as they obtain the needed energy from the large batteries installed in them. Although the current iteration of electric automobiles is already functional, more autonomy, faster charging times and cost reductions are crucial to be able to compete in the market with traditional combustion powered vehicles.[6;7]

All these facts are just some examples that illustrate the essential importance of batteries in today's world. However, crucial materials that are part of key elements of batteries, like some rare earths, are scarce and often located in specific regions of the Earth.[8;9] This is potentially a critical issue, as world politics is highly volatile nowadays. The supply of these materials might be seriously affected or even completely halted. In conclusion, the design of improved batteries, with a "green" perspective, and the search for new materials that could be used in this role, is key for the development of modern human society.

In order to improve the performance of electrochemical devices, battery focused research has often been split into two different approaches: either improving the properties of the electrode or those of the electrolyte. Specifically, ionic liquids (ILs) have been proposed among the most promising materials to be used as components of electrolytes, in either pure form or more commonly as a mixture with other cosolvents.[10–14] The properties of ILs (which will be thoroughly discussed in the following section) make them very suitable to be employed as part of electrochemical devices, and due to their low toxicity they are considered a "green" alternative to the traditionally used molten salts.[15] More recently, hybrid ionogels (mixtures of ILs with other compounds that form a solid-like network, such as polymers) are being considered as the next step forward in the field of IL electrolyte battery research, due to the improved mechanical properties that the polymer compound provides, while retaining the ideal features of the IL.[16–18]

Recently, the scientific approach has changed, and rather than studying each battery component separately, experts have started to study the battery as a whole. In particular, much attention is being put into understanding the electrode-electrolyte interaction. For example,

when an IL-based electrolyte gets in contact with an electrode (or any other heterogeneity), an electric double layer (EDL) is formed.[19] The EDL is roughly composed of successive layers of counterions spanning around 2 nm. At the same time, in the interfacial electrode-electrolyte region, known as the solid electrolyte interphase (SEI), chemical reactions take place as species get reduced or oxidized. However, although much scientific work has been carried out on the matter, how exactly these regions are created and how their composition varies with different electrode and electrolyte combinations is not fully understood yet. In this thesis, we will focus on analyzing the relevant interactions and effects of the EDL.

Although traditionally most of the research has been carried out experimentally,[20–26] in the past decades simulations have arisen as an extremely useful tool to investigate such compounds.[27–34] It does not only have the advantage of circumventing the costs of physically obtaining the materials, which can be quite high for some ILs, but it also allows microscopical analyses that are really hard to achieve experimentally. Thus, investigating the composition and structure of the electrolyte mixtures as well as the formation of the EDL, or the electronic interaction between electrode and electrolyte becomes more accessible and direct than the approach traditional macroscopic experimental techniques provide. In this thesis, we have employed two different computational techniques: molecular dynamics allows extracting the microscopic properties of our IL-based systems at the atomistic level, and when the electronic interactions are relevant, we used *ab-initio* quantum density functional theory. The foundations of both techniques will be detailed in Chapter 2.

1.2 Objectives

In this context, the importance of the research on the field of batteries and other electrochemical devices becomes apparent. As ILs constitute one of the most promising categories of materials to be used as electrolyte components, understanding their nanostructure and dynamics is one of the hottest topics in scientific research. However, there is a relative scarcity of studies that focus on mixtures with polymeric compounds, specially in nanoconfined environments. In this thesis, we will aim to provide more knowledge about the properties of IL mixtures with different compounds, going from a broader view of molecular nanostructure to a more detailed description of electronic interactions. In particular, the specific objectives that were addressed in this thesis were:

- Studying the properties of mixtures of ILs with ammonia and analyzing the effect of including multipolar considerations in the modelling of species in a simulation. Specifically, two different models for ammonia were tested against each other in bulk systems and at the electrochemical interface. This was addressed in the work presented in Chapter 4.

- Understanding the nanostructure and properties of ternary mixtures of ILs with polymeric compounds and metal salts (hybrid ionogels). This accurate description is necessary to develop improved electrolytes for electronic devices. Two studies were carried out for this purpose, and the results are presented in Chapters 5 and 6.

- Unveiling the effects that arise from the presence of a solid interface in contact with the system. This was first analyzed for mixtures of IL with ammonia in the paper included

USC UNIVERSIDADE DE SANTIAGO DE COMPOSTELA

in Chapter 4. Then, it was pioneeringly studied for ternary IL-polymer-salt mixtures in a publication shown in Chapter 6.

- Investigating the electronic interactions between electrode and IL-salt electrolyte and their effects on the properties of the system, starting with a study of the charge transfer process (Chapter 7) and following with a study analyzing how the electronic properties of the electrode might be affected by the presence of ILs and metal atoms (Chapter 8).

1.3 Ionic liquids

In the year 1914, in his laboratory, Paul Walden was attempting to obtain molten salts that were liquid at low enough temperatures so that he could study them with his available experimental setup. He discovered that ethylammonium nitrate had a surprisingly low melting temperature, of 12 °C.[35] This event is generally accepted as the first time an ionic liquid was synthesized.[36] However, this field remained relatively ignored for decades. In 1948 the first ionic liquid related patent was filed by Hurley.[37]. In 1963 the U.S. Air Force Academy started a research program to study thermal batteries composed of ionic liquids.[38] It was not until the 80s that the field really started to attract widespread attention, as researchers started to realize how the exceptional properties of these species could be exploited.[39–41] Ionic liquids (ILs), as the name implies, are just compounds composed of cations and anions, in opposition to traditional liquids that are commonly formed of neutral molecules. The large force of ionic bonding should in principle lead to ILs being solid compounds at ambient temperature. However, the key property that gives rise to the characteristic low melting temperature is the asymmetry and geometric differences between its components. The ions in traditional salts, with their small size, allow for the formation of the usual regular crystal lattices. To obtain a liquid state (molten salts), high temperatures must be achieved. On the other hand, in the case of ILs, the ions are not so similar. Typically, the anion is a relatively small molecule, while cations are characterized by a long alkyl chain. This misalignment between sizes and geometries disturbs the formation of a regular network (see Fig. 1.1) and, indeed, it results in a really large lattice energy. Therefore, liquid is the most energetically favorable state of matter available for these compounds. In the scientific community, ILs are currently defined as ionic compounds whose melting point is below 100 °C.[42]

The number of possible ILs has been estimated to be as high as in the trillions.[43] This stems from the fact that there is a large number of different anions and cations that lead to the formation of an IL when combined, and the amount of possible pairings (or even triplets in more complex ILs with more than 2 ions) skyrockets. As we have already mentioned, in general anions are small and inorganic, while cations are composed large organic chains. This is not always the case, and some of the most common ions do not fit this criteria. Either way, ILs have been traditionally classified into two groups: protic and aprotic. This classification emerges from the difference in the synthethization process. Protic ILs are the product of proton transfer reactions between an acid and a base, this is, a Brønsted reaction.[44] This results in protic ILs having a free H atom that allows for enhanced hydrogen bonding formation, which can impact their properties.[45] On the other hand, if the process of synthesis does not fall into this definition, the IL is classified in the aprotic category.

Creating a common list of properties of ILs is a difficult task due to the sheer size of ILs that exist. However, most of these materials share the following features:

- **Large electrochemical window:** The components of ILs are usually species with large redox potentials, and therefore they can withstand high voltages without undergoing chemical reactions. Typically ILs have electrochemical windows of around 4 or 5 V,[43] but some studies show stabilities larger than 8 V.[46]

- **Good ionic conductivity:** As the components of ILs are of ionic nature, they can be redistributed in an efficient and fast manner when exposed to an electric field. In consequence, the ionic conductivity of ILs is greater than that of other common solvents.[10] In mixtures with other cosolvents, there exist certain concentration ranges where ILs achieve even larger conductivities.[47]

- **Low vapor pressure:** As ILs are formed by ions of opposite charge, the Coulomb forces present in the system are very large. This means that the vaporization process is energetically unfavorable for a large range of temperatures. Indeed, the vapor pressure in ILs is so low that in some cases it is almost undetectable with the current measuring technology.[48]

- **High thermal stability:** In addition to their great electrochemical stability, ILs also present a large range of temperatures in which they remain in the liquid state. This is a product of the low melting temperature that defines these compounds, added to the already discussed low vapor pressure. In fact, for many ILs their upper operational temperature limit is not bound by evaporation. Instead, chemical reactions are responsible for the degradation of the compounds.

- **High viscosity:** Another consequence of the large Coulomb interactions present in these systems is the high viscosities that ILs exhibit.[49] The viscosities are largely affected by factors such as the external temperature[50] or the geometries of the species.[51]

- **Lower risk handling:** The toxicity of the compound greatly varies between different ILs, and is comparable to that of other traditional solvents.[52] However, due to the really low vapor pressure already discussed, the possible leakages are much easier and safer to handle, as almost no harmful emissions to the atmosphere are released. For this reason ILs are usually labelled as “green solvents”.

- **Nanostructuring:** In general, ILs include polar and apolar regions in its ionic components, as specially IL cations are usually amphiphillic molecules. The association of these parts with similar chemical polarity leads to the emergence of several nanodomains, usually referred to as the nanostructure of the liquid. Other cosolvents can easily solvate in the appropriate region that matches their polarity.[53;54] Because of this, ILs present a really high adaptability as universal solvents. In protic ILs, the presence of hydrogen bond networks is also able to affect the nanostructured solvation.[55] In fact, some studies have proven the possibility of tuning ILs to allow or prevent the solvation of a specific compound, earning ILs the title of “designer solvents”.[56]

The collection of the properties mentioned clearly shows why ILs are one of the most promising materials for applications in batteries and other electrochemical devices. Moreover, the large amount of anions and cations available to form ILs almost guarantee that if one property is desired, there will exist a combination that results in an IL that satisfies it.[57;58] This tuning possibility is the final characteristic that further motivates the importance of ILs in this research field.

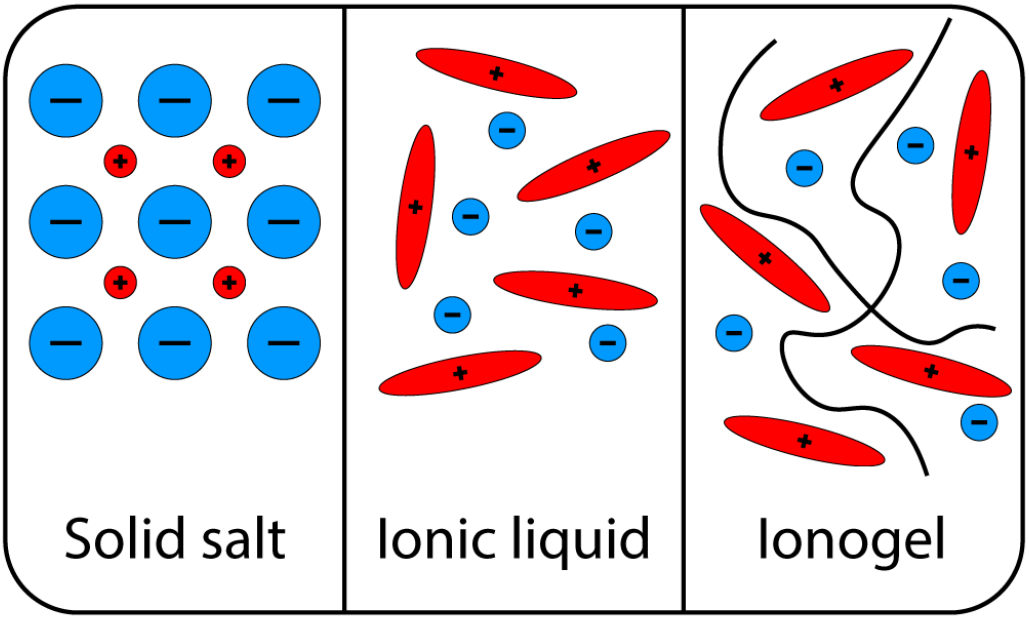


Figure 1.1: Schematic view of the different structures of regular solid salts, ionic liquids and hybrid ionogels respectively.

1.3.1 Hybrid ionogels

In recent times, major research efforts are being devoted to investigate electrolytes that possess liquid state ionic conductivities and solid-like mechanical properties, which would solve issues that traditional electrolytes posses such as high volatility or the ease of handling. For this purpose, additives such as polymers or carbon nanotubes are added to ILs in order to immobilize them (see Fig. 1.1), while keeping their interesting electrical properties. These materials are called hybrid ionogels.[16] Their hybrid characteristic comes from the fact that the properties of the material should be derivable from those of the IL and the compound that forms the solid-like network. There are physical ionogels, in which the cross-linking comes from weak interactions such as hydrogen bonding and hydrophobic interactions, and chemical ionogels, in which the solid network is formed through covalent bonding.[59] This new nature widens the possible applications of the material, with several uses in drug delivery,[60] catalysis,[61] drug detection[62] or, as we have anticipated, solid electrolytes.[18;63;64]

Hybrid ionogels are not the only kind of solid electrolyte that is available. In fact, parallel to these advances, solid polymer electrolytes (SPEs) were developed.[65] These materials are the result of the dissolution of a metal salt (usually a lithium salt) in a polymeric matrix, resulting in an ionically conducting medium. SPEs have the improved mechanical properties that the solid-like behavior entails, such as higher flexibility and thermal and electrochemical stability.[66] However, the ionic conductivity is lower compared to that of the traditional liquid electrolytes. One of the proposed solutions to this issue is to plasticize the polymeric matrix with an IL, improving the conductivity of the material. With this approach, a special kind of hybrid ionogels

is created: the conjunction of IL, metal salt and polymer form ternary mixtures that is known as ternary solid polymer electrolytes (TSPEs).[67] These materials have become one of the most promising candidates for the energy storage and battery technologies future. For these reasons, these kinds of materials will be the core systems analyzed throughout this thesis.

USC
UNIVERSIDADE DE SANTIAGO DE COMPOSTELA

2- Methods

In this chapter the main methods that were used in the development in this thesis will be discussed. As we have previously mentioned, computer simulations are powerful tools that allow the study of the systems from a microscopic perspective, more easily accessible than through physical experiments. In this thesis, we have taken advantage of this methodology to study the systems we were interested on. Basically, a simulation is a virtual replica of a real system that lies within the realms of the computer memory. Added to the fact that some properties of the systems are more readily available with this approach, the main advantage of simulations is the flexibility they provide. Performing different simulations of similar systems, or adjusting the parameters of a given study are somewhat trivial tasks in the simulation regime. This is not the case in the experimental world, where each slight adjustment could lead to high costs of both money and time.

There are computer simulation techniques for very different scales of size and time (see Fig. 2.1), ranging from very large systems, studied via finite elements calculations,[68] to the smallest scale, involving quantum calculations that deal with the electronic distributions of atoms.[69] Each scale comes with its own limitations. Macroscopically oriented techniques allow studying large sizes and time spans, but the details that can be obtained from their description are limited. The most precise techniques, however, are severely affected by the quantity of atoms that can be simulated in a reasonable amount of time, allowing only for the study of really small systems for short amounts of time. The simulations present in this thesis are classified as simulations at the molecular level. In this regime, the individual molecules of each species are explicitly considered in the calculations. The first method we employed is molecular dynamics. In this technique we study systems of a few nanometers of size length and time spans of up to μs with atomic resolution. The second method, density functional theory, lies in a smaller scale (pm and ps in length and time dimensions respectively), and allows considering even the electronic degrees of freedom of the atoms. The basis of both of these techniques, as well as the finer details that they entail, will be discussed in the following sections.

2.1 Molecular dynamics

Molecular dynamics (MD) is the first of the two computational techniques employed in this thesis. It is a simulation method that lies in the atomic level scale, where we follow the time evolution of the position, velocities and forces of a system of particles. Given an initial configuration, this evolution is achieved by integrating Newton's equations of motion. The core idea behind MD is therefore surprisingly simple, but the actual implementation depends on several details that we will discuss in detail. Firstly, the equations of motion cannot be analytically retrieved for the whole simulation time. Instead, the process must be split into several fragments (usually equidistant), called time steps. Then, for each time step, we numerically calculate the updated positions, velocities and forces based on the previous one. The finer the division, the more precise the calculation becomes. However, the number of steps needed to reach the same amount of total simulated time increases, so a compromise must be reached. The typical time step intervals used in MD are 1 or 2 fs. When the simulation process finishes, a complete collection of ordered positions, velocities and forces for all of the atoms present in our system is

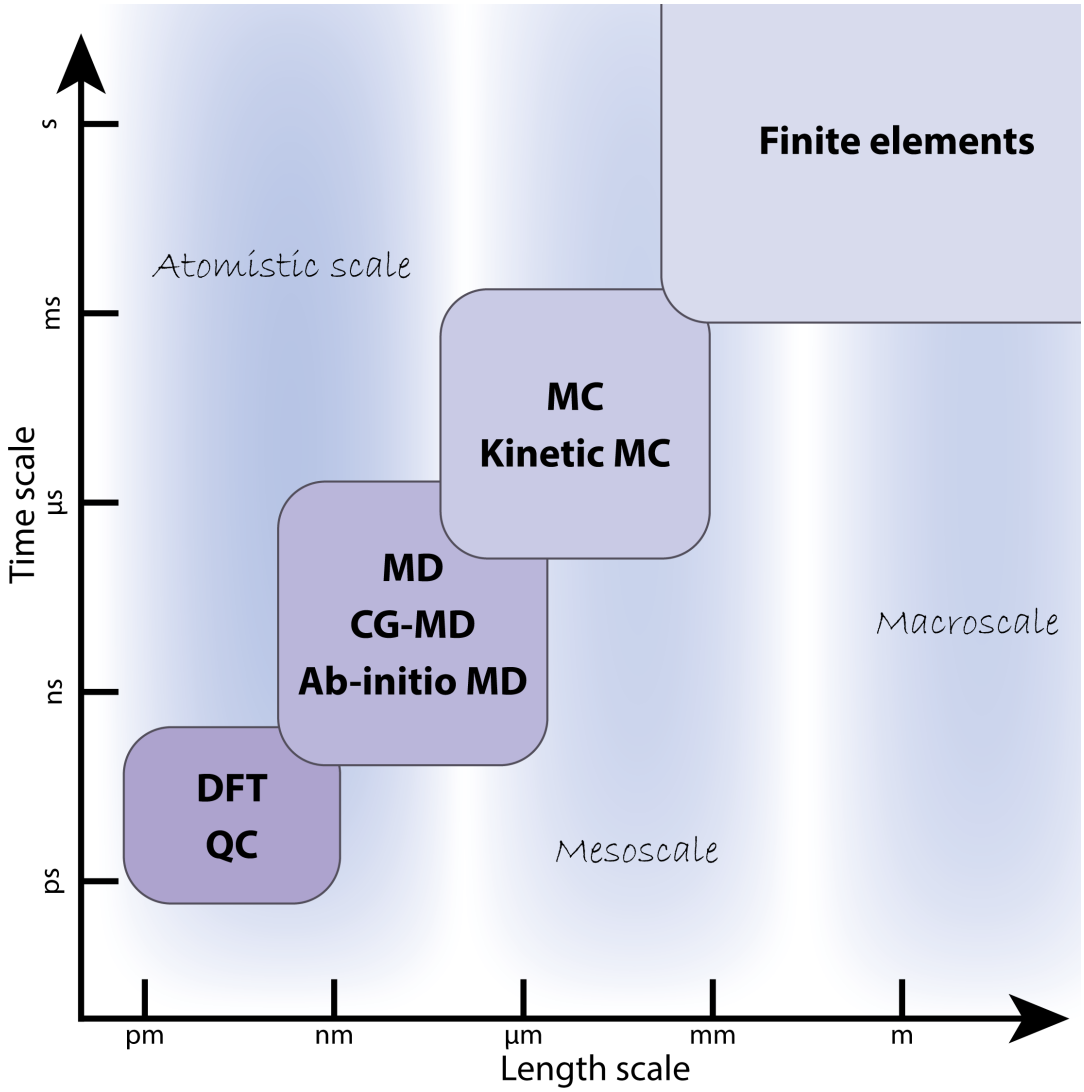


Figure 2.1: Classification of some of the most widely spread simulation techniques according to their spatial and time resolutions.

obtained. With this information, we can retrieve the relevant properties of the system through averages and correlations.

The first element needed in order to be able to perform a simulation is the initial configuration. A good initial configuration is really useful, as it will largely reduce the simulation time needed to obtain a proper model of the system. In order to create the simulation box, where our molecules will be accommodated, its total size must be first approximately obtained from the density of the system. It will also depend on the number of molecules that we desire to include. A typical MD simulation of ILs involves from hundreds to a couple thousand pairs of ions. Usually, in order to study the properties of a liquid, we will work on the bulk regime, *i.e.*, a region far enough from any surface, where the only relevant interactions are those of the molecules in the liquid. Effectively, this leads to a simulation box that is isotropic, without any privileged directions. In practice, the geometry of the box is cubic, and the box length is just the cubic root of the volume. However, if in our simulations we want to include interactions with solid systems, the box geometry must be accommodated to meet the desired configuration. In

many cases, this leads to a parallelepipedal disposition with one privileged axis, although less symmetrical options can be used in more specific environments. After obtaining the simulation box, the actual molecules must be placed inside it. There are mainly two approaches to achieve this task. One could place the molecules following a regular lattice, with the lattice constant set so that the simulation box is completely filled. The main advantage of this technique is the ease of obtaining the configuration. However, this methodology could lead to metastable positions that are not realistic. A better approach is to randomly distribute the molecules in the simulation box. The largest difficulty that this entails is guaranteeing that the molecules do not overlap each other. This problem has already been solved by the scientific community, and several software packages implement this solution. In this thesis, we used the software PACKMOL, developed by Martínez *et al.*[70] As a final step, it is usually useful to give the atoms an initial velocity. This is usually accomplished using generators based on the Maxwell-Boltzman distribution.

Once the initial configuration is set, the configuration that corresponds to the next time step is calculated. Obviously, the new positions will depend on the forces the atoms are subjected to. The collection of all interactions between particles are collected in the force field. There are many force fields available to the scientific community. Each force field is optimized to deal with a certain application, so the selection of a correct force field for the study is key. In this thesis, we have used the OPLS-AA (Optimized Potentials for Liquid Simulations, All-Atom) force field,[71;72] which is a landmark in IL simulations. In the following lines, we will briefly explain the interactions specifically considered by the OPLS-AA force field, but other force fields follow similar patterns. There are two main groups of interactions depending on the range of the interaction: bonded and non-bonded. Bonded interactions deal with the restrictions that involve groups of atoms that belong to the same molecule. Depending on the number of atoms considered, we have the bond interaction (2 atoms), angular interaction (3 atoms) and the torsion interaction of dihedrals (4 atoms). Bonds and angles are modelled using harmonic potentials, while the dihedral potential uses a cosine expansion:

$$V_{\text{bond}} = \sum_{\text{bonds}} K_r \left(r - r_{\text{eq}}\right)^2$$

$$V_{\text{angle}} = \sum_{\text{angles}} K_\theta \left(\theta - \theta_{\text{eq}}\right)^2$$

$$V_{\text{torsion}} = \sum_{\text{dihedrals}} \left(\frac{V_1}{2}\left[1 + cos\left(\phi + \phi_1\right)\right] + \frac{V_2}{2}\left[1 - cos\left(2\phi + \phi_2\right)\right] + \frac{V_3}{2}\left[1 + cos\left(3\phi + \phi_3\right)\right] \right) . \quad (2.1)$$

Non-bonded potentials deal with the long range interactions between atoms. In the case of OPLS-AA, the Coulomb force and the van der Waals dispersive interaction are considered. The dispersive forces are modelled using a Lennard-Jones 12-6 potential. Both interactions also apply to atoms that belong to the same molecule. In order to avoid unphysical effects, they are turned off for atoms that are 2 bonds or less away from each other. If the atoms are exactly 3 bonds apart, the interaction is considered but scaled by a 0.5 factor

USC UNIVERSIDADE DE SANTIAGO DE COMPOSTELA

$$V_{\text{Coulomb}} = \sum_i \sum_{j \neq i} \frac{q_i q_j}{r_{ij}}$$

$$V_{\text{dispersion}} = \sum_i \sum_{j \neq i} 4\varepsilon_{ij} \left[\left(\frac{\sigma_{ij}}{r_{ij}} \right)^{12} - \left(\frac{\sigma_{ij}}{r_{ij}} \right)^{6} \right] . \tag{2.2}$$

A schematic representation of all these interactions is sketched in Fig. 2.2. The total potential is just the sum of all aforementioned terms:

$$V = V_{\text{bond}} + V_{\text{angle}} + V_{\text{torsion}} + V_{\text{Coulomb}} + V_{\text{dispersion}} . \tag{2.3}$$

There are a couple extra concepts that need to be considered. First, in order to completely avoid border effects, periodic boundary conditions (PBCs) must be applied. In practice, this means that a particle that exits the simulation box through one side will immediately reenter it through the opposite one. This concept is equivalent to the creation of infinite replicas of the simulation box that span across all space. The long range interactions that we have discussed will be therefore computed using the smallest possible distance between each pair of atoms. In fact, in order to avoid unphysical results, interactions with particles further away than half the system size box are ignored. Another topic is the possible inclusion of extra constraints that deal with potentially problematic parts of the simulation process. An example could be hydrogen atoms, whose small mass could lead to too large displacements between time steps, causing possible errors. Examples of such constraint algorithms are LINCS[73] and SHAKE.[74]

Now that we can compute the interactions between atoms, we can obtain for each atom the net total force that is acting on them. A quick calculation using Newton's second law grants us the accelerations. From these values, obtaining the position and velocity of each atom in the next time step is possible, and several algorithms have been developed over the years for this purpose. Perhaps the most universally used integration method is the Velocity Verlet algorithm, where the positions and velocities for each atom are obtained based on the previous frame under the transformations detailed below:

$$\begin{aligned} \mathbf{x}\left(t + \Delta t\right) &= \mathbf{x}\left(t\right) + \mathbf{v}\left(t\right) \Delta t + \frac{1}{2} \mathbf{a}\left(t\right) \left(\Delta t\right)^2 \\ \mathbf{v}\left(t + \Delta t\right) &= \mathbf{v}\left(t\right) + \frac{1}{2} \left[\mathbf{a}\left(t\right) + \mathbf{a}\left(t + \Delta t\right) \right] \Delta t . \end{aligned} \tag{2.4}$$

Another popular approach is the Leap Frog algorithm. A sketch of the time evolution of the Leap Frog algorithm is depicted in Fig. 2.3. Its peculiarity is the use of velocities evaluated in half-steps.

$$\begin{aligned} \mathbf{v}\left(t + \frac{1}{2}\Delta t\right) &= \mathbf{v}\left(t - \frac{1}{2}\Delta t\right) + \mathbf{a}\Delta t \\ \mathbf{x}\left(t + \Delta t\right) &= \mathbf{x}\left(t\right) + \mathbf{v}\left(t + \frac{\Delta t}{2}\right) \Delta t . \end{aligned} \tag{2.5}$$

Each of these algorithms have their advantages for the computational implementation, but it can be proved that they lead to the same trajectory.[75] In fact, their formulation imposes by definition the conservation of energy (in other words, these integrators are symplectic). In this thesis, we have chosen to use the Leap Frog algorithm.

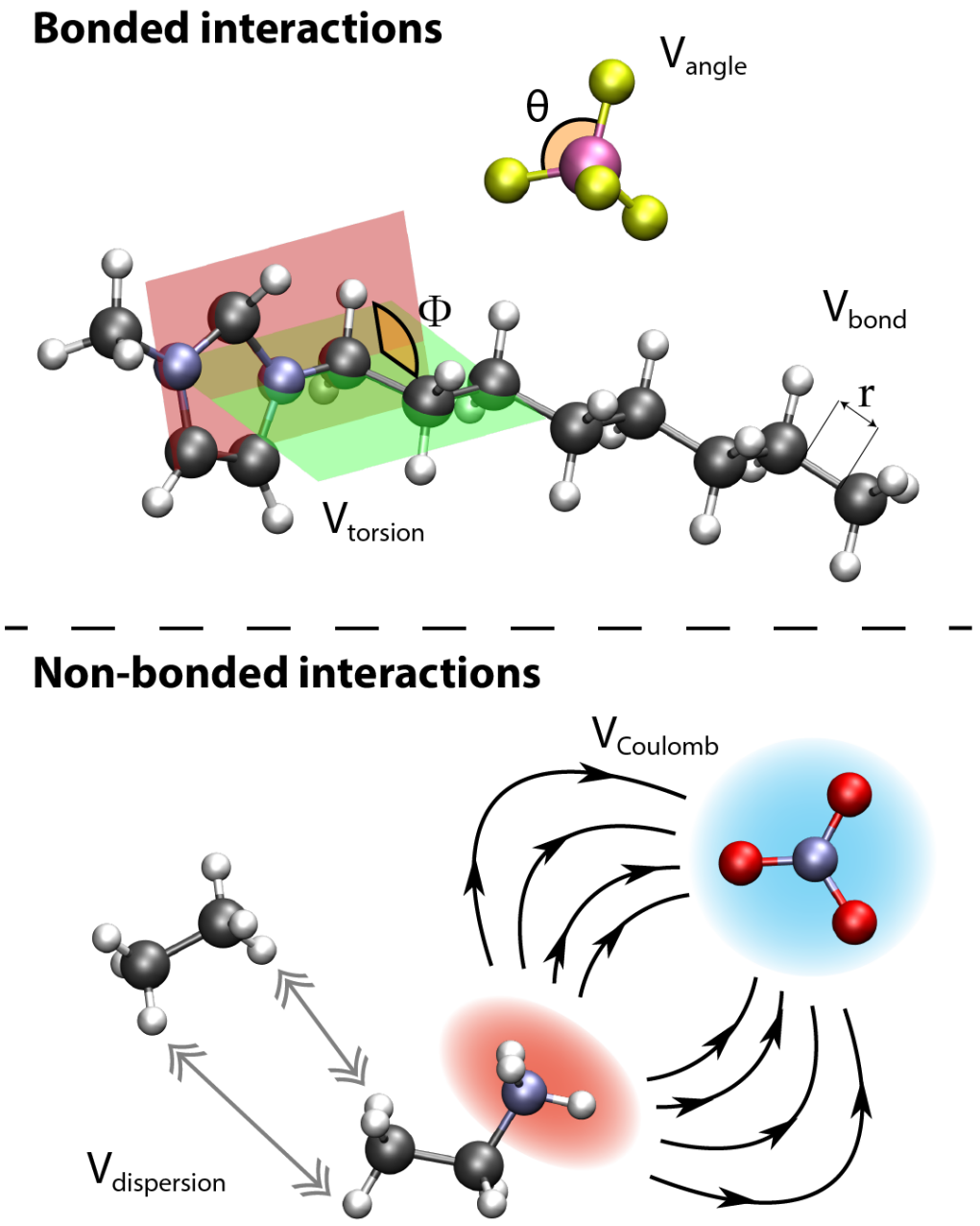


Figure 2.2: Schematic view of the different bonded and non-bonded interactions considered by most current force fields.

USC
UNIVERSIDADE DE SANTIAGO DE COMPOSTELA

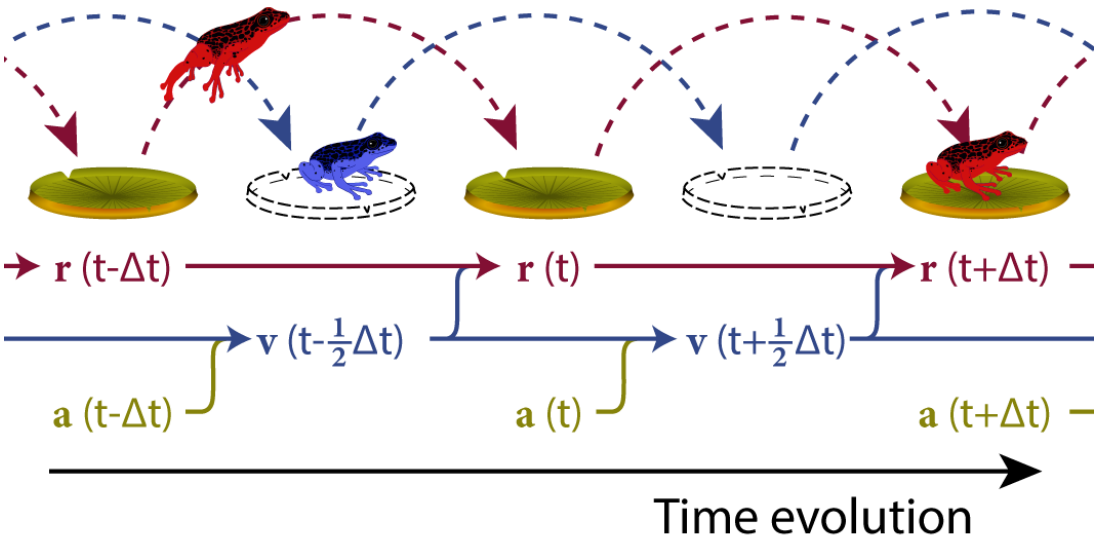


Figure 2.3: Schematic representation of the workflow of the Leap Frog algorithm.

If we naively try to perform a simulation using the discussed methodology we will probably not get reasonable results. The initial configuration, although created by pure randomness, might be deeply unrealistic. This is specially true for charged species, like ILs, where molecules of the same charge sign - although not overlapped - might be too close, generating huge electrostatic forces. If these interactions are large enough, the displacements caused would be too sizeable for the simulation to handle, leading to numerous errors. Either way, the unrealistic start will inevitably render the first steps of the simulations unusable. Any results derived from these steps would simply not be physical. Therefore, the simulation must be run for some time just to arrive at a better stabilized system. In order to assure this, we can monitor some thermodynamic variables, as the total energy, and make sure they converge with simulation time. This step is usually referred to as the stabilization phase. After the correct behavior has been achieved, we can start storing more frequently all the relevant variables, so that we can later extract the properties of the system.

As the stabilization in fact follows the same process as the "real" simulation, it is just as costly computationally. This means that it is in our best interest that this intermediate step is reduced as much as possible. For this purpose, algorithms have been developed to modify the initial configuration and to provide the stabilization with an input that is closer to the realistic system. Two are the main methods widely employed to achieve this goal, which we have made use of in this thesis. Firstly, a steepest descent algorithm displaces all atoms of the system a small distance in the direction of the net force that acts on them. After several iterations, a conjugate gradient algorithm optimizes more accurately the energy of the system via variation of the positions of the atoms. After the two methods are employed, the final configuration obtained is much more realistic and leads to small forces between atoms. The system will then correctly behave when integrating Newton's equations of motion.

The simulation procedure described upon this point conserves the energy of the system by definition. The same can be said about the number of molecules considered. At the same time, we have not provided any tools to modify the size of the simulation box. Therefore, the simu-

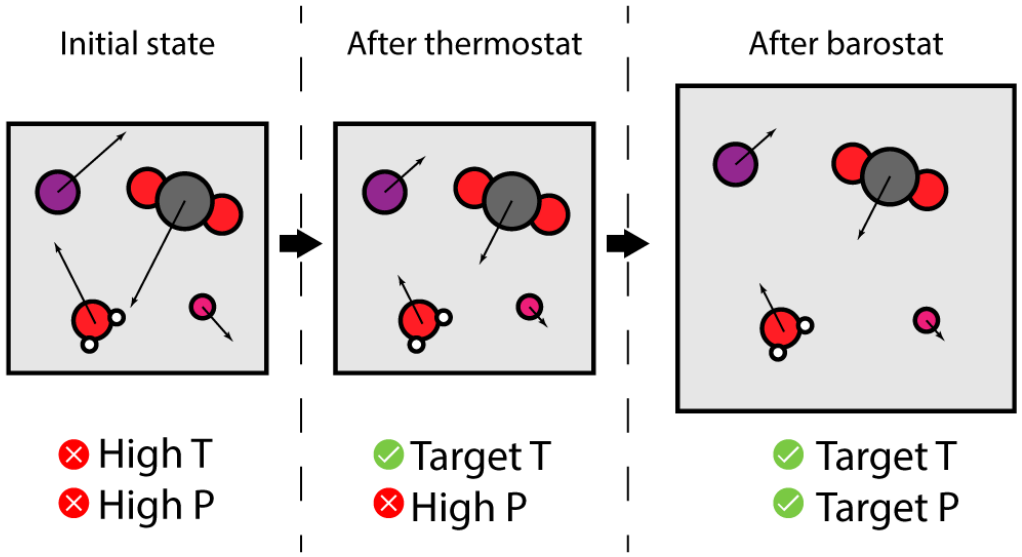


Figure 2.4: Schematic representation of the changes that thermostats and barostats induce in the simulated system.

lation carried out with this procedure will be in the NVE ensemble. However, in some cases, it could be interesting to consider simulations where we can fix the corresponding intensive variables, *i.e.*, the pressure and the temperature. The relationship between the physical experiment and the simulation would then be more direct, facilitating possible comparisons of results, as pressure and temperature conditions on the laboratory are much easier to fix. Thankfully, simulations in different ensembles converge to the same results if properly sampled.

In order to keep the temperature fixed, we need to introduce a new constraint to the system, mimicking a thermostat. Basically, the idea is to rescale the velocities of all particles in the system by a factor, so that the average kinetic energy of the system matches that of the desired temperature. There are many implementations of thermostats available, and in this thesis we have used two options: the v-rescale algorithm[76] and the Nosé-Hoover thermostat[77]. On the topic of pressure, the equivalent to thermostats are the barostats. These constraints are able to modify the simulation box shape and size so that the pressure inside the box resembles the desired one. Effectively, this means that the coordinates of all atoms are rescaled. In this thesis, we have employed the Berendsen[78] and the Parrinello-Rahman[79] barostats. An schematic view of the effect of both these constrains on a simulation step is depicted in Fig. 2.4.

Finally, as we have previously mentioned, simulations that include solid planar interfaces can be really interesting in order to understand the properties of the systems near electrodes. There are different ways to actually implement these interfaces. One of the approaches we have taken in the works present in this thesis is to include the interface atoms explicitly (in our case, carbon atoms forming a graphene sheet). The equations of motion of these atoms are ignored, and so they remain frozen in place throughout the whole simulation. However, the interactions created by their presence are taken into account. In this way, they affect the other atoms of the simulation without being affected themselves. These atoms can also be charged, allowing for the modelling of electrodes of batteries and other electrochemical devices. Notice that the interface, specially if we desire to represent a structure forming a regular lattice like graphene, must be created carefully so that the infinite replicas of the system preserve its geometry. Another

possible approach is to average out the interactions that would arise from the interface, mainly if we are not interested in the effects that might be caused by the details of the surface. This way, if we integrate the 12-6 Lennard-Jones potential over the lateral coordinates, we would obtain a 10-4 potential, which is only a function of the distance to the interface. In this thesis we have used this approach, which is faster computationally, in some stabilization phases of the works that include interfaces, whilst we used the explicit version in the actual production runs.

Although one could theoretically implement all the previously discussed algorithms and create its own MD simulation software, there are several packages readily available to use. One of such packages, that stands out due to its performance and its free access license, is GROMACS.[80;81] In addition to its large parallelization optimizations, GROMACS includes a number of tools that are useful to extract results once the simulation has been completed. In all the works of this thesis performed with MD simulations, GROMACS was the software of choice.

2.2 Density functional theory

Although MD simulations allow us to extract relevant information about the properties of the studied systems at the molecular and even atomic scale, they are not precise enough when we need to consider the electronic component of molecules. Indeed, in MD simulations we do not consider explicitly the electrons of the atoms. As the partial charge of each atom is fixed throughout the simulation, one has to resort to more refined tools to take into account the possible electronic effects that are omitted. One such example is the use of Drude particles to account for polarization effects.[82] Nevertheless, modelling possible electron transfers between molecules, or obtaining detailed information about the electronic states is not possible. For this purpose, one has to turn to a higher level theory where the electron cloud is considered explicitly. One of the most well-known methods to achieve this is the density functional theory (DFT) approach.

The aim of DFT is to solve the time independent Schrödinger equation. In the quantum hamiltonian, the nuclear and electronic interactions must be explicitly considered. In this way, the hamiltonian must include terms for the kinetic energy of nuclei and electrons, the nuclei coulombic interaction, the electronic coulombic interaction and the cross interaction between them.

$$\begin{aligned}\hat{H}|\Psi\rangle = E|\Psi\rangle = \Bigg(& -\sum_i \frac{\hbar^2}{2M_i}\nabla_i^2 + \frac{1}{4\pi\varepsilon_0}\sum_i\sum_{j>i}\frac{Z_i Z_j e^2}{|\mathbf{r}_i-\mathbf{r}_j|} \\ & -\frac{\hbar^2}{2m_e}\sum_\alpha \nabla_\alpha^2 + \frac{1}{4\pi\varepsilon_0}\sum_\alpha\sum_{\beta>\alpha}\frac{e^2}{|\mathbf{r}_\alpha-\mathbf{r}_\beta|} \\ & -\frac{1}{4\pi\varepsilon_0}\sum_i\sum_\alpha\frac{Z_i e^2}{|\mathbf{r}_i-\mathbf{r}_\alpha|}\Bigg)|\Psi\rangle\,. \end{aligned} \tag{2.6}$$

In this expression, the latin indexes run through the nuclear coordinates, while the greek indexes refer to electronic coordinates. Obtaining a solution to this equation proves to be really challenging. A common approximation is to realize that the nuclei movement is orders of magnitude slower than that of electrons. Therefore, they can be considered as fixed, and the electrons

are immersed in an external potential generated by the nuclei. This approach, known as the Born-Opppenheimer approximation,[83] effectively decouples the nuclear and electronic degrees of freedom, so the hamiltonian is simplified to

$$\hat{H} = -\frac{\hbar^2}{2m_e}\sum_{\alpha}\nabla_{\alpha}^2 + \frac{1}{4\pi\varepsilon_0}\sum_{\alpha}\sum_{\beta>\alpha}\frac{e^2}{|\mathbf{r}_\alpha - \mathbf{r}_\beta|} - \frac{1}{4\pi\varepsilon_0}\sum_{i}\sum_{\alpha}\frac{Z_i e^2}{|\mathbf{r}_i - \mathbf{r}_\alpha|}\,. \tag{2.7}$$

Still, even with this approximation, the calculation of the wavefunction proves to be really demanding, specially for systems with many electrons. Some techniques attempt to solve this equation by brute force means, most notably Hartree-Fock methods. However, the computational cost of these approaches is unreasonable for systems with as little as few molecules even for current day technologies.

In DFT, the approach taken is different. It is based around the two theorems enunciated by Hohenberg and Kohn, applicable to systems of electrons immersed in an external potential. They state:[84]

- The external potential, and therefore the total energy, are unique functionals of the electronic density.
- The electronic density corresponds to that of the ground state if and only if this density minimizes the total energy.

These theorems imply that the solution of the Schrödinger equation is no more than an optimization problem, where we need to minimize the total energy of the new system by variations on the electronic density. However, the exact relation between this energy and the density is not given. To solve this issue, Kohn and Sham introduced a fictitious system of non interacting electrons.[85] This system is chosen to produce the same density as the real one. The beauty of this approach is that the system becomes effectively decoupled and, for each fictitious pseudo-electron, we can write an independent equation for their orbitals. In other words, the many body problem has been simplified to many one body problems (see Fig. 2.5). This is much easier to solve, and critically, much faster to compute. The Kohn-Sham equation for each pseudo-electron, which is subjected to an effective potential, is therefore

$$\left(-\frac{\hbar^2}{2m_e}\nabla^2 + V_{\text{eff}}(\mathbf{r})\right)\phi_i(\mathbf{r}) = \varepsilon_i\phi_i(\mathbf{r})\,, \tag{2.8}$$

where ϕ denote the orbitals of each pseudo-electron.

Notice that the formulation until this point remains exact. The effective potential arises from different contributions.

USC UNIVERSIDADE DE SANTIAGO DE COMPOSTELA

$$V_{\text{eff}} = U + V_H + V_{xc}\,. \tag{2.9}$$

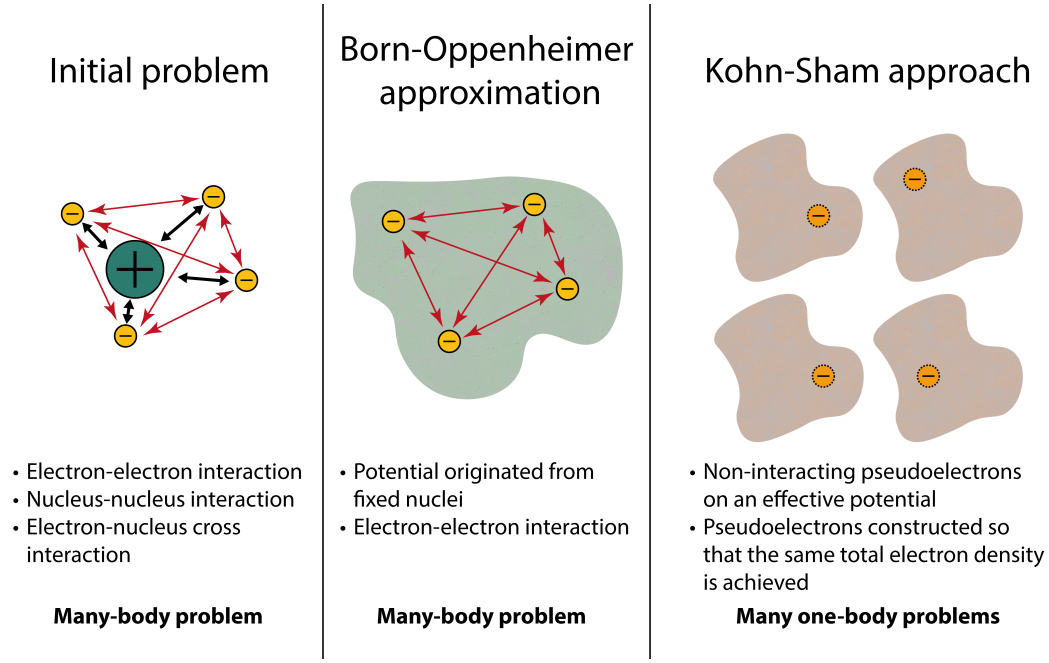


Figure 2.5: Scheme of the different degrees of approximation to the quantum many-body problem.

First, we have the interaction with the external potential, U. The extra terms are traditionally called Hartree energy, V_H, related to electron-electron repulsions, and the exchange correlation energy, V_{xc}. The Hartree energy term is well defined as follows:

$$V_H(\mathbf{r}) = \int \frac{e^2}{|\mathbf{r}-\mathbf{r}'|}\rho(r')\,\mathbf{dr}' = \int \frac{e^2}{|\mathbf{r}-\mathbf{r}'|}\sum_i |\phi_i^2(r')\,|\mathbf{dr}' \tag{2.10}$$

The exchange correlation energy term arises from all many body interactions. This term does not have an exact formulation, and so many approximations have been developed over the years to compute this term. We will now summarize these different approaches.

- **Local density approximation (LDA)** The only system where the exchange correlation term has an exact formulation is the uniform electron gas, where the electron density is constant and equal in all points in space. From this result, the first approximation developed was to consider the corresponding exchange correlation potential for the density present in each point in space. This approximation only depends on the local density, hence it was named "local density approximation".

- **General gradient approximation (GGA)** The first refinement involves the consideration of not only the electronic density but its first derivative for each point of space. One of the most widely used functionals is the Perdew-Burke-Ernzerhoff (PBE) GGA.[86] This was the selected functional in the two contributions included in this thesis where DFT calculations are performed (Chapters 7 and 8).

- **Hybrid orbitals** The current trend in DFT calculations is the use of hybrid orbitals, which arise from empirical mixes between exact results for the exchange energy with LDA and GGA orbitals.

USC UNIVERSIDADE DE SANTIAGO DE COMPOSTELA

After selecting a form for our functional, we already have all the necessary pieces. However, it is easy to realize that the problem at hand is circular. The electronic density is needed to obtain the potentials that appear in the Kohn-Sham equations. However, this electronic density is only accessible through solving these equations. To solve this issue, the usual approach is iterative. We start with a guessed initial density, which is used to solve the equations obtaining a new density. We can repeat the process with this new density (or a mix between both), so that the result is slowly refined (in a convergent way) in successive iterative steps. When the solution to the Kohn-Sham equations is close enough to the one obtained before (which is defined through cutoffs), then we have arrived at the ground state density. This is known as a self consistent field (SCF) calculation.

There is a lengthy list of available software that has been developed over the years to perform DFT calculations. In this thesis, we have performed simulations using the software packages VASP[87;88] (Vienna Ab initio Simulation Package) and Quantum Espresso.[89;90]

USC
UNIVERSIDADE DE SANTIAGO DE COMPOSTELA

Part II

Results

USC
UNIVERSIDADE
DE SANTIAGO
DE COMPOSTELA

3- Summary of the Results

In order to contextualize all the results obtained throughout the development of this doctoral thesis, in this chapter we will detail the path that we followed through these last years, and the reasoning behind all the steps that we decided to take on this journey. The general objective of this thesis was to obtain a detailed understanding of the nanostructure and the relevant interactions present in IL-based electrochemical systems. Specifically, as we were particularly interested in the characterization of electrolytes that are partially composed by ILs, we started our studies by analyzing the properties of a binary mixture of an IL with ammonia, a cosolvent of notable interest in several applications, such as in refrigeration[91], agriculture,[92] or energy storage.[93] This work did not only offer interesting results on their own, but allowed to lay down most of the reference methods that were used in the development of this thesis. That is, molecular dynamics simulations both in bulk conditions and in the presence of an interface. As we have previously mentioned, and will become apparent in the works detailed later, the addition of this interface is crucial since it allows the investigation of the interactions between the electrolyte and the electrodes, which are the key processes that rule the behavior of batteries and other electrochemical devices, and whose full understanding is critical to the field, as it would facilitate the creation of electrochemical devices with largely improved capabilities. After this initial work, we devoted ourselves to the study of the main type of electrolyte that this thesis is centered on: hybrid ionogels. We started by studying a ternary mixture (IL/Li^+ salt/polymer) in bulk conditions. In this work, we mainly focused on understanding the structure of the system, paying special attention to elucidating the role of the polymer, as well as identifying the composition of solvation shell of the Li^+ cations. After having analyzed and understood the properties of this type of electrolytes, we went a step further in the next work and considered graphene-like interfaces in the presence of the electrolyte, mimicking the structure of the electrochemical electrolyte-electrode interface of a battery. There, we studied how the presence of these electrodes modified the structure of ternary IL/Li^+ salt/polymer mixtures. Specifically, we investigated the effect of varying the surface charge of the interfaces, and the different behavior that the ternary mixture exhibited if we replaced the IL cations. After this study, it was clear that the path forward included a more detailed understanding of the interactions that took place at the interface. In order to achieve our goal, and because of the electronic origin of these interactions, we shifted our focus to a more detailed simulation technique that allowed considering the electronic degrees of freedom explicitly. Therefore, we adopted *ab initio* DFT calculations as our new methodology, a well established simulation technique for this type of analysis. As the computational cost increases rapidly when using DFT, the systems now considered must be considerably smaller, and large polymer molecules can not be usually considered explicitly. In a first work, we studied the charge transfer between a metal salt and the electrode as a function of the distance between the two. This interaction was mediated by the presence of an IL pair. Several insertion paths for the metal salt were considered and their differences studied, as well as the dissimilarities that arise when changing the metal cation of the salt (lithium and potassium). Then, in a further work, and the final one in this thesis, we extended our scope to systematically considering more metal atoms of electrochemical interest (sodium, calcium, aluminum and magnesium, as well as the already mentioned lithium). In this work, we were interested to analyze how the presence of the IL and metal salt modified the electronic properties of the surface, such as the band structure, density of states, and electromagnetic and optical properties.

In the following paragraphs, we will delve into the details of each work, such as the motivation, context and main results obtained in each one.

Back in 2019, I had just finished my Masters degree in Physics and I was looking for an emerging opportunity to pursue my academic career. I had began to steadily specialize in the soft matter field through my previous degree studies. Furthermore, at that time, I had already gained some preliminary contact with the fields of ILs and simulations previously, thanks to the support offered by some grants that allowed to conduct collaborations with my current research group during the last years of the Physics and Master in Physics degrees. The group already had an extensive knowledge and expertise after years of working and investigating ILs. It is composed of both an experimental branch and a computationally focused one. Due to my large love for computers, which dates back to my childhood, the choice was easy. Performing and analyzing simulations of these materials with both MD and DFT were the bread and butter of the group, so it was the perfect opportunity for me. Luckily, after those past collaborations, the group still considered me as a promising candidate to keep working with them, and so this thesis program was born.

Quite fortunately, a wonderful opportunity to apply all the skills previously learned, and to become completely familiar with all the simulation techniques needed, arose almost immediately when Prof. R. Lynden-Bell and Prof. A. Stone from Cambridge University were eager to collaborate in an interesting initial study. In this work, the system we considered was a binary mixture between an IL, ethylammonium nitrate ([EA][NO_3]), and a molecular cosolvent, ammonia (NH_3). Ammonia is a key component in a wide array of energy applications,[91–93] so it was a really interesting species to study. However, up to our knowledge no previous studies had been performed that considered mixtures of NH_3 with protic ILs. Moreover, the polar "head" of the ethylammonium cation is chemically similar to the ammonia molecule, which could affect the structure of the mixture, so the appeal of this study was self-evident. There, one of our main objectives was to determine the importance of considering the polarization of the molecules, which is not included by default on the most common traditional force fields. It was already well known that this property greatly affects the dynamics of the systems, but we also wanted to analyze the possible effects on the nanostructure of the mixture. In order not to overcomplicate the analysis, and to better visualize the differences between taking polarization effects into account, we only considered different models for the ammonia molecule, leaving the IL molecules untouched. Indeed, the traditional parametrization of ammonia was compared to a new model. This new representation was achieved with a 6-site model that included two new virtual atoms (particles without mass) and a restructuring of the partial charges of the system, selected in a way that it implicitly included the effects of considering the dipole and quadrupole moment of ammonia. The software CamCASP,[94] based in DFT, was used in order to obtain the aforementioned model. We performed simulations for different mole percents of NH_3 (10, 30 and 50% respectively), which would provide a further comparison analysis. We started our study with a complete characterization of the structural properties of the mixture in bulk conditions. We could observe through the calculation of the radial and spatial distribution functions that the nanostructure was similar in both studied systems, with either NH_3 model considered. $[EA]^+$ was placed in front of the ammonia nitrogen, while the $[NO_3]^-$ anions occupied the space directly above the hydrogens. In fact, NH_3 and $[NO_3]^-$ molecules competed to place in the first solvation shell of $[EA]^+$. The main difference between the models was a much stronger interactions detected between the 6-site one and the other species (specially the $[EA]^+$ polar head), which although did not modify the general structure, it resulted in a much stricter positioning. In

USC DE COMPOSTELA

the NH_3 solvation shell, $[EA]^+$ molecules are placed on top of the nitrogen atom, while $[NO_3]^-$ position themselves near the hydrogen atoms. Concentration did not seem to play an important role in the structure of the mixture. The dynamics of the system were also modified, specially in the case of ammonia, with the 6-site model showing a rattling motion that was not present in the traditional model. After considering the bulk medium, we decided to investigate how the properties of the mixture might be affected when the interaction with an interface is present in the system. For that purpose, we constructed new systems with a graphene wall at each side in the Z axis, with a separation of around 8 nm. The nanostructure analysis revealed that layering (a succession of layers of the different species of the system) took place along this axis, in the region close to the interfaces. NH_3 was the species found the closest to the interface, followed by the IL anion and cation respectively. This picture was obviously modified for charged interfaces. Indeed, as one would expect, anions were more prevalent in the presence of a positively charged interface, while cations occupied the space next to the negatively charged one. However, NH_3 molecules also competed for these positions with the ions. A Fourier transform analysis revealed that a square lattice arrangement of the molecule was formed by the anions in the first layer near the positively charged interface. The orientation and disposition of the different species in the interfacial region was also analyzed, with different results depending on the charge state of the graphene sheet. All these results were collected in a publication, which will be presented in more detail in Chapter 4.

After this initial work, we were ready to move onto studies that resembled more closely the interactions that take place in batteries. In this sense, we were particularly interested on improving the knowledge about ternary mixtures of ILs with metal salts (mainly lithium salts, the most common in batteries) and polymeric matrices. As we have previously mentioned, this new kind of materials is usually referred to as hybrid ionogels. In fact, when dealing with ternary mixtures that include metal salts, the term ternary solid polymer electrolytes (TSPEs) is also often used. Indeed, this kind of material is really promising for a wide array of electrochemical applications, and they are expected to be part of the new generation battery electrolytes. The addition of a polymer to the usual IL-salt binary mixture gelifies the material and confers a series of solid-like properties that provide enhanced mechanical properties and decreased risks such as corrosion and leakages, at the cost of a lower electrical conductivity. However, substantial effort is being focused on improving the understanding of this kind of material in order to improve this slower electronic mobility. In our group, although much work had been done over the years in the IL field, only a few studies were related with polymeric compounds. In that regard, this thesis program was also a first approach to the area. The main objective was to improve the understanding of the nanostructure and interactions that happen in this kind of systems, specially in the presence of the electrode. The importance of this description is vital, so that eventually the design of specific TSPEs with the desired solid properties but with an improved conductivity is achieved by the scientific community. Therefore, the first step in this direction was to investigate bulk simulations of ternary mixtures. Another wonderful opportunity arose to collaborate with colleagues from University of Münster and Helmholtz Institute. The groups of Prof. A. Heuer and Dr. D. Diddens already had a lot of experience in the field of polymeric mixtures, with a large amount of very relevant pieces of work in the matter. This meant that this was a really unique opportunity to dive into this field.

The first challenge that we faced was dealing with the packing of long chains in the simulation box. Most of the software that groups traditionally use to fill the system to obtain the initial configuration (PACKMOL in our case) is flawed when these large molecules are considered.

USC DE COMPOSTELA

The root cause is that periodic boundary conditions are not usually considered in this step, and as a consequence the molecule is only fitted in the system if all of it is contained within the simulation box. This is not a problem when the molecules are an order of magnitude smaller than the whole system, but when large molecules are considered, the only option is to place them near the center of the simulation box. As a consequence, all the other, smaller species get displaced to the sides. This configuration is not well constructed as a starting point for our simulations. One thing to keep in mind when working with these kind of solid-like electrolytes is the greatly reduced dynamics of the system. Therefore, if the initial configuration is not realistic enough, the amount of simulation time needed to arrive at a stable configuration is really long, often unsustainable. Therefore, we developed a tool that extends the functionality of PACKMOL, packing the molecules whilst taking into account the periodic boundary conditions so that we could perform our simulations. Basically, after placing each large molecule at the center of the box, we displaced it via a random vector, and then applied the appropriate PBCs, obtaining the desired result.

We selected polyethylene oxide (PEO) as the polymer in our study as it is one of the most established and best known species. We then performed a study to determine what IL would be a suitable candidate as a cosolvent of PEO. Binary mixtures of IL and PEO were analyzed for several different IL candidates, paying special attention to the formation of clusters of polymers and the values of characteristic polymer properties that point out if the dissolution is optimal. After these considerations, ethylammonium acetate [EA][ACE] came out on top and was selected. The lithium salt [Li][ACE] was chosen to match the anion of the IL. Having decided on the different components of our system, we shifted our focus to understanding the structure of the system, and how the presence of polymer affects the properties of themselves studied binary IL-salt mixtures. The main conclusion we obtained was that the addition of the polymer did not greatly modify the solvation shells of the different species. A really strong Li^+-ACE^- interaction was detected, revealing that they form strong Li^+-ACE_4^- tetrahedral complexes that the polymer network is not able to disturb. Two coordination modes (mono and bidentate) were found. In fact, no preferential adsorption of lithium on PEO was detected, as opposed to other results present in the literature for different mixtures with other ILs. The percentage of Li^+ cations not coordinated with $[ACE]^+$ was determined to be below 1% in all simulated systems. The polymer was in effect acting as a support matrix, holding the mixture together and providing some mechanical advantages, but the properties of the binary mixture remained unaffected. This was further confirmed with the analysis of the hydrogen bond network, which was changed with the relative concentration of salt, but it was not disturbed by the presence of the polymer. These results were summarized in a publication presented in detail in Chapter 5.

The most natural way to continue this research line, and to arrive to an even more detailed representation of the environment around these electrolyte materials in the neighborhood of the electrodes of batteries, was to include a solid interface and study its effect. Really scarce work was conducted in this field up until this point. The only previous study, reported by Lourenço *et al.*,[95] considered a TSPE using an united atoms force field to describe the polymer chains, as opposed to the more detailed all atom force field we considered. At the same time, certain properties such as the orientation of the polymer chains were not studied in that previous publication, so our study was one of the pioneering works in the research of TSPEs in the presence of interfaces. It has to be noted that the dynamics of the system was then even more restricted by the presence of the interface, so the time needed (both simulation time and computation time) reached really large values. The simulations took around 2 to 3 months each in the most powerful

UVa DE COMPLUTELA

machinery of our cluster as well as some of the computers in the Helmholtz Institute of Münster. The simulated times were 500 ns, which is an order of magnitude higher than the typical values for more fluid systems. These long times were selected in order to ensure that a proper scanning of the energetic landscape was performed, once again because of the slow dynamics of the systems. In fact, the mixtures were simulated at 423 K, a relatively high temperature, after doing some preliminary tests at room temperature and observing that the system atoms (specially Li^+ cations) were almost frozen in place. Without barely any dynamics, the higher temperature that we eventually selected was necessary. Furthermore, the charges of all atoms were scaled down to 80% of their values. This is a common practice to preserve structural results and enhance the dynamics of the system without having to resort to polarized simulations, which would take our already really long simulations (in real and simulated time) to unreasonably large simulation times. The system was then much more mobile and we were able to investigate the effects on the nanoconfinement of the system. In this work, we opted to change the IL anion, as the previously considered one restricted too much the movement of Li^+. The direct interaction between lithium and polymer was relatively small, and we were interested in a system where this was not the case. In fact, studies in the literature have shown that the interaction with the polymer backbone can open up new transport mechanisms for the Li^+ cation.[96] In order to achieve this, the usual approach is to select an anion with delocalized charge, and we selected bis(trifluoromethanesulfonyl)imide ($[TFSI]^-$) for this purpose. This ion was accordingly selected as the lithium salt anion. As for the IL cation, we selected two candidates, and performed simulations for both of them to compare the properties. These two cations were 1-butyl-1-methylpyrrolidinium ($[PYR_{14}]^+$) and 1-ethyl-3-methylimidazolium ($[EMIM]^+$).

Once again we were particularly interested in studying the environment of Li^+, as it is the main charge carrier of the system, and its surroundings will dictate how this charge transfer might be carried out. RDFs and coordination numbers showed that Li^+ is mainly coordinated with oxygen atoms, both from the $[TFSI]^-$ and the PEO molecules. In the vicinity of the wall, the fraction of lithium cations coordinated with the polymer further increased. This result was different from what Ebadi *et al.* had found on Li metal surfaces,[95;97] where the opposite effect happened. This difference might be caused by the hydrophobicity of PEO, that enhances its interaction with the graphene surface. In fact, an analysis of the densities of the different species from a lateral view revealed that the polymer accommodated itself in a first layer next to the surface, allowing for Li^+ to be coordinated with its oxygens in this region. Charging the electrodes obviously modified this picture, as the IL counterions placed themselves near the interface with opposite charge. Interestingly, Li^+ cations could only reach the electrode in the $[PYR_{14}]^+$ based systems, a crucial fact that might render them more suitable as potential electrolytes for batteries and other electrochemical devices. In this work, we also analyzed the different orientations that molecules adopted with respect to the interface. Interestingly, the polymer backbone sat mainly parallel to the graphene sheet plane, which ensured a proper contact with the electrode. Once again, this is an effect caused by the enhanced interaction of PEO with the hydrophobic graphene-like surface. This fact was specially true near the positive electrode, as the negatively charged oxygens were strongly attracted to the positive graphene sheet. An analysis of the polymer structure revealed that the radius of gyration of PEO was larger on the vicinity of the interfaces, probably due to some stretching of the polymer backbone in order to maximize the favorable interaction with the graphene interface. Some analyses of the dynamics were also performed, which showed the difference in relative movement freedom between the lateral and perpendicular axis of the simulation box, specially in the interfacial region. With this pioneering

work we shed some light on a number of unknowns in this emerging field, such as the importance of the hydrophobicity/hydrophilicity of the polymer backbone and the electrode material, the general nanostructure of the system or the significance of the selection of an appropriate IL cation. This set a starting reference from which future studies (from our and other researching groups) will emerge. In Chapter 6 a complete discussion of all these results will be presented in detail.

After achieving a deeper understanding of the overall structure, what we sought now was to improve our knowledge about the interactions that take place at the interface. To achieve such a detailed description, we must consider issues where MD simulations are not precise enough, as for example charge transfer between electrolyte and electrode. Indeed, an explicit consideration of the electronic cloud of the molecules is necessary in order to study these environments in depth. Therefore, we deemed it necessary to "lower the scale" and to move into more accurate ab initio methods, such as DFT. The computation time that is needed for DFT simulations scales exponentially with the number of electrons being considered, so the total amount of atoms in the system that might be simulated in a reasonable amount of time is greatly reduced. We move from systems with sizes of around 10 nm in length and tens of thousands of atoms, to systems with 1-2 nm of side length and around a hundred atoms. A side effect of this performance downgrade is that we cannot consider the polymeric long chains explicitly, as they would slow down our simulations beyond any reasonable limits. Note that in our simulations each polymeric chain consists of more than a hundred atoms. Luckily, the polymeric matrix should be just a supporting scaffold to the liquid electrolyte, and not play any relevant role in the electronic interactions of the electrodes. Therefore, we made the compromise to only consider the metal salts and the IL molecules in the presence of the interfaces.

Specifically, in our first DFT study, we investigated how the electron charge transfer takes place between the salt cation and the surface. In order to achieve this, we placed a metal atom at a certain fixed distance from the electrode, and IL molecules in the nearby surroundings. In successive DFT calculations, the distance between the metal atom and the electrode was manually lowered, and the properties of the system such as the total energy or the charge of each species were obtained for each position. This allowed drawing a smooth profile of these quantities, so as to predict if the electron transfer did exist and to determine when it took place. In this study, the selected IL was 1-butyl-3-methylimidazolium tetrafluoroborate ([BMIM][BF_4]), one of the most well-known and studied ILs, and we considered two different salts (whose cation is the metal atom we fix), [Li][BF_4] and [K][BF_4], to investigate the possible differences between compounds. At the same time, two different electrode models and their respective approach routes were considered. On the one hand, we examined a planar electrode composed of one pristine graphene layer, which was approached perpendicularly by the metal atom. This is, the distance between metal and the graphene plane was fixed and lowered in successive DFT simulations. On the other hand, we had a look at an electrode comprised of 3 stacked graphene layers, where the cation approached this interface using a path parallel to the graphene sheets. As there was empty space between the layers, this approach route actually allowed considering intercalation of the metal inside the electrode.

In the first set of simulations, the energetic profiles showed a minimum when the metal is close to the interface and a maximum when it crosses the IL layer. Li^+ achieved a closer minimum to the electrode, which relates to its smaller ionic radius compared to that of K^+. The IL molecules formed a layer that was also actually slightly adjusting its position, moving in the

opposite direction of the metal. We also investigated how the charge of the different species was modified when adjusting the metal position. We could see how there was minimal charge reorganization in the graphene interface, and the metal compound MC_6 (formed by the metal and the closest 6 carbon atoms) did not achieve large enough negative charge at any intermediate distance between the metal and the graphene electrode. Therefore, we could not consider that a successful charge transfer took place. This frustration prompted us to perform the second set of simulations, where the intercalation of the metal inside the electrode was possible. Indeed, when looking at the energetic profile, a clear local minimum appears in a position where Li^+ is found inside the electrode. Interestingly, the IL layer now moved in the same direction as the metal atom, possibly due to the lack of π orbitals from graphene in the IL vicinity that were present in the first set of simulations. The charge obtained by the compound MC_{12} (this time formed by the metal and the 12 closest carbon atoms, from the graphene sheet directly above and below the metal approach path) was deemed enough to consider that charge transfer between electrolyte and electrode took place, and therefore we concluded that the insertion inside the electrode is necessary for this kind of interactions. All the results discussed have been collected in a publication that will be presented in more detail in Chapter 7.

Finally, in the last work presented in this doctoral thesis, we followed this same line of investigation with another DFT study of a metal salt in the presence of an IL and a graphene interface. This time, we were mostly interested in the effects on the electronic properties of the material, such as the band spectra or the density of states. The metal cation choice was systematically broadened to include some other elements (Na, Ca, Mg and Al, added to the Li cation already used in the previous work) that are usually present in salts used in electrolytes in various applications. In total, we had 5 different systems, including a final one without metal for comparison purposes. After a complete ionic relaxation performed via DFT, the analysis started focusing on the charge redistribution that takes place in the system. We could see how the metal is responsible for transferring the charge to the graphene electrode. This charge transfer is different for each metal, explained by the different ionization energies of each atomic element. Particularly, Mg barely transferred any charge. Furthermore, the redistribution of charge in the graphene surface was also different depending on the metal, as Li, Ca and Mg polarized much more markedly the electronic distributions. This charge analysis was completed studying the redistribution of electronic density in the system. As one would expect, the introduction of a metal lead to a depletion of electrons in its surroundings, while mainly the carbons from graphene obtained electron gains. The structure of all the systems was similar, the metal lying between the graphene surface and the IL anion. The exception is the Mg system, where the metal was placed in the same layer as the IL molecules and much further away from the surface. This was consistent with the lack of charge transfer detected, which caused no preference for Mg to stay close to the graphene sheet. Looking at the binding energies, Li based was the more stable system, while Mg exhibited the lowest one.

In order to further investigate the electronic properties, we noticed that the system was actually composed of two parts with clear differences that needed their own analysis tools. On the one hand, we had the solid region, with the graphene surface, where all free electrons lied. We analyzed its band structure and found that the Dirac cone (typical of graphene systems) was always being downshifted, creating a n-type dopant material. This shift did not happen to graphene with just the addition of IL, and is therefore an effect of the metal atom. In fact, we showed that there existed a direct relation between the amount of charge that the metal atom transferred and the degree of shifting that was present. Looking at the band structure, we could

USC DE COMPOSTELA

see that the underlying graphene spectra was still preserved, and just shifted the same way as the dirac cone. Its shape was only modified moderately by the Ca atom, which is the metal atom that transferred the most charge. Moreover, new horizontal lines in the spectra appeared due to the presence of the molecular species.

On the other hand, we had the molecular region, comprised of the IL and metal atoms. We analyzed the partial density of states, revealing which states and orbitals corresponded to which species in the system. There were two systems with states near the Fermi energy level, which would be interesting for electronic device applications. These systems were those considering Mg and Ca. However, in the case of Mg we already described how the charge transfer was frustrated due to the structural positioning of the system. For the Ca system, the relevant state corresponded to the IL cation and not to the metal. The energy gap between the highest occupied molecular orbital and the lowest unoccupied molecular orbital of the systems (often abbreviated in the literature as the HOMO-LUMO gap) revealed once again that Mg was the metal atom that interacted the most with the IL and the least with the graphene surface.

Finally, an analysis of the optical properties of the system was carried out. As the electronic properties of the system were modified by the metal atoms, the optical features of each system were modified accordingly. Different magnitudes were analyzed, such as the dielectric constant, refractive index or the extinction coefficient. All the properties studied showed an anisotropic behavior, with different results for incoming parallel and perpendicular electric field. Collective interactions, for example, were observed just in the parallel case. All the results described until this point will be presented in detail in Chapter 8.

In summary, the complete picture of this novel kind of electrolyte systems obtained from the computational point of view will be drawn by the studies that we have briefly discussed in this section. Each of the following chapters will contain the aforementioned works, where the different approaches and results will be discussed in detail. Moreover, each chapter will be prefaced by a brief summary, which will include a disclosure of my specific contributions to the publication.

USC
UNIVERSIDADE DE SANTIAGO DE COMPOSTELA

4- The interaction of ammonia with the protic ionic liquid ethylammonium nitrate: a simulation study

Summary of the chapter

We started this thesis with a first work in which we analyzed the properties of an ionic liquid mixture. For that purpose, we performed a molecular dynamics study of ammonia solutions in a protic ionic liquid with a structurally similar cation, ethylammonium nitrate. Using two different models of the ammonia molecule, a conventional 4-site model and a 6-site model optimizing the dipolar and quadrupolar electron distributions, we evaluate their effect on the microstructure and single-particle dynamics of these mixtures, as well as on their behavior at the electrochemical interface. Quite significant differences are found on the solvation of ammonia in these dense ionic solvents, the 6-atom model predicting a stronger affinity of solvent molecules for the cations of the solvent as well as a caging effect on NH_3 solvation shells, not predicted by the 4-site model. Finally, we discuss the structure of the liquid layers near charged graphene walls. The structure in the layer next to the wall varies with the charge on the wall and varies with the model used for ammonia.

The post-print version of the publication reproduced in this chapter (including the full list of authors and their affiliations) can be found in appendix A.1, while the corresponding supporting information lies in appendix B.1. At the same time, in appendix C.1. we have included a complete disclosure of the relevant information related to this publication, including the authorization of the journal to reproduce its contents in this thesis, and the contribution of the author of this thesis to the publication.

4.1 Introduction

The change of the lifestyle of people all around the world due to the development of technology has led to a high demand of temperature control devices. In this context, refrigeration engineering is used every day in many different fields including food industry, air conditioning, electronic devices and medical technology.[98–101] Compression refrigerators typically employ hydrofluorocarbons,[102] but the research of efficient refrigeration systems with minimal impact on the environment is leading to an increasing adoption of ammonia as a refrigerant.[91] In the case of absorption refrigeration systems, they usually use a pair of materials (refrigerant/absorbent) that is completely soluble over a wide temperature range, such as a simple salt (lithium bromide or lithium chloride) and water[103] or ammonia (NH_3) and water.[104] However, other absorbents like ionic liquids (ILs) have been proposed as alternatives to avoid the drawbacks of the former working pairs.[105]

ILs are salts that melt below 100 °C. They offer some physical properties, including negligible volatility, wide liquid range and relatively high thermal stability,[106] that make them useful as new absorbents in absorption refrigeration cycles. With the purpose of finding new promising working pairs containing NH_3 as refrigerant and ILs as absorbent, researchers have analyzed several thermodynamical properties such as miscibility, heat capacity and enthalpy of absorp-

tion. For example, Yokozeki *et al.*,[107;108] one of the pioneers in this field, observed extremely high solubilities of ammonia in ILs. Experimental data on the solubilities of NH_3 in ILs has also been reported by Li and coworkers,[109] who concluded that this solubility increases with the increase of alkyl side chain length but decreases with the rise of temperature. More recently, Coronas and coworkers[110–113] reported several studies focusing on this topic. They stated that the presence of a hydroxyl group in the cation structure of the ILs enhances the solubility of ammonia, and they also indicated that 1-(2-hydroxyethyl)-3-methylimidazolium tetrafluoroborate [EtOHmim][BF_4] is a suitable IL as absorbent for ammonia.[111] Working with this IL, they also analyzed its interaction with ammonia and they found that it preferentially occurs through the hydroxyl group in the cation, whereas the interaction through the anion is favored only at lower temperatures.[113] Interestingly, Swarnkar *et al.*[114] tried to avoid one of the problems of ILs, their high viscosity, by using water as a co-solvent, and they obtained a slight decrease in the coefficient of performance but a large decrease in circulation ratio. In addition, several research groups[115–117] performed cyclic voltammetric analysis using glassy carbon and platinum electrodes, respectively, to study the direct electrochemical oxidation of ammonia in several ILs, and they showed that the ammonia cation is formed after oxidation of NH_3.

On the other hand, several computational studies were also proposed to obtain a molecular level understanding of these systems and to predict some thermodynamic properties for conditions under which experiments are difficult to perform. For example, Shi and Maginn[118] performed Monte Carlo (MC) simulations to compute isotherms for ammonia absorption in ethyl-3-methylimidazolium bis(trifluoromethylsulfonyl)imide ([emim][TFSI]) at several temperatures. They observed that NH_3 interacts more strongly with the cation than with the anion due to the strong hydrogen bond that ammonia forms with the hydrogen atoms in the ring of the cation. They also suggested that the cation plays a larger role in determining the NH_3 solubility in ILs. This same conclusion was reported by Kapoor *et al.*[119] by using molecular dynamics (MD) simulations in a study in which they also observed the decrease of the solubility with the temperature. In addition, their results indicated that NH_3 is less soluble in ILs than SO_2 but more than CO_2 and CH_4. Another approach, the COSMO-RS method, was employed by Palomar and coworkers[105;120;121] to elucidate the structural characteristics enhancing the solubility of NH_3 in ILs and, thus, were able to propose the absorbents with the most favorable properties for ammonia capture. In good agreement with previous works, they concluded that attractive hydrogen-bond interactions determine the increasing gas solubility, due to which some conventional ILs (such as [emim][TFSI]) do not seem to be optimum solvents for ammonia absorption since they behave mostly as hydrogen-bond acceptors. Instead, they encourage the use of OH-functionalized cations and propose [EtOHmim][BF_4] and [choline][TFSI] to implement novel NH_3 absorption systems. More recently, Becker *et al.*[122] also carried out MC simulations to predict some thermodynamic properties and estimate the performance of absorption refrigeration cycles using [emim][TFSI] and [emim][SCN] with NH_3, observing a better performance of the former.

However, we are not aware of any studies analyzing the interaction of ammonia and protic ILs, which are well-known for the presence of strong hydrogen bonds between the cation and the anion.[123] On the other hand, the role of quadrupole moment in the rationalization of molecular properties and intermolecular intreactions is well-known,[124] specifically in the case of nonrigid systems such as ammonia for which the role of the vibrational or even rotational effects is usually important. For that purpose we performed MD simulations of mixtures of NH_3 and the most studied protic ionic liquid ethylammonium nitrate (EAN). Thus, in this work we will analyze, for

USC DE COMPOSTELA

the first time, mixtures of ammonia with an IL including a cation with a similar molecular head group NH_3^+. Moreover, we compare two different molecular models for NH_3, a conventional 4-site one and a new 6-site model that describes the electrostatic interactions more accurately by including the dipolar and quadrupolar electron distributions around the nitrogen atom in addition to point charges on the atomic sites.

Ionic liquids and their solutions are of great importance for advanced electrochemical energy storage,[125;126] and ammonia is starting to be considered a key player also in this field because of its use in a thermally regenerative ammonia-based batteries[127;128] or to its role as a high conductivity switch in solid-state lithium batteries.[129] However, there is a total dearth of studies of ammonia-IL mixtures at the electrochemical interface. Therefore, our bulk simulations are extended to investigate the behaviour of ammonia/EAN solutions near charged walls.

4.2 Simulation Details

In this study, we introduce a new molecular model for ammonia that contains a better description of the charge distribution of the ammonia molecules by including a quadrupole and a small dipole on the nitrogen site in addition to site charges. These are modelled by two additional virtual sites with charge but without mass, localized on the symmetry axis of the molecule (0.2646 Å away from the nitrogen). The N-H bond distance is 1.01 Å. The charge of each hydrogen is +0.330e, the nitrogen charge has a value of +2.670e, and the virtual atoms have a charge of -1.7035e and -1.9565e, respectively (see Fig. 4.1). The bond angle is 106.67 degrees.

The model was developed from a DFT electron density calculated with CamCASP[130;131] using the PBE0 functional[132] with asymptotic correction and the aug-cc-pVQZ basis set.[133;134] The atomic multipoles were obtained from iterated stockholder (ISA-GRID) atom densities,[135] and the charges on the atom sites and the two additional sites were initially chosen to reproduce the H atom charges and the N atom charge, dipole and quadrupole. These values were then adjusted slightly to optimise the agreement with the electrostatic potential of the total DFT electron density, calculated on the surface at 1.5 times the van der Waals radii, in order to take into account to some extent the effect of higher multipoles. For comparison, we also employed a conventional ammonia model (4-site model) with bond distances of 1.020 Å, and a nitrogen and hydrogen charge of -1.020e and +0.340e, respectively (Fig. 4.1). This model was reported by Rizzo and Jorgensen in Ref. 136. It must be noted that our ammonia model does not consider proton-transfer reaction effects, which would provide us with results on the behaviour of the mixtures more consistent with reality. But the goal of this work is to analyze the effect of the quadrupole by quantifying the differences between both models from a theoretical point of view. The parametrization of the IL - ethylammonium nitrate (EAN) - is detailed in the supplementary information.

Atomistic MD bulk simulations of mixtures of EAN and ammonia were performed for several concentrations, ranging from 10 to 50mole% ammonia. The concentrations are defined by the number of ammonia molecules divided by the total number of ions. Thus a 50% mixture has equal numbers of cations, anions and ammonia molecules. Each of these simulations was carried out for both ammonia models. Furthermore, bulk simulations were later extended to a nanoconfined environment by placing the mixtures between two rigid graphene walls (one layer thick, situated 8 nanometers apart along the z axis) that were either electrically neutral or charged

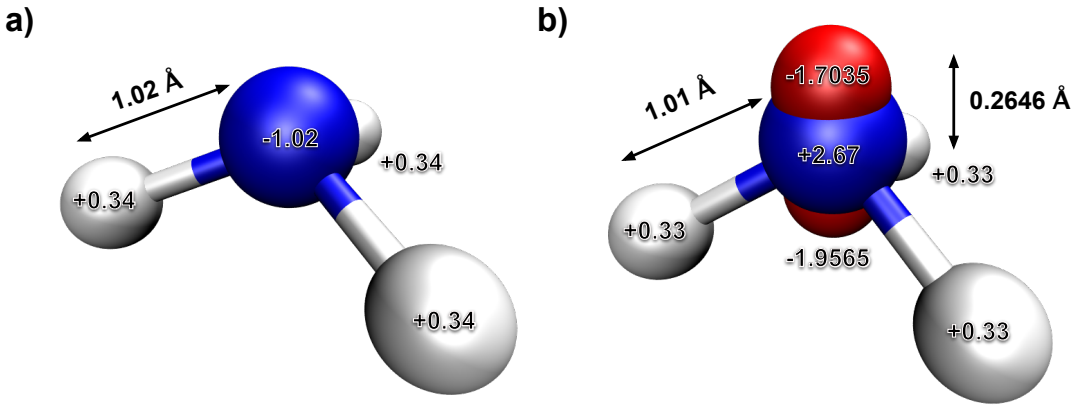


Figure 4.1: Conventional 4-site model (left) and 6-site model (right) for ammonia showing the partial charges and bond distances.

(one positively and one negatively, with charges $\pm 1 e/nm^2$). The total number of molecules was 600 for the 4-site ammonia model simulations and 500 for the 6-site one in the bulk simulations, which was increased to 1200 in both cases for the nanoconfined ones. Bulk simulations were performed in the NPT ensemble (1 atm, 298 K), while nanoconfined simulations were carried out in the NVT one (also at room temperature).

We performed all of the simulations reported in this paper using the open source Gromacs 2016 package[81;137] with the OPLS-AA force field,[72] which includes both intramolecular (bond stretching, dihedral torsion and angle bending) and intermolecular forces (a van der Waals and a Coulomb term). The PACKMOL[70] software was employed to obtain the initial configurations of our simulations, followed by proper minimization and stabilization (at least 10 ns) of the systems. The confined simulations also incorporated an annealing run (1ns) to avoid metastable configurations in which the temperature was linearly increased to 600K and then decreased back to the simulation temperature. The production runs used for the structural analysis were 10 ns long, while in the simulations used for the single-particle dynamics the velocities were saved at each time step (1fs) during runs of 100ps.

4.3 Results and Discussion

In order to understand the structural properties of our mixtures, studying the radial density functions (RDFs) of the system is needed. This function is defined as

$$g(r) = \frac{1}{\rho N} \langle \sum_{ij} \delta\left(r - r_{ij}\right) \rangle \tag{4.1}$$

where ρ is the number density, N the number of particles in the simulation box and the brackets refer to an ensemble average. In Fig. 4.2 the RDFs between nitrogen sites on each of the ions of the IL and the nitrogen sites on ammonia (both models). As can be seen in Fig. 4.2, the

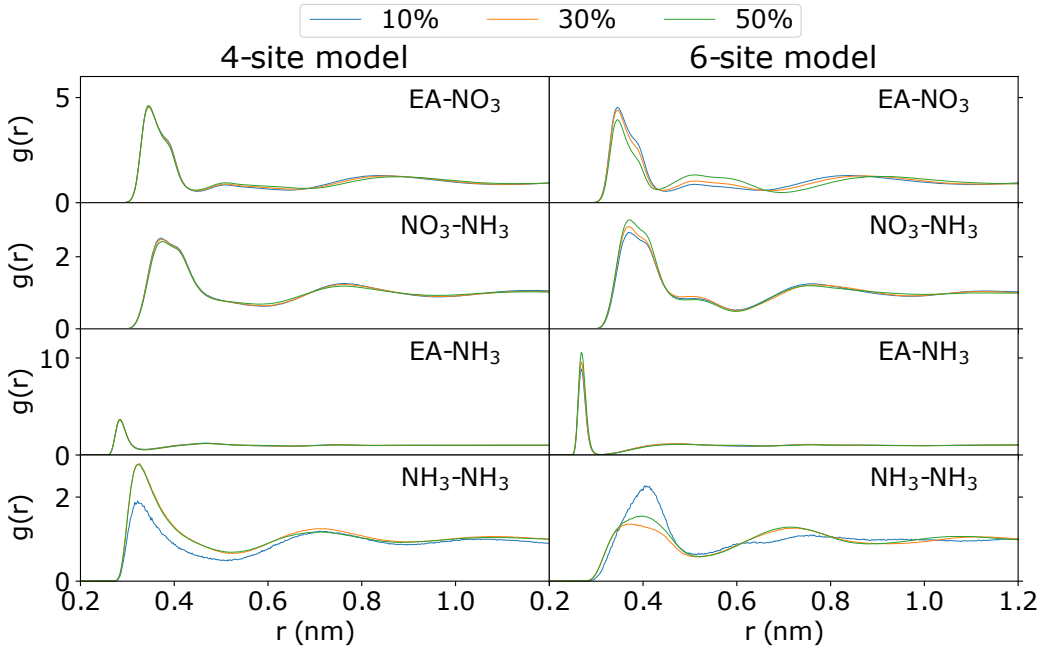


Figure 4.2: Radial distribution functions for the 4-site (left) and 6-site (right) models. From top to bottom, the results are calculated between nitrogen sites on species EA^+ - NO_3^-, NO_3^--NH_3, EA^+-NH_3 and NH_3-NH_3 for three different concentrations of ammonia: 10 mole% (blue), 30 mole% (orange) and 50 mole% (green).

major effect of the 6-site model with electrostatic interactions is the enhancement of EA^+-NH_3 interactions, reflected in a very large increase of the height of the first peak of $g_{EA-\mathrm{NH_3}}$. This leads to a restructuring of the solvation shell of all the species in the mixture as the first solvation shell of EA^+ is enriched with ammonia, expelling the other species to a second layer. This is the origin of the increase of the height of the second peak in $g_{EA-\mathrm{NO_3}}$ and $g_{\mathrm{NH_3}-\mathrm{NH_3}}$, located at 0.65 Å and 0.7 Å, respectively. We can also observe in Fig. 4.2 that the positions of the first peaks are not shifted by the presence of the quadrupole in the ammonia molecule. The position of the EA^+-NO_3^- main peak is 0.35 nm, while the peaks for the NO_3^--NH_3 and EA^+-NH_3 coordinations appear at 0.37 and 0.28 nm, respectively. The effect of the multipolarity is apparent, as the height of the first peak has a dependence on concentration in the 6-site model, a property that does not appear in the 4-site model. Moreover, there is a large increase in the height of the peak between the cation head and the ammonia, which shows an enhanced interaction between these two species when using the quadrupole. This explains the dependence on concentration, as the ammonia molecules effectively compete with the anions occupying the positions in the first shell around the cation, so the EA^+-NO_3^- first peak decreases with increasing ammonia concentration, displacing the anions to a second shell. This preference of ammonia for interacting with the head of the ethylammonium cation is in good agreement with the results reported by Maginn *et al.*,[118] who observed a clear preference for the basic nitrogen of ammonia to associate with the acidic hydrogen on the ring of the imidazolium cation.

In order to complete our structural picture, we calculated spatial distribution functions (SDFs) for the different species in the mixture. As the ammonia is the central point of this work, we decided to obtain the isosurfaces of numerical density of each IL species using the three hydrogens of each ammonia molecule to define a local reference frame. In Fig. 4.3 the

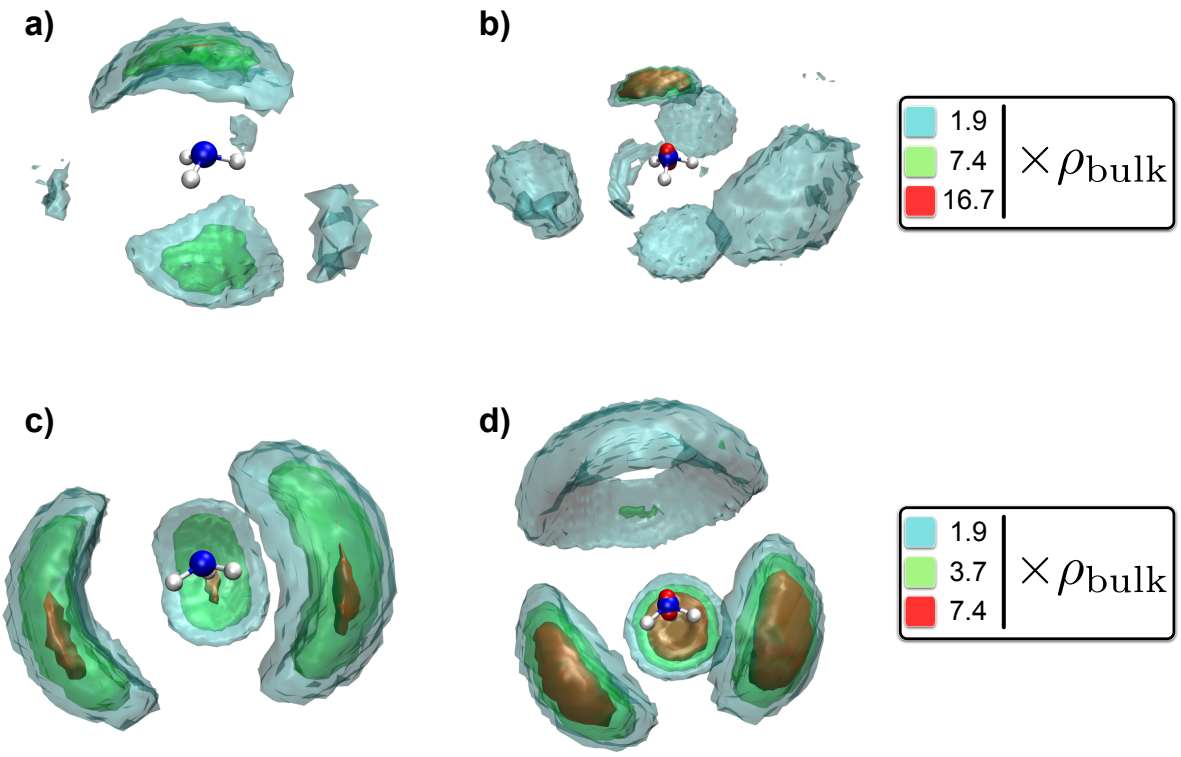


Figure 4.3: Spatial distribution functions of the cation (top) and the anion (bottom) around the NH_3 molecule in both 4-site (left) and 6-site (right) models at a concentration of 50 mole%.

preferential position that each species occupies around ammonia molecules can be observed, as well as the differences between both ammonia models. The pictures correspond to the 50% concentration systems, but the results are analogous in any of them. As we can see, the prevalent position of the cation around ammonia is directly over the nitrogen atom, while other less relevant options appear in the positions that are not in front of an hydrogen. These results were expected due to the charge that each atom carries. Moreover, we can see that the position of the cation is very restricted in the 6-site model, confirming the strong interaction between these molecules that was previously observed in the RDFs. On the other hand, the calculations for the 4-site model show that the nitrogen atoms in the ammonia molecules have the freedom to invert between two metastable positions; one at each side of the plane defined by the three hydrogen atoms. Consequently, the results are an average of these two configurations. This ammonia inversion is known to be rapid at room temperature due to a low and narrow energy barrier, but it has also been observed in condensed phase.[138] This does not occur in the 6-site ammonia, since nitrogen atoms NH_3 interact more strongly with the nitrate and are also restricted by the virtual atoms, so they do not invert. For the anions (Fig. 4.3-c,d), it is clear that the preferential occupied position is that in front of one of the hydrogens, with which they coordinate in a monodentate fashion. In the 4-site model, the position is somewhat diffuse as a consequence of the symmetrical replication, but in the 6-site model the positions are very well defined. In addition, a secondary anion position appears around the space that the cation occupies in front of the nitrogen of the ammonia.

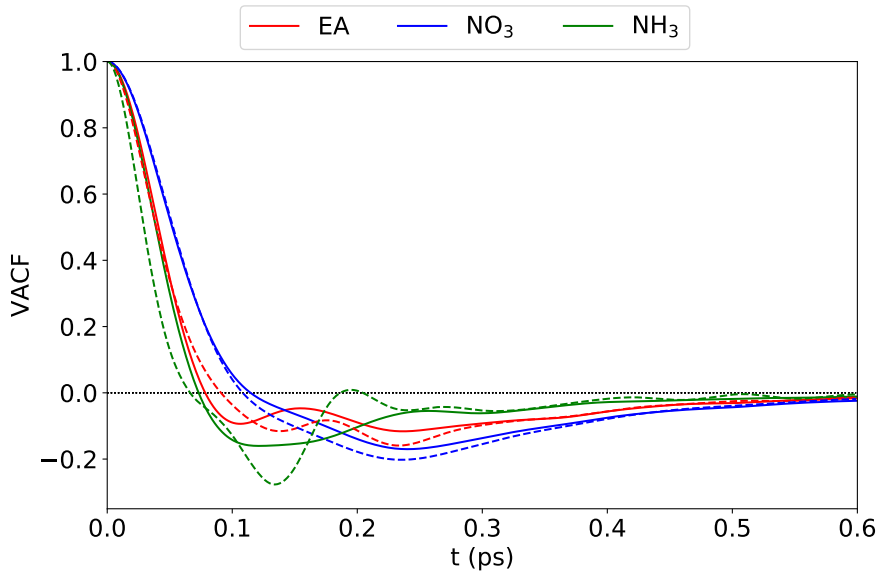


Figure 4.4: Velocity autocorrelation functions of the three species in both 4-site (solid lines) and 6-site (dashed lines) models at a concentration of 50%.

To gain some insight into the single-particle dynamics of our system, we performed a series of calculations to shed light on the behaviour of the system. First of all, we calculated the velocity autocorrelation functions (VACFs) of the species, as shown in Fig. 4.4. This normalized function is defined as

$$C(t) = \frac{\langle \vec{v}(t)\vec{v}(0)\rangle}{\langle \vec{v}(0)\vec{v}(0)\rangle} \tag{4.2}$$

where $\vec{v}$ is the velocity of the centre of mass of the molecule. The results correspond to a 50 mole% concentration of NH_3. As we can see, there is no significant difference in the diffusion of the IL species between the two ammonia models. The contrast shows up when we consider the ammonia VACFs. There is some evidence of caging for all the species as one would expect in a dense liquid, but the 6-site ammonia shows an enhanced rattling motion of the ammonia molecules, which are trapped inside their solvation shells during 0.4 ps before escaping to the bulk. These different observations for the caging of NH_3 molecules are in good agreement with the enhanced interaction between ammonia and cation previously observed in the systems described by the 6-site model by means of $g(r)$'s.

From the VACFs the vibrational density of states (vDOS) can be straightforwardly calculated, since it is directly related to the Fourier transform of the former

$$f(\omega) = \int_0^\infty e^{-i\omega t} C(t) dt, \tag{4.3}$$

and the results are shown in Fig. S1 of the supplementary information for 50% concentrated mixtures. As expected, the differences between systems with different ammonia models are present just in the vDOS of this latter species. For the 6-site model of the ammonia molecule, a new vibrational mode arises related to the motion of the molecule inside its solvation shell that was apparent in the VACFs. Moreover, the first peak is also blue-shifted relative to the

one predicted by the 4-site model, which implies, once again, that the ammonia suffers stronger interactions in the quadrupolar model.

To extend our investigation to the behaviour of these mixtures near charged electrodes, we performed a similar structural and dynamical analysis of this system nanoconfined between two parallel walls, and we then compared the results with those reported for the bulk. We started our structural calculations by obtaining the density profiles of the system, i.e., the number density of each species along the z-axis. Note that these profiles are calculated taking one atom as reference for each species: once again, we chose the nitrogen atoms. The results are plotted in Fig. 4.5. As in bulk systems, the ammonia concentration does not significantly alter the structure of the mixtures, so the results of Fig. 4.5 correspond to a 50 mole% concentration. If we focus on the systems with neutral walls, the first observation is that, with both models ammonia is preferentially adsorbed at the graphene walls. The first layer is composed mainly of ammonia and anions, followed by a cation layer. In the successive electric double layer (EDL) layers, anions and ammonia always occupy the same positions in the z-axis, in accordance with the previous bulk results that suggest that these species compete for the same positions. The EDL formation is clear, as the layers with ions of opposite charge alternate. This layering behaviour has been reported previously in several computational studies,[139–141] although it is somehow controversial.[142] The bulk densities are recovered in the centre of the simulation box (at a distance of about 1.5 nm away from the walls), showing that the walls are sufficiently far apart not to influence each other. The layering effect is enhanced in the simulations with charged walls. In those systems, cations occupy the first layer near the negatively charged wall, while anions do the same in the positively charged one, as expected. There is an overcompensation of charge near the electrodes (overscreening[19]) that attracts the ions of opposite charge forming a second layer, which also overcompensates the charge, giving rise to a third one and so on. The first layer of cations near the negative wall can be seen to be split. This is because the cations have two possible orientations in this layer each represented by a peak (as we will discuss later). Ammonia molecules are attracted to the negatively charged wall and repelled from the positively charged one. This behaviour is explained by the lack of anions near the negative wall, which leaves more room for the ammonia molecules, which compete for position with the anions.

In order to complete the information obtained from the density profiles we analyzed the lateral structure in the innermost layer of the EDL. We obtained the 2D Fourier transform of these layers averaged over time, which provides additional information about the arrangement of the molecules in the xy-plane. The results for the neutral and positively charged walls can be seen in Figs. S2 and S3 of the supplementary information, respectively; whereas the configurations for the negative electrodes are shown in Fig. 4.6. Once again, the concentration does not play a significant role, so for visual clarity we plotted the results just for a 50% concentration. In the neutral simulations, no preferential directions are observed, as the plot is somewhat homogeneous. However, there is a difference between the systems with different ammonia models, as the 4-site NH_3 systems seem to have certain preferential distances. In the simulations with charged walls (Figs. 4.6 and S3) we observe more interesting results. Both IL molecules, anion and cation, form a square lattice in the positively charged wall, but the negatively charged wall structure does not present that kind of arrangement. This can be explained as follows: in the positively charged wall, the first layer is composed of NO_3 molecules, which are small and symmetric. These molecules arrange themselves in a square lattice. This structure allows the subsequent cation layer (specifically, the cations heads) to position in the spaces left by the anions, forming themselves another square lattice. If we consider the two species together, the

USC DE COMPOSTELA

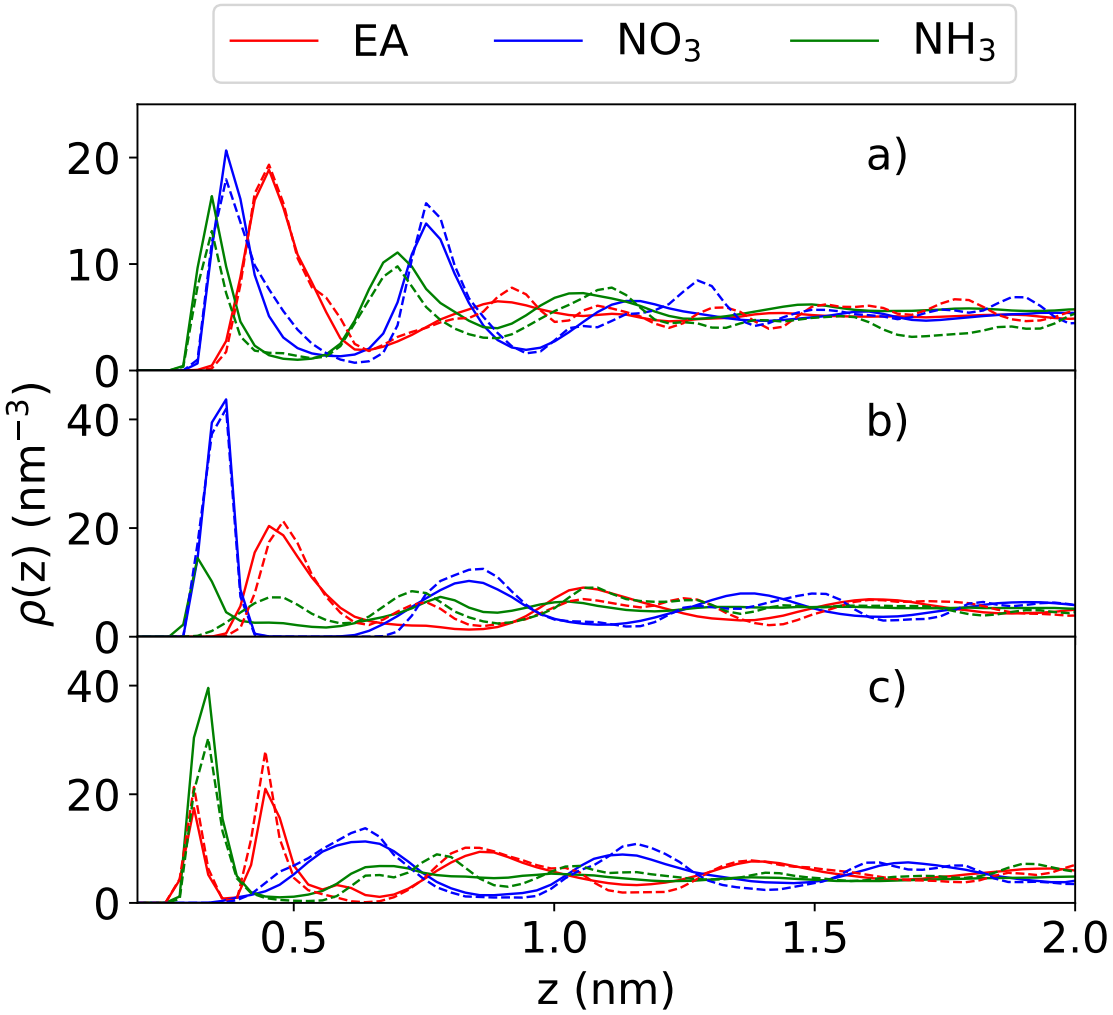


Figure 4.5: Number density profiles for all species near the neutral wall (a), the positive wall (b), and the negative wall (c) in both 4-site (solid lines) and 6-site (dashed lines) models at a 50% ammonia concentration.

lattice would be triangular, which is incidentally the structure that minimizes the energy. Near the negatively charged wall, the first layer is composed of cations, whose chemical structure is much less symmetric, leaving a rather difficult accommodation for the anions, so neither of the species forms a square lattice and this structure is lost. The arrangement of NH_3 molecules does not show a clear pattern on either wall, but this is possibly due to lack of statistics.

To strengthen our deductions about the IL structuring near the graphene walls in the charged systems, we studied the molecular orientation of both ionic species near the walls. We obtained the conditional probability of finding a molecule at a certain orientation and distance from the wall: $P\left(r, cos\left(\theta\right)\right)$, where θ is the angle between a normal vector to the wall and a characteristic vector of the molecule, and r is the minimum distance between the wall and the application point of the vector. For the anion, this vector is normal to the plane where all its atoms lie, being applied on the nitrogen atom; whereas for the cation, the vector starts in the nitrogen and directs towards the center of the triangle formed by the three hydrogen atoms on the EA^+ head. The results are plotted in Fig. S4 of the supplementary information as a 2D-histogram. We also

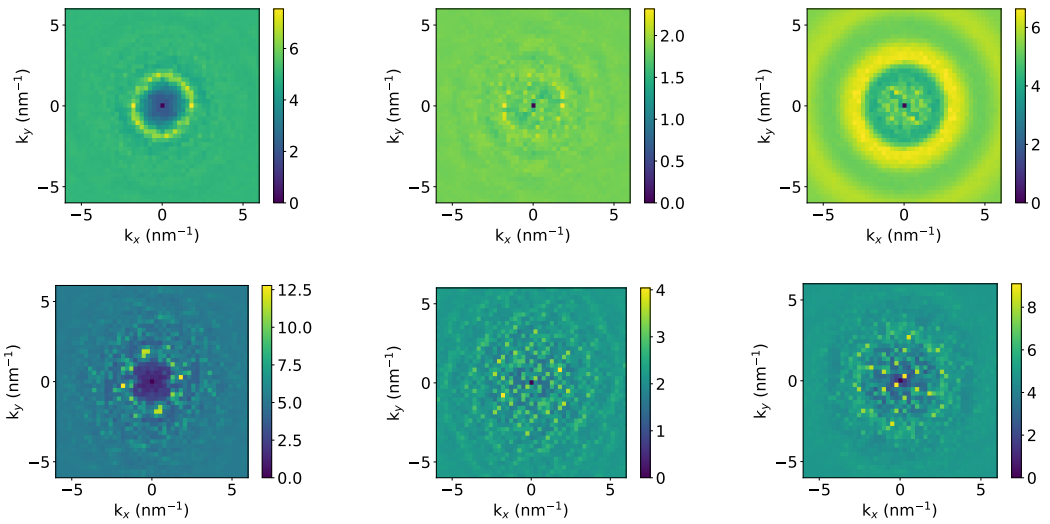


Figure 4.6: Time-averaged 2D Fourier transforms of the x,y components of the positions of the molecules in the first layer near the negatively charged wall for a 50% concentration. The upper row corresponds to the 4-site model systems, while the bottom row contains the results for the 6-site systems. The species represented are, from left to right, cation, anion and ammonia.

plotted in Fig. 4.7 the marginal probability distribution of this conditional probability, obtained by integrating the 2D-distribution between the distances corresponding to the first layer. As we can see, near the positively charged wall (the one with clear structuring) the anions have values of cos(θ) centered around +1 and -1, i. e., θ=0 and θ=2π. For the anion, both situations are indeed the same as the molecular structure is planar. The anions, thus, are oriented parallel to the wall. In the cation case, the values of cos(θ) are centered around -1, indicating that the arrangement of cations is so that the heads (NH_3^+) point towards the wall. this is true for both 4 -site and 6-site model systems, although the cation distribution is sharper in the latter. Near the negatively charged wall, anions follow a more homogeneus distribution but still show a predisposition to position themselves parallel to the wall, with a sharper distribution around the peaks in the 6-site model systems. The cations, as discussed earlier, show two different orientations in the first layer. These orientations are slightly displaced between the systems with different ammonia models.

The single particle dynamics study will be composed of the analysis of the VACFs of the molecules in the first layer of the EDL and the corresponding vDOS, represented respectively in Fig. 4.8 and Fig. S5 (supplementary information). The concentration of ammonia has a slight impact on the collision time of the cation and on the ammonia profiles, but it does not play an important role, so for visual clarity the figures correspond to, once again, a 50% NH_3. The cation profiles do not present significant differences between the systems with different ammonia models or charge walls. The anion profile is, however, altered by charging the walls. The dynamics on the negatively charged wall is similar to that of the neutral ones, but in the positively charged ones, the diffusion is faster. Regarding the dynamics of the NH_3, the details depend on the model we used. Once again, the velocity autocorrelation function of the ammonia molecules shows a caging effect, but the 6-site model ammonia presents enhanced rattling motion.

Introducing charge on the walls also affects somewhat the VACF but they are more pro-

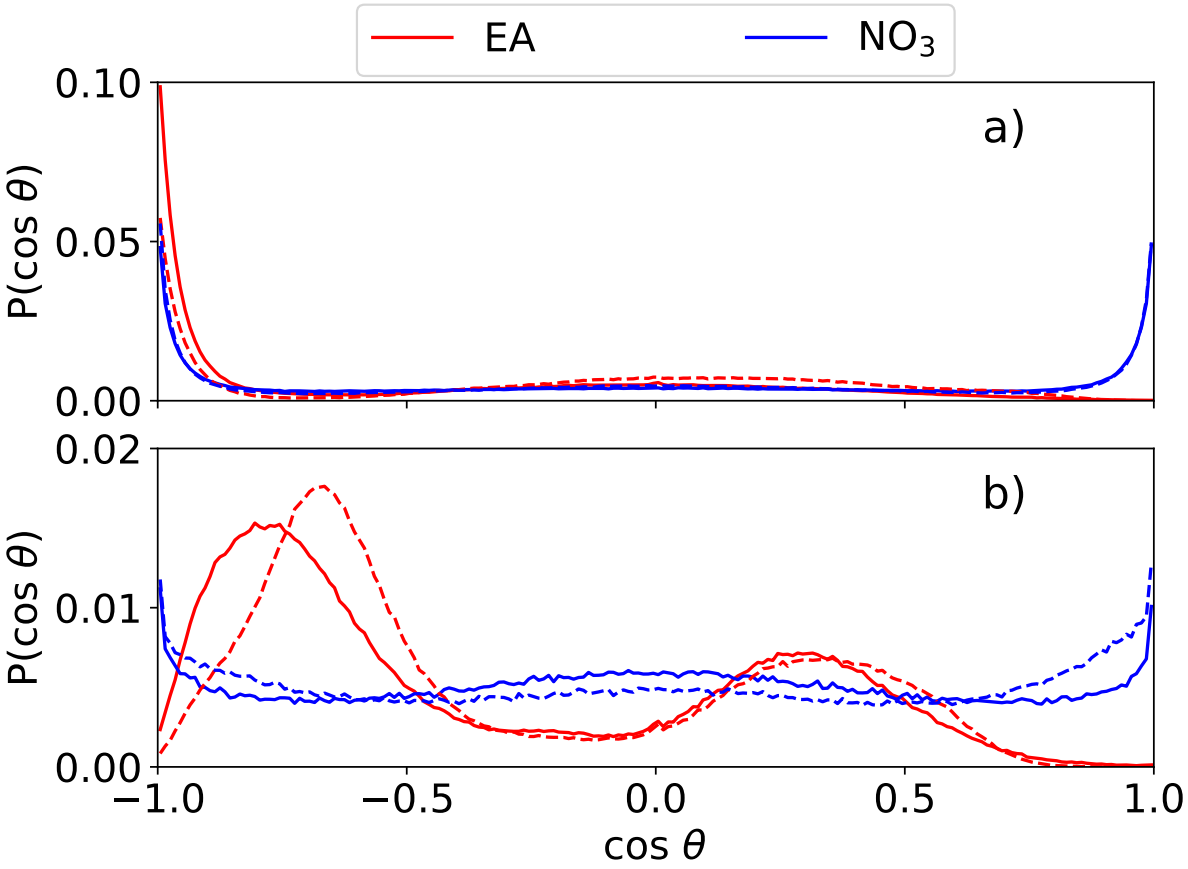


Figure 4.7: Normalized continuous probability density as a function of cos(θ) for cations and anions in the first layer near the a) positively and b) negatively charged walls for bot 4-site (solid line) and 6-site (dashed line) models.

nounced for the 6-site model ammonia dynamics, enhancing the caging effect near the negatively charged wall. This wall is the one that ammonia populates along with cations, and the strong interaction between these species that we observed in the bulk systems is probably responsible for this enhancement.

The vDOS, represented in Fig. S5 of the supplementary information, also includes the bulk results for better comparison. As we can see, the vDOS of the IL species are basically unaffected by the ammonia model. On the other hand, the ammonia profiles show, as we observed in the bulk, a second vibrational mode in the 6-site model, related to those two different motions that the ammonia molecules present. Charging the walls has an effect on the profile of the anion, which is significantly blue-shifted in the proximity of the positively charged wall, indicating stronger interactions due to the opposite charge of the wall.

USC
UNIVERSIDADE DE SANTIAGO DE COMPOSTELA

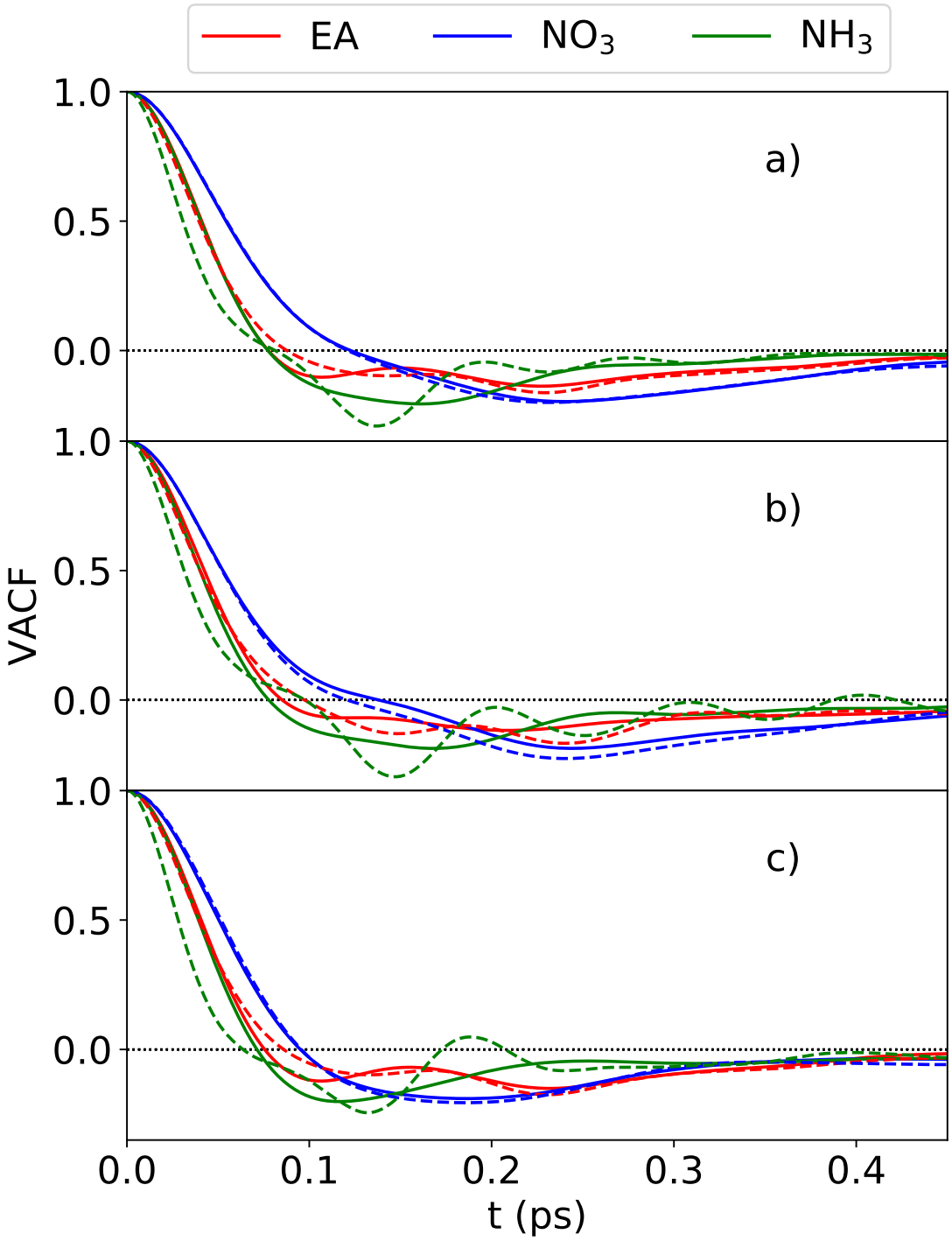


Figure 4.8: Velocity autocorrelation functions of EA^+ (red), NO_3^- (blue) and NH_3 (green) for the first layer near the a) neutral, b) positive and c) negative walls, for both 4-site (solid line) and 6-site (dashed line) models.

UNIVERSIDADE DE SANTIAGO DE COMPOSTELA

4.4 Conclusions

In this work we performed several MD simulations in order to study the structural and dynamical properties of mixtures of a protic ionic liquid, EAN, and ammonia, both in bulk and nanoconfined between either neutral or charged graphene walls, as this system is expected to have important applications in the refrigeration and electrochemical fields.

The main conclusions from the bulk simulations are that NH_3 and NO_3^- compete for the same position around the EA^+ head, and more significantly, the great increase in the interaction between ammonia and cation in the 6-site model compared to the the 4-site model, showing the importance of an accurate description of the molecular charge distribution. This also also leads to significant caging and rattling motion in the single-particle dynamics of the 6-site ammonia dynamics.

In the presence of graphene walls, we can see that ammonia adsorbs near the neutral interfaces, and stays near the negatively charged wall occupying the positions left by the anions. A clear structuring of the IL in the first layer near the positively charged wall is present as the molecules arrange themselves in a square lattice to minimize the energy. Moreover, the 6-site NH_3 model yields to significantly more inhomogenous patterns in the wall adlayer. The dynamic properties of the species are consistent with those of bulk albeit we observe a slight blueshift on the vibrational densities of states.

Future work is already in progress focused on more accurate descriptions of intermolecular interactions, including the effects of polarisability.

Conflict of Interest

There are no conflicts to declare.

Acknowledgments

The financial support of the Spanish Ministry of Economy and Competitiveness (Grants MAT 2017-89239-C2-1-P) is gratefully acknowledged. Moreover, this work was funded by the Xunta de Galicia (ED431D 2017/06, ED431E 2018/08 and GRC ED431C 2016/001). All these research projects were partially supported by FEDER. A. R.-P. and J. M. O.-M. thank the Spanish Ministry of Education for their FPU grants. T. M.-M. thanks the Spanish Ministry of Science, Innovation and Universities for her Juan de la Cierva grant IJC2018-036774-I. Facilities provided by the Galician Supercomputing Centre (CESGA) are also acknowledged.

USC
UNIVERSIDADE DE SANTIAGO DE COMPOSTELA

5- Computational Study of the Structure of Ternary Ionic Liquid/salt/polymer Electrolytes based on Protic Ionic Liquids

Summary of the chapter

As a second step in this thesis development, we shifted our focus into the study of hybrid ionogels. We started with a study in bulk conditions, where we analyzed the properties of an IL/salt/-polymer ternary mixture. In this study, the stability of binary mixtures of several protic ionic liquids (ethylammonium nitrate, ethylammonium acetate and ethylammonium tetrafluoroborate) with polyethylene oxide was studied by means of molecular dynamics simulations. The solubility range was seen to be wider for ethylammonium acetate, and the structure and single-particle dynamics of its ternary mixtures with lithium acetate were then studied. The structure of liquid mixtures of lithium acetate with the ionic liquid was seen to be seldom modified by the addition of the polymer, with very limited hydrogen bonding between the ionic liquid and the polymer taking place. Moreover, lithium was seen to be solvated in the liquid phase forming $[Li(ACE)_4]^{-3}$ tetrahedral complexes irrespective of the presence of the polymer, with very limited binding of metal cations to oxygen atoms in the polymer backbone. Hence, the registered single particle dynamics and lithium transport took place in practically the same way as in the liquid phase with almost no interference of the polymer, contrarily to previously reported results for other ionic liquids.

The post-print version of the publication reproduced in this chapter (including the full list of authors and their affiliations) can be found in appendix A.2, while the corresponding supporting information lies in appendix B.2. At the same time, in appendix C.2. we have included a complete disclosure of the relevant information related to this publication, including the authorization of the journal to reproduce its contents in this thesis, and the contribution of the author of this thesis to the publication.

5.1 Introduction

Ionic liquids (ILs) have proved to be very versatile materials in a wide range of applications including lubricants, catalyzers for chemical reactions, gas storage, electrolytes for batteries or supercapacitors among others.[10;106;143–149] This is mainly due to interesting properties such as very low vapor pressures, high thermal stability, wide electrochemical windows or non-flammability among others. Moreover, these properties can be tuned for a specific task with the right choice of anions and cations forming the IL. Focusing on their good electrochemical properties, ILs have been applied in multiple electrochemical devices, particularly in batteries and supercapacitors.[150;151]

On the other hand, another kind of materials that also have shown to be very promising in this field, mainly because of their mechanical properties, are binary polymer+salt mixtures.[152–155] In order to benefit from the appropriate mechanical properties (rigidity) of these systems, as well as from their relatively high electrical conductivities, lots of efforts have been invested in the study and characterization of ternary polymer+salt+IL ionogels.[96;153;156–158]

USC UNIVERSIDADE DE SANTIAGO DE COMPOSTELA

However, the majority of these studies were focused on the use of ILs based on NTf_2^- anion or imidazolium based cations. Indeed, it has been proved experimentally that the addition of IL to the binary polymer+salt mixtures results in an increment of the ionic conductivity at low salt concentrations.[96;153;157–159] This phenomenon is related to the fact that with the addition of ILs the number of charge carriers increases and, moreover, it acts as plasticizer and induces an enhancement of the segmental motion and the center-of-mass-diffusion of the polymer, the latter contribution becoming irrelevant in the limit of long chains. On the other hand, later theoretical studies supported by molecular dynamics (MD) simulations performed by Diddens *et al.*,[96;157] proved that the ionic diffusion of lithium cations in this kind of ternary mixtures with the IL n-methyl-n-propylpyrrolidinium bis(trifluoromethylsulfonyl)imide, $[PYR_{13}][NTf_2]$, is the cumulative result of four different Li^+ transport mechanisms: Li^+ hopping between adsorption sites along the polymer backbones, hopping between different polymer chains, diffusion along with the polymer in which the lithium cation is adsorbed, and, finally, Li^+ diffusion in the IL+salt binary mixture inside the nanocavities in the polymer matrix. In other words, there is a component of the diffusion that is linked to the Li^+ adsorption in the polymer and another one that is linked to the ionic diffusion inside the IL. More precisely, while for rather low lithium-salt concentrations it was observed that Li^+ preferentially binds to the polyether chain due to the multidentate, crown-ether-like coordination structure,[157] the fraction of lithium ions that are solely coordinated to IL anions becomes more significant at higher lithium salt concentrations,[96] as also observed in nuclear magnetic resonance ^1H microimaging experiments,[160] or when using functionalized coordinating cations.[29] Mogurampelly and Ganesan[158] also studied computationally the structure and diffusion of lithium cations in these ternary systems, but now with an IL based on imidazolium cations (1-butyl-3-methylimidazolium hexafluorophosphate, $[BMIM][PF_6]$). They also reported Li^+ adsorption in the backbones of the polymers and an increment in the diffusion of Li^+ as the IL amount increases. All these studies have focused on ternary mixtures with aprotic ILs (AILs). In this work we are interested in the characterization of the applicability of protic ILs (PILs) in these systems, because their synthesis is more accesible compared with that of AILs. Besides, there are studies that suggest an enhancement of Li^+ transport in PILs.[161] Specifically, using atomistic MD simulations we report the structure of ternary mixtures of a PIL, a lithium salt and polymers with a specific focus on the adsoption of Li^+ cations on the polymer backbones and we compare the results with some previously reported ones for mixtures with different ILs. The IL selected for this study was the ethylammonium acetate ([EA][ACE]), as our results regarding the solubility of our employed polymer (polyethylene oxide, PEO) suggest this IL is the optimal candidate out of three studied ones: [EA][ACE], $[EA][BF_4]$ and $[EA][NO_3]$. We are also interested to see if the IL loading may or may not affect the conductivity in these systems.

In the next section of the paper the simulation details for all the performed steps are presented. There, a new algorithm for the random packing of large molecules inside simulation boxes is also explained. The solubility study and the simulation results are discussed in the section 3. Finally, the main conclusions are summarized in the last section.

5.2 Simulation Details

USC DE SANTIAGO

MD simulations of binary mixtures of PEO and either [EA][ACE], $[EA][BF_4]$ or $[EA][NO_3]$, as well as ternary mixtures of PEO, [EA][ACE] and [Li][ACE] were performed using Gromacs

2019 software.[81;162] The binary systems were simulated to study the miscibility of the polymer-IL mixtures, whereas the most promising IL, [EA][ACE], was employed in the ternary electrolytes to investigate the lithium ion solvation in these materials. We used the OPLS-AA force-field[72] to describe the molecular interactions of PEO, EA, and ACE, while the CL&P force field[27;163;164] (which is compatible with OPLS-AA) was used for BF_4^- and NO_3^-. The parameters for Li^+ were taken from Ref. 165.

To study the miscibility and the phase behaviour of binary PEO-IL mixtures in a first step, we performed Replica Exchange Molecular Dynamics (REMD) simulations with 64 replicas at temperatures between 300 K and 558 K. The individual temperatures were chosen according to the algorithm in Ref. 166. The resulting exchange probability was about 0.2, and an exchange attempt was made every 2 ps. Two different scenarios have been considered: A many-chain system comprised of 20 PEO chains with 20 monomers each and 400 IL ion pairs, as well as a single PEO chain with 20 monomers immersed in 500 IL ion pairs. The REMD simulations at each temperature had a length of 30 ns, amounting to almost 2 μs of total simulation time.

The initial configurations were obtained randomly packing the molecules in a simulation box using the Packmol software.[70] The PEO chains used in the packing process were in a fully stretched conformation. We simulated this very artificial configuration in the NpT ensemble at a temperature of $T = 500$ K and a reference pressure of $p = 100$ bar, maintained by a Berendsen thermostat and barostat,[78] for 10 ns with a time step of 0.5 fs to allow the simulation box size to reduce and obtain a dense system. Electrostatic interactions have been turned off in this step to promote mixing of the system's components, and a cutoff radius of 1.2 nm has been used to truncate the Lennard-Jones interactions. It has to be mentioned that such a low value of the time step (0.5 fs) was required to guarantee the consistency of the solution of the motion equations, due to the initial artificial molecular configuration and high pressures. Then, we simulated an annealing from 500 K to 300 K over 30 ns with an elementary time step of 2 fs to cool down the system, and finally we performed a 120 ns run at room temperature ($T = 300$ K) to stabilize the system. Here, a cutoff radius of 1.4 nm has been used for all nonbonded interactions, and the long-ranged part of the electrostatic interactions has been treated by the particle Mesh Ewald (PME) method[167;168] with a grid spacing of 0.12 nm and sixth-order interpolation.

Bonds involving hydrogen atoms were constrained by the LINCS algorithm.[73] The resulting structures both served as input for the REMD simulations of the binary systems (with [EA][ACE], [EA][BF_4] or [EA][NO_3]) and the conventional MD simulations of the ternary systems (only [EA][ACE], see below for the remaining simulation procedure).

For [EA][ACE], which showed the best miscibility out of the three ILs considered in the REMD simulations (see discussion below), we subsequently performed conventional MD simulations of ternary PEO/[EA][ACE]/[Li][ACE] electrolytes to study the lithium ion coordination and dynamics in these materials. While the OPLS-AA/CL&P force field usually reproduces thermodynamic properties accurately, the main problem of this non-polarizable description is the underestimation of the molecular mobility.[169;170] This means that in order to obtain a realistic molecular configuration starting from a completely random distribution, very long stabilization runs will be needed.

This is even more so when starting from fully stretched chain conformations as in our case, and when studying multiple [Li][ACE] salt concentrations. On the other hand, REMD simulations are costly as well, as typically a larger number of replicas is employed to span a wider

temperature range (see above). Therefore, to obtain realistic polymer structures as input for the ternary systems in a computationally expedient way, we started the simulation process from the well stabilized simulation boxes containing binary PEO/[EA][ACE] that also served as input for the REMD simulations, in which specially the polymer chains have equilibrated, coiled structures.

Another issue that needs to be considered when these configurations are used to create new random initial simulation boxes is related to the periodic boundary conditions (pbcs). We observed that if all the polymer chains were packed randomly inside a simulation box together with the rest of the components, the resulting output at the end of the simulation will contain all the polymers in a central region of the box surrounded by the mixture of the IL and the salt. This is mainly because the software used for the packing does not take into account pbcs and because of the slow motion of the polymers compared with the smaller components in the systems, which are able to occupy much faster the artificially empty space left in the packing process at the edges of the box. To solve this, we encapsulated all the polymer chains in the new simulation boxes using a sequential approach: we first inserted one polymer with a configuration obtained from the previous MD run into an empty cubic box with an estimated side length that reproduces the density of the previous simulation. Then, the position of the polymer was shifted by a random linear vector displacement. To ensure that all atoms were inside the simulation box, pbcs were applied. Then, a new polymer chain (extracted from the previous simulation) was randomly introduced in the free space of this box using Packmol. Once again, all the positions of the polymers in the box were randomly shifted and pbcs were applied. These steps were repeated until all the 20 simulated polymer chains are properly placed inside the box, which is finally filled with the salt and/or IL molecules. With this algorithm we obtained a more realistic random initial configuration without the restriction of the polymer chains being completely inside the simulation box. A representation of the steps of this algorithm is shown in Fig. 5.1. It has to be highlighted that this algorithm can be used to generate initial random configurations for a wide variety of systems, specially when large molecules are involved. An implementation of this algorithm can be found here: [https://github.com/txemaotero/large-molecule-pbc-packing]. The simulation steps from this point include all the standard procedures in a MD simulation. First, an energy minimization of the system using a conjugated gradient algorithm, followed by a short NVE stabilization run of 50 ps and a longer NPT stabilization run of 20 ns, at a temperature of 300 K and 1 atm of pressure. Finally, a NPT production run of 20 ns at 300 K and 1 atm, saving the positions and velocities of the atoms each 1 ps. For the single particle dynamics, shorter simulation runs were performed, each of 1 ns, where the velocities of the atoms were saved in every simulation step, i. e., each 2 fs. It has to be noted that the 20 ns of the production runs are not enough to allow the polymers to significantly change their molecular configuration. So, to cover much more diverse polymer configurations we created 10 random initial simulation boxes following the algorithm mentioned above and simulating each one of them. The final results shown in this manuscript are those from the average for all the production runs starting from different configurations.

We performed simulations following the steps mentioned above for different concentrations of [Li][ACE], i.e., ratios of ionic pairs between [Li][ACE] and [EA][ACE] of {0.1, 0.2, 0.25, 0.5, 0.75, 1}. In all the systems there were 500 ion pairs comprising [EA][ACE] and [Li][ACE] pairs, depending on the desired salt concentration. We also performed simulations without any polymer chain at a molar fraction of 0.1 for further comparison.

USC DE COMPOSTELA

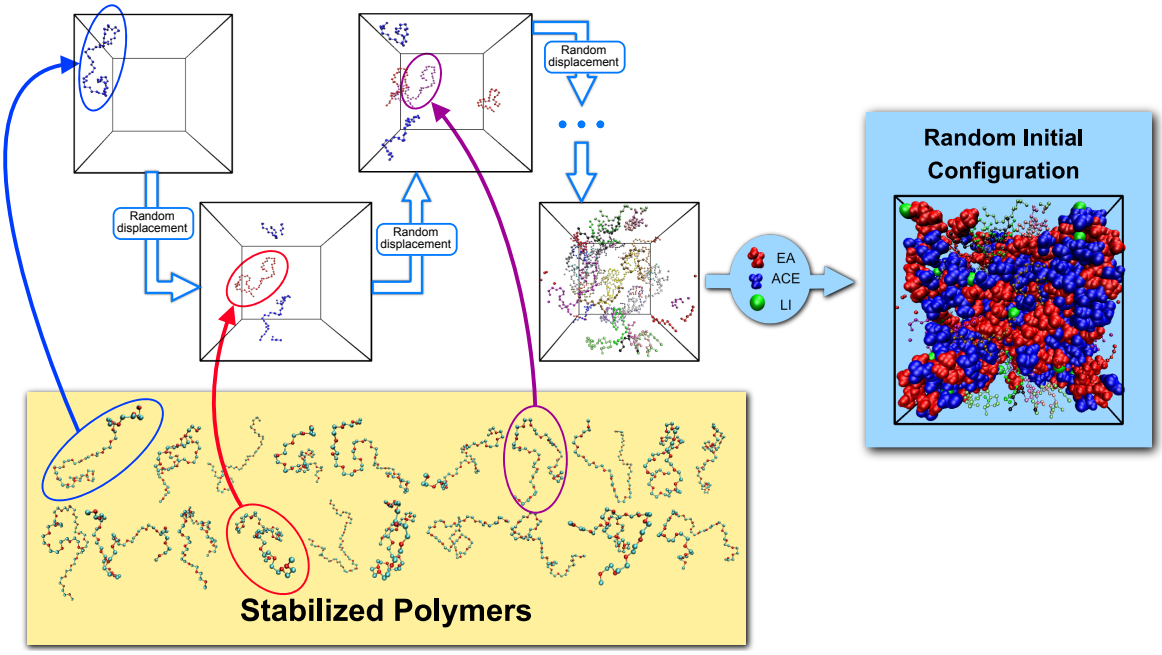


Figure 5.1: A representation of the algorithm used to generate the initial configurations for the simulations. The polymers are represented without the hydrogen atoms as well as using small sizes for the atoms beads for a better visualization.

5.3 Results and Discussion

In a first step, we studied the miscibility and the phase behavior of the binary PEO/[EA][ACE] mixtures, to which end we studied both many-chain systems and single chain systems. Typical snapshots from the REMD simulations for different temperatures between 300 and 500 K are shown in Fig. S1, S2 and S3 in the Supporting Information (SI). Note that only the PEO chains are visible in this representation to be sensitive to any aggregation or crumpling of the polymers. For PEO/[EA][ACE], we observe a minor degree of PEO clustering for all studied temperatures, specially at temperatures of the PEO below 500 K, demonstrating that PEO and the IL appear to be well mixed. In contrast, for PEO/[EA][BF_4] and PEO/[EA][NO_3], aggregation of the PEO chains seemingly sets in already at lower temperatures, although at temperatures below 400 K a certain degree of mixing can be observed. Interestingly, a lower critical solution temperature (LCST) has also been observed for binary PEO/[BMIM][BF_4] mixtures, which was attributed to the existence of hydrogen bond-like interactions between the protons of the imidazolium ring and the PEO oxygen atoms.[171] These interactions become entropically unfavorable at high temperatures, thus minimizing the polymer-IL interface and favoring demixing.[171]

To study these effects in more detail, we also performed REMD simulations of a single PEO chain immersed in the three individual ILs. The corresponding simulation snapshots are depicted in Fig. S4 in the SI. We observe that in PEO/[EA][ACE] the PEO chain has a coiled conformation both at high ($T = 550$ K) and low ($T = 300$ K) temperatures, whereas in PEO/[EA][BF_4] and PEO/[EA][NO_3] the chains rather adopt a crumpled, globular shape, particularly at 300

K, in agreement with our observations for the many-chain system. This is further confirmed in Figure 5.2, which shows the average end-to-end vector R_e and radius of gyration R_g as a function of temperature. In [EA][ACE], the PEO chain has the largest spatial extension, which becomes most pronounced at low temperatures. Contrarily, in [EA][BF_4] and [EA][NO_3], the PEO chains have shorter R_e and R_g, which again becomes most pronounced at low temperatures. In total, the PEO structure in [EA][BF_4] and [EA][NO_3] is rather similar. Figure 5.2 also shows the ratio of the mean squared end-to-end vector and the mean squared radius of gyration, i.e. $\langle R_e^2 \rangle / \langle R_g^2 \rangle$. For an ideal coiled chain, obeying a Gaussian distribution for the segment lengths, $\langle R_e^2 \rangle / \langle R_g^2 \rangle = 6$. In case of PEO/[EA][ACE], a value of six is attained at 300 K, whereas lower values – indicating a more globular structure – are found at higher temperatures, as well as for [EA][BF_4] and [EA][NO_3] throughout the entire temperature range. The phenomenology behind this change from coiled to globular configuration of the polymer in [EA][ACE] when the temperature increases is the same than that behind mixtures of PEO with [BMIM][BF_4],[171] i. e. at high temperatures the hydrogen bonding interactions become entropically unfavorable and thus the IL becomes a bad solvent for the polymer. Choi and Yethiraj supported this hypothesis by calculating the potential of the mean force (PMF) related with the hydrogen bond formation between the cations and the polymer. They showed that at high temperatures the minimum of the PMF indicating the hydrogen bond formation disappeared. To check the if this is the case for the [EA][ACE] we calculated the PMF between N-H groups of the EA^+ and oxygen atoms of the PEO for simulations of a single frozen coiled polymer chain immersed in the IL at 300 and 500 K. The results are shown in Fig. S5 in the SI and it is clear that at high temperatures the coordination of the cation and the polymer becomes very unfavorable in terms of the free energy, which explains the globular PEO configurations at high temperatures. Therefore, we conclude that at ambient temperatures, PEO has the largest solubility in [EA][ACE], and hence chose this IL for our study of the ternary electrolytes.

To characterize how the protic nature of [EA][ACE] IL changes the properties of the ternary polymer gels that we are interested in, specifically the ones related with Li^+ transport mechanisms, relative to previously reported results for similar mixtures with other ILs,[156–158] the first thing that we can analyze is how the presence of the polymer affects the environment of Li^+ cations in the bulk. To do that we have calculated the radial distribution functions (RDFs) between the different molecular species in the system with 10% of lithium salt, with and without the polymer. For the calculation of these functions the position of the center of mass of the molecules was taken as reference point for the distance calculations. These RDFs are plotted in Fig. 5.3. Very minor changes are observed in the Li^+ environment with the addition of polymer. The coordination distance with all the molecular species remains constant, i. e., the peaks of the RDFs are located at the same distance and only a slight increase in the height of the first peaks of the RDFs with ACE^- and EA^+ are registered. This usually means that there is a stronger coordination between the species. However, the normalization for the RDFs in the systems with and without the polymers could be playing a role in this comparison. For a better comparison of this coordination strength we calculate the coordination number of the same species around the Li^+, i. e., the average number of the different molecules around each Li^+ cation. These curves are also represented in Fig. 5.3. Now it is more evident that at short distances (less than 0.5 nm) the coordination is almost identical for all the species. The polymer only causes a slightly weaker coordination between the systems, likely caused by the polymer preventing the homogeneous distribution of one species around another. As one could expect, for larger distances the coordinations are notably higher in the simulations without polymers,

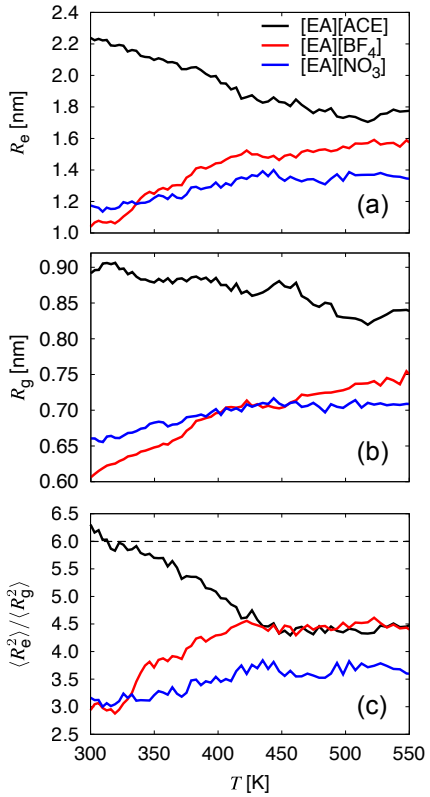


Figure 5.2: Average end-to-end vector R_e (a) and radius of gyration R_g (b) of PEO in the REMD simulations comprising a single PEO chain with 20 monomers and 500 IL ion pairs. The ratio of the two mean squared radii, $\langle R_e^2\rangle/\langle R_g^2\rangle$, is shown in (c). For a Gaussian chain $\langle R_e^2\rangle/\langle R_g^2\rangle = 6$, which is represented with a dashed line.

as there are no regions excluded by the chains and the molecules can fill the whole simulation box. At this point, our results suggest that the structure of the liquid mixture remains the same when the polymer chains are solvated in the system, meaning that Li^+ cations are preferentially coordinated with the IL anions. This is not the case when $[Pyr_{13}][NTf_2]$+$[Li][NTf_2]$ mixtures are considered.[96] Diddens *et al.* reported that, for those systems, when the polymers were added to the IL+salt mixture, a significant fraction of Li^+ cations are preferentially coordinated with the oxygen atoms in the polymer chains instead of with the oxygen atoms in the NTf_2^-. As they pointed out, the main mechanism of transport of Li^+ cations in these ternary systems, specially at high lithium salt concentrations, is through the polymer chains. This difference in behaviour relative to our findings possibly suggests a much higher stability of the Li^+-ACE_4^- tetrahedral complex in PEO-[EA][ACE] mixture compared to $Li^+[NTf_2]_2^-$ linear complexes in PEO-$[Pyr_{13}][NTf_2]$, so lithium cations are not able to break its coordination complexes in the former case. The comparatively stronger Li^+-ACE coordination can be rationalized by the fact that the negative charge is more distributed across the larger NTf_2 anion as compared to ACE, resulting in weaker electrostatic interactions of Li^+ with the latter.

To check if a similar diffusion mechanism of lithium cations through the polymer chains takes place in our systems with [EA][ACE], we studied the coordination of Li^+ with the oxygen atoms of the polymer chains. We represent in Fig. 5.4 the RDFs between the polymers and the rest of the components for all the simulated salt concentrations. The first thing that can be noticed looking at these RDFs is that the change in the molar fraction of lithium salt does not significantly

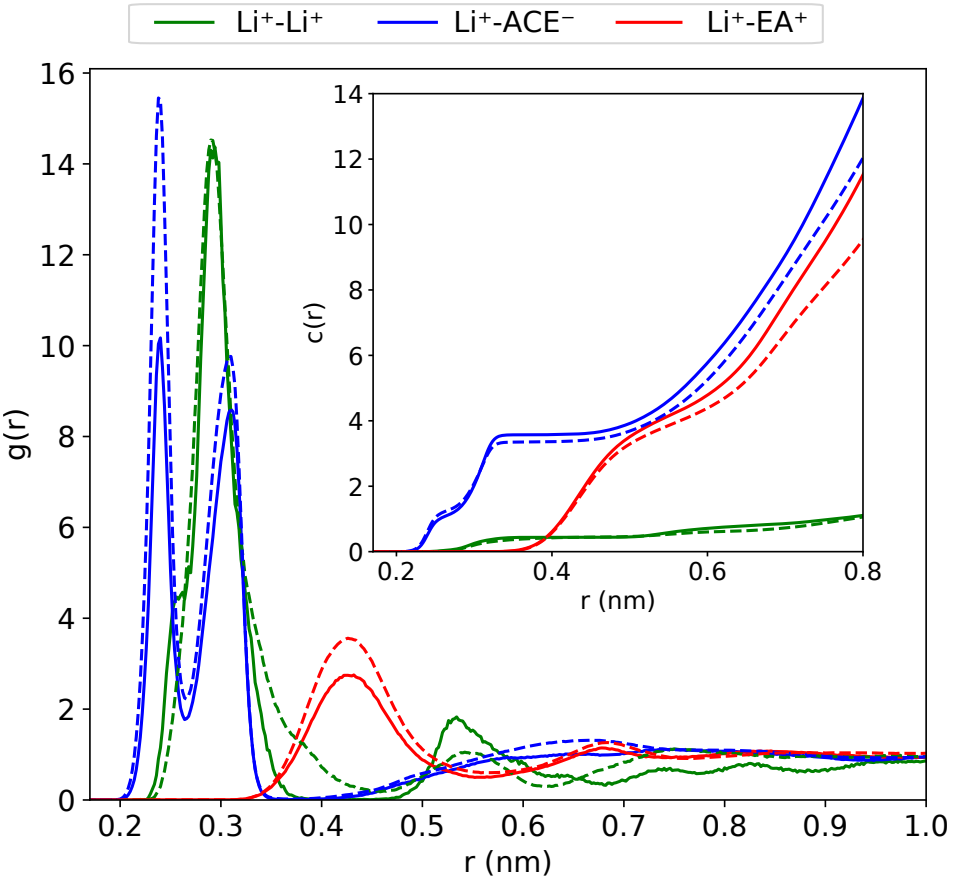


Figure 5.3: RDFs between Li^+ and the other molecular species presented in mixtures with 10% of lithium salt with (dashed lines) and without (solid lines) polymers. The corresponding coordination numbers are also represented in the inset.

affect the ionic distribution around the polymer chains and only slight changes in the height of the first peak in the RDFs with Li^+ are registered. As we indicated before, these changes in the height of the RDFs may be related with changes in the coordination around the polymer, which will be more detailed below in context with Figure 5.8. Another interesting phenomenon that can also be observed is that the RDFs of the ACE^- and EA^+ around the polymers are always below 1 in the studied distances for all the salt concentrations. This means that the probability of finding an ACE^- or an EA^+ around an oxygen atom of the polymer is lower than in the case of a random distribution of ions in the mixture. It must be mentioned that when the molecular distributions around the oxygen atoms of the polymers are analyzed, there is a region that can not be filled with any species due to the presence of the rest of the polymer chain. So, even if any species is randomly distributed around the polymers the values of its RDFs would be lower than 1. In this line, looking at our results, although we cannot ensure that there is an absence of coordination, we can conclude that there is no preferential adsorption of ACE^- or EA^+ on the polymer backbone. Similar distributions were reported by Mogurampelly and Ganesan[158] when similar ternary mixtures of PEO, the [BMIM][PF_6] IL and [Li][PF_6] salt were considered. They reported how the distribution of $BMIM^+$ cations around the polymer chains change when varying the salt percentage. Their results showed that there was indeed a preferential adsorption of the $BMIM^+$ cations around the monomers that was damped down as the salt concentration increased. They also reported the distribution of lithium cations around the monomers showing

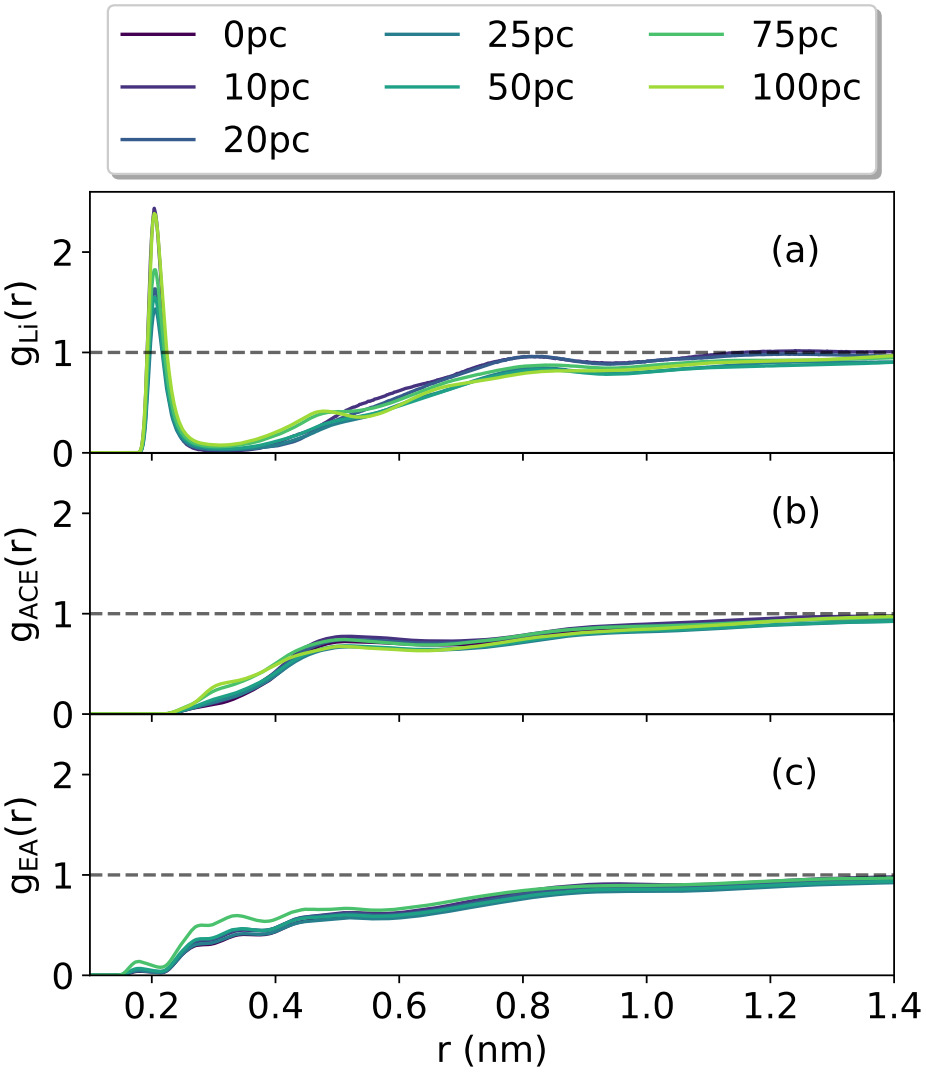


Figure 5.4: RDFs between the oxygen atoms of the polymer chains and the Li^+ (a), ACE^- (b) and EA^+(c) for all the simulated salt concentrations. The horizontal black dashed lines placed at $g(r) = 1$ are represented to mark the ideal distribution.

a very similar distribution as the one that we obtained with a cordination shell located at the same distance but much higher than in our simulations, i. e., their maxima reach values around 23 while ours do not exceed 2.5. So, we can conclude that lithium cations are preferentially solvated in the bulk IL+salt mixture when this IL, [EA][ACE], is used, instead of being adsorbed in the polymer monomers, as it happens when the [BMIM][PF_6] IL is considered. It is also remarkable that the results suggest a better solvation of the polymers in [BMIM][PF_6] than in [EA][ACE] as the polymer-ion interaction showed to be stronger in the first case. Indeed, some works show that PEO has some hydrophobic character,[172] so it could be better solvated in the hydrophobic [BMIM][PF_6].[173] We also took into account the hydrogen bond network present in the system by calculating the mean number of hydrogen bonds per donor molecule (in our case, EA^+). We show the results in Fig. 5.5. As we can see, the amount of hydrogen bonds between the IL components decreases as we increase the salt concentration in the system. This reinforces the idea that the lithium cations are strongly coordinated with the ACE^- anions, removing some

of the hydrogen bonding between EA^+ and ACE^-. As a result, the ethylammonium cation is more free to form some hydrogen bonds with the polymer. The presence of the polymer does not seem to disturb the hydrogen bond network, as the simulations without polymeric chain and a 10% Li^+ concentration has an average of 3.23 hydrogen bonds between EA^+ and ACE^- per EA^+ molecule, a value compatible with those reported earlier.

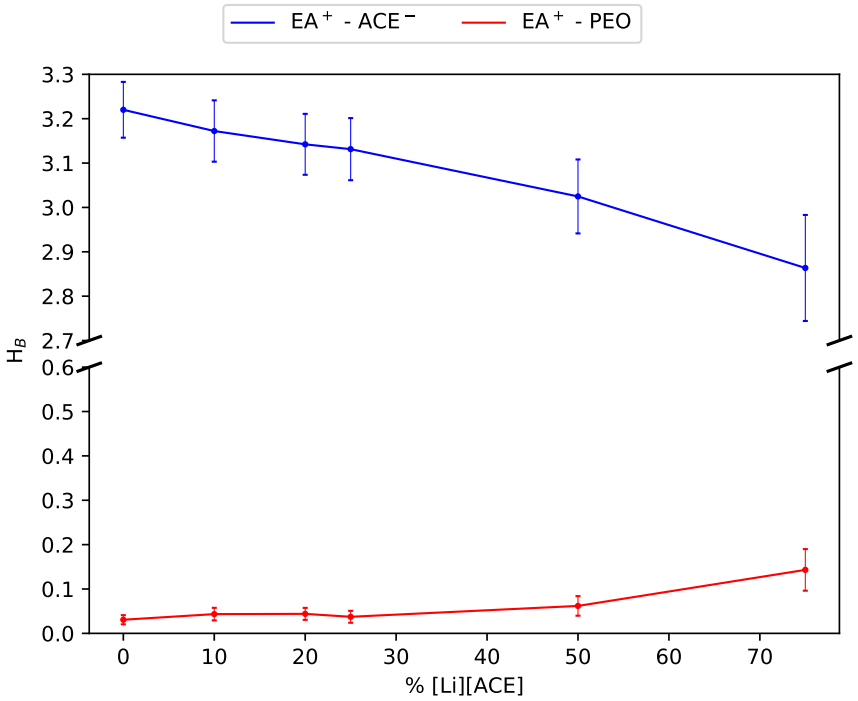


Figure 5.5: Mean number of hydrogen bonds by donor molecule (EA^+) between the EA^+ molecule and the ACE^- anion (blue line) and the EA^+ cation and polymer chains (blue).

Up to now all the results suggest that the addition of polymers to the binary IL+salt mixture considered here does not significantly affect its liquid structure, and lithium cations seem to be the only species that significantly interacts with the polymers, as it was showed by the previously discussed RDFs. In order to have a better insight into the effect of the polymer on the molecular environment of the simulated species we calculated the vibrational power spectrum, which is nothing more than the Fourier transform of the velocity autocorrelation function,

$$\Phi(\omega) = \left(\frac{1}{\sqrt{2\pi}} \int_{-\infty}^{\infty} e^{i\omega t} \langle \vec{v}(0) \cdot \vec{v}(t) \rangle dt \right)^2 . \tag{5.1}$$

This magnitude gives us an idea of the vibrational spectrum of the molecules inside their coordination shells. These spectra for Li^+, EA^+ and ACE^- ions are represented in Fig. 5.6 for the systems with 10% of lithium salt with and without polymers. If the presence of PEO chains induces structural changes in the binary mixture, changes in the molecular environment of each species are expected, which, in turn, translates into differences in the vibrational spectrum (see Ref. 174 for a discussion of how the changes in these spectra can be related with changes in the molecular environment, specially for simulations where complexes with Li^+ close to interfaces are involved). However, the results shown in Fig. 5.6 are almost identical for simulations with and without polymers, and only tiny differences can be seen in the region around 600 cm^{-1} for

the spectrum of Li^+, which are surely related with the coordination mentioned before between Li^+ and the PEO oxygen atoms. Apart from this slight difference, the results are compatible with the hypothesis that PEO does not significantly affect the IL+salt mixture structure in this reported case.

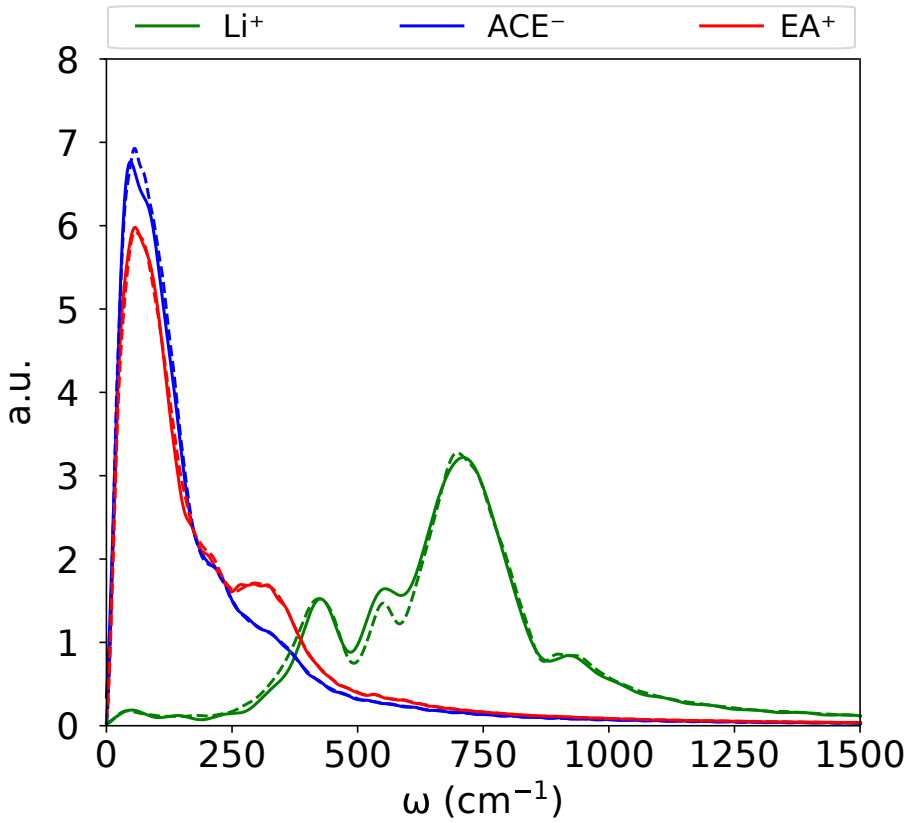


Figure 5.6: Vibrational power spectrum for Li^+, ACE^- and EA^+ ions for the systems with 10% of lithium salt with (dashed lines) and without (solid lines) polymers.

We also used the calculated velocity autocorrelation functions to compute the self-diffusion coefficients of each ionic species as:

$$D_i = \frac{1}{3}\int_0^\infty \langle \vec{v_i}(0) \cdot \vec{v_i}(t) \rangle dt. \tag{5.2}$$

As it was mentioned before, the molecular dynamics is expected to be quite underestimated when non-polarizable force-fields are used. This means that the self-diffusion coefficients calculated with eq. 5.2 are considerably lower than the experimental ones. However, if we suppose that the dynamics of all the ionic species are affected in the same way, a proper qualitative comparison between anions and cations can be made. To perform this comparison we calculated the transference numbers of the charged species:

$$t_i = \frac{\sigma_i}{\sigma}, \tag{5.3}$$

where σ_i is the contribution to the electric conductivity by the ionic specise i and σ is the total electric conductivity of the system. To compute the conductivities we used the Nerst-Einstein

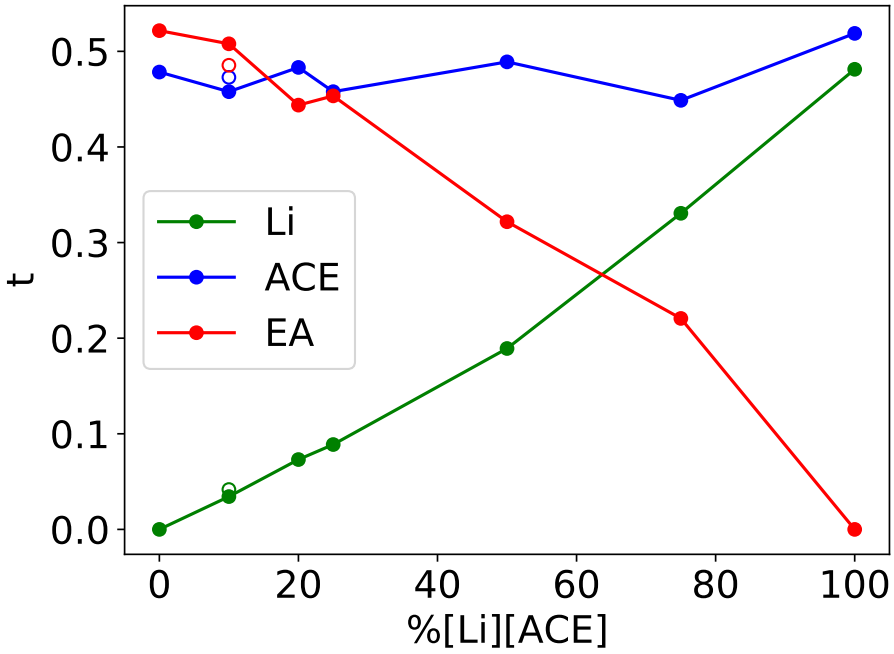


Figure 5.7: Transference numbers for all the ionic species in the simulations with different [Li][ACE] concentration. The numbers for the simulation of 10% of [Li][ACE] without polymer are also represented as empty dots.

approximation:

$$\sigma = \sum_i \sigma_i = \frac{e^2}{V k_B T} \sum_i N_i D_i, \tag{5.4}$$

where e is the charge of the electron, V the volume of the simulation box, k_B the Boltzman constant, T the temperature and N_i the number of i ions in the simulation. Calculating the conductivities in this way has the drawback that anion-cation correlations are not taken into account, so the results should be prudently analyzed, but for the purpose of this study, this level of approximation showed to be accurate enough. The obtained transference numbers for all the simulated [Li][ACE] concentrations as well as those obtained for the 10% without polymer chains are represented in Fig. 5.7. We can see that approximately half the conductivity is associated to the acetate anions and the rest to the cations in the whole range of concentration. Lithium cations gradually replace the role of the EA^+ in the conductivity as the concentration of [Li][ACE] increases. However, the most remarkable conclusion, which can be made looking at the comparative with the numbers from the system without polymer, is that the addition of polymer has a negligible effect in the conductivities of each ion. In other words, the presence of polymer not only leaves the structure of this ILunaffected, but also the essentials of the charge transport mechanism.

The theory developed by Maitra *et al.*[175] and Diddens *et al.*[29;96;157] about Li^+ diffusion in this kind of systems states that one of the keys in the Li^+ transport is its adsorption on the polymer chains. If Li^+ is not adsorbed in the polymer only one of the four transport mechanisms described in Ref. 29;96;157 appears, which is the diffusion of lithium cations in the binary mixture inside the cavities produced upon the entanglement of the polymer chains. To see if the other three mechanisms (hopping between monomers, between different chains and diffusion of

the attached polymer chain) play any role in our systems, we calculated the percentage of lithium cations that can be considered to be adsorbed in the polymers. In view of the already discussed RDFs, we considered that a Li^+ cation is adsorbed at the oxygen atoms of the polymer when it is closer than 3 Å from it. This result must be compared to the percentage of salt that would meet our criteria if Li^+ was distributed homogeneously in the cavities formed by the polymer. Although we know that the lithium cations are mostly coordinated with the anions, this image is equivalent to a mean field description of the structure of the ionic liquid + salt mixtures. To obtain this value, we calculated the free volume left by the polymer chain in our simulation box (FV). After that, we performed the same calculation, but with a twist: the size of the oxygen atoms of the polymers was artificially enlarged to a radius of 3 Å, so that the volume obtained matched exactly the free volume that does not meet our criteria (FV_O). With these two values we can calculate the theoretical percentage of adsorbed Li^+ if they were randomly distributed as:

$$\%\text{Random} = \frac{FV - FV_O}{FV}. \tag{5.5}$$

On the other hand, we can calculate the percentage obtained in the simulations dividing the number of adsorbed Li^+ cations by the total number of Li^+ in each frame and average this magnitude for all the frames in each simulation (%Simulated). We can see the proportion between these two results in Fig. 5.8. The error bars associated to each value correspond to the standard deviation at the average values from the different simulations of each salt concentration. Looking at the figure it seems reasonable to conclude that a random distribution of the Li^+ is compatible with the obtained results in the whole range of salt concentration. This is again in agreement with the picture that we were drawing up to now, i. e., the polymer does not affect significantly the structure of the binary mixture.

To highlight even more the difference of the Li^+ adsorption with that in other ILs we can notice that the average percentage of Li^+ adsorption in all our simulation is around 7%, while Diddens *et al.*[157] reported a 60 % for $[PYR_{13}][NTf_2]$. Moreover, it was reported by them that the addition of IL promotes Li^+ adsorption in the polymer backbone, i. e. the percentage of adsorbed lithium cations increases as the salt percentage in the system decreases. This was also observed by Mogurampelly and Ganesan[158] for systems with $[BMIM][PF_6]$. This is just the opposite behaviour that we observe in our systems, where a slight increase in the adsorption is shown as the amount of salt increases. In the case of the systems with aprotic ILs the addition of IL leads to a situation where the ACE^- anions preferentially coordinate with the IL cations leaving part of the Li^+ cations free to coordinate with the polymer backbone. Mogurampelly and Ganesan[158] supported this hypothesis showing that the distribution of Li^+ around ACE^- revealed weaker interactions as the amount of IL increases, also showing that the number of free Li^+ cations, i. e., those not coordinated with any anion, increased in the same conditions. With the results reported up to now we expect the opposite behaviour for our systems. In Fig. 5.9 the RDFs of Li^+ around ACE^- anions are plotted. These RDFs provide the first evidence that the phenomenology in the ternary mixtures under this study follows the opposite trend that in systems with other ILs. We can see that, as the amount of salt increases the height of the coordination peaks decreases, specially that of the first one, contrary to what happens in the study by Mogurampelly and Ganesan.[158] It has to be mentioned that the double-peak shape of these RDFs is very common in the coordination between Li^+ and its anions and corresponds with two different adsorption sites of Li^+ around anions (see Ref. 176). These two types of coordination, monodentate and bidentate, can be better observed in the spatial distribution depicted in Fig. 5.9. Mogurampelly

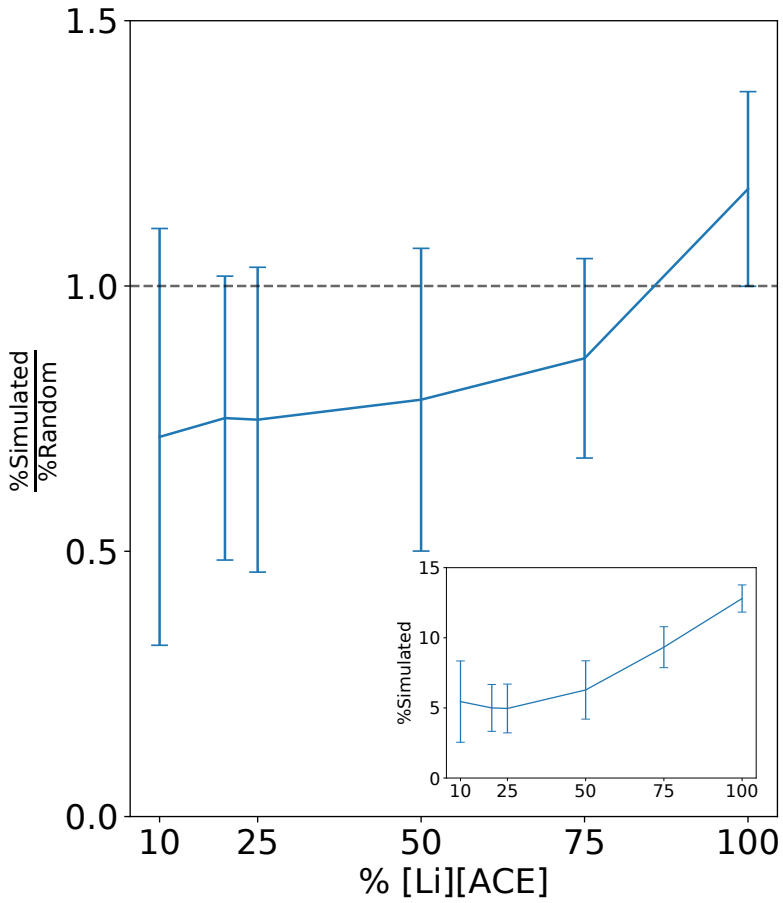


Figure 5.8: Relative Li^+ adsorption compared with random distribution for all the simulated salt concentrations. The horizontal dashed line represents an adsorption compatible with a random distribution. The absolute percentage of coordinated Li^+ is represented in the inset.

and Ganesan also reported a notable decrease in the coordination of Li^+ cation around the IL anions as the amount of salt decreases both in the first and second solvation shell which supported the idea of the release of Li^+ when the amount of IL cations increases. To corroborate that this does take place in our systems we calculated how the amount of ACE^- anions surrounding each Li^+ changes with salt concentration, i. e., the coordination numbers of ACE^- around Li^+. These are also shown in Fig. 5.9. One should expect the amount of ACE^- anions around the Li^+ to decrease significantly if the same phenomenology as with previously studied ILs undergoes our systems. However, we see that it actually increases in the first coordination shell and there is only a slight decrease from 3.7 to 3.3 in the second one when the percentage of IL increases. Moreover, all of these coordination numbers are compatible with the ones obtained for the system without polymer, which again reinforces our hypothesis about the resilience of the structure of the binary mixture upon the addition of polymer. With these results we can conclude that the $[Li(ACE)_4]^{3-}$ complexes formed by the Li^+ and ACE^- anions are so stable that their adsorption on the polymer backbone via interactions wigh oxygens in the polymer backbone does not thermodynamically compensate their breaking up. The last thing that we calculated to support this hypothesis was the fraction of Li^+ cations in the systems that are not coordinated by IL anions, i. e., the percentage of free lithium cations and, indeed, the results obtained for

all the simulated concentrations, were all very close to zero (they range from 0 to 1%), which is another evidence of the high stability of Li^+-ACE^- complexes.

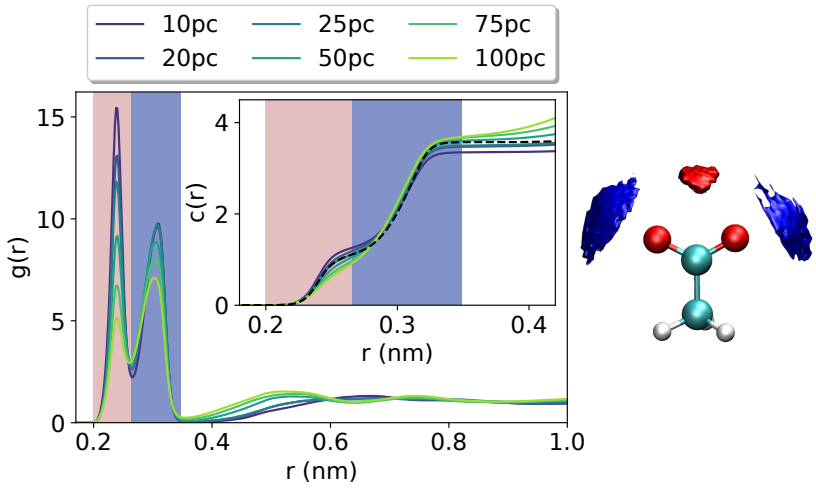


Figure 5.9: RDFs between Li^+ and ACE^-. In the inset the coordination numbers of ACE^- around Li^+ are represented for all the simulated salt concentrations as well as the one corresponding to the system of 10% without polymers. The spatial distribution function of Li^+ around ACE^- for the 20pc system is represented on the right side pointing out the Li^+ adsorption sites. The blue and red regions represent the mono and bidentate coordinations respectively.

5.4 Summary and Conclusion

In this paper we characterize the structure of polymer+salt+PIL ternary mixture using MD simulations focusing on the changes in the Li^+ environment and adsorption compared with previously reported results for similar systems. Firstly, we enumerate the used simulation details as well as the employed packing algorithm that allowed us to insert inside the simulation boxes large molecules such as the polymers taking into account the periodic boundary conditions. The tool that we developed for implementing this task was released as an open source project and we think that it can be very handy to the scientific community for obtaining the initial simulation configurations for a wide variety of systems involving large molecules with slow dynamics.

Our solubility study suggested that the [EA][ACE] was the best candidate to solvate the PEO polymer regarding the results of the radius of gyration and end-to-end distances of the polymers in every considered ILs. Therefore, we performed a series of simulations of ternary mixtures of PEO, [EA][ACE] IL and different percentage of [Li][ACE] salt. Firstly, we analyzed how the environment of Li^+ cations is affected when the polymer is added to the IL+salt mixture. Our results suggested that the polymer presence does not significantly change the molecular environment of the lithium cations pointing out that the polymer acts merely as a holder of the binary mixture. This hypothesis was also supported by the analysis of the ionic structure around the polymer backbones. In this analysis we showed that ethylammonium and acetate ions do not show any preference to be close to the polymer and only a tiny coordination of lithium cations around the polymer oxygens was remarkable. We also corroborated that the molecular environment of the ions remains constant with the addition of polymer calculating the vibrational power spectrum of the different species.

A qualitative study of the transport properties of this system was also done by means of the transference numbers of each ionic species, revealing that the addition of polymer does not affect the transport mechanisms of the considered mixture.

At this point the results deviated considerably from those previously reported with other ILs[96;157;158] and the differences were more obvious when the fraction of adsorbed Li^+ was calculated showing that, when the [EA][ACE] IL is considered, the percentage of adsorbed lithium cations in the polymers' backbones is fully compatible with a random distribution. This completes the picture that describes the polymer as a holder for the considered IL+salt mixture instead of being integrated in the ionic lattice as it happens when other ILs are considered. Moreover, this picture remains constant when the amount of IL changes, i. e., the amount of free lithium cations that could be candidates to be adsorbed in the polymer does not change. This is supported by the coordination results of ACE^- anions around lithium cations. These results showed that the addition of EA^+ cations is not able to break the coordination complexes formed by the ACE^- and Li^+. In summary, the studied system seems to be ideal to get a mechanical supported electrochemical device while keeping the IL properties.

Conflict of Interest

There are no conflicts to declare.

Acknowledgments

The financial support of the Spanish Ministry of Economy and Competitiveness (Projects MAT2017-89239-C2-1-P and MAT2017-89239-C2-2-P) is gratefully acknowledged. Moreover, this work was funded by the Xunta de Galicia (ED431D 2017/06, ED431E 2018/08, GRC ED431C 2016/001 and GRC ED431C 2020/10). All these research projects were partially supported by FEDER. J. M. O-M., A. R-P. and H. M-C. thanks the Spanish Ministry of Education for their FPU grants. A. H. and D. D. thank the German Federal Ministry of Education and Research for financial support through the FestBatt project (grant number 03XP0174B).

USC
UNIVERSIDADE DE SANTIAGO DE COMPOSTELA

6- Ternary solid polymer electrolytes at the electrochemical interface: a computational study

Summary of the chapter

Polymer-based solid-like gel electrolytes have emerged as a promising alternative to improve battery performance. However, there is a scarce of studies of the behavior of these media at the electrochemical interface. Hence, as the third study of this thesis, we pioneeringly focused on improving the current understanding of the properties of these materials when in contact with a solid interface. To achieve it, in this work we reported classical MD simulations of ternary polymer electrolytes composed of poly(ethylene oxide), a lithium salt (lithium bis(trifluoromethanesulfonyl)imide) and different ionic liquids (1-butyl-1-methylpyrrolidinium bis(trifluoromethanesulfonyl)imide and 1-ethyl-3-methylimidazolium bis(trifluoromethanesulfonyl)imide) confined between two charged and uncharged graphene-like surfaces. The molecular solvation of Li^+ ions and their diffusion, as well as the polymer conformational picture were characterized in terms of the radial distribution functions, coordination numbers, numbers density profiles, orientations, displacement variance, polymer radius of gyration and polymer end-to-end distance. Our results show that the layering behavior of the ternary electrolyte in the interfacial region leads to a decrease of Li^+ mobility in the direction perpendicular to the electrodes and high energy barriers that hinder lithium cations to come into direct contact with the graphene-like surface. The nature of the ionic liquid and its concentration were found to influence the structural and dynamic properties at the electrode/electrolyte interface, the electrolyte with low amounts of the pyrrolidinium-based ionic liquid being that with the best performance since it favors the migration of Li^+ cations towards the negative electrode when compared to the imidazolium-based one.

The post-print version of the publication reproduced in this chapter (including the full list of authors and their affiliations) can be found in appendix A.3, while the corresponding supporting information lies in appendix B.3. At the same time, in appendix C.3. we have included a complete disclosure of the relevant information related to this publication, including the authorization of the journal to reproduce its contents in this thesis, and the contribution of the author of this thesis to the publication.

6.1 Introduction

The current digital electronic revolution has gone hand in hand with an ultrarapid growth of the number of portable electronic devices. Li-ion batteries are currently the dominant mobile power sources for these devices, since they have the highest energy per unit weight of the known energy storage systems.[177;178] However, despite significant achievements in the optimization of Li-ion batteries, there are still notable challenges across cost, safety and ageing.[179;180] For example, traditional lithium batteries use liquid electrolytes based on organic carbonates, which are highly flammable and volatile, and can lead to an inhomogeneous deposition of lithium in the form of dendrites.[181]

USC UNIVERSIDADE DE SANTIAGO DE COMPOSTELA

Solid polymer electrolytes (SPEs) have emerged as attractive candidates to solve these safety and life cycle issues. Their main advantages lie in having high flexibility, low-cost and enhanced thermal/electrochemical stabilities.[65;66] Among all the options, poly(ethylene oxide) (PEO) has demonstrated to possess an excellent salt-solvating ability. After being the first polymer electrolyte reported to dissolve Li ions in 1973[182], its potential use in lithium batteries was then explored in the pioneering works of Armand *et al.*[183–185] Although PEO is one of the most studied polymers and most commonly used nowadays, PEO-based SPEs still suffer from lower ionic conductivity compared to conventional liquid electrolytes. While standard SPEs are prepared by dissolving a lithium salt in a polymer matrix, several strategies have been employed to enhance lithium ion mobility. These approaches include, for instance, the use of lithium salts with non coordinating anions such as bis(trifluoromethanesulfonyl)imide (TFSI),[154;155;186–190] the dispersion of nanoparticles[191–193] or the addition of liquid plasticizers such as carbonates,[194;195] among others.

Another feasible solution is to form ternary SPEs (TSPEs) plasticizing the PEO-based SPE with an ionic liquid (IL). ILs are molten salts with melting points below 100 °C containing charge-balanced ions.[36;42] Their properties can be modulated through different combinations of anions and cations, due to which they have been termed "designer solvents". Their features, such as negligible volatility, high chemical and thermal stability, wide electrochemical window and good solubility in various materials,[44;196] make them promising green solvents for various applications including synthesis, catalysis, separation, lubrication, drug delivery or energy storage.[145;151;197] Although many works have considered ILs and their binary metal salt mixtures to be used as electrolytes in high-performance lithium-ion batteries,[198] it has been observed that lithium salts not only usually exhibit poor solubility in ILs, but they also decrease the ionic conductivity of the binary mixtures upon increasing concentration.[199;200] Also, these binary IL/salt electrolytes suffer from large anionic clusters hindering lithium ion transport. However, this inconvenient behaviour is avoided when PEO is also present in the system, since it decouples lithium ions from its solvation shell and changes lithium transport to a PEO-dominated cationic mechanism.[201] As a result, the addition of ILs to SPEs allows improving the conductivity of polymer electrolytes increasing the number of charge carriers and accelerating polymer segmental dynamics, while guaranteeing high safety and good mechanical properties. Thus, it seems that TSPEs will play a fundamental role in the next-generation energy storage technologies.

Mixtures of PEO, lithium salts and pyrrolidinium-based ILs are undoubtedly the most investigated ternary SPE system, although short chain imidazolium IL-cations have also been considered.[156;158;202–206] In addition to the increase in conductivity with IL addition, experiments on TSPEs have also reported aspects such as the effect of the temperature and their interfacial stability on lithium metal.[156;159;160;202–205;207–211] For example, Passerini and coworkers observed that smaller anions such as bisfluorosulfonylimide (FSI) increase electrical conductivity relative to TFSI at the expense of a lower thermal stability.[212] They also highlighted the importance of the ternary SPE composition, since anions and polymers compete for the coordination with lithium cations.[213]

On the other hand, computational methods have been also widely employed over the last decades for the identification and understanding of promising TSPEs, since they allow the analysis of the systems at the molecular level and a straightforward comparison with the experimental measurements.[214;215] In general, density functional theory (DFT) calculations have been

employed to analyze either polymer decomposition on a metal surface[216;217] or the local environment around lithium cations.[190] Molecular dynamics simulations (MD), which are much more abundant, have been mainly devoted to understand the structure of TSPEs and the mechanisms of lithium transport in them.[29;158;160;206;218–220] For example, Heuer and coworkers[157] proved that the enhanced lithium diffusion in TPSEs including pyrrolidinium-based cations is due to the plasticization of the PEO backbone by the IL. Besides, they explained how lithium ion transport mechanism is modified when changing the composition of the TSPE: at high PEO/lithium ratios the three transport mechanisms remain qualitatively the same as compared to binary SPEs [i) diffusion of the cation along the PEO backbone, ii) cooperative motion of the cation with the polymer segments, and iii) cationic transfer between two polymer chains], whereas for low ratios a fourth transport mechanism based on the coordination of lithium with TFSI anions becomes more relevant.[96] Very recently, Paillard and coworkers[211] combined MD simulations with experiments to suggest the use of coordinating anions like trifluoromethanesulfonyl-N-cyanoamide (TFSAM) in TSPEs to accelerate lithium ion transport by re-coupling its dynamics from the polymer to the anion.

Moreover, while the bulk properties of binary and ternary SPEs have been extensively explored, their interfacial behaviour at the proximity of an electrode is scarcely known. The interaction of the electrolyte with the electrode considerably modifies the properties of the liquid relative to their bulk values. However, the electrode/electrolyte interfaces are not well-understood yet. Thus, consideration of structures and processes at the electrolyte/electrode interface is crucial for the optimization of energy storage devices. Concerning binary SPEs,[97;221] it was observed by Thum *et al.*[222] using MD simulations that the presence of a surface does not affect the parallel transport mechanism, but it substantially reduces the lithium-ion diffusion in the direction perpendicular to the interface. To the best of our knowledge, only one work analyzing the interfacial properties of ternary SPEs at a Li-metal surface has been reported up to now.[95] In that case, several combinations of IL cations and anions were tested to tune the structural and dynamic properties at the surface/electrolyte interface, and 1-ethyl-3-methylimidazolium 1,2,3-triazolide ([EMIM][123Triaz]) was observed to show the best performance.

In this work, with the aim of getting a better understanding of the electrode/electrolyte interface, we performed MD simulations of ternary PEO-based electrolytes to analyze their bulk behaviour and the interfacial properties at a graphene-like surface (both under charged and uncharged conditions). The studied ternary system is composed of the polymer PEO; a lithium-based salt, [Li][TFSI]; and an IL. Two different ionic liquids were considered, both sharing the anion with the salt species: [EMIM][TFSI] and [PYR_{14}][TFSI], and for the imidazolium-based TSPE two concentrations were considered. Thus, in this contribution the following questions will be addressed:

- How does the presence of a graphene-like surface influence the structure of the ternary SPE mixtures in the interfacial region? And how does the conformational redistribution depend on the surface charge?
- What is the influence of the IL on the interaction between the lithium cation and the polymer?
- Do the concentration of the TSPE or the structure of the IL cation have any impact on the interfacial properties? Which mixture shows the best potential as battery electrolyte?

USC UNIVERSIDADE DE SANTIAGO DE COMPOSTELA

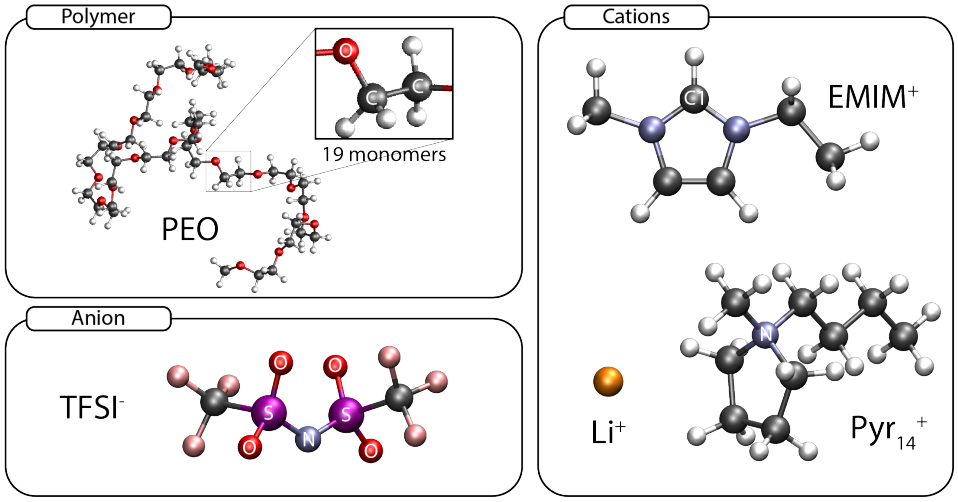


Figure 6.1: 3D models of the species present in the systems. Oxygen, carbon, hydrogen, nitrogen, sulfur, fluorine and lithium atoms are represented in red, black, white, blue, purple, pink and orange, respectively. Relevant sites employed for the calculations in each species are explicitly labeled.

Our findings are presented as follows: In the next section, details about the simulation setup are given. Then, the results are discussed in section 6.3 and, finally, the main conclusions are summarized.

6.2 SIMULATION DETAILS

The reported simulations were carried out using Gromacs 2019.5 software.[80;81] The OPLS-AA[72] force-field was used to describe the molecular interactions of PEO, Li^+ and $EMIM^+$. $PYR_{14}{}^+$ and $TFSI^-$ were parameterized according to the CL&P force field,[27;163;164] which is compatible with OPLS-AA. On the basis of a mean-field approximation, a charge scaling of 0.8 was employed to take into account polarization effects, thus obtaining a better agreement with experiments compared to a full charge model. This methodology has been previously used to investigate SPEs.[155;218]

The polymeric PEO chains were composed of 19 monomers, that is, 20 ether oxygens. Already coiled structures were chosen as the dynamics of the system is very slow. The base ratio between the different species was chosen as 20:2:6, i.e., for each 20 PEO oxygen ethers (1 chain) 2 salt molecules and 6 IL molecules are present. In order to study the influence of IL concentration on the properties of the system, the [EMIM][TFSI]-based setups were also analyzed at an oxygen(PEO)/salt/IL ratio of 20:2:20. The initial configuration was obtained following the algorithm described in Ref. 219 that allows to encapsulate long molecules, such as polymers, in periodic simulation boxes. This method takes advantage of the software package Packmol.[70] Bulk simulations of all these mixtures were carried out using 25 polymer chains and the respective amounts of lithium salt and IL.

The simulation path followed was the one thoroughly described in Ref. 222. It starts with two energy minimizations, using first a steepest descent followed by a conjugated gradients

algorithm. Then, two implicit graphene-like walls were inserted in the z dimension at the ends of the simulation box using the Gromacs tool. These layers interact with the electrolyte as a surface integrated 10-4 Lennard-Jones potential. The lateral box dimensions were fixed throughout the whole preparation and simulation of the systems in order to afterwards adjust to the graphene-like sheet size, ensuring correct periodicity of the C-C bonds. For this purpose, the x and y dimensions were set to 4.9118 and 4.6798 nm, respectively. As the lateral size of the simulation system cannot change, the z dimension will have to be accomodated to recover the correct bulk density. The exact number of molecules of each species can be seen in Table 6.1, and was chosen as to obtain approximately 10 nm between graphene-like walls, which was deemed sufficient to recover bulk conditions in the center of the simulation box.

System	Concentration	n PEO	n [Li][TFSI]	n IL
[Pyr_{14}][TFSI]	20:2:6	45	90	270
[EMIM][TFSI]	20:2:6	51	102	306
[EMIM][TFSI]	20:2:20	21	42	420

Table 6.1: Number of molecules contained in the simulation box for the different systems.

Periodic boundary conditions are applied in the X and Y dimensions. After energy minimization, a 3 ns 273 K NVT and a 3 ns 423 K NVT runs were done as a first attempt to relax unfavourable configurations. Temperature was maintained using a Berendsen thermostat.[78] Then, a series of NPT stabilizations with semi-isotropic berendsen pressure coupling[78] allowed the z-dimension of the box to adapt to reach the right density. An initial NPT run of 3 ns was followed by an annealing at 623 K for 100 ns, eventually followed by a temperature descent to the initial 423 K and another 100 ns of NPT relaxation.

After this procedure, we removed the implicit walls and inserted the real graphene-like surfaces. The carbon atom selected was opls147. The graphene-like surfaces were built using the carbon nanostructure utility of the software package VMD.[223] These graphene-like walls will remain fixed throughout the simulation procedure, so the box dimensions will not further change. The systems were simulated both with no charge on the carbon atoms of the graphene-like walls as well as with a charge density of $\sigma = \pm 1e/\text{nm}^2$, which results in a charge per carbon atom of $\pm 0.0131e$. The atomic charge is kept constant throughout the simulation, and no image charge effects are considered. Coulomb interactions were taken into account using the smooth Particle Mesh Ewald (PME) method[168;224] with the Yeh-Berkowitz correction.[225] Although constant potential conditions would result in a more realistic simulation environment, it is a technique with a much larger computational cost. The main difference in predictions from both techniques comes in the dynamics of the formation of the electric double layer,[226] but the main focus of this work is the structuring of the mixture. Furthermore, it has been previously shown in the literature that for space widths larger than 1.4 nm the constant charge method produces reliable counter-ion concentration results.[227] Adding the extra computational cost to the already long simulations needed for systems with slow dynamics, we deemed appropiate the use of the constant charge technique in this study.

After a final energy minimization was carried out, a 600-ns NVT run applying a Nosé-Hoover thermostat[228] was used as the production run, where we discarded the results from the first 100 ns since they were considered as further stabilization of the system, as can be seen in Fig. S1 of the Supporting Information. For the systems with charged graphene-like surfaces, the configuration after the first 100 ns of the neutral system was selected as a starting point. The

graphene-like surface at $z = 0$ nm is always positively charged, and the other surface is always negatively charged. These systems were simulated in a similar manner as the neutral ones, discarding the first 100 ns of the 600 ns NVT production run. Even though such long simulation times are computationally expensive, they are necessary to allow for the slow dynamics of these systems. Simulations of equivalent systems but without the polymer molecules were carried out for further comparison.

6.3 Results and discussion

6.3.1 Influence of the presence of a graphene-like surface.

In order to analyze the structural properties of the TSPEs, we computed the radial distrubution functions (RDFs) of the different species of the mixture around a Li^+ cation. In this section, these functions were calculated both in bulk and in the interfacial region of the slab model (~ 2 nm from the neutral graphene-like surface), as can be seen in Fig. 6.2. For that purpose, we selected relevant sites of the molecular components (shown in Fig. 6.1) to achieve a comprehensive view of the structural arrangement of the system. Thus, for the IL cation, C1 and N atoms were chosen for the imidazolium and pyrrolidinium rings, respectively, whereas the ones selected for the other species are specified in Fig. 6.2. There, we can clearly observe that Li^+ prioritizes the oxygen atoms from the molecular components, both PEO and $TFSI^-$, thus evidencing a mixed coordination in agreement with previous computational and experimental works on TSPEs.[156;206] Although the Li^+ environment is similar in both configurations, the height of those peaks increases in the presence of the graphene-like surface, specially the coordinations that involve the polymer molecule. This is indicative of the ternary mixtures becoming more ordered when confined due to organization of the molecules in the interfacial region. Other sites of the molecules appear as the following closest atoms as a consequence. Specifically, the two peaks for the $TFSI^-$ nitrogen interaction confirm that Li^+ and $TFSI^-$ coordinate in two different conformations: monodentate and bidentate, which are yielded by the well-known *cis* and *trans* conformations of $TFSI^-$ and are typical of this kind of aggregates.[229;230] It is interesting to note that concentration seems to play a similar role both in the bulk and at the interface, since more IL concentration leads to the bidendate coordination being more abundant. However, no remarkable effects on the height of the peaks concerning the $TFSI^-$ oxygen atoms are induced by increasing the amount of IL.

The cumulative radial distribution functions (CRDFs), i.e. the average number of particles within a distance r around a central molecule, also provide us with information about the spatial distribution. The results for Li^+ solvation are included in the insets of Fig. 6.2. As we can see, in bulk simulations Li^+ coordinates in its first solvation shell with around 3 oxygen atoms of PEO and 3 oxygen atoms of $TFSI^-$ (depending on the system), giving an average coordination number of 6, which is typical for this kind of electrolyte systems.[206] An increase in IL concentration leads to the coordination with $TFSI^-$ taking over and the coordination with the polymer exhibiting the inverse trend, although keeping the total amount of 6 oxygens being coordinated with a Li^+ cation. This change of the coordination environment of lithium cations through a weakening

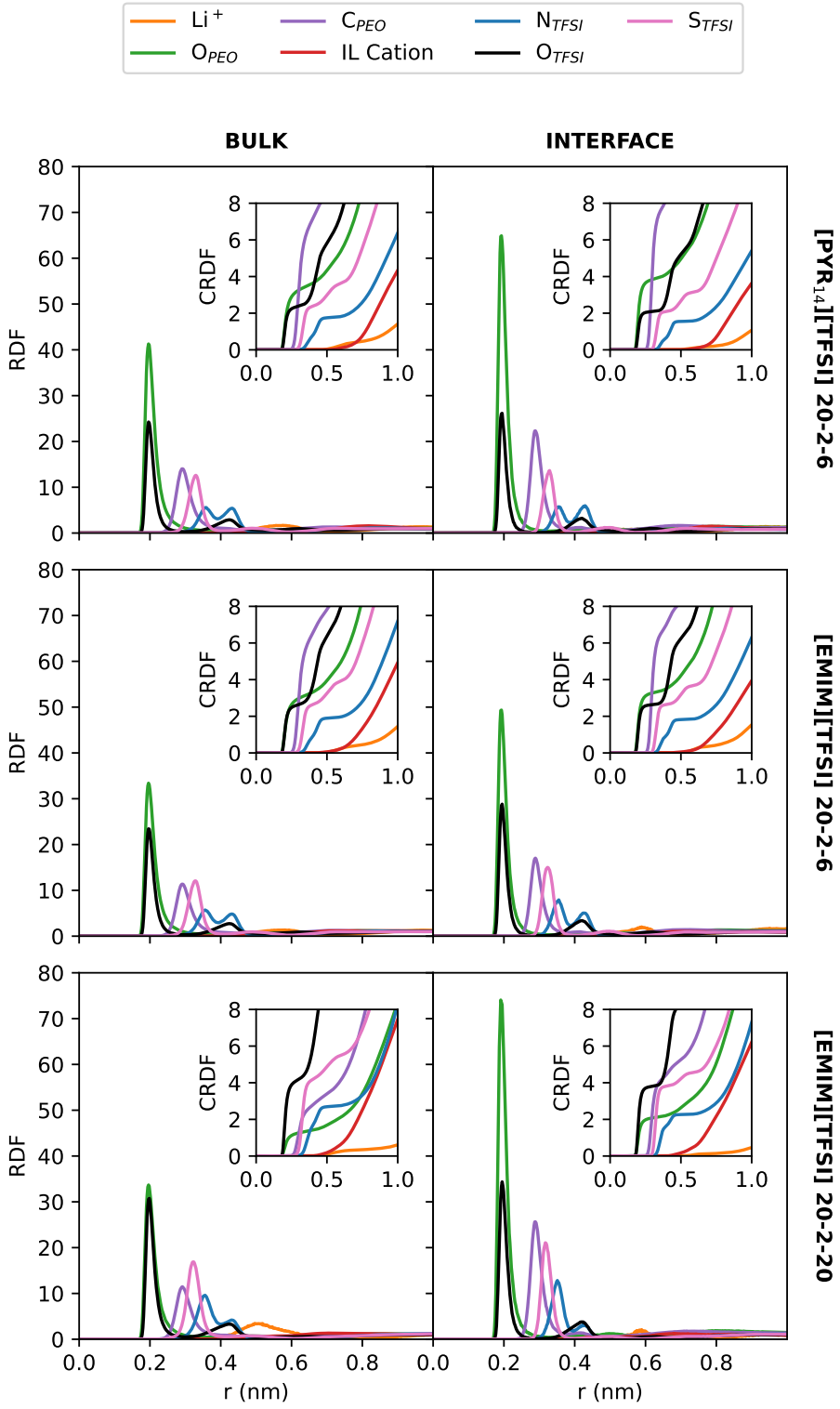


Figure 6.2: RDFs between Li^+ and several atoms of the different molecules in bulk mixtures (left) and in the interfacial region in systems between neutral graphene-like walls (right). The insets show the corresponding cumulative RDF. The representative atoms for $TFSI^-$ and PEO are specified in the legend, whereas C1 and N were chosen for $EMIM^+$ and Pyr_{14}^+, respectively.

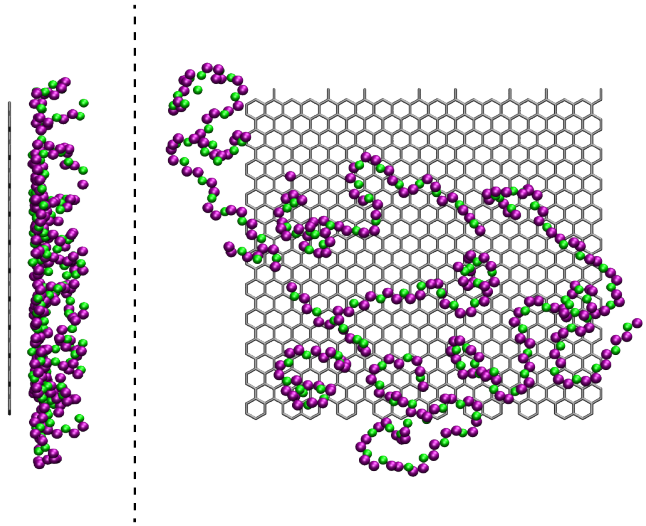


Figure 6.3: Snapshots in the YZ plane (left) and XY plane (right) of the polymer chains closer than $1\ \mathrm{nm}$ to a neutral electrode in mixtures with[Pyr_{14}][TFSI]. Oxygen and carbon atoms are represented in green and purple, respectively.

of the so-called "breathing mode" (the association between Li^+ and PEO) is mainly due to the decrease in the polymer fraction as the IL content increases. This structural picture is slightly modified when the system is under confinement. At the neutral interface the total number of oxygen atoms coordinating a Li^+ cation is maintained, with the "breathing mode" being favoured when compared to the bulk. Thus, the neutral graphene-like surface gets Li^+ preferentially coordinated to the PEO oxygens. The opposite behaviour, that is, an increase in the number of $TFSI^-$ anions in the lithium ion solvation shell when going from the bulk to the interface, was previously reported when introducing a Li metal surface.[95;97] This discrepancy is an effect of the nature of the electrode on its interaction with the polymer. That is, due to the well-known hydrophobicity of graphene,[231;232] this carbon surface shows stronger interactions with the PEO carbon atoms than the Li metal surface, resulting in a larger number of polymers in the interfacial region that are available for coordinating a lithium ion, as it will be shown by the calculation of the number density profiles included in Fig. 6.5. In fact, this can be clearly appreciated in the snapshot included in Fig. 6.3 (right), where the polymers in the proximity of an uncharged graphene-like sheet show to be arranged parallel to the surface, thus maximizing their interaction with the neutral electrode. This will be also confirmed later with the analysis of the orientations.

6.3.2 Influence of the charge of the graphene-like surface.

RDFs and CRDFs in the interfacial regions with charged graphene-like electrodes were calculated with the aim of analyzing the impact of charging the surface. The corresponding plots are shown in Fig. 6.4.

At surface charges of $\sigma = +1e/nm^2$ the interaction between an oxygen of the polymer and a Li^+ cation is always slightly lower than at neutral interfaces, whereas that with an oxygen from $TFSI^-$ anion is greater. In fact, it can be seen that the interaction between lithium and the anion increases when increasing the amount of IL in the ternary mixture due to the presence of

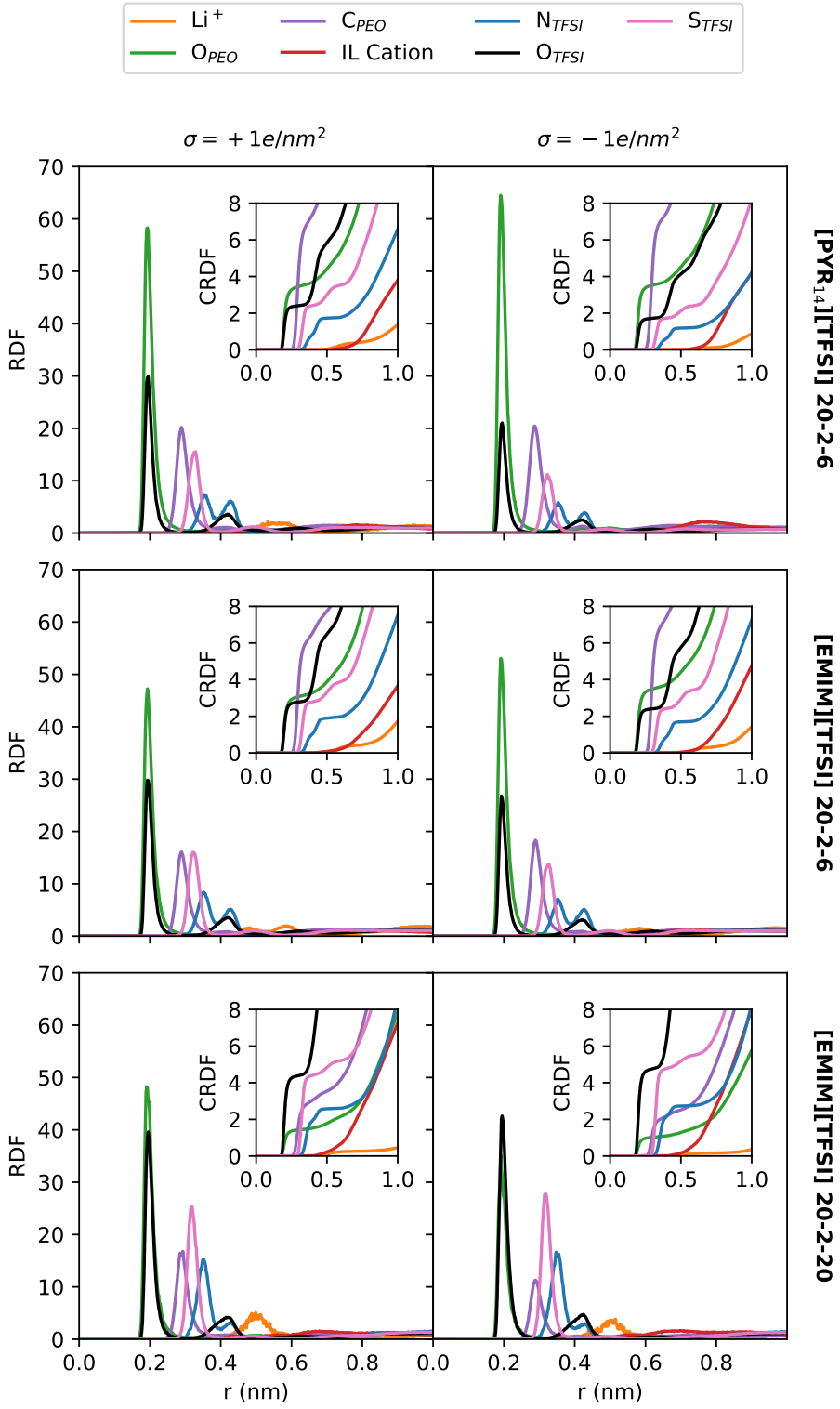


Figure 6.4: RDFs between Li^+ and several atoms of the different molecules in the region near the positively (left) and negatively (right) charged graphene-like surfaces, respectively. The insets show the corresponding cumulative RDF. The representative atoms for $TFSI^-$ and PEO are specified in the legend, whereas C1 and N were chosen for $EMIM^+$ and Pyr_{14}^+, respectively.

a greater amount of $TFSI^-$ anions. Concerning the coordination numbers, in the first solvation shell of lithium ions there are always around $2-3$ oxygens of PEO and $2-4$ oxygens of $TFSI^-$ anions. Since the anions are expected to be located in the neighborhood of the positively charged surface, this could be indicative of Li^+ showing correlated ion motion with the anions in negatively charged Li-containing clusters. This will be explored later with the analysis of the number density profiles.

On the other hand, at surface charges of $\sigma = -1e/nm^2$ and low amounts of IL, the interaction between an oxygen from PEO and a solvated Li^+ ion is stronger than at positively charged surfaces, but it decreases when increasing the concentration. Regarding the interaction of Li^+ with the oxygens of $TFSI^-$ anions, the height of the peaks of the RDF is comparable to that in neutral interfaces, with a tendency of increasing with IL concentration. Lithium coordination numbers with the polymer are 3 (except for the most concentrated mixture), as observed in the vicinity of the positive electrode; whereas those with the anion show an increase with the amount of IL, probably due to a greater number of $TFSI^-$ anions being available for solvating the same number of lithium cations.

As it is well known, the interface leads to a layering of highly concentrated ionic electrolytes due to the interactions between the electrolyte and the surface.[19;233;234] To analyze this effect and shed more light on the microscopic structure of these systems, we also computed the density profile along the z-axis, which are displayed in Fig. 6.5. The first characteristic that is visible there is that some degree of layering in the interfacial region takes place also at neutral surfaces, which is associated to the translation symmetry breaking, but the effect is much more pronounced when charging the graphene-like sheet. In both cases, bulk density is recovered after approximately 2 nm from the carbon surface.

On the other hand, as can be seen in Fig. 6.5 (left) for uncharged graphene-like surfaces, Li^+ atoms are never found in the regions adjacent to the walls, regardless of the IL employed and the concentration of the ternary SPE. Instead, they are located sharing the second layer with $TFSI^-$ anions. In turn, the first layer is mainly occupied by PEO molecules and a small amount of IL ions. This behaviour has been also observed at the interface between SPEs and a Li-metal surface, and it is indicative of a preference of the surface to interact with the electron rich compounds.[95;97] Li^+ cations are more propense to interact with the elctrolyte molecules rather than with the surface atoms. On the other hand, it is also shown in Fig. 6.5 (right) that charging the graphene-like electrode leads to the spontaneous accumulation of counter-ions and the depletion of co-ions near the charged surface, as expected. Interestingly, an inner PEO layer emerges directly attached to the positively charged carbon surface at around 0.3 nm, followed by a dense layer of anions at secondary positions. Concerning the negatively charged surface, a dense layer of IL cations is always formed at approximately 0.4 nm from the graphene-like wall, but some differences can be seen between the different systems. Firstly, for the lowest IL concentrations (20-2-6), lithium cations are able to directly approach the electrode together with some PEOs, which are splitted in several layers, with the pyrrolidinium-based TSPE, but not with the imidazolium-based one. Apparently, with $[Pyr_{14}][TFSI]$, Li^+ is not able to desolvate from the polymer, but these positively charged aggregates are indeed capable of reaching the negative electrode. This can be also observed in the snapshots of Fig. 6.6, where the 1 nm-wide regions from the negative surface are represented for these two mixtures. However, when low amounts of [EMIM][TFSI] are present in the electrolyte, Li^+ seems to keep a strong coordination with $TFSI^-$ anions, as shown by the emerging lithium ion populations at around 0.7 nm and

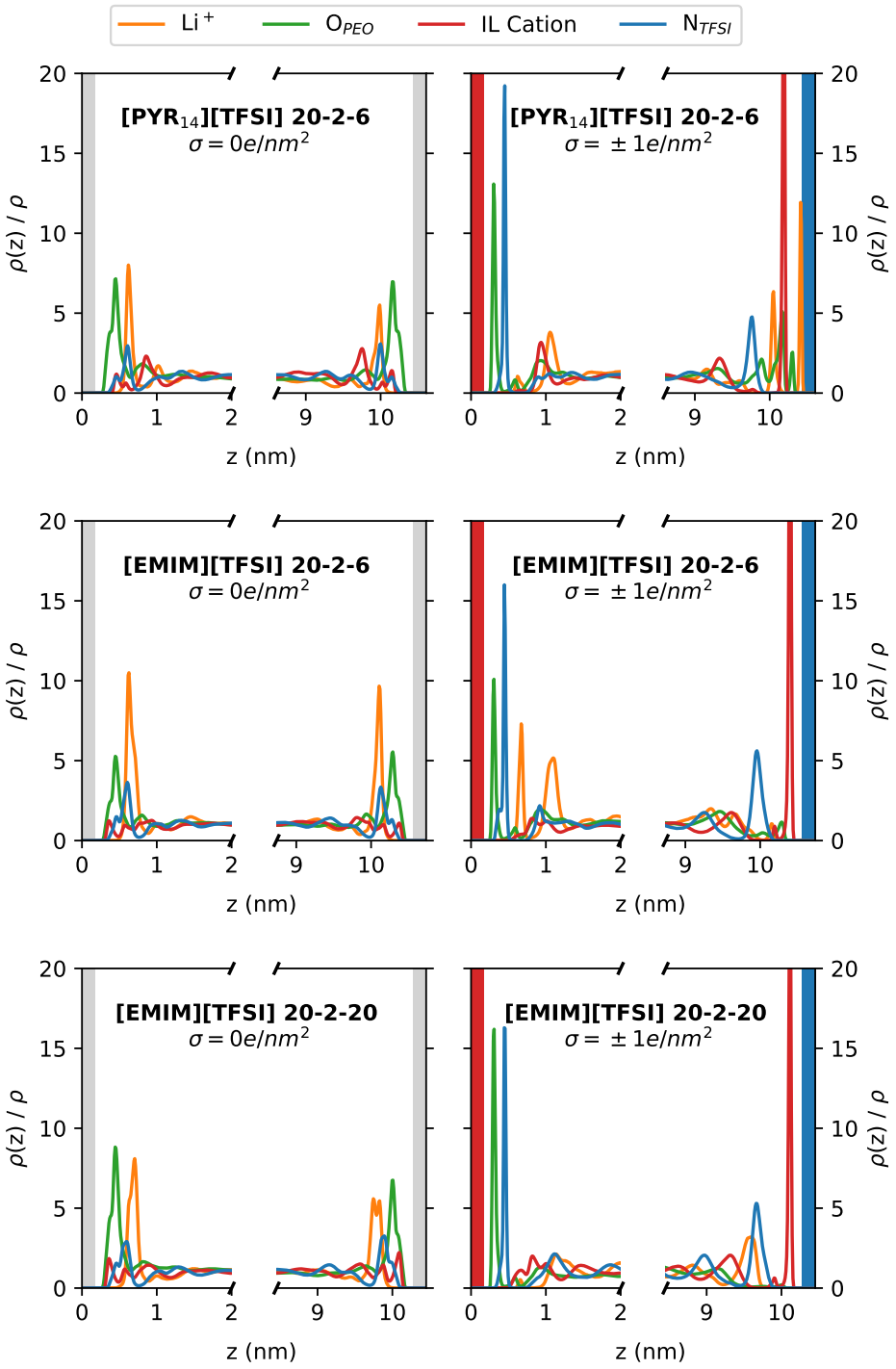


Figure 6.5: Density profiles in the z direction, normalized to the bulk density, for several atoms of the different molecules in systems confined between neutral graphene-like surfaces (left) and charged graphene-like surfaces (right). The representative atoms for $TFSI^-$ and PEO are specified in the legend, whereas C1 and N were chosen for $EMIM^+$ and Pyr_{14}^+, respectively.

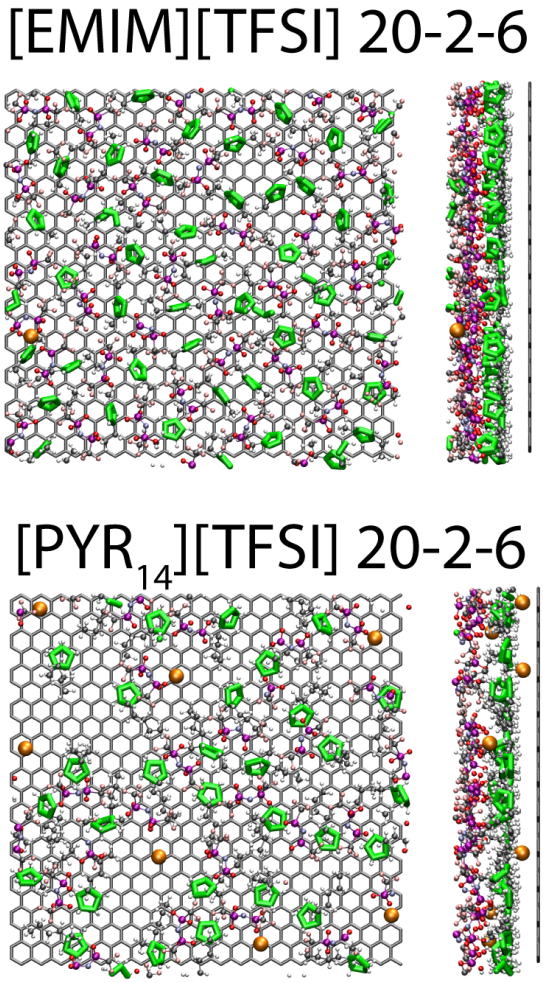


Figure 6.6: Snapshots in the XY plane (left) and YZ plane (right) of the molecules closer than 1 nm to the negative electrode in the [EMIM][TFSI] (top) and [Pyr_{14}][TFSI] (bottom) 20-2-6 systems. Lithium atoms, in orange, and cationic rings, in green, are artificially enlarged for better visual clarity.

1.1 nm from the positively charged graphene-like sheet. This is probably due to the stronger interaction of $TFSI^-$ anions with Pyr_{14}^+ than with $EMIM^+$ that diminishes the degree of anion clustering with Li^+. This can be observed in Fig. S2 of the Supporting Information, where we have plotted the RDFs between the IL ions for binary mixtures of [EMIM][TFSI] with LiTFSI and [Pyr_{14}][TFSI] with the same salt, both with a ratio of 6-2, which corresponds to the lowest IL concentration in the ternary SPEs.

Focusing now on the PEO/[Li][TFSI]/[EMIM][TFSI] electrolyte between charged surfaces, it can be observed in Fig. 6.5 that Li^+ cations are not able to cross the dense layer of $EMIM^+$ and approach the negatively charged carbon surface for any of the tested concentrations. Thus, we try to get a deeper understanding about the movement of Li^+ cations calculating the free energy

profiles of transfering a Li^+ from the bulk to the graphene-like surface as

$$F(z) = -k_B T \ln\left(\frac{\rho_{Li}(z)}{\rho_{Li}(\text{bulk})}\right), \tag{6.1}$$

where k_B is the Boltzmann constant. The free energy profiles obtained for uncharged, positively charged and negatively charged surfaces are included in Fig. 6.7, where we can observe the oscillations due to the layering behaviour of the TSPE in the proximity of the wall. At uncharged surfaces, for all the systems there is an easily accessible first minimum at 0.6 nm followed by a second one at 1 nm. This shows that a given lithium is slightly stabilized at uncharged interfaces, with a larger lifetime in the minimum at 0.6 nm. However, it should be kept in mind that in the neutral slab configuration there is an inner layer composed mainly of PEO and some IL that impedes Li^+ to come into direct contact with the surface.

In the case of positively charged interfaces, the opposite behaviour can be observed for most systems. That is, Li^+ cation has a preference to place at distances larger than 1 nm rather than in the first layer, the only exception being the electrolyte with the lowest amount of [EMIM][TFSI]. In that mixture, Li^+ faces the lowest energy barrier to jump into the first layer. Once it has entered it, the Li^+ ion will stay there for some extended waiting time. This behaviour arises from the strong interaction between Li^+ and the first layer of $TFSI^-$ anions at the positive electrode, as we have seen in Fig. 6.5. At the negative electrode, the height of the free energy barriers increases remarkably in comparison with the previous situations due to a depletion of Li^+ cations in some regions, as shown in Fig. 6.5. Now, free energy barriers are much higher than thermal energy, so the diffusion process towards the negative electrode can be regarded as a rare event, with the $[Pyr_{14}]$[TFSI]-based TSPE showing the highest probability of Li^+ approaching the graphene-like surface. However, if a rare transition from the second layer at 0.6 nm to the innermost one at 0.2 nm takes place, which has been observed to happen 11 times during the whole trajectory, then Li^+ cations are accommodated in a stable position with high energy barriers for escaping from the negative electrode, since for that to happen they must overcome the electrostatic attraction of the electrode.[222] In fact, our simulations show that once Li^+ cations reach the negative electrode, they remain at the innermost layer (on average) during 24.15 ns and 3.00 ns for PYR 20-2-6 and EMIM 20-2-6, respectively.

Another relevant aspect of the TSPEs studies in this work is the particular orientation that the long polymeric chains adopt near the interfaces. As it has been shown in previous studies,[157] the polymer chains allow three new possible channels of Li^+ diffusion in these mixtures: i) motion along with the chain, ii) hopping between chain sites, and iii) hopping between chains. As a result, the orientation of these chains could play an important role on the diffusion of Li^+ cations towards the electrodes. To analyze this feature, we considered the orientations of the different species in the system by computing the probability density distribution of the cosine of the relative angle between a vector normal to the surfaces pointing to the bulk and a characteristic molecular vector. For the IL cation, the vector is normal to the ring and has the geometrical center of the ring as application point. For the polymer, a subdivision of the chains allows to better identify the correct orientation of the chains. Thus, we decided to take multiple vectors between consecutive oxygen sites of PEO, that is, going from one monomer to the next one in a random direction; with the application point of the vector being placed halfway between the two oxygens. For both species, the orientations were calculated only for those molecules whose application point of the characteristic vector lies within the first 2 nm from the charged and uncharged electrodes.

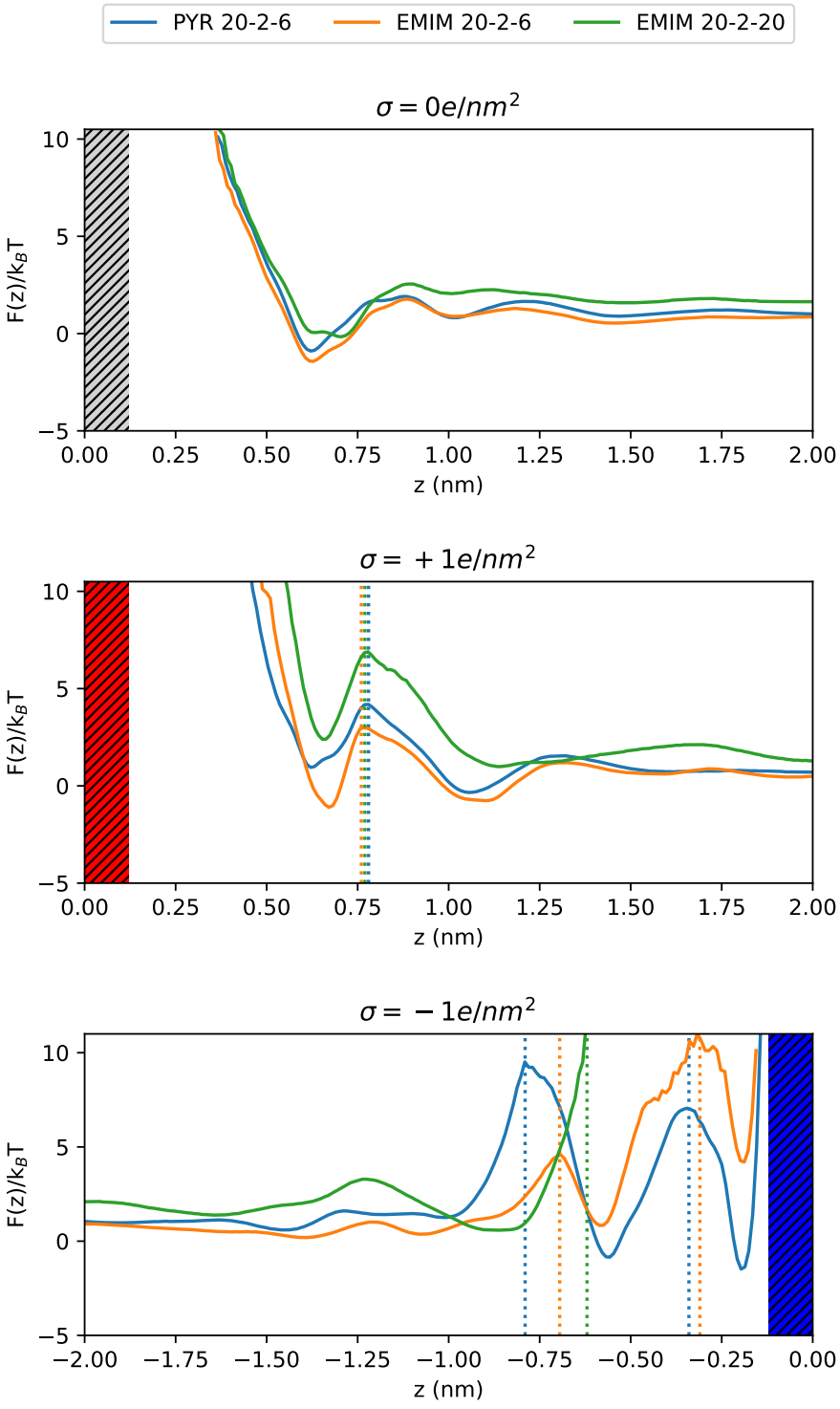


Figure 6.7: Free energy profiles for lithium ions approaching the graphene-like surfaces with neutral (top), positive (center) and negative (bottom) charge densities for the investigated ternary SPEs. Dotted lines show the positions of the barrier for all the concentrations: PYR 20-2-6 (blue), EMIM 20-2-6 (orange) and EMIM 20-2-20 (green). In all cases the corresponding electrode is located at z = 0.0 nm.

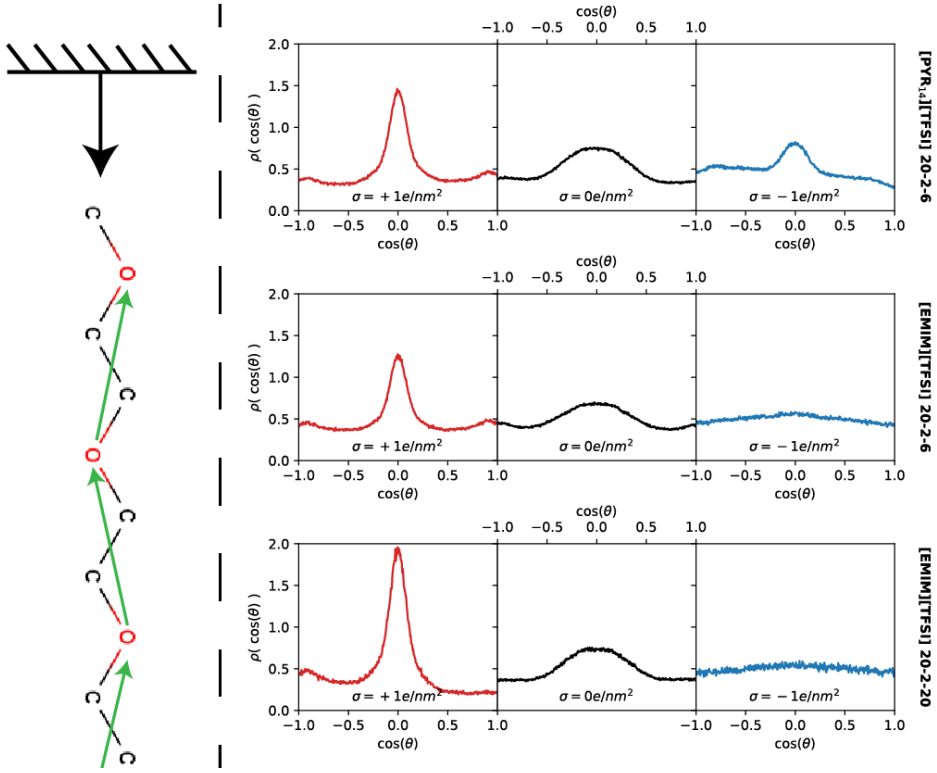


Figure 6.8: Marginal probability density distribution of polymer orientation relative to the vector normal to the graphene-like surface in the interfacial region (up to 2 nm). A scheme depicting the characteristic vectors defined for the polymer is shown on the left.

The orientations of interfacial PEO molecules are plotted in Fig. 6.8. There we can observe higher populations of polymers in the parallel orientations close to the graphene-like surfaces for most of the considered systems, thus trying to maximize their interaction with the carbon atoms of the surface, as it was previously mentioned in the analysis of the effect of confining the SPE. This arrangement is more marked in the vicinity of the positively charged electrode, where we have seen in Fig. 6.5 that PEO is located in the innermost layer followed by a second layer of $TFSI^-$ anions. Probably, the Coulomb attraction between this second anionic layer and the positive electrode is squeezing the polymer against the surface, forcing it to adopt a parallel stacking behaviour. However, in the proximity of the negative graphene-like surface, where the polymer was observed to be less constrained in the z direction, it does not show a preferential orientation in ternary mixtures with [EMIM][TFSI]-based electrolytes because it has more conformational freedom. Neutral graphene-like surfaces also favour a "flat" polymer conformation, in agreement with previous observations for uncharged Li-metal surfaces.[95;97] In addition, the amount of IL and the nature of the IL cation does not seem to affect the orientation of PEO molecules. Fig. S3 of the Supporting Information shows the orientation of the IL cations that are located in the innermost layer. The results suggest that both IL cations have random arrangements relative to a positively charged electrode, whereas cation rings become more parallel to the negatively charged surfaces, in order to get a more efficient accumulation that allows them to overcompensate the charge of the electrode. On the other hand, the orientation of IL cations when adsorbed at neutral surfaces depends on their nature, with imidazolium rings preferring to be parallel regardless the concentration, and pyrrolidinium rings showing no preferential orientation.

The interaction of PEO with the components of the solvent and the graphene-like surfaces can be further analyzed by calculating the radius of gyration (R_g) and the end-to-end distance (d_e), which quantify the chain expansion in the mixture and can be calculated, respectively, as

$$R_g^2 = \left\langle \frac{1}{N} \sum_i |\vec{r}_i - \vec{r}_{cm}|^2 \right\rangle, \tag{6.2}$$

and

$$d_e^2 = \langle |\vec{r}_N - \vec{r}_0|^2 \rangle, \tag{6.3}$$

where N is the number of atoms in a PEO chain, $\vec{r}_N$ and $\vec{r}_0$ are the coordinates of the last and the first atoms of the chain, respectively, and r_{cm} is the center of mass of a chain. The results for the radius of gyration as a function of the position of the polymer along the simulation box axis can be seen in Fig. 6.9, whereas those for the end-to-end distance are included in Fig. S4 of the Supporting Information. In order to obtain these plots, the computed quantities for each chain were asigned to the z coordinate of all of the backbone atoms of said chain (oxygens and carbons). Our findings show that, the radius of gyration increases in the proximity of the neutral and the positively charged walls, which indicates that the PEO backbone is less folded in the interfacial region. This behaviour seems to be in open contradiction with the fact that the O(PEO)-Li^+ interactions were observed to increase close to the graphene-like walls, and the radius of gyration is expected to decrease when increasing those interactions, as previously reported for PEO-based electrolytes confined between Li-metal surfaces.[95;97] However, as it was earlier stated in this work, PEO molecules in the interfacial region strongly interact with the carbon atoms of the wall, which leads to the unfolding of the polymer. In addition, the radius of gyration is also observed to increase close to the negatively charged surface in mixtures with [PYR_{14}][TFSI] due to the enhanced presence of lithium cations and polymer molecules in that interface. In general, the interaction with Li^+ in bulk leads to a globule conformation of the polymer on a local scale. However, globally, the constraint introduced by the graphene-like wall, and the fact that PEO tries to maximize the interaction with both the surface and all the Li^+ cations in the interfacial region, lead to a transition to a coil conformation. In addition, we computed the gyration tensor in order to further confirm this picture. The gyration tensor of a set of N points can be defined as:

$$G_{ij} = \frac{1}{N} \sum_{k=1}^{N} r_i^{(k)} r_j^{(k)}, \tag{6.4}$$

provided that the center of mass of the points is set to zero. The eigenvalues and eigenvectors of this tensor, or more specifically, the square root of these eigenvalues, offer a measure of the shape of the point cloud. In our case, we can see plotted in Fig. S5 the values corresponding to the Z direction as well as those corresponding to directions contained in the XY plane. These values were computed for all polymers and discretized into bins so that we could see the variation of these parameters along the Z axis. As we can see, along all of the simulation box, the square root of the eigenvalues of the XY plane are comparable and substantially larger than that of Z. This once again confirms our view, suggesting that polymer conformations are disk shaped and parallel to the surface. This situation is, as we hinted earlier, even more marked at the vicinity

of the interface, as the value corresponding to the Z direction decreases even further in general.

As it is well known, Li^+ diffusion plays a crucial role on the kinetic process that takes place in battery electrodes, and thus on the performance of energy storage devices. To obtain information on Li^+ dynamics we analyzed the Li^+ cation diffusion by calculating the variance Var$[\Delta z]$ of the displacement vector Δz of these ions as a function of their initial position in z, as described in Ref. 222. The variance of the lithium displacements is calculated as

$$\text{Var}[\Delta z] = \langle \Delta z^2 \rangle - \langle \Delta z \rangle^2, \tag{6.5}$$

with $\langle \Delta z^2 \rangle$ being the mean-square displacement, and $\langle \Delta z \rangle^2$ the square of the mean displacement in the z direction. The brackets indicate average over all the particles of the same species and average over multiple starting times, t_k. Thus, the displacement of a given molecule after a lag-time Δt is

$$\Delta z(\Delta t) = z(t_k + \Delta t) - z(t_k) \tag{6.6}$$

The variance of the displacements in the x and y directions were calculated in the same way and all of them are represented in Fig. 6.10 for a lag-time of 1 ns as a function of the initial position in z.

It can be observed that, regardless of the charge of the electrodes, of the IL cation, and of the amount of IL, the diffusion of Li^+ ions in the direction perpendicular to the graphene-like surface always slows down in the interfacial region, where the formation of layers takes place. At neutral interfaces, the z displacement variance decreases in a similar way for all the systems compared to the bulk, which is consistent with the nearly identical free energy barriers in the neighbourhood of these surfaces, as shown in Fig. 6.7. Charging the electrodes leads to diverse modifications of the z displacement variance in the interfacial region for the different systems. In general, the shortest z displacement variances correspond to those electrolytes with most stable minima in the free energy profiles, which is in agreement with Li^+ cations remaining at the interfaces once they reach that region. These results are indicative of a high interfacial resistance to ionic mobility at both the positively and negatively charged electrode interfaces due to strong interfacial layering. In addition, it can be seen that the bulk behaviour is not 100% recovered in the center of the simulation box, since the displacement variances in the direction perpendicular to the electrodes are always lower than those in the x and y directions.

In the directions parallel to the electrodes, the variance of the displacement shows a much lower degree of dependence with the distance to the carbon interface compared to the perpendicular direction. In addition, Li^+ cation diffusion is slightly faster in the regions of the outer layers of the electric double layer (EDL) and then decreases again in the inner layers, probably due to a constraining effect due to the presence of other species or to the own charge of the electrode. In summary, the molecular conformation at the innermost layer of the EDL inhibits Li^+ transport in the three directions, but their migration towards the electrode suffers a much more marked "locked-in-place" effect once within the interfacial layering.

From the analysis of the displacement variance we can also infer that Li^+ mobility slightly increases with increasing the IL concentration, both between neutral and charged graphene-like surfaces, which can be indicative of the IL acting as a plastizicer. Also, the comparison between both ILs at a proportion of 20-2-6 shows that the addition of [EMIM][TFSI] leads to a moderately enhanced Li^+ dynamics.

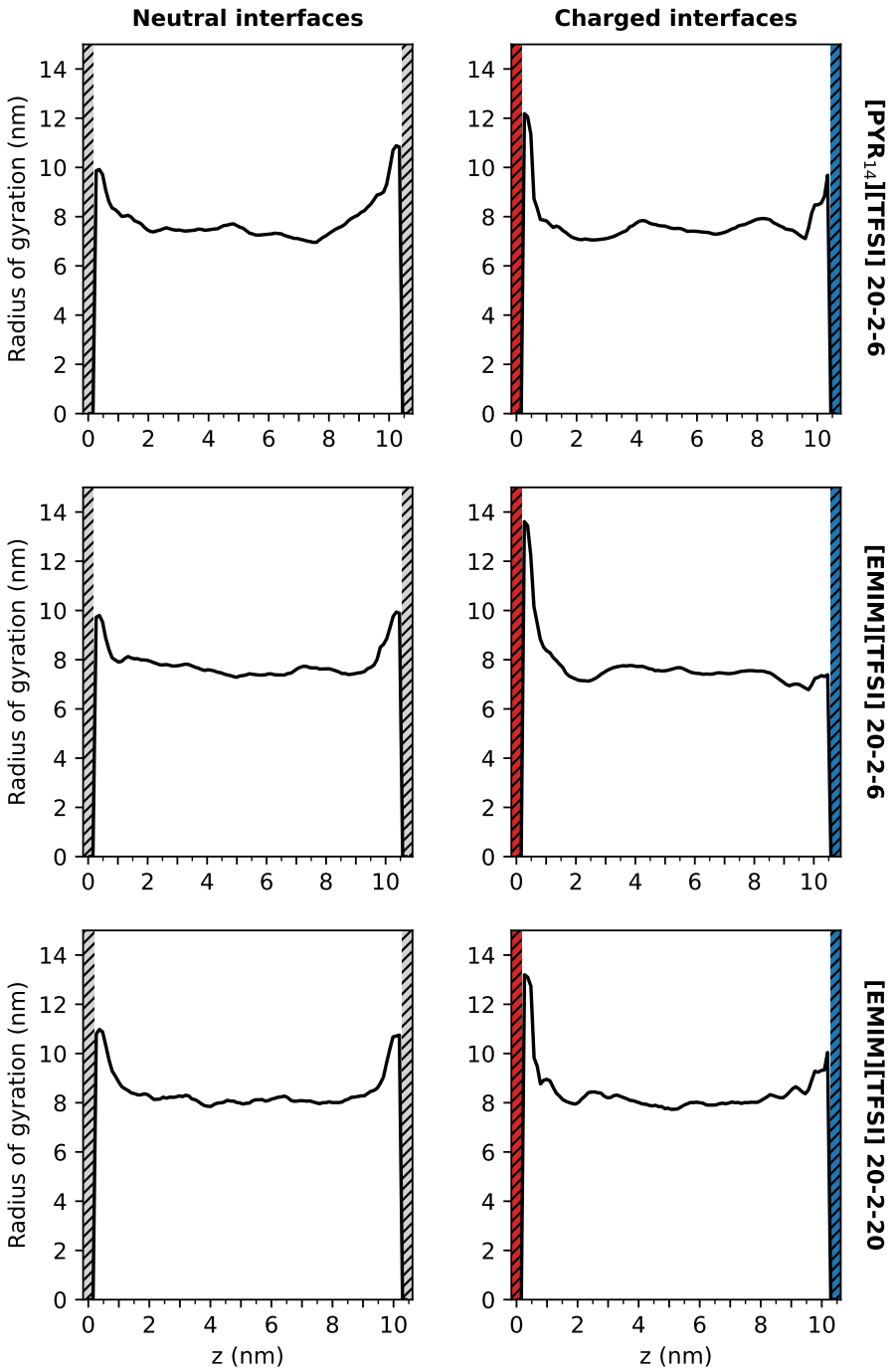


Figure 6.9: Radius of gyration in the z direction for TSPEs confined between neutral (left) and charged (right) graphene-like surfaces.

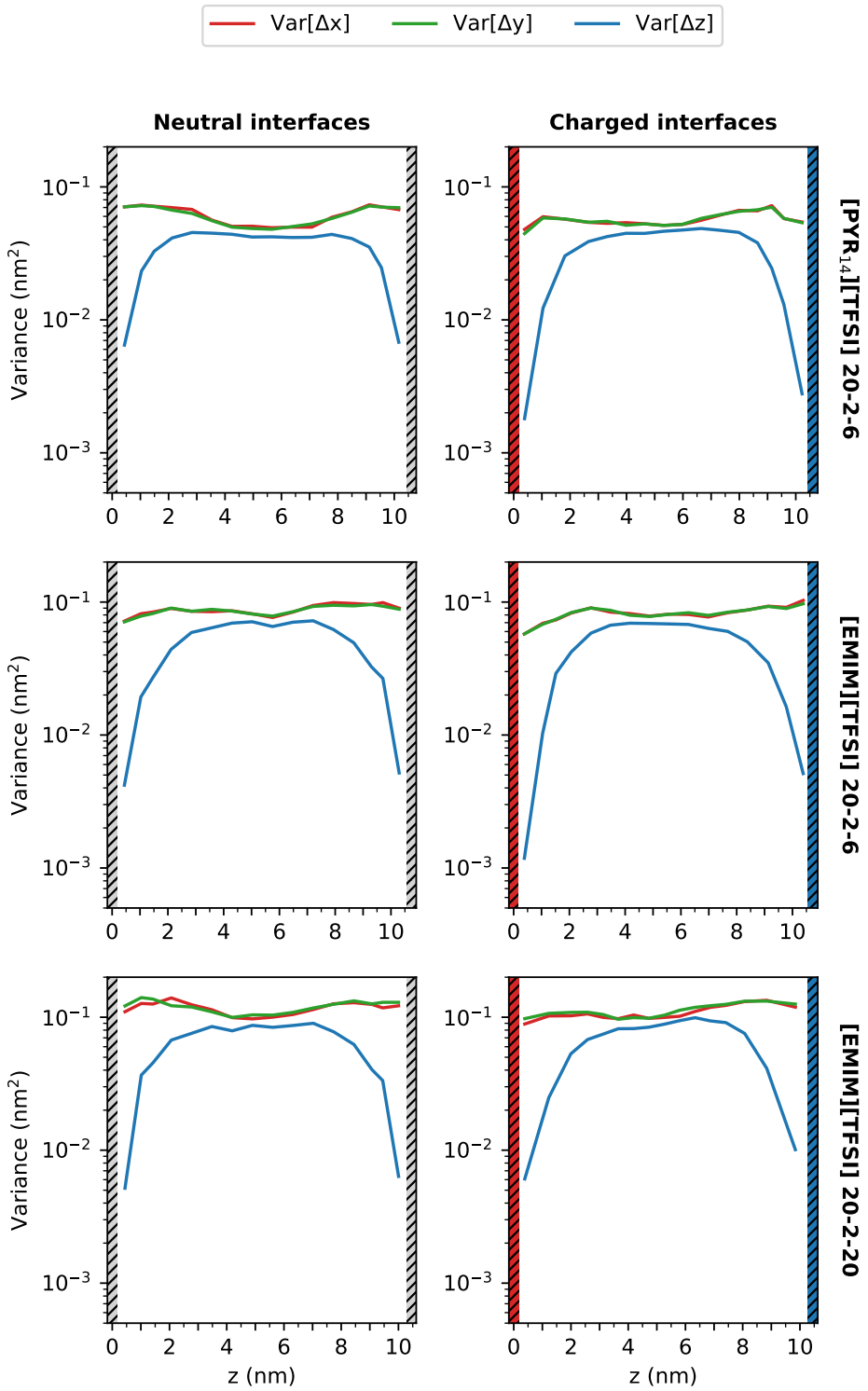


Figure 6.10: Displacement variance (Eq. 6.5) of Li^+ cations in the three directions as a function of the initial position in z for TSPEs confined between neutral (left) and charged (right) graphene-like surfaces.

The variance of the displacements of PEO oxygens are included in Fig. S6 of the Supporting Information. There it can be seen that PEO diffusion shows, in general, the same features as that of Li^+ ions. We can observe the same restraint in the motion perpendicular to the electrodes when the oxygen atoms are located close to the interface. It is interesting to notice that the variance in this direction never reaches values comparable to those of the X and Y directions. This effect is likely due to the much larger size of the PEO chains compared to the other molecular species. This way, the chains could "feel" the presence of the interfaces even when part of it is far away from the electrode.

6.3.3 Influence of adding IL into the binary SPE (PEO/LiTFSI).

As it is well-known, the addition of an IL to a SPE leads to a plasticizing effect that enhances the mobility of the Li^+ cation, which confers ideal properties to the TSPEs. Understanding the role of the IL on the structure of these ternary mixtures is therefore of paramount importance. In this section, we will attempt to shed some light on this issue. Previously, Thum *et al.*[222] reported structural results for a SPE composed of both PEO and [Li][TFSI] in the presence of neutral and charged graphene-like surfaces.

Concerning Li^+ solvation in bulk, the main effect of IL inclusion is the appearance of some degree of coordination with TFSI oxygen atoms, which was hardly present for PEO-LiTFSI binary mixtures, at the expense of decreasing that with PEO oxygens. The total number of 6 oxygens around a given lithium is not changed with the addition of the IL, but the coordination environment of 6 PEO oxygens observed by Thum *et al.*[222] is more markedly modified when increasing the amount of [EMIM][TFSI], even being swung up to a solvation shell composed of 4 and 2 oxygens from TFSI and PEO, respectively, which can be attributed to a dilution of the polymer. In the proximity of graphene-like surfaces, the addition of an IL to the binary SPE affects the surroundings of Li^+ cations in a less pronounced way compared to the bulk, but the results depend on the charge of the electrode. For neutral surfaces, the insertion of an IL leads to Li^+ being surrounded not by 5 PEO oxygens, but instead by 4 and 2 oxygen atoms from PEO and TFSI, respectively. This proportion is reversed with increasing IL concentration. Concerning the positively charged surface, we observed that the interaction with the polymer decreases from 5 PEO oxygens to $3-4$ when including any of the ILs, whereas the number of TFSI oxygens is kept at $2-3$. This shows that the charge of the surface dominates over the addition of IL, as this is the electrode that electrostatically attracts the anions, which increases the interaction between $TFSI^-$ and solvated Li^+. On the other hand, near the negative electrode the structural picture depends on the concentration of IL. At low amounts of IL, the $2-3$ PEO oxygens coordinating a Li^+ observed in binary SPE are kept in ternary mixtures, although the inclusion of IL leads to the incorporation of two TFSI oxygen to the Li^+ first solvation shell. At high [EMIM][TFSI] concentrations the anions take $4-5$ of the 6 interaction sites of Li^+.

The comparison of the number density profiles with those reported by Thum *et al.*[222] reveals that, near neutral graphene-like surfaces, the addition of IL does not markedly modify the composition of the innermost layer of the EDL, which is filled up with anions and polymer molecules. Also, the peak positions of Li^+ do not change relative to those observed by Thum *et al.*.[222] However, while they obtained a similar height for both peaks, in ternary SPEs there is a clear tendency of Li^+ ions to be placed as close as possible to the electrode. On the other hand, the layer that is in direct contact with the positively charged surface is still shared by polymers

and anions regardless the inclusion of IL. Notwithstanding, for low IL concentrations a new position of Li^+ appears at around 0.6 nm, which probably corresponds to those lithiums that are dragged by the anions. With respect to the negative electrode, some noteworthy changes are observed when adding IL to the binary SPE studied by Thum *et al.*[222]. Firstly, the positions close to the surface at which PEO molecules are located in binary mixtures are now occupied by the IL cations in the ternary ones. Secondly, this leads to a competition between Li^+ and IL cations to reach the negatively charged surface that is more remarkable when increasing the amount of IL, as expected. In fact, at the highest [EMIM][TFSI] concentration the negative electrode is observed to be fully impregnated by $EMIM^+$ and nor Li^+ neither PEO are able to get to the innermost layer.

The number density profiles are directly related to the energy landscape that Li^+ has to cross to reach the electrodes. Those free energy profiles are much smoother with the addition of IL, in particular in those systems with neutral graphene-like walls, where the energetic barrier almost vanishes. Previous results reported by Thum *et al.*[222] for neutral surfaces showed a much more layered profile for the binary SPE, where lithium cations need to overcome several barriers before reaching the interfacial region. In the absence of Coulomb interactions with the electrodes that add competing effects into the systems, these smoother energy profiles can be indicative of a reduced degree of ordering with the addition of IL that facilitates the motion of Li^+ through the simulation box towards the surfaces. Although we can not establish a clear connection between the well-known plastizicer effect of the IL from our MD simulations and those of Thum *et al.*[222], the comparison between the free energy profiles at charged interfaces indicates that, for choosing the amount of IL to be added to the binary SPE, a compromise between enhancing PEO and Li^+ motion and how the IL ions are going to compete for the electrodes must be made. In this regard, our results advise to avoid very high IL concentrations.

6.4 Conclusions

In the present work, classical MD simulations were performed for TSPEs (containing the polymer PEO, a lithium salt ([Li][TFSI]) and an IL) confined between two graphene-like surfaces. Two ILs at different concentrations were tested, $[PYR_{14}][TFSI]$ and [EMIM][TFSI], with the aim of determining the optimal composition of the electrolyte system for application in energy storage devices. The structural picture of the molecular species in the interfacial region with both charged and uncharged walls was characterized by the radial distribution functions, the coordination numbers, the number density profiles and the orientations. The dynamics and kinetics of Li^+ motion was analyzed in terms of the variance of the displacement and the free energy profiles. In addition, the PEO conformation was investigated through the calculation of the radius of gyration and the end-to-end distance.

All systems show the typical electrolyte–electrode interfacial layering characteristic. This results in Li^+ being preferentially coordinated with the PEO oxygens instead of with $TFSI^-$ anions in the neighborhood of neutral graphene-like surfaces, which is the opposite behaviour of the one previously observed for Li-metal electrodes. The innermost layer in the neutral interfacial region is mainly composed of PEO molecules, which are arranged parallel to the surface in a "flat" conformation trying to maximize their interaction with the hydrophobic graphene. In the presence of charged graphene-like surfaces, lithium cations more easily approach the negatively charged electrode with the pyrrolidinium-based TSPE, rather than with the imidazolium-based

USC COMPOSTELA

one even for high concentrations, which is probably due to the lower degree of anion clustering with Li^+ in the former case. This allows lithium cations to coordinate with the polymer and reach the negative surface. However, the analysis of the free energy profiles shows that the barriers lithium cations must overcome to come into contact with the negative electrode are much higher than the thermal energy, so the diffusion process can be regarded as a rare event, which, in case of taking place, would lead to very stable Li^+ adsorption. Concerning the dynamics, the diffusion of Li^+ ions in the direction perpendicular to the graphene-like surfaces always slows down regardless of their charge, due to the strong interfacial layering that leads to a high interfacial resistance to ionic mobility.

In summary, although our findings indicate that large amounts of imidazolium-based ILs increase Li^+ mobility due to a plastizicing effect, we also observed that the presence of [PYR_{14}^+] cation energetically favours Li^+ presence at the negative electrode when compared to [$EMIM^+$]. Thus, we suggest the use of low amounts of pyrrolidinium-based ILs as the proper selection of the ternary SPE in order to optimize solid-like battery performance.

Acknowledgements

The financial support of the Spanish Ministry of Science and Innovation (PID2021-126148NA-I00 funded by MCIN/AEI/10.13039/501100011033/FEDER, UE) is gratefully acknowledged. Moreover, this work was funded by the Xunta de Galicia (GRC ED431C 2020/10). A. R. P. thanks the Spanish Ministry of Education for his FPU18/01597 grant. T. M. M. acknowledges her contract funded by the pilot program of the USC for the recruitment of distinguished research personnel—call 2021 under the agreement between the USC and the Santander Bank for 2021–2024. H. M. C. thanks the USC for his "Convocatoria de Recualificación do Sistema Universitario Español-Margarita Salas" postdoctoral grant under the "Plan de Recuperación Transformación" program funded by the Spanish Ministry of Universities with European Union's NextGenerationEU funds. This work was supported by the Fundacão para a Ciência e Tecnologia (FCT) funded by national funds through the FCT/MCTES (PIDDAC)) to CIQUP, Faculty of Science, University of Porto (Project UIDB/00081/2020), IMS-Institute of Molecular Sciences (LA/P/0056/2020). A.H. and D.D. thank the German Federal Ministry of Education and Research (BMBF) for financial support through the projects FestBatt (grant number 03XP0174B) and FestBatt2 (grant number 03XP0435E).

USC
UNIVERSIDADE DE SANTIAGO DE COMPOSTELA

7- Density functional theory of alkali metals at the IL/graphene electrochemical interface

Summary of the chapter

As a final step in our research line, we focused on analyzing the electronic interactions happening at the electrode-electrolyte electrochemical interface. In this work, the mechanism of charge transfer between metal ions and graphene in the presence of an ionic liquid (1-butyl-3-methylimidazolium tetrafluoroborate) was investigated by means of density functional theory calculations. For that purpose, two different comparisons were established: i) the behavior of Li^+ and K^+ when adsorbed onto the basal plane of graphene, and ii) the differences between Li^+ approaching the carbon surface from the basal plane or being intercalated through the edge plane of trilayer graphene. In the first case, it was found that the metal ions must overcome high energy barriers due to their interaction with the ionic liquid before reaching an equilibrium position close to the interface. Also, no significant charge transfer between any of the metals and graphene took place until very close energetically unfavorable distances. The second configuration showed that Li^+ had no equilibrium position in the proximity of the interface but instead when it is inside the electrode, for which it had to cross an energy barrier. In this case, the formation of a LiC_{12} complex was observed, since charge transfer at the equilibrium distance was achieved to a considerable extent. Thus, the interfacial charge transfer resistance on the electrode in energy devices based on ionic liquids clearly depends not only on the binding of the ionic liquid to the metal cations and their ability to form a dense solvation shell around them, but also on the surface topography and its effect on the ion packing on the surface.

The post-print version of the publication reproduced in this chapter (including the full list of authors and their affiliations) can be found in appendix A.4. At the same time, in appendix C.4. we have included a complete disclosure of the relevant information related to this publication, including the authorization of the journal to reproduce its contents in this thesis, and the contribution of the author of this thesis to the publication.

7.1 Introduction

In recent years, substantial efforts have been dedicated to the development of energy storage technologies able to operate safely and efficiently in different environments. Most of the attention has focused on the market-dominant supercapacitors (SCs) and lithium-ion batteries (LIBs).[235;236] Although the electrode is a key factor in achieving high energy and power densities and the last decade has witnessed significant advances in the optimization of high-performance electrode materials, the electrolyte is also an essential component in energy storage systems as the bridge to transport ions between both electrodes.

Focusing on LIBs, the features of the electrode/electrolyte interface as well as the electronic and ionic components of interfacial reactions play a fundamental role in the cycle life and safety of LIBs.[237;238] In this context, benefiting from the advantages of their unique properties such as nonvolatility, high thermal stability, and high ionic conductivity, ionic liquids (ILs) are con-

sidered to be an "environmentally friendly" alternative to conventional electrolytes.[239–244] These molten salts, whose melting points are lower than 100 °C, are comprised of organic cations and inorganic or organic anions that can be paired together in different combinations toward the desired target applications.

The performance of LIBs and other electrochemical devices is governed by the following factors: i) the ion-transport resistance of lithium (Li^+) in the electrolyte during the charge and discharge of the cell, which is strongly affected by the viscosity of the media; ii) the charge-transfer resistance of the electrode/electrolyte interface, which requires a change on the solvation shell of Li^+ in the vicinity of the electrodes; iii) diffusion of lithium ions within the graphene structure (or other active material); and iv) electron transport at the electrode interface. In spite of their wide electrochemical window, the widespread use of ILs in conventional LIBs is limited due to their relatively high ion-transport resistance and to the strong interaction between the anion and Li^+ cation, which affects the intercalation of the latter on an electrode and lowers the performace of the device. In order to make some progress in this respect, the use of mixtures of ILs and organic solvents, e. g. carbonates, is becoming a popular strategy in the search for advanced IL-based electrolytes.[245–247] Yet even with all the attention, the performance of ILs in batteries is far from being optimized and they still require a lot of work concerning the structure of the IL/electrode interface, the ion-transport dynamics and the interfacial electrochemical reactions in order to become go-to electrolytes in energy storage. All these issues will be addressed in the following sections.

Up to now, there has been much effort in improving the interface with sophisticated experiments, but computer simulations also play a key role in analyzing interfacial issues in batteries (for an overview see Refs. 150;248 and references therein). Before starting with the description of our work, we consider appropriate to the reader to include a brief description of the major advances that have been made in this field during the last years.

7.1.1 Structural transitions

As it was previously said, understanding and controlling the formation and the properties of the electrical double layer (EDL) is fundamental for the use of ILs in electrochemical applications; not only in SCs, where electrical energy is stored via the counter-ion adsorption at the electrode surface, but also in batteries. The performance, safety, and life cycle of these devices strongly depend, in general, on interfacial processes and, in particular, on the formation of the solid-electrolyte interphase (SEI), which is the product of electrolyte reduction on the negative electrode surface. The structure of the EDL is highly associated with the formation of the SEI and, since the EDL forms prior to the SEI, the possibility of regulating the latter by modifying the structure of the former through the choice of the electrolytes has been explored.[249–251]

As pointed out by Kornyshev and Qiao,[252] in systems with a high density of ions like ILs, it is necessary to take into account the 3D nature of the EDL instead of just focusing in the distribution of ions in the direction normal to the surface. That is, the lateral restructuring of those ions absorbed into the electrodes upon surface charging must be considered along with the information in the third dimension, since the alternating layers of anions and cations can affect the transitions in the layer adjacent to the electrode.

These voltage-induced ordering transitions at the interface have been observed by means of experimental techniques,[206;253–269] such as scanning tunneling microscopy (STM), and also by simulations (extensive literature in the topic has been reviewed in Ref. 270). For example, the first experimental evidence of 2D phase transitions was reported by Pan and Freyland[253] in 2006 at the 1-butyl-3-methylimidazolium hexafluorophosphate ([BMIM][PF_6])/Au(111) interface. By using STM they demonstrated the change from PF_6^- anions forming Moiré-like patterns to a $(\sqrt{3} \times \sqrt{3})$ phase with varying the applied potential. While most of the experiments focused on these phenomena of 2D phase formation and transitions in gold, some researchers also studied the evolution of the Stern layer nanostructure of ILs in graphite.[268;269]

Concerning computational techniques, molecular dynamics (MD) simulations has been the most employed method when it comes to analyzing interfacial structural transitions.[34;141;271–282] Madden and coworkers[271;272] were the first ones reporting potential-induced phase transitions of a molten salt (LiCl) layer adsorbed on a metallic aluminum electrode by means of computer simulations in which the polarization of both the ions and the metal atoms was included. Concerning ILs, Merlet *et al.*[273] took a big step forward on this subject when they found peaks in the differential capacitance that were directly linked with the structural changes in the interfacial region. When examining the in-plane order of [BMIM][PF_6] adsorbed on graphite electrodes, they observed a transition of the first interfacial layer from a disordered state at low and high potentials to an ordered lattice-like state at intermediate voltages. More recently, Montes-Campos *et al.*[278–280] performed MD simulations of 1-butyl-3-methylimidazolium tetrafluoroborate ([BMIM][BF_4]) confined between graphene walls under a large variety of conditions, such as mixtures with water/alcohols, mixtures with $LiBF_4$ and defected electrodes. Their results showed the transition from solid-like (hexagonal) patterns to fluid-like (stripes) ones in the Stern layer when modifying the charge density. Some other authors also observed a transition in the interfacial behaviour of ILs when increasing the surface charge density, going from a multilayered structure with multiple alternating layers of co-ions and counter-ions to an ordered monolayer of densely packed counter-ions with a Moiré-like structure, which coexists with apparently non-structured IL further in the direction perpendicular to the electrode.[34;281;282]

Ion layering/packing and the presence of those patterns at the IL/electrode interface is expected to have a deep impact on the free energy barriers for an ion approaching the electrode, on the rate of redox reactions and on the friction behaviour. Then, the manipulation of the 3D packing of ions is of great technological interest to achieve more efficient energy storage.

7.1.2 Ion desolvation & charge-transfer

To obtain a high performance of batteries, lots of experimental works focused on interfacial ion (mainly lithium, but also sodium and potassium) transfer between the electrode and the electrolyte, both for typical electrolytes[283–289] and for ILs.[290–293] They all observed that ion transfer at the interface was a slow process with high activation barriers. These activation energies at the electrode/electrolyte interface were directly related to the desolvation energy of an ion from the solvent. Thus, the stripping of the ion primary solvation sheath and SEI chemistry were found to play an importante role in charge-transfer kinetics.

USC UNIVERSIDADE DE SANTIAGO DE COMPOSTELA

Several computational studies analyzed the differences between the ion coordination envir-

onment at the bulk and the interface regions, and the conclusions also supported the hypothesis of an energy penalty for metal ions to come into direct contact with charged electrodes.[95;294–298] This resistance to ion transport at the electrolyte/electrode interface was found to be more relevant for IL-based electrolytes than for carbonate electrolytes. For example, Ivaništšev *et al.*[294] employed MD simulations with the aim of understanting the role of ion solvation in the formation of the interfacial free energy barriers. For that purpose, they compared the behaviour of Li^+ and K^+ at a negatively charged graphene surface in [BMIM][BF_4] and its mixtures with $LiBF_4$ and KBF_4. The results showed strong interactions between Li^+ and IL anions that significantly increased the height of the free energy barriers compared to K^+. This lower desolvation penalty for K^+ with respect to other carrier ions like Li^+ or Na^+ is due to its weakest Lewis acidity,[289] and can have important implications in the development of beyond-lithium batteries. Moreover, Ivaništšev *et al.*[294] also reported that both alkali ions remained partially solvated by the BF_4^- even at the point of direct contact with the surface, which leads to positive values of the free energy minima that correspond to the contact of the ions with the electrode. Density functional theory (DFT) and ab initio molecular dynamics (AIMD) calculations are usually employed in this field to study ion adsorption energies, charge transferred to the electrode, solvation effects, interfacial decomposition of the electrolyte, composition and structure of the SEI and also diffusion rates of Li^+ in the electrode region and SEI layer.[299–307] In particular, Varela and coworkers[300] pioneeringly considered the charge transfer between Li^+ or Mg^{2+} and a graphene wall placing the metal ions at different distances to the wall and in different kinds of environments, including vacuum, a fluorine atom and an IL. They stated that a complete charge transfer to the surface took place in all the systems, with some kind of catalyzing effect of the IL making the charge transfer process to start at longer distances than in the other two environments.

However, despite all these research efforts, the truth is that in a dense, liquid-like IL environment, the organization of the ions at the electrified solid-IL interface still remains somehow complex and not exactly understood. With this article we aim at increasing the knowledge about the electronic distribution and transport at interfaces, with the general purpose of overcoming the charge-transfer resistance barrier and promoting ion conduction at the electrode/electrolyte interface for designing novel highly efficient next generation ionic devices.

In this work, the electron transfer between Li^+ and K^+ and the basal plane of graphene as a function of the distance between those cations and the interface was evaluated in a first set of simulations using DFT. The analysis has been performed in the presence of an ionic pair of 1-butyl-3-methylimidazolium tetrafluoroborate ([BMIM][BF_4]) to account for the transfer reaction in ILs. This IL has been chosen for being one of the most popular and for comparison with the results obtained in some of our previous studies.[294;300] In addition, the results for Li^+ were compared with a second set of simulations modelling the charge transfer between this cation and the edge plane of trilayer graphene. In this case, an additional BF_4^- anion was added in order to preserve electroneutrality. The adsorption of metal atoms on graphene and other carbon structures has been previously studied from the computational point of view. However, to the best of our knowledge, a work in which the mechanism of charge transfer between metal ions and graphene in the presence of an IL has not been performed yet accounting for the usual oxidation state of the metals (+1) and allowing a full relaxation of the whole system. Under these more realistic conditions we analyzed the adsorption process as a function of the nature of the alkali metal, and as well as of the crystallographic face from which ion intercalation takes place. All these simulations try to contribute to build a microscopic understanding of the interface ionics and the interface electronics of these advanced densely ionic electrolytes.

The structure of the paper is as follows. The essential technical details of the computational method used are sketched in section II, our results are presented and discussed in section III, and in section IV we summarise our main conclusions.

7.2 Computational details

All DFT calculations were carried out using the Vienna AB initio Simulation Package (VASP, version 5.4.4).[87;88;308;309] The projector-augmented wave (PAW)[310] method was used, and the electron exchange–correlation was described by the generalised gradient approximation (GGA) of Perdew-Burke-Ernzerhoff (PBE).[86] The DFT-D2 method of Grimme *et al.*[311] was applied to account for dispersion effects. This combination has been shown to produce results in very good agreement with experimental ones for IL-based systems,[312;313] and PBE has been succesfully employed in simulations of ILs at interfaces.[299;300] For the calculation of atomic partial charges Bader charge analysis was employed in all the simulations.[314–317] We have chosen this method because it gives reliable charges; however, there are many other options like Mulliken, NBO analysis or ESP fitting, whose adoption could quantitatively modify some results reported here.

Our simulations are divided in two blocks regarding the approach route that the metal ion follows toward the electrode. As stated in the previous section, in the first set of simulations, the movement of the metal cation was considered in the direction perpendicular to the basal plane of graphene; whereas in the second set the displacement was done facing the edge plane of trilayer graphene.

In the first set of simulations, the $BMIM^+$ cation, the BF_4^- anion and the metal atoms (Li^+ or K^+) were optimised in a supercell whose X and Y dimensions match the simulated graphene sheet (composed of 50 C atoms), and a region of vacuum of 40 Å in the Z direction in order to avoid influence from periodic replicas. For the integration over the first Brillouin zone, a $2 \times 2 \times 1$ gamma-centered k-point set with a Gaussian smearing of 0.1 eV was employed. In order to take into account the usual oxidation state of the metals in an electrochemical device, the system was simulated with a total charge of $+1e$.

The initial configurations were constructed from previous MD simulations of [BMIM][BF_4] confined between graphene walls. Then, we placed the metal ion at a given distance from the surface and the whole system was fully relaxed so that the total energy was converged to 10^{-5} eV. The salt cations were then moved along the direction normal to the graphene layer from 1.3 to 6.1 Å in 0.2 Å increments. During these simulation the Z coordinates of the metal atoms and the carbon atoms of the graphene were fixed during the relaxation in order to be able to set the graphene-metal distance. Moreover, in order to speed-up the relaxation process the output of one distance was fed as initial configuration of the following distance (after displacing the metal atom).

In the second set of simulations, the metal ion (Li^+) approached the electrode perpendicular to the edge plane. The electrode was now comprised by three graphene layers (a total of 96 C atoms, 32 per layer) separated 3.6 Å in the Y direction. The graphene layers were not arranged in a typical Bernal stacking of graphite (ABA); instead, they are forming a simple hexagonal vertical stacking (AAA). This electrode structure has already been explored in previous works.[318;319] The interlayer distance was selected after performing an auxiliary simulation, where lithium was placed between two layers and the mean distance between equivalent carbon

USC DE COMPOSTELA

atoms was measured.

The supercell X and Y dimensions were once again selected in order to preserve the periodicity of the system. In the Z direction, a further vacuum region of 18.5 Å (for a total Z dimension of 25.524 Å) ensured once more no possible influence from periodic replicas. The integration technique was identical to the one used in the previous set.

The electrolyte, now comprised of a $BMIM^+$ cation, two BF_4^- anions and the Li^+ metal ion, was once again fully relaxed, and several Li^+ positions were sampled in the Z direction, from 8.2 Å to -2.1 Å (negative distance is to be interpreted as the Li^+ cation being inside the electrode), for a total of 52 distances. The Li^+ Y coordinate is 1.8 Å, so that it approaches and penetrates the electrode from a zig-zag edge at a symmetric distance from the two bottom layers. Since the extra anion ensures the electroneutrality, the system was simulated as neutral.

7.3 Results

We start the analysis with the first set of simulations. In these simulations the metallic atom (Li^+ and K^+) approaches the graphene interface from the basal plane. This setup replicates the same kind of system present in most of the classical MD simulations of ILs at the interface. Moreover, it is a similar analysis to the one performed by Gómez-González *et al.*[300] with the distinction that their configuration represents the process of a metallic atom, with initial oxidation state 0, approaching the interface and oxidizing. On the other hand, in our simulations the initial oxidation state of the metal is already $+1$ and it is not expected to change throughout the simulated process, in a similar fashion to the process that takes place in a common LIB. Therefore, in the simulation presented in this manuscript we are not particularly interested in changes in the oxidation state of the metal. Instead, we focus on the energetic of the adsorption process and the possible changes in the electronic density of the interface, in particular the possible creation of lithium and potassium carbides.

In order to study the energetics of the adsorption process, we analyzed the energy profiles of the system as function of the position of the metallic atom, represented in Fig. 7.1. These profiles show a similar behaviour for both metals, with a minimum close to the interface, followed by an energy barrier. The origin of this profile can be easily interpreted by looking at the atomic configurations at different distances from the interface. These configuration are represented in Fig. 7.2 at four different distances: the closest distance to the interface, the distance at the energy minimum, the distance at the energy maximum, and the furthest simulated distance. As can be seen there, the maximum of the energy is achieved when the metal atom goes through the middle of the IL layer, while the minimum is achieved when Li^+ or K^+ are placed between the interface and the IL. It is interesting that even though the IL is able to move freely in the relaxation process, its movement is not the same as that of the metal. In fact, it suffers the opposite movement than the metal, decreasing its distance a little bit when the lithium and potassium atoms are further away. This means that the interaction of the IL with the interface is strong enough to withstand the effect of the metal movement without changing its relative position with the interface. It must be also noted that the energy keeps decreasing after 6 Å, but since there are no more IL layers we consider that the configurations further than this point are not realistic, and due only to the design of the simulation box.

While the general characteristics of the energy profiles for Li^+ and K^+ are the same we

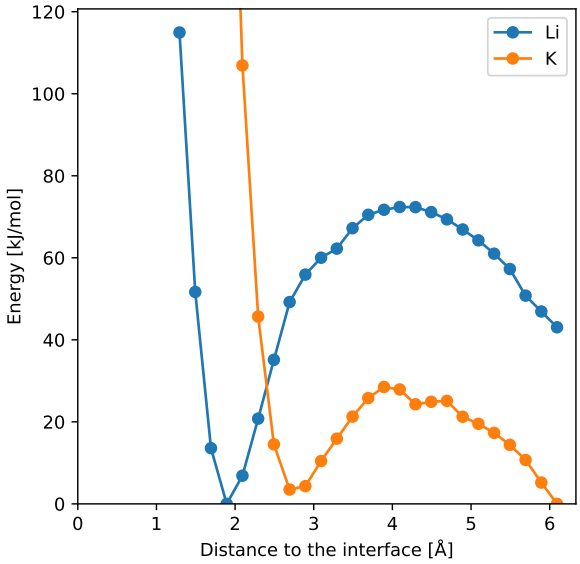


Figure 7.1: Energy profiles for Li^+ (blue) and K^+ (orange) approaching the basal plane of graphene in the presence of a pair of [BMIM][BF_4] as a function of the distance to the interface.

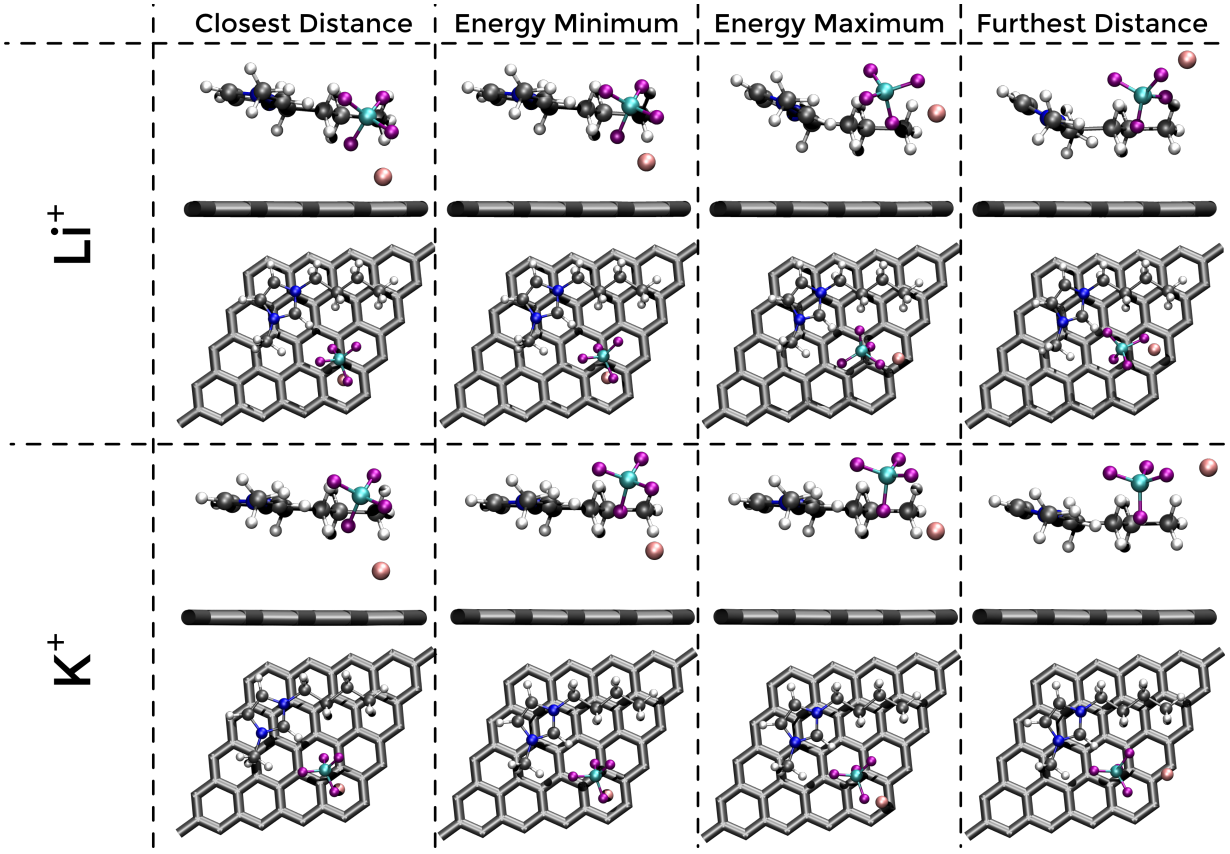


Figure 7.2: Snapshots of the arrangements of the ions on top of the basal plane of graphene for several distances between Li^+ (top) and K^+ (bottom) and the interface.

can see see some quantitative differences between them. The first difference is the equilibrium distance of the metal, being quite lower for the lithium system (1.7 Å vs 2.7 Å). This difference can be easily explained due to the difference in their ionic radius, approximately 1.51 Å for the K^+ and 0.73 Å for the Li^+,[320] which can explain the 1 Å difference in the equilibrium position. The position of the energy maximum of the barrier does not suffer profound changes. This is due to the origin of this maximum being the position at which the ion goes through the middle of the IL layer, which does not suffer deep changes when the metal is changed. There is, however, a big difference in the height of the barrier relative to the equilibrium configuration. This effect can be also caused by the difference in size of both ions. The greater charge density of lithium causes a stronger interaction with the IL and, therefore, increases the energy penalty of crossing the IL layer. The increased energy barrier for the lithium could be also due to the greater electrostriction ability of this ion caused by its more intense electric field at the surface. This very same effect has been also reported in classical MD simulations. For example, Ivaništšev *et al.*[294] reported a decrease of around a 50% in the energy barrier when Li^+ was exchanged with K^+. If we compare these profiles to the ones calculated by Ivaništšev *et al.*,[294] we can conclude that both processes are qualitatively the same. There are some minor differences in the equilibrium distance of the metal and some quantitative differences in the height of the barrier. This difference in the barrier can be due to two different effects. The first one is that the ratio metal/IL is much higher in the results presented in this manuscript and the second one is that the classical MD simulation cannot account for all the effects present in the real system, specifically it does not take into account the polarizability of the electronic densities around the metals. We should also take into account that the high dielectric constant of [BMIM][BF_4][321] could have an impact on the height of the barrier due to the screening of the Coulombic interactions that would decrease it. More extensive simulations would be needed in order to properly estimate this quantitatively. Nevertheless, we can conclude that MD simulations can capture accurately enough the interfacial ionics.

We also studied the electrode/electrolyte interface from an electronic point of view. In Fig. 7.3 we represent the total charge of the different species in the simulation. As can be seen there, there is no significant charge transfer between any of the species in the system (metal, anion, cation and graphene) at distances greater than 2 Å. There seems to be some charge transfer between the metal and the graphene at very short distances, but these configurations are heavily unfavorable from an energetic point of view. We can analyze the effect that the metal has on the six carbon atoms of the graphene closest to the metal equilibrium configuration in order to discard the formation of carbides. As can be seen in Fig. 7.3, the total charge of these atoms does indeed decrease when the metal approaches the interface, but at the equilibrium distance the charge is not high enough to be considered a MC_6 complex. It is interesting that both metals create a similar localization of charge when at their equilibrium distance. This can be confirmed also by the partial charge distribution on the graphene, which is shown in Fig 7.4. As can be seen there, there is not a clear rearrangement of the charge distribution around the metal when this atom is at its equilibrium distance. Moreover, the effect of the metal in the charge distribution seems to be similar to the effect of the IL ions. This is compatible with results reported by Zhour *et al.*,[299;322] who observed a greater charge redistribution for a simulation of pure IL at the interface compared to a simulation with the same IL and potassium. Therefore, we can conclude from these simulations that the metal is not able to cause profound effects on the electronic structure of the interface from an structural point of view.

In order to check if the presence of the metal inside the electrode structure is needed to observe the formation of carbides, a second set of simulations was performed. Salanne and

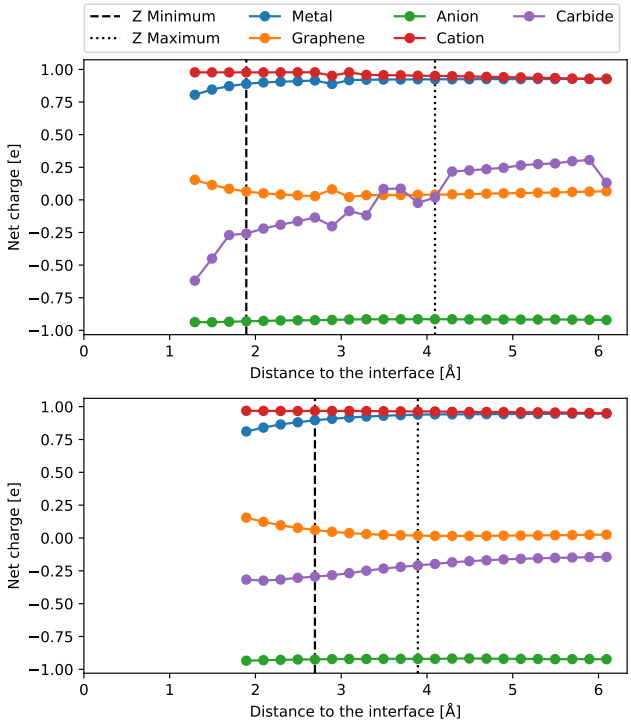


Figure 7.3: Net charges of the different species present in the system as a function of the Li^+ (top) and K^+ (bottom) distance to the basal plane of graphene. Carbide stands for the 6 carbon atoms of the graphene closest to the metal.

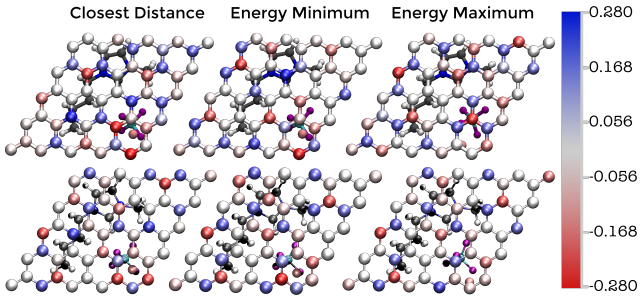


Figure 7.4: Charge distribution on the graphene for the simulations of Li^+ (top) and K^+ (bottom) appraching the basal plane of graphene in the presence of a pair of [BMIM][BF_4].

USC UNIVERSIDADE DE SANTIAGO DE COMPOSTELA

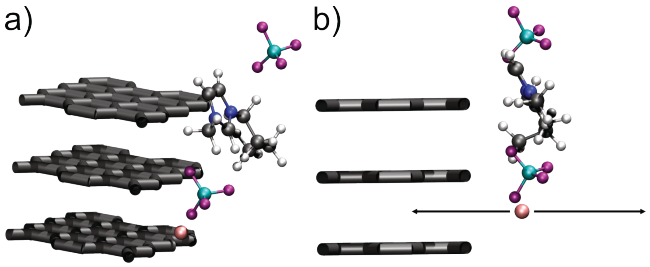


Figure 7.5: Snapshots of the configuration for the simulations of Li^+ approaching the edge plane trilayer graphene in the presence of a pair of [BMIM][BF_4] and an additional BF_4^-, (a) general view and (b) lateral view.

coworkers[323;324] replicated this state in classical MD by introducing holes on the graphene layers to allow the entrance and diffusion of the ions in the electrode. Replicating this system in DFT would be extremely computing intense. Therefore, we have chosen to insert the lithium from the edge plane instead of the basal one, specifically through the zig-zag edge (see Fig. 7.5), and therefore letting the metal penetrate inside the carbon structure.

In Fig. 7.6 we represent the energy profile of the system, as well as the net charge of the species of the system. There, we can see that the system can achieve an equilibrium state in which the lithium is inside the electrode, after having overcome the energy barrier. This energetic obstacle is significantly larger than that of the basal plane simulations. However, we believe that the height of this energy barrier could be artificially large, as the carbon atoms of the graphene layers were set as frozen for the entire simulation to preserve the electrode structure. The lack of relaxation of these atoms could account for the larger relative energy differences. Therefore, the profile should be interpreted in qualitative terms. We can also see that there is no equilibrium position when the lithium is close to the interface, opposed to the behaviour we observed in the previous results for the basal plane. Moreover, the IL follows the motion of the Li^+ atom, which could account for the increse in energy at long distances due to the the unrealistic removal of the IL from the interface. When the lithium is far away from the interface, the IL does not place itself nearer to the electrode, which could be an effect of the lack of interaction with π-orbitals that are not present in the edge plane. These results are consistent with the behaviour observed by Vatamanu *et al.*[325] when they analyzed by means of MD simulations the influence of the electrode surface topography on the differential capacitance and the EDL structure. They compared the potential energy of the ions in the inner Helmholtz layer of an IL in contact with the basal face of graphite with that in the proximity of the graphite edge plane; and they observed that the intermolecular potential energy of the ions was lower for the flat surface. This indicates that near the basal plane of graphite the interactions of the ions with their surroundings are stronger and they have a greater ability to optimize their packing.

If we analyze the carbide formation, we can focus on the charge of the carbon atoms that lie near the lithium atom when it is placed inside the carbon structure. As we can see, the charge decreases as Li^+ enters the electrode, and indeed reaches a considerable magnitude (-0.6e) at the lithium equilibrium distance, which although it is not a negative charge of -1e, it is enough to consider that a LiC_{12} complex has been created. This is also shown in Fig. 7.7, in which we include the charge distribution of the 12 carbons closest to Li^+ when it is located at its equilibrium position inside the electrode. Therefore we can conclude that the insertion of the metal ion is necessary to reproduce the carbide complexes that are created in a LIB.[326] This difference in the electronic behaviour of the interface has been also reported experimentally. Compton *et al.*[327;328]

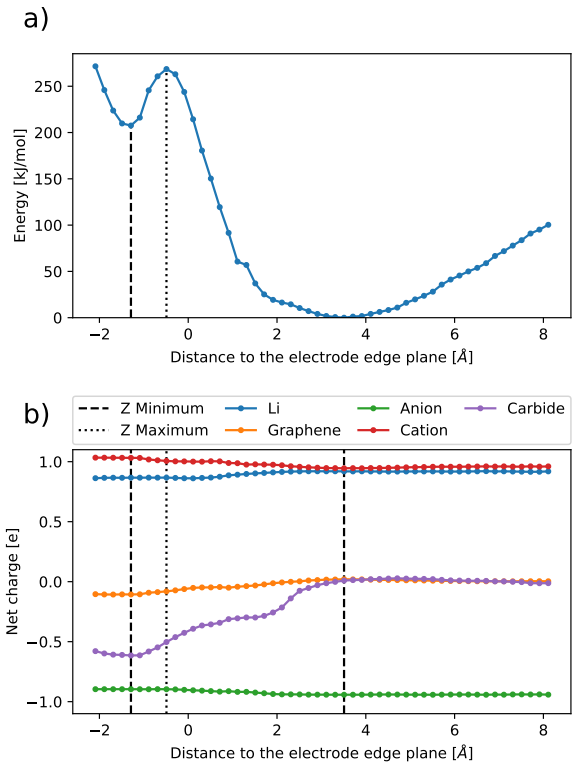


Figure 7.6: Energy profile (a) and total net charge of the different species present in the system (b) for Li^+ approaching the edge plane of trilayer graphene in the presence of a pair of [BMIM][BF_4] and an additional BF_4^-, in both cases as a function of the distance to the interface. Carbide stands for the 12 nearest carbon atoms to the lithium position inside the electrode. Negative distances mean that Li^+ is located inside the electrode.

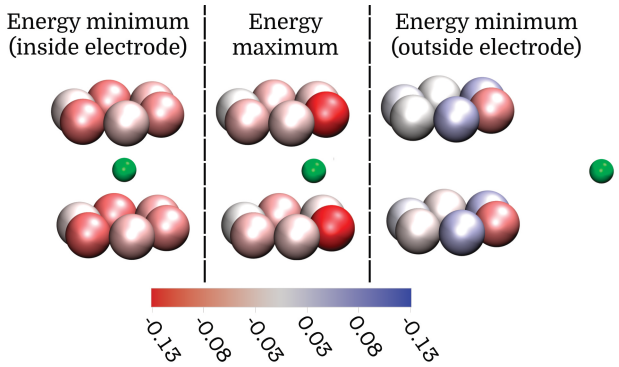


Figure 7.7: Charge distribution on the 12 carbon atoms surrounding the equilibrium position of the Li^+ inside the interface. The other atoms were hidden for an clearer view of the distribution.

have previously shown that graphite exhibits very different charge transfer kinetics between its two crystallographic faces, with a rate of electron transfer being much greater at the edge plane sites than at the basal plane.

7.4 Conclusions

DFT calculations have been performed with the purpose of studying the effect of the choice of the metal salt (Li^+ and K^+) added to an IL-based electrolyte and of the crystallographic orientation of the electrode surface on the interfacial resistance. Our main findings can be summarized in the following points:

- Both Li^+ and K^+ are adsorbed at the interface with high energy barriers (around 70 kJ/mol and 30 kJ/mol, respectively) in order to come to the basal plane of graphene. This energy maximum corresponds to the moment at which the metal ions go through the IL, which does not change its distance to the electrode when moving the metal due to greater interactions with the former. Hence, both energy profiles show a minimum close to the interface, whose location depends on their ionic radius.

- Neither Li^+ nor K^+ lead to a significant charge transfer with the graphene layer until very close distances which are not energetically favourable, and the formation of LiC_6 complexes is not observed.

- When Li^+ approaches the electrode from the edge plane of trilayer graphene, it must cross a high energy barrier before finding an equilibrium position once located inside the carbon structure instead of in the outside vicinity.

- A considerable charge transfer is observed at the equilibrium position when Li^+ is inserted from the edge plane. In this case the creation of a LiC_{12} complex can be stated.

Solving this high interfacial resistance of ion transport characteristic of IL-based electrolytes is crucial for their use as electrolytes in energy storage devices. For this purpose, the ionic and electronic behaviour at the electrode/electrolyte interface must be fully elucidated. We hope that the discussion in this article will contribute to a comprehensive understanding of the interactions at the interface for further optimization of IL-based energy devices.

Acknowledgments

The financial support of the Spanish Ministry of Economy and Competitiveness (Projects MAT2017-89239-C2-1-P and MAT2017-89239-C2-2-P) is gratefully acknowledged. Moreover, this work was funded by the Xunta de Galicia (ED431E 2018/08 and GRC ED431C 2020/10). All these research projects were partially supported by FEDER. A. R-P. thanks the Spanish Ministry of Education for his FPU grant. T. M. M. thanks her contract funded by the pilot program of the USC for the recruitment of distinguished research personnel - call 2021, under the agreement between the USC and the Santander Bank, for 2021-2024. Facilities provided by the Galician Supercomputing Centre (CESGA) are also acknowledged. Prof. L. M. Varela is acknowledged for fruitful discussions and suggestions during the preparation of the manuscript.

7.5 Data Availability Statement

The data that support the findings of this study are available from the corresponding author upon reasonable request.

USC
UNIVERSIDADE DE SANTIAGO DE COMPOSTELA

8- Ionic liquid/metal salt mixtures at the graphene interface: a density functional theory approach

Summary of the chapter

In order to complement the previous work, in this final study we had a look at the interactions of graphene sheets with metal cations, which are of large relevance because of the modifications that are produced in the electrochemical properties of the 2D surface. Therefore, we have studied the adsorption of a mixture of an ionic liquid and a metal salt on a graphene surface by means of first-principles calculations. Several metals (including most of the common cations currently used in batteries) were chosen in order to analyze the effect they have on the optoelectronic properties of the graphene monolayer and to understand the trends in their adsorption behavior. We characterized the ground state configurations in terms of their binding energies and the distance between the metal atom and the graphene layer. From the analysis of the charge transfer behavior, calcium and magnesium were identified as the species that transfer the highest and the lowest amount of charge, respectively, which is related to their ionization energies. Band structure diagrams and projected density of states calculations also showed that the energy shift of the Dirac cone increases with increasing the degree of charge transfer. In addition, a stronger interaction of magnesium with the ionic liquid compared to the other metal atoms was observed. The analysis of several electromagnetic parameters indicated an anisotropic behavior for electric fields polarized both perpendicular and parallel to the graphene layer. Our density functional theory study offers fundamental insights into the adsorption behavior of ionic liquids mixed with metal ions on monolayer graphene.

The post-print version of the publication reproduced in this chapter (including the full list of authors and their affiliations) can be found in appendix A.5, while the corresponding supporting information lies in appendix B.4. At the same time, in appendix C.5. we have included a complete disclosure of the relevant information related to this publication, including the authorization of the journal to reproduce its contents in this thesis, and the contribution of the author of this thesis to the publication.

8.1 Introduction

In recent years, scientific emphasis has been focused on the unique optical, electronic, mechanical and chemical properties of 2D materials.[329;330] Among them, the most studied one is undoubtedly graphene, which has become a central topic of research interest due to its high carrier mobility, extraordinary strength, high thermal conductivity and excellent optical properties.[331–333] All of them can be tuned through different methods like impurity doping, designed defects, adsorption or chemical functionalization.[334–339] This versatility has enabled graphene to hold great potential for a virtually unlimited range of applications, including electronics,[340] energy,[341] medicine,[342] sensors[343] and light processing.[344]

An interesting aspect of graphene sheets lies in their interaction with metal cations due to the change in electronic and mechanical properties, thus providing new functionalities and widening

their use in many fields. Metals interacting with graphene have been thoroughly studied and analyzed by means of both experimental studies[345–347] and computational calculations based on first-principles density functional theory (DFT).[348–359] Among the latter, Olsson *et al.*[360] studied the adsorption and migration of several alkali atoms on pristine and defective graphene surfaces, and they reported more favourable adsorption energies for Li and K ions than for Na. Similarly, Mendoza-Cortes and coworkers[361;362] showed how to modify the electronic properties of bilayer graphene with the intercalation of transition metals. This study found that the Dirac point was pushed down below the Fermi energy level in all the intercalated structures except for vanadium, which had the Dirac cone in its band structure.

Among all the works addressing the adsorption of molecules on a graphene surface, ionic liquids (ILs) are emerging as a relevant field of study due to their attractive properties for a great number of applications. These salts that are mainly composed of cations and anions and have melting points below 100 °C, offer high thermal stability, high ionic conductivity, negligible volatility, and structural and physicochemical designability through appropriate selection of the ions.[36;363] Because of these benefits, their efficient utilization in synthesis, catalysis, electrochemistry, gas separation, tribology, pharmaceuticals and energy storage devices has been exhaustively tested in the last decades.[126;151;364–366] Thus, the growing interest on understanding the adsorption mechanism of ILs on different surfaces has led to numerous experimental investigations in this area.[367–369] Alongside the experimental efforts, computational methods such as those based on electronic structure have been widely employed to analyse the properties and interactions of ILs with a large panel of surfaces, including graphene (or its derivatives) and other 2D materials,[370–374] polycyclic aromatic hydrocarbons,[375;376] and metal interfaces[377–379]; with the purpose of finding their influence on the electronic properties of the surface,[322;380–383] and evaluate their potential use in applications such as exfoliation[384–386] or energy storage devices.[387–392] For example, Kamath and coworkers[381–383] performed a series of calculations to compare the adsorption characteristics of different ILs on graphene, defective graphene and fluorographene surfaces. They observed that the presence of defects on the graphene nanoflakes increases the binding energy of ILs by about 10% in comparison with pristine graphene and hexagonal boron-nitride nanosheets. However, fluorinated graphene strongly decreases the binding energy compared to them.

Nevertheless, even though ILs are promising electrolytes for energy storage devices, there is still scarce information about their interfacial interactions with graphene substrate and the electronic structure upon adsorption when it comes to their mixtures with metal atoms. Up to our knowledge, there is only one publication in which the effect of the adsorption of an imidazolium-based IL mixed with a potassium salt on the electronic and optical properties of graphene and borophene was considered.[299] The authors reported a downward shift of the Dirac cones relative to their Fermi level for both structures due to the electron transferred from potassium to the 2D-materials. Also, they observed that the presence of the IL increased the charge transferred from the metal atom to the graphene/borophene sheets when compared to its adsorption on pristine materials.

Thus, in this work a comprehensive investigation was carried out by means of DFT simulations to shed some light on the interaction mechanism between IL-metal salt mixtures and the graphene substrate. This computational technique was chosen due to its capability of producing highly accurate results that can be compared to experimental findings[393] and because it takes into account interactions that are not accessible by means of other techniques such as MD.

The screening of several metal atoms (lithium (Li), sodium (Na), magnesium (Mg), calcium (Ca) and aluminum (Al)) allowed us to compare the electronic and optical properties avoiding more costly trial-and-error experimental measurements, which is of fundamental importance for optimizing the performance and efficiency of a new generation of electronics, optoelectronics and energy storage devices. The IL employed in this study was 1-butyl-3-methylimidazolium tetrafluoroborate ([BMIM][BF_4]), which was chosen with the purpose of comparison with the same hybrid system doped with potassium that was previously reported by some members of our group.[299] Also, the potential of this IL as a suitable electrolyte (pure or in mixtures) for energy storage devices such as supercapacitors or lithium-ion batteries has been often considered.[394;395]

In this study, we investigate the role played by the metal atoms doping the IL in the adsorption mechanism and the interaction with monolayer graphene. Of particular interest is to understand the effect of their atomic radius or valence on several electronic and optical properties, such as binding energy, charge transfer, electron density difference (EDD), band structure, partial density of states (PDOS), real and imaginary dielectric functions (ε), electron energy loss function (EELS, L), real and imaginary refractive index (n), reflectivity (R) and absorption coefficient (α). All the optical properties are studied for parallel and perpendicular (to the graphene layer) incoming electromagnetic radiation.

The paper is organized as follows: the details of the computational and theoretical methodology are given in Section 8.2, the results are presented and discussed in Section 8.3, and finally, in Section 8.4 we summarize our main conclusions.

8.2 Simulations details

In this work, we performed DFT calculations to study the effect of the adsorption of a metal atom in a system composed of a 2D graphene layer with an IL ([BMIM][BF_4]) already adsorbed. We explored 5 different metallic species (lithium, sodium, magnesium, calcium and aluminum) to unveil the effect of properties such as atomic radius or valence. All calculations were conducted using Quantum-ESPRESSO (QE) package,[89;90;396] which is based on plane wave pseudopotentials. For all the calculations in this work, we used the ultrasoft pseudopotentials. To describe the electron exchange-correlation energy we employed the generalised gradient approximation (GGA) of Perdew-Burke-Ernzerhoff (PBE).[86] Cutoffs of 50 Ry and 400 Ry in kinetic energy and charge density were deemed sufficient to achieve proper convergence.

A 5×5 supercell for graphene (2.47 Å lattice constant) was chosen as it approximately covers the surface of one anion-cation pair of the IL, amounting to a total of 50 carbon atoms. This graphene layer was set up perpendicular to the z-axis. To ensure proper decoupling from periodic replicas, a buffer spacing of 30 Å in the z-direction was established. After a relaxation of the system, the IL was placed in the cell according to previous molecular dynamics (MD) simulations.[174] Another relaxation was carried out, and then the metal atom was added to the resulting configuration. We therefore had 5 equivalent systems (graphene/IL/metal) that were all of them relaxed once again. A snapshot of one of these systems is shown in Fig. 8.1.

Self consistency threshold was set to 10^{-6} Ry. In order to efficiently sample the Brillouin zone of the different structures, Methfessel-Paxton smearing[397] was used in conjunction with a $20\times20\times1$ Γ-centered k-point mesh and a gaussian spreading of 0.01 Ry. It was checked in previous works performed by our group[299;322] that tightening the threshold and/or the k-points

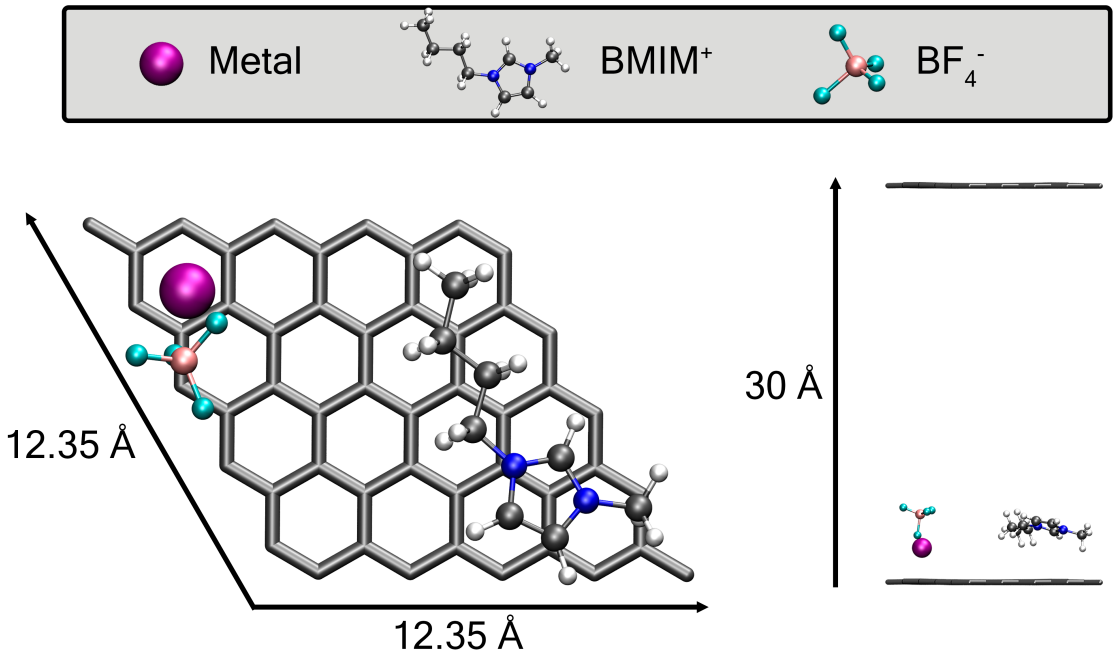


Figure 8.1: Top and side views of a snapshot of one of the simulated systems.

criteria does not lead to remarkable differences in the obtained results. This exact mesh was also used for the density of states (DOS) calculations. However, norm-conserving pseudopotentials in a $7\times7\times1$ mesh disposition were employed for the computation of optical properties. These properties can all be derived from the complex dielectric function as described in Refs. 299;322. As the first Brillouin zone of the considered system is hexagonal, the most convenient path to explore for the band structure, according to the corresponding high symmetry points, is the $\Gamma \rightarrow$ M $\rightarrow$ K $\rightarrow \Gamma$ path, along 91 different k-points. This choice is well-established in the literature, as it is commonly used in studies of band structures for graphene and related structures. In order to obtain the charge of the atoms, Bader charge analysis[398] was used. In order to obtain the necessary .cube file, Quantum Espressos pp.x software was used.

8.3 Results and Discussion

8.3.1 Electronic properties

A Bader charge analysis[398] was carried out in order to determine the induced charge transfer to the graphene surface atoms that emerges from the adsorption of the IL and a metal atom. In Fig. 8.2 we can observe that there is a redistribution of electric charge in the graphene sheet when compared with the metal absent configuration.[322] The most salient feature is that Li and Ca atoms induce high polarity in some of their close neighbouring carbons. In the case of Mg,

	Charge (e)				Ionization energy	
System	Graphene	IL cation	IL anion	Metal	1st IE	2nd IE
G/IL/Li	-0.90	0.95	-0.95	0.90	5.39	75.64
G/IL/Na	-0.91	0.94	-0.94	0.90	5.14	47.29
G/IL/Mg	-0.20	0.88	-1.01	0.32	7.65	15.03
G/IL/Ca	-1.46	0.85	-0.91	1.52	6.11	11.87
G/IL/Al	-0.86	0.95	-1.16	1.07	5.99	18.83
G/IL/K	-0.91	0.95	-0.94	0.90	4.34	31.63

Table 8.1: Total charge of the different species after Bader analysis of the relaxed configurations. Values for simulations with K obtained from Ref. 299 are included for comparison. First and second ionization energies (IE, in eV) for each element from Ref. 399 are also included.

a high induced polarization is also observed in some carbon atoms, which is originated not only from the presence of the metal but also from that of the IL ions, since the three of them are located at the same distance from the 2D surface. On the other hand, the presence of Na and Al leads to a more homogeneous distribution of the charge, as it was also previously observed for K.[299] However, a situation in which every positively charged site is neighbored by negatively charged carbon atoms was only predicted for lithium. As it can be seen in Table 8.1, in general the metal is the species that transfers approximately all its charge to the graphene sheet, while the IL ions suffer almost no modification and keep their bulk charge of $\pm$1e. Although, a detailed comparison between the charge of cation and anion in the different systems after adsorption indicates that the cation always tends to become less positive, whereas the anion usually tends to be less negative except for mixtures with magnesium and, mainly, with aluminum, where it gains charge. Moreover, the total transfer of charge from magnesium to graphene is predictably low, which can be explained in terms of the ionization energies (IE) included in Table 8.1, and from where it can be inferred that only those atoms whose first IE are close to or lower than approximately 6 eV are able to transfer an electron to graphene. In particular, Mg has a stable closed-shell configuration, which explains its large first IE and the difficulty to remove an electron. On the other hand, calcium and, specially, aluminum atoms, despite being located in a more advantageous position than Mg, do not transfer all their free electrons to the graphene. In the first case, Ca has the smallest second IE, which explains the fact that this metal transfers the largest amount of charge to the surface. However, the second IE is still too high for removing two electrons from Ca. For Al, after losing one electron, it achieves a stable electron configuration. Thus, the first electron is relatively easy to remove from aluminum, but the second one is much more difficult to remove from the 1+ charge-state aluminum ion.

We have also calculated the binding energies (ΔE) of the metal atoms on a graphene sheet with an IL already adsorbed on it as

$$\Delta E = E_{G/IL/M} - E_{G/IL} - E_M \tag{8.1}$$

where $E_{G/IL/M}$ is the total energy of the graphene layer with the adsorbed IL and the metal atom, $E_{G/IL}$ is the total energy of the graphene layer with the adsorbed IL and E_M is the total energy of the isolated metal atom. Following this criteria, a negative binding energy is associated to a stable configuration, whereas a positive one is an indication of an unfavourable adsorption on the assembly graphene/IL and the metal atom preferring to remain in its atomic state.

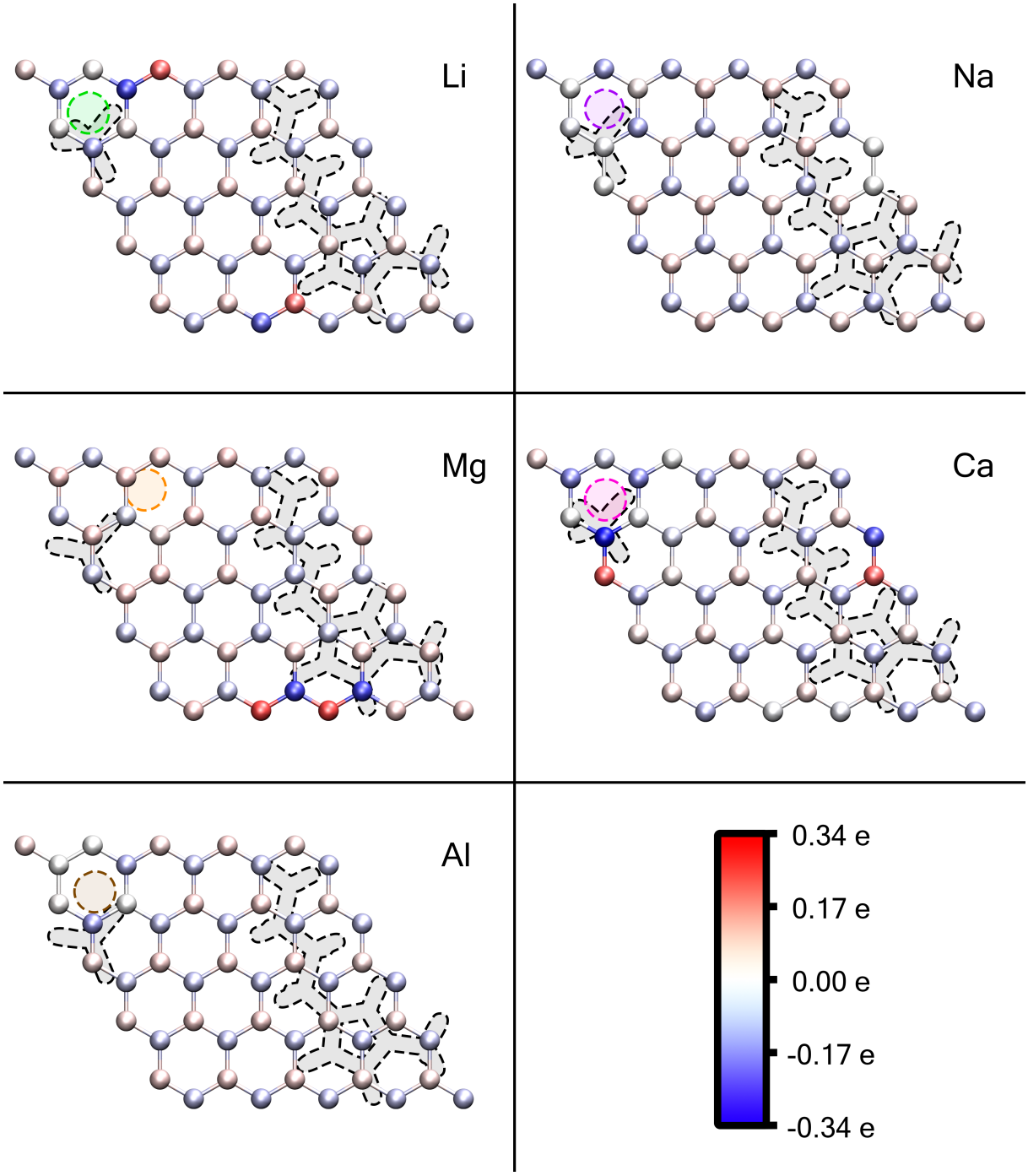


Figure 8.2: Charge of the carbon atoms of graphene induced by the presence of the IL and the different metals calculated using Bader charge analysis. Dashed outlines show the position of the IL and the corresponding metal in each system. The respective sizes of the metals have been increased for clarity purposes.

USC
UNIVERSIDADE DE SANTIAGO DE COMPOSTELA

	ΔE (eV)	d_{MC} (Å)	d_{MA} (Å)	d_{MR} (Å)	d_{MT} (Å)
G/IL/Li	-3.21	1.97	2.48	6.17	5.34
G/IL/Na	-2.40	2.37	2.83	6.18	5.53
G/IL/Mg	-0.76	4.63	3.25	7.47	5.38
G/IL/Ca	-2.89	2.11	2.95	6.36	5.60
G/IL/Al	-2.20	2.59	3.12	6.23	5.36
G/IL/K	-2.25	2.69	3.18	6.64	5.60

Table 8.2: Binding energy (ΔE) and distance between the metal atom and i) its nearest carbon atom (d_{MC}), ii) the center of mass of the anion (d_{MA}), iii) the center of mass of the imidazolium ring (d_{MR}), and iv) the terminal carbon of the imidazolium tail (d_{MT}) for each of the studied systems. Values for simulations with K obtained from Ref. 299 are included for comparison.

Adsorption energies and structural properties such as the distance between the metal atom and i) its nearest carbon atom (d_{MC}), ii) the center of mass of the anion (d_{MA}), iii) the center of mass of the imidazolium ring (d_{MR}), and iv) the terminal carbon of the imidazolium tail (d_{MT}) are summarized in Table 8.2. All the metal atoms lie at a distance of about 2 Å from the graphene sheet except magnesium, which is further away from the surface. For visual reference, see Fig. S1 of the Supporting Information, which contains snapshots of all the systems. This is likely related to the lower binding energy of this particular metal in comparison with the rest. In this way, the magnesium atom accommodates itself in the same plane as the IL components, but at a further straight line distance from them than the other metals. However, all the other systems share a quite similar geometrical disposition, with the metal being positioned between the graphene sheet and the BF_4^- anion. In addition, we can observe that lithium is the atom more strongly adsorbed on the surface in the presence of the IL, which is in agreement with trends previously reported for the adsorption of metal atoms on pristine graphene.[352;360;400] These observations are coherent with the previous charge transfer analysis. Indeed, Mg is the species located the furthest from the surface because of its vanishing charge transfer ability. For this metal it is not energetically favourable to stay in this electronically highly reactive region, whereas the rest of the metals are located close to graphene because they are capable of transferring electrons to it. Some degree of charge transfer from the Mg atom at distances longer than 4 Å has been previously reported in the presence of an ionic liquid.[300]

The electronic behaviour was further examined through the charge density difference ($\Delta\rho$) defined as

$$\Delta\rho = \rho_{G/IL/M} - \rho_{G/IL} - \rho_M \,, \tag{8.2}$$

where $\rho_{G/IL/M}$, $\rho_{G/IL}$ and ρ_M are the total charge densities of the relaxed system with IL and metal adsorbed on graphene, the system with IL adsorbed on the 2D surface and the isolated metal, respectively. Lateral views of the charge density differences for the different metals are provided in Fig. 8.3. An isovalue of ± 0.017 e/Å^3 was considered for the calculation of the diagrams, in which the electron gain and loss configurations are represented by blue and red isosurfaces, respectively. Top views of the same systems are included in the Supporting Information (Fig. S2).

Charge densities of the systems presented in Fig. 8.3 indicate that the addition of metal atoms modifies not only the electron distribution in the anion and the cation, but also that of the C atoms of graphene lying below the metals. The effect on electronic density difference

is similar for all the systems, with metal atoms acquiring an electron loss configuration and C atoms around them showing gain of electrons, as indicated by the red isosurface covering all the metals and the blue one accumulated below them, respectively. This ionic interaction is consistent with the picture previously reported for potassium.[299] Moreover, this effect affects boths sides of the surface layer in the systems that showcase greater charge transfer, specially in the case of calcium.

Before starting the analysis of the electronic states of the system, we must take into account that the system is composed of two clearly differentiated parts. The first one is the solid region, which is composed by the graphene and contains the free electrons. The second one is the molecular region, which is composed by the ionic liquid and the metal atom. The difference between these regions is not only a matter of denomination, but they require different tools for their analysis. Therefore, we will first analyze the band structure of the system, focusing on the graphene. Then, we will analyze the highest occupied molecular orbital (HOMO) and the lowest unoccupied molecular orbital (LUMO) of the molecular region and we will use these values to analyze the possible charge transfer between both regions.

The band structure diagrams for all the metals adsorbed on the G/IL systems are shown in Fig. 8.4, in which the energies are relative to the Fermi level. In order to determine the effect of the metal atoms on the electronic structure, band structure diagrams of pristine graphene are also depicted (black lines) and, for the sake of comparison, they are shifted in such a way that the Dirac cones of both configurations are overlapped. As it is well known, graphene is a semimetal whose conduction and valence bands meet at the Dirac points. On the other hand, it was previously reported that the Dirac cones at the Fermi energy of this 2D material do not suffer any shift upon adsorption of this IL.[322] As it can be seen in Fig. 8.4, in all cases the adsorption of metal atoms downshifts the Dirac cone below the Fermi level, thus confirming that the charge is donated from the metal to the graphene surface. Therefore, all the metal atoms act like n-type dopants. We can also observe that the band structure of the pristine graphene is approximately conserved in most of the systems. For example, in Fig. 8.4, where the band structure of the configuration with Mg is represented, the bands corresponding to the periodic part of the system completely coincide, whereas the bands with new molecular levels arise in the form of horizontal bands. In the opposite way, Ca shows to be the atom that induces a larger modification of the bands associated with the periodic part, as it is the metal that transfers the largest amount of charge to the graphene surface. This analysis of the band structure diagrams is also indicative of the degree of charge transfer resistance of these systems and how it varies with the metal atom of the electrolyte.

To analyze this effect, the energy shifts as a function of the charge of the 2D layer are plotted in Fig. 8.5. There we can observe that the greater the degree of charge transfer, the larger the shift in energy, confirming the direct relationship. Previously reported values for K[299] are similar to those of Li, Na and Al; whereas Ca and Mg atoms tend to have the largest and the smallest electron transfer and energy shifts, respectively.

To further understand the effect of mixtures of [BMIM][BF_4] and that of the metal atoms on the electronic structure of graphene, we calculated the total (DOS) and projected density of states (PDOS) of the different systems, which are shown in Fig. 8.6 for energies values relative to the Fermi level within the range $[-5, +5]$ eV. Molecular HOMO-3, HOMO-2, HOMO-1, HOMO, LUMO, LUMO+1, LUMO+2 and LUMO+3 states are also represented and, since some of them are overlapping, each of the energy levels are included in Table S1 of the Supporting Information

USC DE COMPOSTELA

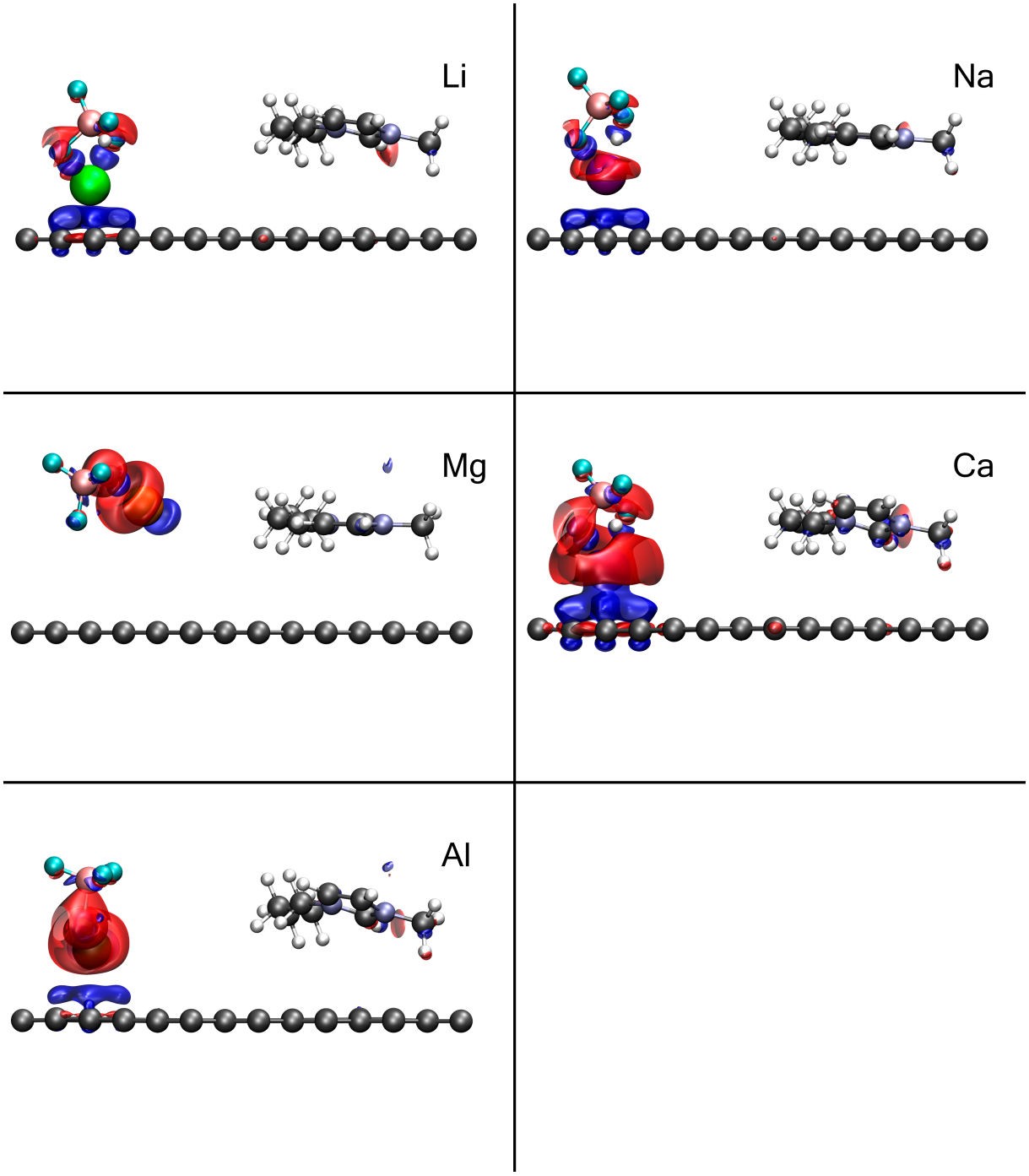


Figure 8.3: Lateral views of the electronic density difference between the system with metal and IL, and the system with no metal and the system with only metal. Regions depicted in red/blue correspond to isosurfaces of value ± 0.017 e/Å^3, and therefore represent electron depletion/accumulation, respectively. The respective sizes of the metals have been increased for clarity purposes.

USC
UNIVERSIDADE DE SANTIAGO DE COMPOSTELA

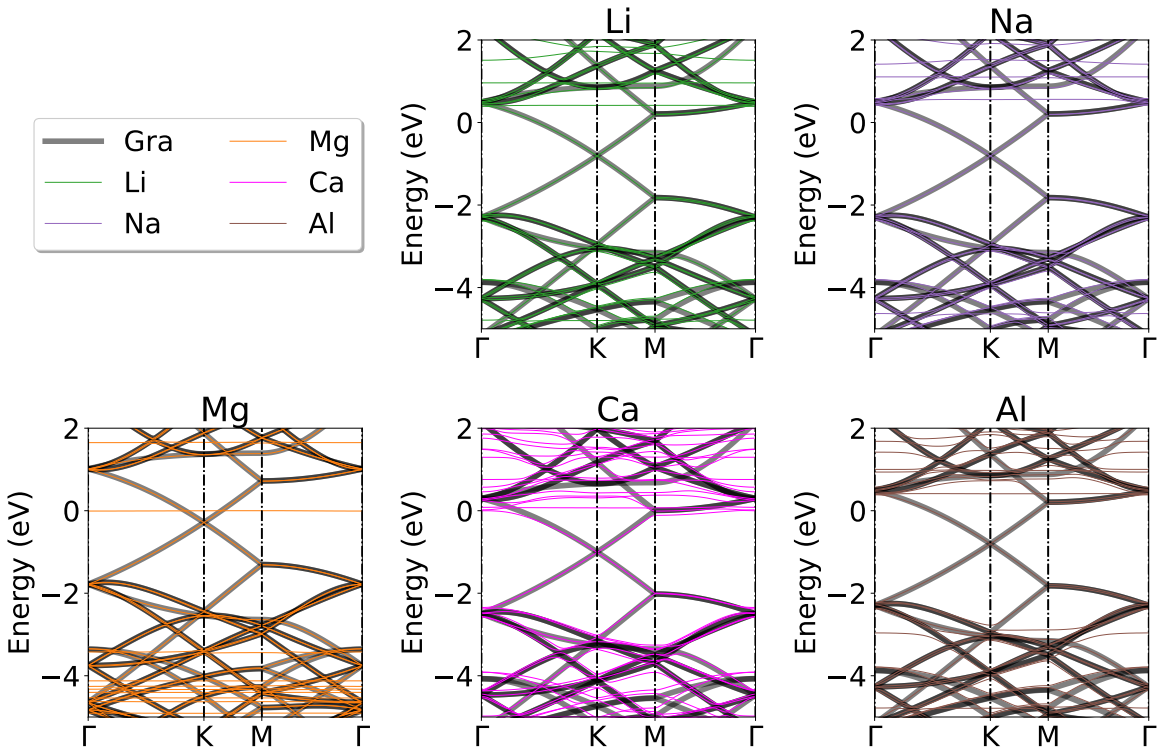


Figure 8.4: Band structure diagrams of the different systems, in which Fermi energy is taken as a reference for the energy level. In a wider black line, the band structure of pristine graphene is positioned so that the Dirac cones are overlapped.

(the color-code shows to which species the state belongs). In addition, DOS and PDOS within an energy interval of $[-20, +6]$ eV are also included in the Supporting Information (Fig. S3), where it can be seen that the states of both the anion and the cation of the IL notably contribute to the valence states of the systems. For each system, we can easily distinguish the Dirac point, at which the DOS is zero. Below the Fermi level the DOS is almost equivalent to that of graphene up to energies around -3 or -4 eV (depending on the system), where the HOMO level of $[BMIM]^+$ cation (which shows the characteristic "flatline" behaviour of molecular systems) lies, and, for mixtures with magnesium and aluminum, also a state of the metal. For mixtures with Mg, this state is superposed with states from the IL ions, and they lie approximately at the Fermi level, which is also very close to the Dirac point. Still, the Dirac point is clearly visible. Due to this feature, we could consider Mg as an interesting option for electronic devices, but it must be remembered that this is the atom adsorbed at the longest distance from the graphene surface. The system with Ca also forms a state at its Fermi level, but in this case it belongs to the IL cation. For the other three systems, the states between the Dirac point and the Fermi level are mostly from graphene. States for Li, Na and Ca lie at approximately 1.6, 1.5 and 0.4 eV above the Fermi energy, respectively, all of them being unoccupied. Moreover, Al has its *3s* and *3p* states at around -3 and 1 eV, respectively. This valence *p* peak being above the Fermi level confirms that close to one electron is transferred from Al to the 2D surface. Notice that a core assumption of PDOS is the projection of the total states on atomic orbitals. In the case of Ca, the dense electronic cloud surrounding it overlaps with that of graphene, as seen in Fig. 8.3. Therefore,

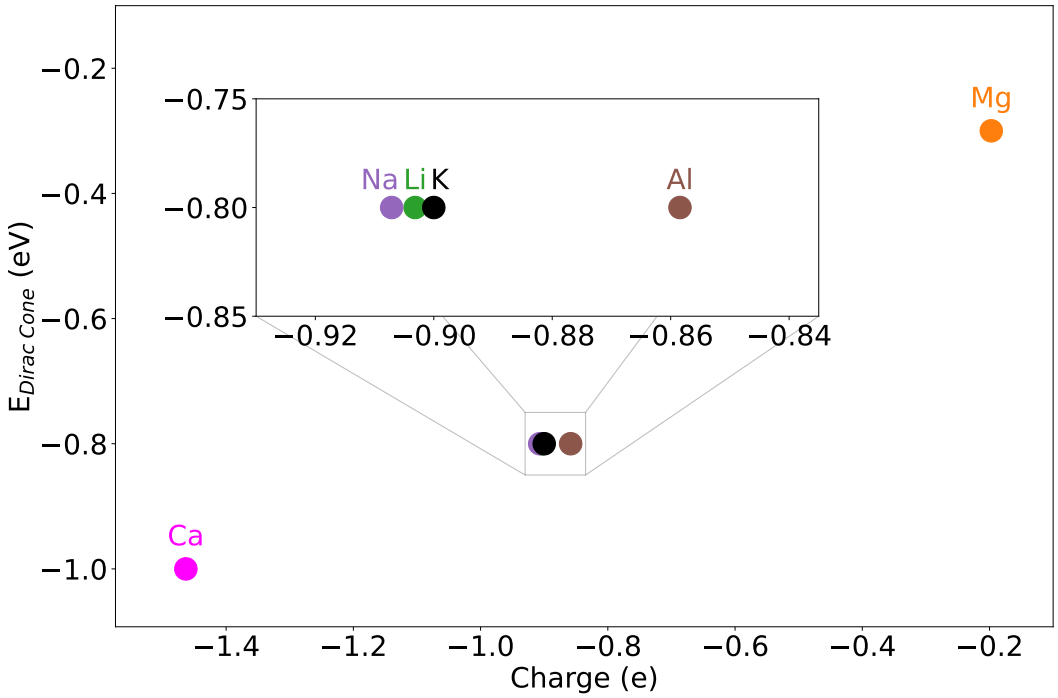


Figure 8.5: Energy shift of the Dirac cone as a function of the charge transferred to the graphene surface for each system. For clarity purposes, a zoom was added as an inset to facilitate the view of some points. Values for simulations with K obtained from Ref. 299 are included for comparison.

this projection is hampered and this approximation becomes less accurate. As a result, although the total DOS does reflect the presence of the Dirac cone in this system (as previously seen in the band structure in Fig. 8.4), some states corresponding to the graphene PDOS near the Dirac cone are missing.

The stability and interaction strength of the metal adsorbed on the G/IL system can be explored through the HOMO and LUMO orbitals, which are represented in Figs. S4 and S5 of the Supporting Information, respectively, with the aim of providing a graphical perspective of the orbitals involved. This was calculated by locally integrating the DOS in a energy band around the HOMO and LUMO states, respectively. The energy difference between these orbitals is known as the HOMO-LUMO energy gap, ΔE_{HL}, and can be calculated as

$$\Delta E_{HL} = E_{LUMO} - E_{HOMO} \tag{8.3}$$

Through the DOS we can analyze the changes in ΔE_{HL} due to molecular interactions, which are tabulated in Table 8.3. From the $\Delta E_{HL} \approx 5$ eV value previously reported by Kazem *et al.*[322] for [BMIM][BF_4] adsorbed on graphene, our simulations show an increase upon adsorption of lithium or sodium. This increase in the HOMO-LUMO gap is mainly accomplished by a substantial decrease in the HOMO energy. On the other hand, ΔE_{HL} was found to decrease for the other three metals (magnesium, calcium and aluminum), which is principally achieved by a remarkable decrease in the LUMO energy. Once again, the more substantial change in

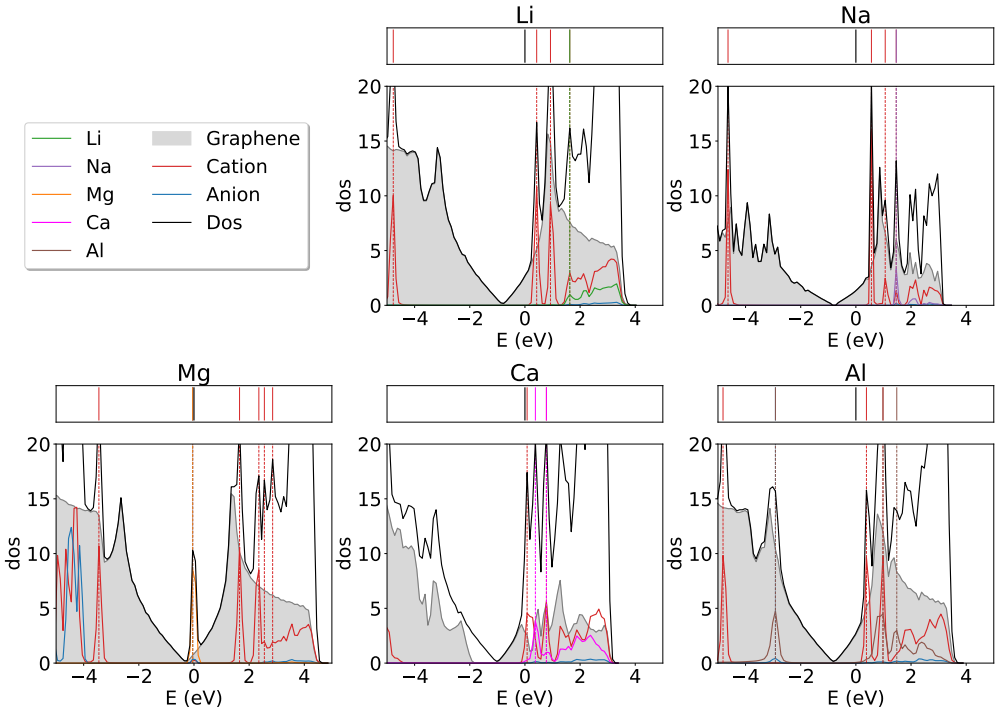


Figure 8.6: DOS and PDOS of the different systems. On top of each plot: molecular HOMO-3, HOMO-2, HOMO-1, HOMO, LUMO, LUMO+1, LUMO+2 and LUMO+3 states that are within the considered energy interval. The color indicates to which species the state belongs. Fermi energy is taken as reference for the energy level.

	ΔE_{HL} (eV)
G/IL/Li	5.20
G/IL/Na	5.20
G/IL/Mg	1.70
G/IL/Ca	4.70
G/IL/Al	3.30
G/IL/K	5.00

Table 8.3: HOMO-LUMO energy gap for the different studied systems. Value for simulations with K obtained from Ref. 299 is included for comparison.

the HOMO-LUMO gap energy is observed for magnesium, which indicates a strong interaction of the metal with the IL, and is consistent with magnesium being located in the same plane of [BMIM][BF_4].

8.3.2 Optical properties

USC UNIVERSIDADE DE SANTIAGO DE COMPOSTELA

As mentioned earlier, the adsorption of metal atoms on the G/IL structure modifies the

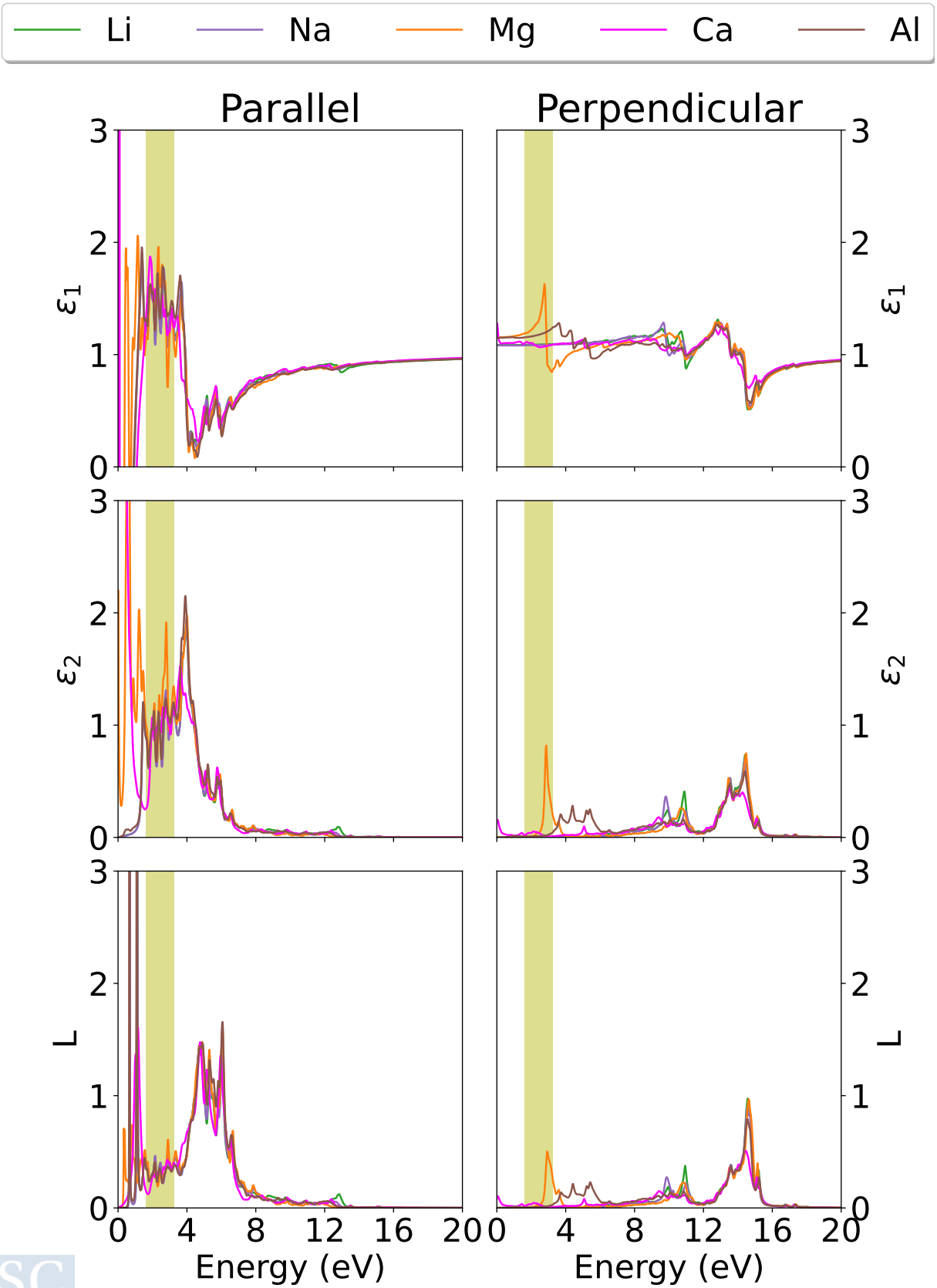
electronic properties of the system, which, in turn, leads to completely different optical characteristics. In this section we investigate several electromagnetic parameters such as the dielectric constant (ε), the electron energy loss spectroscopy (EELS, L), refractive index (n), extinction coefficient (κ), reflectivity (R) and absorption coefficient (α) for the perpendicular and parallel polarization to the graphene layer, which are of fundamental importance for many technological applications. The considered frequency interval for the calculation of the optical parameters is taken from 0 to 20 eV, and the corresponding graphs are included in Figs. 8.7 and 8.8. In addition, since the visible range is of particular interest, in Figs. S6 and S7 of the Supporting Information only the region between 1.63 and 3.26 eV is plotted.

The dielectric coefficient is a complex magnitude, $\varepsilon(\omega) = \varepsilon_1(\omega) + i\varepsilon_2(\omega)$, whose real and imaginary parts are related through the conventional Kramers-Kronig transformations.[401] The former is related to the amount of energy stored by the system, whereas the latter is related to its dissipation of energy. From this function, the refractive index, extinction coefficient, reflectivity and absorption coefficient can be easily calculated as it was explained in detail elsewhere.[299;322;402;403].

The real and imaginary parts of the dielectric coefficient as a function of the frequency for all the considered structures are shown in Fig. 8.7 for both perpendicular and parallel incident electric field. We can clearly observe an anisotropic behaviour of this magnitude for the different polarizations of light. In particular, this figure shows that for parallel electric field, the excitations, which are indicated by the peaks of ε_2, are located in the low-energy region. On the contrary, they are mainly observed in the high-frequency one for perpendicular electric field, except for Mg that also has an excitation energy at 2.85 eV. Thus, when the polarization of the electric field is parallel, the imaginary part for Li, Na and Al shows a similar behavior to that previously reported for K,[299] with the metals screening the peaks of G/IL below the visible range. However, both Ca and Mg exhibit very intense transitions in this regime. Concerning the perpendicular polarization, a small peak is observed near zero due to the adsorption of Ca and, in addition to the aforementioned peak for Mg, Al shows that some transitions are possible at energies around 5 eV. Then, all the systems have excitation energies situated at around $(10-11)$ eV and 14 eV, thus confirming that the transitions associated to the out-of-plane polarization are prevalent at higher energies.

Focusing now on the real part of the dielectric function, Fig. 8.7 indicates that for the perpendicular electric field the changes are detected for Ca, Mg and Al at the same energies as for the imaginary one. In the case of in-plane polarization, remarkable modifications compared to the G/IL system are observed at low frequencies mainly for Li, Na and Al, since their curves do not take positive values, contrary to what was previously observed for K.[299] By definition, the plasma frequency is the one at which the real part of the dielectric function cancels, $\varepsilon_1(\omega_p) = 0$. At these frequencies, ε_1 changes its sign[404] and this behavior corresponds to the collective excitations of the electrons. Thus, in Fig. 8.7 we can see that for perpendicular polarization there are no plasma frequencies, whereas for parallel polarization three plasma frequencies are induced by the presence of Mg at the interface, two by Ca and one by the rest of the metals. This shows that there are no collective excitations for perpendicular polarization but, for parallel one, the systems absorb the incoming electromagnetic radiation.[404]

In Fig. 8.7 it can be also noticed that the static dielectric constant, which is the real part of the dielectric function at zero frequency, $\varepsilon_1(0)$, is remarkably modified by the adsorption of the metal with respect to the configuration G/IL[322] under in-plane polarization of the electric field.



USC
UNIVERSIDADE DE SANTIAGO DE COMPOSTELA

Figure 8.7: Real (ε_1) and imaginary (ε_2) parts of the dielectric function and EELS (L) for the different systems with parallel (left) and perpendicular (right) electric field. Shaded stripes represent the optical region.

This can be due to an increase in the number of free electrons by the addition of the metal,[404] which plays an important role for parallel polarization and implies that the metal-doped system dissipates more energy. On the other hand, for out-of-plane polarization, $\varepsilon_1(0)$ shows quite similar behavior compared to the G/IL system. In particular, it remains unchanged for Li and Na (1.08 and 1.09, respectively), it is slightly increased for Al and Mg (1.15 and 1.16, respectively), and takes the largest value (1.28) when Ca is adsorbed.

The EELS (L), which provides us with information about the collective excitation of the electrons, is also depicted in Figs. 8.7 and S4 for parallel and perpendicular polarization. The peaks in $L(\omega)$ correspond to 2D plasmons and are due to intraband transitions. Under in-plane electric field two peaks appear at 0.65 and 1.15 eV (in a similar way to what was found for K[299]) as expected, since they correspond to the dips in the dielectric function. The first one is for Li, Na and Al, whereas the second one is also registered for Ca. For its part, the adsorption of Mg also causes a peak at lower energies (0.35 eV). For out-of-plane electric field, new peaks with respect to G/IL[322] are found for Mg, Ca and Al at the same energies as for the dielectric function.

The complex refractive index compares the propagation of an electromagnetic wave in vacuum and in given material. The optical refractive index, $n(\omega)$ (which represents the real part of the complex refractive index and is necessary for the optical devices), and the extinction coefficient, $\kappa(\omega)$ (which represents its imaginary part), as a function of energy can be both determined from the real and imaginary parts of the dielectric function as described in.[299]

From Figs. 8.8 and S5, it can be seen that the refractive index has an anisotropic behaviour. For parallel polarization the behavior observed for Li, Na and Al is similar to the one previously reported for the adsorption of K,[299] with $n(\omega)$ reaching values close to zero in the lowest frequency interval of $[0, 1]$ eV. Mg shows similar characteristics, but its refractive index goes to zero at lower frequencies and it reaches a maximum value of 1.65 at 0.6 eV. For Ca, an intense peak of 9.5 is obtained at 0.06 eV and it seems to be the metal that modifies the least the shape of the curve that was observed for G/IL.[299] It must be noted that for energies larger than about 4 eV the refractive index value is less than one, due to the phase velocity of the electromagnetic field being higher than the speed of light in vacuum. The features for perpendicular polarization are similar for all the metals other than Mg, which shows the highest value (1.3) at 2.8 eV. In this case, the static refractive index at vanishing frequencies (i.e. $n(0)$), takes values of 1.04 for Li and Na, 1.07 for Mg and Al, and 1.13 for Ca, thus validating the relation $n(0) = \sqrt{\varepsilon_1(0)}$. These values point out that the mobility of electrons increases after adsorption of Ca compared to the other metals. Moreover, when a material exhibits a refractive index that varies based on the polarization of light, it is referred to as birefringent. In our systems, the difference between $n(\omega)$ in parallel and perpendicular directions to the graphene plane is ca. 0.2 in the visible range and, prominent changes take place in the low-frequency region specially for Ca.

Concerning the extinction coefficient, which indicates the degree of attenuation of the electromagnetic waves when propagating through the material, is as well clearly anisotropic. For the in-plane polarization, the adsorption of Mg causes the first minimum to move towards lower energies compared to Li, Na and Al, whereas doping with Ca shows the opposite effect. In addition, $\kappa(\omega)$ dramatically increases at low frequencies for all the metal atoms with respect to G/IL and it goes to zero when the frequency exceeds ~ 13 eV, in a similar way to what happens in the presence of K.[299] In the case of out-of-plane polarization, the main difference arises again for Mg and Al, which show peaks at ~ 2.9 eV and in the region around 5 eV, respectively.

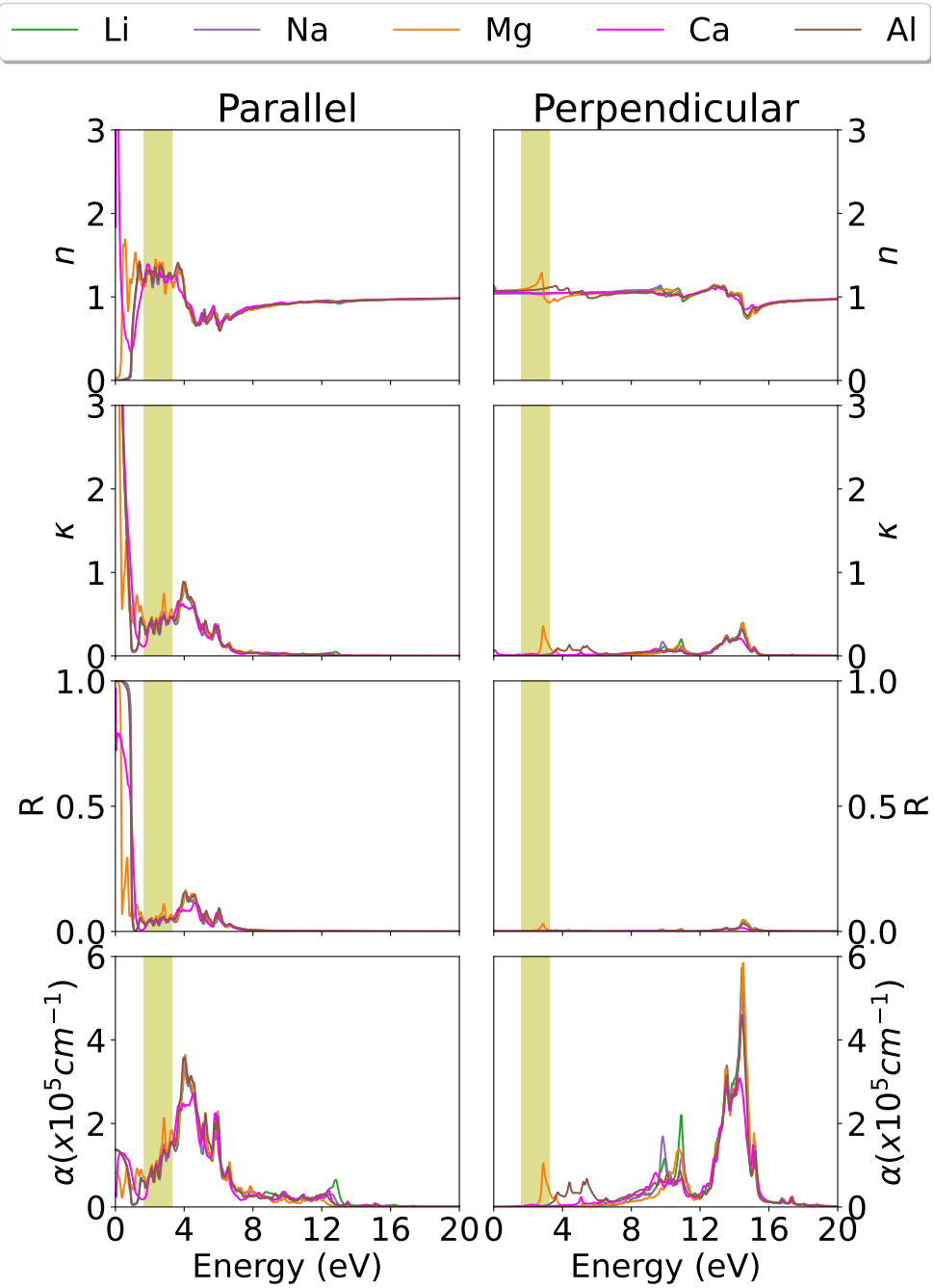


Figure 8.8: Refractive index (n), extinction coefficient (κ), reflectivity (R) and absorption coefficient (α) for the different systems with parallel (left) and perpendicular (right) electric field. Shaded stripes represent the optical region.

USC UNIVERSIDADE DE SANTIAGO DE COMPOSTELA

Thus, we can state that different choices of the doping metal atom allow tuning the refractive index and the extinction coefficient in the low electron energy region for different applications.

Optical reflectivity (R) and absorption (α) coefficients were also calculated as detailed in[299] and analyzed in Figs. 8.8 and S5. Firstly, the reflectivity parameter shows prominent reflection at low frequencies for parallel incident electric field (from 0 to 0.4 eV for Mg, and from 0 to 1.1 eV for the rest of the metals). Then, in the visible range, R is shown to be below 20% and it vanishes at 7.6 eV. On the other hand, for perpendicular incident electric field the calculated reflectivity is zero in almost all the considered energy range, and it does not exceed a 5% in any case. Once again, Mg is the only metal atom that shows a peak within the visible range at 2.9 eV.

With regard to the absorption coefficient, it clearly follows the same behavior as the extinction coefficient. The results for the parallel polarization indicate that the absorption in the presence of all the metals starts at very low frequencies, and it increases at higher energies reaching a maximum value at around 4 eV. All the changes observed at low frequencies in the in-plane optical parameters with respect to the G/IL system[299] are due to the free electrons being the ones excited and contributing to optical transitions. The variation of the number of free electrons with metal-doping and the electron transfer process from the metal to graphene not only induce modifications in the electronic properties, but are also behind the effects observed in the near-zero frequency region for a parallel electric field. For perpendicular polarization, there is an overall increasing tendency for all the metals up to ~ 14.5 eV, before α starts to decrease. This is due to the bound electrons being able to oscillate with increasing frequency when increasing the energy of the incident electric field just up to a given value, after which the absorption process decreases. Looking at $\alpha(\omega)$ and $\kappa(\omega)$ we can confirm that these materials are transparent for energies above 18 eV.

8.4 CONCLUSIONS

In this work, we employed plane wave DFT calculations to analyze how the electronic and optical properties of a graphene 2D surface are modified by the adsorption of an ionic liquid ([BMIM][BF_4]) mixed with a metal salt. Several metals of different valence and ionic radius (Li, Na, Mg, Ca, Al) were selected in order to shed some light on how the features of the systems are affected by these parameters.

A Bader charge analysis showed that most metals transfer 1 electron to the graphene surface, regardless of their valence. The ionization energy seems to be responsible for this behaviour, as it prevents the electron exchange on Mg, the metal with the highest 1st IE, and induces the second electron transfer on Ca, whose 2nd IE is the lowest. This effect can also be observed in a structural analysis, where all the metals other than Mg are adsorbed near the 2D surface while sharing their electrons, with lithium adsorption being the most stable one and magnesium having the lowest binding energy.

From the charge density difference we confirmed that metal atoms acquired an electron loss configuration and carbon atoms around them showed gain of electrons. In addition, the redistribution of electric charge in the graphene surface was observed to be homogeneous with the adsorption of Na and Al, whereas the other metals induced high polarization in their neighbouring carbon atoms. A band structure analysis showed that our system has two well differentiated

parts: the 2D surface and the molecular complex, which is formed by the IL and the metal. The band structure of pristine graphene is conserved, but the Dirac cone is downshifted below the Fermi level as a consequence of the charge transfer. Moreover, new molecular levels arise in the system. The partial density of states also revealed some key differences between these systems. The metals that show more states close to the Dirac cone are Mg and Ca. However, the ionization of Mg is highly unlikely, which leads to its accommodation further from the surface.

Concerning the optical properties, all the magnitudes analyzed show an anisotropic behavior for the different polarizations of light. The adsorption of Mg and Ca leads to different features compared to the other metals, the former due to being positioned at great distances and the latter due to its larger charge transfer to graphene. Different plasma frequencies are induced depending on the metal at the interface for parallel polarization, whereas there are no collective excitations of the electrons for perpendicular polarization were found. Also, the analysis of the static refractive index showed that the mobility of the electrons is increased when Ca is adsorbed compared to the other metals.

We hope that this work will shed some light on the possibility to tune the optoelectronic properties of graphene using ionic liquids and metal salts and provide a basis for the development of novel electrochemical and photonic devices. Further study employing more realistic electrodes such as metal oxide surfaces, and analyzing how the metal atom intercalation and alloy formation are affected by the findings reported in this work is now in progress.

Conflict of Interest

There are no conflicts to declare.

Acknowledgments

The financial support of the Spanish Ministry of Science and Innovation (PID2021-126148NA-I00 funded by MCIN/AEI/10.13039/501100011033/FEDER, UE) is gratefully acknowledged. Moreover, this work was funded by the Xunta de Galicia (GRC ED431C 2020/10). A. R.-P. and J.M.O.-M. thank the Spanish Ministry of Education for their FPU grant. C. D. R. F. thanks the support of Xunta de Galicia through the grant ED481A-2018/032. T. M. M. acknowledges her contract funded by the pilot program of the USC for the recruitment of distinguished research personnel—call 2021 under the agreement between the USC and the Santander Bank for 2021–2024. H.M.C. thanks the USC for his ””Convocatoria de Recualificación do Sistema Universitario Español-Margarita Salas” postdoctoral grant under the ”Plan de Recuperación Transformación” program funded by the Spanish Ministry of Universities with European Union’s NextGenerationEU funds. This work was supported by the Fundacão para a Ciência e Tecnologia (FCT) (funded by national funds through the FCT/MCTES (PIDDAC)) to CIQUP, Faculty of Science, University of Porto (Project UIDB/00081/2020), IMS-Institute of Molecular Sciences (LA/P/0056/2020). Facilities provided by the Galician Supercomputing Centre (CESGA) are also acknowledged.

USC
UNIVERSIDADE DE SANTIAGO DE COMPOSTELA

Part III

Conclusions

USC
UNIVERSIDADE
DE SANTIAGO
DE COMPOSTELA

9- Conclusions and Future Perspectives

9.1 Conclusions

The main conclusions that are derived from the studies contained in this thesis are:

1. The consideration of multipolar effects in simulation studies has implications not only on the dynamics but also on the structure of IL mixtures. We have reported MD simulations of a mixture of IL with ammonia where the NH_3 models lead to different levels of interaction between species, specially between ammonia and the IL cation. Furthermore, the inclusion of an interface lead to the preferential adsorption of NH_3 at the electrode vicinity.

2. Our MD studies show that the interaction between metal salt cations and polymer chains in hybrid ionogels is restricted if the interaction between the metal cation and the IL/salt anions is strong, leading to the formation of complexes that are strongly bound throughout the simulation. This way, the polymer presence does not disturb the molecular environment of the binary mixture, acting just as a supporting matrix. This can be prevented by the selection of an anion with more delocalized charge. We have shown how then Li^+ molecules coordinate strongly with oxygen atoms, including those of the PEO polymeric backbone.

3. The interaction of TSPEs with the electrode interface depends on the specific species employed. PEO concentration is increased in the neighborhood of the interface because of its hydrophobic nature, leading to an increase in Li^+ coordination. This is opposite to previously reported results with Li metal solid electrodes. Due to this enhanced interaction, PEO chains are oriented parallel to the electrode. The choice of IL cation is also relevant, as only some species allow Li^+ cations reaching the electrode.

4. The intercalation of the metal cation inside the electrode is necessary for a meaningful charge transfer to occur. This was reported in a DFT study where two different approach paths were considered. Neither Li^+ nor K^+ lead to a significant enough charge transfer when approaching a graphene electrode in the direction normal to the interface. However, the insertion of Li^+ through the edge plane of a trilayer graphene electrode did achieve it.

5. The interaction of metal salts with electrodes is dependent on the considered species. We have reported how the ionization energy is likely the main reason behind the different amounts of charge transfer that take place. The presence of the metal downshifts the band structure of the system, proportionally to the amount of charge transfer. New molecular levels appear in the system, which are placed closer to the Dirac cone in the case of Mg and Ca.

USC UNIVERSIDADE DE SANTIAGO DE COMPOSTELA

9.2 Future Perspectives

In the years ahead, we will further develop these research lines with finer refinements to the techniques employed. On the one hand, we must consider more explicitly the polarization of the different molecules in MD studies, as the properties obtained, specially the dynamic ones, might be affected. This should include the electrode atoms as well, which would need to consider fluctuating charges that reflect the real state of the simulation. Methods such as image charge or gaussian distributions allow for constant potential simulations instead of constant charge, which would also be a step further in making the systems more realistic. Up until now, most of these considerations were very computationally expensive, to the point where we had to discard using them, as the simulations were already long enough. However, many simulation software packages have been updated and upgraded, greatly improving the performance of these techniques in the recent years. Therefore, in the future, it might be possible to explicitly consider all these quirks even when working with large systems. In fact, a novel technique that has gained a lot of traction lately is the consideration of neural network derived force fields. In brief, the neural network is trained with more accurate techniques, such as DFT, and then it is used to feed to the MD simulation the appropriate forces. Although not purely *ab initio*, it is a great complement to *ab initio* MD simulations - while being orders of magnitude faster. In the coming years, all these different avenues will be explored.

On the other hand, ILs are currently trending materials in other fields, specially in energy storage. Improving the knowledge about mixtures of ILs with cosolvents of interest, specially gases such as hydrogen or nitrogen is critical. Evaluating their potential to store gases, explaining the mechanisms behind the relevant interactions in the mixture or unveiling the possible effects of nanoconfinement are examples of relevant areas where research work is needed. In this regard, we have already published different computational studies on the matter, with more planned for the near future.

USC
UNIVERSIDADE DE SANTIAGO DE COMPOSTELA

List of Figures

1.1 Schematic view of the different structures of regular solid salts, ionic liquids and hybrid ionogels respectively. 6

2.1 Classification of some of the most widely spread simulation techniques according to their spatial and time resolutions. 9
2.2 Schematic view of the different bonded and non-bonded interactions considered by most current force fields. 12
2.3 Schematic representation of the workflow of the Leap Frog algorithm. 13
2.4 Schematic representation of the changes that thermostats and barostats induce in the simulated system. 14
2.5 Scheme of the different degrees of approximation to the quantum many-body problem. 17

4.1 Conventional 4-site model (left) and 6-site model (right) for ammonia showing the partial charges and bond distances. 31
4.2 Radial distribution functions for the 4-site (left) and 6-site (right) models. From top to bottom, the results are calculated between nitrogen sites on species EA^+ - NO_3^-, NO_3^--NH_3, EA^+-NH_3 and NH_3-NH_3 for three different concentrations of ammonia: 10 mole% (blue), 30 mole% (orange) and 50 mole% (green). 32
4.3 Spatial distribution functions of the cation (top) and the anion (bottom) around the NH_3 molecule in both 4-site (left) and 6-site (right) models at a concentration of 50 mole%. 33
4.4 Velocity autocorrelation functions of the three species in both 4-site (solid lines) and 6-site (dashed lines) models at a concentration of 50%. 34
4.5 Number density profiles for all species near the neutral wall (a), the positive wall (b), and the negative wall (c) in both 4-site (solid lines) and 6-site (dashed lines) models at a 50% ammonia concentration. 36
4.6 Time-averaged 2D Fourier transforms of the x,y components of the positions of the molecules in the first layer near the negatively charged wall for a 50% concentration. The upper row corresponds to the 4-site model systems, while the bottom row contains the results for the 6-site systems. The species represented are, from left to right, cation, anion and ammonia. 37
4.7 Normalized continuous probability density as a function of $\cos(\theta)$ for cations and anions in the first layer near the a) positively and b) negatively charged walls for bot 4-site (solid line) and 6-site (dashed line) models. 38
4.8 Velocity autocorrelation functions of EA^+ (red), NO_3^- (blue) and NH_3 (green) for the first layer near the a) neutral, b) positive and c) negative walls, for both 4-site (solid line) and 6-site (dashed line) models. 39

USC UNIVERSIDADE DE SANTIAGO DE COMPOSTELA

5.1 A representation of the algorithm used to generate the initial configurations for the simulations. The polymers are represented without the hydrogen atoms as well as using small sizes for the atoms beads for a better visualization. 45

5.2 Average end-to-end vector R_e (a) and radius of gyration R_g (b) of PEO in the REMD simulations comprising a single PEO chain with 20 monomers and 500 IL ion pairs. The ratio of the two mean squared radii, $\langle R_e^2 \rangle / \langle R_g^2 \rangle$, is shown in (c). For a Gaussian chain $\langle R_e^2 \rangle / \langle R_g^2 \rangle = 6$, which is represented with a dashed line. 47

5.3 RDFs between Li^+ and the other molecular species presented in mixtures with 10% of lithium salt with (dashed lines) and without (solid lines) polymers. The corresponding coordination numbers are also represented in the inset. 48

5.4 RDFs between the oxygen atoms of the polymer chains and the Li^+ (a), ACE^- (b) and EA^+(c) for all the simulated salt concentrations. The horizontal black dashed lines placed at $g(r) = 1$ are represented to mark the ideal distribution. 49

5.5 Mean number of hydrogen bonds by donor molecule (EA^+) between the EA^+ molecule and the ACE− anion (blue line) and the EA^+ cation and polymer chains (blue). 50

5.6 Vibrational power spectrum for Li^+, ACE^- and EA^+ ions for the systems with 10% of lithium salt with (dashed lines) and without (solid lines) polymers. 51

5.7 Transference numbers for all the ionic species in the simulations with different [Li][ACE] concentration. The numbers for the simulation of 10% of [Li][ACE] without polymer are also represented as empty dots. 52

5.8 Relative Li^+ adsorption compared with random distribution for all the simulated salt concentrations. The horizontal dashed line represents an adsorption compatible with a random distribution. The absolute percentage of coordinated Li^+ is represented in the inset. 54

5.9 RDFs between Li^+ and ACE^-. In the inset the coordination numbers of ACE^- around Li^+ are represented for all the simulated salt concentrations as well as the one corresponding to the system of 10% without polymers. The spatial distribution function of Li^+ around ACE^- for the 20pc system is represented on the right side pointing out the Li^+ adsorption sites. The blue and red regions represent the mono and bidentate coordinations respectively. 55

6.1 3D models of the species present in the systems. Oxygen, carbon, hydrogen, nitrogen, sulfur, fluorine and lithium atoms are represented in red, black, white, blue, purple, pink and orange, respectively. Relevant sites employed for the calculations in each species are explicitly labeled. 60

6.2 RDFs between Li^+ and several atoms of the different molecules in bulk mixtures (left) and in the interfacial region in systems between neutral graphene-like walls (right). The insets show the corresponding cumulative RDF. The representative atoms for $TFSI^-$ and PEO are specified in the legend, whereas C1 and N were chosen for $EMIM^+$ and $Pyr_{14}{}^+$, respectively. 63

6.3 Snapshots in the YZ plane (left) and XY plane (right) of the polymer chains closer than 1 nm to a neutral electrode in mixtures with[Pyr_{14}][TFSI]. Oxygen and carbon atoms are represented in green and purple, respectively. 64

6.4 RDFs between Li^+ and several atoms of the different molecules in the region near the positively (left) and negatively (right) charged graphene-like surfaces, respectively. The insets show the corresponding cumulative RDF. The representative atoms for $TFSI^-$ and PEO are specified in the legend, whereas C1 and N were chosen for $EMIM^+$ and $Pyr_{14}{}^+$, respectively. 65
6.5 Density profiles in the z direction, normalized to the bulk density, for several atoms of the different molecules in systems confined between neutral graphene-like surfaces (left) and charged graphene-like surfaces (right). The representative atoms for $TFSI^-$ and PEO are specified in the legend, whereas C1 and N were chosen for $EMIM^+$ and $Pyr_{14}{}^+$, respectively. 67
6.6 Snapshots in the XY plane (left) and YZ plane (right) of the molecules closer than 1 nm to the negative electrode in the [EMIM][TFSI] (top) and [Pyr_{14}][TFSI] (bottom) 20-2-6 systems. Lithium atoms, in orange, and cationic rings, in green, are artificially enlarged for better visual clarity. 68
6.7 Free energy profiles for lithium ions approaching the graphene-like surfaces with neutral (top), positive (center) and negative (bottom) charge densities for the investigated ternary SPEs. Dotted lines show the positions of the barrier for all the concentrations: PYR 20-2-6 (blue), EMIM 20-2-6 (orange) and EMIM 20-2-20 (green). In all cases the corresponding electrode is located at z = 0.0 nm. 70
6.8 Marginal probability density distribution of polymer orientation relative to the vector normal to the graphene-like surface in the interfacial region (up to 2 nm). A scheme depicting the characteristic vectors defined for the polymer is shown on the left. 71
6.9 Radius of gyration in the z direction for TSPEs confined between neutral (left) and charged (right) graphene-like surfaces. 74
6.10 Displacement variance (Eq. 6.5) of Li^+ cations in the three directions as a function of the initial position in z for TSPEs confined between neutral (left) and charged (right) graphene-like surfaces. 75

7.1 Energy profiles for Li^+ (blue) and K^+ (orange) approaching the basal plane of graphene in the presence of a pair of [BMIM][BF_4] as a function of the distance to the interface. 85
7.2 Snapshots of the arrangements of the ions on top of the basal plane of graphene for several distances between Li^+ (top) and K^+ (bottom) and the interface. 85
7.3 Net charges of the different species present in the system as a function of the Li^+ (top) and K^+ (bottom) distance to the basal plane of graphene. Carbide stands for the 6 carbon atoms of the graphene closest to the metal. 87
7.4 Charge distribution on the graphene for the simulations of Li^+ (top) and K^+ (bottom) appraching the basal plane of graphene in the presence of a pair of [BMIM][BF_4]. . 87
7.5 Snapshots of the configuration for the simulations of Li^+ approaching the edge plane trilayer graphene in the presence of a pair of [BMIM][BF_4] and an additional $BF_4{}^-$, (a) general view and (b) lateral view. 88
7.6 Energy profile (a) and total net charge of the different species present in the system (b) for Li^+ approaching the edge plane of trilayer graphene in the presence of a pair of [BMIM][BF_4] and an additional $BF_4{}^-$, in both cases as a function of the distance to the interface. Carbide stands for the 12 nearest carbon atoms to the lithium position inside the electrode. Negative distances mean that Li^+ is located inside the electrode. 89

USC UNIVERSIDADE DE SANTIAGO DE COMPOSTELA

7.7 Charge distribution on the 12 carbon atoms surrounding the equilibrium position of the Li^+ inside the interface. The other atoms were hidden for an clearer view of the distribution. 89

8.1 Top and side views of a snapshot of one of the simulated systems. 95
8.2 Charge of the carbon atoms of graphene induced by the presence of the IL and the different metals calculated using Bader charge analysis. Dashed outlines show the position of the IL and the corresponding metal in each system. The respective sizes of the metals have been increased for clarity purposes. 97
8.3 Lateral views of the electronic density difference between the system with metal and IL, and the system with no metal and the system with only metal. Regions depicted in red/blue correspond to isosurfaces of value ± 0.017 e/Å^3, and therefore represent electron depletion/accumulation, respectively. The respective sizes of the metals have been increased for clarity purposes. 100
8.4 Band structure diagrams of the different systems, in which Fermi energy is taken as a reference for the energy level. In a wider black line, the band structure of pristine graphene is positioned so that the Dirac cones are overlapped. 101
8.5 Energy shift of the Dirac cone as a function of the charge transferred to the graphene surface for each system. For clarity purposes, a zoom was added as an inset to facilitate the view of some points. Values for simulations with K obtained from Ref. 299 are included for comparison. 102
8.6 DOS and PDOS of the different systems. On top of each plot: molecular HOMO-3, HOMO-2, HOMO-1, HOMO, LUMO, LUMO+1, LUMO+2 and LUMO+3 states that are within the considered energy interval. The color indicates to which species the state belongs. Fermi energy is taken as reference for the energy level. 103
8.7 Real (ε_1) and imaginary (ε_2) parts of the dielectric function and EELS (L) for the different systems with parallel (left) and perpendicular (right) electric field. Shaded stripes represent the optical region. 105
8.8 Refractive index (n), extinction coefficient (κ), reflectivity (R) and absorption coefficient (α) for the different systems with parallel (left) and perpendicular (right) electric field. Shaded stripes represent the optical region. 107

USC UNIVERSIDADE DE SANTIAGO DE COMPOSTELA

List of Tables

6.1 Number of molecules contained in the simulation box for the different systems. . . 61

8.1 Total charge of the different species after Bader analysis of the relaxed configurations. Values for simulations with K obtained from Ref. 299 are included for comparison. First and second ionization energies (IE, in eV) for each element from Ref. 399 are also included. 96

8.2 Binding energy (ΔE) and distance between the metal atom and i) its nearest carbon atom (d_{MC}), ii) the center of mass of the anion (d_{MA}), iii) the center of mass of the imidazolium ring (d_{MR}), and iv) the terminal carbon of the imidazolium tail (d_{MT}) for each of the studied systems. Values for simulations with K obtained from Ref. 299 are included for comparison. 98

8.3 HOMO-LUMO energy gap for the different studied systems. Value for simulations with K obtained from Ref. 299 is included for comparison. 103

USC
UNIVERSIDADE DE SANTIAGO DE COMPOSTELA

Part IV

Appendix

USC
UNIVERSIDADE
DE SANTIAGO
DE COMPOSTELA

A- Post-Print Version of the Publications

In the following pages we include the post-print version of the publications used in this thesis:

- The interaction of ammonia with the protic ionic liquid ethylammonium nitrate: A simulation study
- Computational study of the structure of ternary ionic liquid/salt/polymer electrolytes based on protic ionic liquids
- Ternary solid polymer electrolytes at the electrochemical interface: a computational study
- Density functional theory of alkali metals at the IL/graphene electrochemical interface
- Ionic liquid/metal salt mixtures at the graphene interface: A density functional theory approach

USC
UNIVERSIDADE DE SANTIAGO DE COMPOSTELA

Journal of Molecular Liquids 320 (2020) 114437

Contents lists available at ScienceDirect

Journal of Molecular Liquids

journal homepage: www.elsevier.com/locate/molliq

The interaction of ammonia with the protic ionic liquid ethylammonium nitrate: A simulation study

Alejandro Rivera-Pousa [a], José M. Otero-Mato [a], Alberto Coronas [b], Anthony J. Stone [c], Ruth M. Lynden-Bell [c], Trinidad Méndez-Morales [a,d,*], Luis M. Varela [a,**]

[a] Grupo de Nanomateriais, Fotónica e Materia Branda, Departamento de Física de Partículas, Universidade de Santiago de Compostela, Campus Vida s/n, E-15782 Santiago de Compostela, Spain
[b] Rovira i Virgili University, Mechanical Engineering Dept., Av. Països Catalans, 26, 43007 Tarragona, Spain
[c] Department of Chemistry, University of Cambridge, Lensfield Road, Cambridge CB2 1EW, UK
[d] Departamento de Física Aplicada, Facultade de Ciencias, Universidade de Vigo, E-36310 Vigo, Spain

ARTICLE INFO

Article history:
Received 30 July 2020
Received in revised form 21 September 2020
Accepted 23 September 2020
Available online 30 September 2020

Keywords:
Ammonia solutions
Protic ionic liquids
Microstructure
Single-particle dynamics
Electrochemical interface

ABSTRACT

In this paper, we present a molecular dynamics study of ammonia solutions in a protic ionic liquid with a structurally similar cation, ethylammonium nitrate. Using two different models of the ammonia molecule, a conventional 4-site model and a 6-site model optimizing the dipolar and quadrupolar electron distributions, we evaluate their effect on the microstructure and single-particle dynamics of these mixtures, as well as on their behaviour at the electrochemical interface. Quite significant differences are found on the solvation of ammonia in these dense ionic solvents, the 6-atom model predicting a stronger affinity of solvent molecules for the cations of the solvent as well as a caging effect on NH_3 solvation shells, not predicted by the 4-site model. Finally, we discuss the structure of the liquid layers near charged graphene walls. The structure in the layer next to the wall varies with the charge on the wall and varies with the model used for ammonia.

© 2020 Elsevier B.V. All rights reserved.

1. Introduction

The change of the lifestyle of people all around the world due to the development of technology has led to a high demand of temperature control devices. In this context, refrigeration engineering is used every day in many different fields including food industry, air conditioning, electronic devices and medical technology [1–4]. Compression refrigerators typically employ hydrofluorocarbons [5], but the research of efficient refrigeration systems with minimal impact on the environment is leading to an increasing adoption of ammonia as a refrigerant [6]. In the case of absorption refrigeration systems, they usually use a pair of materials (refrigerant/absorbent) that is completely soluble over a wide temperature range, such as a simple salt (lithium bromide or lithium chloride) and water [7] or ammonia (NH_3) and water [8]. However, other absorbents like ionic liquids (ILs) have been proposed as alternatives to avoid the drawbacks of the former working pairs [9].

ILs are salts that melt below 100 °C. They offer some physical properties, including negligible volatility, wide liquid range and relatively high thermal stability [10], that make them useful as new absorbents in absorption refrigeration cycles. With the purpose of finding new promising working pairs containing NH_3 as refrigerant and ILs as absorbent, researchers have analyzed several thermodynamical properties such as miscibility, heat capacity and enthalpy of absorption. For example, Yokozeki et al. [11,12], one of the pioneers in this field, observed extremely high solubilities of ammonia in ILs. Experimental data on the solubilities of NH_3 in ILs has also been reported by Li and coworkers [13], who concluded that this solubility increases with the increase of alkyl side chain length but decreases with the rise of temperature. More recently, Coronas and coworkers [14–17] reported several studies focusing on this topic. They stated that the presence of a hydroxyl group in the cation structure of the ILs enhances the solubility of ammonia, and they also indicated that 1-(2-hydroxyethyl)-3-methylimidazolium tetrafluoroborate [EtOHmim][BF_4] is a suitable IL as absorbent for ammonia [15]. Working with this IL, they also analyzed its interaction with ammonia and they found that it preferentially occurs through the hydroxyl group in the cation, whereas the interaction through the anion is favored only at lower temperatures [17]. Interestingly, Swarnkar et al. [18] tried to avoid one of the problems of ILs, their high viscosity, by using water as a co-solvent, and they obtained a slight decrease in the coefficient of performance, but a large decrease in circulation ratio. In addition, several research groups [19–21] performed cyclic voltammetric analysis using glassy carbon and platinum electrodes,

* Correspondence to: T. Méndez-Morales, Departamento de Física Aplicada, Facultade de Ciencias, Universidade de Vigo, E-36310 Vigo, Spain.
** Corresponding author.
E-mail addresses: trinidad.mendez@usc.es (T. Méndez-Morales), luismiguel.varela@usc.es (L.M. Varela).

USC UNIVERSIDADE DE SANTIAGO DE COMPOSTELA

https://doi.org/10.1016/j.molliq.2020.114437
0167-7322/© 2020 Elsevier B.V. All rights reserved.

respectively, to study the direct electrochemical oxidation of ammonia in several ILs, and they showed that the ammonia cation is formed after oxidation of NH_3.

On the other hand, several computational studies were also proposed to obtain a molecular level understanding of these systems and to predict some thermodynamic properties for conditions under which experiments are difficult to perform. For example, Shi and Maginn [22] performed Monte Carlo (MC) simulations to compute isotherms for ammonia absorption in ethyl-3-methylimidazolium bis (trifluoromethylsulfonyl)imide ([emim][TFSI]) at several temperatures. They observed that NH_3 interacts more strongly with the cation than with the anion due to the strong hydrogen bond that ammonia forms with the hydrogen atoms in the ring of the cation. They also suggested that the cation plays a larger role in determining the NH_3 solubility in ILs. This same conclusion was reported by Kapoor et al. [23] by using molecular dynamics (MD) simulations in a study in which they also observed the decrease of the solubility with the temperature. In addition, their results indicated that NH_3 is less soluble in ILs than SO_2, but more than CO_2 and CH_4. Another approach, the COSMO-RS method, was employed by Palomar and coworkers [9,24,25] to elucidate the structural characteristics enhancing the solubility of NH_3 in ILs and, thus, was able to propose the absorbents with the most favorable properties for ammonia capture. In good agreement with previous works, they concluded that attractive hydrogen-bond interactions determine the increasing gas solubility, due to which some conventional ILs (such as [emim][TFSI]) do not seem to be optimum solvents for ammonia absorption since they behave mostly as hydrogen-bond acceptors. Instead, they encourage the use of OH-functionalized cations and propose [EtOHmim][BF_4] and [choline][TFSI] to implement novel NH_3 absorption systems. More recently, Becker et al. [26] also carried out MC simulations to predict some thermodynamic properties and estimate the performance of absorption refrigeration cycles using [emim][TFSI] and [emim][SCN] with NH_3, observing a better performance of the former.

However, we are not aware of any studies analyzing the interaction of ammonia and protic ILs, which are well-known for the presence of strong hydrogen bonds between the cation and the anion [27]. On the other hand, the role of quadrupole moment in the rationalization of molecular properties and intermolecular interactions is well-known [28], specifically in the case of nonrigid systems such as ammonia, for which the role of the vibrational or even rotational effects is usually important. For that purpose we performed MD simulations of mixtures of NH_3 and the most studied protic ionic liquid ethylammonium nitrate (EAN). Thus, in this work we will analyze, for the first time, mixtures of ammonia with an IL including a cation with a similar molecular head group NH_3^+. Moreover, we compare two different molecular models for NH_3, a conventional 4-site one and a new 6-site model that describes the electrostatic interactions more accurately by including the dipolar and quadrupolar electron distributions around the nitrogen atom in addition to point charges on the atomic sites.

Ionic liquids and their solutions are of great importance for advanced electrochemical energy storage [29,30], and ammonia is starting to be considered a key player also in this field because of its use in a thermally regenerative ammonia-based batteries [31,32] or to its role as a high conductivity switch in solid-state lithium batteries [33]. However, there is a total dearth of studies of ammonia-IL mixtures at the electrochemical interface. Therefore, our bulk simulations are extended to investigate the behaviour of ammonia/EAN solutions near charged walls.

2. Simulation details

In this study, we introduce a new molecular model for ammonia that contains a better description of the charge distribution of the ammonia molecules by including a quadrupole and a small dipole on the nitrogen site in addition to site charges. These are modelled by two additional virtual sites with charge but without mass, localized on the symmetry axis of the molecule (0.2646 Å away from the nitrogen). The N—H bond distance is 1.01 Å. The charge of each hydrogen is +0.330e, the nitrogen charge has a value of +2.670e, and the virtual atoms have a charge of −1.7035e and −1.9565e, respectively (see Fig. 1). The bond angle is 106.67°.

The model was developed from a DFT electron density calculated with CamCASP [34,35] using the PBE0 functional [36] with asymptotic correction and the aug-cc-pVQZ basis set [37,38]. The atomic multipoles were obtained from iterated stockholder (ISA-GRID) atom densities [39], and the charges on the atom sites and the two additional sites were initially chosen to reproduce the H atom charges and the N atom charge, dipole and quadrupole. These values were then adjusted slightly to optimize the agreement with the electrostatic potential of the total DFT electron density, calculated on the surface at 1.5 times the van der Waals radii, in order to take into account to some extent the effect of higher multipoles. For comparison, we also employed a conventional ammonia model (4-site model) with bond distances of 1.020 Å, and a nitrogen and hydrogen charge of −1.020e and +0.340e, respectively (Fig. 1). This model was reported by Rizzo and Jorgensen in Ref. [40]. It must be noted that our ammonia model does not consider proton-transfer reaction effects, which would provide us with results on the behaviour of the mixtures more consistent with reality. But the goal of this work is to analyze the effect of the quadrupole by quantifying the differences between both models from a theoretical point of view. The parametrization of the IL - ethylammonium nitrate (EAN) - is detailed in the Supplementary information.

Atomistic MD bulk simulations of mixtures of EAN and ammonia were performed for several concentrations, ranging from 10 to 50 mol % ammonia. The concentrations are defined by the number of ammonia molecules divided by the total number of ions. Thus a 50% mixture has equal numbers of cations, anions and ammonia molecules. Each of these simulations was carried out for both ammonia models. Furthermore, bulk simulations were later extended to a nanoconfined environment by placing the mixtures between two rigid graphene walls (one layer thick, situated 8 nm apart along the z axis) that were either

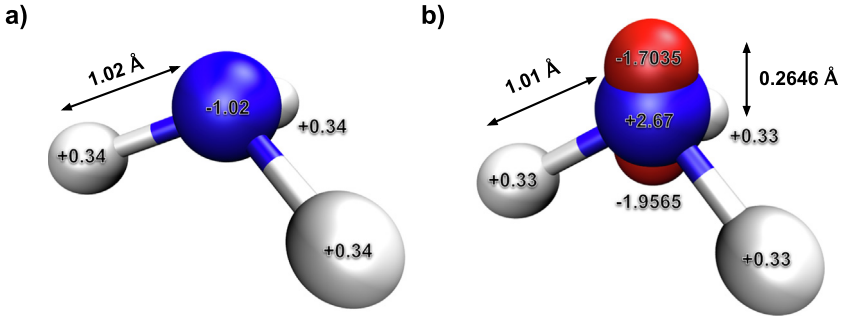


Fig. 1. Conventional 4-site model (left) and 6-site model (right) for ammonia showing the partial charges and bond distances.

electrically neutral or charged (one positively and one negatively, with charges $\pm 1e/nm^2$). The total number of molecules was 600 for the 4-site ammonia model simulations and 500 for the 6-site one in the bulk simulations, which was increased to 1200 in both cases for the nanoconfined ones. Bulk simulations were performed in the NPT ensemble (1 atm, 298 K), while nanoconfined simulations were carried out in the NVT one (also at room temperature).

We performed all of the simulations reported in this paper using the open source Gromacs 2016 package [41,42] with the OPLS-AA force field, [43] which includes both intramolecular (bond stretching, dihedral torsion and angle bending) and intermolecular forces (a van der Waals and a Coulomb term). The PACKMOL [44] software was employed to obtain the initial configurations of our simulations, followed by proper minimization and stabilization (at least 10 ns) of the systems. The confined simulations also incorporated an annealing run (1 ns) to avoid metastable configurations in which the temperature was linearly increased to 600 K and then decreased back to the simulation temperature. The production runs used for the structural analysis were 10 ns long, while in the simulations used for the single-particle dynamics the velocities were saved at each time step (1 fs) during runs of 100 ps.

3. Results and discussion

In order to understand the structural properties of our mixtures, studying the radial density functions (RDFs) of the system is needed. This function is defined as

$$g(r) = \frac{1}{\rho N}\left\langle \sum_{ij} \delta(r - r_{ij}) \right\rangle \quad (1)$$

where ρ is the number density, N the number of particles in the simulation box and the brackets refer to an ensemble average. In Fig. 2 the RDFs between nitrogen sites on each of the ions of the IL and the nitrogen sites on ammonia (both models). As can be seen in Fig. 2, the major effect of the 6-site model with electrostatic interactions is the enhancement of EA^+-NH_3 interactions, reflected in a very large increase of the height of the first peak of g_{EA-NH3}. This leads to a restructuring of the solvation shell of all the species in the mixture as the first solvation shell of EA^+ is enriched with ammonia, expelling the other species to a second layer. This is the origin of the increase of the height of the second peak in g_{EA-NO3} and $g_{NH3-NH3}$, located at 0.65 Å and 0.7 Å, respectively. We can also observe in Fig. 2 that the positions of the first peaks are not shifted by the presence of the quadrupole in the ammonia molecule. The position of the EA^+-NO_3^- main peak is 0.35 nm, while the peaks for the NO_3^--NH_3 and EA^+-NH_3 coordinations appear at 0.37 and 0.28 nm, respectively. The effect of the multipolarity is apparent, as the height of the first peak has a dependence on concentration in the 6-site model, a property that does not appear in the 4-site model. Moreover, there is a large increase in the height of the peak between the cation head and the ammonia, which shows an enhanced interaction between these two species when using the quadrupole. This explains the dependence on concentration, as the ammonia molecules effectively compete with the anions occupying the positions in the first shell around the cation, so the EA^+-NO_3^- first peak decreases with increasing ammonia concentration, displacing the anions to a second shell. This preference of ammonia for interacting with the head of the ethylammonium cation is in good agreement with the results reported by Maginn et al. [22], who observed a clear preference for the basic nitrogen of ammonia to associate with the acidic hydrogen on the ring of the imidazolium cation.

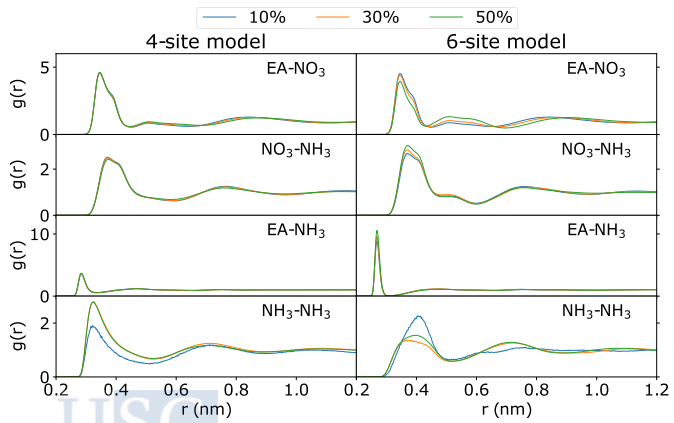


Fig. 2. Radial distribution functions for the 4-site (left) and 6-site (right) models. From top to bottom, the results are calculated between nitrogen sites on species EA^+ — NO_3^-, NO_3^--NH_3, EA^+-NH_3 and NH_3-NH_3 for three different concentrations of ammonia: 10 mol% (blue), 30 mol% (orange) and 50 mol% (green).

In order to complete our structural picture, we calculated spatial distribution functions (SDFs) for the different species in the mixture. As the ammonia is the central point of this work, we decided to obtain the isosurfaces of numerical density of each IL species using the three hydrogens of each ammonia molecule to define a local reference frame. In Fig. 3 the preferential position that each species occupies around ammonia molecules can be observed, as well as the differences between both ammonia models. The pictures correspond to the 50% concentration systems, but the results are analogous in any of them. As we can see, the prevalent position of the cation around ammonia is directly over the nitrogen atom, while other less relevant options appear in the positions that are not in front of a hydrogen. These results were expected due to the charge that each atom carries. Moreover, we can see that the position of the cation is very restricted in the 6-site model, confirming the strong interaction between these molecules that was previously observed in the RDFs. On the other hand, the calculations for the 4-site model show that the nitrogen atoms in the ammonia molecules have the freedom to invert between two metastable positions; one at each side of the plane defined by the three hydrogen atoms. Consequently, the results are an average of these two configurations. This ammonia inversion is known to be rapid at room temperature due to a low and narrow energy barrier, but it has also been observed in condensed phases [45]. This does not occur in the 6-site ammonia, since nitrogen atoms NH_3 interact more strongly with the nitrate and are also restricted by the virtual atoms, so they do not invert. For the anions (Fig. 3c, d), it is clear that the preferentially occupied position is that in front of one of the hydrogens, with which they coordinate in a monodentate fashion. In the 4-site model, the position is somewhat diffuse as a consequence of the symmetrical replication, but in the 6-site model the positions are very well defined. In addition, a secondary anion position appears around the space that the cation occupies in front of the nitrogen of the ammonia.

To gain some insight into the single-particle dynamics of our system, we performed a series of calculations to shed light on its behaviour. First of all, we calculated the velocity autocorrelation functions (VACFs) of the species in the mixture, as shown in Fig. 4. This normalized function is defined as

$$C(t) = \frac{\langle \vec{v}(t)\vec{v}(0)\rangle}{\langle \vec{v}(0)\vec{v}(0)\rangle} \quad (2)$$

where $\vec{v}$ is the velocity of the center of mass of the molecule. The results correspond to a 50 mol% concentration of NH_3. As we can see, there is no significant difference in the diffusion of the IL species between the two ammonia models. The contrast shows up when we consider the ammonia VACFs. There is some evidence of caging for all the species as one would expect in a dense liquid, but the 6-site ammonia shows an enhanced rattling motion of the ammonia molecules, which are trapped inside their solvation shells during 0.4 ps before escaping to the bulk.

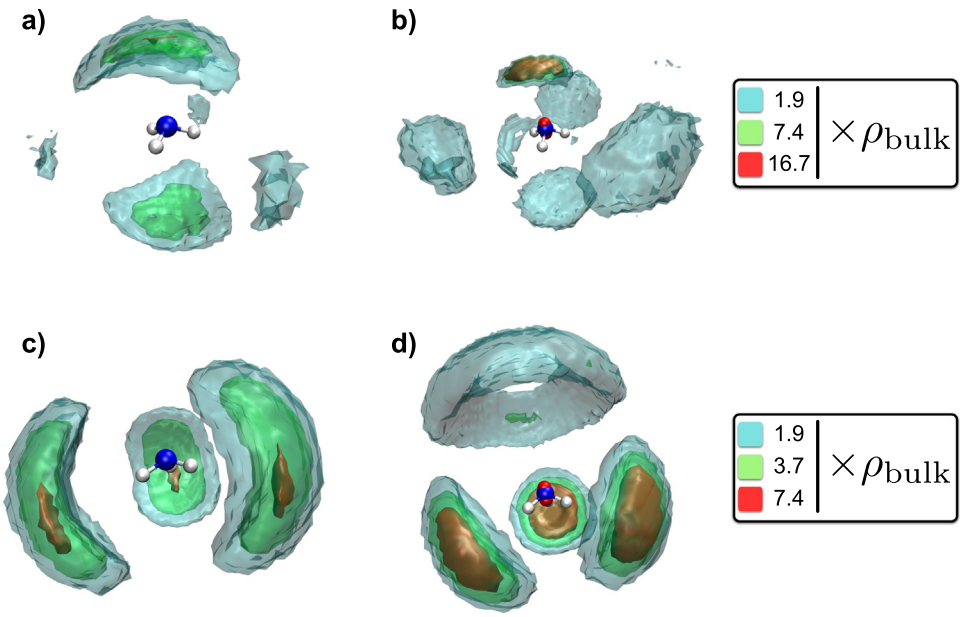


Fig. 3. Spatial distribution functions of the cation (top) and the anion (bottom) around the NH_3 molecule in both 4-site (left) and 6-site (right) models at a concentration of 50 mol%.

These different observations for the caging of NH_3 molecules are in good agreement with the enhanced interaction between ammonia and the IL cation previously observed in the systems described by the 6-site model by means of $g(r)$'s.

From the VACFs the vibrational density of states (vDOS) can be straightforwardly calculated, since it is the Fourier transform of the former

$$f(\omega) = \int_0^\infty e^{-i\omega t} C(t) dt, \tag{3}$$

and the results are shown in Fig. S1 of the Supplementary information for 50% concentrated mixtures. As expected, the differences between systems with different ammonia models are present just in the vDOS of this latter species. For the 6-site model of the ammonia molecule, a new vibrational mode arises related to the motion of the molecule inside its solvation shell that was apparent in the VACFs. Moreover, the first peak is also blue-shifted relative to the one predicted by the 4-site model, which implies, once again, that the ammonia suffers stronger interactions in the quadrupolar model.

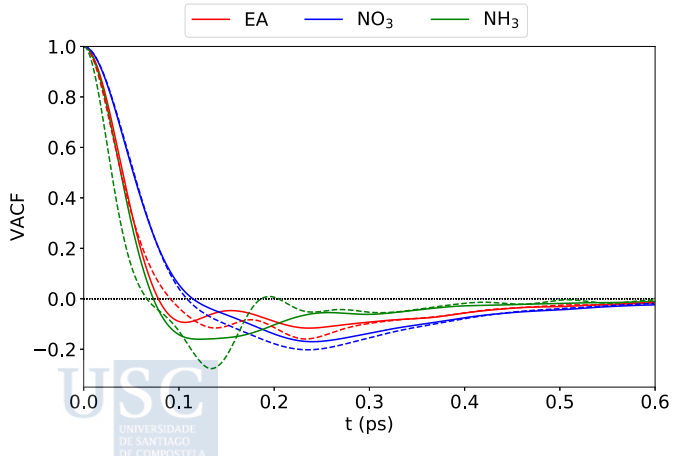


Fig. 4. Velocity autocorrelation functions of the three species in both 4-site (solid lines) and 6-site (dashed lines) models at a concentration of 50%.

To extend our investigation to the behaviour of these mixtures near charged electrodes, we performed a similar structural and dynamical analysis of this system nanoconfined between two parallel walls, and we then compared the results with those reported for the bulk. We started our structural calculations by obtaining the density profiles of the system, i.e., the number density of each species along the z-axis. Note that these profiles are calculated taking one atom as reference for each species: once again, we chose the nitrogen atoms. The results are plotted in Fig. 5. As in bulk systems, the ammonia concentration does not significantly alter the structure of the mixtures, so the results of Fig. 5 correspond to a 50 mol% concentration. If we focus on the systems with neutral walls, the first observation is that, with both models ammonia is preferentially adsorbed at the graphene walls. The first layer is composed mainly of ammonia and anions, followed by a cation layer. In the successive electric double layer (EDL) layers, anions and

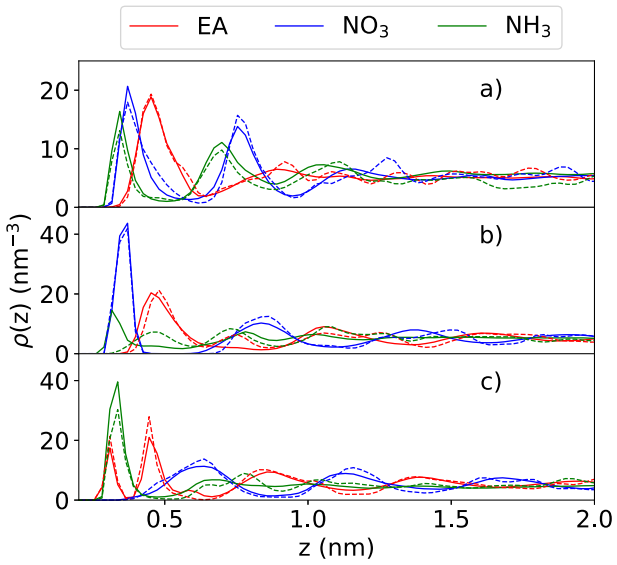


Fig. 5. Number density profiles for all species near the neutral wall (a), the positive wall (b), and the negative wall (c) in both 4-site (solid lines) and 6-site (dashed lines) models at a 50% ammonia concentration.

ammonia always occupy the same positions in the z-axis, in accordance with the previous bulk results that suggest that these species compete for the same positions. The EDL formation is clear, as the layers with ions of opposite charge alternate. This layering behaviour has been reported previously in several computational studies [46–48], although it is somehow controversial [49]. The bulk densities are recovered in the center of the simulation box (at a distance of about 1.5 nm away from the walls), showing that the walls are sufficiently far apart not to influence each other. The layering effect is enhanced in the simulations with charged walls. In those systems, cations occupy the first layer near the negatively charged wall, while anions do the same in the positively charged one, as expected. There is an over-compensation of charge near the electrodes (overscreening [50]) that attracts the ions of opposite charge forming a second layer, which also overcompensates the charge, giving rise to a third one and so on. The first layer of cations near the negative wall can be seen to be split. This is because the cations have two possible orientations in this layer each represented by a peak (as we will discuss later). Ammonia molecules are attracted to the negatively charged wall and repelled from the positively charged one. This behaviour is explained by the lack of anions near the negative wall, which leaves more room for the ammonia molecules, which compete for position with the anions.

In order to complete the information obtained from the density profiles we analyzed the lateral structure in the innermost layer of the EDL. We obtained the 2D Fourier transform of these layers averaged over time, which provides additional information about the arrangement of the molecules in the *xy*-plane. The results for the neutral and positively charged walls can be seen in Figs. S2 and S3 of the Supplementary information, respectively; whereas the configurations for the negative electrodes are shown in Fig. 6. Once again, the concentration does not play a significant role, so for visual clarity we plotted the results just for a 50% concentration. In the neutral simulations, no preferential directions are observed, as the plot is somewhat homogeneous. However, there is a difference between the systems with different ammonia models, as the 4-site NH_3 systems seem to have certain preferential distances. In the simulations with charged walls (Figs. 6 and S3) we observe more interesting results. Both IL molecules, anion and cation, form a square lattice in the positively charged wall, but the negatively charged wall structure does not present that kind of arrangement. This can be explained as follows: in the positively charged wall, the first layer is composed of NO_3^- anions, which are small and symmetric. These anions arrange themselves in a square lattice. This structure allows the subsequent cation layer (specifically, the cations heads) to position in the spaces left by the anions, forming themselves another square lattice. If we consider the two species together, the lattice would be triangular, which is incidentally the structure that minimizes the energy. Near the negatively charged wall, the first layer is composed of cations, whose chemical structure is much less symmetric, leaving a rather difficult accommodation for the anions, so neither of the species forms a square lattice and this structure is lost. The arrangement of NH_3 molecules does not show a clear pattern on either wall, but this is possibly due to lack of statistics.

To strengthen our deductions about the IL structuring near the graphene walls in the charged systems, we studied the molecular orientation of both ionic species near the walls. We obtained the conditional probability of finding a molecule at a certain orientation and distance from the wall: $P(r,\cos(\theta))$, where θ is the angle between a normal vector to the wall and a characteristic vector of the molecule, and r is the minimum distance between the wall and the application point of the vector. For the anion, this vector is normal to the plane where all its atoms lie, being applied on the nitrogen atom; whereas for the cation, the vector starts in the nitrogen and points towards the center of the triangle formed by the three hydrogen atoms on the EA^+ head. The results are plotted in Fig. S4 of the Supplementary information as a 2D-histogram. We also plotted in Fig. 7 the marginal probability distribution of this conditional probability, obtained by integrating the 2D-distribution between the distances corresponding to the first layer. As we can see, near the positively charged wall (the one with clear structuring) the anions have values of $\cos\theta$ centered around $+1$ and -1, i.e., $\theta = 0$ and $\theta = 2\pi$. For the anion, both situations are indeed the same as the molecular structure is planar. The anions, thus, are oriented parallel to the wall. In the cation case, the values of $\cos\theta$ are centered around -1, indicating that the arrangement of cations is so that the heads (NH_3^+) point towards the wall. This is true for both 4 -site and 6-site model systems, although the cation distribution is sharper in the latter. Near the negatively charged wall, anions follow a more homogenous distribution but still show a predisposition to position themselves parallel to

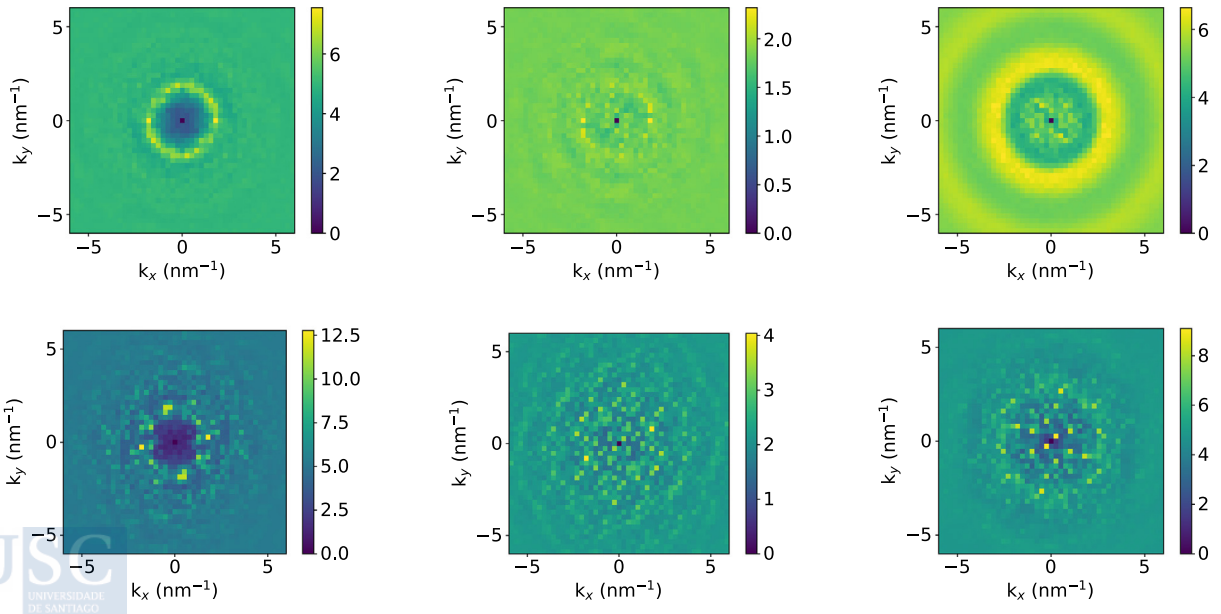


Fig. 6. Time-averaged 2D Fourier transforms of the x,y components of the positions of the molecules in the first layer near the negatively charged wall for a 50% concentration. The upper row corresponds to the 4-site model systems, while the bottom row contains the results for the 6-site systems. The species represented are, from left to right, cation, anion and ammonia.

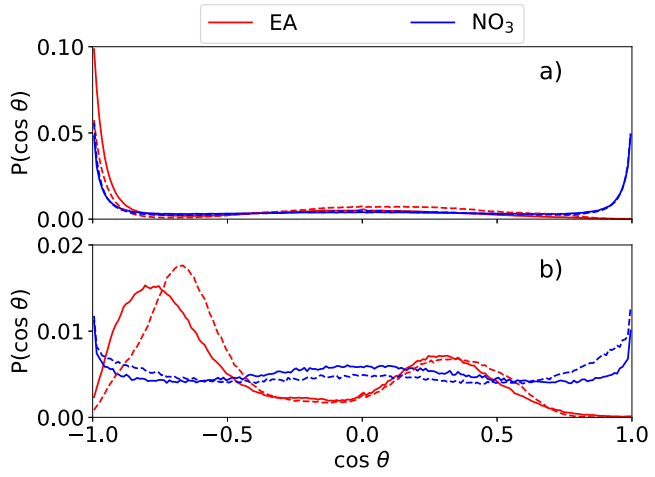


Fig. 7. Normalized continuous probability density as a function of cos(θ) for cations and anions in the first layer near the a) positively and b) negatively charged walls for both 4-site (solid line) and 6-site (dashed line) models.

the wall, with a sharper distribution around the peaks in the 6-site model systems. The cations, as discussed earlier, show two different orientations in the first layer. These orientations are slightly displaced between the systems with different ammonia models.

The single particle dynamics study will be composed of the analysis of the VACFs of the molecules in the first layer of the EDL and the corresponding vDOS, represented respectively in Figs. 8 and S5 (Supplementary information). The concentration of ammonia has a slight impact on the collision time of the cation and on the ammonia profiles, but it does not play an important role, so for visual clarity the figures correspond to, once again, a 50% NH_3. The cation profiles do not present significant differences between the systems with different ammonia models or charge walls. The anion profile is, however, altered by charging the walls. The dynamics on the negatively charged wall is similar to that of the neutral ones, but in the positively charged walls, the diffusion is faster. Regarding the dynamics of NH_3, the details depend on the model we used. Once again, the velocity autocorrelation function of the ammonia molecules shows a caging effect, but the 6-site model ammonia presents enhanced rattling motion.

Introducing charge on the walls also affects somewhat the VACF but they are more pronounced for the 6-site model ammonia dynamics, enhancing the caging effect near the negatively charged wall. This wall is the one that ammonia populates along with cations, and the strong interaction between these species that we observed in the bulk systems is probably responsible for this enhancement.

The vDOS, represented in Fig. S5 of the Supplementary information, also includes the bulk results for better comparison. As we can see, the vDOS of the IL species are basically unaffected by the ammonia model. On the other hand, the ammonia profiles show, as we observed in the bulk, a second vibrational mode in the 6-site model, related to those two different motions that the ammonia molecules present. Charging the walls has an effect on the profile of the anion, which is significantly blue-shifted in the proximity of the positively charged wall, indicating stronger interactions due to the opposite charge of the wall.

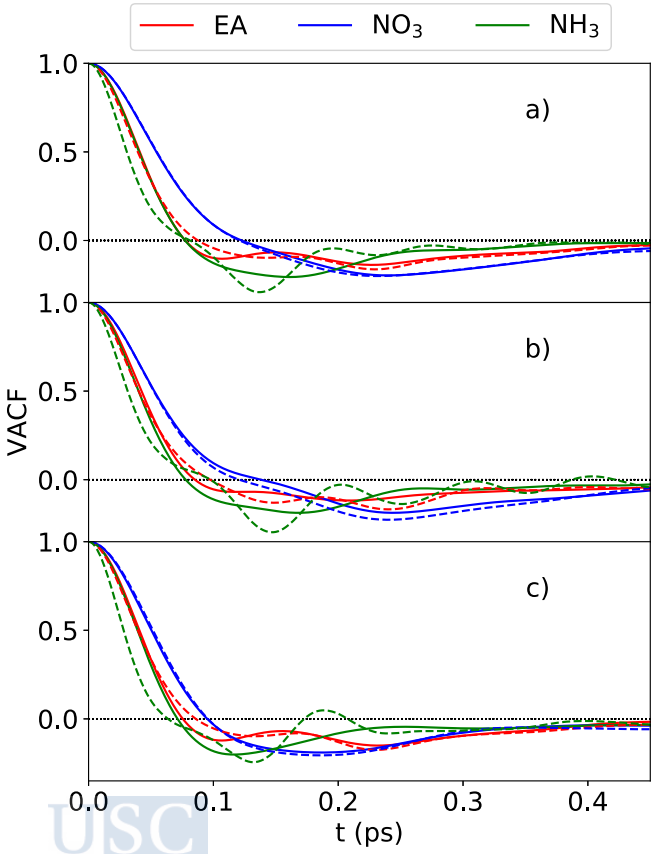


Fig. 8. Velocity autocorrelation functions of EA^+ (red), NO_3^- (blue) and NH_3 (green) for the first layer near the a) neutral, b) positive and c) negative walls, for both 4-site (solid line) and 6-site (dashed line) models.

4. Conclusions

In this work we performed several MD simulations in order to study the structural and dynamical properties of mixtures of a protic ionic liquid, EAN, and ammonia, both in bulk and nanoconfined between either neutral or charged graphene walls, as this system is expected to have important applications in the refrigeration and electrochemical fields.

The main conclusions from the bulk simulations are that NH_3 and NO_3^- compete for the same position around the EA^+ head, and more significantly, the great increase in the interaction between ammonia and cation in the 6-site model compared to the 4-site model, showing the importance of an accurate description of the molecular charge distribution. This also leads to significant caging and rattling motion in the single-particle dynamics of the 6-site ammonia dynamics.

In the presence of graphene walls, we can see that ammonia adsorbs near the neutral interfaces, and stays near the negatively charged wall occupying the positions left by the anions. A clear structuring of the IL in the first layer near the positively charged wall is present as the molecules arrange themselves in a square lattice to minimize the energy. Moreover, the 6-site NH_3 model yields to significantly more inhomogenous patterns in the wall adlayer. The dynamic properties of the species are consistent with those of bulk albeit we observe a slight blueshift on the vibrational densities of states.

Future work is already in progress focused on more accurate descriptions of intermolecular interactions, including the effects of polarisability.

CRediT authorship contribution statement

Alejandro Rivera-Pousa: Conceptualization, Methodology, Software, Validation, Formal analysis, Investigation, Data curation, Writing - original draft, Writing - review & editing, Visualization, Funding acquisition. **José M. Otero-Mato:** Conceptualization, Methodology, Software, Validation, Formal analysis, Investigation, Data curation, Writing - original draft, Writing - review & editing, Visualization, Funding acquisition.

Alberto Coronas: Writing - original draft, Writing - review & editing. **Anthony J. Stone:** Software, Formal analysis, Writing - original draft, Writing - review & editing. **Ruth M. Lynden-Bell:** Conceptualization, Methodology, Writing - original draft, Writing - review & editing. **Trinidad Méndez-Morales:** Conceptualization, Methodology, Writing - original draft, Writing - review & editing, Supervision, Funding acquisition. **Luis M. Varela:** Conceptualization, Methodology, Writing - original draft, Writing - review & editing, Supervision, Project administration, Funding acquisition.

Declaration of competing interest

The authors declare that they have no known competing financial interests or personal relationships that could have appeared to influence the work reported in this paper.

Acknowledgments

The financial support of the Spanish Ministry of Economy and Competitiveness (Grants MAT 2017-89239-C2-1-P) is gratefully acknowledged. Moreover, this work was funded by the Xunta de Galicia (ED431D 2017/06, ED431E 2018/08 and GRC ED431C 2016/001). All these research projects were partially supported by FEDER. A. R.-P. and J. M. O.-M. thank the Spanish Ministry of Education for their FPU grants. T. M.-M. thanks the Spanish Ministry of Science, Innovation and Universities for her Juan de la Cierva grant IJC2018-036774-I. Facilities provided by the Galician Supercomputing Centre (CESGA) are also acknowledged.

Appendix A. Supplementary data

Supplementary data to this article can be found online at https://doi.org/10.1016/j.molliq.2020.114437.

References

[1] D. Smith, Cooling electronic devices installed in a subsurface environment (2017). US Patent 9,593,876.
[2] R.-R. He, H.-Y. Zhong, Y. Cai, D. Liu, F.-Y. Zhao, Theoretical and experimental investigations of thermoelectric refrigeration box used for medical service, Procedia Engineering 205 (2017) 1215–1222.
[3] H. Wan, T. Cao, Y. Hwang, S. Oh, A review of recent advancements of variable refrigerant flow air-conditioning systems, Appl. Therm. Eng. 169 (2020) 112893.
[4] S. Tassou, J. Lewis, Y. Ge, A. Hadawey, I. Chaer, A review of emerging technologies for food refrigeration applications, Appl. Therm. Eng. 30 (2010) 263–276.
[5] S.V. Shaik, T.A. Babu, Theoretical performance investigation of vapour compression refrigeration system using HFC and HC refrigerant mixtures as alternatives to replace R22, Energy Procedia 109 (2017) 235–242.
[6] A. Pearson, Refrigeration with ammonia, Int. J. Refrig. 31 (2008) 545–551.
[7] P. Srikhirin, S. Aphornratana, S. Chungpaibulpatana, A review of absorption refrigeration technologies, Renew. Sust. Energ. Rev. 5 (2001) 343–372.
[8] D. Zheng, L. Dong, W. Huang, X. Wu, N. Nie, A review of imidazolium ionic liquids research and development towards working pair of absorption cycle, Renew. Sust. Energ. Rev. 37 (2014) 47–68.
[9] E. Ruiz, V. Ferro, J. de Riva, D. Moreno, J. Palomar, Evaluation of ionic liquids as absorbents for ammonia absorption refrigeration cycles using cosmo-based process simulations, Appl. Energy 123 (2014) 281–291.
[10] P. Wasserscheid, T. Welton, Ionic Liquids in Synthesis, John Wiley & Sons, 2008.
[11] A. Yokozeki, M.B. Shiflett, Vapor–liquid equilibria of ammonia + ionic liquid mixtures, Appl. Energy 84 (2007) 1258–1273.
[12] A. Yokozeki, M.B. Shiflett, Ammonia solubilities in room-temperature ionic liquids, Ind. Eng. Chem. Res. 46 (2007) 1605–1610.
[13] G. Li, Q. Zhou, X. Zhang, L. Wang, S. Zhang, J. Li, Solubilities of ammonia in basic imidazolium ionic liquids, Fluid Phase Equilib. 297 (2010) 34–39.
[14] M. Berdasco, A. Coronas, M. Vallès, Study of the adiabatic absorption process in polymeric hollow fiber membranes for ammonia/water absorption refrigeration systems, Appl. Therm. Eng. 137 (2018) 594–607.
[15] A. Cera-Manjarres, D. Salavera, A. Coronas, Vapour pressure measurements of ammonia/ionic liquids mixtures as suitable alternative working fluids for absorption refrigeration technology, Fluid Phase Equilib. 476 (2018) 48–60.
[16] M.S. Larrechi, A. Cera-Manjarres, A. Coronas, Ranking the solubility of ammonia in ionic liquids using near infrared spectroscopy and multivariate curve resolution, Spectrochim. Acta A Mol. Biomol. Spectrosc. 215 (2019) 88–96.
[17] M.S. Larrechi, A. Cera-Manjarres, D. Salavera, A. Coronas, Quantitative analysis of the interaction of ammonia with 1-(2-hydroxyethyl)-3-methylimidazolium tetrafluoroborate ionic liquid. Understanding the volumetric and transport properties of their mixtures, J. Mol. Liq. 301 (2020) (112440(1)–112440(11).
[18] S.K. Swarnkar, S.S. Murthy, R.L. Gardas, G. Venkatarathnam, Performance of a vapour absorption refrigeration system operating with ionic liquid-ammonia combination with water as cosolvent, Appl. Therm. Eng. 72 (2014) 250–257.
[19] X. Ji, D.S. Silvester, L. Aldous, C. Hardacre, R.G. Compton, Mechanistic studies of the electro-oxidation pathway of ammonia in several room-temperature ionic liquids, J. Phys. Chem. C 111 (2007) 9562–9572.
[20] X. Ji, C.E. Banks, D.S. Silvester, L. Aldous, C. Hardacre, R.G. Compton, Electrochemical ammonia gas sensing in nonaqueous systems: a comparison of propylene carbonate with room temperature ionic liquids, Electroanalysis 19 (2007) 2194–2201.
[21] M. Buzzeo, D. Giovanelli, N. Lawrence, C. Hardacre, K. Seddon, R. Compton, Elucidation of the electrochemical oxidation pathway of ammonia in dimethylformamide and the room temperature ionic liquid, 1-ethyl-3-methylimidazolium bis (trifluoromethylsulfonyl)imide, Electroanalysis 16 (2004) 888–896.
[22] W. Shi, E.J. Maginn, Molecular simulation of ammonia absorption in the ionic liquid 1-ethyl-3-methylimidazolium bis(trifluoromethylsulfonyl)imide ([emim][Tf2N]), AICHE J. 55 (2009) 2414–2421.
[23] U. Kapoor, A. Banerjee, J.K. Shah, Evaluation of the predictive capability of ionic liquid force fields for CH_4, CO_2, NH_3, and SO_2 phase equilibria, Fluid Phase Equilib. 492 (2019) 161–173.
[24] J. Palomar, M. Gonzalez-Miquel, J. Bedia, F. Rodriguez, J.J. Rodriguez, Task-specific ionic liquids for efficient ammonia absorption, Sep. Purif. Technol. 82 (2011) 43–52.
[25] J. Bedia, J. Palomar, M. Gonzalez-Miquel, F. Rodriguez, J.J. Rodriguez, Screening ionic liquids as suitable ammonia absorbents on the basis of thermodynamic and kinetic analysis, Sep. Purif. Technol. 95 (2012) 188–195.
[26] T.M. Becker, M. Wang, A. Kabra, S.H. Jamali, M. Ramdin, C.A.I.F. David Dubbeldam, T.J.H. Vlugt, Absorption refrigeration cycles with ammonia–ionic liquid working pairs studied by molecular simulation, Ind. Eng. Chem. Res. 57 (2018) 5442–5452.
[27] M.S. Miran, H. Kinoshita, T. Yasuda, M.A.B.H. Susanz, M. Watanabe, Hydrogen bonds in protic ionic liquids and their correlation with physicochemical properties, Chem. Commun. 47 (2011) 12676–12678.
[28] P. Piecuch, V. Špirko, J. Paldus, Molecular quadrupole moment function of ammonia, J. Chem. Phys. 105 (1996) 11068–11074.
[29] M. Radiom, Ionic liquid–solid interface and applications in lubrication and energy storage, Curr. Opin. Colloid Interface Sci. 39 (2019) 148–161.
[30] H. Liu, H. Yu, Ionic liquids for electrochemical energy storage devices applications, J. Mater. Sci. Technol. 35 (2019) 674–686.
[31] F. Zhang, J. Liu, W. Yanga, B.E. Logan, A thermally regenerative ammonia-based battery for efficient harvesting of low-grade thermal energy as electrical power, Energy Environ. Sci. 8 (2015) 343–349.
[32] X. Zhu, M. Rahimi, C.A. Gorski, B. Logan, A thermally-regenerative ammonia-based flow battery for electrical energy recovery from waste heat, Chem. Sus. Chem. 9 (2016) 873–879.
[33] T. Zhang, Y. Wang, T. Song, H. Miyaoka, K. Shinzato, H. Miyaoka, T. Ichikawa, S. Shi, X. Zhang, S. Isobe, N. Hashimoto, Y. Kojima, Ammonia, a switch for controlling high ionic conductivity in lithium borohydride ammoniates, Joule 15 (2018) 1522–1533.
[34] A.J. Misquitta, A.J. Stone, Ab initio atom–atom potentials using Cam-CASP: theory and application to many-body models for the pyridine dimer, J. Chem. Theor. Comp. 12 (2016) 4184–4208.
[35] A.J. Misquitta, A.J. Stone, CamCASP: A Program for Studying Intermolecular Interactions and for the Calculation of Molecular Properties in Distributed Form, https://gitlab.com/anthonyjs/camcasp.
[36] C. Adamo, V. Barone, Toward reliable density functional methods without adjustable parameters: the PBE0 model, J. Chem. Theor. Comp. 110 (1999) 6158–6170.
[37] T.H. Dunnin Jr., Gaussian-basis sets for use in correlated molecular calculations. 1. The atoms boron throuch neon and hydrogen, J. Chem. Phys. 90 (1989) 1007–1023.
[38] R.A. Kendall, T.H. Dunnin Jr., R.J. Harrison, Electron-affinities of the 1st row atoms revisited - systematic basis sets and wave functions, J. Chem. Phys. 96 (1992) 6796–6806.
[39] A.J. Misquitta, A.J. Stone, F. Fazelli, Distributed multipoles from a robust basis-space implementation of the iterated stockholder atoms procedure, J. Chem. Theor. Comp. 12 (2014) (4184–42085405–5418).
[40] R.C. Rizzo, W.L. Jorgensen, Opls all-atom model for amines: resolution of the amine hydration problem, J. Am. Chem. Soc. 121 (1999) 4827–4836.
[41] M.J. Abraham, T. Murtola, R. Schulz, S. Páll, J.C. Smith, B. Hess, E. Lindahl, Gromacs: high performance molecular simulations through multi-level parallelism from laptops to supercomputers, SoftwareX 1 (2015) 19–25.
[42] D. van der Spoel, E. Lindahl, B. Hess, A. Van Buuren, E. Apol, P. Meulenhoff, D. Tieleman, A. Sijbers, K. Feenstra, R. Van Drunen, et al., Gromacs user manual version 4.0, Nijenborgh 4 (2005) 9747.
[43] W.L. Jorgensen, D.S. Maxwell, J. Tirado-Rives, Development and testing of the opls all-atom force field on conformational energetics and properties of organic liquids, J. Am. Chem. Soc. 118 (1996) 11225–11236.
[44] L. Martínez, R. Andrade, E.G. Birgin, J.M. Martínez, Packmol: a package for building initial configurations for molecular dynamics simulations, J. Comput. Chem. 30 (2009) 2157–2164.
[45] C. Girardet, A. Lakhlifi, NH_3 inversion in condensed media. Static, dynamic, and inhomogeneous environmental effects on the internal tunneling, J. Chem. Phys. 91 (1989) 2172–2180.
[46] G. Feng, J. Zhang, R. Qiao, Microstructure and capacitance of the electrical double layers at the interface of ionic liquids and planar electrodes, J. Phys. Chem. C 113 (2009) 4549–4559.

[47] Q. Dou, M. Sha, H. Fu, G. Wu, Molecular dynamics simulation of the interfacial structure of [cnmim][PF_6] adsorbed on a graphite surface: effects of temperature and alkyl chain length, J. Phys. Condens. Matter 23 (2011) 175001.
[48] S.A. Kislenko, I.S. Samoylov, R.H. Amirov, Molecular dynamics simulation of the electrochemical interface between a graphite surface and the ionic liquid [bmim][PF_6], Phys. Chem. Chem. Phys. 11 (2009) 5584–5590.
[49] M.A. Gebbie, M. Valtiner, X. Banquy, E.T. Fox, W.A. Henderson, J.N. Israelachvili, Ionic liquids behave as dilute electrolyte solutions, Proc. Natl. Acad. Sci. U. S. A. 110 (2013) 9674–9679.
[50] M.Z. Bazant, B.D. Storey, A.A. Kornyshev, Double layer in ionic liquids: overscreening versus crowding, Phys. Rev. Lett. 106 (2011) 046102.

USC UNIVERSIDADE DE SANTIAGO DE COMPOSTELA

Journal of Molecular Liquids 333 (2021) 115883

Contents lists available at ScienceDirect

Journal of Molecular Liquids

journal homepage: www.elsevier.com/locate/molliq

Computational study of the structure of ternary ionic liquid/salt/polymer electrolytes based on protic ionic liquids

José M. Otero-Mato [a,1], Alejandro Rivera-Pousa [a,1], Hadrián Montes-Campos [a], Oscar Cabeza [b], A. Heuer [c,d], D. Diddens [d], Luis M. Varela [a,*]

[a] Grupo de Nanomateriais, Fotónica e Materia Branda, Departamento de Física de Partículas, Universidade de Santiago de Compostela, Campus Vida s/n E-15782, Santiago de Compostela, Spain
[b] Facultade de Ciencias, Universidade da Coruña, Campus A Zapateira s/n E-15008, A Coruña, Spain
[c] Institute of Physical Chemistry, University of Münster, Corrensstraße 28/30, 48149 Münster, Germany
[d] Helmholtz-Institute Münster (HI MS), Ionics in Energy Storage, Forschungszentrum Jülich GmbH, Corrensstraße 46, 48149 Münster, Germany

ARTICLE INFO

Article history:
Received 11 January 2021
Received in revised form 26 February 2021
Accepted 8 March 2021
Available online 11 March 2021

Keywords:
Ionic liquids
Polymer electrolytes
Structure
Lithium
Molecular dynamics simulation

ABSTRACT

The stability of binary mixtures of several protic ionic liquids (ethylammonium nitrate, ethylammonium acetate and ethylammonium tetrafluoroborate) with polyethylene oxide is studied by means of molecular dynamics simulations. The solubility range is seen to be wider for ethylammonium acetate, and the structure and single-particle dynamics of its ternary mixtures with lithium acetate are then studied. The structure of liquid mixtures of lithium acetate with the ionic liquid is seen to be seldom modified by the addition of the polymer, with very limited hydrogen bonding between the ionic liquid and the polymer taking place. Moreover, lithium is seen to be solvated in the liquid phase forming $[Li(ACE)_4]^{-3}$ tetrahedral complexes irrespective of the presence of the polymer, with very limited binding of metal cations to oxygen atoms in the polymer backbone. Hence, the registered single particle dynamics and lithium transport takes place in practically the same way as in the liquid phase with almost no interference of the polymer, contrarily to previously reported results for other ionic liquids.
© 2021 Elsevier B.V. All rights reserved.

1. Introduction

Ionic liquids (ILs) have proved to be very versatile materials in a wide range of applications including lubricants, catalyzers for chemical reactions, gas storage, electrolytes for batteries or supercapacitors among others [1–9]. This is mainly due to interesting properties such as very low vapor pressures, high thermal stability, wide electrochemical windows or non-flammability among others. Moreover, these properties can be tuned for a specific task with the right choice of anions and cations forming the IL. Focusing on their good electrochemical properties, ILs have been applied in multiple electrochemical devices, particularly in batteries and supercapacitors [10,11].

On the other hand, another kind of materials that also have shown to be very promising in this field, mainly because of their mechanical properties, are binary polymer+salt mixtures [12–15]. In order to benefit from the appropriate mechanical properties (rigidity) of these systems, as well as from their relatively high electrical conductivities, lots of efforts have been invested in the study and characterization of ternary polymer+salt+IL ionogels [13,16–19]. However, the majority of these studies were focused on the use of ILs based on N-methyl-N-propylpyrrolidinium bis(trifluoromethylsulfonyl)imide anion, NTf_2^-, or imidazolium based cations. Indeed, it has been proved experimentally that the addition of IL to the binary polymer+salt mixtures results in an increment of the ionic conductivity at low salt concentrations [13,17–20]. This phenomenon is related to the fact that with the addition of ILs the number of charge carriers increases and, moreover, it acts as plasticizer and induces an enhancement of the segmental motion and the center-of-mass-diffusion of the polymer, the latter contribution becoming irrelevant in the limit of long chains. On the other hand, later theoretical studies supported by molecular dynamics (MD) simulations performed by Diddens et al. [17,18], proved that the ionic diffusion of lithium cations in this kind of ternary mixtures with the IL $[PYR_{13}][NTf_2]$ is the cumulative result of four different Li^+ transport mechanisms: Li^+ hopping between adsorption sites along the polymer backbones, hopping between different polymer chains, diffusion along with the polymer in which the lithium cation is adsorbed, and, finally, Li^+ diffusion in the IL + salt binary mixture inside the nanocavities in the polymer matrix. In other words, there is a component of the diffusion that is linked to the Li^+ adsorption in the polymer and another one that is linked to the ionic diffusion inside the IL. More precisely, while for rather low lithium-salt concentrations it was observed that Li^+ preferentially binds to the polyether chain due to the multidentate, crown-ether-like coordination structure [17], the fraction of lithium ions that are solely coordinated to IL anions becomes more significant

* Corresponding author.
E-mail address: luismiguel.varela@usc.es (L.M. Varela).
[1] Contributed equally to this work.

USC UNIVERSIDADE DE SANTIAGO DE COMPOSTELA

https://doi.org/10.1016/j.molliq.2021.115883
0167-7322/© 2021 Elsevier B.V. All rights reserved.

at higher lithium salt concentrations [18], as also observed in nuclear magnetic resonance ^{1}H microimaging experiments [21], or when using functionalized coordinating cations [22]. Mogurampelly and Ganesan [19] also studied computationally the structure and diffusion of lithium cations in these ternary systems, but now with an IL based on imidazolium cations (1-butyl-3-methylimidazolium hexafluorophosphate, [BMIM][PF_6]). They also reported Li^+ adsorption in the backbones of the polymers and an increment in the diffusion of Li^+ as the IL amount increases. All these studies have focused on ternary mixtures with aprotic ILs (AILs). In this work we are interested in the characterization of the applicability of protic ILs (PILs) in these systems, because their synthesis is more accesible compared with that of AILs. Besides, there are studies that suggest an enhancement of Li^+ transport in PILs [23]. Specifically, using atomistic MD simulations we report the structure of ternary mixtures of a PIL, a lithium salt and polymers with a specific focus on the adsorption of Li^+ cations on the polymer backbones and we compare the results with some previously reported ones for mixtures with different ILs. The IL selected for this study was the ethylammonium acetate ([EA][ACE]), as our results regarding the solubility of our employed polymer (polyethylene oxide, PEO) suggest this IL is the optimal candidate out of three studied ones: [EA][ACE], [EA][BF_4] and [EA][NO_3]. We are also interested to see if the IL loading may or may not affect the conductivity in these systems.

In the next section of the paper the simulation details for all the performed steps are presented. There, a new algorithm for the random packing of large molecules inside simulation boxes is also explained. The solubility study and the simulation results are discussed in the section 3. Finally, the main conclusions are summarized in the last section.

2. Simulation details

MD simulations of binary mixtures of PEO and either [EA][ACE], [EA][BF_4] or [EA][NO_3], as well as ternary mixtures of PEO, [EA][ACE] and [Li][ACE] were performed using Gromacs 2019 [24,25]. The binary systems were simulated to study the miscibility of the polymer-IL mixtures, whereas the most promising IL, [EA][ACE], was employed in the ternary electrolytes to investigate the lithium ion solvation in these materials. We used the OPLS-AA force-field [26] to describe the molecular interactions of PEO, EA^+, and ACE^+, while the CL&P force field [27–29] (which is compatible with OPLS-AA) was used for BF_4^- and NO_3^-. The parameters for Li^+ were taken from Ref. [30].

To study the miscibility and the phase behaviour of binary PEO-IL mixtures in a first step, we performed Replica Exchange Molecular Dynamics (REMD) simulations with 64 replicas at temperatures between 300 K and 558 K. The individual temperatures were chosen according to the algorithm in Ref. 31. The resulting exchange probability was about 0.2, and an exchange attempt was made every 2 ps. Two different scenarios have been considered: A many-chain system comprised of 20 PEO chains with 20 monomers each and 400 IL ion pairs, as well as a single PEO chain with 20 monomers immersed in 500 IL ion pairs. The REMD simulations at each temperature had a length of 30 ns, amounting to almost 2 μs of total simulation time.

The initial configurations were obtained by randomly packing the molecules in a simulation box using the Packmol software [32]. The PEO chains used in the packing process were in a fully stretched conformation. We simulated this very artificial configuration in the *NpT* ensemble at a temperature of $T = 500$ K and a reference pressure of $p = 100$ bar, maintained by a Berendsen thermostat and barostat [33], for 10 ns with a time step of 0.5 f. to allow the simulation box size to reduce and obtain a dense system. Electrostatic interactions have been turned off in this step to promote mixing of the system's components, and a cutoff radius of 1.2 nm has been used to truncate the Lennard-Jones interactions. It has to be mentioned that such a low value of the time step (0.5 fs) was required to guarantee the consistency of the solution of the motion equations, due to the initial artificial molecular configuration and high pressures, which are strongly related to the high forces that therefore appear in these equations. Then, we simulated an annealing from 500 K to 300 K over 30 ns with an elementary time step of 2 f. to cool down the system, and finally we performed a 120 ns run at room temperature ($T = 300$ K) to stabilize the system. Here, a cutoff radius of 1.4 nm has been used for all nonbonded interactions, and the long-ranged part of the electrostatic interactions has been treated by the particle Mesh Ewald (PME) method [34,35] with a grid spacing of 0.12 nm and sixth-order interpolation.

Bonds involving hydrogen atoms were constrained by the LINCS algorithm [36]. The resulting structures both served as input for the REMD simulations of the binary systems (with [EA][ACE], [EA][BF_4] or [EA][NO_3]) and the conventional MD simulations of the ternary systems (only [EA][ACE], see below for the remaining simulation procedure).

For [EA][ACE], which showed the best miscibility out of the three ILs considered in the REMD simulations (see discussion below), we subsequently performed conventional MD simulations of ternary PEO/[EA][ACE]/[Li][ACE] electrolytes to study the lithium ion coordination and dynamics in these materials. While the OPLS-AA/CL&P force field usually reproduces thermodynamic properties accurately, the main problem of this non-polarizable description is the underestimation of the molecular mobility [37,38]. This means that in order to obtain a realistic molecular configuration starting from a completely random distribution, very long stabilization runs will be needed.

This is even more so when starting from fully stretched chain conformations as in our case, and when studying multiple [Li][ACE] salt concentrations. On the other hand, REMD simulations are costly as well, as typically a larger number of replicas is employed to span a wider temperature range (see above). Therefore, to obtain realistic polymer structures as input for the ternary systems in a computationally expedient way, we started the simulation process from the well stabilized simulation boxes containing binary PEO/[EA][ACE] that also served as input for the REMD simulations, in which especially the polymer chains have equilibrated, coiled structures.

Another issue that needs to be considered when these configurations are used to create new random initial simulation boxes is related to the periodic boundary conditions (pbcs). We observed that if all the polymer chains were packed randomly inside a simulation box together with the rest of the components, the resulting output at the end of the simulation will contain all the polymers in a central region of the box surrounded by the mixture of the IL and the salt. This is mainly because the software used for the packing does not take into account pbcs and because of the slow motion of the polymers compared with the smaller components in the systems, which are able to occupy much faster the artificially empty space left in the packing process at the edges of the box. To solve this, we encapsulated all the polymer chains in the new simulation boxes using a sequential approach: we first inserted one polymer with a configuration obtained from the previous MD run into an empty cubic box with an estimated side length that reproduces the density of the previous simulation. Then, the position of the polymer was shifted by a random linear vector displacement. To ensure that all atoms were inside the simulation box, pbcs were applied. Then, a new polymer chain (extracted from the previous simulation) was randomly introduced in the free space of this box using Packmol. Once again, all the positions of the polymers in the box were randomly shifted and pbcs were applied. These steps were repeated until all the 20 simulated polymer chains are properly placed inside the box, which is finally filled with the salt and/or IL molecules. With this algorithm we obtained a more realistic random initial configuration without the restriction of the polymer chains being completely inside the simulation box. A representation of the steps of this algorithm is shown in Fig. 1. It has to be highlighted that this algorithm can be used to generate initial random configurations for a wide variety of systems, specially when large molecules are involved. An implementation of this algorithm can be found here: [https://github.com/txemaotero/large-molecule-pbc-packing]. The simulation steps from this point include all the standard procedures in a MD simulation. First, an energy minimization of the system using a

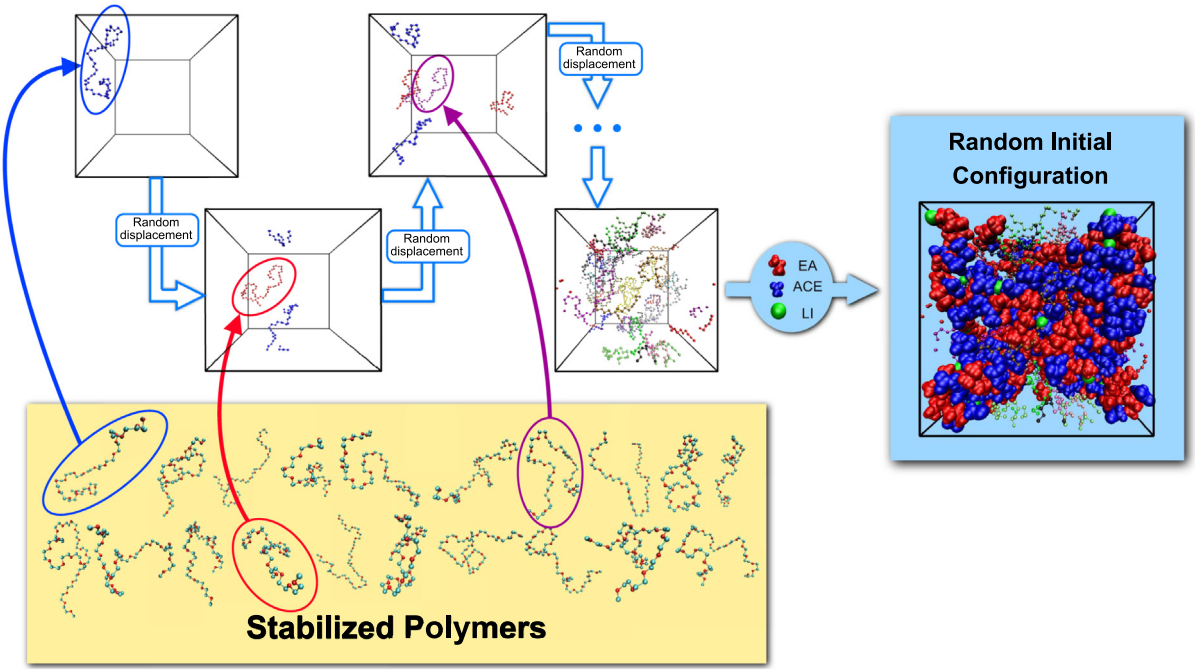


Fig. 1. A representation of the algorithm used to generate the initial configurations for the simulations. The polymers are represented without the hydrogen atoms as well as using small sizes for the atoms beads for a better visualization.

conjugated gradient algorithm, followed by a short NVE stabilization run of 50 ps and a longer NPT stabilization run of 20 ns, at a temperature of 300 K and 1 atm of pressure. Finally, a NPT production run of 20 ns at 300 K and 1 atm, saving the positions and velocities of the atoms each 1 ps. For the single particle dynamics, shorter simulation runs were performed, each of 1 ns, where the velocities of the atoms were saved in every simulation step, i. e., each 2 fs. It has to be noted that the 20 ns of the production runs are not enough to allow the polymers to significantly change their molecular configuration. So, to cover much more diverse polymer configurations we created 10 random initial simulation boxes following the algorithm mentioned above and simulating each one of them. The final results shown in this manuscript are those from the average for all the production runs starting from different configurations.

We performed simulations following the steps mentioned above for different concentrations of [Li][ACE], i.e., ratios of ionic pairs between [Li][ACE] and [EA][ACE] of {0.1, 0.2, 0.25, 0.5, 0.75, 1}. In all the systems there were 500 ion pairs comprising [EA][ACE] and [Li][ACE] pairs, depending on the desired salt concentration. We also performed simulations without any polymer chain at a molar fraction of 0.1 for further comparison.

3. Results and discussion

In a first step, we studied the miscibility and the phase behaviour of the binary PEO/[EA][ACE] mixtures, to which end we studied both many-chain systems and single chain systems. Typical snapshots from the REMD simulations for different temperatures between 300 and 500 K are shown in Fig. S1, S2 and S3 in the Supporting Information (SI). Note that only the PEO chains are visible in this representation to be sensitive to any aggregation or crumpling of the polymers. For PEO/[EA][ACE], we observe a minor degree of PEO clustering for all studied temperatures, specially at temperatures of the PEO below 500 K, demonstrating that PEO and the IL appear to be well mixed. In contrast, for PEO/[EA][BF_4] and PEO/[EA][NO_3], aggregation of the PEO chains seemingly sets in already at lower temperatures, although at temperatures below 400 K a certain degree of mixing can be observed. Interestingly, a lower critical solution temperature (LCST) has also been observed for binary PEO/[BMIM][BF_4] mixtures, which was attributed to the existence of hydrogen bond-like interactions between the protons of the imidazolium ring and the PEO oxygen atoms [39]. These interactions become entropically unfavorable at high temperatures, thus minimizing the polymer-IL interface and favoring demixing [39].

To study these effects in more detail, we also performed REMD simulations of a single PEO chain immersed in the three individual ILs. The corresponding simulation snapshots are depicted in Fig. S4 in the SI. We observe that in PEO/[EA][ACE] the PEO chain has a coiled conformation both at high ($T = 550$ K) and low ($T = 300$ K) temperatures, whereas in PEO/[EA][BF_4] and PEO/[EA][NO_3] the chains rather adopt a crumpled, globular shape, particularly at 300 K, in agreement with our observations for the many-chain system. This is further confirmed in Fig. 2, which shows the average end-to-end vector R_e and radius of gyration R_g as a function of temperature. In [EA][ACE], the PEO chain has the largest spatial extension, which becomes most pronounced at low temperatures. Contrarily, in [EA][BF_4] and [EA][NO_3], the PEO chains have shorter R_e and R_g, which again becomes most pronounced at low temperatures. In total, the PEO structure in [EA][BF_4] and [EA][NO_3] is rather similar. Fig. 2 also shows the ratio of the mean squared end-to-end vector and the mean squared radius of gyration, i.e. $\langle R_e^2\rangle/\langle R_g^2\rangle$. For an ideal coiled chain, obeying a Gaussian distribution for the segment lengths, $\langle R_e^2\rangle/\langle R_g^2\rangle = 6$. In case of PEO/[EA][ACE], a value of six is attained at 300 K, whereas lower values – indicating a more globular structure – are found at higher temperatures, as well as for [EA][BF_4] and [EA][NO_3] throughout the entire temperature range. The phenomenology behind this change from coiled to globular configuration of the polymer in [EA][ACE] when the temperature increases is the same than that behind mixtures of PEO with [BMIM][BF_4] [39], i.e., at high temperatures the hydrogen bonding interactions become entropically unfavorable and thus the IL becomes a bad solvent for the polymer. Choi and Yethiraj supported this hypothesis by calculating the potential of the mean force (PMF) related with the hydrogen bond formation between the cations and the polymer. They showed that at high temperatures the minimum of the PMF indicating the hydrogen bond formation disappeared. To check if this is the case for [EA][ACE] we calculated the PMF between

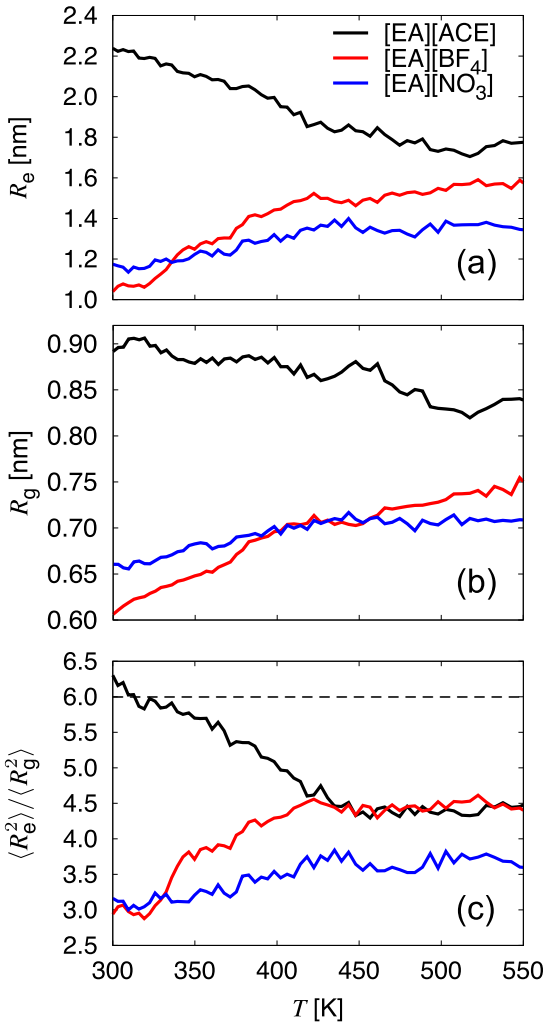


Fig. 2. Average end-to-end vector R_e (a) and radius of gyration R_g (b) of PEO in the REMD simulations comprising a single PEO chain with 20 monomers and 500 IL ion pairs. The ratio of the two mean squared radii, $\langle R_e^2\rangle/\langle R_g^2\rangle$, is shown in (c). For a Gaussian chain $\langle R_e^2\rangle/\langle R_g^2\rangle = 6$, which is represented with a dashed line.

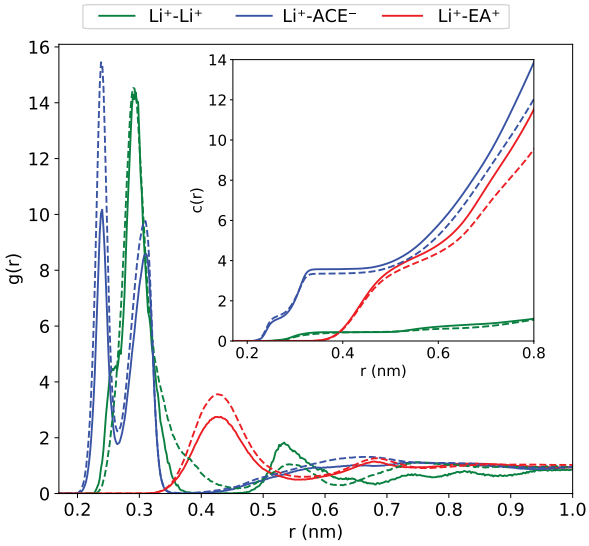


Fig. 3. RDFs between Li^+ and the other molecular species presented in mixtures with 10% of lithium salt with (dashed lines) and without (solid lines) polymers. The corresponding coordination numbers are also represented in the inset.

N—H groups of the EA^+ and oxygen atoms of the PEO for simulations of a single frozen coiled polymer chain immersed in the IL at 300 and 500 K. The results are shown in Fig. S5 in the SI and it is clear that at high temperatures the coordination of the cation and the polymer becomes very unfavorable in terms of the free energy, which explains the globular PEO configurations at high temperatures. Therefore, we conclude that at ambient temperatures, PEO has the largest solubility in [EA][ACE], and hence chose this IL for our study of the ternary electrolytes.

To characterize how the protic nature of [EA][ACE] IL changes the properties of the ternary polymer gels that we are interested in, specifically the ones related with Li^+ transport mechanisms, relative to previously reported results for similar mixtures with other ILs [16,17,19], the first thing that we can analyze is how the presence of the polymer affects the environment of Li^+ cations in the bulk. To do that we have calculated the radial distribution functions (RDFs) between the different molecular species in the system with 10% of lithium salt, with and without the polymer. For the calculation of these functions the position of the center of mass of the molecules was taken as reference point for the distance calculations. These RDFs are plotted in Fig. 3. Very minor changes are observed in the Li^+ environment with the addition of polymer. The coordination distance with all the molecular species remains constant, i.e., the peaks of the RDFs are located at the same distance and only a slight increase in the height of the first peaks of the RDFs with ACE^- and EA^+ are registered. This usually means that there is a stronger coordination between the species. However, the normalization for the RDFs in the systems with and without the polymers could be playing a role in this comparison. For a better comparison of this coordination strength we calculate the coordination number of the same species around the Li^+, i.e., the average number of the different molecules around each Li^+ cation. These curves are also represented in Fig. 3. Now it is more evident that at short distances (less than 0.5 nm) the coordination is almost identical for all the species. The polymer only causes a slightly weaker coordination between the systems, likely caused by the polymer preventing the homogeneous distribution of one species around another. As one could expect, for larger distances the coordinations are notably higher in the simulations without polymers, as there are no regions excluded by the chains and the molecules can fill the whole simulation box. At this point, our results suggest that the structure of the liquid mixture remains the same when the polymer chains are solvated in the system, meaning that Li^+ cations are preferentially coordinated with the IL anions. This is not the case when $[Pyr_{13}][NTf_2]$ + $[Li][NTf_2]$ mixtures are considered [18]. Diddens et al. reported that, for those systems, when the polymers were added to the IL + salt mixture, a significant fraction of Li^+ cations are preferentially coordinated with the oxygen atoms in the polymer chains instead of with the oxygen atoms in the NTf_2^-. As they pointed out, the main mechanism of transport of Li^+ cations in these ternary systems, specially at low lithium salt concentrations, is through the polymer chains. This difference in behaviour relative to our findings possibly suggests a much higher stability of the Li^+-ACE_4^- tetrahedral complex in PEO-[EA][ACE] mixture compared to $Li^+[NTf_2]_2^-$ linear complexes in PEO-$[Pyr_{13}][NTf_2]$, so lithium cations are not able to break its coordination complexes in the former case. The comparatively stronger Li^+-ACE^- coordination can be rationalized by the fact that the negative charge is more distributed across the larger NTf_2 anion as compared to ACE^-, resulting in weaker electrostatic interactions of Li^+ with the latter.

To check if a similar diffusion mechanism of lithium cations through the polymer chains takes place in our systems with [EA][ACE], we studied the coordination of Li^+ with the oxygen atoms of the polymer chains. We represent in Fig. 4 the RDFs between the polymers and the rest of the components for all the simulated salt concentrations. The first thing that can be noticed looking at these RDFs is that the change

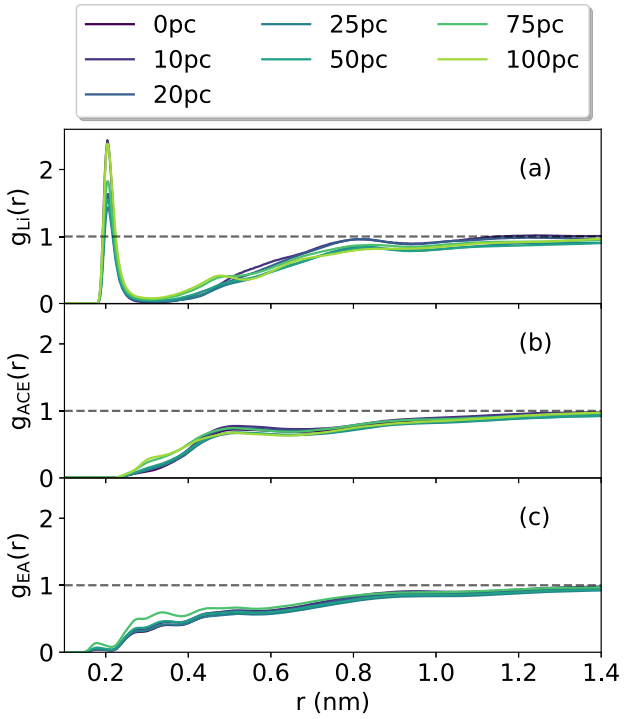


Fig. 4. RDFs between the oxygen atoms of the polymer chains and the Li^+ (a), ACE^- (b) and EA^+(c) for all the simulated salt concentrations. The horizontal black dashed lines placed at $g(r) = 1$ are represented to mark the ideal distribution.

in the molar fraction of lithium salt does not significantly affect the ionic distribution around the polymer chains and only slight changes in the height of the first peak in the RDFs with Li^+ are registered. As we indicated before, these changes in the height of the RDFs may be related with changes in the coordination around the polymer, which will be more detailed below in context with Fig. 8. Another interesting phenomenon that can also be observed is that the RDFs of the ACE^- and EA^+ around the polymers are always below 1 in the studied distances for all the salt concentrations. This means that the probability of finding an ACE^- or an EA^+ around an oxygen atom of the polymer is lower than in the case of a random distribution of ions in the mixture. It must be mentioned that when the molecular distributions around the oxygen atoms of the polymers are analyzed, there is a region that can not be filled with any species due to the presence of the rest of the polymer chain. So, even if any species is randomly distributed around the polymers the values of its RDFs would be lower than 1. In this line, looking at our results, although we cannot ensure that there is an absence of coordination, we can conclude that there is no preferential adsorption of ACE^- or EA^+ on the polymer backbone. Similar distributions were reported by Mogurampelly and Ganesan [19] when similar ternary mixtures of PEO, the [BMIM][PF_6] IL and [Li][PF_6] salt were considered. They reported how the distribution of $BMIM^+$ cations around the polymer chains change when varying the salt percentage. Their results showed that there was indeed a preferential adsorption of the $BMIM^+$ cations around the monomers that was damped down as the salt concentration increased. They also reported the distribution of lithium cations around the monomers showing a very similar distribution as the one that we obtained with a coordination shell located at the same distance but much higher than in our simulations, i.e., their maxima reach values around 23 while ours do not exceed 2.5. So, we can conclude that lithium cations are preferentially solvated in the bulk IL + salt mixture when this IL, [EA][ACE], is used, instead of being adsorbed in the polymer monomers, as it happens when the [BMIM][PF_6] IL is considered. It is also remarkable that the results suggest a better solvation of the polymers in [BMIM][PF_6] than in [EA][ACE] as the polymer-ion interaction showed to be stronger in the first case. Indeed, some works show that PEO has some hydrophobic character [40], so it could be better solvated in the hydrophobic [BMIM][PF_6] [41]. We also took into account the hydrogen bond network present in the system by calculating the mean number of hydrogen bonds per donor molecule (in our case, EA^+). We show the results in Fig. 5. As we can see, the amount of hydrogen bonds between the IL components decreases as we increase the salt concentration in the system. This reinforces the idea that the lithium cations are strongly coordinated with the ACE^- anions, removing some of the hydrogen bonding between EA^+ and ACE^-. As a result, the ethylammonium cation is more free to form some hydrogen bonds with the polymer. The presence of the polymer does not seem to disturb the hydrogen bond network, as the simulations without polymeric chain and a 10% Li^+ concentration has an average of 3.23 hydrogen bonds between EA^+ and ACE^- per EA^+ molecule, a value compatible with those reported earlier.

Up to now all the results suggest that the addition of polymers to the binary IL + salt mixture considered here does not significantly affect its liquid structure, and lithium cations seem to be the only species that significantly interacts with the polymers, as it was showed by the previously discussed RDFs. In order to have a better insight into the effect of the polymer on the molecular environment of the simulated species we calculated the vibrational power spectrum, which is nothing more than the Fourier transform of the velocity autocorrelation function,

$$\Phi(\omega) = \left(\frac{1}{\sqrt{2\pi}}\int_{-\infty}^{\infty} e^{i\omega t}\langle\vec{v}(0)\cdot\vec{v}(t)\rangle dt\right)^2. \quad (1)$$

This magnitude gives us an idea of the vibrational spectrum of the molecules inside their coordination shells. These spectra for Li^+, EA^+ and ACE^- ions are represented in Fig. 6 for the systems with 10% of lithium salt with and without polymers. If the presence of PEO chains induces structural changes in the binary mixture, changes in the molecular environment of each species are expected, which, in turn, translates into differences in the vibrational spectrum (see Ref. 42 for a discussion of how the changes in these spectra can be related with changes in the molecular environment, specially for simulations where complexes with Li^+ close to interfaces are involved). However, the results shown in Fig. 6 are almost identical for simulations with and without polymers, and only tiny differences can be seen in the region around 600 cm^{-1} for the spectrum of Li^+, which are surely related with the coordination mentioned before between Li^+ and the PEO

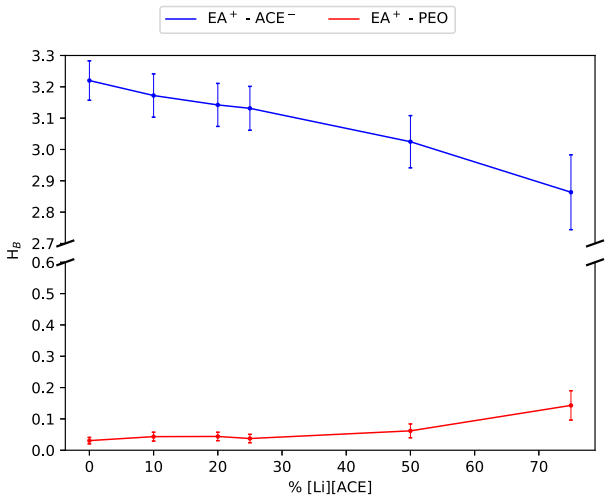


Fig. 5. Mean number of hydrogen bonds per donor molecule (EA^+) between the EA^+ molecule and the ACE^- anion (blue line) and the EA^+ cation and polymer chains (blue).

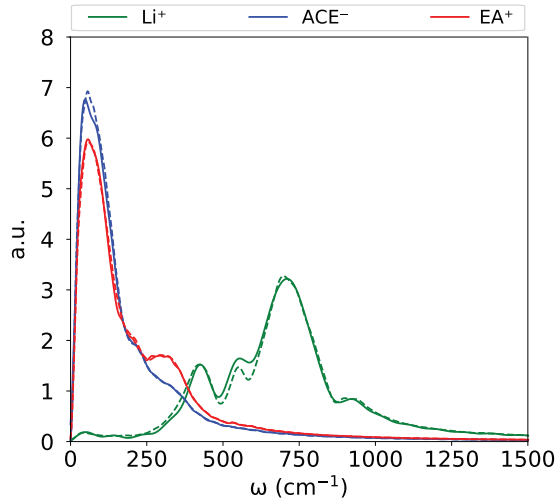


Fig. 6. Vibrational power spectrum for Li^+, ACE^- and EA^+ ions for the systems with 10% of lithium salt with (dashed lines) and without (solid lines) polymers.

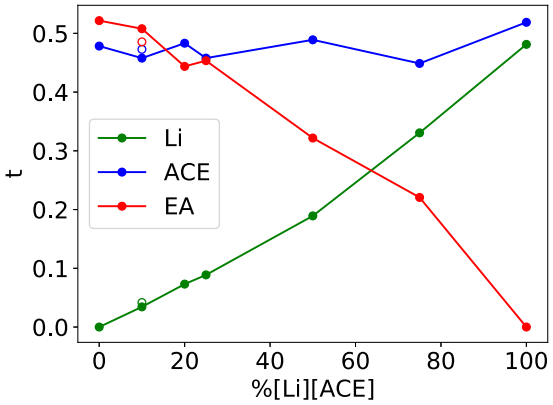


Fig. 7. Transport numbers for all the ionic species in the simulations with different [Li][ACE] concentration. The numbers for the simulation of 10% of [Li][ACE] without polymer are also represented as empty dots.

oxygen atoms. Apart from this slight difference, the results are compatible with the hypothesis that PEO does not significantly affect the IL + salt mixture structure in this reported case.

We also used the calculated velocity autocorrelation functions to compute the self-diffusion coefficients of each ionic species as:

$$D_i = \frac{1}{3}\int_0^\infty \langle \vec{v}_i(0)\cdot\vec{v}_i(t)\rangle dt. \quad (2)$$

As it was mentioned before, the molecular dynamics is expected to be quite underestimated when non-polarizable force-fields are used. This means that the self-diffusion coefficients calculated with eq. 2 are considerably lower than the experimental ones. However, if we suppose that the dynamics of all the ionic species are affected in the same way, a proper qualitative comparison between anions and cations can be made. To perform this comparison we calculated the transport numbers of the charged species:

$$t_i = \frac{\sigma_i}{\sigma}, \quad (3)$$

where σ_i is the contribution to the electric conductivity by the ionic species i and σ is the total electric conductivity of the system. To compute the conductivities we used the Nernst-Einstein approximation:

$$\sigma = \sum_i \sigma_i = \frac{e^2}{VK_BT}\sum_i N_i D_i, \quad (4)$$

where e is the charge of the electron, V the volume of the simulation box, k_B the Boltzman constant, T the temperature and N_i the number of i ions in the simulation. Calculating the conductivities in this way has the drawback that correlations between different ions are not taken into account, so the results should be prudently analyzed, but for the purpose of this study, this level of approximation showed to be accurate enough. The obtained transport numbers for all the simulated [Li][ACE] concentrations as well as those obtained for the 10% without polymer chains are represented in Fig. 7. We can see that approximately half the conductivity is associated to the acetate anions and the rest to the cations in the whole range of concentration. Lithium cations gradually replace the role of the EA^+ in the conductivity as the concentration of [Li][ACE] increases. However, the most remarkable conclusion, which can be made looking at the comparative with the numbers from the system without polymer, is that the addition of polymer has a negligible effect in the conductivities of each ion. In other words, the presence of polymer not only leaves the structure of this IL unaffected, but also the essentials of the charge transport mechanism.

The theory developed by Maitra et al. [43] and Diddens et al. [17,18,22] about Li^+ diffusion in this kind of systems states that one of the keys in the Li^+ transport is its adsorption on the polymer chains. If Li^+ is not adsorbed in the polymer only one of the four transport mechanisms described in Ref. [17, 18, 22] appears, which is the diffusion of lithium cations in the binary mixture inside the cavities produced upon the entanglement of the polymer chains. To see if the other three mechanisms (hopping between monomers, between different chains and diffusion of the attached polymer chain) play any role in our systems, we calculated the percentage of lithium cations that can be considered to be adsorbed in the polymers. In view of the already discussed RDFs, we considered that a Li^+ cation is adsorbed at the oxygen atoms of the polymer when it is closer than 3 Å from it. This result must be compared to the percentage of salt that would meet our criteria if Li^+ was distributed homogeneously in the cavities formed by the polymer. Although we know that the lithium cations are mostly coordinated with the anions, this image is equivalent to a mean field description of the structure of the ionic liquid + salt mixtures. To obtain this value, we calculated the free volume left by the polymer chain in our simulation box (FV). After that, we performed the same calculation, but with a twist: the size of the oxygen atoms of the polymers was artificially enlarged to a radius of 3 Å, so that the volume obtained matched exactly the free volume that does not meet our criteria (FV_O). With these two values we can calculate the theoretical percentage of adsorbed Li^+ if they were randomly distributed as:

$$\%\text{Random} = \frac{FV - FV_O}{FV}. \quad (5)$$

On the other hand, we can calculate the percentage obtained in the simulations dividing the number of adsorbed Li^+ cations by the total number of Li^+ in each frame and average this magnitude for all the frames in each simulation (%Simulated). We can see the proportion between these two results in Fig. 8. The error bars associated to each value correspond to the standard deviation at the average values from the different simulations of each salt concentration. Looking at the figure it seems reasonable to conclude that a random distribution of the Li^+ is compatible with the obtained results in the whole range of salt concentration. This is again in agreement with the picture that we were drawing up to now, i.e., the polymer does not affect significantly the structure of the binary mixture.

To highlight even more the difference of the Li^+ adsorption with that in other ILs we can notice that the average percentage of Li^+ adsorption in all our simulation is around 7%, while Diddens et al. [17] reported a

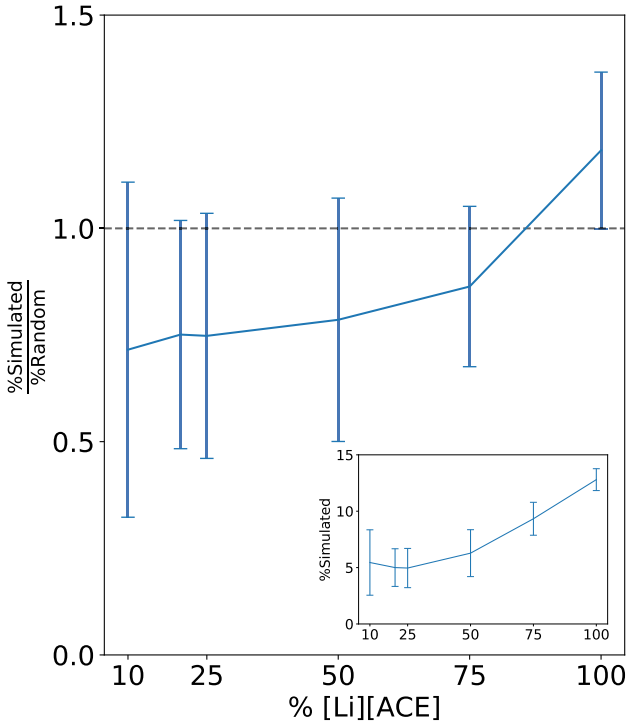


Fig. 8. Relative Li^+ adsorption compared with random distribution for all the simulated salt concentrations. The horizontal dashed line represents an adsorption compatible with a random distribution. The absolute percentage of coordinated Li^+ is represented in the inset.

value of 60% for $[PYR_{13}][NTf_2]$. Moreover, it was reported by them that the addition of IL promotes Li^+ adsorption in the polymer backbone, i. e. the percentage of adsorbed lithium cations increases as the salt percentage in the system decreases. This was also observed by Mogurampelly and Ganesan [19] for systems with $[BMIM][PF_6]$. This is just the opposite behaviour that we observe in our systems, where a slight increase in the adsorption is shown as the amount of salt increases. In the case of the systems with aprotic $[PYR_{13}][NTf_2]$.the addition of IL leads to a situation where the anions preferentially coordinate with the IL cations leaving part of the Li^+ cations free to coordinate with the polymer backbone. Mogurampelly and Ganesan [19] supported this hypothesis showing that the distribution of Li^+ around PF_6^- revealed weaker interactions as the amount of IL increases, also showing that the number of free Li^+ cations, i.e., those not coordinated with any anion, increased in the same conditions. With the results reported up to now we expect the opposite behaviour for our systems. In Fig. 9 the RDFs of Li^+ around ACE^- anions are plotted. These RDFs provide the first evidence that the phenomenology in the ternary mixtures under this study follows the opposite trend that in systems with other ILs. We can see that, as the amount of salt increases the height of the coordination peaks decreases, specially that of the first one, contrary to what happens in the study by Mogurampelly and Ganesan [19]. It has to be mentioned that the double-peak shape of these RDFs is very common in the coordination between Li^+ and its anions and corresponds with two different adsorption sites of Li^+ around anions (see Ref. 44). These two types of coordination, monodentate and bidentate, can be better observed in the spatial distribution depicted in Fig. 9. Mogurampelly and Ganesan also reported a notable decrease in the coordination of Li^+ cation around the IL anions as the amount of salt decreases both in the first and second solvation shell which supported the idea of the release of Li^+ when the amount of IL cations increases. To corroborate that this does take place in our systems we calculated how the amount of ACE^- anions surrounding each Li^+ changes with salt concentration, i. e., the coordination numbers of ACE^- around Li^+. These are also shown in Fig. 9. One should expect the amount of ACE^- anions around the Li^+ to decrease significantly if the same phenomenology as with previously studied ILs undergoes our systems. However, we see that it actually increases in the first coordination shell and there is only a slight decrease from 3.7 to 3.3 in the second one when the percentage of IL increases. Moreover, all of these coordination numbers are compatible with the ones obtained for the system without polymer, which again reinforces our hypothesis about the resilience of the structure of the binary mixture upon the addition of polymer. With these results we can conclude that the $[Li(ACE)_4]^{3-}$ complexes formed by the Li^+ and ACE^- anions are so stable that their adsorption on the polymer backbone via interactions with oxygens in the polymer backbone does not thermodynamically compensate their breaking up. The last thing that we calculated to support this hypothesis was the fraction of Li^+ cations in the systems that are not coordinated by IL anions, i.e., the percentage of free lithium cations and, indeed, the results obtained for all the simulated concentrations, were all very close to zero (they range from 0 to 1%), which is another evidence of the high stability of Li^+- - ACE^- complexes.

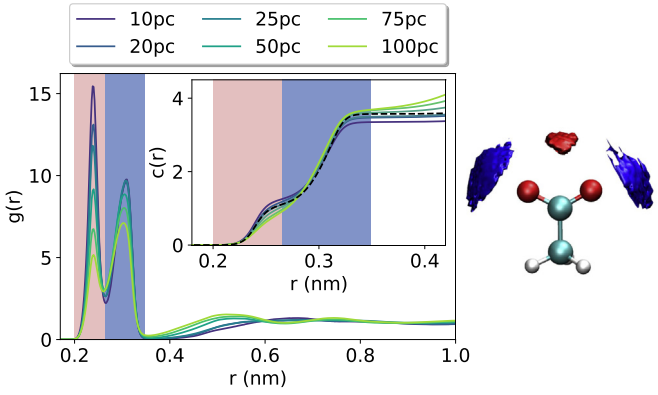


Fig. 9. RDFs between Li^+ and ACE^-. In the inset the coordination numbers of ACE^- around Li^+ are represented for all the simulated salt concentrations as well as the one corresponding to the system of 10% without polymers. The spatial distribution function of Li^+ around ACE^- for the 20pc system is represented on the right side pointing out the Li^+ adsorption sites. The blue and red regions represent the mono and bidentate coordinations respectively.

4. Summary and conclusion

In this paper we characterize the structure of polymer+salt+PIL ternary mixtures using MD simulations focusing on the changes in the Li^+ environment and adsorption compared with previously reported results for similar systems. Firstly, we enumerate the used simulation details as well as the employed packing algorithm that allowed us to insert inside the simulation boxes large molecules such as the polymers taking into account the periodic boundary conditions. The tool that we developed for implementing this task was released as an open source project and we think that it can be very handy to the scientific community for obtaining the initial simulation configurations for a wide variety of systems involving large molecules with slow dynamics.

Our solubility study suggested that the [EA][ACE] was the best candidate to solvate the PEO polymer regarding the results of the radius of gyration and end-to-end distances of the polymers in every considered ILs. Therefore, we performed a series of simulations of ternary mixtures of PEO, [EA][ACE] IL and different percentages of [Li][ACE] salt. Firstly, we analyzed how the environment of Li^+ cations is affected when the polymer is added to the IL + salt mixture. Our results suggested that the polymer presence does not significantly change the molecular environment of the lithium cations pointing out that the polymer acts merely as a holder of the binary mixture. This hypothesis was also supported by

the analysis of the ionic structure around the polymer backbones. In this analysis we showed that ethylammonium and acetate ions do not show any preference to be close to the polymer and only a tiny coordination of lithium cations around the polymer oxygens was remarkable. We also corroborated that the molecular environment of the ions remains constant with the addition of polymer calculating the vibrational power spectrum of the different species. A qualitative study of the transport properties of this system was also done by means of the ideal transport numbers of each ionic species, revealing that the addition of polymer does not affect the transport mechanisms of the considered mixture. At this point the results deviated considerably from those previously reported with other ILs [17–19] and the differences were more obvious when the fraction of adsorbed Li^+ was calculated showing that, when the [EA][ACE] IL is considered, the percentage of adsorbed lithium cations in the polymers' backbones is fully compatible with a random distribution. This completes the picture that describes the polymer as a holder for the considered IL + salt mixture instead of being integrated in the ionic lattice as it happens when other ILs are considered. Moreover, this picture remains constant when the amount of IL changes, i.e., the amount of free lithium cations that could be candidates to be adsorbed in the polymer does not change. This is supported by the coordination results of ACE^- anions around lithium cations. These results showed that the addition of EA^+ cations is not able to break the coordination complexes formed by the ACE^- and Li^+. In summary, the studied system seems to be ideal to get a mechanically supported electrochemical device while keeping the IL properties.

Declaration of Competing Interest

There are no conflicts to declare.

Acknowledgments

The financial support of the Spanish Ministry of Economy and Competitiveness (Projects MAT2017-89239-C2-1-P and MAT2017-89239-C2-2-P) is gratefully acknowledged. Moreover, this work was funded by the Xunta de Galicia (ED431D 2017/06, ED431E 2018/08, GRC ED431C 2016/001 and GRC ED431C 2020/10). All these research projects were partially supported by FEDER. J. M. O-M., A. R-P. and H. M-C. thanks the Spanish Ministry of Education for their FPU grants. A. H. and D. D. thank the German Federal Ministry of Education and Research for financial support through the FestBatt project (grant number 03XP0174B).

Appendix A. Supplementary data

Supplementary data to this article can be found online at https://doi.org/10.1016/j.molliq.2021.115883.

References

[1] H. Zhao, S.V. Malhotra, Applications of ionic liquids in organic synthesis, Aldrichim. Acta. 35 (2002) 75–83.
[2] R.D. Rogers, K.R. Seddon, Ionic Liquids: Industrial Applications for Green Chemistry, ACS Publications, 2002.
[3] N.V. Plechkova, K.R. Seddon, Applications of ionic liquids in the chemical industry, Chem. Soc. Rev. 37 (2008) 123–150.
[4] C. Reichardt, T. Welton, Solvents and Solvent Effects in Organic Chemistry, John Wiley & Sons, 2011.
[5] P. Wasserscheid, T. Welton, Ionic Liquids in Synthesis, John Wiley & Sons, 2008.
[6] I. Minami, Ionic liquids in tribology, Molecules 14 (2009) 2286–2305.
[7] M. Galiński, A. Lewandowski, I. Stepniak, Ionic liquids as electrolytes, Electrochim. Acta 51 (2006) 5567–5580.
[8] A. Matic, B. Scrosati, Ionic liquids for energy applications, MRS Bullet. 38 (2013) 533–537.
[9] M. Armand, F. Endres, D.R. MacFarlane, H. Ohno, B. Scrosati, Ionic-liquid materials for the electrochemical challenges of the future, Nat. Mater. 8 (2009) 621–629.
[10] M.V. Fedorov, A.A. Kornyshev, Ionic liquids at electrified interfaces, Chem. Rev. 114 (2014) 2978–3036.
[11] D.R. MacFarlane, N. Tachikawa, M. Forsyth, J.M. Pringle, P.C. Howlett, G.D. Elliott, J.H. Davis, M. Watanabe, P. Simon, C.A. Angell, Energy applications of ionic liquids, Energy Environ. Sci. 7 (2014) 232–250.
[12] H. Ohno, Molten salt type polymer electrolytes, Electrochim. Acta 46 (2001) 1407–1411.
[13] J.-H. Shin, W.A. Henderson, S. Passerini, Peo-based polymer electrolytes with ionic liquids and their use in lithium metal-polymer electrolyte batteries, J. Electrochem. Soc. 152 (2005) A978.
[14] O. Borodin, G.D. Smith, Mechanism of ion transport in amorphous poly (ethylene oxide)/litfsi from molecular dynamics simulations, Macromolecules 39 (2006) 1620–1629.
[15] N. Molinari, J.P. Mailoa, B. Kozinsky, Effect of salt concentration on ion clustering and transport in polymer solid electrolytes: a molecular dynamics study of peo–litfsi, Chem. Mater. 30 (2018) 6298–6306.
[16] Y. Kumar, S. Hashmi, G. Pandey, Lithium ion transport and ion–polymer interaction in peo based polymer electrolyte plasticized with ionic liquid, Solid State Ionics 201 (2011) 73–80.
[17] D. Diddens, A. Heuer, Lithium ion transport mechanism in ternary polymer electrolyte-ionic liquid mixtures: a molecular dynamics simulation study, ACS Macro Lett. 2 (2013) 322–326.
[18] D. Diddens, A. Heuer, Simulation study of the lithium ion transport mechanism in ternary polymer electrolytes: the critical role of the segmental mobility, J. Phys. Chem. B 118 (2014) 1113–1125.
[19] S. Mogurampelly, V. Ganesan, Structure and mechanisms underlying ion transport in ternary polymer electrolytes containing ionic liquids, J. Chem. Phys. 146 (2017), 074902, .
[20] J.-H. Shin, W.A. Henderson, C. Tizzani, S. Passerini, S.-S. Jeong, K.-W. Kim, Characterization of solvent-free polymer electrolytes consisting of ternary peo–litfsi–pyr14 tfsi, J. Electrochem. Soc. 153 (2006) A1649.
[21] M. Casalegno, F. Castiglione, G. Raos, G.B. Appetecchi, S. Passerini, A. Mele, E. Ragg, Magnetic resonance imaging and molecular dynamics characterization of ionic liquid in poly(ethylene oxide)-based polymer electrolytes, ACS Appl. Mater. Interfaces 12 (2020) 23800–23811.
[22] D. Diddens, E. Paillard, A. Heuer, Improving the lithium ion transport in polymer electrolytes by functionalized ionic-liquid additives: simulations and modeling, J. Electrochem. Soc. 164 (2017) E3225–E3231.
[23] T. Vogl, S. Menne, R.-S. Kühnel, A. Balducci, The beneficial effect of protic ionic liquids on the lithium environment in electrolytes for battery applications, J. Mater. Chem. A 2 (2014) 8258–8265.
[24] M.J. Abraham, T. Murtola, R. Schulz, S. Páll, J.C. Smith, B. Hess, E. Lindahl, Gromacs: high performance molecular simulations through multi-level parallelism from laptops to supercomputers, SoftwareX 1 (2015) 19–25.
[25] B. Hess, C. Kutzner, D. Van Der Spoel, E. Lindahl, Gromacs 4: algorithms for highly efficient, load-balanced, and scalable molecular simulation, J. Chem. Theory Comput. 4 (2008) 435–447.
[26] W.L. Jorgensen, D.S. Maxwell, J. Tirado-Rives, Development and testing of the opls all-atom force field on conformational energetics and properties of organic liquids, J. Am. Chem. Soc. 118 (1996) 11225–11236.
[27] J.N. Canongia Lopes, J. Deschamps, A.A.H. Pádua, Modeling ionic liquids using a systematic all-atom force field, J. Phys. Chem. B 108 (2004) 2038–2047.
[28] A.A. Padua, M.F. Costa Gomes, J.N. Canongia Lopes, Molecular solutes in ionic liquids: a structural perspective, Acc. Chem. Res. 40 (2007) 1087–1096.
[29] J.N.C. Lopes, A.A. Pádua, Cl&p: a generic and systematic force field for ionic liquids modeling, Theor. Chem. Accounts 131 (2012) 1129.
[30] J. Åqvist, Ion-water interaction potentials derived from free energy perturbation simulations, J. Phys. Chem. 94 (1990) 8021–8024.
[31] A. Patriksson, D. van der Spoel, A temperature predictor for parallel tempering simulations, Phys. Chem. Chem. Phys. 10 (2008) 2073–2077.
[32] L. Martnez, R. Andrade, E.G. Birgin, J.M. Martínez, Packmol: a package for building initial configurations for molecular dynamics simulations, J. Comput. Chem. 30 (2009) 2157–2164.
[33] H.J. Berendsen, J.V. Postma, W.F. van Gunsteren, A. DiNola, J.R. Haak, Molecular dynamics with coupling to an external bath, J. Chem. Phys. 81 (1984) 3684–3690.
[34] T. Darden, D. York, L. Pedersen, Particle mesh ewald: an n·log (n) method for ewald sums in large systems, J. Chem. Phys. 98 (1993) 10089–10092.
[35] U. Essmann, L. Perera, M.L. Berkowitz, T. Darden, H. Lee, L.G. Pedersen, A smooth particle mesh ewald method, J. Chem. Phys. 103 (1995) 8577–8593.
[36] B. Hess, H. Bekker, H.J. Berendsen, J.G. Fraaije, Lincs: a linear constraint solver for molecular simulations, J. Comput. Chem. 18 (1997) 1463–1472.
[37] V. Lesch, H. Montes-Campos, T. Méndez-Morales, L.J. Gallego, A. Heuer, C. Schröder, L.M. Varela, Molecular dynamics analysis of the effect of electronic polarization on the structure and single-particle dynamics of mixtures of ionic liquids and lithium salts, J. Chem. Phys. 145 (2016) 204507.
[38] T. Yan, C.J. Burnham, M.G. Del Pópolo, G.A. Voth, Molecular dynamics simulation of ionic liquids: the effect of electronic polarizability, J. Phys. Chem. B 108 (2004) 11877–11881.
[39] E. Choi, A. Yethiraj, Entropic mechanism for the lower critical solution temperature of poly (ethylene oxide) in a room temperature ionic liquid, ACS Macro Lett. 4 (2015) 799–803.
[40] J. Israelachvili, The different faces of poly (ethylene glycol), Proc. Natl. Acad. Sci. U. S. A. 94 (1997) 8378–8379.
[41] M.H. Ghatee, A.R. Zolghadr, Local depolarization in hydrophobic and hydrophilic ionic liquids/water mixtures: car–parrinello and classical molecular dynamics simulation, J. Phys. Chem. C 117 (2013) 2066–2077.
[42] V. Gómez-González, J.M. Otero-Mato, H. Montes-Campos, X. García-Andrade, A. García-Fuente, A. Vega, J. Carrete, O. Cabeza, L.J. Gallego, L.M. Varela, Borophene

vs. graphene interfaces: Tuning the electric double layer in ionic liquids, J. Mol. Liq. 303 (2020) 112647.
[43] A. Maitra, A. Heuer, Cation transport in polymer electrolytes: a microscopic approach, Phys. Rev. Lett. 98 (2007) 227802.
[44] T. Mendez-Morales, J. Carrete, S. Bouzon-Capelo, M. Perez-Rodriguez, O. Cabeza, L.J. Gallego, L.M. Varela, Md simulations of the formation of stable clusters in mixtures of alkaline salts and imidazolium-based ionic liquids, J. Phys. Chem. B 117 (2013) 3207–3220.

USC UNIVERSIDADE DE SANTIAGO DE COMPOSTELA

Macromolecules

Open Access
This article is licensed under CC-BY 4.0

pubs.acs.org/Macromolecules
Article

Ternary Solid Polymer Electrolytes at the Electrochemical Interface: A Computational Study

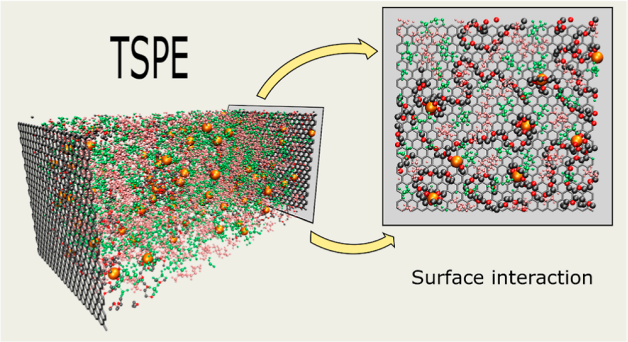
Alejandro Rivera-Pousa, José Manuel Otero-Mato, Hadrian Montes-Campos,* Trinidad Méndez-Morales, Diddo Diddens, Andreas Heuer, and Luis Miguel Varela*

Cite This: *Macromolecules* 2024, 57, 3921−3936

Read Online

ACCESS | Metrics & More | Article Recommendations | Supporting Information

ABSTRACT: Polymer-based solid-like gel electrolytes have emerged as a promising alternative to improve battery performance. However, there is a scarcity of studies on the behavior of these media at the electrochemical interface. In this work, we report classical MD simulations of ternary polymer electrolytes composed of poly(ethylene oxide), a lithium salt [lithium bis(trifluoromethanesulfonyl)imide], and different ionic liquids [1-butyl-1-methylpyrrolidinium bis(trifluoromethanesulfonyl)-imide and 1-ethyl-3-methylimidazolium bis-(trifluoromethanesulfonyl)imide] confined between two charged and uncharged graphene-like surfaces. The molecular solvation of Li^+ ions and their diffusion as well as the polymer conformational picture were characterized in terms of the radial distribution functions, coordination numbers, number density profiles, orientations, displacement variance, polymer radius of gyration, and polymer end-to-end distance. Our results show that the layering behavior of the ternary electrolyte in the interfacial region leads to a decrease of Li^+ mobility in the direction perpendicular to the electrodes and high energy barriers that hinder lithium cations from coming into direct contact with the graphene-like surface. The nature of the ionic liquid and its concentration were found to influence the structural and dynamic properties at the electrode/electrolyte interface, the electrolyte with low amounts of the pyrrolidinium-based ionic liquid being that with the best performance since it favors the migration of Li^+ cations toward the negative electrode when compared to the imidazolium-based one.



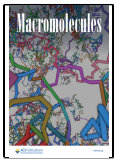
INTRODUCTION

The current digital electronic revolution has gone hand in hand with the rapid growth of the number of portable electronic devices. Li-ion batteries are currently the dominant mobile power sources for these devices, since they have the highest energy per unit weight of the known energy storage systems.[1,2] However, despite significant achievements in the optimization of Li-ion batteries, there are still notable challenges across cost, safety, and aging.[3,4] For example, traditional lithium batteries use liquid electrolytes based on organic carbonates, which are highly flammable and volatile, and can lead to an inhomogeneous deposition of lithium in the form of dendrites.[5]

Solid polymer electrolytes (SPEs) have emerged as attractive candidates to solve these safety and life cycle issues. Their main advantages lie in having high flexibility, low cost, and enhanced thermal/electrochemical stabilities.[6,7] Among all the options, poly(ethylene oxide) (PEO) has been demonstrated to possess an excellent salt-solvating ability. After being the first polymer electrolyte reported to dissolve Li ions in 1973,[8] its potential use in lithium batteries was then explored in the pioneering works of Armand et al.[9−11] Although PEO is one of the most studied polymers and most commonly used nowadays, PEO-based SPEs still suffer from lower ionic conductivity compared to conventional liquid electrolytes. While standard SPEs are prepared by dissolving a lithium salt in a polymer matrix, several strategies have been employed to enhance lithium-ion mobility. These approaches include, for instance, the use of lithium salts with noncoordinating anions such as bis(trifluoromethanesulfonyl)-imide (TFSI),[12−18] the dispersion of nanoparticles,[19−21] or the addition of liquid plasticizers such as carbonates,[22,23] among others.

Another feasible solution is to form ternary SPEs (TSPEs) by plasticizing the PEO-based SPE with an ionic liquid (IL). ILs are molten salts with melting points below 100 °C containing charge-balanced ions.[24,25] Their properties can be modulated through different combinations of anions and cations, due to which they have been termed "designer solvents". Their features,

Received: December 29, 2023
Revised: March 31, 2024
Accepted: April 9, 2024
Published: April 29, 2024



Downloaded via UNIV DE SANTIAGO DE COMPOSTELA on May 20, 2024 at 09:36:41 (UTC).
See https://pubs.acs.org/sharingguidelines for options on how to legitimately share published articles.

ACS Publications
© 2024 The Authors. Published by American Chemical Society

https://doi.org/10.1021/acs.macromol.3c02669
Macromolecules 2024, 57, 3921−3936

such as negligible volatility, high chemical and thermal stability, wide electrochemical window, and good solubility in various materials,[26,27] make them promising green solvents for various applications including synthesis, catalysis, separation, lubrication, drug delivery, or energy storage.[28−30] Although many works have considered ILs and their binary metal salt mixtures to be used as electrolytes in high-performance lithium-ion batteries,[31] it has been observed that lithium salts not only usually exhibit poor solubility in ILs but also decrease the ionic conductivity of the binary mixtures upon increasing concentration.[32,33] Also, these binary IL/salt electrolytes suffer from large anionic clusters, hindering lithium-ion transport. However, this inconvenient behavior is avoided when PEO is also present in the system, since it decouples lithium ions from its solvation shell and changes lithium transport to a PEO-dominated cationic mechanism.[34] As a result, the addition of ILs to SPEs allows improving the conductivity of polymer electrolytes, increasing the number of charge carriers and accelerating polymer segmental dynamics, while guaranteeing high safety and good mechanical properties. Thus, it seems that TSPEs will play a fundamental role in next-generation energy storage technologies.

Mixtures of PEO, lithium salts, and pyrrolidinium-based ILs are undoubtedly the most investigated TSPE system, although short-chain imidazolium IL cations have also been considered.[35−41] In addition to the increase in conductivity with IL addition, experiments on TSPEs have also reported aspects such as the effect of the temperature and their interfacial stability on lithium metal.[35−38,40,42−48] For example, Passerini and coworkers observed that smaller anions such as bis(fluorosulfonyl)imide (FSI) increase electrical conductivity relative to TFSI at the expense of a lower thermal stability.[49] They also highlighted the importance of the TSPE composition, since anions and polymers compete for the coordination with lithium cations.[50]

On the other hand, computational methods have been also widely employed over the last decades for the identification and understanding of promising TSPEs, since they allow the analysis of the systems at the molecular level and a straightforward comparison with the experimental measurements.[51,52] In general, density functional theory (DFT) calculations have been employed to analyze either polymer decomposition on a metal surface[53,54] or the local environment around lithium cations.[17] Molecular dynamics (MD) simulations, which are much more abundant, have been mainly devoted to understand the structure of TSPEs and the mechanisms of lithium transport in them.[39,41,45,55−58] For example, Diddens and Heuer and coworkers[59] proved that the enhanced lithium diffusion in TPSEs including pyrrolidinium-based cations is due to the plasticization of the PEO backbone by the IL. Besides, they explained how the lithium-ion transport mechanism is modified when changing the composition of the TSPE: at high PEO/lithium ratios, the three transport mechanisms remain qualitatively the same as compared to binary SPEs [(i) diffusion of the cation along the PEO backbone, (ii) cooperative motion of the cation with the polymer segments, and (iii) cationic transfer between two polymer chains], whereas for low ratios, a fourth transport mechanism based on the coordination of lithium with TFSI anions becomes more relevant.[60] Very recently, Paillard and coworkers[48] combined MD simulations with experiments to suggest the use of coordinating anions like trifluoromethanesulfonyl-*N*-cyanoamide in TSPEs to accelerate lithium-ion transport by recoupling its dynamics from the polymer to the anion.

Moreover, while the bulk properties of binary and ternary SPEs have been extensively explored, their interfacial behavior at the proximity of an electrode is scarcely known. The interaction of the electrolyte with the electrode considerably modifies the properties of the liquids relative to their bulk values. However, the electrode/electrolyte interfaces are not well-understood yet. Thus, consideration of the structures and processes at the electrolyte/electrode interface is crucial for the optimization of energy storage devices. Concerning binary SPEs,[61,62] it was observed by Thum et al.[63] using MD simulations that the presence of a surface does not affect the parallel transport mechanism, but it substantially reduces the lithium-ion diffusion in the direction perpendicular to the interface. To the best of our knowledge, only one work analyzing the interfacial properties of TSPEs at a Li-metal surface has been reported up until now.[64] In that case, several combinations of IL cations and anions were tested to tune the structural and dynamic properties at the surface/electrolyte interface, and 1-ethyl-3-methylimidazolium 1,2,3-triazolide ([EMIM][123Triaz]) was observed to show the best performance.

In this work, with the aim of getting a better understanding of the electrode/electrolyte interface, we performed MD simulations of ternary PEO-based electrolytes to analyze their bulk behavior and the interfacial properties at a graphene-like surface (both under charged and uncharged conditions). The studied ternary system is composed of the polymer PEO; a lithium-based salt, [Li][TFSI]; and an IL. Two different ILs were considered, both sharing the anion with the salt species: [EMIM][TFSI] and [PYR_{14}][TFSI], and for the imidazolium-based TSPE, two concentrations were considered. Thus, in this contribution, the following questions will be addressed:

- How does the presence of a graphene-like surface influence the structure of the TSPE mixtures in the interfacial region? Moreover, how does the conformational redistribution depend on the surface charge?
- What is the influence of the IL on the interaction between the lithium cation and the polymer?
- Does the concentration of the TSPE or the structure of the IL cation have any impact on the interfacial properties? Which mixture shows the best potential as battery electrolytes?

Our findings are presented as follows: In the next section, details of the simulation setup are given. Then, the results are discussed in the section and, finally, the main conclusions are summarized.

SIMULATION DETAILS

The reported simulations were carried out using Gromacs 2019.5 software.[65,66] The OPLS-AA[67] force field was used to describe the molecular interactions of PEO, Li^+, and $EMIM^+$. PYR_{14}^+ and $TFSI^-$ were parameterized according to the CL&P force field,[68−70] which is compatible with OPLS-AA. On the basis of a mean-field approximation, a charge scaling of 0.8 was employed to take into account polarization effects, thus obtaining a better agreement with experiments compared to a full charge model. This methodology has been previously used to investigate SPEs.[18,55]

The polymeric PEO chains were composed of 19 monomers, that is, 20 ether oxygens. Already coiled structures were chosen as the dynamics of the system is very slow. The base ratio

https://doi.org/10.1021/acs.macromol.3c02669
Macromolecules 2024, 57, 3921−3936

between the different species was chosen as 20:2:6, i.e., for each 20 PEO oxygen ethers (1 chain), 2 salt molecules and 6 IL molecules are present. In order to study the influence of the IL concentration on the properties of the system, the [EMIM][TFSI]-based setups were also analyzed at an oxygen(PEO)/salt/IL ratio of 20:2:20. The initial configuration was obtained following the algorithm described in ref 56 that allows encapsulation of long molecules, such as polymers, in periodic simulation boxes. This method takes advantage of the software package Packmol.[71] Bulk simulations of all of these mixtures were carried out using 25 polymer chains and the respective amounts of lithium salt and IL.

The simulation path followed was the one thoroughly described in ref 63. It starts with two energy minimizations, using first a steepest descent followed by a conjugated gradients algorithm. Then, two implicit graphene-like walls were inserted in the z dimension at the ends of the simulation box using the Gromacs tool. These layers interact with the electrolyte as a surface-integrated 10-4 Lennard-Jones potential. The lateral box dimensions were fixed throughout the whole preparation and simulation of the systems in order to afterward adjust to the graphene-like sheet size, ensuring correct periodicity of the C−C bonds. For this purpose, the x and y dimensions were set to 4.9118 and 4.6798 nm, respectively. As the lateral size of the simulation system cannot change, the z dimension will have to be accommodated to recover the correct bulk density. The exact number of molecules of each species can be seen in Table 1 and was chosen as to obtain approximately 10 nm between graphene-like walls, which was deemed sufficient to recover bulk conditions in the center of the simulation box.

Table 1. Number of Molecules Contained in the Simulation Box for the Different Systems

system	concentration	n PEO	n [Li][TFSI]	n IL
[Pyr_{14}][TFSI]	20:2:6	45	90	270
[EMIM][TFSI]	20:2:6	51	102	306
[EMIM][TFSI]	20:2:20	21	42	420

Periodic boundary conditions are applied in the x and y dimensions. After energy minimization, 3 ns 273 K *NVT* and 3 ns 423 K *NVT* runs were done as a first attempt to relax unfavorable configurations. The temperature was maintained using a Berendsen thermostat.[72] Then, a series of *NPT* stabilizations with semi-isotropic Berendsen pressure coupling[72] allowed the z dimension of the box to adapt to reach the right density. An initial NPT run of 3 ns was followed by an annealing at 623 K for 100 ns, eventually followed by a temperature decrease to the initial 423 K and another 100 ns of NPT relaxation.

After this procedure, we removed the implicit walls and inserted the real graphene-like surfaces. The carbon atom selected was opls147. The graphene-like surfaces were built using the carbon nanostructure utility of the software package VMD.[73] These graphene-like walls will remain fixed throughout the simulation procedure; therefore, the box dimensions will not further change. The systems were simulated both with no charge on the carbon atoms of the graphene-like walls as well as with a charge density of $\sigma = \pm 1e/\text{nm}^2$, which results in a charge per carbon atom of $\pm 0.0131e$. The atomic charge is kept constant throughout the simulation, and no image charge effects are considered. Coulomb interactions were taken into account using the smooth particle mesh Ewald (PME) method[74,75] with the Yeh−Berkowitz correction.[76] Although constant potential conditions would result in a more realistic simulation environment, it is a technique with a much larger computational cost. The main difference in predictions from both techniques comes in the dynamics of the formation of the electric double layer,[77] but the main focus of this work is the structuring of the mixture. Furthermore, it has been previously shown in the literature that for space widths larger than 1.4 nm, the constant charge method produces reliable counterion concentration results.[78] Adding the extra computational cost to the already long simulations needed for systems with slow dynamics, we deemed appropriate the use of the constant charge technique in this study.

After a final energy minimization was carried out, a 600 ns *NVT* run applying a Nosé−Hoover thermostat[79] was used as the production run, where we discarded the results from the first 100 ns since they were considered as further stabilization of the system, as can be seen in Figure S1 of the Supporting Information. For the systems with charged graphene-like surfaces, the configuration after the first 100 ns of the neutral system was selected as a starting point. The graphene-like surface at $z = 0$ nm is always positively charged, and the other surface is always negatively charged. These systems were simulated in a manner similar to that for the neutral ones, discarding the first 100 ns of the 600 ns *NVT* production run. Even though such long simulation times are computationally

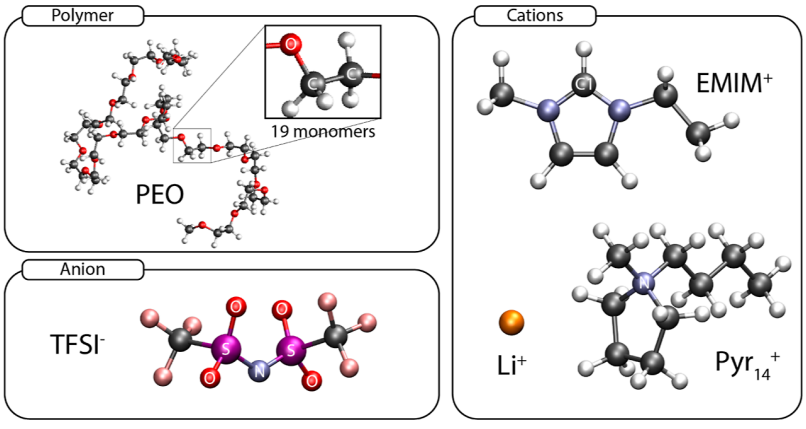


Figure 1. 3D models of the species present in the systems. Oxygen, carbon, hydrogen, nitrogen, sulfur, fluorine, and lithium atoms are represented in red, black, white, blue, purple, pink, and orange, respectively. Relevant sites employed for the calculations in each species are explicitly labeled.

https://doi.org/10.1021/acs.macromol.3c02669
Macromolecules 2024, 57, 3921−3936

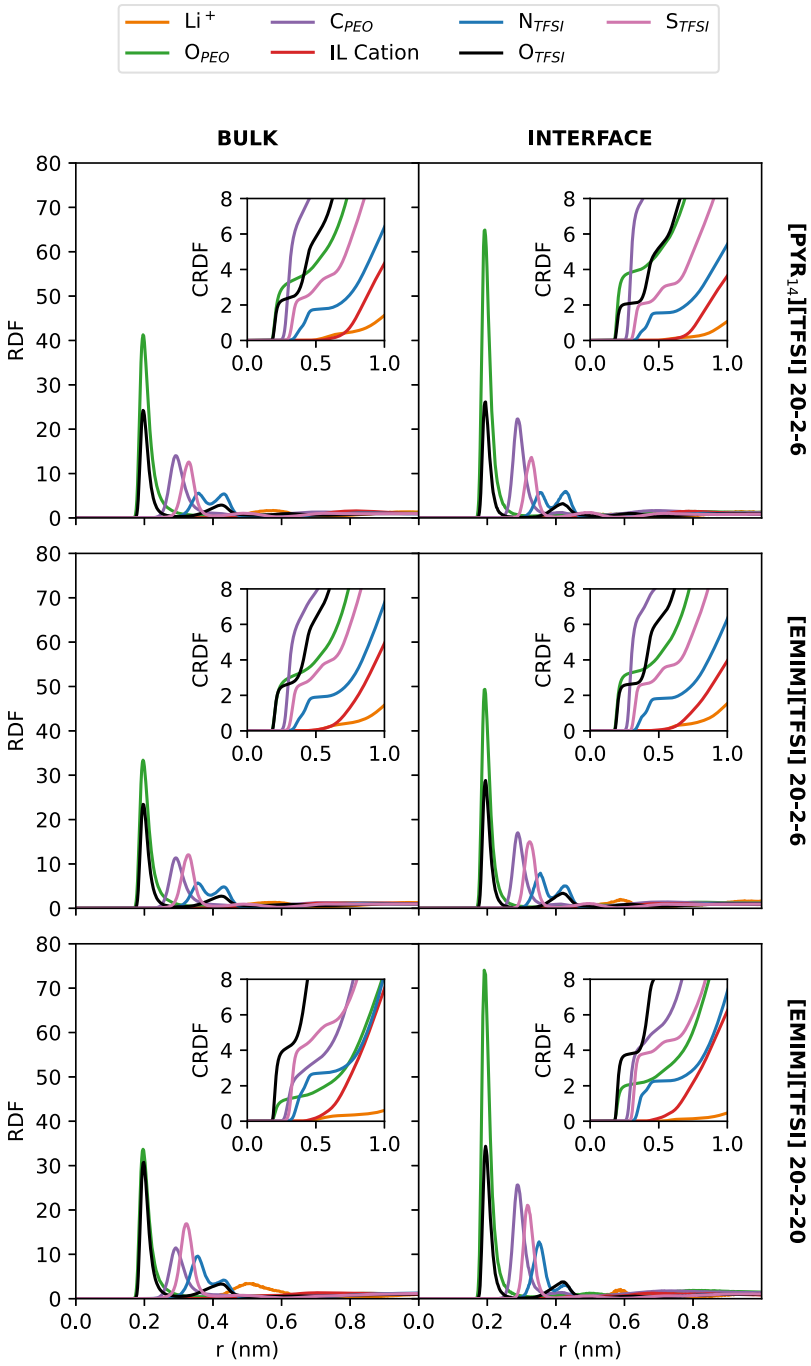


Figure 2. RDFs between Li^+ and several atoms of the different molecules in bulk mixtures (left) and in the interfacial region in systems between neutral graphene-like walls (right). The insets show the corresponding cumulative RDF. The representative atoms for $TFSI^-$ and PEO are specified in the legend, whereas C1 and N were chosen for $EMIM^+$ and Pyr_{14}^+, respectively.

expensive, they are necessary to allow for slow dynamics of these systems. Simulations of equivalent systems but without the polymer molecules were carried out for further comparison.

RESULTS AND DISCUSSION

Influence of the Presence of a Graphene-like Surface.

In order to analyze the structural properties of the TSPEs, we computed the radial distribution functions (RDFs) of the different species of the mixture around a Li^+ cation. In this section, these functions were calculated both in bulk and in the interfacial region of the slab model (~2 nm from the neutral graphene-like surface), as seen in Figure 2. For that purpose, we selected relevant sites of the molecular components (shown in Figure 1) to achieve a comprehensive view of the structural arrangement of the system. Thus, for the IL cation, C1 and N atoms were chosen for the imidazolium and pyrrolidinium rings, respectively, whereas those selected for the other species are specified in Figure 2. There we can clearly observe that Li^+ prioritizes the oxygen atoms from the molecular components, both PEO and $TFSI^-$, thus evidencing a mixed coordination in agreement with previous computational and experimental works on TSPEs.[38,41] Although the Li^+ environment is similar in both

https://doi.org/10.1021/acs.macromol.3c02669
Macromolecules 2024, 57, 3921−3936

configurations, the height of those peaks increases in the presence of the graphene-like surface, especially the coordinations that involve the polymer molecule. This is indicative of the ternary mixtures becoming more ordered when confined due to organization of the molecules in the interfacial region. Other sites of the molecules appear as the following closest atoms as a consequence. Specifically, the two peaks for the $TFSI^-$ nitrogen interaction confirm that Li^+ and $TFSI^-$ coordinate in two different conformations: monodentate and bidentate, which are yielded by the well-known *cis* and *trans* conformations of $TFSI^-$ and are typical of this kind of aggregate.[80,81] It is interesting to note that concentration seems to play a similar role both in the bulk and at the interface since more IL concentration leads to the bidentate coordination being more abundant. However, no remarkable effects on the height of the peaks concerning the $TFSI^-$ oxygen atoms are induced by increasing the amount of IL.

The cumulative RDFs (CRDFs), i.e., the average number of particles within a distance r around a central molecule, also provide us with information about the spatial distribution. The results for Li^+ solvation are included in the insets of Figure 2. As we can see, in bulk simulations, Li^+ coordinates in its first solvation shell with around 3 oxygen atoms of PEO and 3 oxygen atoms of $TFSI^-$ (depending on the system), giving an average coordination number of 6, which is typical for this kind of electrolyte system.[41] An increase in IL concentration leads to the coordination with $TFSI^-$ taking over and the coordination with the polymer exhibiting the inverse trend, although keeping the total amount of 6 oxygens being coordinated with a Li^+ cation. This change in the coordination environment of lithium cations through a weakening of the so-called "breathing mode" (the association between Li^+ and PEO) is mainly due to the decrease in the polymer fraction as the IL content increases. This structural picture is slightly modified when the system is under confinement. At the neutral interface, the total number of oxygen atoms coordinating a Li^+ cation is maintained, with the "breathing mode" being favored when compared to the bulk. Thus, the neutral graphene-like surface gets Li^+ preferentially coordinated to the PEO oxygens. The opposite behavior, that is, an increase in the number of $TFSI^-$ anions in the lithium-ion solvation shell when going from the bulk to the interface, was previously reported when introducing a Li-metal surface.[62,64] This discrepancy is an effect of the nature of the electrode on its interaction with the polymer. That is, due to the well-known hydrophobicity of graphene,[82,83] this carbon surface shows stronger interactions with the PEO carbon atoms than the Li-metal surface, resulting in a larger number of polymers in the interfacial region that are available for coordinating a lithium ion, as it will be shown by the calculation of the number density profiles included in Figure 5. In fact, this can be clearly appreciated in the snapshot included in Figure 3 (right), where the polymers in the proximity of an uncharged graphene-like sheet are shown to be arranged parallel to the surface, thus maximizing their interaction with the neutral electrode. This will be also confirmed later with the analysis of the orientations.

Influence of the Charge of the Graphene-like Surface. RDFs and CRDFs in the interfacial regions with charged graphene-like electrodes were calculated with the aim of analyzing the impact of charging the surface. The corresponding plots are shown in Figure 4.

At surface charges of $\sigma = +1e/nm^2$, the interaction between an oxygen of the polymer and a Li^+ cation is always slightly lower than that at neutral interfaces, whereas that with an oxygen from the $TFSI^-$ anion is greater. In fact, it can be seen that the

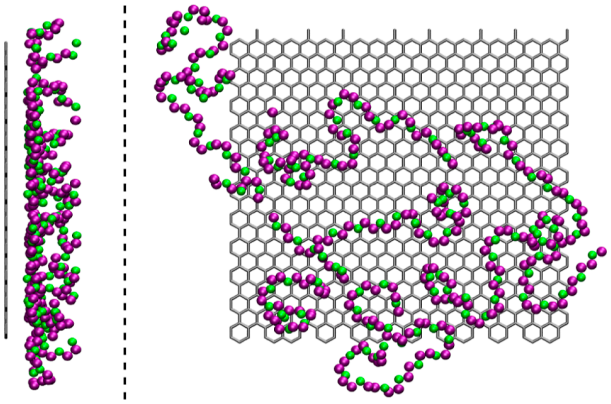


Figure 3. Snapshots in the *YZ* plane (left) and *XY* plane (right) of the polymer chains closer than 1 nm to a neutral electrode in mixtures with $[Pyr_{14}][TFSI]$. Oxygen and carbon atoms are represented in green and purple, respectively.

interaction between lithium and the anion increases when increasing the amount of IL in the ternary mixture due to the presence of a greater number of $TFSI^-$ anions. Concerning the coordination numbers, in the first solvation shell of lithium ions, there are always around 2−3 oxygens of PEO and 2−4 oxygens of $TFSI^-$ anions. Since the anions are expected to be located in the neighborhood of the positively charged surface, this could be indicative of Li^+ showing correlated ion motion with the anions in negatively charged Li-containing clusters. This will be explored later with an analysis of the number density profiles.

On the other hand, at surface charges of $\sigma = -1e/nm^2$ and low amounts of IL, the interaction between an oxygen from PEO and a solvated Li^+ ion is stronger than at positively charged surfaces, but it decreases when increasing the concentration. Regarding the interaction of Li^+ with the oxygens of $TFSI^-$ anions, the height of the peaks of the RDF is comparable to that in neutral interfaces, with a tendency to increase with IL concentration. Lithium coordination numbers with the polymer are 3 (except for the most concentrated mixture), as observed in the vicinity of the positive electrode, whereas those with the anion show an increase with the amount of IL, probably due to a greater number of $TFSI^-$ anions being available for solvating the same number of lithium cations.

As it is well-known, the interface leads to a layering of highly concentrated ionic electrolytes due to the interactions between the electrolyte and the surface.[84−86] To analyze this effect and shed more light on the microscopic structure of these systems, we also computed the density profiles along the z-axis, which are displayed in Figure 5. The first characteristic that is visible there is that some degree of layering in the interfacial region takes place also at neutral surfaces, which is associated with the translation symmetry breaking, but the effect is much more pronounced when charging the graphene-like sheet. In both cases, bulk density is recovered after approximately 2 nm from the carbon surface.

On the other hand, as can be seen in Figure 5 (left) for uncharged graphene-like surfaces, Li^+ atoms are never found in the regions adjacent to the walls, regardless of the IL employed and the concentration of the TSPE. Instead, they are located sharing the second layer with $TFSI^-$ anions. In turn, the first layer is mainly occupied by PEO molecules and a small amount of IL ions. This behavior has been also observed at the interface between SPEs and a Li-metal surface, and it is indicative of a

https://doi.org/10.1021/acs.macromol.3c02669
Macromolecules 2024, 57, 3921−3936

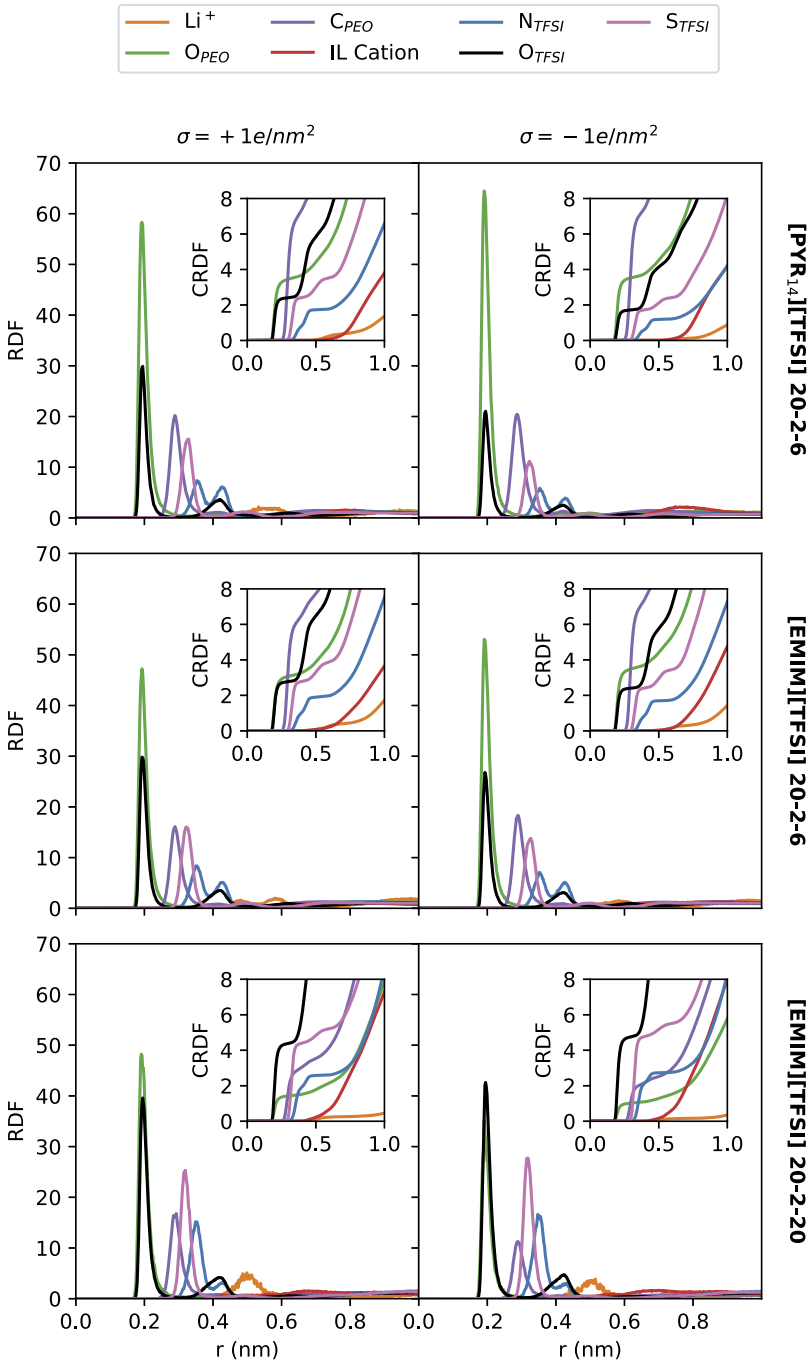


Figure 4. RDFs between Li^+ and several atoms of the different molecules in the region near the positively (left) and negatively (right) charged graphene-like surfaces, respectively. The insets show the corresponding cumulative RDF. The representative atoms for $TFSI^-$ and PEO are specified in the legend, whereas C1 and N were chosen for $EMIM^+$ and Pyr_{14}^+, respectively.

preference of the surface to interact with the electron-rich compounds.[62,64] Li^+ cations are more likely to interact with the electrolyte molecules rather than with the surface atoms. On the other hand, it is also shown in Figure 5 (right) that charging the graphene-like electrode leads to the spontaneous accumulation of counterions and the depletion of co-ions near the charged surface, as expected. Interestingly, an inner PEO layer emerges directly attached to the positively charged carbon surface at around 0.3 nm, followed by a dense layer of anions at secondary positions. Concerning the negatively charged surface, a dense layer of IL cations is always formed at approximately 0.4 nm from the graphene-like wall, but some differences can be seen between the different systems. First, for the lowest IL concentrations (20−2−6), lithium cations are able to directly approach the electrode together with some PEOs, which are split in several layers, with the pyrrolidinium-based TSPE but not with the imidazolium-based one. Apparently, with $[Pyr_{14}]$-[TFSI], Li^+ is not able to desolvate from the polymer, but these positively charged aggregates are indeed capable of reaching the negative electrode. This can be also observed in the snapshots of Figure 6, where the 1 nm-wide regions from the negative surface are represented for these two mixtures. However, when low

https://doi.org/10.1021/acs.macromol.3c02669
Macromolecules 2024, 57, 3921−3936

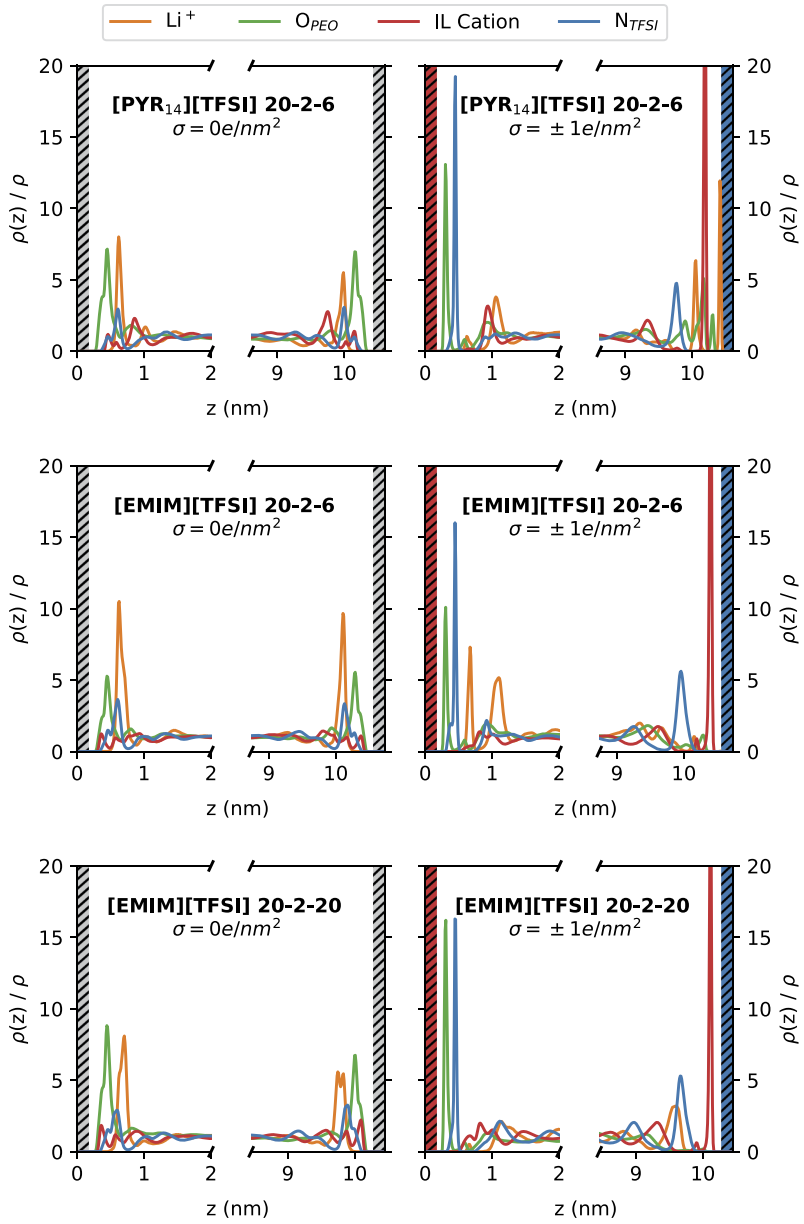


Figure 5. Density profiles in the z direction, normalized to the bulk density, for several atoms of the different molecules in systems confined between neutral graphene-like surfaces (left) and charged graphene-like surfaces (right). The representative atoms for $TFSI^-$ and PEO are specified in the legend, whereas C1 and N were chosen for $EMIM^+$ and Pyr_{14}^+, respectively.

amounts of [EMIM][TFSI] are present in the electrolyte, Li^+ seems to keep a strong coordination with $TFSI^-$ anions, as shown by the emerging lithium-ion populations at around 0.7 and 1.1 nm from the positively charged graphene-like sheet. This is probably due to the stronger interaction of $TFSI^-$ anions with Pyr_{14}^+ than with $EMIM^+$ that diminishes the degree of anion clustering with Li^+. This can be observed in Figure S2 of the Supporting Information, where we have plotted the RDFs between the IL ions for binary mixtures of [EMIM][TFSI] with LiTFSI and [Pyr_{14}][TFSI] with the same salt, both with a ratio of 6:2, which corresponds to the lowest IL concentration in the TSPEs.

Focusing now on the PEO/[Li][TFSI]/[EMIM][TFSI] electrolyte between charged surfaces, it can be observed in Figure 5 that Li^+ cations are not able to cross the dense layer of $EMIM^+$ and approach the negatively charged carbon surface for any of the tested concentrations. Thus, we try to get a deeper understanding about the movement of Li^+ cations calculating the free-energy profiles of transferring a Li^+ from the bulk to the graphene-like surface as

$$F(z) = -k_B T \ln\left(\frac{\rho_{Li}(z)}{\rho_{Li}(\text{bulk})}\right) \quad (1)$$

where k_B is the Boltzmann constant. The free-energy profiles obtained for uncharged, positively charged, and negatively charged surfaces are included in Figure 7, where we can observe the oscillations due to the layering behavior of the TSPE in the proximity of the wall. At uncharged surfaces, for all the systems, there is an easily accessible first minimum at 0.6 nm followed by a second one at 1 nm. This shows that a given lithium is slightly stabilized at uncharged interfaces, with a larger lifetime in the

https://doi.org/10.1021/acs.macromol.3c02669
Macromolecules 2024, 57, 3921−3936

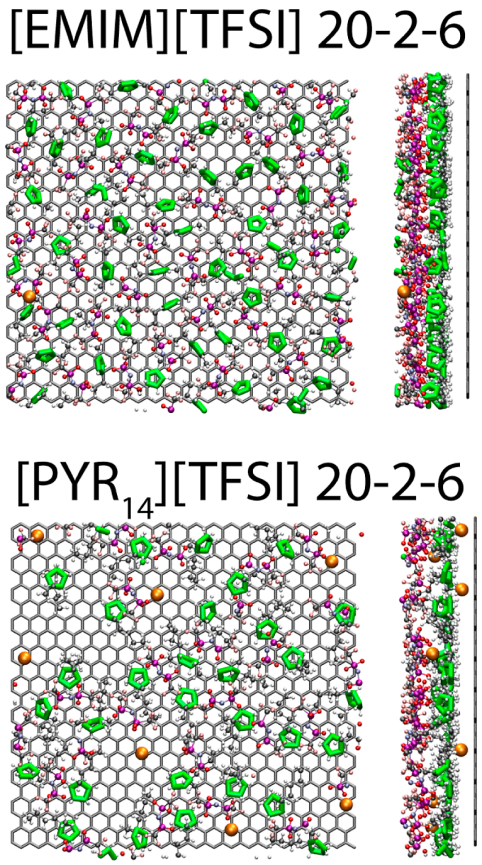


Figure 6. Snapshots in the *XY* plane (left) and *YZ* plane (right) of the molecules closer than 1 nm to the negative electrode in the [EMIM][TFSI] (top) and [Pyr_{14}][TFSI] (bottom) 20−2−6 systems. Lithium atoms, in orange, and cationic rings, in green, are artificially enlarged for better visual clarity.

minimum at 0.6 nm. However, it should be kept in mind that in the neutral slab configuration, there is an inner layer composed mainly of PEO and some IL that impedes Li^+ from coming into direct contact with the surface.

In the case of positively charged interfaces, the opposite behavior can be observed for most systems. That is, the Li^+ cation has a preference to place at distances larger than 1 nm rather than in the first layer, the only exception being the electrolyte with the lowest amount of [EMIM][TFSI]. In that mixture, Li^+ faces the lowest energy barrier to jump into the first layer. Once it has entered it, the Li^+ ion will stay there for some extended waiting time. This behavior arises from the strong interaction between Li^+ and the first layer of $TFSI^-$ anions at the positive electrode, as we have seen in Figure 5. At the negative electrode, the height of the free-energy barriers increases remarkably in comparison to the previous situations due to a depletion of Li^+ cations in some regions, as shown in Figure 5. Now, free-energy barriers are much higher than thermal energy, so the diffusion process toward the negative electrode can be regarded as a rare event, with the [Pyr_{14}][TFSI]-based TSPE showing the highest probability of Li^+ approaching the graphene-like surface. However, if a rare transition from the second layer at 0.6 nm to the innermost one at 0.2 nm takes place, which has been observed to happen 11 times during the whole trajectory, then Li^+ cations are accommodated in a stable position with high energy barriers for escaping from the negative electrode, since for that to happen, they must overcome the electrostatic attraction of the electrode.[63] In fact, our simulations show that once Li^+ cations reach the negative electrode, they remain at the innermost layer (on average) during 24.15 and 3.00 ns for PYR 20−2−6 and EMIM 20−2−6, respectively.

Another relevant aspect of the TSPE studies in this work is the particular orientation that the long polymeric chains adopt near the interfaces. As it has been shown in previous studies,[59] the polymer chains allow three new possible channels of Li^+ diffusion in these mixtures: (i) motion along with the chain, (ii) hopping between chain sites, and (iii) hopping between chains. As a result, the orientation of these chains could play an important role in the diffusion of Li^+ cations toward the electrodes. To analyze this feature, we considered the orientations of the different species in the system by computing the probability density distribution of the cosine of the relative angle between a vector normal to the surfaces pointing to the bulk and a characteristic molecular vector. For the IL cation, the vector is normal to the ring and has the geometrical center of the ring as the application point. For the polymer, a subdivision of the chains allows better identification of the correct orientation of the chains. Thus, we decided to take multiple vectors between consecutive oxygen sites of PEO, that is, going from one monomer to the next one in a random direction, with the application point of the vector being placed halfway between the two oxygens. For both species, the orientations were calculated only for those molecules whose application point of the characteristic vector lies within the first 2 nm from the charged and uncharged electrodes.

The orientations of the interfacial PEO molecules are plotted in Figure 8. There we can observe higher populations of polymers in the parallel orientations close to the graphene-like surfaces for most of the considered systems, thus trying to maximize their interaction with the carbon atoms of the surface, as was previously mentioned in the analysis of the effect of confining the SPE. This arrangement is more marked in the vicinity of the positively charged electrode, where we have seen in Figure 5 that PEO is located in the innermost layer followed by a second layer of $TFSI^-$ anions. Probably, the Coulomb attraction between this second anionic layer and the positive electrode is squeezing the polymer against the surface, forcing it to adopt a parallel stacking behavior. However, in the proximity of the negative graphene-like surface, where the polymer was observed to be less constrained in the *z* direction, it does not show a preferential orientation in ternary mixtures with [EMIM][TFSI]-based electrolytes because it has more conformational freedom. Neutral graphene-like surfaces also favor a "flat" polymer conformation, in agreement with previous observations for uncharged Li-metal surfaces.[62,64] In addition, the amount of IL and the nature of the IL cation do not seem to affect the orientation of PEO molecules. Figure S3 of the Supporting Information shows the orientation of the IL cations that are located in the innermost layer. The results suggest that both IL cations have random arrangements relative to a positively charged electrode, whereas cation rings become more parallel to the negatively charged surfaces in order to get a more efficient accumulation that allows them to overcompensate the charge of the electrode. On the other hand, the orientation of IL cations when adsorbed at neutral surfaces depends on their nature, with imidazolium rings preferring to be parallel regardless of the concentration and pyrrolidinium rings showing no preferential orientation.

The interaction of PEO with the components of the solvent and the graphene-like surfaces can be further analyzed by

https://doi.org/10.1021/acs.macromol.3c02669
Macromolecules 2024, 57, 3921−3936

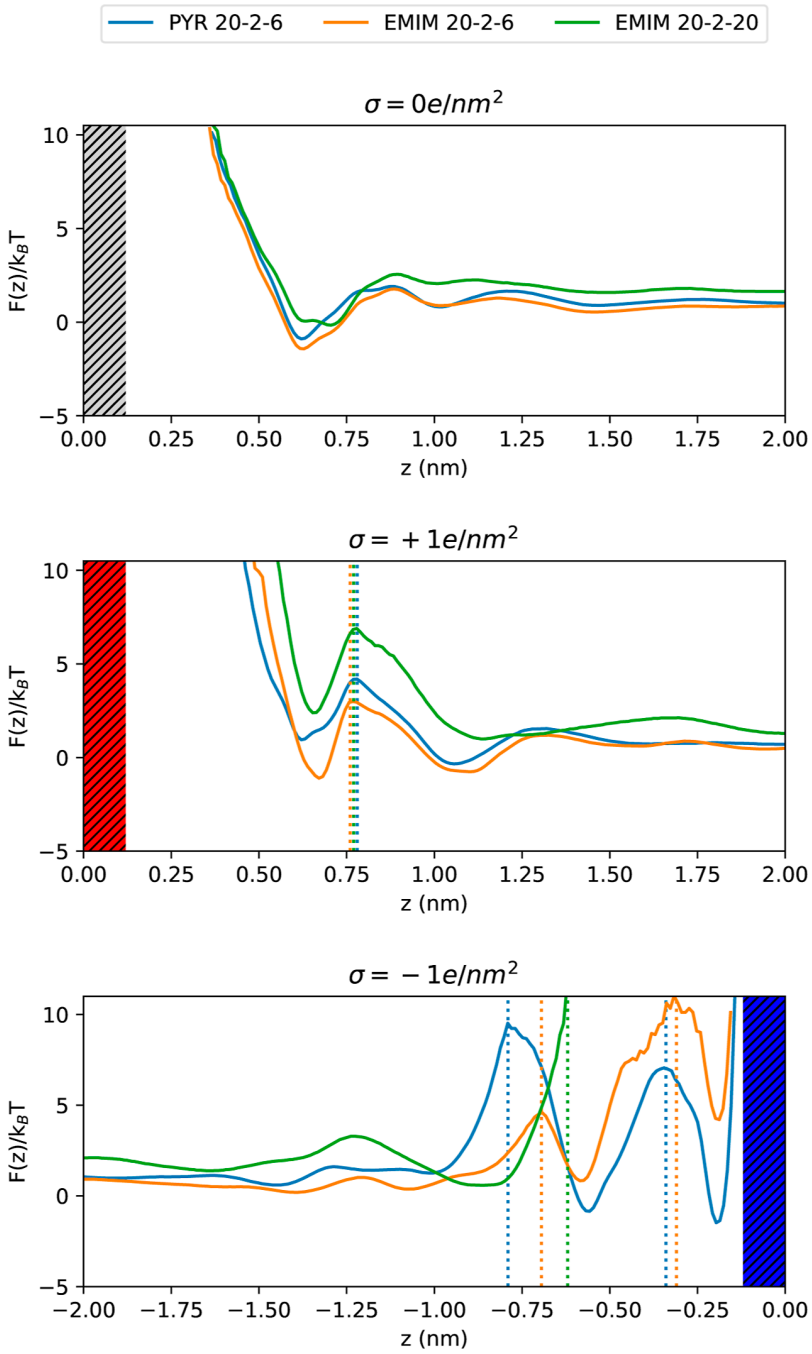


Figure 7. Free-energy profiles for lithium ions approaching the graphene-like surfaces with neutral (top), positive (center), and negative (bottom) charge densities for the investigated TSPEs. Dotted lines show the positions of the barrier for all the concentrations: PYR 20−2−6 (blue), EMIM 20−2−6 (orange), and EMIM 20−2−20 (green). In all cases, the corresponding electrode is located at z = 0.0 nm.

calculating the radius of gyration (R_g) and the end-to-end distance (d_e), which quantify the chain expansion in the mixture and can be calculated, respectively, as

$$R_g^2 = \langle \frac{1}{N} \sum_i |\vec{r}_i - \vec{r}_{cm}|^2 \rangle \quad (2)$$

and

$$d_e^2 = \langle |\vec{r}_N - \vec{r}_0|^2 \rangle \quad (3)$$

where N is the number of atoms in a PEO chain, $\vec{r}_N$ and $\vec{r}_0$ are the coordinates of the last and the first atoms of the chain, respectively, and r_{cm} is the center of mass of a chain. The results for the radius of gyration as a function of the position of the polymer along the simulation box axis can be seen in Figure 9, whereas those for the end-to-end distance are included in Figure S4 of the Supporting Information. In order to obtain these plots, the computed quantities for each chain were assigned to the z coordinate of all of the backbone atoms of the said chain (oxygens and carbons). Our findings show that the radius of gyration increases in the proximity of the neutral and the positively charged walls, which indicates that the PEO backbone is less folded in the interfacial region. This behavior seems to be

https://doi.org/10.1021/acs.macromol.3c02669
Macromolecules 2024, 57, 3921−3936

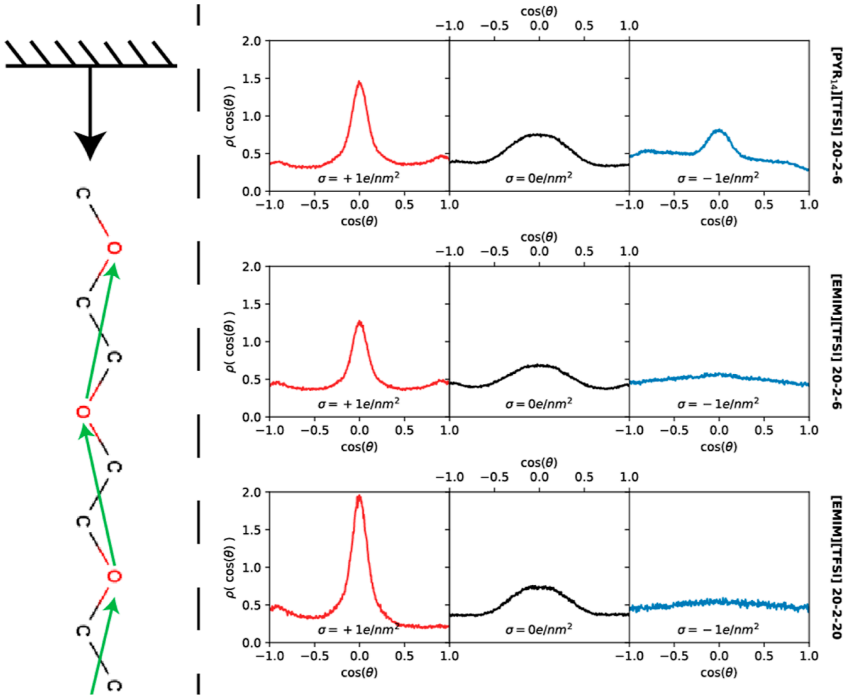


Figure 8. Marginal probability density distribution of polymer orientation relative to the vector normal to the graphene-like surface in the interfacial region (up to 2 nm). A scheme depicting the characteristic vectors defined for the polymer is shown on the left.

in open contradiction with the fact that the O(PEO)−Li^+ interactions were observed to increase close to the graphene-like walls, and the radius of gyration is expected to decrease when increasing those interactions, as previously reported for PEO-based electrolytes confined between Li-metal surfaces.[62,64] However, as previously stated in this work, PEO molecules in the interfacial region strongly interact with the carbon atoms of the wall, which leads to the unfolding of the polymer. In addition, the radius of gyration is also observed to increase close to the negatively charged surface in mixtures with $[PYR_{14}]$-[TFSI] due to the enhanced presence of lithium cations and polymer molecules in that interface. In general, the interaction with Li^+ in the bulk leads to a globule conformation of the polymer on a local scale. However, globally, the constraint introduced by the graphene-like wall and the fact that PEO tries to maximize the interaction with both the surface and all the Li^+ cations in the interfacial region lead to a transition to a coil conformation. In addition, we computed the gyration tensor in order to further confirm this picture. The gyration tensor of a set of N points can be defined as

$$G_{ij} = \frac{1}{N}\sum_{k=1}^{N} r_i^{(k)} r_j^{(k)} \tag{4}$$

provided that the center of mass of the points is set to zero. The eigenvalues and eigenvectors of this tensor, or more specifically, the square root of these eigenvalues, offer a measure of the shape of the point cloud. In our case, we can see plotted in Figure S5 the values corresponding to the Z direction as well as those corresponding to directions contained in the XY plane. These values were computed for all polymers and discretized into bins so that we could see the variation of these parameters along the Z axis. As we can see, throughout the simulation box, the square root of the eigenvalues of the XY plane is comparable and substantially larger than that of Z. This once again confirms our view, suggesting that polymer conformations are disk-shaped and parallel to the surface. This situation is, as we hinted earlier, even more marked at the vicinity of the interface as the value corresponding to the Z direction decreases even further in general.

As is well-known, Li^+ diffusion plays a crucial role in the kinetic process that takes place in battery electrodes and thus in the performance of energy storage devices. To obtain information on Li^+ dynamics, we analyzed the Li^+-cation diffusion by calculating the variance $\mathrm{Var}[\Delta z]$ of the displacement vector Δz of these ions as a function of their initial position in z, as described in ref 63. The variance of the lithium displacements is calculated as

$$\mathrm{Var}[\Delta z] = \langle \Delta z^2 \rangle - \langle \Delta z \rangle^2 \tag{5}$$

with $\langle \Delta z^2 \rangle$ being the mean-square displacement, and $\langle \Delta z \rangle^2$ the square of the mean displacement in the z direction. The brackets indicate the average over all of the particles of the same species and the average over multiple starting times, t_k. Thus, the displacement of a given molecule after a lag-time Δt is

$$\Delta z(\Delta t) = z(t_k + \Delta t) - z(t_k) \tag{6}$$

The variance of the displacements in the x and y directions were calculated in the same way and all of them are represented in Figure 10 for a lag-time of 1 ns as a function of the initial position in z.

It can be observed that, regardless of the charge of the electrodes, of the IL cation, and of the amount of IL, the diffusion of Li^+ ions in the direction perpendicular to the graphene-like surface always slows in the interfacial region, where the formation of layers takes place. At neutral interfaces, the z displacement variance decreases in a similar way for all the systems compared to the bulk, which is consistent with the nearly identical free-energy barriers in the neighborhood of these surfaces, as shown in Figure 7. Charging the electrodes

https://doi.org/10.1021/acs.macromol.3c02669
Macromolecules 2024, 57, 3921−3936

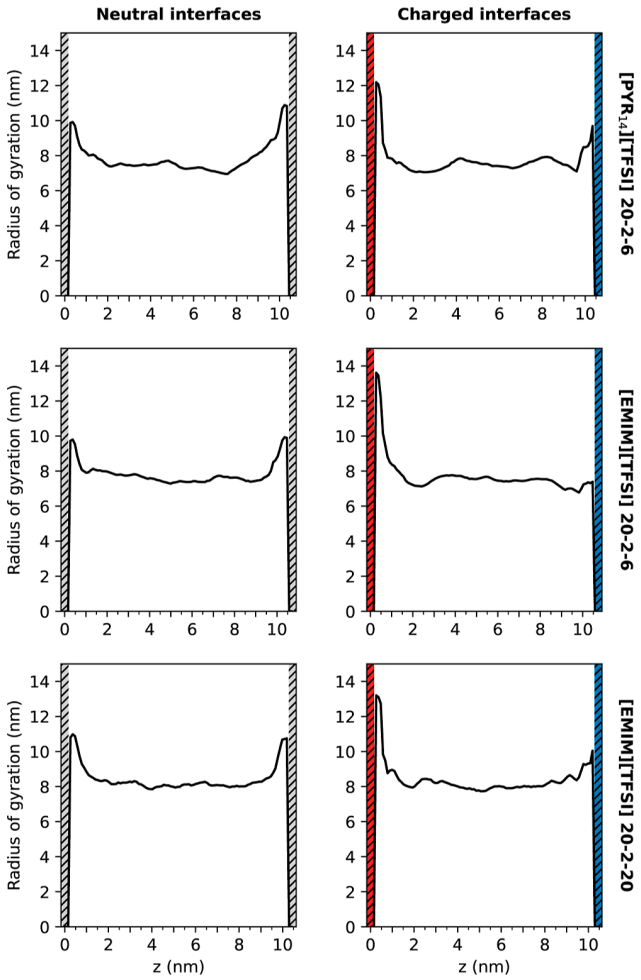


Figure 9. Radius of gyration in the z direction for TSPEs confined between neutral (left) and charged (right) graphene-like surfaces.

leads to diverse modifications of the z displacement variance in the interfacial region for different systems. In general, the shortest z displacement variances correspond to those electrolytes with the most stable minima in the free-energy profiles, which is in agreement with Li^+ cations remaining at the interfaces once they reach that region. These results are indicative of a high interfacial resistance to ionic mobility at both the positively and negatively charged electrode interfaces due to strong interfacial layering. In addition, it can be seen that the bulk behavior is not 100% recovered in the center of the simulation box, since the displacement variances in the direction perpendicular to the electrodes are always lower than those in the x and y directions.

In the directions parallel to the electrodes, the variance of the displacement shows a much lower degree of dependence with the distance to the carbon interface compared to the perpendicular direction. In addition, Li^+-cation diffusion is slightly faster in the regions of the outer layers of the electric double layer (EDL) and then decreases again in the inner layers, probably due to a constraining effect due to the presence of other species or to the own charge of the electrode. In summary, the molecular conformation at the innermost layer of the EDL inhibits Li^+ transport in the three directions, but their migration toward the electrode suffers a much more marked "locked-in-place" effect once within the interfacial layering.

From the analysis of the displacement variance, we can also infer that Li^+ mobility slightly increases with increasing IL concentration, both between neutral and charged graphene-like surfaces, which can be indicative of the IL acting as a plasticizer. Also, the comparison between both ILs at a proportion of 20−2−6 shows that the addition of [EMIM][TFSI] leads to moderately enhanced Li^+ dynamics.

The variance of the displacements of PEO oxygens is included in Figure S6 of the Supporting Information. There it can be seen that PEO diffusion shows, in general, the same features as those of Li^+ ions. We can observe the same restraint in the motion perpendicular to the electrodes when the oxygen atoms are located close to the interface. It is interesting to notice that the variance in this direction never reaches values comparable to those of the x and y directions. This effect is likely due to the much larger size of the PEO chains compared to the other molecular species. This way, the chains could "feel" the presence of the interfaces even when part of it is far away from the electrode.

Influence of Adding IL into the Binary SPE (PEO/LiTFSI). As is well-known, the addition of an IL to an SPE leads to a plasticizing effect that enhances the mobility of the Li^+ cation, which confers ideal properties to the TSPEs. Understanding the role of the IL in the structure of these ternary mixtures is therefore of paramount importance. In this section, we will attempt to shed some light on this issue. Previously, Thum et al.[63] reported structural results for an SPE composed of both PEO and [Li][TFSI] in the presence of neutral and charged graphene-like surfaces.

Concerning Li^+ solvation in bulk, the main effect of IL inclusion is the appearance of some degree of coordination with TFSI oxygen atoms, which was hardly present for PEO−LiTFSI binary mixtures at the expense of decreasing that with PEO oxygens. The total number of 6 oxygens around a given lithium is not changed with the addition of the IL, but the coordination environment of 6 PEO oxygens observed by Thum et al.[63] is more markedly modified when increasing the amount of [EMIM][TFSI], even being swung up to a solvation shell composed of 4 and 2 oxygens from TFSI and PEO, respectively, which can be attributed to a dilution of the polymer. In the proximity of graphene-like surfaces, the addition of an IL to the binary SPE affects the surroundings of Li^+ cations in a less pronounced way compared with the bulk, but the results depend on the charge of the electrode. For neutral surfaces, the insertion of an IL leads to Li^+ being surrounded not by 5 PEO oxygens but instead by 4 and 2 oxygen atoms from PEO and TFSI, respectively. This proportion is reversed with increasing IL concentration. Concerning the positively charged surface, we observed that the interaction with the polymer decreases from 5 PEO oxygens to 3−4 when including any of the ILs, whereas the number of TFSI oxygens is kept at 2−3. This shows that the charge of the surface dominates over the addition of the IL, as this is the electrode that electrostatically attracts the anions, which increases the interaction between $TFSI^-$ and solvated Li^+. On the other hand, near the negative electrode, the structural picture depends on the concentration of IL. At low amounts of IL, the 2−3 PEO oxygens coordinating a Li^+ observed in the binary SPE are kept in ternary mixtures, although the inclusion of IL leads to the incorporation of two TFSI oxygens to the Li^+ first solvation shell. At high [EMIM][TFSI] concentrations, the anions take 4−5 of the 6 interaction sites of Li^+.

The comparison of the number density profiles with those reported by Thum et al.[63] reveals that, near neutral graphene-

https://doi.org/10.1021/acs.macromol.3c02669
Macromolecules 2024, 57, 3921−3936

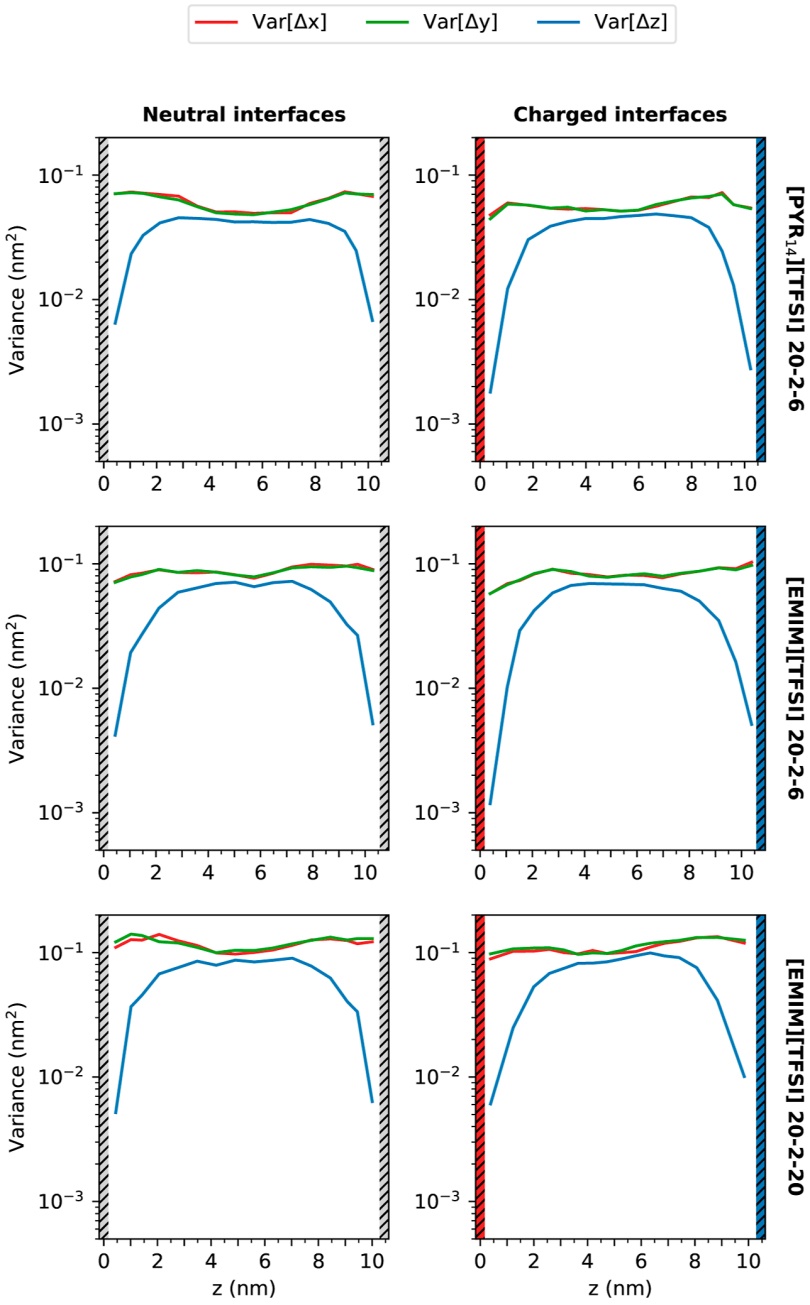


Figure 10. Displacement variance (eq 5) of Li^+ cations in the three directions as a function of the initial position in z for TSPEs confined between neutral (left) and charged (right) graphene-like surfaces.

like surfaces, the addition of IL does not markedly modify the composition of the innermost layer of the EDL, which is filled up with anions and polymer molecules. Also, the peak positions of Li^+ do not change relative to those observed by Thum et al.[63] However, while they obtained a similar height for both peaks, in TSPEs, there is a clear tendency of Li^+ ions to be placed as close as possible to the electrode. On the other hand, the layer that is in direct contact with the positively charged surface is still shared by polymers and anions regardless of the inclusion of IL. Notwithstanding, for low IL concentrations, a new position of Li^+ appears at around 0.6 nm, which probably corresponds to those lithiums that are dragged by the anions. With respect to the negative electrode, some noteworthy changes are observed when adding IL to the binary SPE studied by Thum et al.[63] First, the positions close to the surface at which PEO molecules are located in binary mixtures are now occupied by the IL cations in the ternary ones. Second, this leads to a competition between Li^+ and IL cations to reach the negatively charged surface, which is more remarkable when increasing the amount of IL, as expected. In fact, at the highest [EMIM][TFSI] concentration, the negative electrode is observed to be fully impregnated by $EMIM^+$ and Li^+ and neither PEO is able to get to the innermost layer.

The number density profiles are directly related to the energy landscape that Li^+ has to cross to reach the electrodes. Those free-energy profiles are much smoother with the addition of IL, in particular, in those systems with neutral graphene-like walls, where the energetic barrier almost vanishes. Previous results

https://doi.org/10.1021/acs.macromol.3c02669
Macromolecules 2024, 57, 3921−3936

reported by Thum et al.[63] for neutral surfaces showed a much more layered profile for the binary SPE, where lithium cations need to overcome several barriers before reaching the interfacial region. In the absence of Coulomb interactions with the electrodes that add competing effects into the systems, these smoother energy profiles can be indicative of a reduced degree of ordering with the addition of IL that facilitates the motion of Li^+ through the simulation box toward the surfaces. Although we cannot establish a clear connection between the well-known plasticizer effect of the IL from our MD simulations and those of Thum et al.,[63] the comparison between the free-energy profiles at charged interfaces indicates that, for choosing the amount of IL to be added to the binary SPE, a compromise between enhancing PEO and Li^+ motion and how the IL ions are going to compete for the electrodes must be made. In this regard, our results advise us to avoid very high IL concentrations.

CONCLUSIONS

In the present work, classical MD simulations were performed for TSPEs [containing the polymer PEO, a lithium salt ([Li][TFSI]), and an IL] confined between two graphene-like surfaces. Two ILs at different concentrations were tested, $[PYR_{14}][TFSI]$ and [EMIM][TFSI], with the aim of determining the optimal composition of the electrolyte system for application in energy storage devices. The structural picture of the molecular species in the interfacial region with both charged and uncharged walls was characterized by the RDFs, the coordination numbers, the number density profiles, and the orientations. The dynamics and kinetics of Li^+ motion were analyzed in terms of the variance of the displacement and the free-energy profiles. In addition, the PEO conformation was investigated through calculation of the radius of gyration and the end-to-end distance.

All systems show the typical electrolyte−electrode interfacial layering characteristic. This results in Li^+ being preferentially coordinated with the PEO oxygens instead of with $TFSI^-$ anions in the neighborhood of neutral graphene-like surfaces, which is the opposite behavior of the one previously observed for Li-metal electrodes. The innermost layer in the neutral interfacial region is mainly composed of PEO molecules, which are arranged parallel to the surface in a "flat" conformation trying to maximize their interaction with the hydrophobic graphene. In the presence of charged graphene-like surfaces, lithium cations more easily approach the negatively charged electrode with the pyrrolidinium-based TSPE, rather than with the imidazolium-based one even for high concentrations, which is probably due to the lower degree of anion clustering with Li^+ in the former case. This allows lithium cations to coordinate with the polymer and reach the negative surface. However, the analysis of the free-energy profiles shows that the barriers lithium cations must overcome to come into contact with the negative electrode are much higher than the thermal energy, so the diffusion process can be regarded as a rare event, which, in the case of taking place, would lead to very stable Li^+ adsorption. Concerning the dynamics, the diffusion of Li^+ ions in the direction perpendicular to the graphene-like surfaces always slows down regardless of their charge due to the strong interfacial layering that leads to a high interfacial resistance to ionic mobility.

In summary, although our findings indicate that large amounts of imidazolium-based ILs increase Li^+ mobility due to a plasticizing effect, we also observed that the presence of the $[PYR_{14}^+]$ cation energetically favors Li^+ presence at the negative electrode when compared to $[EMIM^+]$. Thus, we suggest the use of low amounts of pyrrolidinium-based ILs as the proper selection of the TSPE in order to optimize solid-like battery performance.

ASSOCIATED CONTENT

Supporting Information

The Supporting Information is available free of charge at https://pubs.acs.org/doi/10.1021/acs.macromol.3c02669.

RDFs of binary mixtures IL + LiTFSI, orientations of both IL cations, and displacement variance of PEO oxygens (PDF)

AUTHOR INFORMATION

Corresponding Authors

Hadrian Montes-Campos − *Grupo de Nanomateriais, Fotónica e Materia Branda, Departamento de Física de Partículas, Universidade de Santiago de Compostela, E-15782 Santiago de Compostela, Spain; Instituto de Materiais (iMATUS), Universidade de Santiago de Compostela, E-15706 Santiago de Compostela, Spain; CIQUP, Institute of Molecular Sciences (IMS)—Departamento de Química e Bioquímica, Faculdade de Ciências da Universidade do Porto, 4169-007 Porto, Portugal;* orcid.org/0000-0001-9861-8076; Email: hadrian.montes@usc.es

Luis Miguel Varela − *Grupo de Nanomateriais, Fotónica e Materia Branda, Departamento de Física de Partículas, Universidade de Santiago de Compostela, E-15782 Santiago de Compostela, Spain; Instituto de Materiais (iMATUS), Universidade de Santiago de Compostela, E-15706 Santiago de Compostela, Spain;* orcid.org/0000-0002-0569-0042; Email: luismiguel.varela@usc.es

Authors

Alejandro Rivera-Pousa − *Grupo de Nanomateriais, Fotónica e Materia Branda, Departamento de Física de Partículas, Universidade de Santiago de Compostela, E-15782 Santiago de Compostela, Spain; Instituto de Materiais (iMATUS), Universidade de Santiago de Compostela, E-15706 Santiago de Compostela, Spain;* orcid.org/0000-0001-6820-7823

José Manuel Otero-Mato − *Grupo de Nanomateriais, Fotónica e Materia Branda, Departamento de Física de Partículas, Universidade de Santiago de Compostela, E-15782 Santiago de Compostela, Spain; Instituto de Materiais (iMATUS), Universidade de Santiago de Compostela, E-15706 Santiago de Compostela, Spain;* orcid.org/0000-0001-6718-2011

Trinidad Méndez-Morales − *Grupo de Nanomateriais, Fotónica e Materia Branda, Departamento de Física de Partículas, Universidade de Santiago de Compostela, E-15782 Santiago de Compostela, Spain; Instituto de Materiais (iMATUS), Universidade de Santiago de Compostela, E-15706 Santiago de Compostela, Spain;* orcid.org/0000-0002-9795-6302

Diddo Diddens − *Helmholtz-Institute Münster (HI MS), Ionics in Energy Storage, Forschungszentrum Jülich GmbH, 48149 Münster, Germany;* orcid.org/0000-0002-2137-1332

Andreas Heuer − *Helmholtz-Institute Münster (HI MS), Ionics in Energy Storage, Forschungszentrum Jülich GmbH, 48149 Münster, Germany; Institute of Physical Chemistry, University of Münster, 48149 Münster, Germany*

Complete contact information is available at: https://pubs.acs.org/10.1021/acs.macromol.3c02669

https://doi.org/10.1021/acs.macromol.3c02669
Macromolecules 2024, 57, 3921−3936

Notes

The authors declare no competing financial interest.

■ ACKNOWLEDGMENTS

The financial support of the Spanish Ministry of Science and Innovation (PID2021-126148NA-I00 funded by MCIN/AEI/10.13039/501100011033/FEDER, UE) is gratefully acknowledged. Moreover, this work was funded by the Xunta de Galicia (GRC ED431C 2020/10). A.R.-P. thanks the Spanish Ministry of Education for his FPU18/01597 grant. T.M.-M. acknowledges her contract funded by the pilot program of the USC for the recruitment of distinguished research personnel—call 2021 under the agreement between the USC and the Santander Bank for 2021−2024. H.M.-C. thanks the USC for his "Convocatoria de Recualificación do Sistema Universitario Español-Margarita Salas" postdoctoral grant under the "Plan de Recuperación Transformación" program funded by the Spanish Ministry of Universities with European Union's NextGenerationEU funds. This work was supported by the Fundacão para a Ciência e Tecnologia (FCT) funded by national funds through the FCT/MCTES (PIDDAC) to CIQUP, Faculty of Science, University of Porto (project UIDB/00081/2020), IMS-Institute of Molecular Sciences (LA/P/0056/2020). A.H. and D.D. thank the German Federal Ministry of Education and Research (BMBF) for financial support through the projects FestBatt (grant number 03XP0174B) and FestBatt2 (grant number 03XP0435E).

■ REFERENCES

(1) Dutta, A.; Mitra, S.; Basak, M.; Banerjee, T. A comprehensive review on batteries and supercapacitors: development and challenges since their inception. *Energy Storage* **2023**, *5*, No. e339.
(2) Manthiram, A. An outlook on lithium ion battery technology. *ACS Cent. Sci.* **2017**, *3*, 1063−1069.
(3) Masias, A.; Marcicki, J.; Paxton, W. A. Opportunities and challenges of lithium ion batteries in automotive applications. *ACS Energy Lett.* **2021**, *6*, 621−630.
(4) Etacheri, V.; Marom, R.; Elazari, R.; Salitra, G.; Aurbach, D. Challenges in the development of advanced Li-ion batteries: a review. *Energy Environ. Sci.* **2011**, *4*, 3243−3262.
(5) Xiao, J. How lithium dendrites form in liquid batteries. *Science* **2019**, *366*, 426−427.
(6) An, Y.; Han, X.; Liu, Y.; Azhar, A.; Na, J.; Nanjundan, A. K.; Wang, S.; Yu, J.; Yamauchi, Y. Progress in Solid Polymer Electrolytes for Lithium-Ion Batteries and Beyond. *Small* **2022**, *18*, 2103617.
(7) Agrawal, R.; Pandey, G. Solid polymer electrolytes: materials designing and all-solid-state battery applications: an overview. *J. Phys. D* **2008**, *41*, 223001.
(8) Fenton, D.; Parker, J.; Wright, P. Complexes of alkali metal ions with poly(ethylene oxide). *Polymer* **1973**, *14*, 589.
(9) Armand, M.; Chabagno, J.; Duclot, M. l. others Fast ion transport in solids: electrodes and electrolytes. In *Proceedings of the International Conference on Fast Ion Transport in Solids; Electrodes, and Electrolytes, Lake Geneva, Wisconsin, USA, May 21−25. 1979*.
(10) Armand, M. Polymer solid electrolytes-an overview. *Solid State Ionics* **1983**, *9−10*, 745−754.
(11) Berthier, C.; Gorecki, W.; Minier, M.; Armand, M.; Chabagno, J.; Rigaud, P. Microscopic investigation of ionic conductivity in alkali metal salts-poly (ethylene oxide) adducts. *Solid State Ionics* **1983**, *11*, 91−95.
(12) Tominaga, Y.; Yamazaki, K.; Nanthana, V. Effect of anions on lithium ion conduction in poly (ethylene carbonate)-based polymer electrolytes. *J. Electrochem. Soc.* **2015**, *162*, A3133−A3136.
(13) Do, C.; Lunkenheimer, P.; Diddens, D.; Götz, M.; Weiß, M.; Loidl, A.; Sun, X.-G.; Allgaier, J.; Ohl, M. Li+ transport in poly (ethylene oxide) based electrolytes: neutron scattering, dielectric spectroscopy, and molecular dynamics simulations. *Phys. Rev. Lett.* **2013**, *111*, 018301.
(14) Diddens, D.; Heuer, A.; Borodin, O. Understanding the lithium transport within a rouse-based model for a PEO/LiTFSI polymer electrolyte. *Macromolecules* **2010**, *43*, 2028−2036.
(15) Borodin, O.; Smith, G. D. Mechanism of ion transport in amorphous poly (ethylene oxide)/LiTFSI from molecular dynamics simulations. *Macromolecules* **2006**, *39*, 1620−1629.
(16) Mao, G.; Saboungi, M.-L.; Price, D. L.; Armand, M. B.; Howells, W. Structure of liquid PEO-LiTFSI electrolyte. *Phys. Rev. Lett.* **2000**, *84*, 5536−5539.
(17) Costa, L. T.; Siqueira, L. J.; Nicolau, B. G.; Ribeiro, M. C. Raman spectra of polymer electrolytes based on poly (ethylene glycol) dimethyl ether, lithium perchlorate, and the ionic liquid 1-butyl-3-methylimidazolium hexafluorophosphate. *Vib. Spectrosc.* **2010**, *54*, 155−158.
(18) Molinari, N.; Mailoa, J. P.; Kozinsky, B. Effect of salt concentration on ion clustering and transport in polymer solid electrolytes: a molecular dynamics study of peo−litfsi. *Chem. Mater.* **2018**, *30*, 6298−6306.
(19) Croce, F.; Appetecchi, G.; Persi, L.; Scrosati, B. Nanocomposite polymer electrolytes for lithium batteries. *Nature* **1998**, *394*, 456−458.
(20) Croce, F.; Persi, L.; Ronci, F.; Scrosati, B. Nanocomposite polymer electrolytes and their impact on the lithium battery technology. *Solid State Ionics* **2000**, *135*, 47−52.
(21) Song, S.; Wu, Y.; Tang, W.; Deng, F.; Yao, J.; Liu, Z.; Hu, R.; Alamusi; Wen, Z.; Lu, L.; et al. Composite Solid Polymer Electrolyte with Garnet Nanosheets in Poly(ethylene oxide). *ACS Sustain. Chem. Eng.* **2019**, *7*, 7163−7170.
(22) Manuel Stephan, A. Review on gel polymer electrolytes for lithium batteries. *Eur. Polym. J.* **2006**, *42*, 21−42.
(23) Rüther, T.; Bhatt, A. I.; Best, A. S.; Harris, K. R.; Hollenkamp, A. F. Electrolytes for lithium (sodium) batteries based on ionic liquids: Highlighting the key role played by the anion. *Batteries Supercaps* **2020**, *3*, 793−827.
(24) Lei, Z.; Chen, B.; Koo, Y. M.; MacFarlane, D. R. Introduction: Ionic Liquids. *Chem. Rev.* **2017**, *117*, 6633−6635.
(25) Welton, T. Ionic liquids: a brief history. *Biophys. Rev.* **2018**, *10*, 691−706.
(26) Greaves, T. L.; Drummond, C. J. Protic ionic liquids: properties and applications. *Chem. Rev.* **2008**, *108*, 206−237.
(27) Zhang, S.; Sun, N.; He, X.; Lu, X.; Zhang, X. Physical properties of ionic liquids: database and evaluation. *J. Phys. Chem. Ref. Data* **2006**, *35*, 1475−1517.
(28) Plechkova, N. V.; Seddon, K. R. Applications of ionic liquids in the chemical industry. *Chem. Soc. Rev.* **2008**, *37*, 123−150.
(29) MacFarlane, D. R.; Tachikawa, N.; Forsyth, M.; Pringle, J. M.; Howlett, P. C.; Elliott, G. D.; Davis, J. H.; Watanabe, M.; Simon, P.; Angell, C. A. Energy applications of ionic liquids. *Energy Environ. Sci.* **2014**, *7*, 232−250.
(30) Marrucho, I.; Branco, L.; Rebelo, L. Ionic liquids in pharmaceutical applications. *Annu. Rev. Chem. Biomol.* **2014**, *5*, 527−546.
(31) Borgel, V.; Markevich, E.; Aurbach, D.; Semrau, G.; Schmidt, M. On the application of ionic liquids for rechargeable Li batteries: High voltage systems. *J. Power Sources* **2009**, *189*, 331−336.
(32) Vallet, P.; Bouzón-Capelo, S.; Méndez-Morales, T.; Gómez-González, V.; Arosa, Y.; de la Fuente, R.; López-Lago, E.; Rodríguez, J. R.; Gallego, L. J.; Parajó, J. J.; et al. On the physical properties of mixtures of nitrate salts and protic ionic liquids. *J. Mol. Liq.* **2022**, *350*, 118483.
(33) Asenbauer, J.; Ben Hassen, N.; McCloskey, B. D.; Prausnitz, J. M. Solubilities and ionic conductivities of ionic liquids containing lithium salts. *Electrochim. Acta* **2017**, *247*, 1038−1043.
(34) Rosenwinkel, M. P.; Schönhoff, M. Polymer-Induced Inversion of the Li+ Drift Direction in Ionic Liquid-Based Ternary Polymer Electrolytes. *Macromol. Chem. Phys.* **2022**, *223*, 2100320.
(35) Chaurasia, S. K.; Saroj, A. L.; Shalu; Singh, V. K.; Tripathi, A.; Gupta, A.; Verma, Y.; Singh, R. Studies on structural, thermal and AC

https://doi.org/10.1021/acs.macromol.3c02669
Macromolecules 2024, 57, 3921−3936

conductivity scaling of PEO-LiPF6 polymer electrolyte with added ionic liquid [BMIMPF6]. *AIP Adv.* **2015**, *5*, 077178.
(36) Kim, Y. H.; Cheruvally, G.; Choi, J. W.; Ahn, J. H.; Kim, K. W.; Ahn, H. J.; Choi, D. S.; Song, C. E. Electrochemical Properties of PEO-Based Polymer Electrolytes Blended with Different Room Temperature Ionic Liquids. *Macromol. Symp.* **2007**, *249*−*250*, 183−189.
(37) Choi, J.-W.; Cheruvally, G.; Kim, Y.-H.; Kim, J.-K.; Manuel, J.; Raghavan, P.; Ahn, J.-H.; Kim, K.-W.; Ahn, H.-J.; Choi, D. S.; et al. Poly(ethylene oxide)-based polymer electrolyte incorporating room-temperature ionic liquid for lithium batteries. *Solid State Ionics* **2007**, *178*, 1235−1241.
(38) Kumar, Y.; Hashmi, S.; Pandey, G. Lithium ion transport and ion−polymer interaction in PEO based polymer electrolyte plasticized with ionic liquid. *Solid State Ionics* **2011**, *201*, 73−80.
(39) Mogurampelly, S.; Ganesan, V. Structure and mechanisms underlying ion transport in ternary polymer electrolytes containing ionic liquids. *J. Chem. Phys.* **2017**, *146*, 074902.
(40) Zhu, C.; Cheng, H.; Yang, Y. Electrochemical characterization of two types of PEO-based polymer electrolytes with room-temperature ionic liquids. *J. Electrochem. Soc.* **2008**, *155*, A569.
(41) Costa, L. T.; Sun, B.; Jeschull, F.; Brandell, D. Polymer-ionic liquid ternary systems for Li-battery electrolytes: Molecular dynamics studies of LiTFSI in a EMIm-TFSI and PEO blend. *J. Chem. Phys.* **2015**, *143*, 024904.
(42) Atik, J.; Diddens, D.; Thienenkamp, J. H.; Brunklaus, G.; Winter, M.; Paillard, E. Cation-assisted lithium-ion transport for high-performance peo-based ternary solid polymer electrolytes. *Angew. Chem., Int. Ed.* **2021**, *60*, 11919−11927.
(43) Atik, J.; Thienenkamp, J. H.; Brunklaus, G.; Winter, M.; Paillard, E. Ionic liquid plasticizers comprising solvating cations for lithium metal polymer batteries. *Electrochim. Acta* **2021**, *398*, 139333.
(44) Widstrom, M. D.; Ludwig, K. B.; Matthews, J. E.; Jarry, A.; Erdi, M.; Cresce, A. V.; Rubloff, G.; Kofinas, P. Enabling high performance all-solid-state lithium metal batteries using solid polymer electrolytes plasticized with ionic liquid. *Electrochim. Acta* **2020**, *345*, 136156.
(45) Casalegno, M.; Castiglione, F.; Raos, G.; Appetecchi, G. B.; Passerini, S.; Mele, A.; Ragg, E. Magnetic Resonance Imaging and Molecular Dynamics Characterization of Ionic Liquid in Poly (ethylene oxide)-Based Polymer Electrolytes. *ACS Appl. Mater. Interfaces* **2020**, *12*, 23800−23811.
(46) Shin, J.-H.; Henderson, W. A.; Tizzani, C.; Passerini, S.; Jeong, S.-S.; Kim, K.-W. Characterization of Solvent-Free Polymer Electrolytes Consisting of Ternary PEO−LiTFSI−PYR[sub 14] TFSI. *J. Electrochem. Soc.* **2006**, *153*, A1649.
(47) Ma, F.; Zhang, Z.; Yan, W.; Ma, X.; Sun, D.; Jin, Y.; Chen, X.; He, K. Solid polymer electrolyte based on polymerized ionic liquid for high performance all-solid-state lithium-ion batteries. *ACS Sustain. Chem. Eng.* **2019**, *7*, 4675−4683.
(48) Hoffknecht, J.-P.; Wettstein, A.; Atik, J.; Krause, C.; Thienenkamp, J.; Brunklaus, G.; Winter, M.; Diddens, D.; Heuer, A.; Paillard, E. Coordinating Anions "to the Rescue" of the Lithium Ion Mobility in Ternary Solid Polymer Electrolytes Plasticized With Ionic Liquids. *Adv. Energy Mater.* **2023**, *13*, 2202789.
(49) de Vries, H.; Jeong, S.; Passerini, S. Ternary polymer electrolytes incorporating pyrrolidinium-imide ionic liquids. *RSC Adv.* **2015**, *5*, 13598−13606.
(50) Joost, M.; Kunze, M.; Jeong, S.; Schönhoff, M.; Winter, M.; Passerini, S. Ionic mobility in ternary polymer electrolytes for lithium-ion batteries. *Electrochim. Acta* **2012**, *86*, 330−338.
(51) Johansson, P. Computational modelling of polymer electrolytes: What do 30 years of research efforts provide us today? *Electrochim. Acta* **2015**, *175*, 42−46.
(52) Mogurampelly, S.; Borodin, O.; Ganesan, V. Computer simulations of ion transport in polymer electrolyte membranes. *Annu. Rev. Chem. Biomol.* **2016**, *7*, 349−371.
(53) Ebadi, M.; Marchiori, C.; Mindemark, J.; Brandell, D.; Araujo, C. M. Assessing structure and stability of polymer/lithium-metal interfaces from first-principles calculations. *J. Mater. Chem. A* **2019**, *7*, 8394−8404.
(54) Mirsakiyeva, A.; Ebadi, M.; Araujo, C. M.; Brandell, D.; Broqvist, P.; Kullgren, J. Initial steps in PEO decomposition on a Li metal electrode. *J. Phys. Chem. C* **2019**, *123*, 22851−22857.
(55) Fischer, M.; Heuer, A.; Diddens, D. Structure and Transport Properties of Poly (ethylene oxide)-Based Cross-Linked Polymer Electrolytes- A Molecular Dynamics Simulations Study. *Macromolecules* **2022**, *55*, 10229−10242.
(56) Otero-Mato, J. M.; Rivera-Pousa, A.; Montes-Campos, H.; Cabeza, O.; Heuer, A.; Diddens, D.; Varela, L. M. Computational study of the structure of ternary ionic liquid/salt/polymer electrolytes based on protic ionic liquids. *J. Mol. Liq.* **2021**, *333*, 115883.
(57) Chattoraj, J.; Diddens, D.; Heuer, A. Effects of ionic liquids on cation dynamics in amorphous polyethylene oxide electrolytes. *J. Chem. Phys.* **2014**, *140*, 024906.
(58) Diddens, D.; Paillard, E.; Heuer, A. Improving the lithium ion transport in polymer electrolytes by functionalized ionic-liquid additives: simulations and modeling. *J. Electrochem. Soc.* **2017**, *164*, E3225−E3231.
(59) Diddens, D.; Heuer, A. Lithium ion transport mechanism in ternary polymer electrolyte-ionic liquid mixtures: A molecular dynamics simulation study. *ACS Macro Lett.* **2013**, *2*, 322−326.
(60) Diddens, D.; Heuer, A. Simulation study of the lithium ion transport mechanism in ternary polymer electrolytes: the critical role of the segmental mobility. *J. Phys. Chem. B* **2014**, *118*, 1113−1125.
(61) Xu, C.; Sun, B.; Gustafsson, T.; Edström, K.; Brandell, D.; Hahlin, M. Interface layer formation in solid polymer electrolyte lithium batteries: an XPS study. *J. Mater. Chem. A* **2014**, *2*, 7256−7264.
(62) Ebadi, M.; Costa, L. T.; Araujo, C. M.; Brandell, D. Modelling the polymer electrolyte/Li-metal interface by molecular dynamics simulations. *Electrochim. Acta* **2017**, *234*, 43−51.
(63) Thum, A.; Diddens, D.; Heuer, A. Impact of Charged Surfaces on the Structure and Dynamics of Polymer Electrolytes: Insights from Atomistic Simulations. *J. Phys. Chem. C* **2021**, *125*, 25392−25403.
(64) Lourenço, T. C.; Ebadi, M.; Brandell, D.; Da Silva, J. L.; Costa, L. T. Interfacial structures in ionic liquid-based ternary electrolytes for lithium-metal batteries: a molecular dynamics study. *J. Phys. Chem. B* **2020**, *124*, 9648−9657.
(65) Abraham, M. J.; Murtola, T.; Schulz, R.; Páll, S.; Smith, J. C.; Hess, B.; Lindahl, E. GROMACS: High performance molecular simulations through multi-level parallelism from laptops to supercomputers. *SoftwareX* **2015**, *1*−*2*, 19−25.
(66) Berendsen, H. J.; van der Spoel, D.; van Drunen, R. GROMACS: A message-passing parallel molecular dynamics implementation. *Comput. Phys. Commun.* **1995**, *91*, 43−56.
(67) Jorgensen, W. L.; Maxwell, D. S.; Tirado-Rives, J. Development and testing of the OPLS all-atom force field on conformational energetics and properties of organic liquids. *J. Am. Chem. Soc.* **1996**, *118*, 11225−11236.
(68) Canongia Lopes, J. N.; Deschamps, J.; Pádua, A. A. H. Modeling ionic liquids using a systematic all-atom force field. *J. Phys. Chem. B* **2004**, *108*, 2038−2047.
(69) Canongia Lopes, J. N.; Pádua, A. A. CL&P: A generic and systematic force field for ionic liquids modeling. *Theor. Chem. Acc.* **2012**, *131*, 1129.
(70) Pádua, A. A. H.; Costa Gomes, M. F.; Canongia Lopes, J. N. Molecular solutes in ionic liquids: a structural perspective. *Acc. Chem. Res.* **2007**, *40*, 1087−1096.
(71) Martínez, L.; Andrade, R.; Birgin, E. G.; Martínez, J. M. PACKMOL: A package for building initial configurations for molecular dynamics simulations. *J. Comput. Chem.* **2009**, *30*, 2157−2164.
(72) Berendsen, H. J.; Postma, J. P. M.; Van Gunsteren, W. F.; DiNola, A.; Haak, J. R. Molecular dynamics with coupling to an external bath. *J. Chem. Phys.* **1984**, *81*, 3684−3690.
(73) Humphrey, W.; Dalke, A.; Schulten, K. VMD: visual molecular dynamics. *J. Mol. Graphics* **1996**, *14*, 33−38.
(74) Darden, T.; York, D.; Pedersen, L. Particle mesh Ewald: An N log (N) method for Ewald sums in large systems. *J. Chem. Phys.* **1993**, *98*, 10089−10092.

https://doi.org/10.1021/acs.macromol.3c02669
Macromolecules 2024, 57, 3921−3936

(75) Essmann, U.; Perera, L.; Berkowitz, M. L.; Darden, T.; Lee, H.; Pedersen, L. G. A smooth particle mesh Ewald method. *J. Chem. Phys.* **1995**, *103*, 8577−8593.
(76) Yeh, I.-C.; Berkowitz, M. L. Ewald summation for systems with slab geometry. *J. Chem. Phys.* **1999**, *111*, 3155−3162.
(77) Merlet, C.; Péan, C.; Rotenberg, B.; Madden, P. A.; Simon, P.; Salanne, M. Simulating supercapacitors: Can we model electrodes as constant charge surfaces? *J. Phys. Chem. Lett.* **2013**, *4*, 264−268.
(78) Yang, J.; Bo, Z.; Yang, H.; Qi, H.; Kong, J.; Yan, J.; Cen, K. Reliability of Constant Charge Method for Molecular Dynamics Simulations on EDLCs in Nanometer and Sub-Nanometer Spaces. *ChemElectroChem* **2017**, *4*, 2486−2493.
(79) Evans, D. J.; Holian, B. L. The nose−hoover thermostat. *J. Chem. Phys.* **1985**, *83*, 4069−4074.
(80) Tong, J.; Wu, S.; Von Solms, N.; Liang, X.; Huo, F.; Zhou, Q.; He, H.; Zhang, S. The effect of concentration of lithium salt on the structural and transport properties of ionic liquid-based electrolytes. *Front. Chem.* **2020**, *7*, 945.
(81) Nasrabadi, A. T.; Ganesan, V. Structure and transport properties of lithium-doped aprotic and protic ionic liquid electrolytes: Insights from molecular dynamics simulations. *J. Phys. Chem. B* **2019**, *123*, 5588−5600.
(82) Leenaerts, O.; Partoens, B.; Peeters, F. Water on graphene: Hydrophobicity and dipole moment using density functional theory. *Phys. Rev. B* **2009**, *79*, 235440.
(83) Zhang, X.; Wan, S.; Pu, J.; Wang, L.; Liu, X. Highly hydrophobic and adhesive performance of graphene films. *J. Mater. Chem.* **2011**, *21*, 12251−12258.
(84) Perkin, S.; Albrecht, T.; Klein, J. Layering and shear properties of an ionic liquid, 1-ethyl-3-methylimidazolium ethylsulfate, confined to nano-films between mica surfaces. *Phys. Chem. Chem. Phys.* **2010**, *12*, 1243−1247.
(85) Hayes, R.; Borisenko, N.; Tam, M. K.; Howlett, P. C.; Endres, F.; Atkin, R. Double layer structure of ionic liquids at the Au (111) electrode interface: an atomic force microscopy investigation. *J. Phys. Chem. C* **2011**, *115*, 6855−6863.
(86) Bazant, M. Z.; Storey, B. D.; Kornyshev, A. A. Double layer in ionic liquids: Overscreening versus crowding. *Phys. Rev. Lett.* **2011**, *106*, 046102.

USC UNIVERSIDADE DE SANTIAGO DE COMPOSTELA

https://doi.org/10.1021/acs.macromol.3c02669
Macromolecules 2024, 57, 3921−3936

The Journal of Chemical Physics

RESEARCH ARTICLE | JANUARY 06 2022

Density functional theory of alkali metals at the IL/graphene electrochemical interface

Special Collection: The Chemical Physics of the Electrode-Electrolyte Interface

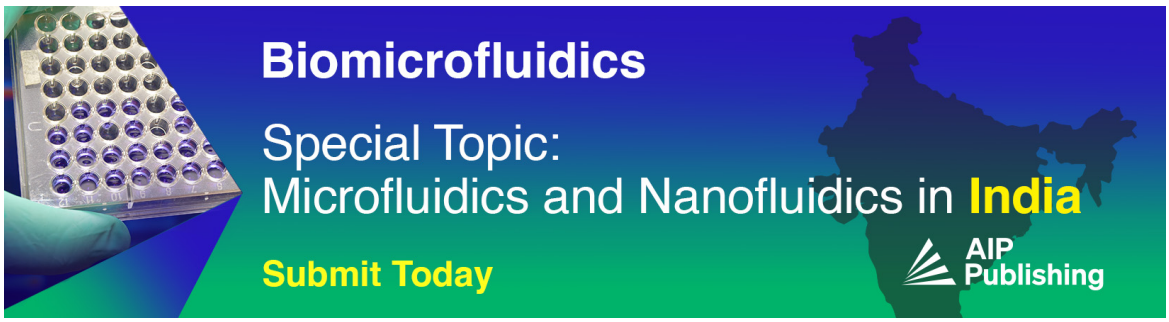
H. Montes-Campos ; A. Rivera-Pousa ; T. Méndez-Morales

Check for updates

J. Chem. Phys. 156, 014706 (2022)
https://doi.org/10.1063/5.0077449

View Online
Export Citation
CrossMark

17 January 2024 10:07:37



AIP Publishing

The Journal of Chemical Physics ARTICLE scitation.org/journal/jcp

Density functional theory of alkali metals at the IL/graphene electrochemical interface

Cite as: J. Chem. Phys. 156, 014706 (2022); doi: 10.1063/5.0077449
Submitted: 2 November 2021 • Accepted: 15 December 2021 •
Published Online: 6 January 2022

View Online Export Citation CrossMark

H. Montes-Campos,[a] A. Rivera-Pousa, and T. Méndez-Morales[a]

AFFILIATIONS

Grupo de Nanomateriais, Fotónica e Materia Branda, Departamento de Física de Partículas, Universidade de Santiago de Compostela, Campus Vida s/n, E-15782 Santiago de Compostela, Spain

Note: This paper is part of the JCP Special Topic on The Chemical Physics of the Electrode–Electrolyte Interface.
[b]**Author to whom correspondence should be addressed:** hadrian.montes@usc.es and trinidad.mendez@usc.es

ABSTRACT

The mechanism of charge transfer between metal ions and graphene in the presence of an ionic liquid (1-butyl-3-methylimidazolium tetrafluoroborate) is investigated by means of density functional theory calculations. For that purpose, two different comparisons are established: (i) the behavior of Li^+ and K^+ when adsorbed onto the basal plane of graphene and (ii) the differences between Li^+ approaching the carbon surface from the basal plane and being intercalated through the edge plane of trilayer graphene. In the first case, it is found that the metal ions must overcome high energy barriers due to their interaction with the ionic liquid before reaching an equilibrium position close to the interface. In addition, no significant charge transfer between any of the metals and graphene takes place until very close energetically unfavorable distances. The second configuration shows that Li^+ has no equilibrium position in the proximity of the interface but instead has an equilibrium position when it is inside the electrode for which it has to cross an energy barrier. In this case, the formation of a LiC_{12} complex is observed since the charge transfer at the equilibrium distance is achieved to a considerable extent. Thus, the interfacial charge transfer resistance on the electrode in energy devices based on ionic liquids clearly depends not only on the binding of the ionic liquid to the metal cations and their ability to form a dense solvation shell around them but also on the surface topography and its effect on the ion packing on the surface.

Published under an exclusive license by AIP Publishing. https://doi.org/10.1063/5.0077449

17 January 2024 10:07:37

I. INTRODUCTION

In recent years, substantial efforts have been dedicated to the development of energy storage technologies able to operate safely and efficiently in different environments. Most of the attention has been focused on the market-dominant supercapacitors (SCs) and lithium-ion batteries (LIBs).[1,2] Although the electrode is a key factor in achieving high energy and power densities and the last decade has witnessed significant advances in the optimization of high-performance electrode materials, the electrolyte is also an essential component in energy storage systems as the bridge to transport ions between both electrodes.

Focusing on LIBs, the features of the electrode/electrolyte interface as well as the electronic and ionic components of interfacial reactions play a fundamental role in the life cycle and safety of LIBs.[3,4] In this context, benefiting from the advantages of their unique properties such as nonvolatility, high thermal stability, and high ionic conductivity, ionic liquids (ILs) are considered to be an "environmentally friendly" alternative to conventional electrolytes.[5–10] These molten salts, whose melting points are lower than 100 °C, are comprised of organic cations and inorganic or organic anions that can be paired together in different combinations toward the desired target applications.

The performance of LIBs and other electrochemical devices is governed by the following factors: (i) the ion-transport resistance of lithium (Li^+) in the electrolyte during the charging and discharging of the cell, which is strongly affected by the viscosity of the media; (ii) the charge-transfer resistance of the electrode/electrolyte interface, which requires a change in the solvation shell of Li^+ in the vicinity of the electrodes; (iii) diffusion of lithium ions within the graphene structure (or other active material); and (iv) electron transport at the electrode interface. Despite their wide electrochemical window, the widespread use of ILs in conventional LIBs is limited due to their relatively high ion-transport resistance and the strong interaction between the anion and Li^+ cation, which affects the intercalation of

USC UNIVERSIDADE DE SANTIAGO DE COMPOSTELA

Published under an exclusive license by AIP Publishing

the latter on an electrode and lowers the performance of the device. In order to make some progress in this respect, the use of mixtures of ILs and organic solvents, e.g., carbonates, is becoming a popular strategy in the search for advanced IL-based electrolytes.[11–13] Yet even with all the attention, the performance of ILs in batteries is far from being optimized, and they still require a lot of work concerning the structure of the IL/electrode interface, the ion-transport dynamics, and the interfacial electrochemical reactions in order to become go-to electrolytes in energy storage. All these issues will be addressed in Secs. I A and I B.

Up to now, there has been much effort in improving the interface with sophisticated experiments, but computer simulations also play a key role in analyzing interfacial issues in batteries (for an overview, see Refs. 14 and 15 and references therein). Before starting with the description of our work, we consider it is appropriate to the reader to include a brief description of the major advances that have been made in this field during the last few years.

A. Structural transitions

As previously said, understanding and controlling the formation and the properties of the electrical double layer (EDL) is fundamental for the use of ILs in electrochemical applications not only in SCs, where the electrical energy is stored via the counter-ion adsorption at the electrode surface, but also in batteries. The performance, safety, and life cycle of these devices strongly depend, in general, on interfacial processes and, in particular, on the formation of the solid-electrolyte interphase (SEI), which is the product of electrolyte reduction on the negative electrode surface. The structure of the EDL is highly associated with the formation of the SEI, and since the EDL forms prior to the SEI, the possibility of regulating the latter by modifying the structure of the former through the choice of the electrolytes has been explored.[16–18]

As pointed out by Kornyshev and Qiao,[19] in systems with a high density of ions such as ILs, it is necessary to take into account the 3D nature of the EDL instead of just focusing on the distribution of ions in the direction normal to the surface. That is, the lateral restructuring of those ions absorbed into the electrodes upon surface charging must be considered along with the information in the third dimension since the alternating layers of anions and cations can affect the transitions in the layer adjacent to the electrode.

These voltage-induced ordering transitions at the interface have been observed by means of experimental techniques,[20–37] such as scanning tunneling microscopy (STM), and also by simulations (the extensive literature on the topic has been reviewed in Ref. 38). For example, the first experimental evidence of 2D phase transitions was reported by Pan and Freyland[20] in 2006 at the 1-butyl-3-methylimidazolium hexafluorophosphate ([BMIM][PF_6])/Au(111) interface. By using STM, they demonstrated the change from PF_6^- anions forming Moiré-like patterns to a $(\sqrt{3} \times \sqrt{3})$ phase with varying applied potential. While most of the experiments focused on these phenomena of 2D phase formation and transitions in gold, some researchers also studied the evolution of the Stern layer nanostructure of ILs in graphite.[36,37]

Concerning computational techniques, molecular dynamics (MD) simulations have been the most employed method when it comes to analyzing interfacial structural transitions.[39–52] Madden and co-workers[39,40] were the first ones reporting potential-induced phase transitions of a molten salt (LiCl) layer adsorbed on a metallic aluminum electrode by means of computer simulations in which the polarization of both the ions and the metal atoms was included. Concerning ILs, Merlet *et al.*[41] took a big step forward on this subject when they found peaks in the differential capacitance that were directly linked with the structural changes in the interfacial region. When examining the in-plane order of [BMIM][PF_6] adsorbed on graphite electrodes, they observed a transition of the first interfacial layer from a disordered state at low and high potentials to an ordered lattice-like state at intermediate voltages. More recently, Montes-Campos *et al.*[47–49] performed MD simulations of 1-butyl-3-methylimidazolium tetrafluoroborate ([BMIM][BF_4]) confined between graphene walls under a large variety of conditions, such as mixtures with water/alcohols, mixtures with $LiBF_4$, and defected electrodes. Their results showed the transition from solid-like (hexagonal) patterns to fluid-like (stripes) ones in the Stern layer when modifying the charge density. Some other authors also observed a transition in the interfacial behavior of ILs when increasing the surface charge density, going from a multilayered structure with multiple alternating layers of co-ions and counter-ions to an ordered monolayer of densely packed counter-ions with a Moiré-like structure, which coexists with apparently non-structured IL further in the direction perpendicular to the electrode.[50–52]

Ion layering/packing and the presence of those patterns at the IL/electrode interface are expected to have a deep impact on the free energy barriers for an ion approaching the electrode, on the rate of redox reactions, and on the friction behavior. Then, the manipulation of the 3D packing of ions is of great technological interest to achieve more efficient energy storage.

B. Ion desolvation and charge transfer

To obtain a high performance of batteries, lots of experimental works focused on interfacial ion (mainly lithium, but also sodium and potassium) transfer between the electrode and the electrolyte, both for typical electrolytes[53–59] and for ILs.[60–63] They all observed that ion transfer at the interface was a slow process with high activation barriers. These activation energies at the electrode/electrolyte interface were directly related to the desolvation energy of an ion from the solvent. Thus, the stripping of the ion primary solvation sheath and SEI chemistry were found to play an important role in charge-transfer kinetics.

Several computational studies analyzed the differences between the ion coordination environment at the bulk and the interface regions, and the conclusions also supported the hypothesis of an energy penalty for metal ions to come into direct contact with charged electrodes.[64–69] This resistance to ion transport at the electrolyte/electrode interface was found to be more relevant for IL-based electrolytes than for carbonate electrolytes. For example, Ivanistsev *et al.*[64] employed MD simulations with the aim of understanding the role of ion solvation in the formation of the interfacial free energy barriers. For that purpose, they compared the behavior of Li^+ and K^+ at a negatively charged graphene surface in [BMIM][BF_4] and its mixtures with $LiBF_4$ and KBF_4. The results showed strong interactions between Li^+ and IL anions that significantly increased the height of the free energy barriers compared

17 January 2024 10:07:37

USC UNIVERSIDADE DE SANTIAGO DE COMPOSTELA

Published under an exclusive license by AIP Publishing

to K^+. This lower desolvation penalty for K^+ with respect to other carrier ions such as Li^+ or Na^+ is due to its weakest Lewis acidity[59] and can have important implications in the development of beyond-lithium batteries. Moreover, Ivanistsev *et al.*[64] also reported that both alkali ions remained partially solvated by the BF_4^- even at the point of direct contact with the surface, which leads to positive values of the free energy minima that correspond to the contact of the ions with the electrode. Density functional theory (DFT) and *ab initio* molecular dynamics (AIMD) calculations are usually employed in this field to study ion adsorption energies, charge transferred to the electrode, solvation effects, interfacial decomposition of the electrolyte, composition and structure of the SEI, and also diffusion rates of Li^+ in the electrode region and SEI layer.[70–78] In particular, Varela and co-workers[71] pioneeringly considered the charge transfer between Li^+ or Mg^{2+} and a graphene wall, placing the metal ions at different distances to the wall and in different kinds of environments, including vacuum, a fluorine atom, and an IL. They stated that a complete charge transfer to the surface took place in all the systems with some kind of catalyzing effect of the IL making the charge transfer process to start at longer distances than in the other two environments.

However, despite all these research efforts, the truth is that in a dense, liquid-like IL environment, the organization of the ions at the electrified solid–IL interface still remains somehow complex and not exactly understood. With this article, we aim at increasing the knowledge about the electronic distribution and transport at interfaces with the general purpose of overcoming the charge-transfer resistance barrier and promoting ion conduction at the electrode/electrolyte interface for designing novel highly efficient next generation ionic devices.

In this work, the electron transfer between Li^+ and K^+ and the basal plane of graphene as a function of the distance between those cations and the interface was evaluated in a first set of simulations using DFT. The analysis has been performed in the presence of an ionic pair of 1-butyl-3-methylimidazolium tetrafluoroborate ([BMIM][BF_4]) to account for the transfer reaction in ILs. This IL has been chosen for being one of the most popular and for comparison with the results obtained in some of our previous studies.[64,71] In addition, the results for Li^+ were compared with a second set of simulations modeling the charge transfer between this cation and the edge plane of trilayer graphene. In this case, an additional BF_4^- anion was added in order to preserve electroneutrality. The adsorption of metal atoms on graphene and other carbon structures has been previously studied from the computational point of view. However, to the best of our knowledge, a work in which the mechanism of charge transfer between metal ions and graphene in the presence of an IL is investigated has not been performed yet, accounting for the usual oxidation state of the metals (+1) and allowing a full relaxation of the whole system. Under these more realistic conditions, we analyzed the adsorption process as a function of the nature of the alkali metal as well as of the crystallographic face from which ion intercalation takes place. All these simulations try to contribute to build a microscopic understanding of the interface ionics and the interface electronics of these advanced densely ionic electrolytes.

This paper is structured as follows: The essential technical details of the computational method used are sketched in Sec. II, our results are presented and discussed in Sec. III, and in Sec. IV, we summarize our main conclusions.

II. COMPUTATIONAL DETAILS

All DFT calculations were carried out using the Vienna *Ab initio* Simulation Package (VASP, version 5.4.4).[79–82] The projector-augmented wave (PAW)[83] method was used, and the electron exchange–correlation was described by the generalized gradient approximation (GGA) of Perdew–Burke–Ernzerhoff (PBE).[84] The DFT-D2 method of Grimme[85] was applied to account for dispersion effects. This combination has been shown to produce results in very good agreement with experimental ones for IL-based systems,[86,87] and PBE has been successfully employed in simulations of ILs at interfaces.[70,71] For the calculation of atomic partial charges, Bader charge analysis was employed in all the simulations.[88–91] We have chosen this method because it gives reliable charges; however, there are many other options such as Mulliken, NBO analysis, or ESP fitting, whose adoption could quantitatively modify some results reported here.

Our simulations are divided in two blocks regarding the approach route that the metal ion follows toward the electrode. As stated in Sec. I B, in the first set of simulations, the movement of the metal cation was considered in the direction perpendicular to the basal plane of graphene, whereas in the second set, the displacement was done facing the edge plane of trilayer graphene.

In the first set of simulations, the $BMIM^+$ cation, the BF_4^- anion, and the metal atoms (Li^+ or K^+) were optimized in a supercell whose X and Y dimensions match the simulated graphene sheet (composed of 50 C atoms) and a region of vacuum of 40 Å in the Z direction in order to avoid influence from periodic replicas. For the integration over the first Brillouin zone, a $2 \times 2 \times 1$ gamma-centered k-point set with a Gaussian smearing of 0.1 eV was employed. In order to take into account the usual oxidation state of the metals in an electrochemical device, the system was simulated with a total charge of $+1e$.

The initial configurations were constructed from previous MD simulations of [BMIM][BF_4] confined between graphene walls. Then, we placed the metal ion at a given distance from the surface, and the whole system was fully relaxed so that the total energy was converged to 10^{-5} eV. The salt cations were then moved along the direction normal to the graphene layer from 1.3 to 6.1 Å in 0.2 Å increments. During these simulations, the Z coordinates of the metal atoms and the carbon atoms of the graphene were fixed during the relaxation in order to be able to set the graphene–metal distance. Moreover, in order to speed-up the relaxation process, the output of one distance was fed as the initial configuration of the following distance (after displacing the metal atom).

In the second set of simulations, the metal ion (Li^+) approached the electrode perpendicular to the edge plane. The electrode was now composed of three graphene layers (a total of 96 C atoms, 32 per layer) separated 3.6 Å in the Y direction. The graphene layers were not arranged in a typical Bernal stacking of graphite (ABA); instead, they are forming a simple hexagonal vertical stacking (AAA). This electrode structure has already been explored in previous studies.[92,93] The interlayer distance was selected after performing an auxiliary simulation, where lithium was placed between

17 January 2024 10:07:37

USC UNIVERSIDADE DE SANTIAGO DE COMPOSTELA

Published under an exclusive license by AIP Publishing

two layers and the mean distance between equivalent carbon atoms was measured.

The supercell X and Y dimensions were once again selected in order to preserve the periodicity of the system. In the Z direction, a further vacuum region of 18.5 Å (for a total Z dimension of 25.524 Å) ensured once more no possible influence from periodic replicas. The integration technique was identical to the one used in the previous set.

The electrolyte, now comprised a $BMIM^+$ cation, two BF_4^- anions, and the Li^+ metal ion, was once again fully relaxed, and several Li^+ positions were sampled in the Z direction from 8.2 to −2.1 Å (the negative distance is to be interpreted as the Li^+ cation being inside the electrode) for a total of 52 distances. The Li^+ Y coordinate is 1.8 Å so that it approaches and penetrates the electrode from a zig-zag edge at a symmetric distance from the two bottom layers. Since the extra anion ensures the electroneutrality, the system was simulated as neutral.

III. RESULTS

We start the analysis with the first set of simulations. In these simulations, the metallic atom (Li^+ and K^+) approaches the graphene interface from the basal plane. This setup replicates the same kind of system present in most of the classical MD simulations of ILs at the interface. Moreover, it is a similar analysis to the one performed by Gómez-González *et al.*[71] with the distinction that their configuration represents the process of a metallic atom, with the initial oxidation state 0, approaching the interface and oxidizing. On the other hand, in our simulations, the initial oxidation state of the metal is already +1, and it is not expected to change throughout the simulated process in a similar fashion to the process that takes place in a common LIB. Therefore, in the simulation presented in this article, we are not particularly interested in changes in the oxidation state of the metal. Instead, we focus on the energetic of the adsorption process and the possible changes in the electronic density of the interface, in particular the possible creation of lithium and potassium carbides.

In order to study the energetics of the adsorption process, we analyzed the energy profiles of the system as function of the position of the metallic atom, presented in Fig. 1. These profiles show a similar behavior for both metals with a minimum close to the interface, followed by an energy barrier. The origin of this profile can be easily interpreted by looking at the atomic configurations at different distances from the interface. These configurations are presented in Fig. 2 at four different distances: the closest distance to the interface, the distance at the energy minimum, the distance at the energy maximum, and the furthest simulated distance. As shown there, the maximum of the energy is achieved when the metal atom goes through the middle of the IL layer, while the minimum is achieved when Li^+ or K^+ is placed between the interface and the IL. It is interesting that even though the IL is able to move freely in the relaxation process, its movement is not the same as that of the metal. In fact, it suffers the opposite movement than the metal, decreasing its distance a little bit when the lithium and potassium atoms are further away. This means that the interaction of the IL with the interface is strong enough to withstand the effect of the metal movement without changing its relative position with the interface. It must be also noted that the energy keeps decreasing after 6 Å, but since there

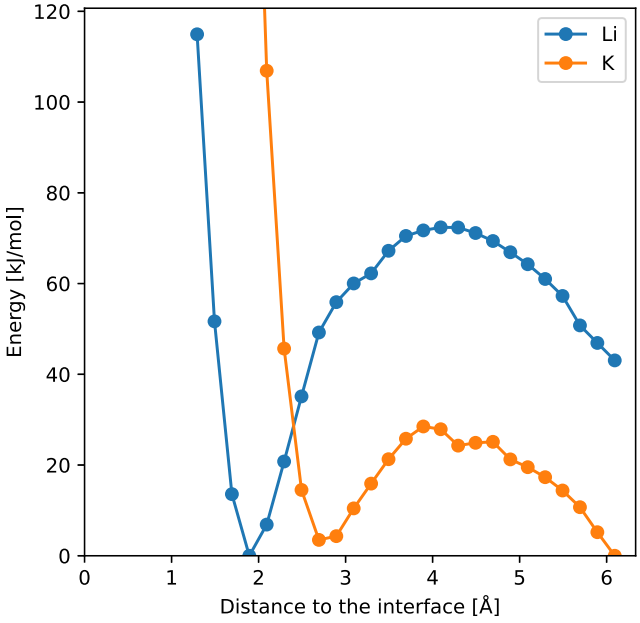


FIG. 1. Energy profiles for Li^+ (blue) and K^+ (orange) approaching the basal plane of graphene in the presence of a pair of [BMIM][BF_4] as a function of the distance to the interface.

are no more IL layers, we consider that the configurations further than this point are not realistic and only due to the design of the simulation box.

While the general characteristics of the energy profiles for Li^+ and K^+ are the same, we can see some quantitative differences between them. The first difference is the equilibrium distance of the metal, being quite lower for the lithium system (1.7 vs 2.7 Å). This difference can be easily explained due to the difference in their ionic radius, ~1.51 Å for the K^+ and 0.73 Å for the Li^+,[94] which can explain the 1 Å difference in the equilibrium position. The position of the energy maximum of the barrier does not suffer profound changes. This is due to the origin of this maximum being the position at which the ion goes through the middle of the IL layer, which does not suffer deep changes when the metal is changed. There is, however, a big difference in the height of the barrier relative to the equilibrium configuration. This effect can be also caused by the difference in the size of both ions. The greater charge density of lithium causes a stronger interaction with the IL and therefore increases the energy penalty of crossing the IL layer. The increased energy barrier for the lithium could be also due to the greater electrostriction ability of this ion caused by its more intense electric field at the surface. This very same effect has been also reported in classical MD simulations. For example, Ivanistsev *et al.*[64] reported a decrease of around 50% in the energy barrier when Li^+ was exchanged with K^+. If we compare these profiles to the ones calculated by Ivanistsev *et al.*,[64] we can conclude that both processes are qualitatively the same. There are some minor differences in the equilibrium distance of the metal and some quantitative differences in the height of the barrier. This difference in the barrier can be due to two different effects. The first one is that the ratio metal/IL is much higher in the results presented in this

17 January 2024 10:07:37

USC UNIVERSIDADE DE SANTIAGO DE COMPOSTELA

Published under an exclusive license by AIP Publishing

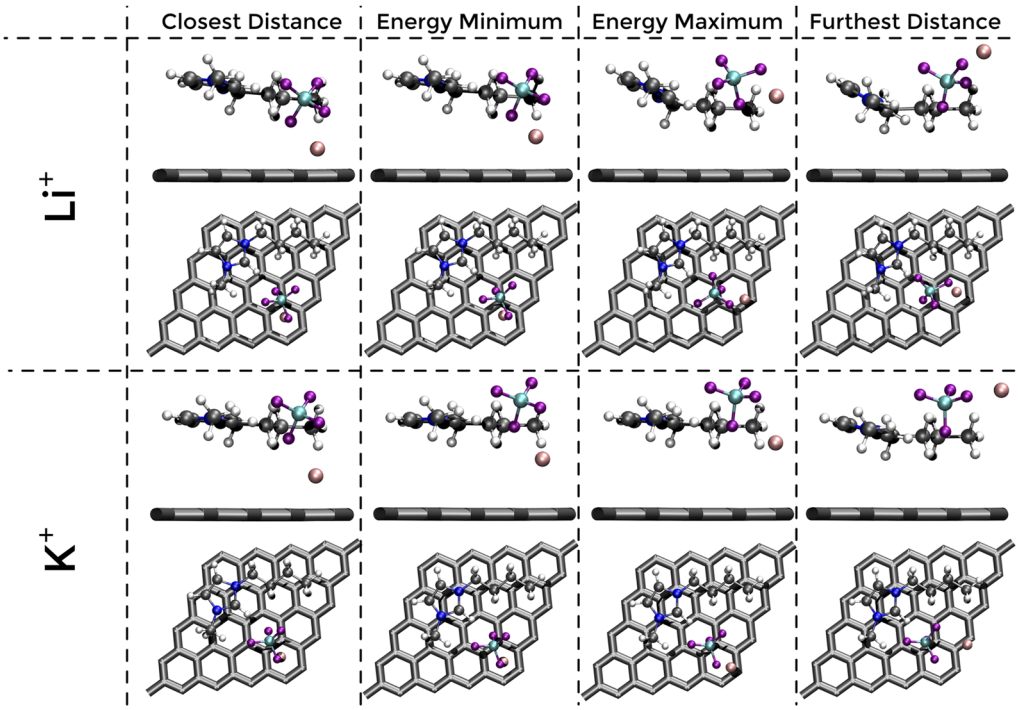


FIG. 2. Snapshots of the arrangements of the ions on top of the basal plane of graphene for several distances between Li^+ (top) and K^+ (bottom) and the interface.

article, and the second one is that the classical MD simulation cannot account for all the effects present in the real system; specifically, it does not take into account the polarizability of the electronic densities around the metals. We should also take into account that the high dielectric constant of [BMIM][BF_4][95] could have an impact on the height of the barrier due to the screening of the Coulombic interactions that would decrease it. More extensive simulations would be needed in order to properly estimate this quantitatively. Nevertheless, we can conclude that MD simulations can capture accurately enough the interfacial ionics.

We also studied the electrode/electrolyte interface from an electronic point of view. In Fig. 3, we represent the total charge of the different species in the simulation. As shown there, there is no significant charge transfer between any of the species in the system (metal, anion, cation, and graphene) at distances greater than 2 Å. There seems to be some charge transfer between the metal and the graphene at very short distances, but these configurations are heavily unfavorable from an energetic point of view. We can analyze the effect that the metal has on the six carbon atoms of the graphene closest to the metal equilibrium configuration in order to discard the formation of carbides. As shown in Fig. 3, the total charge of these atoms does indeed decrease when the metal approaches the interface, but at the equilibrium distance, the charge is not high enough to be considered a MC_6 complex. It is interesting that both metals create a similar localization of charge when at their equilibrium distance. This can be confirmed also by the partial charge distribution on graphene, which is shown in Fig. 4. As shown there, there is no clear rearrangement of the charge distribution around the metal when this atom is at its equilibrium distance. Moreover, the effect of the metal in the charge distribution seems to be similar to the effect of the IL ions. This is compatible with results reported by Zhour *et al.*,[70,96] who observed a greater charge redistribution for a simulation of pure IL at the interface compared to a simulation with the same IL and potassium. Therefore, we can conclude from these simulations that the metal is not able to cause profound effects on the electronic structure of the interface from a structural point of view.

In order to check if the presence of the metal inside the electrode structure is needed to observe the formation of carbides, a second set of simulations was performed. Salanne and co-workers[97,98] replicated this state in classical MD by introducing holes on the graphene layers to allow the entrance and diffusion of the ions in the electrode. Replicating this system in DFT would be extremely intense computing. Therefore, we have chosen to insert the lithium from the edge plane instead of the basal one, specifically through the zig-zag edge (see Fig. 5) and thus letting the metal penetrate inside the carbon structure.

In Fig. 6, we represent the energy profile of the system as well as the net charge of the species of the system. There, we can see that the system can achieve an equilibrium state in which the lithium is inside the electrode after having overcome the energy barrier. This energetic obstacle is significantly larger than that of the basal plane simulations. However, we believe that the height of this energy barrier could be artificially large as the carbon atoms of the graphene layers were set as frozen for the entire simulation to preserve the electrode structure. The lack of relaxation of these atoms could account for the larger relative energy differences. Therefore, the profile should be interpreted in qualitative terms. We can also see that there is no equilibrium position when lithium is close to the

17 January 2024 10:07:37

USC UNIVERSIDADE DE SANTIAGO DE COMPOSTELA

Published under an exclusive license by AIP Publishing

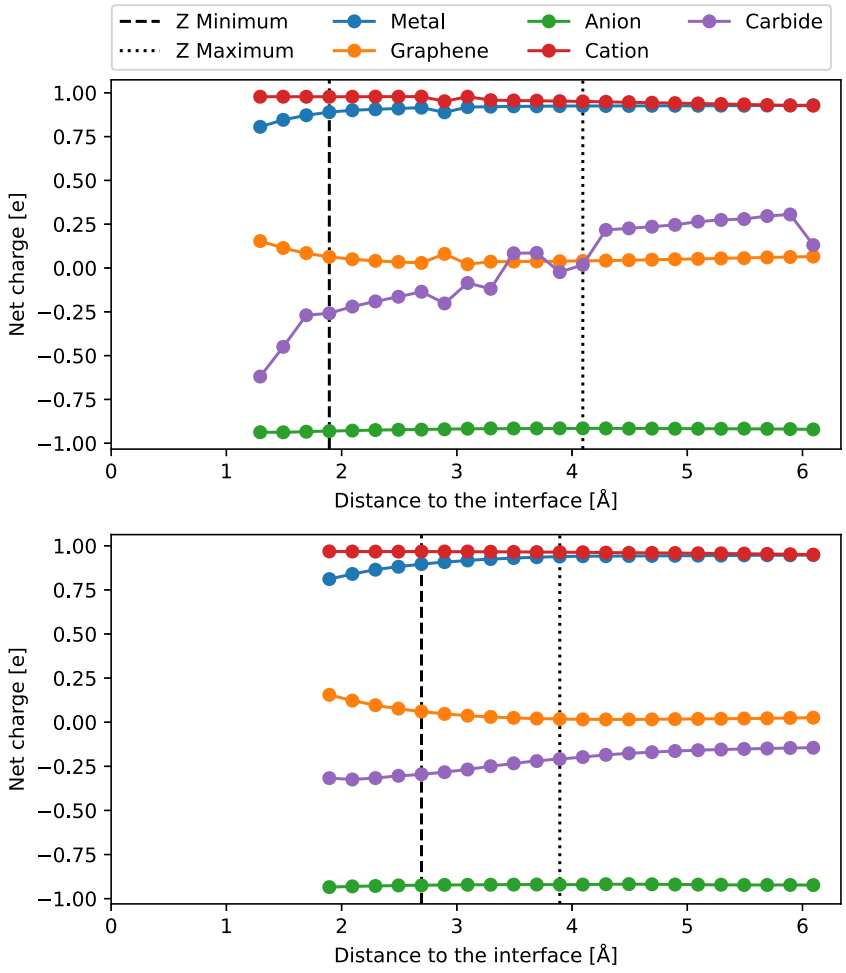


FIG. 3. Net charges of the different species present in the system as a function of the Li^+ (top) and K^+ (bottom) distance to the basal plane of graphene. Carbide stands for the six carbon atoms of graphene closest to the metal.

interface, opposed to the behavior we observed in the previous results for the basal plane. Moreover, the IL follows the motion of the Li^+ atom, which could account for the increase in the energy at long distances due to the unrealistic removal of the IL from the interface. When the lithium is far away from the interface, the IL does not place itself nearer to the electrode, which could be an effect of the lack of interaction with π-orbitals that are not present in the edge plane. These results are consistent with the behavior observed by Vatamanu *et al.*[99] when they analyzed by means of MD simulations the influence of the electrode surface topography on the

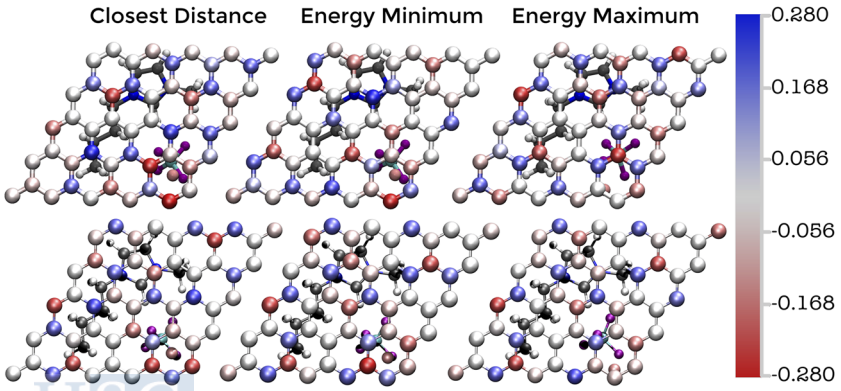


FIG. 4. Charge distribution on graphene for the simulations of Li^+ (top) and K^+ (bottom) approaching the basal plane of graphene in the presence of a pair of [BMIM][BF_4].

17 January 2024 10:07:37

Published under an exclusive license by AIP Publishing

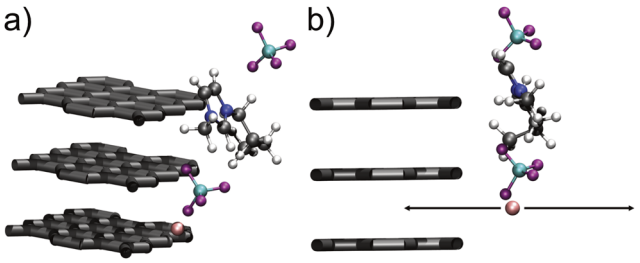


FIG. 5. Snapshots of the configuration for the simulations of Li^+ approaching the edge plane trilayer graphene in the presence of a pair of [BMIM][BF_4] and an additional BF_4^-: (a) general view and (b) lateral view.

differential capacitance and the EDL structure. They compared the potential energy of the ions in the inner Helmholtz layer of an IL in contact with the basal face of graphite with that in the proximity of the graphite edge plane; and they observed that the intermolecular potential energy of the ions was lower for the flat surface. This indicates that near the basal plane of graphite, the interactions of the ions with their surroundings are stronger and they have a greater ability to optimize their packing.

If we analyze the carbide formation, we can focus on the charge of the carbon atoms that lie near the lithium atom when it is placed inside the carbon structure. As shown, the charge decreases as Li^+ enters the electrode and, indeed, reaches a considerable magnitude (−0.6e) at the lithium equilibrium distance, which, although it is not

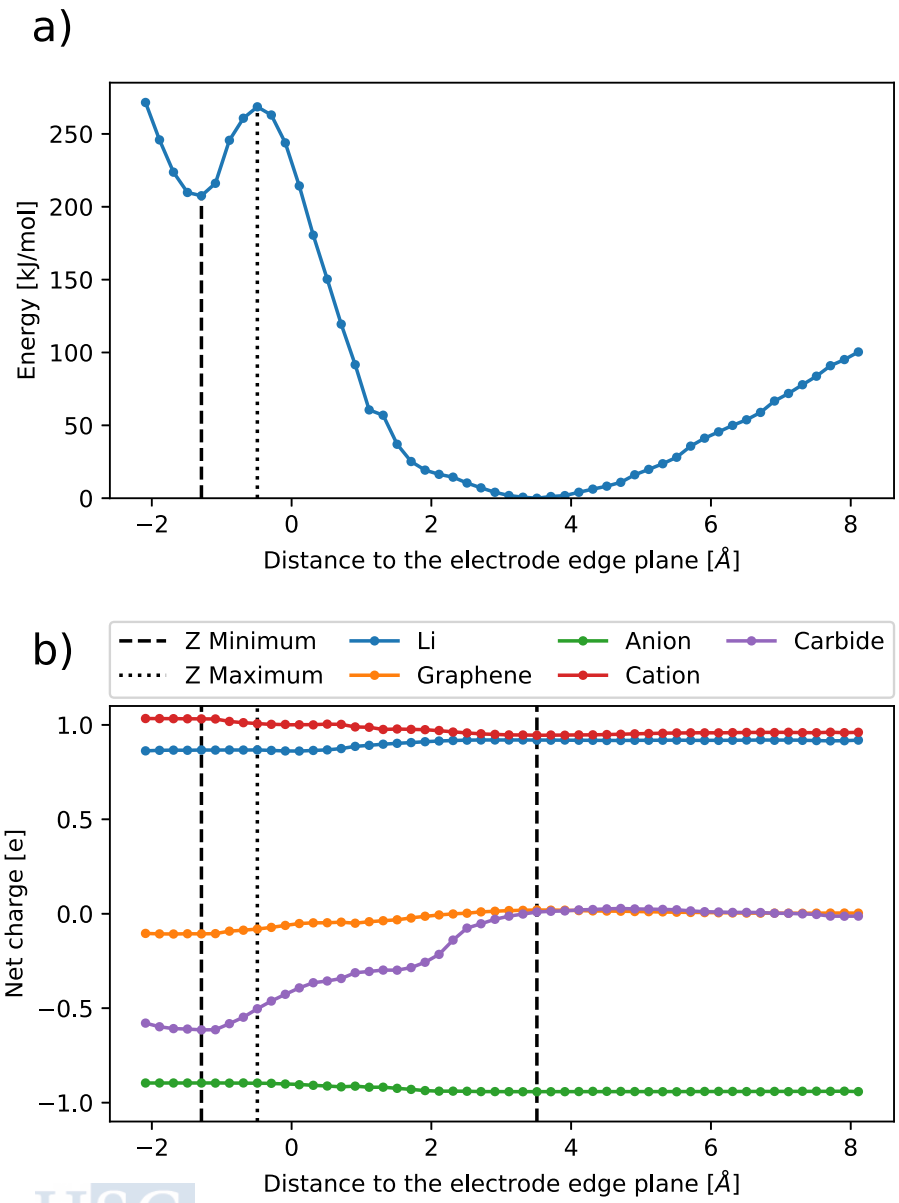


FIG. 6. Energy profile (a) and total net charge of the different species present in the system (b) for Li^+ approaching the edge plane of trilayer graphene in the presence of a pair of [BMIM][BF_4] and an additional BF_4^- in both cases as a function of the distance to the interface. Carbide stands for the 12 nearest carbon atoms to the lithium position inside the electrode. Negative distances mean that Li^+ is located inside the electrode.

17 January 2024 10:07:37

USC UNIVERSIDADE DE SANTIAGO DE COMPOSTELA

Published under an exclusive license by AIP Publishing

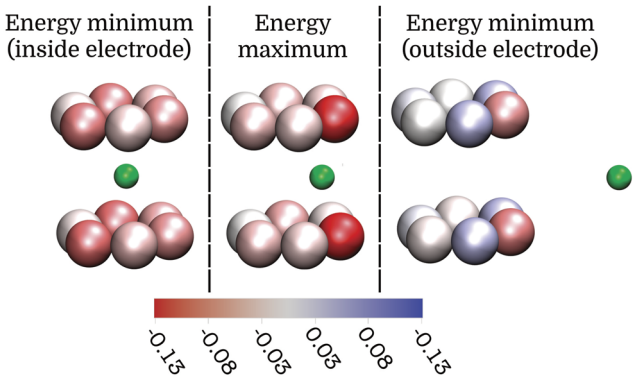


FIG. 7. Charge distribution on the 12 carbon atoms surrounding the equilibrium position of the Li^+ inside the interface. The other atoms were hidden for a clearer view of the distribution.

a negative charge of −1e, is enough to consider that a LiC_{12} complex has been created. This is also shown in Fig. 7 in which we include the charge distribution of the 12 carbons closest to Li^+ when it is located at its equilibrium position inside the electrode. Therefore, we can conclude that the insertion of the metal ion is necessary to reproduce the carbide complexes that are created in a LIB.[100] This difference in the electronic behavior of the interface has been also reported experimentally. Compton *et al.*[101,102] have previously shown that graphite exhibits very different charge transfer kinetics between its two crystallographic faces with a rate of electron transfer being much greater at the edge plane sites than at the basal plane.

IV. CONCLUSIONS

DFT calculations have been performed with the purpose of studying the effect of the choice of the metal salt (Li^+ and K^+) added to an IL-based electrolyte and of the crystallographic orientation of the electrode surface on the interfacial resistance. Our main findings can be summarized in the following points:

- Both Li^+ and K^+ are adsorbed at the interface with high energy barriers (around 70 and 30 kJ/mol, respectively) in order to come to the basal plane of graphene. This energy maximum corresponds to the moment at which the metal ions go through the IL, which does not change its distance to the electrode when moving the metal due to greater interactions with the former. Hence, both energy profiles show a minimum close to the interface, whose location depends on their ionic radius.
- Neither Li^+ nor K^+ leads to a significant charge transfer with the graphene layer until very close distances that are not energetically favorable, and the formation of LiC_6 complexes is not observed.
- When Li^+ approaches the electrode from the edge plane of trilayer graphene, it must cross a high energy barrier before finding an equilibrium position once located inside the carbon structure instead of in the outside vicinity.
- A considerable charge transfer is observed at the equilibrium position when Li^+ is inserted from the edge plane. In this case, the creation of a LiC_{12} complex can be stated.

Solving this high interfacial resistance of ion transport characteristic of IL-based electrolytes is crucial for their use as electrolytes in energy storage devices. For this purpose, the ionic and electronic behavior at the electrode/electrolyte interface must be fully elucidated. We hope that the discussion in this article will contribute to a comprehensive understanding of the interactions at the interface for further optimization of IL-based energy devices.

ACKNOWLEDGMENTS

The financial support of the Spanish Ministry of Economy and Competitiveness (Project Nos. MAT2017-89239-C2-1-P and MAT2017-89239-C2-2-P) is gratefully acknowledged. Moreover, this work was funded by the Xunta de Galicia (Grant Nos. ED431E 2018/08 and GRC ED431C 2020/10). All these research projects were partially supported by FEDER. A.R.P. acknowledges the Spanish Ministry of Education for his FPU grant. T.M.M. acknowledges her contract funded by the pilot program of the USC for the recruitment of distinguished research personnel—call 2021 under the agreement between the USC and the Santander Bank for 2021–2024. Facilities provided by the Galician Supercomputing Centre (CESGA) are also acknowledged. Professor L. M. Varela is thanked for fruitful discussions and suggestions during the preparation of the manuscript.

AUTHOR DECLARATIONS

Conflict of Interest

The authors have no conflicts to disclose.

Author Contributions

All authors contributed equally to this work.

DATA AVAILABILITY

The data that support the findings of this study are available from the corresponding author upon reasonable request.

REFERENCES

[1]X. Yu and A. Manthiram, Energy Environ. Sci. **11**, 527 (2018).
[2]L. Miao, Z. Song, D. Zhu, L. Li, L. Gan, and M. Liu, Mater. Adv. **1**, 945 (2020).
[3]M. Gauthier, T. J. Carney, A. Grimaud, L. Giordano, N. Pour, H.-H. Chang, D. P. Fenning, S. F. Lux, O. Paschos, C. Bauer, F. Maglia, S. Lupart, P. Lamp, and Y. Shao-Horn, J. Phys. Chem. Lett. **6**, 4653 (2015).
[4]J. Kasnatscheew, R. Wagner, M. Winter, and I. Cekic-Laskovic, Top Curr. Chem. **16**(1), 376 (2018).
[5]H. Matsumoto, in *2014 IEEE International Nanoelectronics Conference (INEC)* (IEEE, 2014), pp. 1–4.
[6]S. Marullo, F. D'Anna, C. Rizzo, and F. Billeci, Org. Biomol. Chem. **19**, 2076 (2021).
[7]S. Pan, M. Yao, J. Zhang, B. Li, C. Xing, X. Song, P. Su, and H. Zhang, Front. Chem. **8**(1), 261 (2020).
[8]M. Watanabe, M. L. Thomas, S. Zhang, K. Ueno, T. Yasuda, and K. Dokko, Chem. Rev. **117**, 7190 (2017).
[9]K. Karuppasamy, J. Theerthagiri, D. Vikraman, C.-J. Yim, S. Hussain, R. Sharma, T. Maiyalagan, J. Qin, and H.-S. Kim, Polymers **12**(4), 918 (2020).

17 January 2024 10:07:37

Published under an exclusive license by AIP Publishing

[10]X. Wang, M. Salari, D.-e. Jiang, J. Chapman Varela, B. Anasori, D. J. Wesolowski, S. Dai, M. W. Grinstaff, and Y. Gogotsi, Nat. Rev. Mater. **5**, 787 (2020).
[11]N. Dupré, P. Moreau, E. De Vito, L. Quazuguel, M. Boniface, H. Kren, P. Bayle-Guillemaud, and D. Guyomard, Chem. Mater. **29**, 8132 (2017).
[12]T. Vogl, S. Menne, and A. Balducci, Phys. Chem. Chem. Phys. **16**, 25014 (2014).
[13]L. T. M. Le, T. D. Vo, K. H. P. Ngo, S. Okada, F. Alloin, A. Garg, and P. M. L. Le, J. Mol. Liq. **271**, 769 (2018).
[14]M. V. Fedorov and A. A. Kornyshev, Chem. Rev. **114**, 2978 (2014).
[15]R. Hayes, G. G. Warr, and R. Atkin, Chem. Rev. **115**, 6357 (2015).
[16]K. Huang, S. Bi, B. Kurt, C. Xu, L. Wu, Z. Li, G. Feng, and X. Zhang, Angew. Chem., Int. Ed. **60**, 19232 (2021).
[17]Z. Yu, H. Wang, X. Kong, W. Huang, Y. Tsao, D. G. Mackanic, K. Wang, X. Wang, W. Huang, S. Choudhury, Y. Zheng, C. V. Amanchukwu, S. T. Hung, Y. Ma, E. G. Lomeli, J. Qin, Y. Cui, and Z. Bao, Nat. Energy **5**, 526 (2020).
[18]C. Yan, H.-R. Li, X. Chen, X.-Q. Zhang, X.-B. Cheng, R. Xu, J.-Q. Huang, and Q. Zhang, J. Am. Chem. Soc. **141**, 9422 (2019).
[19]A. A. Kornyshev and R. Qiao, J. Phys. Chem. C **118**, 18285 (2014).
[20]G.-B. Pan and W. Freyland, Chem. Phys. Lett. **427**, 96 (2006).
[21]D. Borissov, C. L. Aravinda, and W. Freyland, J. Phys. Chem. B **109**, 11606 (2005).
[22]Y. Liu, Y. Zhang, G. Wu, and J. Hu, J. Am. Chem. Soc. **128**, 7456 (2006).
[23]Y.-Z. Su, Y.-C. Fu, J.-W. Yan, Z.-B. Chen, and B.-W. Mao, Angew. Chem., Int. Ed. **48**, 5148 (2009).
[24]Y.-Z. Su, J.-W. Yan, M.-G. Li, Z.-X. Xie, B.-W. Mao, and Z.-Q. Tian, Z. Phys. Chem. **226**, 979 (2012).
[25]Y. Su, J. Yan, M. Li, M. Zhang, and B. Mao, J. Phys. Chem. C **117**, 205 (2013).
[26]F. Buchner, K. Forster-Tonigold, B. Uhl, D. Alwast, N. Wagner, H. Farkhondeh, A. Groß, and R. J. Behm, ACS Nano **7**, 7773 (2013).
[27]T. Cremer, M. Stark, A. Deyko, H.-P. Steinrück, and F. Maier, Langmuir **27**, 3662 (2011).
[28]R. Foulston, S. Gangopadhyay, C. Chiutu, P. Moriarty, and R. G. Jones, Phys. Chem. Chem. Phys. **14**, 6054 (2012).
[29]L. Tamam, B. M. Ocko, H. Reichert, and M. Deutsch, Phys. Rev. Lett. **106**(19), 197801 (2011).
[30]W. Freyland, Phys. Chem. Chem. Phys. **10**, 923 (2008).
[31]G.-B. Pan and W. Freyland, Phys. Chem. Chem. Phys. **9**, 3286 (2007).
[32]R. Wen, B. Rahn, and O. M. Magnussen, Angew. Chem., Int. Ed. **54**, 6062 (2015).
[33]R. Costa, C. M. Pereira, and A. Fernando Silva, Electrochem. Commun. **57**, 10 (2015).
[34]N. Borisenko, R. Atkin, A. Lahiri, S. Z. E. Abedin, and F. Endres, J. Phys.: Condens. Matter **26**(28), 284111 (2014).
[35]F. Endres, N. Borisenko, S. Z. El Abedin, R. Hayes, and R. Atkin, Faraday Discuss. **154**, 221 (2012).
[36]A. Elbourne, S. McDonald, K. Voïchovsky, F. Endres, G. G. Warr, and R. Atkin, ACS Nano **9**, 7608 (2015).
[37]D. Ebeling, S. Bradler, B. Roling, and A. Schirmeisen, J. Phys. Chem. C **120**, 11947 (2016).
[38]B. Rotenberg and M. Salanne, J. Phys. Chem. Lett. **6**, 4978 (2015).
[39]M. Pounds, S. Tazi, M. Salanne, and P. A. Madden, J. Phys.: Condens. Matter **21**(42), 424109 (2009).
[40]S. Tazi, M. Salanne, C. Simon, P. Turq, M. Pounds, and P. A. Madden, J. Phys. Chem. B **114**, 8453 (2010).
[41]C. Merlet, D. T. Limmer, M. Salanne, R. van Roij, P. A. Madden, D. Chandler, and B. Rotenberg, J. Phys. Chem. C **118**, 18291 (2014).
[42]S. A. Kislenko, I. S. Samoylov, and R. H. Amirov, Phys. Chem. Chem. Phys. **11**, 5584 (2009).
[43]S. Begic, E. Jónsson, F. Chen, and M. Forsyth, Phys. Chem. Chem. Phys. **19**, 30010 (2017).
[44]J. Le Ma, Q. Meng, and J. Fan, Phys. Chem. Chem. Phys. **20**, 8054 (2018).
[45]B. Docampo-Álvarez, V. Gómez-González, H. M.-C. andJ, M. Otero-Mato, T. Méndez-Morales, O. Cabeza, L. J. Gallego, R. M. Lynden-Bell, V. B. Ivanistsev, M. V. Fedorov, and L. M. Varela, J. Phys.: Condens. Matter **28**(46), 464001 (2016).
[46]V. Gómez-González, B. Docampo-Álvarez, T. Méndez-Morales, O. Cabeza, V. B. Ivaništšev, M. V. Fedorov, L. J. Gallego, and L. M. Varela, Phys. Chem. Chem. Phys. **19**, 846 (2017).
[47]H. Montes-Campos, J. M. Otero-Mato, T. Méndez-Morales, O. Cabeza, L. J. Gallego, A. Ciach, and L. M. Varela, Phys. Chem. Chem. Phys. **19**, 24505 (2017).
[48]J. M. Otero-Mato, H. Montes-Campos, O. Cabeza, D. Diddens, A. Ciach, L. J. Gallego, and L. M. Varela, Phys. Chem. Chem. Phys. **20**, 30412 (2018).
[49]H. Montes-Campos, J. M. Otero-Mato, R. C. Longo, O. Cabeza, L. J. Gallego, and L. M. Varela, J. Mol. Liq. **289**(1), 111083 (2019).
[50]V. Ivanistsev, K. Kirchner, T. Kirchner, and M. V. Fedorov, J. Phys.: Condens. Matter **27**(1), 102101 (2015).
[51]K. Kirchner, T. Kirchner, V. Ivaništšev, and M. V. Fedorov, Electrochim. Acta **110**, 762 (2013).
[52]V. Ivanistsev and M. V. Fedorov, Electrochem. Soc. Interface **23**, 65 (2014).
[53]T. Abe, H. Fukuda, Y. Iriyama, and Z. Ogumi, J. Electrochem. Soc. **151**, A1120 (2004).
[54]Y. Yamada, Y. Iriyama, T. Abe, and Z. Ogumi, Langmuir **25**, 12766 (2009).
[55]A. von Cresce and K. Xu, ECS Solid State Lett. **14**, A154 (2011).
[56]A. von Wald Cresce, O. Borodin, and K. Xu, J. Phys. Chem. C **116**, 26111 (2012).
[57]K. Xu, A. von Cresce, and U. Lee, Langmuir **26**, 11538 (2010).
[58]K. Xu and A. von Wald Cresce, J. Mater. Res. **27**, 2327 (2012).
[59]M. Zhou, P. Bai, X. Ji, J. Yang, C. Wang, and Y. Xu, Adv. Mat. **33**(7), 2003741 (2021).
[60]M.-T. F. Rodrigues, X. Lin, H. Gullapalli, M. W. Grinstaff, and P. M. Ajayan, J. Power Sources **330**, 84 (2016).
[61]A. M. Smith and S. Perkin, J. Phys. Chem. Lett. **6**, 4857 (2015).
[62]Y. Ishihara, K. Miyazaki, T. Fukutsuka, and T. Abe, J. Electrochem. Soc. **161**, A1939 (2014).
[63]F. Sagane, T. Abe, and Z. Ogumi, J. Electrochem. Soc. **159**, A1766 (2012).
[64]V. Ivanistsev, T. Méndez-Morales, R. M. Lynden-Bell, O. Cabeza, L. J. Gallego, L. M. Varela, and M. V. Fedorov, Phys. Chem. Chem. Phys. **18**, 1302 (2016).
[65]S. W. Coles, M. Mishin, S. Perkin, M. V. Fedorov, and V. B. Ivaništšev, Phys. Chem. Chem. Phys. **19**, 11004 (2017).
[66]T. C. Lourenço, M. Ebadi, D. Brandell, J. L. F. Da Silva, and L. T. Costa, J. Phys. Chem. B **124**, 9648 (2020).
[67]J. B. Haskins, J. J. Wu, and J. W. Lawson, J. Phys. Chem. C **120**, 11993 (2016).
[68]G. D. Smith, O. Borodin, S. P. Russo, R. J. Rees, and A. F. Hollenkamp, Phys. Chem. Chem. Phys. **11**, 9884 (2009).
[69]J. Vatamanu, O. Borodin, and G. D. Smith, J. Phys. Chem. C **116**, 1114 (2012).
[70]K. Zhour, J. M. Otero-Mato, F. E. H. Hassan, H. Fahs, M. Vaezzadeh, E. López-Lago, L. J. Gallego, and L. M. Varela, J. Mol. Liq. **321**(1), 114759 (2021).
[71]V. Gómez-González, A. García-Fuente, A. Vega, J. Carrete, O. Cabeza, L. J. Gallego, and L. M. Varela, J. Phys. Chem. C **122**, 15070 (2018).
[72]L. E. Camacho-Forero, T. W. Smith, and P. B. Balbuena, J. Phys. Chem. C **121**, 182 (2016).
[73]C. Wei, K. Jiang, T. Fang, and X. Liu, J. Mol. Liq. **338**(1), 116641 (2021).
[74]A. Budi, A. Basile, G. Opletal, A. F. Hollenkamp, A. S. Best, R. J. Rees, A. I. Bhatt, A. P. O'Mullane, and S. P. Russo, J. Phys. Chem. C **116**, 19789 (2012).
[75]H. Yildirim, J. B. Haskins, C. W. Bauschlicher, and J. W. Lawson, J. Phys. Chem. C **121**, 28214 (2017).
[76]B. V. Merinov, S. V. Zybin, S. Naserifar, S. Morozov, J. Oppenheim, W. A. Goddard, J. Lee, J. H. Lee, H. E. Han, Y. C. Choi, and S. H. Kim, J. Phys. Chem. Lett. **10**, 4577 (2019).
[77]B. V. Merinov, S. Naserifar, S. V. Zybin, S. Morozov, W. A. Goddard, J. Lee, J. H. Lee, H. E. Han, Y. C. Choi, and S. H. Kim, J. Chem. Phys. **152**(3), 031101 (2020).
[78]J. Clarke-Hannaford, M. Breedon, A. S. Best, and M. J. S. Spencer, Phys. Chem. Chem. Phys. **21**, 10028 (2019).
[79]G. Kresse and J. Hafner, Phys. Rev. B **47**, 558 (1993).
[80]G. Kresse and J. Furthmüller, Phys. Rev. B **54**, 11169 (1996).
[81]G. Kresse and J. Furthmüller, Comput. Mater. Sci. **6**, 15 (1996).
[82]G. Kresse and D. Joubert, Phys. Rev. B **59**, 1758 (1999).
[83]P. E. Blöchl, Phys. Rev. B **50**, 17953 (1994).
[84]J. P. Perdew, K. Burke, and M. Ernzerhof, Phys. Rev. Lett. **77**, 3865 (1996).
[85]S. Grimme, J. Comput. Chem. **27**, 1787 (2006).

17 January 2024 10:07:37

Published under an exclusive license by AIP Publishing

[86]M. Kim, T. Gould, E. I. Izgorodina, D. Rocca, and S. Lebègue, Phys. Chem. Chem. Phys. **23**, 25558 (2021).
[87]A. Thomas, K. R. Maiyelvaganan, S. Kamalakannan, and M. Prakash, ACS Omega **4**, 22655 (2019).
[88]G. Henkelman, A. Arnaldsson, and H. Jónsson, Comput. Mater. Sci. **36**, 354 (2006).
[89]E. Sanville, S. D. Kenny, R. Smith, and G. Henkelman, J. Comput. Chem. **28**, 899 (2007).
[90]W. Tang, E. Sanville, and G. Henkelman, J. Phys.: Condens. Matter **21**, 084204 (2009).
[91]M. Yu and D. R. Trinkle, J. Chem. Phys. **134**, 064111 (2011).
[92]K. Persson, Y. Hinuma, Y. S. Meng, A. Van der Ven, and G. Ceder, Phys. Rev. B **82**, 125416 (2010).
[93]E. Lee and K. A. Persson, Nano Lett. **12**, 4624 (2012).
[94]R. D. Shannon, Acta Crystallogr., Sect. A: Cryst. Phys., Diffr., Theor. Gen. Crystallogr. **32**, 751 (1976).
[95]A. Stoppa, J. Hunger, R. Buchner, G. Hefter, A. Thoman, and H. Helm, J. Phys. Chem. B **112**, 4854 (2008).
[96]K. Zhour, J. M. Otero-Mato, F. E. H. Hassan, H. Fahs, M. Vaezzadeh, E. López-Lago, L. J. Gallego, and L. M. Varela, J. Mol. Liq. **316**, 113803 (2020).
[97]T. Mendez-Morales, M. Burbano, M. Haefele, B. Rotenberg, and M. Salanne, J. Chem. Phys. **148**(19), 193812 (2018).
[98]T. Méndez-Morales, N. Ganfoud, Z. Li, M. Haefele, B. Rotenberg, and M. Salanne, Energy Storage Mater. **17**, 88 (2019).
[99]J. Vatamanu, L. Cao, O. Borodin, D. Bedrov, and G. D. Smith, J. Phys. Chem. Lett. **2**, 2267 (2011).
[100]F. Chevallier, F. Poli, B. Montigny, and M. Letellier, Carbon **61**, 140 (2013).
[101]C. E. Banks, T. J. Davies, G. G. Wildgoose, and R. G. Compton, Chem. Commun. **2005**, 829.
[102]L. Xiao, E. J. F. Dickinson, G. G. Wildgoose, and R. G. Compton, Electroanalysis **22**, 269 (2010).

17 January 2024 10:07:37

USC UNIVERSIDADE DE SANTIAGO DE COMPOSTELA

Published under an exclusive license by AIP Publishing

Journal of Molecular Liquids 392 (2023) 123460

Contents lists available at ScienceDirect

Journal of Molecular Liquids

journal homepage: www.elsevier.com/locate/molliq

Ionic liquid/metal salt mixtures at the graphene interface: A density functional theory approach

Alejandro Rivera-Pousa [a,b], José M. Otero-Mato [a], Carlos Damián Rodríguez-Fernández [a,c], Kazem Zhour [d], Hadrián Montes-Campos [a,b,e,*], Trinidad Méndez-Morales [a,b,*], Luis M. Varela [a,b]

[a] Grupo de Nanomateriais, Fotónica e Materia Branda, Departamento de Física de Partículas, Universidade de Santiago de Compostela, Campus Vida s/n, E-15782, Santiago de Compostela, Spain
[b] Instituto de Materiais (iMATUS), Universidade de Santiago de Compostela, Avenida do Mestre Mateo 25, E-15782, Santiago de Compostela, Spain
[c] Departamento de Física e Ciencias da Terra, Universidade da Coruña, Campus de A Zapateira s/n, E-15071, A Coruña, Spain
[d] Institute of Physical Chemistry, University of Münster, Corrensstraße 28/30, 48149, Münster, Germany
[e] CIQUP, Institute of Molecular Sciences (IMS)—Departamento de Química e Bioquímica, Faculdade de Ciências da Universidade do Porto, Rua Campo Alegre, 4169-007, Porto, Portugal

ARTICLE INFO

Keywords:
Ionic liquids
Graphene
Metal atoms adsorption
Density functional theory
Optoelectronic properties

ABSTRACT

The interaction of graphene sheets with metal cations is very relevant because of the modifications that are induced in the electrochemical properties of the 2D material. Ionic liquids are a promising kind of materials with several applications in electrochemical devices, so understanding how they affect the graphene-metal interaction is key for their practical implementation. Therefore, we have studied the adsorption of a mixture of an ionic liquid and a metal salt on a graphene surface by means of first-principles calculations. Several metals were chosen to analyze the effect they have on the optoelectronic properties of the graphene monolayer and to understand the trends in their adsorption behavior. We have characterized the ground state configurations in terms of their binding energies and the distance between the metal atom and the graphene layer. From the analysis of the charge transfer behavior, calcium and magnesium have been identified as the species that transfer the highest and the lowest amount of charge, respectively, which is related to their ionization energies. Band structure diagrams and projected density of states calculations also show that the energy shift of the Dirac cone increases with the degree of charge transfer. In addition, a stronger interaction of magnesium with the ionic liquid compared to that of other metal atoms was observed. The analysis of several electromagnetic parameters indicated an anisotropic behavior for electric fields polarized both perpendicular and parallel to the graphene layer. Our density functional theory study offers fundamental insights into the adsorption behavior of ionic liquids mixed with metal ions on monolayer graphene.

1. Introduction

In recent years, scientific emphasis has been focused on the unique optical, electronic, mechanical and chemical properties of 2D materials [1,2]. Among them, the most studied one is undoubtedly graphene, which has become a central topic of research interest due to its high carrier mobility, extraordinary strength, high thermal conductivity and excellent optical properties [3–5]. All of them can be tuned through different methods like impurity doping, designed defects, adsorption or chemical functionalization [6–11]. This versatility has enabled graphene to hold great potential for a virtually unlimited range of applications, including electronics [12], energy [13], medicine [14], sensors [15] and light processing [16].

An interesting aspect of graphene sheets lies in their interaction with metal cations due to the change in electronic and mechanical properties, thus providing new functionalities and widening their use in many fields. Metals interacting with graphene have been thoroughly studied and analyzed by means of both experimental studies [17–19] and computational calculations based on first-principles density functional theory (DFT) [20–31]. Among the latter, Olsson et al. [32] studied the adsorption and migration of several alkali atoms on pristine and defective graphene surfaces, and they reported more favorable adsorption

* Corresponding authors.
E-mail addresses: hadrian.montes@usc.es (H. Montes-Campos), trinidad.mendez@usc.es (T. Méndez-Morales).

https://doi.org/10.1016/j.molliq.2023.123460
Received 30 June 2023; Received in revised form 29 September 2023; Accepted 29 October 2023
Available online 4 November 2023
0167-7322/© 2023 The Author(s). Published by Elsevier B.V. This is an open access article under the CC BY-NC-ND license (http://creativecommons.org/licenses/by-nc-nd/4.0/).

energies for Li^+ and K^+ ions than for Na^+. Similarly, Mendoza-Cortes and coworkers [33,34] showed how to modify the electronic properties of bilayer graphene with the intercalation of transition metals. This study found that the Dirac point was pushed down below the Fermi energy level in all the intercalated structures except for vanadium, which had the Dirac cone in its band structure.

Among all the works addressing the adsorption of molecules on a graphene surface, ionic liquids (ILs) are emerging as a relevant field of study due to their attractive properties for a great number of applications. These salts that are mainly composed of cations and anions and have melting points below 100 °C, offer high thermal stability, high ionic conductivity, negligible volatility, and structural and physicochemical tunability through appropriate selection of the ions [35,36]. Because of these benefits, their efficient utilization in synthesis, catalysis, electrochemistry, gas separation, tribology, pharmaceuticals and energy storage devices has been exhaustively tested in the last decades [37–41]. Thus, the growing interest on understanding the adsorption mechanism of ILs on different surfaces has led to numerous experimental investigations in this area [42–44]. Alongside the experimental efforts, computational methods such as those based on electronic structure have been widely employed to analyse the properties and interactions of ILs with a large panel of surfaces, including graphene (or its derivatives) and other 2D materials [45–49], polycyclic aromatic hydrocarbons [50,51], and metal interfaces [52–54]; with the purpose of elucidating their influence on the electronic properties of the surface [55–59], and evaluate their potential use in applications such as exfoliation [60–62] or energy storage devices [63–68]. For example, Kamath and coworkers [57–59] performed a series of calculations to compare the adsorption characteristics of different ILs on graphene, defective graphene and fluorographene surfaces. They observed that the presence of defects on the graphene nanoflakes increases the binding energy of ILs by about 10% in comparison with pristine graphene and hexagonal boron-nitride nanosheets. However, fluorinated graphene strongly decreases the binding energy compared to them.

Nevertheless, even though ILs are promising electrolytes for energy storage devices, there is still scarce information about their interfacial interactions with graphene substrate and the electronic structure upon adsorption when it comes to their mixtures with metal atoms. Up to our knowledge, there is only one publication in which the effect of the adsorption of an imidazolium-based IL mixed with a potassium salt on the electronic and optical properties of graphene and borophene was considered [69]. The authors reported a downward shift of the Dirac cones relative to their Fermi level for both structures due to the electron transferred from potassium to the 2D-materials. Also, they observed that the presence of the IL increased the charge transferred from the metal atom to the graphene/borophene sheets when compared to its adsorption on pristine materials.

Thus, in this work a comprehensive investigation was carried out by means of DFT simulations to shed some light on the interaction mechanism between IL-metal salt mixtures and the graphene substrate. This computational technique was chosen due to its capability of producing highly accurate results that can be compared to experimental findings [70,71] and because it takes into account interactions that are not accessible by means of other techniques such as MD. The screening of several metal atoms (lithium (Li), sodium (Na), magnesium (Mg), calcium (Ca), and aluminum (Al)) allowed us to compare the electronic and optical properties avoiding more costly trial-and-error experimental measurements, which is of fundamental importance for optimizing the performance and efficiency of a new generation of electronic, optoelectronic and energy storage devices. The IL employed in this study was 1-butyl-3-methylimidazolium tetrafluoroborate ([BMIM][BF_4]), which was chosen with the purpose of comparison with the same hybrid system doped with potassium that was previously reported by some members of our group [69]. Also, the potential of this IL as a suitable electrolyte (pure or in mixtures) for energy storage devices such as supercapacitors or lithium-ion batteries has been often considered [72,73].

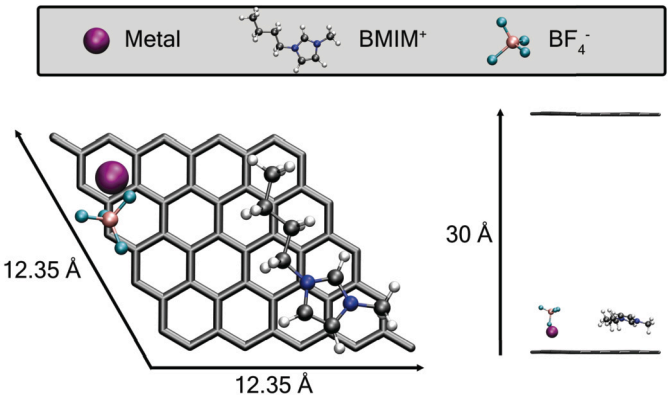


Fig. 1. Top and side views of a snapshot of one of the simulated systems.

In this study, we investigate the role played by the metal atoms doping the IL in the adsorption mechanism and the interaction with monolayer graphene. Of particular interest is to understand the effect of their atomic radius or valence on several electronic and optical properties, such as binding energy, charge transfer, electron density difference (EDD), band structure, partial density of states (PDOS), real and imaginary dielectric functions (ε), electron energy loss function (EELS, L), real and imaginary refractive index (n), reflectivity (R) and absorption coefficient (α). All the optical properties are studied for parallel and perpendicular (to the graphene layer) incoming electromagnetic radiation.

The paper is organized as follows: the details of the computational and theoretical methodology are given in Section 2, the results are presented and discussed in Section 3, and finally, in Section 4 we summarize our main conclusions.

2. Simulations details

In this work, we performed DFT calculations to study the effect of the adsorption of a metal atom in a system composed of a 2D graphene layer with an IL ([BMIM][BF_4]) already adsorbed. We explored 5 different metal species (lithium, sodium, magnesium, calcium and aluminum) to unveil the effect of properties such as atomic radius or valence. All calculations were conducted using Quantum-ESPRESSO (QE) package [74–76], which is based on plane wave pseudopotentials. For all the calculations in this work, we used the ultrasoft pseudopotentials. To describe the electron exchange-correlation energy, we employed the generalized gradient approximation (GGA) of Perdew-Burke-Ernzerhoff (PBE) [77]. Cutoffs of 50 Ry and 400 Ry in kinetic energy and charge density were deemed sufficient to achieve proper convergence.

A 5×5 supercell for graphene (2.47 Å lattice constant) was chosen as it approximately covers the surface of one anion-cation pair of the IL, comprising a total of 50 carbon atoms. This graphene layer was set up perpendicular to the z-axis. To ensure proper decoupling from periodic replicas, a buffer spacing of 30 Å in the z-direction was established. After a relaxation of the system, the IL was placed in the cell according to previous molecular dynamics (MD) simulations [78]. Another relaxation was carried out, and then the metal atom was added to the resulting configuration. We therefore had 5 equivalent systems (graphene/IL/metal) that were all of them relaxed once again. A snapshot of one of these systems is shown in Fig. 1.

Self consistency threshold was set to 10^{-6} Ry. In order to efficiently sample the Brillouin zone of the different structures, Methfessel-Paxton smearing [79] was used in conjunction with a 20×20×1 Γ-centered k-point mesh and a gaussian spreading of 0.01 Ry. It was checked in previous works performed by our group [55,69] that tightening the threshold and/or the k-points criteria does not lead to remarkable differences in

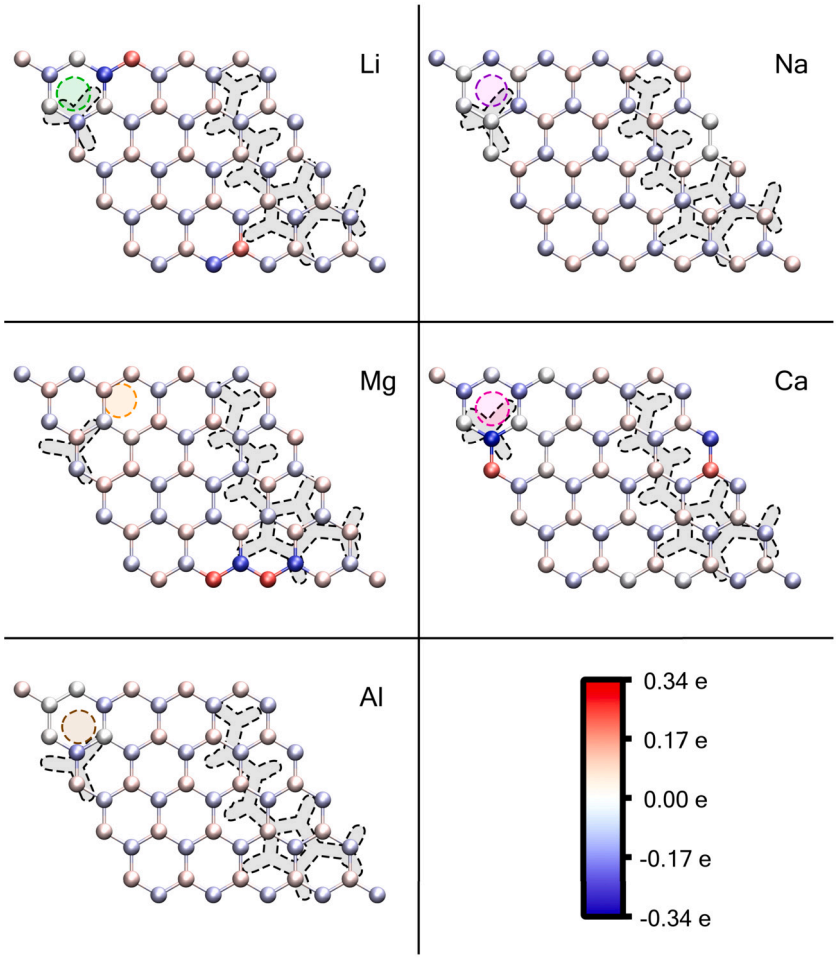


Fig. 2. Charge of the carbon atoms of graphene induced by the presence of the IL and the different metals calculated using Bader charge analysis. Dashed outlines show the position of the IL and the corresponding metal in each system. The respective sizes of the metals have been increased for clarity purposes.

the obtained results. The same mesh was also used for the density of states (DOS) calculations. However, norm-conserving pseudopotentials in a 7×7×1 mesh disposition were employed for the computation of optical properties. These properties can all be derived from the complex dielectric function as described in Refs. [55,69]. As the first Brillouin zone of the considered system is hexagonal, the most convenient path to explore for the band structure, according to the corresponding high symmetry points, is the Γ → M → K → Γ path, along 91 different k-points. This choice is well-established in the literature [80–84], as it is commonly used in studies of band structures for graphene and related structures. In order to obtain the charge of the atoms, Bader charge analysis [85] was employed, and the necessary .cube file was obtained with Quantum Espresso's pp.x code.

Table 1
Total charge of the different species after Bader analysis of the relaxed configurations. Values for simulations with K obtained from Ref. [69] are included for comparison. First and second ionization energies (IE, in eV) for each element from Ref. [86] are also included.

	Charge (e)				Ionization energy	
System	Graphene	IL cation	IL anion	Metal	1st IE	2nd IE
G/IL/Li	-0.90	0.95	-0.95	0.90	5.39	75.64
G/IL/Na	-0.91	0.94	-0.94	0.90	5.14	47.29
G/IL/Mg	-0.20	0.88	-1.01	0.32	7.65	15.03
G/IL/Ca	-1.46	0.85	-0.91	1.52	6.11	11.87
G/IL/Al	-0.86	0.95	-1.16	1.07	5.99	18.83
G/IL/K	-0.91	0.95	-0.94	0.90	4.34	31.63

3. Results and discussion

3.1. Electronic properties

A Bader charge analysis [85] was carried out in order to determine the induced charge transfer to the graphene surface atoms that emerges from the adsorption of the IL and a metal atom. In Fig. 2 we can observe that there is a redistribution of electric charge in the graphene sheet when compared with the metal absent configuration [55]. The most remarkable feature is that Li and Ca atoms induce high polarity in some of their close neighboring carbons. In the case of Mg, a high induced polarization is also observed in some carbon atoms, which is originated not only from the presence of the metal but also from that of the IL ions, since the three of them are located at the same distance from the 2D surface. On the other hand, the presence of Na and Al leads to a more homogeneous distribution of the charge, as it was also previously observed for K [69]. However, a situation in which every positively charged site is surrounded by negatively charged carbon atoms was only predicted for lithium. As it can be seen in Table 1, in general the metal is the species that transfers approximately all its charge to the graphene sheet, while the IL ions suffer almost no modification and keep their bulk charge of ±1e. However, a detailed comparison between the charge of cation and anion in the different systems after adsorption indicates that the cation always tends to become less positive, whereas the anion usually tends to be less negative except for mixtures with magnesium and, mainly, with aluminum, where it gains charge. Moreover, the total transfer of charge from magnesium to graphene is predictably

Table 2
Binding energy (ΔE) and distance between the metal atom and i) its nearest carbon atom (d_{MC}), ii) the center of mass of the anion (d_{MA}), iii) the center of mass of the imidazolium ring (d_{MR}), and iv) the terminal carbon of the imidazolium tail (d_{MT}) for each of the studied systems. Values for simulations with K obtained from Ref. [69] are included for comparison.

	ΔE (eV)	d_{MC} (Å)	d_{MA} (Å)	d_{MR} (Å)	d_{MT} (Å)
G/IL/Li	-3.21	1.97	2.48	6.17	5.34
G/IL/Na	-2.40	2.37	2.83	6.18	5.53
G/IL/Mg	-0.76	4.63	3.25	7.47	5.38
G/IL/Ca	-2.89	2.11	2.95	6.36	5.60
G/IL/Al	-2.20	2.59	3.12	6.23	5.36
G/IL/K	-2.25	2.69	3.18	6.64	5.60

low, which can be explained in terms of the ionization energies (IE) included in Table 1, and from where it can be inferred that only those atoms whose first IE are close to or lower than approximately 6 eV are able to transfer an electron to graphene. In particular, Mg has a stable closed-shell configuration, which explains its large first IE and the difficulty to remove an electron. On the other hand, calcium and, specially, aluminum atoms, despite being located in a more advantageous position than Mg, do not transfer all their free electrons to the graphene. In the first case, Ca has the smallest second IE, which explains the fact that this metal transfers the largest amount of charge to the surface. However, the second IE is still too high for removing two electrons from Ca. For Al, after losing one electron, it achieves a stable electron configuration. Thus, the first electron is relatively easy to remove from aluminum, but the second one is much more difficult to remove from the 1+ charge-state aluminum ion.

We have also calculated the binding energies (ΔE) of the metal atoms on a graphene sheet with an IL already adsorbed on it as

$$\Delta E = E_{\mathrm{G/IL/M}} - E_{\mathrm{G/IL}} - E_{\mathrm{M}}, \tag{1}$$

where $E_{\mathrm{G/IL/M}}$ is the total energy of the graphene layer with the adsorbed IL and the metal atom, $E_{\mathrm{G/IL}}$ is the total energy of the graphene layer with the adsorbed IL, and E_{M} is the total energy of the isolated metal atom. Following these criteria, a negative binding energy is associated to a stable configuration, whereas a positive one is an indication of an unfavorable adsorption on the assembly graphene/IL and the metal atom preferring to remain in its atomic state.

Adsorption energies and structural properties such as the distance between the metal atom and i) its nearest carbon atom (d_{MC}), ii) the center of mass of the anion (d_{MA}), iii) the center of mass of the imidazolium ring (d_{MR}), and iv) the terminal carbon of the imidazolium tail (d_{MT}) are summarized in Table 2. All the metal atoms lie at a distance of about 2 Å from the graphene sheet except magnesium, which is further away from the surface. For visual reference, see Fig. S1 of the Supporting Information, which contains snapshots of all the systems. This is likely related to the lower binding energy of this particular metal in comparison with the rest. In this way, the magnesium atom accommodates itself in the same plane as the IL components, but at a further straight line distance from them than the other metals. However, all the other systems share a quite similar geometrical disposition, with the metal being placed between the graphene sheet and the BF_4^- anion. In addition, we can observe that lithium is the atom more strongly adsorbed on the surface in the presence of the IL, which is in agreement with trends previously reported for the adsorption of metal atoms on pristine graphene [24,32,87]. These observations are coherent with the previous charge transfer analysis. Indeed, Mg is the species located the furthest from the surface because of its vanishing charge transfer ability. For this metal it is not energetically favorable to stay in this electronically highly reactive region, whereas the rest of the metals are located close to graphene because they are capable of transferring electrons to it. Some degree of charge transfer from the Mg atom at distances longer than 4 Å has been previously reported in the presence of an ionic liquid [88].

The electronic behavior was further examined through the charge density difference ($\Delta\rho$) defined as

$$\Delta\rho = \rho_{\mathrm{G/IL/M}} - \rho_{\mathrm{G/IL}} - \rho_{\mathrm{M}}, \tag{2}$$

where $\rho_{\mathrm{G/IL/M}}$, $\rho_{\mathrm{G/IL}}$ and ρ_{M} are the total charge densities of the relaxed system with IL and metal adsorbed on graphene, the system with IL adsorbed on the 2D surface and the isolated metal, respectively. Lateral views of the charge density differences for the different metals are provided in Fig. 3. An isovalue of $\pm 0.017\ \mathrm{e/Å^3}$ was considered for the calculation of the diagrams, in which the electron gain and loss configurations are represented by blue and red isosurfaces, respectively. Top views of the same systems are included in the Supporting Information (Fig. S2).

Charge densities of the systems presented in Fig. 3 indicate that the addition of metal atoms modifies not only the electron distribution in the anion and the cation, but also that of the C atoms of graphene lying below the metals. The effect on electronic density difference is similar for all the systems, with metal atoms acquiring an electron loss configuration and C atoms around them showing gain of electrons, as indicated by the red isosurface covering all the metals and the blue one accumulated below them, respectively. This ionic interaction is consistent with the picture previously reported for potassium [69]. Moreover, this effect affects both sides of the surface layer in the systems that showcase greater charge transfer, specially in the case of calcium.

Before starting the analysis of the electronic states of the system, we must take into account that the system is composed of two clearly differentiated parts. The first one is the solid region, which is composed by the graphene and contains the free electrons. The second one is the molecular region, which is composed by the ionic liquid and the metal atom. The difference between these regions is not only a matter of denomination, but they require different tools for their analysis. Therefore, we will first analyze the band structure of the system, focusing on the graphene. Then, we will analyze the highest occupied molecular orbital (HOMO) and the lowest unoccupied molecular orbital (LUMO) of the molecular region and we will use these values to analyze the possible charge transfer between both regions.

The band structure diagrams for all the metals adsorbed on the G/IL systems are shown in Fig. 4, in which the energies are relative to the Fermi level. In order to determine the effect of the metal atoms on the electronic structure, band structure diagrams of pristine graphene are also depicted (black lines) and, for the sake of comparison, they are shifted in such a way that the Dirac cones of both configurations are overlapped. As it is well known, graphene is a semimetal whose conduction and valence bands meet at the Dirac points. On the other hand, it was previously reported that the Dirac cones at the Fermi energy of this 2D material do not suffer any shift upon adsorption of this IL [55]. As it can be seen in Fig. 4, in all cases the adsorption of metal atoms downshifts the Dirac cone below the Fermi level, thus confirming that the charge is donated from the metal to the graphene surface. Therefore, all the metal atoms act like n-type dopants. We can also observe that the band structure of the pristine graphene is approximately conserved in most of the systems. For example, in Fig. 4, where the band structure of the configuration with Mg is represented, the bands corresponding to the periodic part of the system completely coincide, whereas the bands with new molecular levels arise in the form of horizontal bands. In the opposite way, Ca shows to be the atom that induces a larger modification of the bands associated with the periodic part, as it is the metal that transfers the largest amount of charge to the graphene surface. This analysis of the band structure diagrams is also indicative of the degree of charge transfer resistance of these systems and how it varies with the metal atom of the electrolyte.

To analyze this effect, the energy shifts as a function of the charge of the 2D layer are plotted in Fig. 5. There, we can observe that the greater

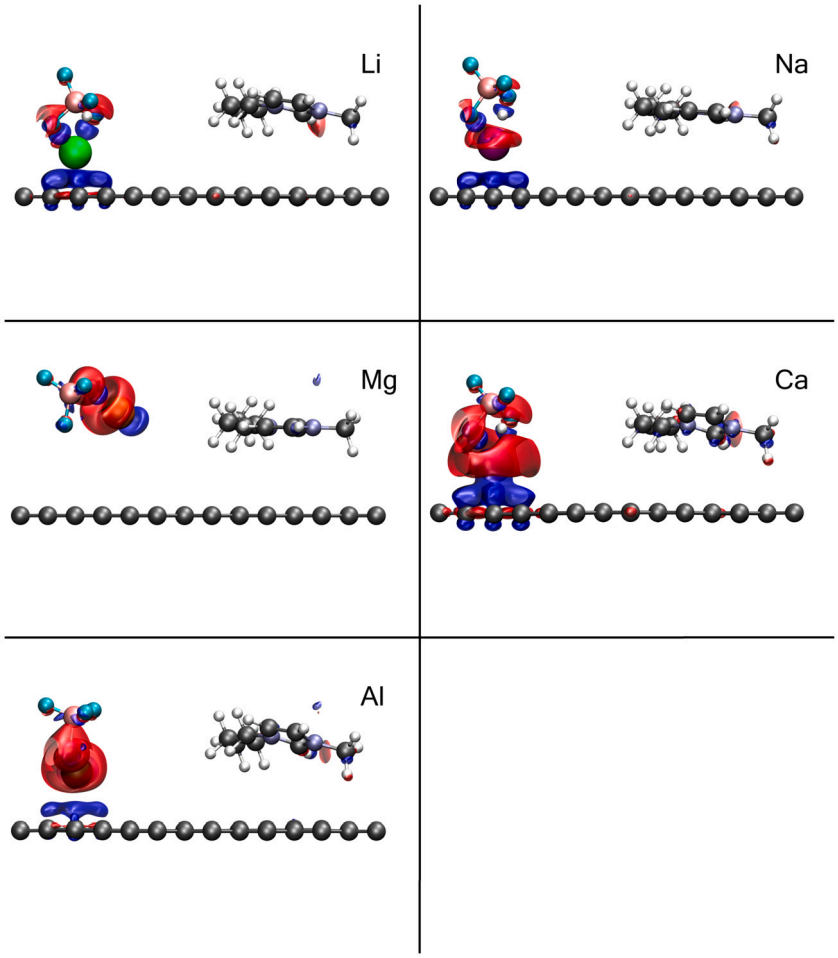


Fig. 3. Lateral views of the electronic density difference between the system with metal and IL, and the system with no metal and the system with only metal. Regions depicted in red/blue correspond to isosurfaces of value $\pm 0.017\ e/Å^3$, and therefore represent electron depletion/accumulation, respectively. The respective sizes of the metals have been increased for clarity purposes.

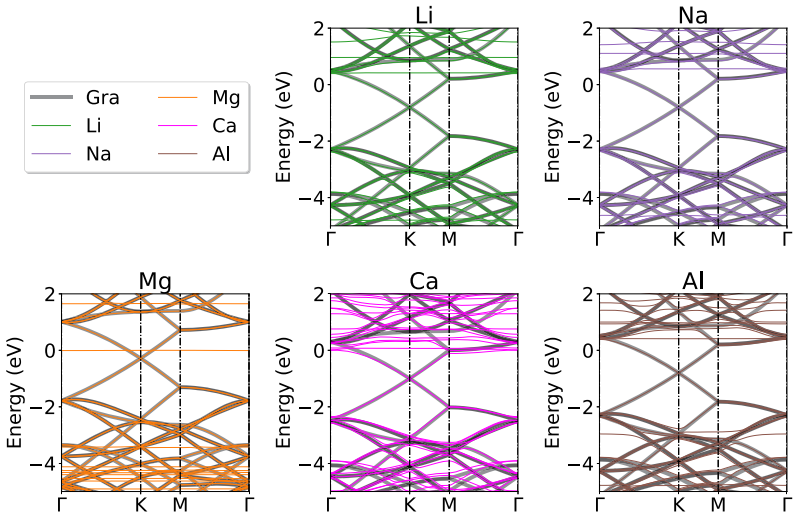


Fig. 4. Band structure diagrams of the different systems, in which the Fermi energy is taken as a reference for the energy level. In a wider black line, the band structure of pristine graphene is positioned so that the Dirac cones are overlapped.

the degree of charge transfer, the larger the shift in energy, confirming the direct relationship. Previously reported values for K [69] are similar to those of Li, Na and Al; whereas Ca and Mg atoms tend to have the largest and the smallest electron transfer and energy shifts, respectively.

To further understand the effect of mixtures of [BMIM][BF_4] and that of the metal atoms on the electronic structure of graphene, we calculated the total (DOS) and projected density of states (PDOS) of the different systems, which are shown in Fig. 6 for energies values relative

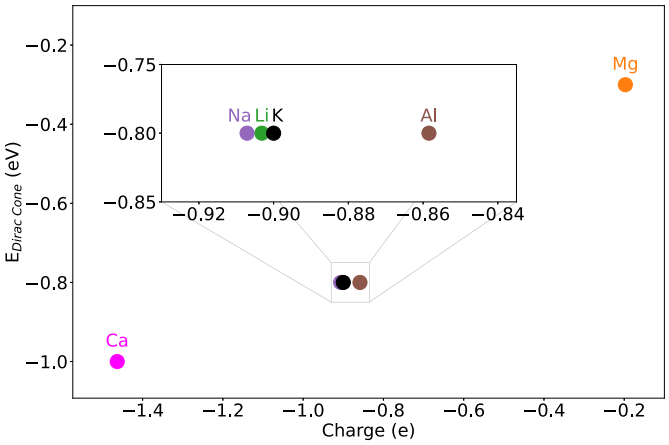


Fig. 5. Energy shift of the Dirac cone as a function of the charge transferred to the graphene surface for each system. For clarity purposes, a zoom was added as an inset to facilitate the view of some points. Values for simulations with K obtained from Ref. [69] are included for comparison.

to the Fermi level within the range $[-5, +5]$ eV. Molecular HOMO-3, HOMO-2, HOMO-1, HOMO, LUMO, LUMO+1, LUMO+2 and LUMO+3 states are also represented and, since some of them are overlapping, each of the energy levels are included in Table S1 of the Supporting Information (the color-code shows to which species the state belongs). In addition, DOS and PDOS within an energy interval of $[-20, +6]$ eV are also included in the Supporting Information (Fig. S3), where it can be seen that the states of both the anion and the cation of the IL notably contribute to the valence states of the systems. For each system, we can easily distinguish the Dirac point, at which the DOS is zero. Below the Fermi level the DOS is almost equivalent to that of graphene up to energies around -3 or -4 eV (depending on the system), where the HOMO level of $[BMIM]^+$ cation (which shows the characteristic "flatline" behavior of molecular systems) lies, and, for mixtures with magnesium and aluminum, also a state of the metal. For mixtures with Mg, this state is superposed with states from the IL ions, and they lie approximately at the Fermi level, which is also very close to the Dirac point. Still, the Dirac point is clearly visible. Due to this feature, we could consider Mg as an interesting option for electronic devices, but it must be remembered that this is the atom adsorbed at the longest distance from the graphene surface. The system with Ca also forms a state at its Fermi level, but in this case it belongs to the IL cation. For the other three systems, the states between the Dirac point and the Fermi level are mostly from graphene. States for Li, Na and Ca lie at approximately 1.6, 1.5 and 0.4 eV above the Fermi energy, respectively, all of them being unoccupied. Moreover, Al has its *3s* and *3p* states at around -3 and 1 eV, respectively. This valence *p* peak being above the Fermi level confirms that close to one electron is transferred from Al to the 2D surface. Notice that a core assumption of PDOS is the projection of the total states on atomic orbitals. In the case of Ca, the dense electronic cloud surrounding it overlaps with that of graphene, as seen in Fig. 3. Therefore, this projection is hampered and this approximation becomes less accurate. As a result, although the total DOS does reflect the presence of the Dirac cone in this system (as previously seen in the band structure in Fig. 4), some states corresponding to the graphene PDOS near the Dirac cone are missing.

The stability and interaction strength of the metal adsorbed on the G/IL system can be explored through the HOMO and LUMO orbitals, which are represented in Figs. S4 and S5 of the Supporting Information, respectively, with the aim of providing a graphical perspective of the orbitals involved. This was calculated by locally integrating the DOS in an energy band around the HOMO and LUMO states, respectively. The energy difference between these orbitals is known as the HOMO-LUMO energy gap, ΔE_{HL}, and can be calculated as

$$\Delta E_{\mathrm{HL}} = E_{\mathrm{LUMO}} - E_{\mathrm{HOMO}} \tag{3}$$

Through the DOS we can analyze the changes in ΔE_{HL} due to molecular interactions, which are tabulated in Table 3. From the $\Delta E_{HL} \approx 5$ eV value previously reported by Zhour et al. [55] for $[BMIM][BF_4]$ adsorbed on graphene, our simulations show an increase upon adsorption of lithium or sodium. This increase in the HOMO-LUMO gap is mainly accomplished by a substantial decrease in the HOMO energy. On the other hand, ΔE_{HL} was found to decrease for the other three metals (magnesium, calcium and aluminum), which is principally achieved by a remarkable decrease in the LUMO energy. Once again, the more substantial change in the HOMO-LUMO gap energy is observed for magnesium, which indicates a strong interaction of the metal with the IL, and is consistent with magnesium being located in the same plane of $[BMIM][BF_4]$.

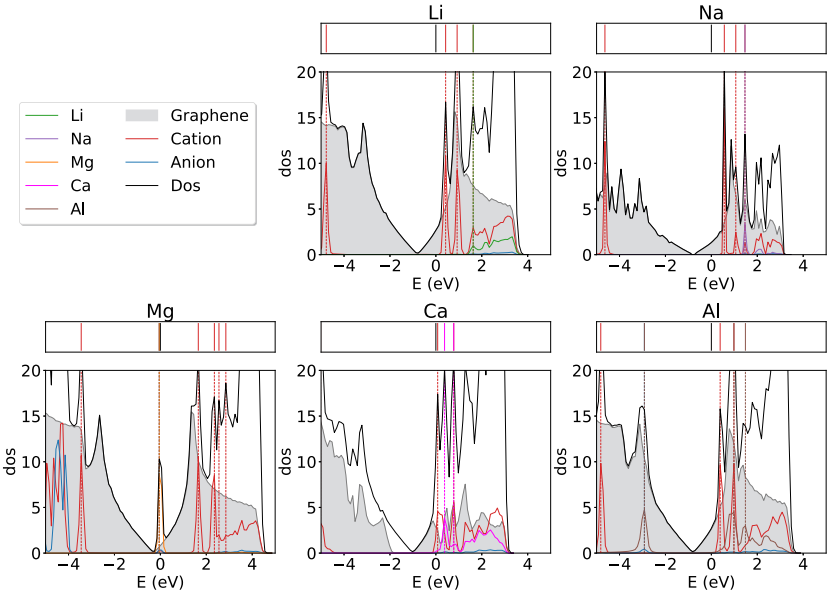


Fig. 6. DOS and PDOS of the different systems. On top of each plot: molecular HOMO-3, HOMO-2, HOMO-1, HOMO, LUMO, LUMO+1, LUMO+2 and LUMO+3 states that are within the considered energy interval. The color indicates to which species the state belongs. Fermi energy is taken as reference for the energy level.

Table 3
HOMO-LUMO energy gap for the different studied systems. Value for simulations with K obtained from Ref. [69] is included for comparison.

	ΔE_{HL} (eV)
G/IL/Li	5.20
G/IL/Na	5.20
G/IL/Mg	1.70
G/IL/Ca	4.70
G/IL/Al	3.30
G/IL/K	5.00

3.2. Optical properties

As mentioned earlier, the adsorption of metal atoms on the G/IL structure modifies the electronic properties of the system, which, in turn, leads to completely different optical characteristics. In this section, we investigate several electromagnetic parameters such as the dielectric constant (ε), the electron energy loss spectrum (EELS, L), refractive index (n), extinction coefficient (κ), reflectivity (R) and absorption coefficient (α) for the perpendicular and parallel polarization to the graphene layer, which are of fundamental importance for many technological applications. The considered frequency interval for the calculation of the optical parameters is taken from 0 to 20 eV, and the corresponding graphs are included in Figs. 7 and 8. In addition, since the visible range is of particular interest, in Figs. S6 and S7 of the Supporting Information only the region between 1.63 and 3.26 eV is plotted.

The dielectric coefficient is a complex magnitude, $\varepsilon(\omega) = \varepsilon_1(\omega) + i\varepsilon_2(\omega)$, whose real and imaginary parts are related through the conventional Kramers-Kronig relations [89]. The former is related to the amount of energy stored by the system, whereas the latter is related to its dissipation of energy. From this function, the refractive index, extinction coefficient, reflectivity and absorption coefficient can be easily calculated as it was explained in detail elsewhere [55,69,90,91].

The real and imaginary parts of the dielectric coefficient as a function of the frequency for all the considered structures are shown in Fig. 7 for both perpendicular and parallel incident electric field. We can clearly observe an anisotropic behavior of this magnitude for the different polarizations of light. In particular, this figure shows that for parallel electric field, the excitations, which are indicated by the peaks of ε_2, are located in the low-energy region. On the contrary, they are mainly observed in the high-frequency one for perpendicular electric field, except for Mg that also has an excitation energy at 2.85 eV. Thus, when the polarization of the electric field is parallel, the imaginary part for Li, Na and Al shows a similar behavior to that previously reported for K [69], with the metals screening the peaks of G/IL below the visible range. However, both Ca and Mg exhibit very intense transitions in this regime. Concerning the perpendicular polarization, a small peak is observed near zero due to the adsorption of Ca and, in addition to the aforementioned peak for Mg, Al shows that some transitions are possible at energies around 5 eV. Then, all the systems have excitation energies situated at around (10 – 11) eV and 14 eV, thus confirming that the transitions associated to the out-of-plane polarization are prevalent at higher energies.

Focusing now on the real part of the dielectric function, Fig. 7 indicates that for the perpendicular electric field the changes are detected for Ca, Mg and Al at the same energies as for the imaginary one. In the case of in-plane polarization, remarkable modifications compared to the G/IL system are observed at low frequencies mainly for Li, Na and Al, since their curves do not take positive values, contrary to what was previously observed for K [69]. By definition, the plasma frequency is the one at which the real part of the dielectric function cancels, $\varepsilon_1(\omega_p) = 0$. At these frequencies, ε_1 changes its sign [92] and this behavior corresponds to the collective excitations of the electrons. Thus, in Fig. 7

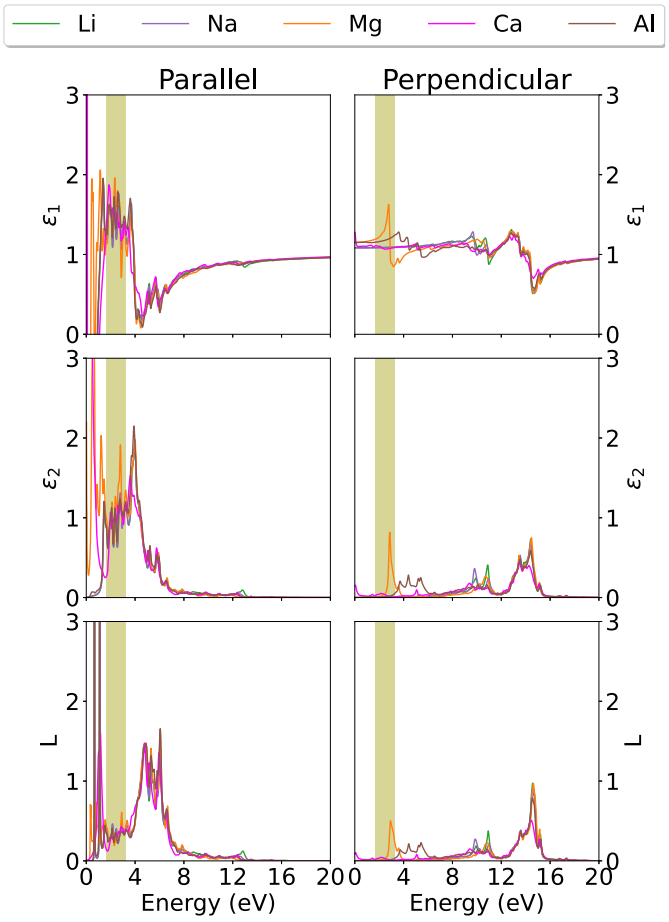


Fig. 7. Real (ε_1) and imaginary (ε_2) parts of the dielectric function and EELS (L) for the different systems with parallel (left) and perpendicular (right) electric field. Shaded stripes represent the optical region.

we can see that for perpendicular polarization there are no plasma frequencies, whereas for parallel polarization three plasma frequencies are induced by the presence of Mg at the interface, two by Ca and one by the rest of the metals. This shows that there are no collective excitations for perpendicular polarization but, for parallel one, the systems absorb the incoming electromagnetic radiation [92].

In Fig. 7 it can be also noticed that the static dielectric constant, which is the real part of the dielectric function at zero frequency, $\varepsilon_1(0)$, is remarkably modified by the adsorption of the metal with respect to the configuration G/IL [55] under in-plane polarization of the electric field. This can be due to an increase in the number of free electrons by the addition of the metal [92], which plays an important role for parallel polarization and implies that the metal-doped system dissipates more energy. On the other hand, for out-of-plane polarization, $\varepsilon_1(0)$ shows quite similar behavior compared to the G/IL system. In particular, it remains unchanged for Li and Na (1.08 and 1.09, respectively), it is slightly increased for Al and Mg (1.15 and 1.16, respectively), and takes the largest value (1.28) when Ca is adsorbed.

The EELS (L), which provides us with information about the collective excitation of the electrons, is also depicted in Figs. 7 and S4 for parallel and perpendicular polarization. The peaks in $L(\omega)$ correspond to 2D plasmons and are due to intraband transitions. Under in-plane electric field, two peaks appear at 0.65 and 1.15 eV (in a similar way to what was found for K [69]), as expected, since they correspond to the dips in the dielectric function. The first one is for Li, Na and Al, whereas the second one is also registered for Ca. For its part, the adsorption of Mg also causes a peak at lower energies (0.35 eV). For out-of-plane elec-

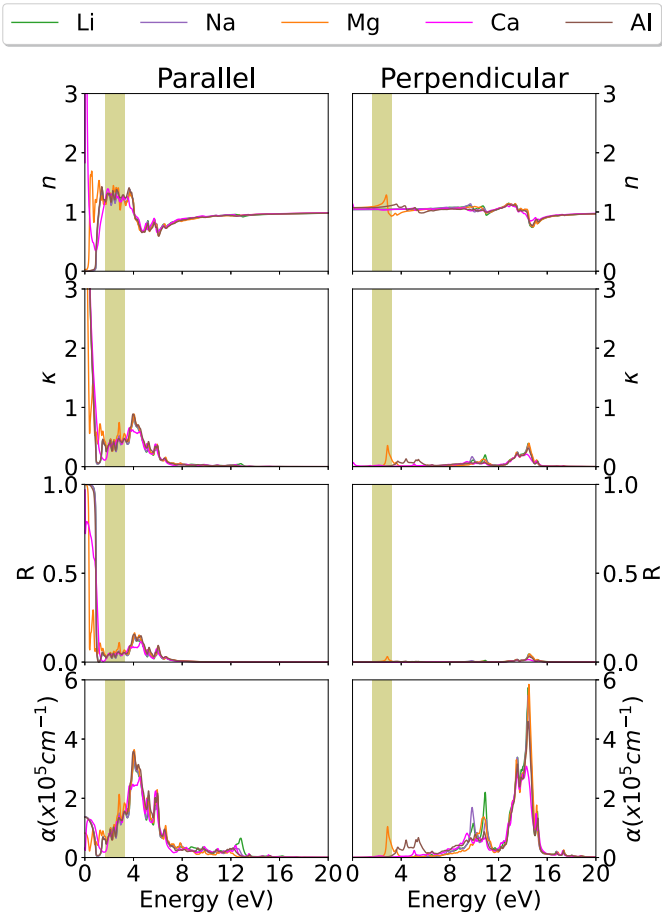


Fig. 8. Refractive index (n), extinction coefficient (κ), reflectivity (R) and absorption coefficient (α) for the different systems with parallel (left) and perpendicular (right) electric field. Shaded stripes represent the optical region.

tric field, new peaks with respect to G/IL [55] are found for Mg, Ca and Al at the same energies as for the dielectric function.

The complex refractive index compares the propagation of an electromagnetic wave in vacuum and in a given material. The optical refractive index, $n(\omega)$ (which represents the real part of the complex refractive index and is necessary for the optical devices), and the extinction coefficient, $\kappa(\omega)$ (which represents its imaginary part), as a function of energy can be both determined from the real and imaginary parts of the dielectric function as described in [69].

From Figs. 8 and S5, it can be seen that the refractive index has an anisotropic behavior. For parallel polarization the behavior observed for Li, Na and Al is similar to the one previously reported for the adsorption of K [69], with $n(\omega)$ reaching values close to zero in the lowest frequency interval of $[0, 1]$ eV. Mg shows similar characteristics, but its refractive index goes to zero at lower frequencies and it reaches a maximum value of 1.65 at 0.6 eV. For Ca, an intense peak of 9.5 is obtained at 0.06 eV and it seems to be the metal that modifies the least the shape of the curve that was observed for G/IL [69]. It must be noted that for energies larger than about 4 eV the refractive index value is less than one, due to the phase velocity of the electromagnetic field being higher than the speed of light in vacuum. The features for perpendicular polarization are similar for all the metals other than Mg, which shows the highest value (1.3) at 2.8 eV. In this case, the static refractive index at vanishing frequencies (i.e. $n(0)$), takes values of 1.04 for Li and Na, 1.07 for Mg and Al, and 1.13 for Ca, thus validating the relation $n(0) = \sqrt{\varepsilon_1(0)}$. These values point out that the mobility of electrons increases after adsorption of Ca compared to the other metals. Moreover, when a material exhibits a refractive index that varies based on the polarization of light, it is referred to as birefringent. In our systems, the difference between the parallel and perpendicular $n(\omega)$ is ca. 0.2 in the visible range, and prominent changes take place in the low-frequency region, specially for Ca.

Concerning the extinction coefficient, which indicates the degree of attenuation of the electromagnetic waves when propagating through the material, is as well clearly anisotropic. For the in-plane polarization, the adsorption of Mg causes the first minimum to move towards lower energies compared to Li, Na and Al, whereas doping with Ca shows the opposite effect. In addition, $\kappa(\omega)$ dramatically increases at low frequencies for all the metal atoms with respect to G/IL and it goes to zero when the frequency exceeds ~ 13 eV, in a similar way to what happens in the presence of K [69]. In the case of the out-of-plane polarization, the main difference arises again for Mg and Al, which show peaks at ~ 2.9 eV and in the region around 5 eV, respectively. Thus, we can state that different choices of the doping metal atom allow tuning the refractive index and the extinction coefficient in the low electron energy region for different applications.

Optical reflectivity (R) and absorption (α) coefficients were also calculated as detailed in [69] and analyzed in Figs. 8 and S5. Firstly, the reflectivity parameter shows prominent reflection at low frequencies for parallel incident electric field (from 0 to 0.4 eV for Mg, and from 0 to 1.1 eV for the rest of the metals). Then, in the visible range, R is shown to be below 20% and it vanishes at 7.6 eV. On the other hand, for perpendicular incident electric field the calculated reflectivity is zero in almost all the considered energy range, and it does not exceed a 5% in any case. Once again, Mg is the only metal atom that shows a peak within the visible range at 2.9 eV.

With regard to the absorption coefficient, it clearly follows the same behavior as the extinction coefficient. The results for the parallel polarization indicate that the absorption in the presence of all the metals starts at very low frequencies, and it increases at higher energies reaching a maximum value at around 4 eV. All the changes observed at low frequencies in the in-plane optical parameters with respect to the G/IL system [69] are due to the free electrons being the ones excited and contributing to optical transitions. The variation of the number of free electrons with metal-doping and the electron transfer process from the metal to graphene not only induce modifications in the electronic properties, but are also behind the effects observed in the near-zero frequency region for a parallel electric field. For perpendicular polarization, there is an overall increasing tendency for all the metals up to ~ 14.5 eV, before α starts to decrease. This is due to the bound electrons being able to oscillate with increasing frequency when increasing the energy of the incident electric field just up to a given value, after which the absorption process decreases. Looking at $\alpha(\omega)$ and $\kappa(\omega)$ we can confirm that these materials are transparent only for energies above 18 eV.

4. Conclusions

In this work, we employed plane wave DFT calculations to analyze how the electronic and optical properties of a graphene 2D surface are modified by the adsorption of an ionic liquid ([BMIM][BF_4]) mixed with a metal salt. Several metals of different valence and ionic radius (Li, Na, Mg, Ca, Al) were selected in order to shed some light on how the features of the systems are affected by these parameters.

A Bader charge analysis showed that most metals transfer 1 electron to the graphene surface, regardless of their valence. The ionization energy seems to be responsible for this behavior, as it prevents the electron exchange on Mg, the metal with the highest 1st IE, and induces the second electron transfer on Ca, whose 2nd IE is the lowest. This effect can also be observed in a structural analysis, where all the metals other than Mg are adsorbed near the 2D surface while sharing their electrons, with lithium adsorption being the most stable one and magnesium having the lowest binding energy.

From the charge density difference we confirmed that metal atoms acquired an electron loss configuration and carbon atoms around them showed gain of electrons. In addition, the redistribution of electric charge in the graphene surface was observed to be homogeneous with the adsorption of Na and Al, whereas the other metals induced high polarization in their neighboring carbon atoms. A band structure analysis showed that our system has two well differentiated parts: the 2D surface and the molecular complex, which is formed by the IL and the metal. The band structure of pristine graphene is conserved, but the Dirac cone is downshifted below the Fermi level as a consequence of the charge transfer. Moreover, new molecular levels arise in the system. The partial density of states also revealed some key differences between these systems. The metals that show more states close to the Dirac cone are Mg and Ca. However, the ionization of Mg is highly unlikely, which leads to its accommodation further from the surface.

Concerning the optical properties, all the magnitudes analyzed show an anisotropic behavior for the different polarizations of light. The adsorption of Mg and Ca leads to different features compared to the other metals, the former due to being positioned at great distances and the latter due to its larger charge transfer to graphene. Different plasma frequencies are induced depending on the metal at the interface for parallel polarization, whereas no collective excitations of the electrons for perpendicular polarization were found. Also, the analysis of the static refractive index showed that the mobility of the electrons is increased when Ca is adsorbed compared to the other metals.

We hope that this work will contribute to the current research on the possibility to tune the optoelectronic properties of graphene using ionic liquids and metal salts and provide a basis for the development of novel electrochemical and photonic devices. Further study employing more realistic electrodes such as metal oxide surfaces, and analyzing how the metal atom intercalation and alloy formation are affected by the findings reported in this work is now in progress.

CRediT authorship contribution statement

Alejandro Rivera-Pousa: Formal analysis, Investigation, Methodology, Software, Validation, Visualization, Writing – original draft, Writing – review & editing. **José M. Otero-Mato:** Formal analysis, Investigation, Methodology, Software, Validation, Writing – review & editing. **Carlos Damián Rodríguez-Fernández:** Formal analysis, Investigation, Methodology, Software, Validation, Writing – review & editing. **Kazem Zhour:** Formal analysis, Investigation, Methodology, Software, Validation, Writing – review & editing. **Hadrián Montes-Campos:** Conceptualization, Formal analysis, Investigation, Methodology, Project administration, Software, Supervision, Validation, Visualization, Writing – original draft, Writing – review & editing. **Trinidad Méndez-Morales:** Conceptualization, Formal analysis, Investigation, Methodology, Project administration, Software, Supervision, Validation, Visualization, Writing – original draft, Writing – review & editing. **Luis M. Varela:** Conceptualization, Formal analysis, Funding acquisition, Project administration, Supervision, Visualization, Writing – review & editing.

Declaration of competing interest

The authors declare that they have no known competing financial interests or personal relationships that could have appeared to influence the work reported in this paper.

Data availability

Data will be made available on request.

Acknowledgements

The financial support of the Spanish Ministry of Science and Innovation (PID2021-126148NA-I00 funded by MCIN/AEI/10.13039/501100011033/FEDER, UE) is gratefully acknowledged. Moreover, this work was funded by the Xunta de Galicia (GRC ED431C 2020/10). A. R.-P. and J.M.O.-M. thank the Spanish Ministry of Education for their FPU grants (FPU16/01500 and FPU18/01597). C. D. R. F. thanks the support of Xunta de Galicia through the grant ED481A-2018/032. T. M. M. acknowledges her contract funded by the pilot program of the USC for the recruitment of distinguished research personnel—call 2021 under the agreement between the USC and the Santander Bank for 2021–2024. H.M.C. thanks the USC for his "Convocatoria de Recualificación do Sistema Universitario Español-Margarita Salas" postdoctoral grant under the "Plan de Recuperación Transformación" program funded by the Spanish Ministry of Universities with European Union's NextGenerationEU funds. This work was supported by the Fundação para a Ciência e a Tecnologia (FCT) (funded by national funds through the FCT/MCTES (PIDDAC)) to CIQUP, Faculty of Science, University of Porto (Project UIDB/00081/2020), IMS-Institute of Molecular Sciences (LA/P/0056/2020). Facilities provided by the Galician Supercomputing Centre (CESGA) are also acknowledged.

Appendix A. Supplementary material

Supplementary material related to this article can be found online at https://doi.org/10.1016/j.molliq.2023.123460.

References

[1] Z. Xie, B. Zhang, Y. Ge, Y. Zhu, G. Nie, Y. Song, C.-K. Lim, H. Zhang, P.N. Prasad, Chemistry, functionalization, and applications of recent monoelemental two-dimensional materials and their heterostructures, Chem. Rev. 122 (2022) 1127–1207.
[2] H. Qiao, H. Liu, Z. Huang, R. Hu, Q. Ma, J. Zhong, X. Qi, Tunable electronic and optical properties of 2d monoelemental materials beyond graphene for promising applications, Energy Environ. Mat. 4 (2021) 522–543.
[3] L.A. Falkovsky, Optical properties of graphene, J. Phys. Conf. Ser. 129 (2008) 012004.
[4] D.G. Papageorgiou, I.A. Kinloch, R.J. Young, Mechanical properties of graphene and graphene-based nanocomposites, Prog. Mater. Sci. 90 (2017) 75–127.
[5] A.H. Castro Neto, F. Guinea, N.M.R. Peres, K.S. Novoselov, A.K. Geim, The electronic properties of graphene, Rev. Mod. Phys. 81 (2009) 109–162.
[6] N.R. Abdullah, B.J. Abdullah, C.-S. Tang, V. Gudmundsson, Properties of bc6n monolayer derived by first-principle computation: influences of interactions between dopant atoms on thermoelectric and optical properties, Mater. Sci. Semicond. Process. 135 (2021) 106073.
[7] M. Rafique, Y. Shuai, I. Ahmed, R. Shaikh, M.A. Tunio, Tailoring electronic and optical parameters of bilayer graphene through boron and nitrogen atom co-substitution; an ab-initio study, Appl. Surf. Sci. 480 (2019) 463–471.
[8] G. Ambrosio, G. Drera, G.D. Santo, L. Petaccia, L. Daukiya, A. Brown, B. Hirsch, S.D. Feyter, L. Sangaletti, S. Pagliara, Interface chemistry of graphene/cu grafted by 3, 4,5-tri-methoxyphenyl, Sci. Rep. 10 (2020) 1–9.
[9] V. Kumar, R. Santosh, First-principle calculations of structural, electronic, optical and thermodynamical properties of fluorinated graphene, Mater. Sci. Eng. B 246 (2019) 127–135.
[10] M.Y. Hanna, I. Santoso, M.A.U. Absor, The role of the oxygen impurity on the electronic properties of monolayer graphene: a density-functional study, J. Phys. Conf. Ser. 1011 (2018) 012071.
[11] T. Sruthi, T. Kartick, Route to achieving enhanced quantum capacitance in functionalized graphene based supercapacitor electrodes, J. Phys. Condens. Matter 31 (2019) 475502.
[12] R. You, Y.-Q. Liu, Y.-L. Hao, D.-D. Han, Y.-L. Zhang, Z. You, Laser fabrication of graphene-based flexible electronics, Adv. Mater. 32 (2020) 1901981.
[13] A. Olabi, M.A. Abdelkareem, T. Wilberforce, E.T. Sayed, Application of graphene in energy storage device – a review, Renew. Sustain. Energy Rev. 135 (2021) 110026.
[14] S. Priyadarsini, S. Mohanty, S. Mukherjee, S. Basu, M. Mishra, Graphene and graphene oxide as nanomaterials for medicine and biology application, J. Nanostruct. Chem. 8 (2018) 123–137.
[15] Y. Qiao, X. Li, T. Hirtz, G. Deng, Y. Wei, M. Li, S. Ji, Q. Wu, J. Jian, F. Wu, et al., Graphene-based wearable sensors, Nanoscale 11 (2019) 18923–18945.
[16] F. Larki, Y. Abdi, P. Kameli, H. Salamati, An effort towards full graphene photodetectors, Photonic Sens. (2022) 1–37.
[17] S. Alvin, H.S. Cahyadi, J. Hwang, W. Chang, S.K. Kwak, J. Kim, Revealing the intercalation mechanisms of lithium, sodium, and potassium in hard carbon, Adv. Energy Mater. 10 (2020) 2000283.
[18] Y. Li, Y. Lu, P. Adelhelm, M.-M. Titirici, Y.-S. Hu, Intercalation chemistry of graphite: alkali metal ions and beyond, Chem. Soc. Rev. 48 (2019) 4655–4687.

[19] X. Liu, Y. Han, J.W. Evans, A.K. Engstfeld, R.J. Behm, M.C. Tringides, M. Hupalo, H.-Q. Lin, L. Huang, K.-M. Ho, et al., Growth morphology and properties of metals on graphene, Prog. Surf. Sci. 90 (2015) 397–443.
[20] S.K. Gupta, H.R. Soni, P.K. Jha, Electronic and phonon bandstructures of pristine few layer and metal doped graphene using first principles calculations, AIP Adv. 3 (2013) 032117.
[21] M. Xu, H. Wang, S. Sun, H. Li, X. Li, Y. Chen, Y. Ni, First-principles study of metal atoms adsorption on 2d dumbbell c4n, Phys. Status Solidi B 257 (2020) 1900205.
[22] M. Rafique, Y. Shuai, H.-P. Tan, M. Hassan, Manipulating intrinsic behaviors of graphene by substituting alkaline earth metal atoms in its structure, RSC Adv. 7 (2017) 16360–16370.
[23] A.C.F. Serraon, J.A.D. Del Rosario, P.-Y. Abel Chuang, M.N. Chong, Y. Morikawa, A.A.B. Padama, J.D. Ocon, Alkaline earth atom doping-induced changes in the electronic and magnetic properties of graphene: a density functional theory study, RSC Adv. 11 (2021) 6268–6283.
[24] K.T. Chan, J.B. Neaton, M.L. Cohen, First-principles study of metal adatom adsorption on graphene, Phys. Rev. B 77 (2008) 235430.
[25] S. Ullah, P.A. Denis, F. Sato, Adsorption and diffusion of alkali-atoms (li, na, and k) on ben dual doped graphene, Int. J. Quant. Chem. 119 (2019) e25900.
[26] A.P. Durajski, K.M. Skoczylas, R. Szczęśniak, Superconductivity in bilayer graphene intercalated with alkali and alkaline earth metals, Phys. Chem. Chem. Phys. 21 (2019) 5925–5931.
[27] C.S. Praveen, S. Piccinin, S. Fabris, Adsorption of alkali adatoms on graphene supported by the au/ni(111) surface, Phys. Rev. B 92 (2015) 075403.
[28] O. Farkad, R. Takassa, F. Elfatouaki, S. Hassine, Y. Ijdiyaou, E. Ibnouelghazi, D. Abouelaoualim, Structural, electronic and optical properties of ab bilayer graphene intercalated by sr atom: a first principles study, Diam. Relat. Mater. 126 (2022) 109082.
[29] T. Kaneko, R. Saito, First-principles study on interlayer state in alkali and alkaline earth metal atoms intercalated bilayer graphene, Surf. Sci. 665 (2017) 1–9.
[30] Y. Shuai, M. Rafique, M. Moazam Baloch, M. Ali Tunio, I. Ahmed, Dft study on tailoring the structural, electronic and optical properties of bilayer graphene through metalloids intercalation, Chem. Phys. 536 (2020) 110828.
[31] Z. Wang, S.M. Selbach, T. Grande, Van der Waals density functional study of the energetics of alkali metal intercalation in graphite, RSC Adv. 4 (2014) 4069–4079.
[32] E. Olsson, G. Chai, M. Dove, Q. Cai, Adsorption and migration of alkali metals (li, na, and k) on pristine and defective graphene surfaces, Nanoscale 11 (2019) 5274–5284.
[33] S. Pakhira, K.P. Lucht, J.L. Mendoza-Cortes, Dirac cone in two dimensional bilayer graphene by intercalation with v, nb, and ta transition metals, J. Chem. Phys. 148 (2018) 064707.
[34] S. Pakhira, J.L. Mendoza-Cortes, Tuning the Dirac cone of bilayer and bulk structure graphene by intercalating first row transition metals using first-principles calculations, J. Phys. Chem. C 122 (2018) 4768–4782.
[35] E. Kianfar, S. Mafi, Ionic liquids: properties, application, and synthesis, Fine Chem. Eng. (2021) 22–31.
[36] T. Welton, Ionic liquids: a brief history, Biophys. Rev. 10 (2018) 691–706.
[37] M.B. Shiflett, Commercial Applications of Ionic Liquids, vol. 605, Springer, 2020.
[38] H. Liu, H. Yu, Ionic liquids for electrochemical energy storage devices applications, J. Mater. Sci. Technol. 35 (2019) 674–686.
[39] D.R. MacFarlane, N. Tachikawa, M. Forsyth, J.M. Pringle, P.C. Howlett, G.D. Elliott, J.H. Davis, M. Watanabe, P. Simon, C.A. Angell, Energy applications of ionic liquids, Energy Environ. Sci. 7 (2014) 232–250.
[40] G. Kaur, H. Kumar, M. Singla, Diverse applications of ionic liquids: a comprehensive review, J. Mol. Liq. (2022) 118556.
[41] A.J. Greer, J. Jacquemin, C. Hardacre, Industrial applications of ionic liquids, Molecules 25 (2020) 5207.
[42] Q. Gao, Y. Zhang, S. Xu, A. Laaksonen, Y. Zhu, X. Ji, X. Lu, Physicochemical properties and structure of fluid at nano-/micro-interface: progress in simulation and experimental study, in: SI: Molecular Thermodynamics for Green Engineering, Green Energy Environ. 5 (2020) 274–285.
[43] S. Aldroubi, N. Brun, I. Bou Malham, A. Mehdi, When graphene meets ionic liquids: a good match for the design of functional materials, Nanoscale 13 (2021) 2750–2779.
[44] P. Snapp, J.M. Kim, C. Cho, J. Leem, M.F. Haque, S. Nam, Interaction of 2d materials with liquids: wettability, electrochemical properties, friction, and emerging directions, NPG Asia Mater. 12 (2020) 1–16.
[45] R. Talaei, B. Khalili, M. Mokhtary, Modulation of opto-electronic properties of the functionalized hexagonal boron nitride nanosheets with tunable aryl alkyl ionic liquids (taails): defect based analysis, J. Mol. Liq. 304 (2020) 112696.
[46] V. Anithaa, R. Shankar, S. Vijayakumar, Structural and electronic properties of graphene and its derivatives physisorbed by ionic liquids, Diam. Relat. Mater. 109 (2020) 108005.
[47] C. Herrera, R. Alcalde, M. Atilhan, S. Aparicio, Theoretical study on amino acid-based ionic pairs and their interaction with carbon nanostructures, J. Phys. Chem. C 118 (2014) 9741–9757.
[48] M. Shyama, S. Lakshmipathi, Adsorption properties of amino acid-based ionic liquids (aails) on edge fluorinated graphene surface–a dft study, Mol. Simul. 47 (2021) 1066–1077.
[49] Y. He, Y. Guo, F. Yan, T. Yu, L. Liu, X. Zhang, T. Zheng, Density functional theory study of adsorption of ionic liquids on graphene oxide surface, Chem. Eng. Sci. 245 (2021) 116946.
[50] A. Ruzanov, M. Lembinen, H. Ers, J.M. Garcia de la Vega, I. Lage-Estebanez, E. Lust, V.B. Ivanistsev, Density functional theory study of ionic liquid adsorption on circumcoronene shaped graphene, J. Phys. Chem. C 122 (2018) 2624–2631.
[51] D. Wagle, G. Kamath, G.A. Baker, Elucidating interactions between ionic liquids and polycyclic aromatic hydrocarbons by quantum chemical calculations, J. Phys. Chem. C 117 (2013) 4521–4532.
[52] T.P.C. Klaver, M. Luppi, M.H.F. Sluiter, M.C. Kroon, B.J. Thijsse, Dft study of 1, 3-dimethylimidazolium tetrafluoroborate on al and cu(111) surfaces, J. Phys. Chem. C 115 (2011) 14718–14730.
[53] H. Valencia, M. Kohyama, S. Tanaka, H. Matsumoto, Ab initio study of emim-bf 4 crystal interaction with a li (100) surface as a model for ionic liquid/li interfaces in li-ion batteries, J. Chem. Phys. 131 (2009) 244705.
[54] C. Wei, K. Jiang, T. Fang, X. Liu, Effects of anions and alkyl chain length of imidazolium-based ionic liquids at the au (111) surface on interfacial structure: a first-principles study, Green Chem. Eng. 2 (2021) 402–411.
[55] K. Zhour, J.M. Otero-Mato, F.E.H. Hassan, H. Fahs, M. Vaezzadeh, E. López-Lago, L.J. Gallego, L.M. Varela, Electronic and optical properties of borophene and graphene with an adsorbed ionic liquid: a density functional theory study, J. Mol. Liq. 316 (2020) 113803.
[56] L. Zhu, A. Fu, The influence of ionic liquids adsorption on the electronic and optical properties of phosphorene and arsenene with different phases: a computational study, Molecules 27 (2022) 2518.
[57] M. Shakourian-Fard, Z. Jamshidi, A. Bayat, G. Kamath, Meta-hybrid density functional theory study of adsorption of imidazolium- and ammonium-based ionic liquids on graphene sheet, J. Phys. Chem. C 119 (2015) 7095–7108.
[58] M. Shakourian-Fard, G. Kamath, The effect of defect types on the electronic and optical properties of graphene nanoflakes physisorbed by ionic liquids, Phys. Chem. Chem. Phys. 19 (2017) 4383–4395.
[59] M. Shakourian-Fard, S.M. Taimoory, V. Semeniuchenko, G. Kamath, J.F. Trant, The effect of ionic liquid adsorption on the electronic and optical properties of fluorographene nanosheets, J. Mol. Liq. 268 (2018) 206–214.
[60] R. Bari, G. Tamas, F. Irin, A.J. Aquino, M.J. Green, E.L. Quitevis, Direct exfoliation of graphene in ionic liquids with aromatic groups, Colloids Surf. A, Physicochem. Eng. Asp. 463 (2014) 63–69.
[61] G. García, M. Atilhan, S. Aparicio, In silico rational design of ionic liquids for the exfoliation and dispersion of boron nitride nanosheets, Phys. Chem. Chem. Phys. 18 (2016) 1212–1224.
[62] M. Shakourian-Fard, G. Kamath, Z. Jamshidi, Trends in physisorption of ionic liquids on boron-nitride sheets, J. Phys. Chem. C 118 (2014) 26003–26016.
[63] G. García, M. Atilhan, S. Aparicio, Adsorption of choline benzoate ionic liquid on graphene, silicene, germanene and boron-nitride nanosheets: a dft perspective, Phys. Chem. Chem. Phys. 17 (2015) 16315–16326.
[64] M. Lalitha, S. Lakshmipathi, Interface energetics of $[Emim]^+[X]^-$ and $[Bmim]^+[X]^-$ (X= BF_4, Cl, PF_6, TfO, Tf_2N) based ionic liquids on graphene, defective graphene, and graphyne surfaces, J. Mol. Liq. 236 (2017) 124–134.
[65] Y. Lu, Y. Hong, Z. Xu, H. Liu, Interfacial interactions and structures of imidazolium-based ionic liquids on black phosphorus surface from first-principles, J. Mol. Liq. 335 (2021) 116562.
[66] Y. Lu, Y. Xu, L. Lu, Z. Xu, H. Liu, Interfacial interactions and structures of protic ionic liquids on a graphite surface: a first-principles study and comparison with aprotic ionic liquids, Phys. Chem. Chem. Phys. 23 (2021) 18338–18348.
[67] M. Shakourian-Fard, H.R. Ghenaatian, G. Kamath, S.M. Taimoory, Unraveling the effect of nitrogen doping on graphene nanoflakes and the adsorption properties of ionic liquids: a dft study, J. Mol. Liq. 312 (2020) 113400.
[68] Y. Tang, W. Huai, H. Li, X. Mao, J. Xie, J.Y. Lee, A. Fu, Adsorption of [bf4]- anion-based ionic liquids on phosphorene, arsenene, and antimonene: a density functional theory study, Int. J. Quant. Chem. 121 (2021) e26668.
[69] K. Zhour, J.M. Otero-Mato, F.E.H. Hassan, H. Fahs, M. Vaezzadeh, E. López-Lago, L.J. Gallego, L.M. Varela, Tuning the hybrid borophene-/graphene-ionic liquid interface: effect of metal cations on the electronic and photonic properties, J. Mol. Liq. 321 (2021) 114759.
[70] B. Mandal, S. Chakrabarti, A.K. Thakur, Dft simulation of nafesno4 structure, electronic and electrochemical properties validated by experimental results, Comput. Mater. Sci. 192 (2021) 110401.
[71] A.H. Mashhadzadeh, M. Ghanbari, A. Koochaki, S. Seyyedbarzegar, M.G. Ahangari, Experiment and theory for acetylene adsorption in transformer oil, J. Mol. Struct. 1230 (2021) 129860.
[72] H.M. Coromina, B. Adeniran, R. Mokaya, D.A. Walsh, Bridging the performance gap between electric double-layer capacitors and batteries with high-energy/high-power carbon nanotube-based electrodes, J. Mater. Chem. A 4 (2016) 14586–14594.
[73] M.-C. Liu, C. Lu, Y. Xu, Y.-X. Hu, J. Li, H. Zhang, Y.-S. Zhang, B.-M. Zhang, L.-B. Kong, W.-W. Liu, et al., Three-dimensional interconnected reticular porous carbon from corn starch by a sample sol–gel method toward high-performance supercapacitors with aqueous and ionic liquid electrolytes, ACS Sustain. Chem. Eng. 7 (2019) 18690–18699.
[74] P. Giannozzi, S. Baroni, N. Bonini, M. Calandra, R. Car, C. Cavazzoni, D. Ceresoli, G.L. Chiarotti, M. Cococcioni, I. Dabo, et al., Quantum espresso: a modular and open-source software project for quantum simulations of materials, J. Phys. Condens. Matter 21 (2009) 395502.

[75] P. Giannozzi, O. Andreussi, T. Brumme, O. Bunau, M.B. Nardelli, M. Calandra, R. Car, C. Cavazzoni, D. Ceresoli, M. Cococcioni, et al., Advanced capabilities for materials modelling with quantum espresso, J. Phys. Condens. Matter 29 (2017) 465901.
[76] P. Giannozzi, O. Baseggio, P. Bonfà, D. Brunato, R. Car, I. Carnimeo, C. Cavazzoni, S. De Gironcoli, P. Delugas, F. Ferrari Ruffino, et al., Quantum espresso toward the exascale, J. Chem. Phys. 152 (2020) 154105.
[77] J.P. Perdew, K. Burke, M. Ernzerhof, Generalized gradient approximation made simple, Phys. Rev. Lett. 77 (1996) 3865.
[78] V. Gomez-Gonzalez, J.M. Otero-Mato, H. Montes-Campos, X. Garcia-Andrade, A. Garcia-Fuente, A. Vega, J. Carrete, O. Cabeza, L.J. Gallego, L.M. Varela, Borophene vs. graphene interfaces: tuning the electric double layer in ionic liquids, J. Mol. Liq. 303 (2020) 112647.
[79] M. Methfessel, A. Paxton, High-precision sampling for Brillouin-zone integration in metals, Phys. Rev. B 40 (1989) 3616.
[80] F. Zhang, B. Sahu, H. Min, A.H. MacDonald, Band structure of a b c-stacked graphene trilayers, Phys. Rev. B 82 (2010) 035409.
[81] A.R. Botello-Mendez, S.M.-M. Dubois, A. Lherbier, J.-C. Charlier, Achievements of dft for the investigation of graphene-related nanostructures, Acc. Chem. Res. 47 (2014) 3292–3300.
[82] J.A. Fürst, J.G. Pedersen, C. Flindt, N.A. Mortensen, M. Brandbyge, T.G. Pedersen, A.-P. Jauho, Electronic properties of graphene antidot lattices, New J. Phys. 11 (2009) 095020.
[83] S. Paavilainen, M. Ropo, J. Nieminen, J. Akola, E. Rasanen, Coexisting honeycomb and Kagome characteristics in the electronic band structure of molecular graphene, Nano Lett. 16 (2016) 3519–3523.
[84] G. Gui, J. Li, J. Zhong, Band structure engineering of graphene by strain: first-principles calculations, Phys. Rev. B 78 (2008) 075435.
[85] R.F.W. Bader, Atoms in molecules, Acc. Chem. Res. 18 (1985) 9–15.
[86] D.R. Lide, CRC Handbook of Chemistry and Physics, 84th edition, CRC Press, 2003.
[87] Z.H. Zhu, G.Q. Lu, Comparative study of li, na, and k adsorptions on graphite by using ab initio method, Langmuir 20 (2004) 10751–10755.
[88] V. Gómez-González, A. Garcìa-Fuente, A. Vega, J. Carrete, O. Cabeza, L. Gallego, L. Varela, Density functional study of charge transfer at the graphene/ionic liquid interface, J. Phys. Chem. C 122 (2018) 15070–15077.
[89] B.A. Boukamp, A linear Kronig-Kramers transform test for immittance data validation, J. Electrochem. Soc. 142 (1995) 1885.
[90] P. Nath, S. Chowdhury, D. Sanyal, D. Jana, Ab-initio calculation of electronic and optical properties of nitrogen and boron doped graphene nanosheet, Carbon 73 (2014) 275–282.
[91] F. Wooten, Optical Properties of Solids, Citeseer, 1972.
[92] S. Chowdhury, A. Majumdar, D. Jana, Electronic and optical properties of the supercell of 8-pmmn borophene modified on doping by h, li, be, and c: a dft approach, Appl. Phys. A 125 (2019) 1–14.

USC UNIVERSIDADE DE SANTIAGO DE COMPOSTELA

B- Supplementary Information

In the following pages we include the Supplementary information for the following articles:

- The interaction of ammonia with the protic ionic liquid ethylammonium nitrate: A simulation study
- Computational study of the structure of ternary ionic liquid/salt/polymer electrolytes based on protic ionic liquids
- Ternary solid polymer electrolytes at the electrochemical interface: a computational study
- Ionic liquid/metal salt mixtures at the graphene interface: A density functional theory approach

USC
UNIVERSIDADE DE SANTIAGO DE COMPOSTELA

The interaction of ammonia with the protic ionic liquid ethylammonium nitrate: a simulation study

Alejandro Rivera-Pousa[a], José M. Otero-Mato[a], Alberto Coronas[b], Anthony J. Stone[c], Ruth M. Lynden-Bell[c], Trinidad Méndez-Morales[a,d,*], Luis M. Varela[a,**]

[a] *Grupo de Nanomateriais, Fotónica e Materia Branda, Departamento de Física de Partículas, Universidade de Santiago de Compostela, Campus Vida s/n E-15782, Santiago de Compostela, Spain*
[b] *Rovira i Virgili University, Mechanical Engineering Dept., Av. Països Catalans, 26, 43007 Tarragona, Spain*
[c] *Department of Chemistry, University of Cambridge, Lensfield Road, Cambridge CB2 1EW, UK*
[d] *Departamento de Física Aplicada, Facultade de Ciencias, Universidade de Vigo, E-36310 Vigo, Spain*

Simulation Details

The ethylammonium molecule was parameterized by using the partial charges previously evaluated by Choe *et al.* [1] using the 6-31G** method, while the LJ parameters were reported by Umebayashi *et al.* [2]. On the other hand, the nitrate anion was modelled as a set of seven sites, three of them being heavy sites and the other four virtual. The heavy sites carry no charge, but each of them is associated with 1/3 of the total mass of the ion and placed in such a way they yield the right tensor of inertia. In contrast, virtual sites are massless but have partial charges of $q_N = +0.794$ for the nitrogen atom and $q_O = -0.598$ for the oxygen atoms [3], whose LJ parameters are, respectively, $\sigma_N = 3.496 \cdot 10^{-1}$ nm, $\varepsilon_N = 7.1128 \cdot 10^{-1}$ kJ/mol, $\sigma_O = 3.175 \cdot 10^{-1}$ nm and $\varepsilon_O = 8.7864 \cdot 10^{-1}$ kJ/mol; and were fitted in order to reproduce the experimental density of the pure IL.

Temperature is maintained constant by applying a V-rescale thermostat [4] with a coupling constant of 0.1 ps and 0.5 ps, for the bulk and confined sim-

*Corresponding author
**Corresponding author

USC UNIVERSIDADE DE SANTIAGO DE COMPOSTELA

ulations, respectively. Pressure control in the bulk systems was performed by using the Parrinello-Rahman barostat [5] with a relaxation time of 1 ps. In these bulk simulations long-range electrostatic interactions were calculated by using the particle-mesh Ewald (PME) [6] method with a cutoff of 1.1 nm, and the same cutoff distance was considered for LJ interactions. In the confined systems, these cutoffs were varied to 1.3 nm and 1 nm, respectively. The linear constraint solver (LINCS) algorithm [7, 8] was used to hold the bonds rigid. We employed periodic boundary conditions along the three directions and Yeh-Berkowitz corrections were included for the slab geometry [9, 10].

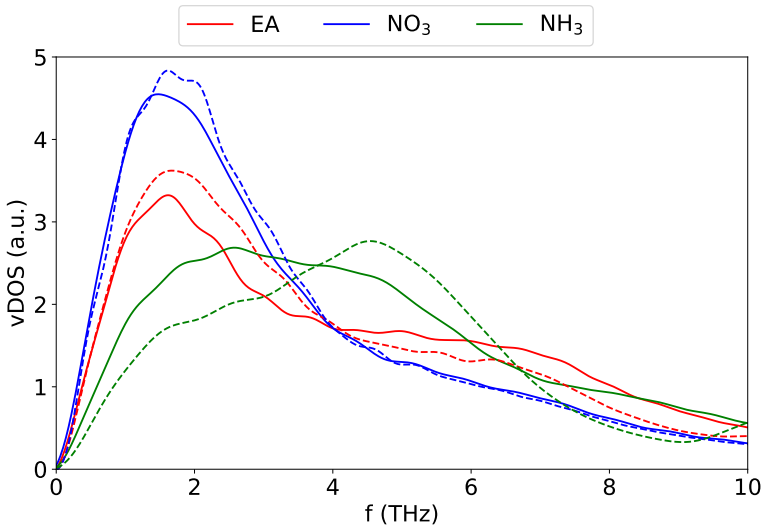


Figure S1: Vibrational density of states for both 4-site (solid lines) and 6-site (dashed lines) models at a 50% ammonia concentration.

USC UNIVERSIDADE DE SANTIAGO DE COMPOSTELA

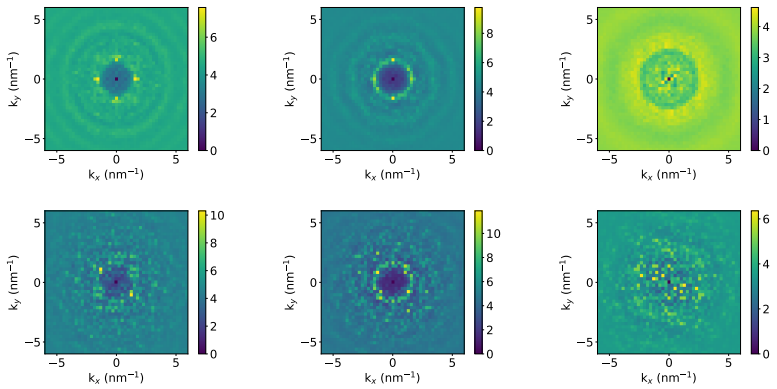


Figure S2: Time-averaged 2D Fourier transforms of the first layer positions in the neutral simulations for a 50% concentration. The upper row corresponds to the 4-site model systems, while the bottom row contains the results for the 6-site systems. The species represented are, from left to right, cation, anion and ammonia.

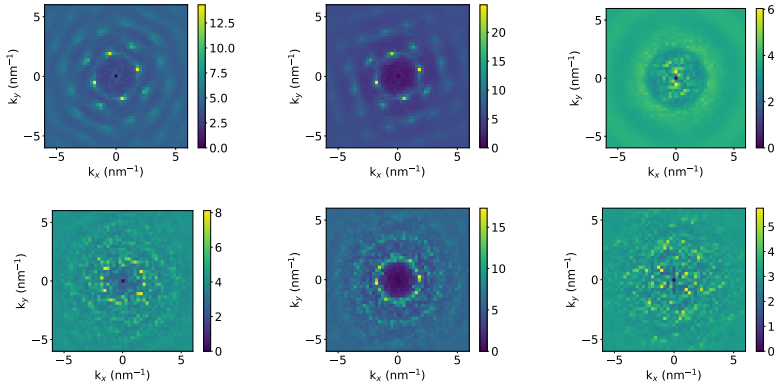


Figure S3: Time-averaged 2D Fourier transforms of the first layer positions near the positively charged wall for a 50% concentration. The upper row corresponds to the 4-site model systems, while the bottom row contains the results for the 6-site systems. The species represented are, from left to right, cation, anion and ammonia.

References

[1] J. Choe, K. Kim, S. Chang, Computer simulations on molecular recognition of alkylamines by ester derivatives of p-tert-butylcalix[6]arene, Bull. Korean Chem. Soc. 21 (2000) 200–206.

[2] Y. Umebayashi, W.-L. Chung, T. Mitsugi, S. Fukuda, M. Takeuchi, K. Fu-

USC UNIVERSIDADE DE SANTIAGO DE COMPOSTELA

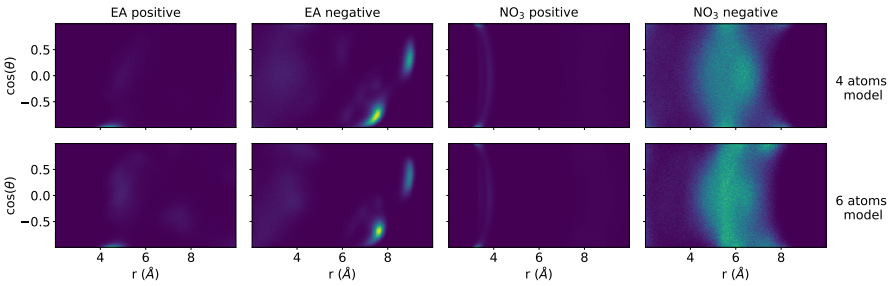


Figure S4: 2D-histogram of the orientations by distance of the molecules from the charged walls. The first two columns corresponds to the cation orientations, near the positively charged wall (first column) and the negatively charged wall (second column). The anion results are plotted in the third (positively charged wall) and fourth (negatively charged wall) columns. The upper row corresponds to the 4-site model systems, while the bottom row contains the results for the 6-site systems.

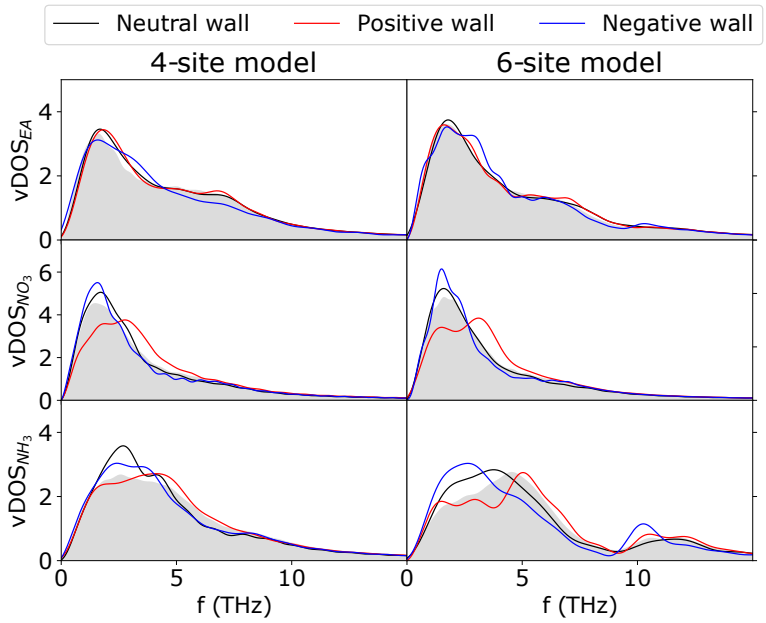


Figure S5: Vibrational densities of states of the three species in both mixtures confined between neutral and charged walls, for a 50% concentration of NH_3. The grey coloured area corresponds to the bulk results.

jii, T. Takamuku, R. Kanzaki, S. Ishiguro, Liquid structure and the ion-ion interactions of ethylammonium nitrate ionic liquid studied by large angle x-ray scattering and molecular dynamics simulations, J. Comput. Chem.

USC UNIVERSIDADE DE SANTIAGO DE COMPOSTELA

Jpn. 7 (2008) 125–134.

[3] S. V. Sambasivarao, O. Acevedo, Development of opls-aa force field parameters for 68 unique ionic liquids, J. Chem. Theory Comput. 5 (2009) 1038–1050.

[4] G. Bussi, D. Donadio, M. Parrinello, Canonical sampling through velocity rescaling, J. Chem. Phys. 126 (2007) 014101(1)–014101(7).

[5] M. Parrinello, A. Rahman, Polymorphic transitions in single crystals: A new molecular dynamics method, J. Appl. Phys. 52 (1981) 7182–7190.

[6] T. Darden, D. York, L. Pedersen, Particle mesh ewald: An n·log(n) method for ewald sums in large systems, J. Chem. Phys. 98 (1993) 10089–10094.

[7] B. Hess, H. Bekker, H. J. C. Berendsen, J. G. E. M. Fraaije, Lincs: A linear constraint solver for molecular simulations, J. Comp. Chem. 18 (1997) 1463–1472.

[8] B. Hess, P-lincs: A parallel linear constraint solver for molecular simulation, J. Chem. Theory Comp. 4 (2007) 116–122.

[9] I. Yeh, M. L. Berkowitz, Ewald summation for systems with slab geometry, J. Chem. Phys. 111 (1999) 3155–3162.

[10] I. Yeh, M. L. Berkowitz, Effects of the polarizability and water density constraint on the structure of water near charged surfaces: Molecular dynamics simulations, J. Chem. Phys. 112 (2000) 10491–10495.

USC UNIVERSIDADE DE SANTIAGO DE COMPOSTELA

Supplementary Information for : "Computational Study of the Structure of Ternary Ionic Liquid/salt/polymer Electrolytes based on Protic Ionic Liquid"

José M. Otero-Mato[a,1], Alejandro Rivera-Pousa[a,1], Hadrián Montes-Campos[a], Oscar Cabeza[b], D. Diddens[c], A. Heuer[c], Luis M. Varela[a,*]

[a] *Grupo de Nanomateriais, Fotónica e Materia Branda, Departamento de Física de Partículas, Universidade de Santiago de Compostela, Campus Vida s/n E-15782, Santiago de Compostela, Spain*
[b] *Facultade de Ciencias, Universidade da Coruña, Campus A Zapateira s/n E-15008, A Coruña, Spain*
[c] *Helmholtz-Institute Münster (HI MS), Ionics in Energy Storage, Forschungszentrum Jülich GmbH, Corrensstraße 46, 48149 Münster, Germany*

*Corresponding author
[1] Contributed equally to this work.

USC UNIVERSIDADE DE SANTIAGO DE COMPOSTELA

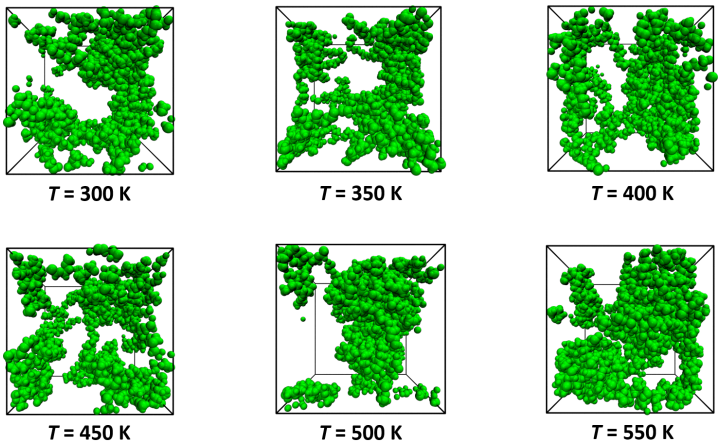


Figure S1: Simulation snapshots from the REMD simulations comprising 20 PEO chains with 20 monomers each and 400 [EA][ACE] ion pairs at various temperatures. PEO is colored green, all ions are invisible for better representation.

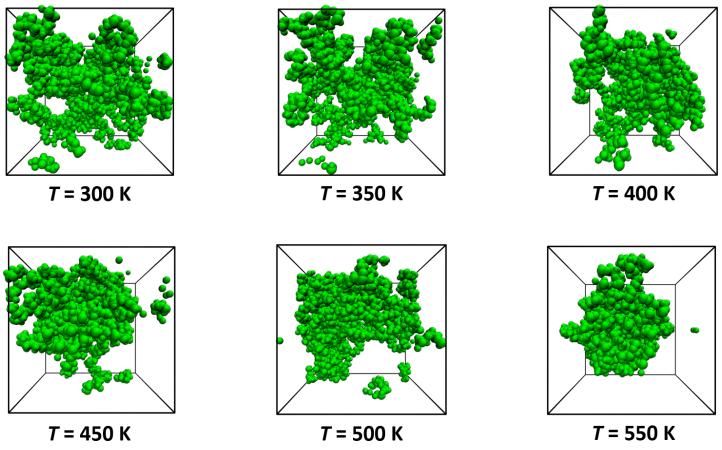


Figure S2: Simulation snapshots from the REMD simulations comprising 20 PEO chains with 20 monomers each and 400 [EA][BF_4] ion pairs at various temperatures. PEO is colored green, all ions are invisible for better representation.

USC UNIVERSIDADE DE SANTIAGO DE COMPOSTELA

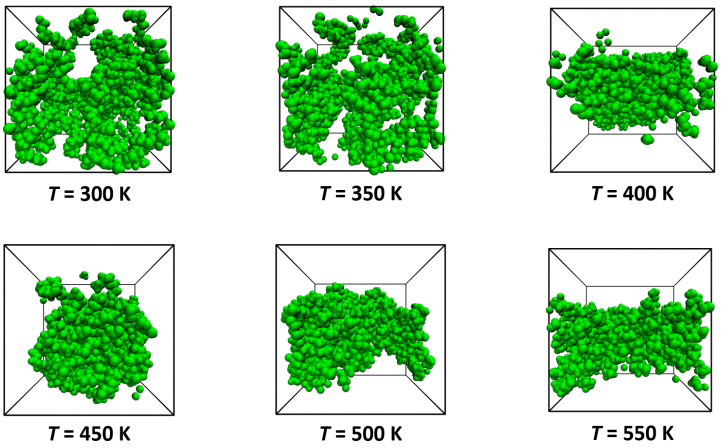


Figure S3: Simulation snapshots from the REMD simulations comprising 20 PEO chains with 20 monomers each and 400 [EA][NO_3] ion pairs at various temperatures. PEO is colored green, all ions are invisible for better representation.

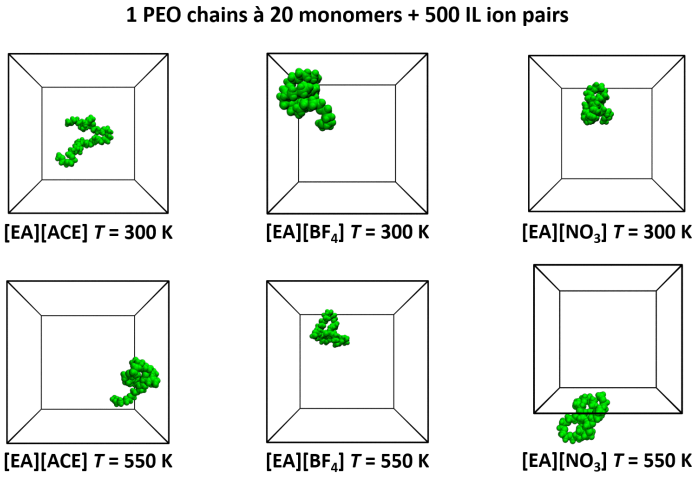


Figure S4: Simulation snapshots from the REMD simulations comprising a single PEO chain with 20 monomers and 500 IL ion pairs for [EA][ACE], [EA][BF_4], and [EA][NO_3] at $T = 300$ K and 550 K. PEO is colored green, all ions are invisible for better representation.

USC UNIVERSIDADE DE SANTIAGO DE COMPOSTELA

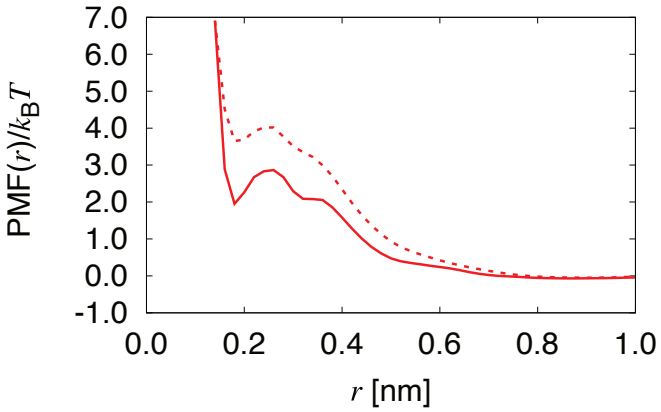


Figure S5: Potential of the mean force between the N-H groups of the EA^+ and the oxygen atoms of a frozen PEO chain immersed in [EA][ACE] at 300 K (solid line) and 500 K (dashed line).

USC
UNIVERSIDADE DE SANTIAGO DE COMPOSTELA

Supporting Information:

Ternary solid polymer electrolytes at the electrochemical interface: a computational study

Alejandro Rivera-Pousa,[†,‡] José Manuel Otero-Mato,[†,‡] Hadrián Montes-Campos,[*,†,‡,¶] Trinidad Méndez-Morales,[†,‡] Diddo Diddens,[§] Andreas Heuer,[‖,§] and Luis Miguel Varela[*,†,‡]

†*Grupo de Nanomateriais, Fotónica e Materia Branda, Departamento de Física de Partículas, Universidade de Santiago de Compostela, Campus Vida s/n, E-15782, Santiago de Compostela, Spain*

‡*Instituto de Materiais (iMATUS), Universidade de Santiago de Compostela, Avenida do Mestre Mateo 25, E-15782, Santiago de Compostela, Spain*

¶*CIQUP, Institute of Molecular Sciences (IMS)—Departamento de Química e Bioquímica, Faculdade de Ciências da Universidade do Porto, Rua Campo Alegre, 4169-007, Porto, Portugal*

§*Helmholtz-Institute Münster (HI MS), Ionics in Energy Storage, Forschungszentrum Jülich GmbH, Corrensstraße 46, 48149 Münster, Germany*

‖*Institute of Physical Chemistry, University of Münster, Corrensstraße 28/30, 48149, Münster, Germany*

E-mail: hadrian.montes@usc.es; luismiguel.varela@usc.es

Results and Discussion

USC UNIVERSIDADE DE SANTIAGO DE COMPOSTELA

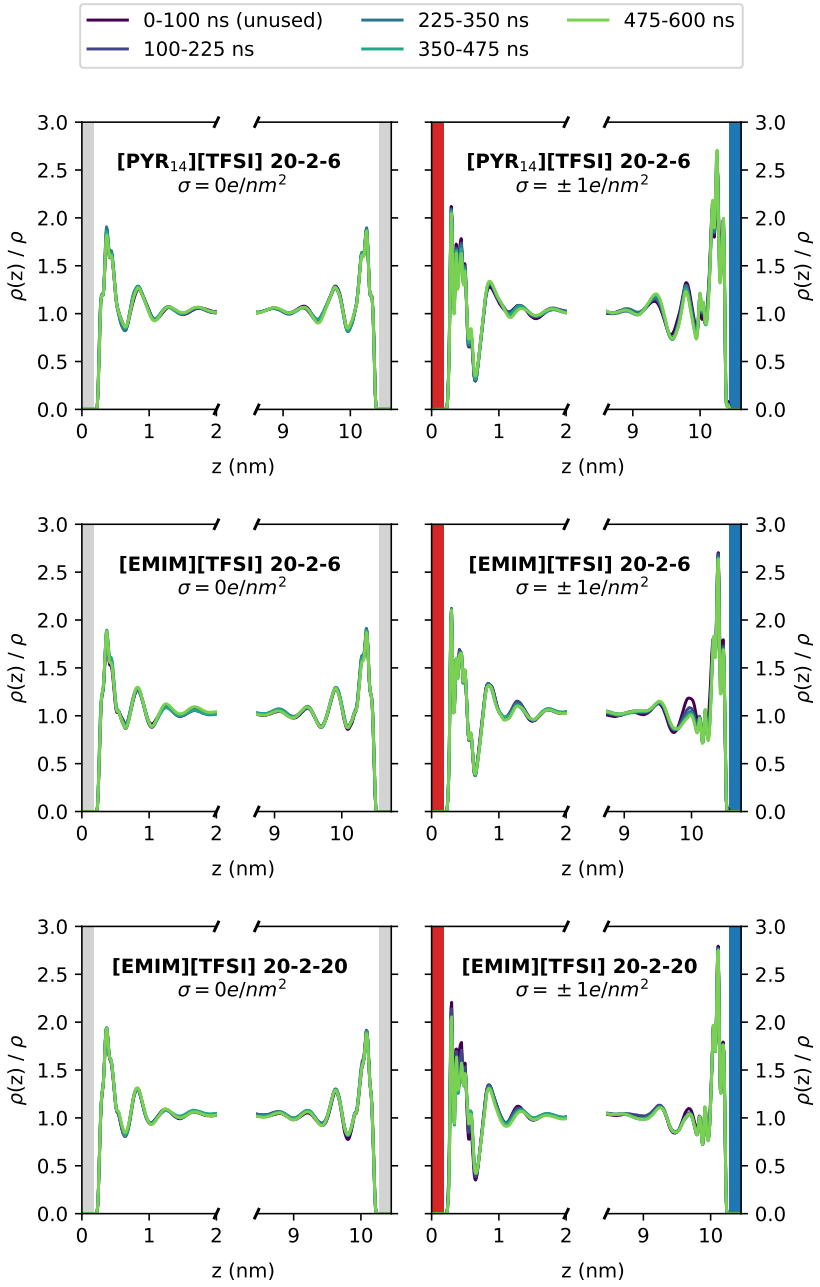


Figure S1: Evolution of the density profiles along the Z axis of the whole simulation system. It can be seen that for the first 100 ns the system is not well stabilized yet, and thus that interval time is discarded from the production run.

USC
UNIVERSIDADE DE SANTIAGO DE COMPOSTELA

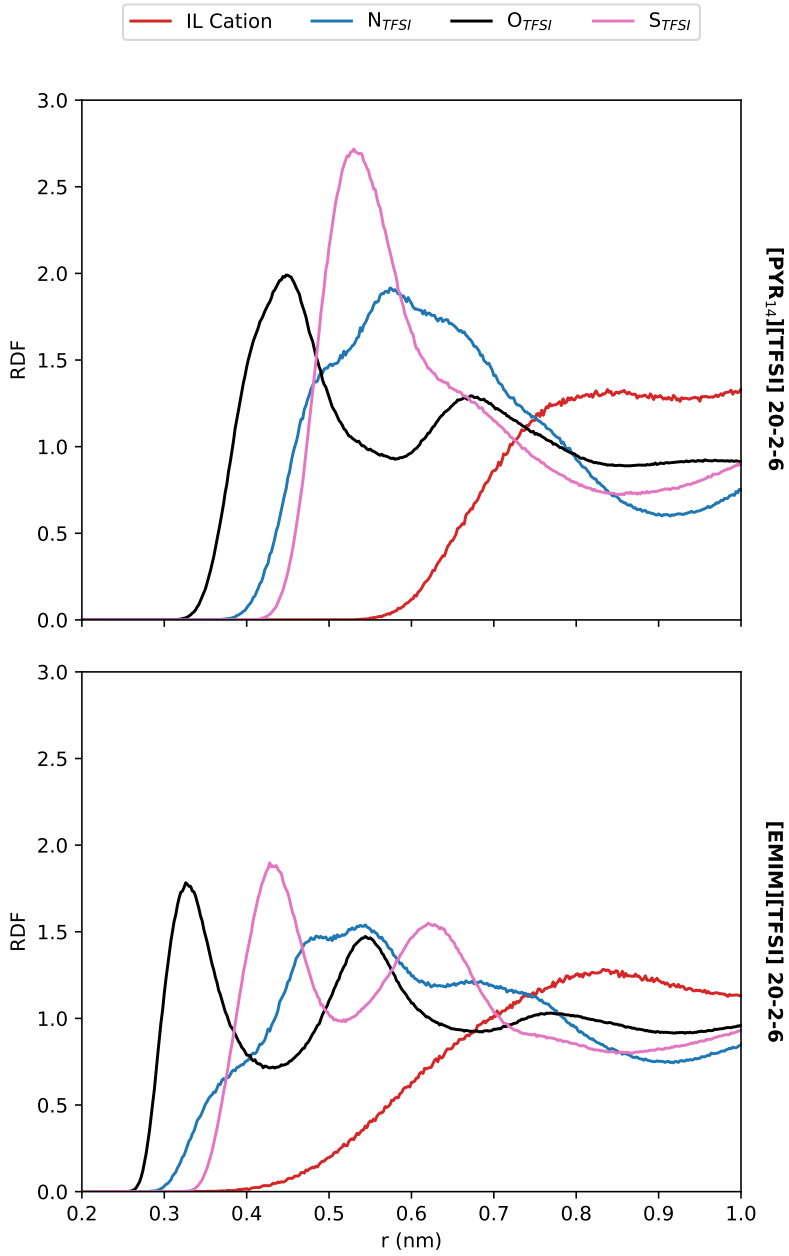


Figure S2: Radial distribution functions between (top) $[Pyr_{14}]^+$ cation and $TFSI^-$ anion and (bottom) $[EMIM]^+$ cation and $TFSI^-$ anion, both in binary mixtures with LiTFSI. The ratio salt/IL is 2-6, which corresponds to the lowest IL concentration in ternary SPEs.

USC
UNIVERSIDADE DE SANTIAGO DE COMPOSTELA

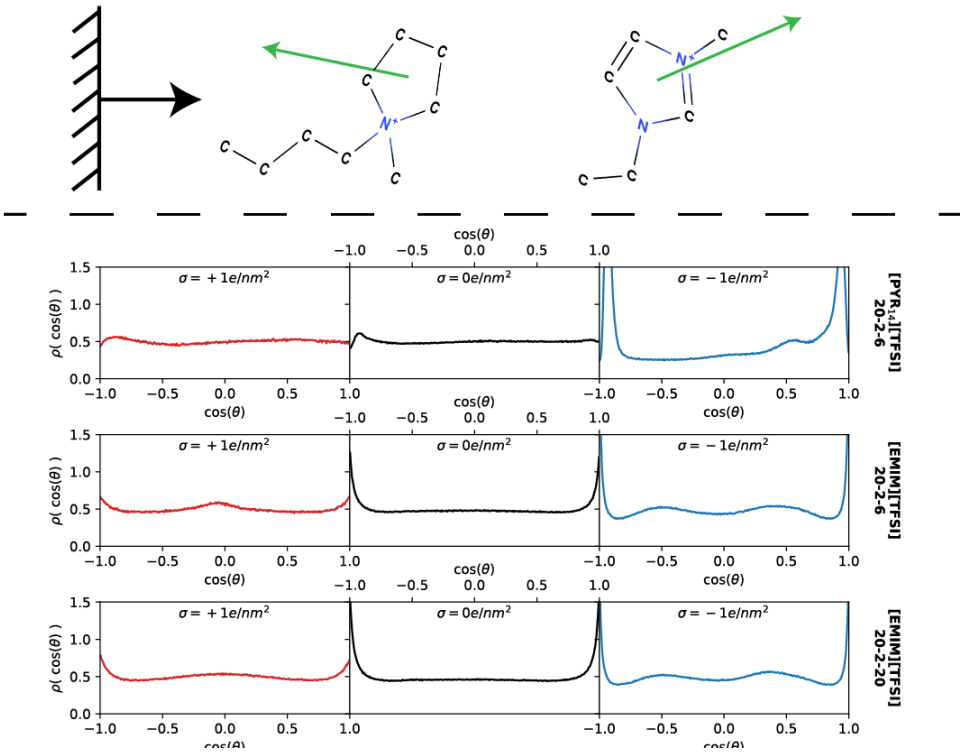


Figure S3: Marginal probability density distribution of IL cation orientation with respect to a vector normal to the graphene-like surface and pointing to the bulk, in the interfacial region (up to 2 nm). The characteristic vectors of the cations are schematized on top of the figure.

USC
UNIVERSIDADE DE SANTIAGO DE COMPOSTELA

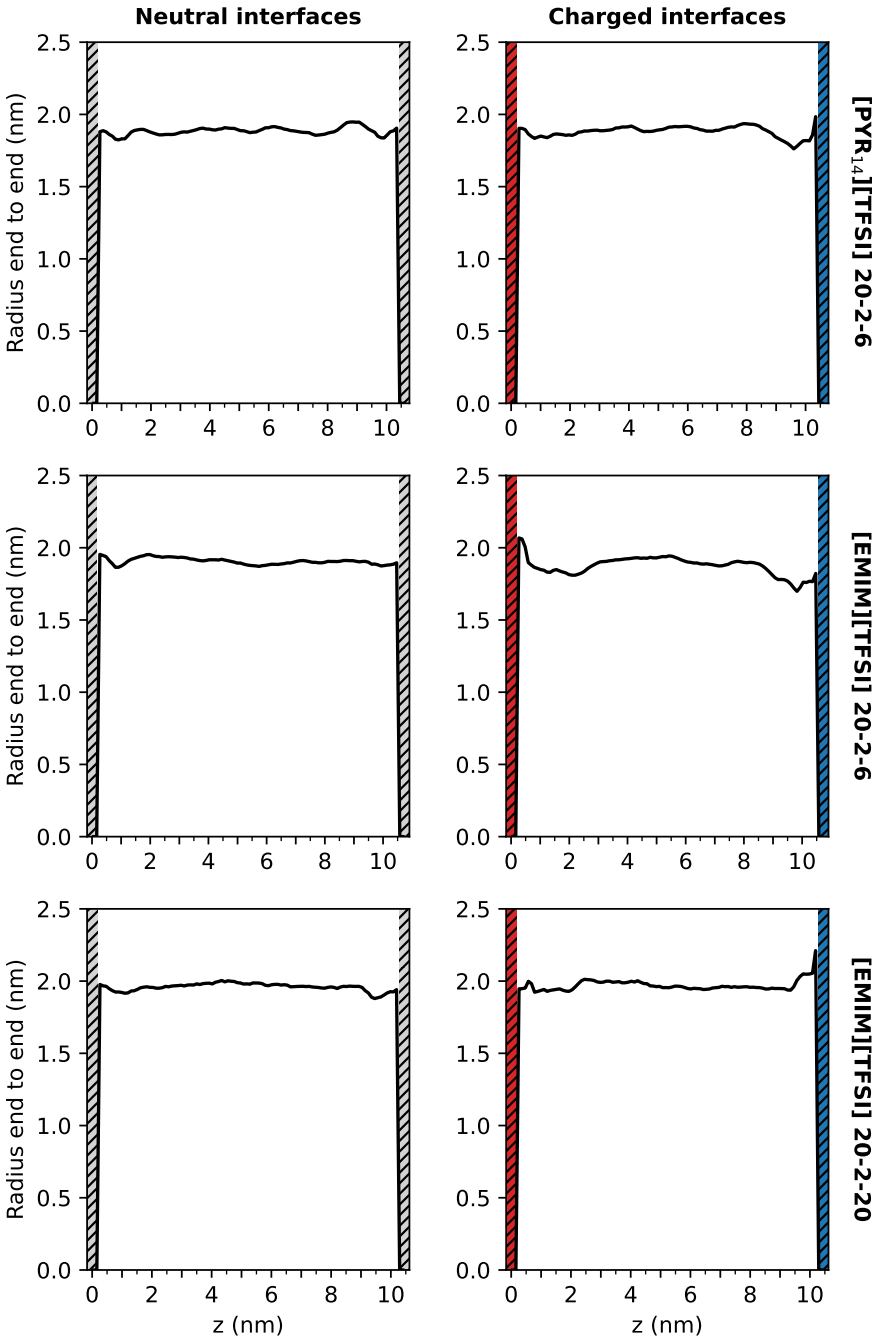


Figure S4: End-to-end distance in the z direction for TSPEs confined between neutral (left) and charged (right) graphene-like surfaces.

USC
UNIVERSIDADE DE SANTIAGO DE COMPOSTELA

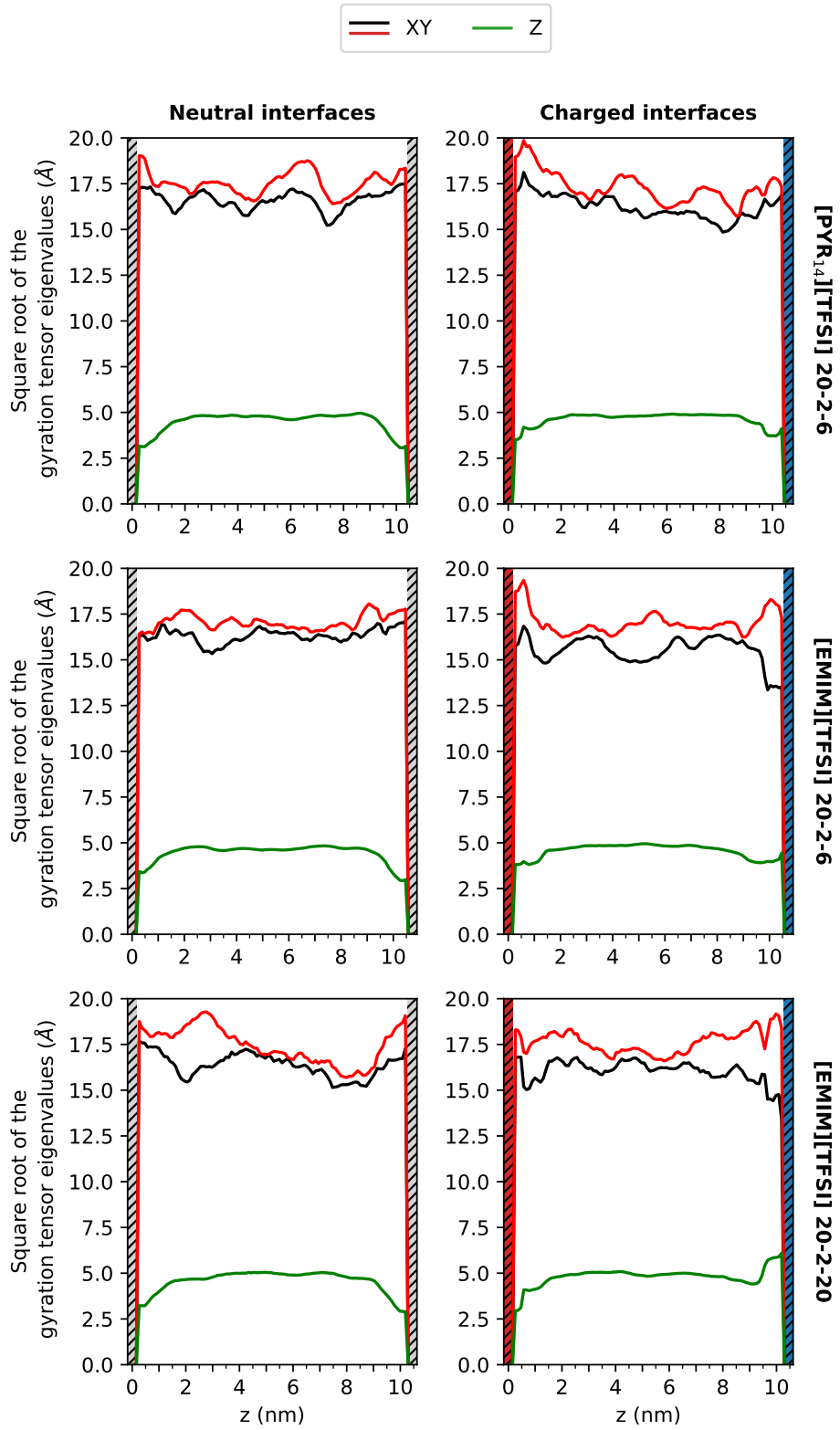


Figure S5: Square root of the eigenvalues of the gyration tensor corresponding to the Z direction (green) and directions contained in the XY plane (red and black) for TSPEs confined between neutral (left) and charged (right) graphene-like surfaces.

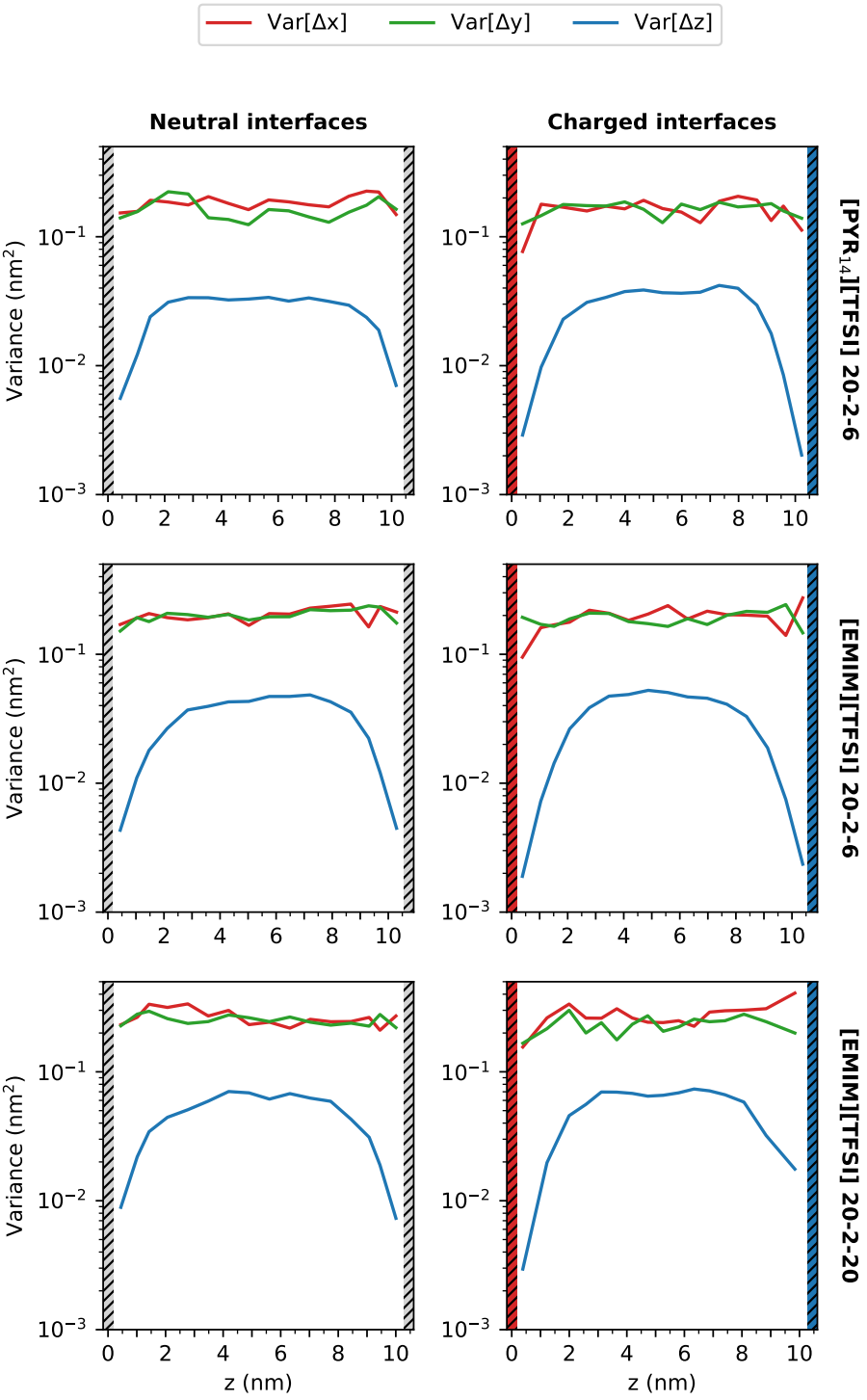


Figure S6: Displacement variance of PEO oxygens in the three directions as a function of the initial position in z for TSPEs confined between neutral (left) and charged (right) graphene-like surfaces.

Supporting Information
Ionic liquid/metal salt mixtures at the graphene interface: a density functional theory approach

Alejandro Rivera-Pousa[a,b], José M. Otero-Mato[a], Carlos Damián Rodríguez-Fernández[a,c], Kazem Zhour[d], Hadrián Montes-Campos[a,b,e,*], Trinidad Méndez-Morales[a,b,**], Luis M. Varela[a,b]

[a] *Grupo de Nanomateriais, Fotónica e Materia Branda, Departamento de Física de Partículas, Universidade de Santiago de Compostela, Campus Vida s/n, E-15782, Santiago de Compostela, Spain*
[b] *Instituto de Materiais (iMATUS), Universidade de Santiago de Compostela, Avenida do Mestre Mateo 25, E-15782, Santiago de Compostela, Spain*
[c] *Departamento de Física e Ciencias da Terra, Universidade da Coruña, Campus de A Zapateira s/n, E-15071, A Coruña, Spain*
[d] *Institute of Physical Chemistry, University of Münster, Corrensstraße 28/30, 48149, Münster, Germany*
[e] *CIQUP, Institute of Molecular Sciences (IMS)—Departamento de Química e Bioquímica, Faculdade de Ciências da Universidade do Porto, Rua Campo Alegre, 4169-007, Porto, Portugal*

Results and Discussion

*hadrian.montes@usc.es
**trinidad.mendez@usc.es

USC UNIVERSIDADE DE SANTIAGO DE COMPOSTELA

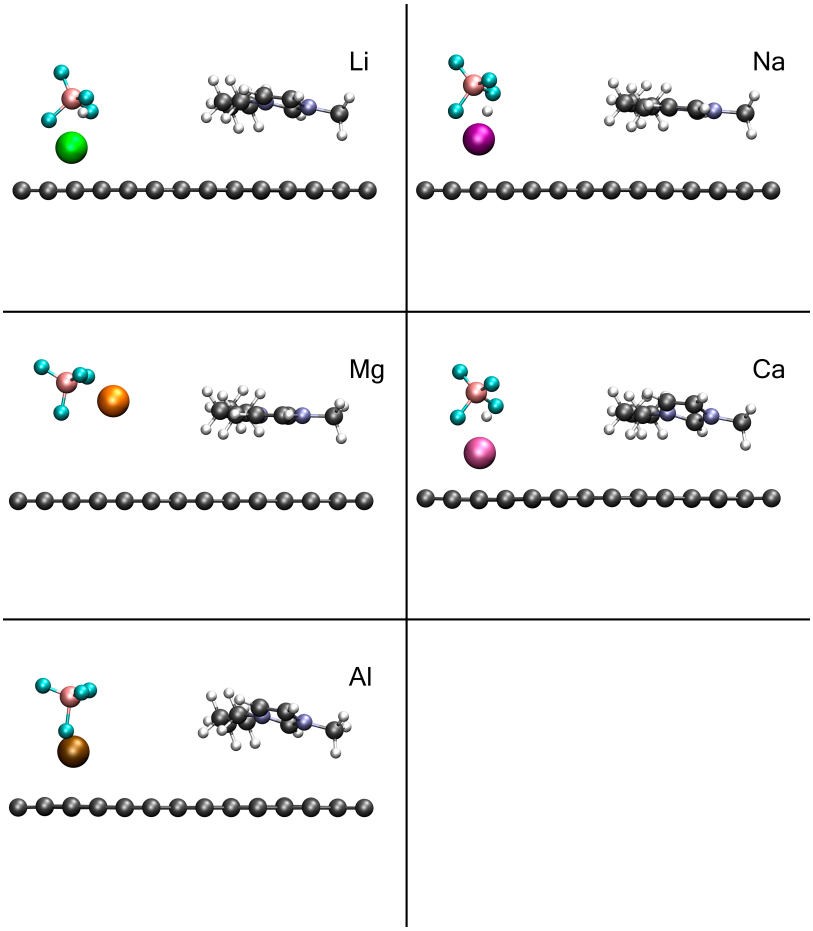


Figure S1: Side views of the relaxed configurations of the different systems. The respective sizes of the metals have been increased for clarity purposes.

USC
UNIVERSIDADE DE SANTIAGO DE COMPOSTELA

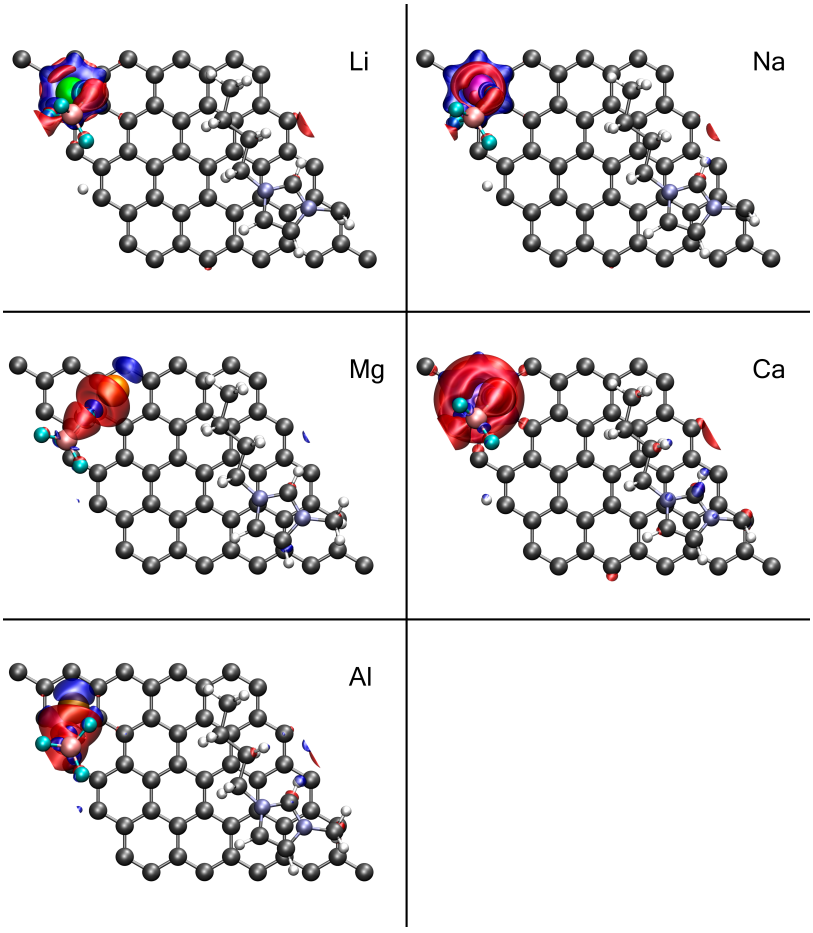


Figure S2: Top views of the electronic density difference between the system with metal and IL, and the system with no metal and the system with only metal. Regions depicted in red/blue correspond to isosurfaces of value ± 0.017 e/Å^3, and therefore represent electron depletion/accumulation compared to the no-metal counterpart, respectively. The respective sizes of the metals have been increased for clarity purposes.

USC UNIVERSIDADE DE SANTIAGO DE COMPOSTELA

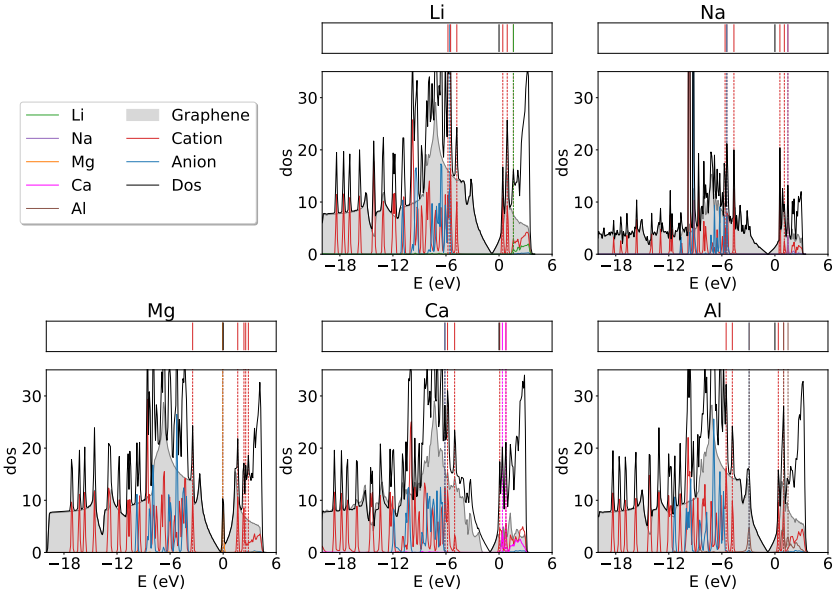


Figure S3: DOS and PDOS of the different systems. On top of each plot: molecular HOMO-3, HOMO-2, HOMO-1, HOMO, LUMO, LUMO+1, LUMO+2 and LUMO+3 states. The color indicates to which species the state belongs. Fermi energy is taken as reference for the energy level.

	G/IL/Li	G/IL/Na	G/IL/Mg	G/IL/Ca	G/IL/Al
HOMO -3 (eV)	-5.77	-5.64	-3.45	-5.82	-5.52
HOMO -2 (eV)	-5.57	-5.44	-0.05	-5.82	-4.82
HOMO -1 (eV)	-5.47	-5.44	-0.05	-5.02	-2.92
HOMO (eV)	-4.77	-4.64	-0.05	-4.62	-2.92
LUMO (eV)	0.43	0.56	1.65	0.08	0.38
LUMO +1 (eV)	0.93	1.06	2.35	0.28	0.98
LUMO +2 (eV)	1.63	1.46	2.55	0.38	0.98
LUMO +3 (eV)	1.63	1.46	2.85	0.78	1.48

Table S1: Energy values (relative to the Fermi level) of the first four HOMO and LUMO molecular states. In red and blue, IL cation and anion states respectively. In teal, the corresponding metal states.

USC UNIVERSIDADE DE SANTIAGO DE COMPOSTELA

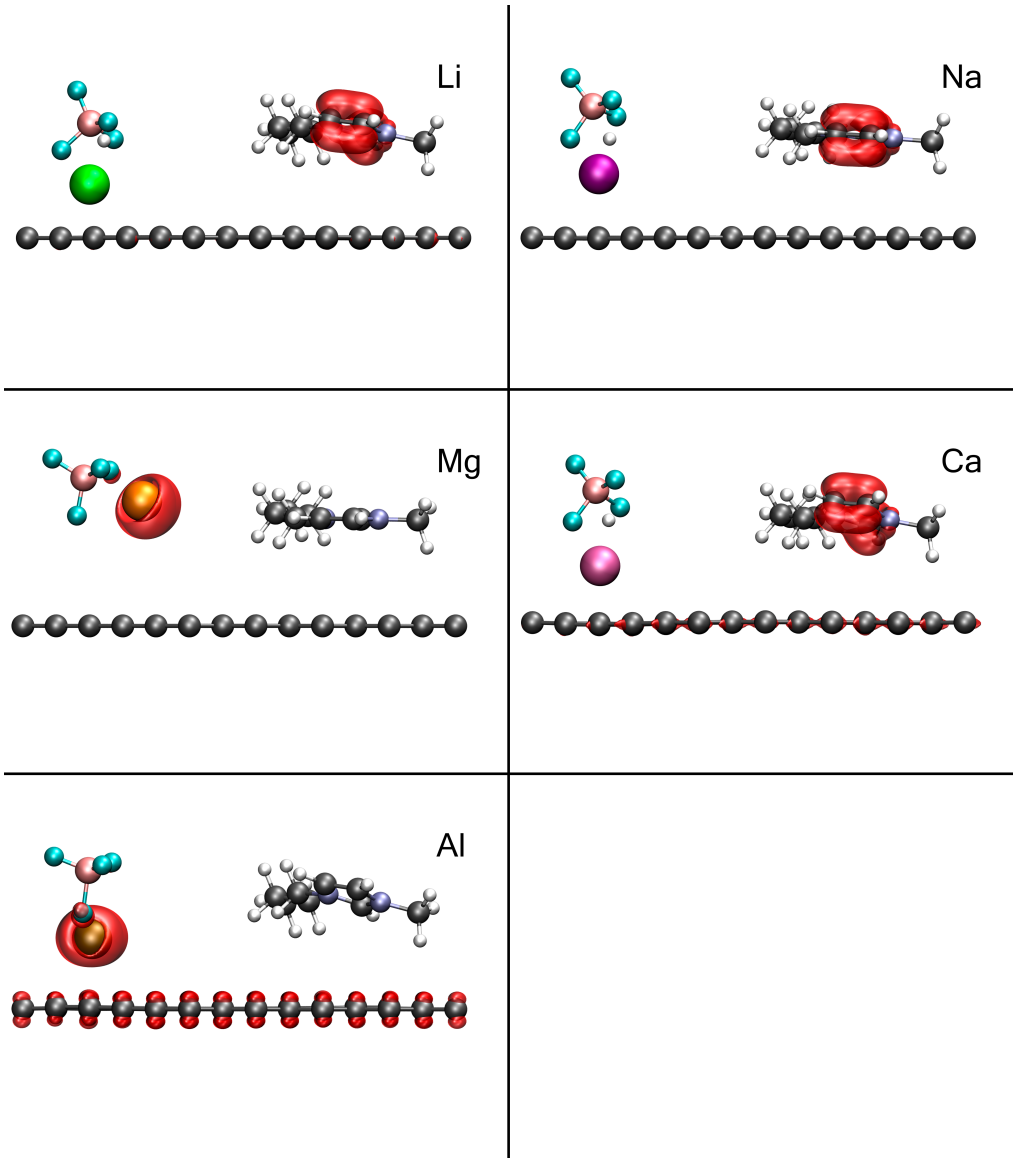


Figure S4: Lateral views of the integrated local density of states around the HOMO state for each of the considered systems.

USC
UNIVERSIDADE DE SANTIAGO DE COMPOSTELA

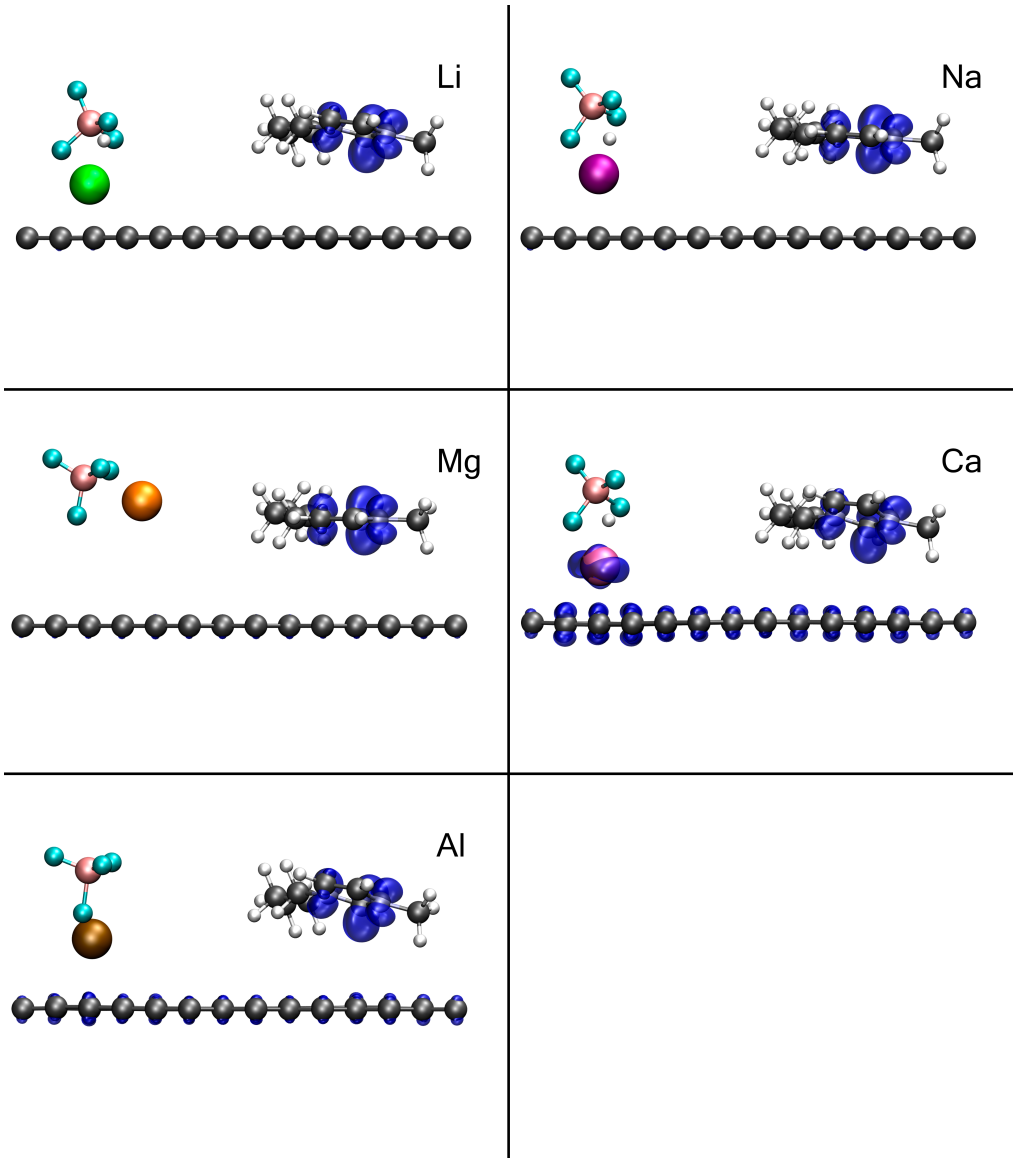
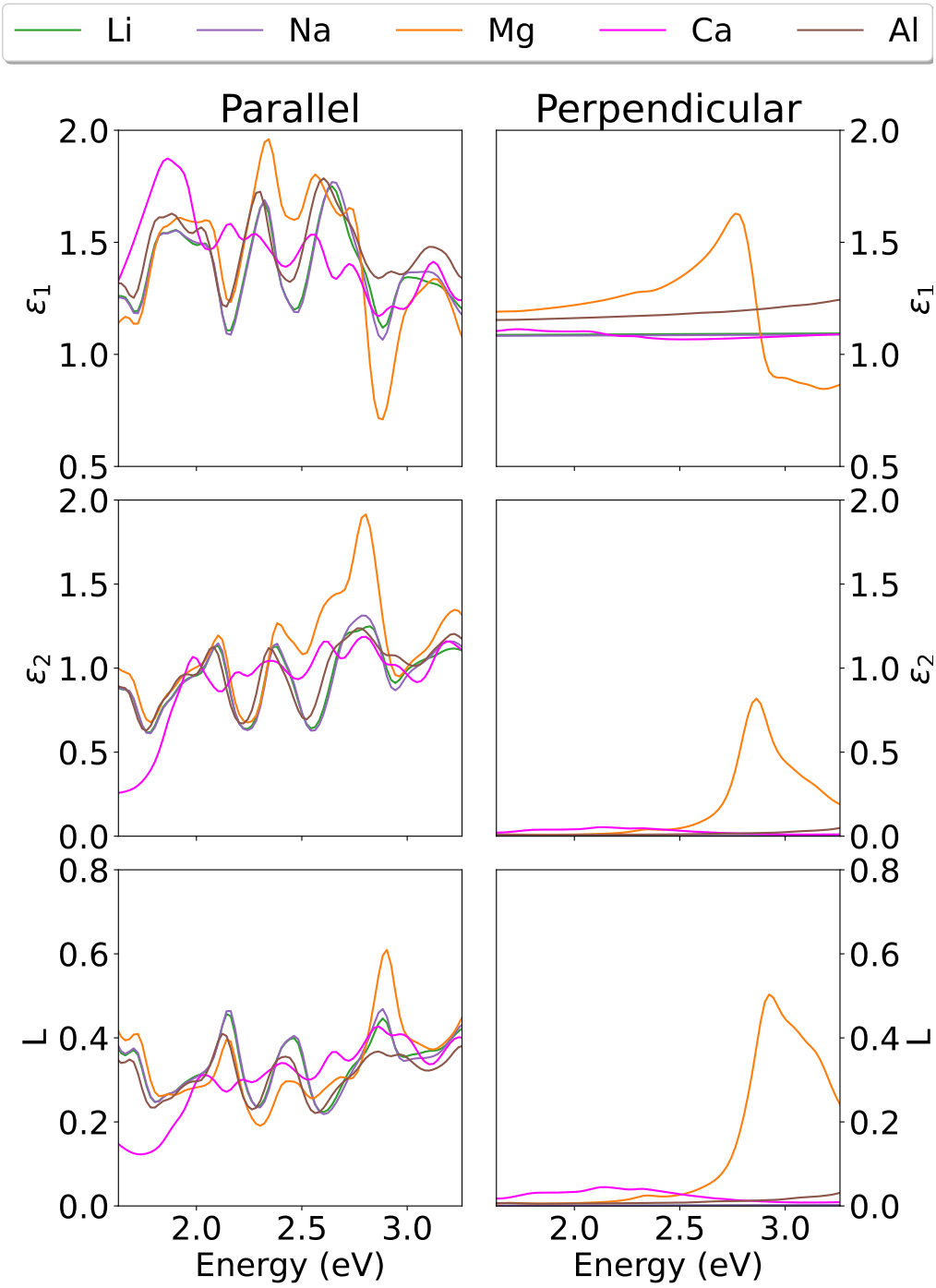


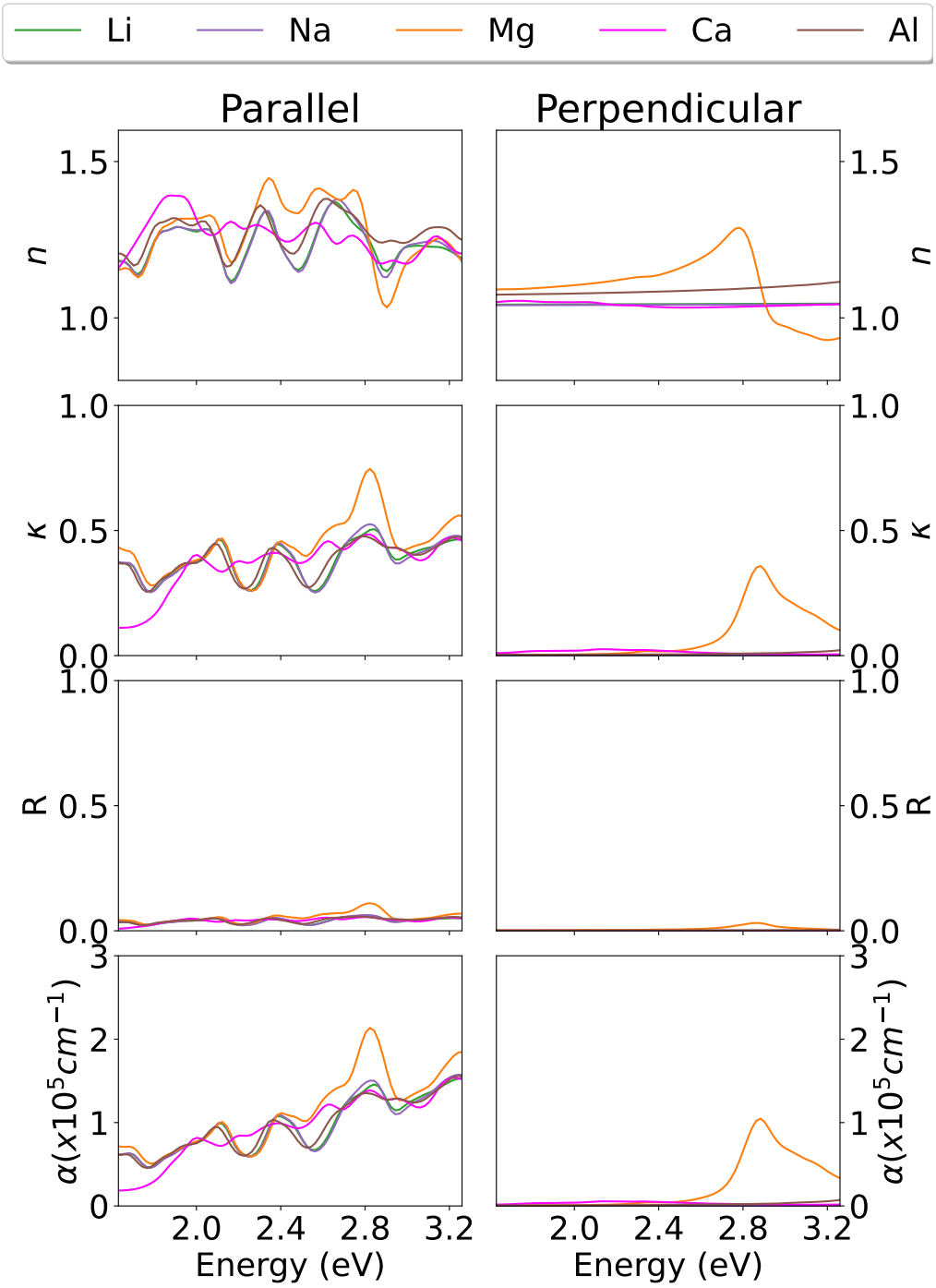
Figure S5: Lateral views of the integrated local density of states around the LUMO state for each of the considered systems.

USC
UNIVERSIDADE DE SANTIAGO DE COMPOSTELA



USC UNIVERSIDADE DE SANTIAGO DE COMPOSTELA

Figure S6: Real (ε_1) and imaginary (ε_2) parts of the dielectric function and EELS (L) for the different systems with parallel (left) and perpendicular (right) electric field.



USC UNIVERSIDADE DE SANTIAGO DE COMPOSTELA

Figure S7: Refractive index (n), extinction coefficient (κ), reflectivity (R) and absorption coefficient (α) for the different systems with parallel (left) and perpendicular (right) electric field.

C- Information of the publications

The relevant information about the different publications contained in this thesis is included in the following pages. Moreover, the authorizations of the journals for the content reproduction of the post-print versions of the articles are also included:

- The interaction of ammonia with the protic ionic liquid ethylammonium nitrate: A simulation study
- Computational study of the structure of ternary ionic liquid/salt/polymer electrolytes based on protic ionic liquids
- Ternary solid polymer electrolytes at the electrochemical interface: a computational study
- Density functional theory of alkali metals at the IL/graphene electrochemical interface
- Ionic liquid/metal salt mixtures at the graphene interface: A density functional theory approach

USC
UNIVERSIDADE DE SANTIAGO DE COMPOSTELA

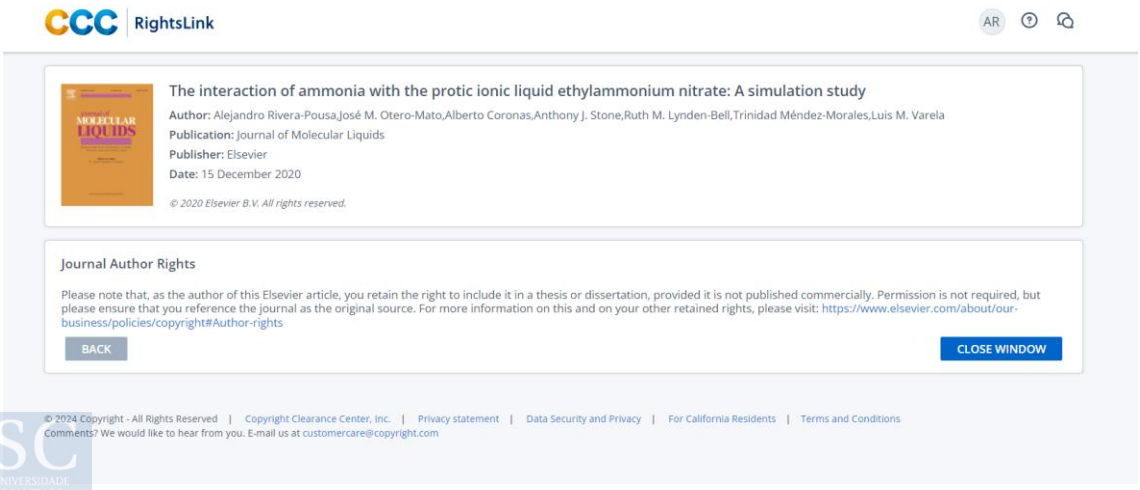
The interaction of ammonia with the protic ionic liquid ethylammonium nitrate: A simulation study

- **Authors:** Alejandro Rivera-Pousa, José M Otero-Mato, Alberto Coronas, Anthony J Stone, Ruth M Lynden-Bell, Trinidad Méndez-Morales, Luis M Varela
- **Journal:** Journal of Molecular Liquids
- **Publisher:** Elsevier
- **ISSN:** 0167-7322
- **Volume:** 320
- **Pages:** 114437
- **Year:** 2020
- **DOI:** https://doi.org/10.1016/j.molliq.2020.114437
- **Journal information (2020):**
    - **Impact factor:** 6.165
    - **Category:** Physics, atomic, molecular & chemical
    - **Ranking inside category:** 4/37

- **Contribution of the author to this thesis to the publication:**

  The author contributed, according to the CRediT contribution classification, with: Conceptualization, Methodology, Software, Validation, Formal analysis, Investigation, Data curation, Writing - original draft, Writing - review & editing, Visualization, Funding acquisition.

The reproduction of the contents of this publication in the present thesis was authorized by the journal, as can be seen in the snapshot below:



USC UNIVERSIDADE DE SANTIAGO DE COMPOSTELA

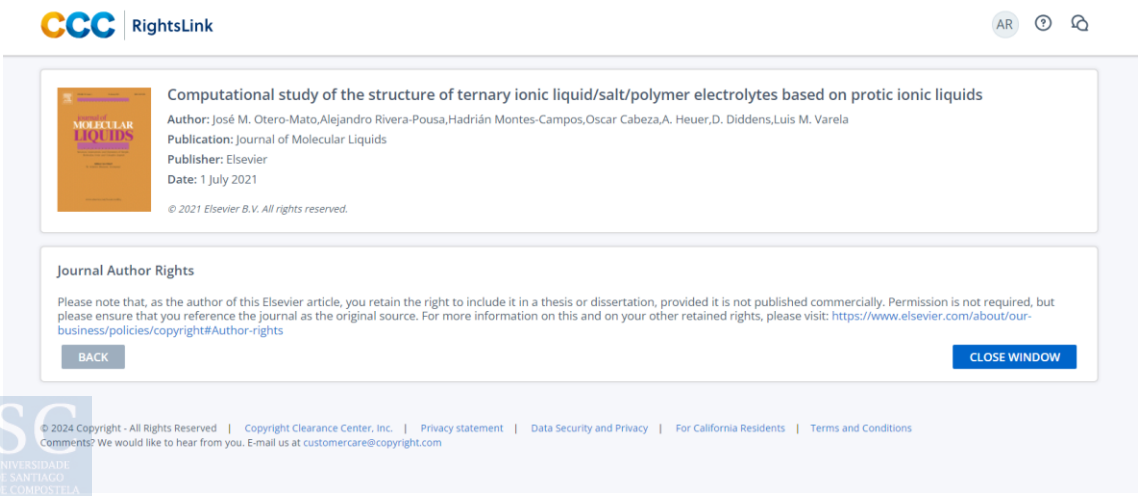
Computational study of the structure of ternary ionic liquid/salt/polymer electrolytes based on protic ionic liquids

- **Authors:** José M Otero-Mato, Alejandro Rivera-Pousa, Hadrián Montes-Campos, Oscar Cabeza, Andreas Heuer, Diddo Diddens, Luis M Varela
- **Journal:** Journal of Molecular Liquids
- **Publisher:** Elsevier
- **ISSN:** 0167-7322
- **Volume:** 333
- **Pages:** 115883
- **Year:** 2021
- **DOI:** https://doi.org/10.1016/j.molliq.2021.115883
- **Journal information (2021):**
    - **Impact factor:** 6.633
    - **Category:** Physics, atomic, molecular & chemical
    - **Ranking inside category:** 6/36

- **Contribution of the author to this thesis to the publication:**

The author contributed, according to the CRediT contribution classification, with: Conceptualization, Methodology, Software, Validation, Formal analysis, Investigation, Data Curation, Writing – Original Draft, Writing – Review & Editing, Visualization.

The reproduction of the contents of this publication in the present thesis was authorized by the journal, as can be seen in the snapshot below:



USC UNIVERSIDADE DE SANTIAGO DE COMPOSTELA

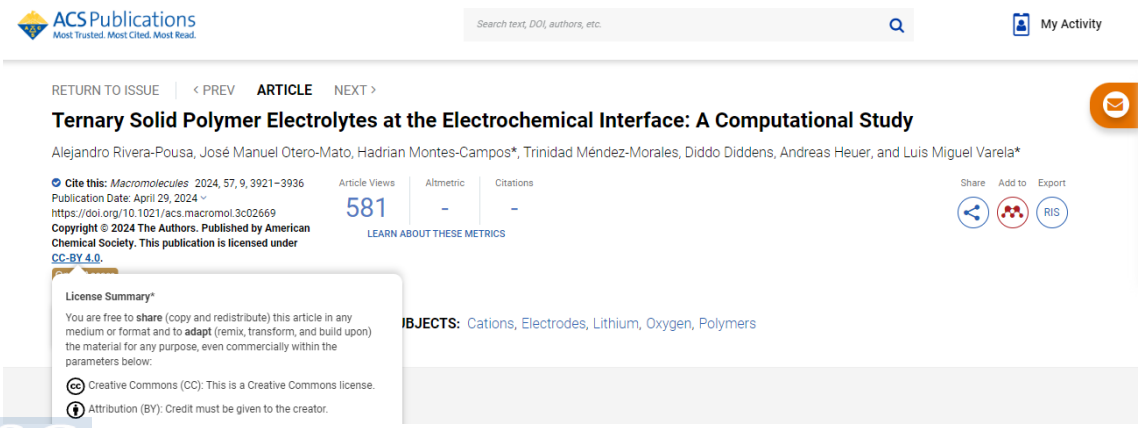
Ternary Solid Polymer Electrolytes at the Electrochemical Interface: A Computational Study

- **Authors:** Alejandro Rivera-Pousa, José M Otero-Mato, Hadrián Montes-Campos, Trinidad Méndez-Morales, Diddo Diddens, Andreas Heuer, Luis M Varela
- **Journal:** Macromolecules
- **Publisher:** ACS Publications
- **ISSN:** 0024-9297
- **Volume(issue):** 57(9)
- **Pages:** 3921-3936
- **Year:** 2024
- **DOI:** https://doi.org/10.1021/acs.macromol.3c02669
- **Journal information (2023):**
    - **Impact factor:** 5.1
    - **Category:** Polymer science
    - **Ranking inside category:** 11/94

- **Contribution of the author to this thesis to the publication:**

The author contributed, according to the CRediT contribution classification, with: Conceptualization, Methodology, Software, Validation, Formal analysis, Investigation, Data Curation, Writing – Original Draft, Writing – Review & Editing, Visualization.

The reproduction of the contents of this publication in the present thesis was authorized by the journal, as the publication is open source under the Creative Commons license CC-BY 4.0, as can be seen in the snapshot below:



Density functional theory of alkali metals at the IL/graphene electrochemical interface

- **Authors:** Hadrián Montes-Campos, Alejandro Rivera-Pousa, Trinidad Méndez-Morales
- **Journal:** The Journal of Chemical Physics
- **Publisher:** AIP Publishing
- **ISSN:** 0021-9606
- **Volume(issue):** 156(1)
- **Pages:** 014706
- **Year:** 2022
- **DOI:** https://doi.org/10.1063/5.0077449
- **Journal information (2022):**
    - **Impact factor:** 4.4
    - **Category:** Physics, atomic, molecular & chemical
    - **Ranking inside category:** 8/35
- **Contribution of the author to this thesis to the publication:**

The author contributed, according to the CRediT contribution classification, with: Conceptualization, Methodology, Software, Validation, Formal analysis, Investigation, Data Curation, Writing – Original Draft, Writing – Review & Editing, Visualization.

This article was reproduced from: Montes-Campos, H., Rivera-Pousa, A., & Méndez-Morales, T. (2022). Density functional theory of alkali metals at the IL/graphene electrochemical interface. *The Journal of Chemical Physics*, *156*(1), with the permission of AIP Publishing.

The reproduction of the contents of publications in AIP Publishing can be reused for a thesis or dissertation by the authors of the publication without asking for explicit permission, as can be checked in the following link (consulted on 17/07/2024):

https://publishing.aip.org/resources/researchers/rights-and-permissions/permissions/

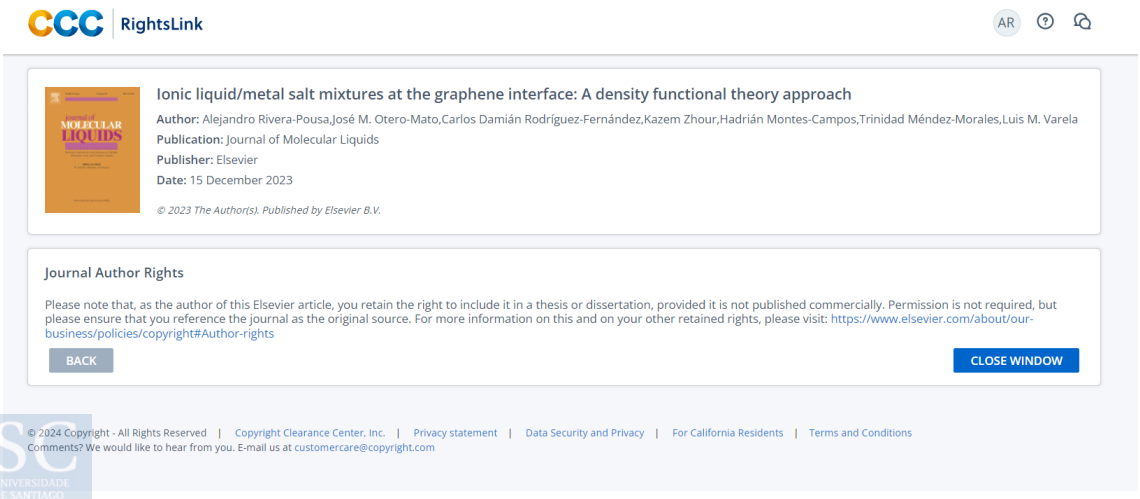
USC UNIVERSIDADE DE SANTIAGO DE COMPOSTELA

Ionic liquid/metal salt mixtures at the graphene interface: A density functional theory approach

- **Authors:** Alejandro Rivera-Pousa, José M Otero-Mato, Carlos Damián Rodríguez-Fernández, Kazem Zhour, Hadrián Montes-Campos, Trinidad Méndez-Morales, Luis M Varela
- **Journal:** Journal of Molecular Liquids
- **Publisher:** Elsevier
- **ISSN:** 0167-7322
- **Volume:** 392
- **Pages:** 123460
- **Year:** 2023
- **DOI:** https://doi.org/10.1016/j.molliq.2023.123460
- **Journal information (2023):**
    - **Impact factor:** 5.3
    - **Category:** Physics, atomic, molecular & chemical
    - **Ranking inside category:** 6/40
- **Contribution of the author to this thesis to the publication:**

The author contributed, according to the CRediT contribution classification, with: Formal analysis, Investigation, Methodology, Software, Validation, Visualization, Writing – original draft, Writing – review & editing.

The reproduction of the contents of this publication in the present thesis was authorized by the journal, as can be seen in the snapshot below:



USC UNIVERSIDADE DE SANTIAGO DE COMPOSTELA

Bibliography

[1] Total population according to The World Bank DataBank. https://data.worldbank.org/indicator/SP.POP.TOTL. Accessed: 2024-05-29.

[2] Population percentage with access to electricity according to The World Bank DataBank. https://data.worldbank.org/indicator/EG.ELC.ACCS.ZS. Accessed: 2024-05-29.

[3] Population percentage with access to mobile phones according to The World Bank DataBank. https://data.worldbank.org/indicator/IT.CEL.SETS.P2. Accessed: 2024-05-29.

[4] Electric power consumption per capita according to The World Bank DataBank. https://data.worldbank.org/indicator/EG.USE.ELEC.KH.PC. Accessed: 2024-05-29.

[5] Zealan Hoover, Florian Nägele, Evan Polymeneas, and Shivika Sahdev. How charging in buildings can power up the electric-vehicle industry. *McKinsey*, 9:1–8, 2021.

[6] Jia Ying Yong, Vigna K. Ramachandaramurthy, Kang Miao Tan, and Nadarajah Mithulananthan. A review on the state-of-the-art technologies of electric vehicle, its impacts and prospects. *Renew. Sustain. Energy Rev.*, 49:365–385, 2015.

[7] Beatriz Junquera, Blanca Moreno, and Roberto Álvarez. Analyzing consumer attitudes towards electric vehicle purchasing intentions in Spain: Technological limitations and vehicle confidence. *Technol Forecast Soc.*, 109:6–14, 2016.

[8] Rajive Ganguli and Douglas R. Cook. Rare earths: A review of the landscape. *MRS Energy & Sustainability*, 5:E9, 2018.

[9] Georgios Charalampides, Konstantinos I. Vatalis, Baklavaridis Apostoplos, and Benetis Ploutarch-Nikolas. Rare earth elements: industrial applications and economic dependency of Europe. *Proc. Econ. Financ.*, 24:126–135, 2015.

[10] Maciej Galiński, Andrzej Lewandowski, and Izabela Stępniak. Ionic liquids as electrolytes. *Electrochim Acta*, 51(26):5567–5580, 2006.

[11] Andrzej Lewandowski and Agnieszka Świderska-Mocek. Ionic liquids as electrolytes for Li-ion batteries—An overview of electrochemical studies. *J. Power Sources*, 194(2):601–609, 2009.

[12] Erlendur Jónsson. Ionic liquids as electrolytes for energy storage applications–A modelling perspective. *Energy Storage Mater.*, 25:827–835, 2020.

[13] J. N. Barisci, Gordon G. Wallace, Douglas Robert Macfarlane, and R. H. Baughman. Investigation of ionic liquids as electrolytes for carbon nanotube electrodes. *Electrochem Commun.*, 6(1):22–27, 2004.

[14] Maria Taige, Diana Hilbert, and Thomas J. S. Schubert. Mixtures of ionic liquids as possible electrolytes for lithium ion batteries. *Zeitschrift für physikalische Chemie*, 226(2):129–139, 2012.

[15] Martyn J. Earle and Kenneth R. Seddon. Ionic liquids. Green solvents for the future. *Pure Appl. Chem.*, 72(7):1391–1398, 2000.

[16] Jean Le Bideau, Lydie Viau, and André Vioux. Ionogels, ionic liquid based hybrid materials. *Chem. Soc. Rev.*, 40(2):907–925, 2011.

[17] Ji Wei Suen, Naveen Kumar Elumalai, Sujan Debnath, Nabisab Mujawar Mubarak, Chye Ing Lim, and Mohan M. Reddy. The role of interfaces in ionic liquid-based hybrid materials (ionogels) for sensing and energy applications. *Adv. Mater. Interfaces*, 9(34):2201405, 2022.

[18] Xiaowei Li, Sijian Li, Zhengxi Zhang, Jun Huang, Li Yang, and Shin-ichi Hirano. High-performance polymeric ionic liquid–silica hybrid ionogel electrolytes for lithium metal batteries. *J. Mater. Chem. A*, 4(36):13822–13829, 2016.

[19] Martin Z. Bazant, Brian D. Storey, and Alexei A. Kornyshev. Double layer in ionic liquids: Overscreening versus crowding. *Phys. Rev. Lett.*, 106(4):046102, 2011.

[20] Alessandro Triolo, Olga Russina, Hans-Jurgen Bleif, and Emanuela Di Cola. Nanoscale segregation in room temperature ionic liquids. *J. Phys. Chem. B*, 111(18):4641–4644, 2007.

[21] Olga Russina, Alessandro Triolo, Lorenzo Gontrani, and Ruggero Caminiti. Mesoscopic structural heterogeneities in room-temperature ionic liquids. *J. Phys. Chem. Lett.*, 3(1):27–33, 2012.

[22] Jorge F. B. Pereira, Álvaro S. Lima, Mara G. Freire, and João A. P. Coutinho. Ionic liquids as adjuvants for the tailored extraction of biomolecules in aqueous biphasic systems. *Green Chem.*, 12(9):1661–1669, 2010.

[23] Mara G. Freire, Catarina M. S. S. Neves, Pedro J. Carvalho, Ramesh L. Gardas, Ana M. Fernandes, Isabel M. Marrucho, Luís M. N. B. F. Santos, and Joao A. P. Coutinho. Mutual solubilities of water and hydrophobic ionic liquids. *J. Phys. Chem. B*, 111(45):13082–13089, 2007.

[24] Lucy R. Griffin, Kathryn L. Browning, Stuart M. Clarke, Alexander M. Smith, Susan Perkin, M. W. A. Skoda, and Sarah E. Norman. Direct measurements of ionic liquid layering at a single mica–liquid interface and in nano-films between two mica–liquid interfaces. *Phys. Chem. Chem. Phys.*, 19(1):297–304, 2017.

[25] J. Vila, P. Ginés, J. M. Pico, C. Franjo, E. Jiménez, L. M. Varela, and O. Cabeza. Temperature dependence of the electrical conductivity in EMIM-based ionic liquids: evidence of Vogel–Tamman–Fulcher behavior. *Fluid Phase Equilibr*, 242(2):141–146, 2006.

[26] Andrea Mele, Chieu D. Tran, and Silvia H. De Paoli Lacerda. The Structure of a Room-Temperature Ionic Liquid with and without Trace Amounts of Water: The Role of C-H··· O and C- H··· F Interactions in 1-n-Butyl-3-Methylimidazolium Tetrafluoroborate. *Angew. Chem. Int. Ed.*, 42(36):4364–4366, 2003.

[27] Agilio A. H. Padua, Margarida F. Costa Gomes, and Jose N. A. Canongia Lopes. Molecular solutes in ionic liquids: a structural perspective. *Accounts Chem. Res.*, 40(11):1087–1096, 2007.

USC UNIVERSIDADE DE SANTIAGO DE COMPOSTELA

[28] José N. A. Canongia Lopes and Agílio A. H. Pádua. Nanostructural organization in ionic liquids. *J. Phys. Chem. B*, 110(7):3330–3335, 2006.

[29] Diddo Diddens, Elie Paillard, and Andreas Heuer. Improving the lithium ion transport in polymer electrolytes by functionalized ionic-liquid additives: simulations and modeling. *J. Electrochem Soc.*, 164(11):E3225, 2017.

[30] Trinidad Mendez-Morales, Jesus Carrete, Oscar Cabeza, Luis J. Gallego, and Luis M. Varela. Molecular dynamics simulation of the structure and dynamics of water–1-alkyl-3-methylimidazolium ionic liquid mixtures. *J. Phys. Chem. B*, 115(21):6995–7008, 2011.

[31] Mathieu Salanne. Simulations of room temperature ionic liquids: from polarizable to coarse-grained force fields. *Phys. Chem. Chem. Phys.*, 17(22):14270–14279, 2015.

[32] Barbara Kirchner, Oldamur Hollóczki, Jose Nuno Canongia Lopes, and Agílio A. H. Pádua. Multiresolution calculation of ionic liquids. *Wiley Interdiscip. Rev. Comput. Mol. Sci.*, 5(2):202–214, 2015.

[33] Dmitry Bedrov, Jean-Philip Piquemal, Oleg Borodin, Alexander D. MacKerell Jr, Benoît Roux, and Christian Schröder. Molecular dynamics simulations of ionic liquids and electrolytes using polarizable force fields. *Chem. Rev.*, 119(13):7940–7995, 2019.

[34] Kathleen Kirchner, Tom Kirchner, V. Ivaništšev, and Maxim V. Fedorov. Electrical double layer in ionic liquids: Structural transitions from multilayer to monolayer structure at the interface. *Electrochim Acta*, 110:762–771, 2013.

[35] P. I. Walden. Ueber die Molekulargrosse und elektrische Leitfahigkeit einiger geschmolzenen Salze. *Известия Российской академии наук. Серия математическая*, 8(6):405–422, 1914.

[36] Tom Welton. Ionic liquids: a brief history. *Biophysical reviews*, 10(3):691–706, 2018.

[37] F. H. Hurley. patent nr 4446331, 1948.

[38] John S. Wilkes. Ionic liquids in perspective: the past with an eye toward the industrial future. ACS Publications, 2002.

[39] D. Fennell Evans, Shaw-Horng Chen, George W. Schriver, and Edward M. Arnett. Thermodynamics of solution of nonpolar gases in a fused salt. Hydrophobic bonding behavior in a nonaqueous system. *J. Am. Chem. Soc.*, 103(2):481–482, 1981.

[40] Frank Pacholec, Hal T. Butler, and Colin F. Poole. Molten organic salt phase for gas-liquid chromatography. *Anal. Chem.*, 54(12):1938–1941, 1982.

[41] John S. Wilkes, Joseph A. Levisky, Robert A. Wilson, and Charles L. Hussey. Dialkylimidazolium chloroaluminate melts: a new class of room-temperature ionic liquids for electrochemistry, spectroscopy and synthesis. *Inorg. Chem.*, 21(3):1263–1264, 1982.

[42] Zhigang Lei, Biaohua Chen, Yoon-Mo Koo, and Douglas R. MacFarlane. Introduction: ionic liquids, 2017. PMID: 28535681.

[43] John D. Holbrey and K. R. Seddon. Ionic liquids. *Clean products and processes*, 1(4):223–236, 1999.

[44] Tamar L. Greaves and Calum J. Drummond. Protic ionic liquids: properties and applications. *Chem. Rev.*, 108(1):206–237, 2008.

[45] Heather E. Bailey, Yong-Lei Wang, and Michael D. Fayer. Impact of hydrogen bonding on the dynamics and structure of protic ionic liquid/water binary mixtures. *J. Phys. Chem. B*, 121(36):8564–8576, 2017.

[46] Erik Piatti, Luca Guglielmero, Giorgio Tofani, Andrea Mezzetta, Lorenzo Guazzelli, Felicia D'Andrea, Stefano Roddaro, and Christian Silvio Pomelli. Ionic liquids for electrochemical applications: Correlation between molecular structure and electrochemical stability window. *J. Mol. Liq.*, 364:120001, 2022.

[47] J. Vila, P. Gines, E. Rilo, O. Cabeza, and L. M. Varela. Great increase of the electrical conductivity of ionic liquids in aqueous solutions. *Fluid Phase Equilibr*, 247(1-2):32–39, 2006.

[48] Marisa A. A. Rocha, João A. P. Coutinho, and Luís M. N. B. F. Santos. Vapor pressures of 1, 3-dialkylimidazolium bis (trifluoromethylsulfonyl) imide ionic liquids with long alkyl chains. *J. Chem. Phys.*, 141(13), 2014.

[49] Guangren Yu, Dachuan Zhao, Lu Wen, Shendu Yang, and Xiaochun Chen. Viscosity of ionic liquids: Database, observation, and quantitative structure-property relationship analysis. *AIChE Journal*, 58(9):2885–2899, 2012.

[50] Mohammad Hadi Ghatee, Morteza Zare, Amin Reza Zolghadr, and Fatemeh Moosavi. Temperature dependence of viscosity and relation with the surface tension of ionic liquids. *Fluid Phase Equilibr*, 291(2):188–194, 2010.

[51] Elena Gómez, Noelia Calvar, Ángeles Domínguez, and Eugénia A. Macedo. Synthesis and temperature dependence of physical properties of four pyridinium-based ionic liquids: Influence of the size of the cation. *J. Chem. Thermodyn*, 42(11):1324–1329, 2010.

[52] Thi Phuong Thuy Pham, Chul-Woong Cho, and Yeoung-Sang Yun. Environmental fate and toxicity of ionic liquids: a review. *Water Res.*, 44(2):352–372, 2010.

[53] Christopher Hardacre, John D. Holbrey, Mark Nieuwenhuyzen, and Tristan G. A. Youngs. Structure and solvation in ionic liquids. *Accounts Chem. Res.*, 40(11):1146–1155, 2007.

[54] Jared L. Anderson, Jie Ding, Thomas Welton, and Daniel W. Armstrong. Characterizing ionic liquids on the basis of multiple solvation interactions. *J. Am. Chem. Soc.*, 124(47):14247–14254, 2002.

[55] Kun Dong and Suojiang Zhang. Hydrogen bonds: a structural insight into ionic liquids. *Chemistry–A European Journal*, 18(10):2748–2761, 2012.

[56] Michael Freemantle. Designer solvents-Ionic liquids may boost clean technology development. *Chemical & engineering news*, 76(13):32–37, 1998.

USC

[57] Congmin Wang, Xiaoyan Luo, Huimin Luo, De-en Jiang, Haoran Li, and Sheng Dai. Tuning the basicity of ionic liquids for equimolar CO 2 capture. *Angew. Chem.*, 21(123):5020–5024, 2011.

[58] Ki-Sub Kim, Jeong Won Kang, and Seong-Pil Kang. Tuning ionic liquids for hydrate inhibition. *Chem. Commun.*, 47(22):6341–6343, 2011.

[59] Chandramouli Manasa, Vrushabendra Basavanna, and Srikantamurthy Ningaiah. Ionic liquid-based hybrid materials: Ionogel review. *Biointerface Res. Appl. Chem*, 13:391, 2023.

[60] Muzammil Kuddushi, Nehal K. Patel, Sargam Rajput, Omar A. El Seoud, Jitendra P. Mata, and Naved I. Malek. Temperature-Responsive Low Molecular Weight Ionic Liquid Based Gelator: An Approach to Fabricate an Anti-Cancer Drug-Loaded Hybrid Ionogel. *ChemSystemsChem*, 2(5):e1900053, 2020.

[61] Xiaolin Wang, Qiao Yang, Yixue Cao, Haibin Hao, Junhan Zhou, and Jingcheng Hao. Metallosurfactant ionogels in imidazolium and protic ionic liquids as precursors to synthesize nanoceria as catalase mimetics for the catalytic decomposition of H2O2. *Chemistry–A European Journal*, 22(49):17857–17865, 2016.

[62] Faezeh Ghorbanizamani, Hichem Moulahoum, Emine Guler Celik, and Suna Timur. Ionic liquid-hydrogel hybrid material for enhanced electron transfer and sensitivity towards electrochemical detection of methamphetamine. *J. Mol. Liq.*, 361:119627, 2022.

[63] Jin Hong Lee, Albert S. Lee, Jong-Chan Lee, Soon Man Hong, Seung Sang Hwang, and Chong Min Koo. Hybrid ionogel electrolytes for high temperature lithium batteries. *J. Mater. Chem. A*, 3(5):2226–2233, 2015.

[64] Aurélie Guyomard-Lack, Julio Abusleme, Patrick Soudan, Bernard Lestriez, Dominique Guyomard, and Jean Le Bideau. Hybrid silica–polymer ionogel solid electrolyte with tunable properties. *Adv. Energy Mater.*, 4(8):1301570, 2014.

[65] R. C. Agrawal and G. P. Pandey. Solid polymer electrolytes: materials designing and all-solid-state battery applications: an overview. *J. Phys. D Appl. Phys.*, 41(22):223001, 2008.

[66] Yong An, Xue Han, Yuyang Liu, Alowasheeir Azhar, Jongbeom Na, Ashok Kumar Nanjundan, Shengping Wang, Jingxian Yu, and Yusuke Yamauchi. Progress in solid polymer electrolytes for lithium-ion batteries and beyond. *Small*, 18(3):2103617, 2022.

[67] Irene Osada, Henrik de Vries, Bruno Scrosati, and Stefano Passerini. Ionic-liquid-based polymer electrolytes for battery applications. *Angew. Chem. Int. Ed.*, 55(2):500–513, 2016.

[68] George F. Pinder and William G. Gray. *Finite element simulation in surface and subsurface hydrology*. Elsevier, 2013.

[69] E. Heifets, E. A. Kotomin, and Roberto Orlando. Hartree-Fock simulation of the Ag/MgO interface structure. *J. Phys. Condens. Matter*, 8(36):6577, 1996.

[70] Leandro Martínez, Ricardo Andrade, Ernesto G. Birgin, and José Mario Martínez. PACKMOL: a package for building initial configurations for molecular dynamics simulations. *J. Comput. Chem.*, 30(13):2157–2164, 2009.

[71] William L. Jorgensen and Julian Tirado-Rives. The OPLS [optimized potentials for liquid simulations] potential functions for proteins, energy minimizations for crystals of cyclic peptides and crambin. *J. Am. Chem. Soc.*, 110(6):1657–1666, 1988.

[72] William L. Jorgensen, David S. Maxwell, and Julian Tirado-Rives. Development and testing of the OPLS all-atom force field on conformational energetics and properties of organic liquids. *J. Am. Chem. Soc.*, 118(45):11225–11236, 1996.

[73] Berk Hess, Henk Bekker, Herman J. C. Berendsen, and Johannes G. E. M. Fraaije. LINCS: A linear constraint solver for molecular simulations. *J. Comput. Chem.*, 18(12):1463–1472, 1997.

[74] Jean-Paul Ryckaert, Giovanni Ciccotti, and Herman J. C. Berendsen. Numerical integration of the cartesian equations of motion of a system with constraints: molecular dynamics of n-alkanes. *J. Comput. Phys.*, 23(3):327–341, 1977.

[75] Jiří Kolafa and Martin Lísal. Time-reversible velocity predictors for verlet integration with velocity-dependent right-hand side. *J. Chem. Theory Comput.*, 7(11):3596–3607, 2011.

[76] Giovanni Bussi, Davide Donadio, and Michele Parrinello. Canonical sampling through velocity rescaling. *J. Chem. Phys.*, 126(1):014101(1)–014101(7), 2007.

[77] William G. Hoover. Canonical dynamics: Equilibrium phase-space distributions. *Phys. Rev. A*, 31(3):1695, 1985.

[78] Herman J. C. Berendsen, J. P. M. van Postma, Wilfred F. Van Gunsteren, A. R. H. J. DiNola, and Jan R. Haak. Molecular dynamics with coupling to an external bath. *J. Chem. Phys.*, 81(8):3684–3690, 1984.

[79] Michele Parrinello and Aneesur Rahman. Polymorphic transitions in single crystals: A new molecular dynamics method. *J. Appl. Phys.*, 52(12):7182–7190, 1981.

[80] Herman J. C. Berendsen, David van der Spoel, and Rudi van Drunen. GROMACS: A message-passing parallel molecular dynamics implementation. *Comput. Phys. Commun.*, 91(1-3):43–56, 1995.

[81] Mark James Abraham, Teemu Murtola, Roland Schulz, Szilárd Páll, Jeremy C. Smith, Berk Hess, and Erik Lindahl. GROMACS: High performance molecular simulations through multi-level parallelism from laptops to supercomputers. *SoftwareX*, 1:19–25, 2015.

[82] Guillaume Lamoureux and Benoıt Roux. Modeling induced polarization with classical Drude oscillators: Theory and molecular dynamics simulation algorithm. *J. Chem. Phys.*, 119(6):3025–3039, 2003.

[83] Max Born and W. Heisenberg. Zur quantentheorie der molekeln. *Original Scientific Papers Wissenschaftliche Originalarbeiten*, pages 216–246, 1985.

USC

[84] Pierre Hohenberg and Walter Kohn. Inhomogeneous electron gas. *Phys. Rev.*, 136(3B):B864, 1964.

[85] Walter Kohn and Lu Jeu Sham. Self-consistent equations including exchange and correlation effects. *Phys. Rev.*, 140(4A):A1133, 1965.

[86] John P. Perdew, Kieron Burke, and Matthias Ernzerhof. Generalized gradient approximation made simple. *Phys. Rev. Lett.*, 77(18):3865, 1996.

[87] Georg Kresse and Jürgen Hafner. Ab initio molecular dynamics for liquid metals. *Phys. Rev. B*, 47(1):558, 1993.

[88] Georg Kresse and Jürgen Furthmüller. Efficiency of ab-initio total energy calculations for metals and semiconductors using a plane-wave basis set. *Nato. Sc. S. Ss. Iii. C. S.*, 6(1):15–50, 1996.

[89] Paolo Giannozzi, Stefano Baroni, Nicola Bonini, Matteo Calandra, Roberto Car, Carlo Cavazzoni, Davide Ceresoli, Guido L. Chiarotti, Matteo Cococcioni, Ismaila Dabo, et al. QUANTUM ESPRESSO: a modular and open-source software project for quantum simulations of materials. *J. Phys. Condens. Matter*, 21(39):395502, 2009.

[90] Paolo Giannozzi, Oliviero Andreussi, Thomas Brumme, Oana Bunau, M. Buongiorno Nardelli, Matteo Calandra, Roberto Car, Carlo Cavazzoni, Davide Ceresoli, Matteo Cococcioni, et al. Advanced capabilities for materials modelling with Quantum ESPRESSO. *J. Phys. Condens. Matter*, 29(46):465901, 2017.

[91] Andy Pearson. Refrigeration with ammonia. *Int. J. Refrigeration*, 31(4):545–551, 2008.

[92] L. B. Fenn and L. R. Hossner. Ammonia volatilization from ammonium or ammonium-forming nitrogen fertilizers. *Advances in soil science*, pages 123–169, 1985.

[93] S. Giddey, S. P. S. Badwal, C. Munnings, and M. J. A. S. C. Dolan. Ammonia as a renewable energy transportation media. *ACS Sustainable Chemistry & Engineering*, 5(11):10231–10239, 2017.

[94] Alston J. Misquitta and Anthony J. Stone. Ab initio atom–atom potentials using CamCASP: Theory and application to many-body models for the pyridine dimer. *J. Chem. Theory Comput.*, 12(9):4184–4208, 2016.

[95] Tuanan C. Lourenço, Mahsa Ebadi, Daniel Brandell, Juarez L. F. Da Silva, and Luciano T. Costa. Interfacial structures in ionic liquid-based ternary electrolytes for lithium-metal batteries: a molecular dynamics study. *J. Phys. Chem. B*, 124(43):9648–9657, 2020.

[96] Diddo Diddens and Andreas Heuer. Simulation study of the lithium ion transport mechanism in ternary polymer electrolytes: the critical role of the segmental mobility. *J. Phys. Chem. B*, 118(4):1113–1125, 2014.

[97] Mahsa Ebadi, Luciano T. Costa, C. Moyses Araujo, and Daniel Brandell. Modelling the polymer electrolyte/Li-metal interface by molecular dynamics simulations. *Electrochim Acta*, 234:43–51, 2017.

[98] David Smith. Cooling electronic devices installed in a subsurface environment. 2017. US Patent 9,593,876.

[99] Rong-Rong He, Huai-Yu Zhong, Yang Cai, Di Liu, and Fu-Yun Zhao. Theoretical and Experimental Investigations of Thermoelectric Refrigeration Box Used for Medical Service. *Procedia Engineer*, 205:1215–1222, 2017.

[100] Hanlong Wan, Tao Cao, Yunho Hwang, and Saikee Oh. A review of recent advancements of variable refrigerant flow air-conditioning systems. *Appl. Therm. Eng.*, 169:112893, 2020.

[101] S.A. Tassou, J.S. Lewis, Y.T. Ge, A. Hadawey, and I. Chaer. A review of emerging technologies for food refrigeration applications. *Appl. Therm. Eng.*, 30(4):263–276, 2010.

[102] Sharmas Vali Shaik and T.P. Ashok Babu. Theoretical Performance Investigation of Vapour Compression Refrigeration System Using HFC and HC Refrigerant Mixtures as Alternatives to Replace R22. *Enrgy. Proced.*, 109:235–242, 2017.

[103] Pongsid Srikhirin, Satha Aphornratana, and Supachart Chungpaibulpatana. A review of absorption refrigeration technologies. *Renew. Sust. Energ. Rev.*, 5(4):343–372, 2001.

[104] Danxing Zheng, Li Dong, Weijia Huang, Xianghong Wu, and Nan Nie. A review of imidazolium ionic liquids research and development towards working pair of absorption cycle. *Renew. Sust. Energ. Rev.*, 37:47–68, 2014.

[105] E. Ruiz, V.R. Ferro, J. de Riva, D. Moreno, and J. Palomar. Evaluation of ionic liquids as absorbents for ammonia absorption refrigeration cycles using COSMO-based process simulations. *Appl. Energy*, 123:281–291, 2014.

[106] Peter Wasserscheid and Thomas Welton. *Ionic liquids in synthesis*. John Wiley & Sons, 2008.

[107] A. Yokozeki and Mark B. Shiflett. Vapor–liquid equilibria of ammonia + ionic liquid mixtures. *Appl. Energy*, 84:1258–1273, 2007.

[108] A. Yokozeki and Mark B. Shiflett. Ammonia Solubilities in Room-Temperature Ionic Liquids. *Ind. Eng. Chem. Res.*, 46(5):1605–1610, 2007.

[109] Guihua Li, Qing Zhou, Xiangping Zhang, Lei Wang, Suojiang Zhang, and Jianwei Li. Solubilities of ammonia in basic imidazolium ionic liquids. *Fluid Phase Equilib.*, 297:34–39, 2010.

[110] M. Berdasco, A. Coronas, and M. Vallès. Study of the adiabatic absorption process in polymeric hollow fiber membranes for ammonia/water absorption refrigeration systems. *Appl. Therm. Eng.*, 137(5):594–607, 2018.

[111] Andry Cera-Manjarres, Daniel Salavera, and Alberto Coronas. Vapour pressure measurements of ammonia/ionic liquids mixtures as suitable alternative working fluids for absorption refrigeration technology. *Fluid Phase Equilib.*, 476:48–60, 2018.

USC UNIVERSIDADE DE SANTIAGO DE COMPOSTELA

[112] M. Soledad Larrechi, Andry Cera-Manjarres, and Alberto Coronas. Ranking the solubility of ammonia in ionic liquids using near infrared spectroscopy and multivariate curve resolution. *Spectrochim. Acta A Mol. Biomol. Spectrosc.*, 215:88–96, 2019.

[113] M. Soledad Larrechi, Andry Cera-Manjarres, Daniel Salavera, and Alberto Coronas. Quantitative analysis of the interaction of ammonia with 1-(2-hydroxyethyl)-3-methylimidazolium tetrafluoroborate ionic liquid. Understanding the volumetric and transport properties of their mixtures. *J. Mol. Liq.*, 301:112440(1)–112440(11), 2020.

[114] Sumit K. Swarnkar, S. Srinivasa Murthy, Ramesh L. Gardas, and G. Venkatarathnam. Performance of a vapour absorption refrigeration system operating with ionic liquid-ammonia combination with water as cosolvent. *Appl. Therm. Eng.*, 72(2):250–257, 2014.

[115] Xiaobo Ji, Debbie S. Silvester, Leigh Aldous, Christopher Hardacre, and Richard G. Compton. Mechanistic Studies of the Electro-oxidation Pathway of Ammonia in Several Room-Temperature Ionic Liquids. *J. Phys. Chem. C*, 111(26):9562–9572, 2007.

[116] Xiaobo Ji, Craig E. Banks, Debbie S. Silvester, Leigh Aldous, Christopher Hardacre, and Richard G. Compton. Electrochemical Ammonia Gas Sensing in Nonaqueous Systems: A Comparison of Propylene Carbonate with Room Temperature Ionic Liquids. *Electroanal*, 19(21):2194–2201, 2007.

[117] Marisa C. Buzzeo, Debora Giovanelli, Nathan S. Lawrence, Christopher Hardacre, Kenneth R. Seddon, and Richard G. Compton. Elucidation of the Electrochemical Oxidation Pathway of Ammonia in Dimethylformamide and the Room Temperature Ionic Liquid, 1-Ethyl-3-methylimidazolium bis(trifluoromethylsulfonyl)imide. *Electroanal*, 16(11):888–896, 2004.

[118] Wei Shi and Edward J. Maginn. Molecular simulation of ammonia absorption in the ionic liquid 1-ethyl-3-methylimidazolium bis(trifluoromethylsulfonyl)imide ([emim][Tf2N]). *AIChE J.*, 55(9):2414–2421, 2009.

[119] Utkarsh Kapoor, Atiya Banerjee, and Jindal K. Shah. Evaluation of the predictive capability of ionic liquid force fields for CH_4, CO_2, NH_3, and SO_2 phase equilibria. *Fluid Phase Equilib.*, 492:161–173, 2019.

[120] Jose Palomar, Maria Gonzalez-Miquel, Jorge Bedia, Francisco Rodriguez, and Juan J. Rodriguez. Task-specific ionic liquids for efficient ammonia absorption. *Sep. Purif. Technol.*, 82:43–52, 2011.

[121] Jorge Bedia, Jose Palomar, Maria Gonzalez-Miquel, Francisco Rodriguez, and Juan J. Rodriguez. Screening ionic liquids as suitable ammonia absorbents on the basis of thermodynamic and kinetic analysis. *Sep. Purif. Technol.*, 95:188–195, 2012.

[122] Tim M. Becker, Meng Wang, Abhishek Kabra, Seyed Hossein Jamali, Mahinder Ramdin, Carlos A. Infante Ferreira David Dubbeldam, and Thijs J. H. Vlugt. Absorption Refrigeration Cycles with Ammonia–Ionic Liquid Working Pairs Studied by Molecular Simulation. *Ind. Eng. Chem. Res.*, 57(15):5442–5452, 2018.

[123] Muhammed Shah Miran, Hiroshi Kinoshita, Tomohiro Yasuda, Md. Abu Bin Hasan Susanz, and Masayoshi Watanabe. Hydrogen bonds in protic ionic liquids and their correlation with physicochemical properties. *Chem. Commun.*, 47:12676–12678, 2011.

[124] P. Piecuch, V. Špirko, and J. Paldus. Molecular quadrupole moment function of ammonia. *J. Chem. Phys.*, 105(24):11068–11074, 1996.

[125] M. Radiom. Ionic liquid–solid interface and applications in lubrication and energy storage. *Curr. Opin. Colloid Interface Sci.*, 39:148–161, 2019.

[126] H. Liu and H. Yu. Ionic liquids for electrochemical energy storage devices applications. *J. Mater. Sci. Technol.*, 35(4):674–686, 2019.

[127] F. Zhang, J. Liu, W. Yanga, and B. E. Logan. A thermally regenerative ammonia-based battery for efficient harvesting of low-grade thermal energy as electrical power. *Energy Environ. Sci.*, 8(1):343–349, 2015.

[128] X. Zhu, M. Rahimi, C. A. Gorski, and B. Logan. A Thermally-Regenerative Ammonia-Based Flow Battery for Electrical Energy Recovery from Waste Heat. *Chem. Sus. Chem.*, 9(8):873–879, 2016.

[129] T. Zhang, Y. Wang, T. Song, H. Miyaoka, K. Shinzato, H. Miyaoka, T. Ichikawa, S. Shi, X. Zhang, S. Isobe, N. Hashimoto, and Y. Kojima. Ammonia, a Switch for Controlling High Ionic Conductivity in Lithium Borohydride Ammoniates. *Joule*, 15(8):1522–1533, 2018.

[130] Alston J. Misquitta and Anthony J. Stone. Ab initio atom–atom potentials using CamCASP: Theory and application to many-body models for the pyridine dimer. *J. Chem. Theor. Comp.*, 12:4184–4208, 2016.

[131] Alston J. Misquitta and Anthony J. Stone. CamCASP: a program for studying intermolecular interactions and for the calculation of molecular properties in distributed form . *https://gitlab.com/anthonyjs/camcasp*, 12:4184–4208, 2016.

[132] Carlo Adamo and Vincenzo Barone. Toward reliable density functional methods without adjustable parameters: The PBE0 model. *J. Chem. Theor. Comp.*, 110:6158–6170, 1999.

[133] T. H. Dunnin Jr. Gaussian-basis sets for use in correlated molecular calculations.1. The atoms boron throuch neon and hydrogen . *J. Chem. Phys.*, 90(2):1007–1023, 1989.

[134] R. A. Kendall, T. H. Dunnin Jr., and R. J. Harrison. Electron-affinities of the 1st row atoms revisited - systematic basis sets and wave functions. *J. Chem. Phys.*, 96(9):6796–6806, 1992.

[135] Alston J. Misquitta, Anthony J. Stone, and F. Fazelli. Distributed Multipoles from a Robust Basis-Space Implementation of the Iterated Stockholder Atoms Procedure. *J. Chem. Theor. Comp.*, 12:4184–42085405–5418, 2014.

[136] Robert C. Rizzo and William L. Jorgensen. OPLS all-atom model for amines: resolution of the amine hydration problem. *J. Am. Chem. Soc.*, 121(20):4827–4836, 1999.

USC

[137] David van der Spoel, E. Lindahl, Berk Hess, A. R. Van Buuren, E. Apol, P. J. Meulenhoff, D. P. Tieleman, A. L. T. M. Sijbers, K. A. Feenstra, R. Van Drunen, et al. Gromacs user manual version 4.0. *Nijenborgh*, 4:9747, 2005.

[138] C. Girardet and A. Lakhlifi. NH_3 inversion in condensed media. Static, dynamic, and inhomogeneous environmental effects on the internal tunneling. *J. Chem. Phys.*, 91(4):2172–2180, 1989.

[139] G. Feng, J. S. Zhang, and R. Qiao. Microstructure and capacitance of the electrical double layers at the interface of ionic liquids and planar electrodes. *J. Phys. Chem. C*, 113(11):4549–4559, 2009.

[140] Q. Dou, M. L. Sha, H. Y. Fu, and G. Z. Wu. Molecular dynamics simulation of the interfacial structure of [Cnmim][PF_6] adsorbed on a graphite surface: effects of temperature and alkyl chain length. *J. Phys. Condens. Matter*, 23(17):175001, 2011.

[141] Sergey A. Kislenko, Igor S. Samoylov, and Ravil H. Amirov. Molecular dynamics simulation of the electrochemical interface between a graphite surface and the ionic liquid [BMIM][PF_6]. *Phys. Chem. Chem. Phys.*, 11(27):5584–5590, 2009.

[142] Matthew A. Gebbie, Markus Valtiner, Xavier Banquy, Eric T. Fox, Wesley A. Henderson, and Jacob N. Israelachvili. Ionic liquids behave as dilute electrolyte solutions. *Proc. Natl. Acad. Sci. USA*, 110(24):9674–9679, 2013.

[143] Hua Zhao and Sanjay V. Malhotra. Applications of ionic liquids in organic synthesis. *Aldrichim. Acta.*, 2002.

[144] Robin D. Rogers and Kenneth R. Seddon. *Ionic liquids: industrial applications for green chemistry*. ACS Publications, 2002.

[145] Natalia V. Plechkova and Kenneth R. Seddon. Applications of ionic liquids in the chemical industry. *Chem. Soc. Rev.*, 37(1):123–150, 2008.

[146] Christian Reichardt and Thomas Welton. *Solvents and solvent effects in organic chemistry*. John Wiley & Sons, 2011.

[147] Ichiro Minami. Ionic liquids in tribology. *Molecules*, 14(6):2286–2305, 2009.

[148] Aleksandar Matic and Bruno Scrosati. Ionic liquids for energy applications. *MRS Bullet.*, 38:533–537, 7 2013.

[149] Michel Armand, Frank Endres, Douglas R. MacFarlane, Hiroyuki Ohno, and Bruno Scrosati. Ionic-liquid materials for the electrochemical challenges of the future. *Nat. Mater.*, 8(8):621–629, 2009.

[150] Maxim V. Fedorov and Alexei A. Kornyshev. Ionic liquids at electrified interfaces. *Chem. Rev.*, 114(5):2978–3036, 2014.

[151] Douglas R. MacFarlane, Naoki Tachikawa, Maria Forsyth, Jennifer M. Pringle, Patrick C. Howlett, Gloria D. Elliott, James H. Davis, Masayoshi Watanabe, Patrice Simon, and C. Austen Angell. Energy applications of ionic liquids. *Energ. Environ. Sci.*, 7(1):232–250, 2014.

[152] Hiroyuki Ohno. Molten salt type polymer electrolytes. *Electrochim Acta*, 46(10-11):1407–1411, 2001.

[153] Joon-Ho Shin, Wesley A. Henderson, and Stefano Passerini. PEO-based polymer electrolytes with ionic liquids and their use in lithium metal-polymer electrolyte batteries. *J. Electrochem Soc.*, 152(5):A978, 2005.

[154] Oleg Borodin and Grant D. Smith. Mechanism of ion transport in amorphous poly (ethylene oxide)/LiTFSI from molecular dynamics simulations. *Macromolecules*, 39(4):1620–1629, 2006.

[155] Nicola Molinari, Jonathan P. Mailoa, and Boris Kozinsky. Effect of salt concentration on ion clustering and transport in polymer solid electrolytes: a molecular dynamics study of peo–litfsi. *Chem. Mater.*, 30(18):6298–6306, 2018.

[156] Yogesh Kumar, S. A. Hashmi, and G. P. Pandey. Lithium ion transport and ion–polymer interaction in PEO based polymer electrolyte plasticized with ionic liquid. *Solid State Ionics*, 201(1):73–80, 2011.

[157] Diddo Diddens and Andreas Heuer. Lithium ion transport mechanism in ternary polymer electrolyte-ionic liquid mixtures: A molecular dynamics simulation study. *ACS Macro Letters*, 2(4):322–326, 2013.

[158] Santosh Mogurampelly and Venkat Ganesan. Structure and mechanisms underlying ion transport in ternary polymer electrolytes containing ionic liquids. *J. Chem. Phys.*, 146(7):074902, 2017.

[159] Joon-Ho Shin, Wesley A. Henderson, Cosimo Tizzani, Stefano Passerini, Sang-Sik Jeong, and Ki-Won Kim. Characterization of solvent-free polymer electrolytes consisting of ternary PEO–LiTFSI–PYR14 TFSI. *J. Electrochem Soc.*, 153(9):A1649, 2006.

[160] Mosè Casalegno, Franca Castiglione, Guido Raos, Giovanni Battista Appetecchi, Stefano Passerini, Andrea Mele, and Enzio Ragg. Magnetic Resonance Imaging and Molecular Dynamics Characterization of Ionic Liquid in Poly(ethylene oxide)-Based Polymer Electrolytes. *ACS Appl. Mater. Interfaces*, 12(21):23800–23811, 2020.

[161] Thomas Vogl, Sebastian Menne, Ruben-Simon Kühnel, and Andrea Balducci. The beneficial effect of protic ionic liquids on the lithium environment in electrolytes for battery applications. *J. Mater. Chem. A*, 2(22):8258–8265, 2014.

[162] Berk Hess, Carsten Kutzner, David Van Der Spoel, and Erik Lindahl. GROMACS 4: algorithms for highly efficient, load-balanced, and scalable molecular simulation. *J. Chem. Theory Comput.*, 4(3):435–447, 2008.

[163] José N. Canongia Lopes, Johnny Deschamps, and Agílio A. H. Pádua. Modeling ionic liquids using a systematic all-atom force field. *J. Phys. Chem. B*, 108(6):2038–2047, 2004.

[164] José N. Canongia Lopes and Agílio A. H. Pádua. CL&P: A generic and systematic force field for ionic liquids modeling. *Theor. Chem. Acc.*, 131(3):1129, 2012.

USC

[165] Johan Åqvist. Ion-water interaction potentials derived from free energy perturbation simulations. *J. Phys. Chem.*, 94(21):8021–8024, 1990.

[166] Alexandra Patriksson and David van der Spoel. A temperature predictor for parallel tempering simulations. *Phys. Chem. Chem. Phys.*, 10(15):2073–2077, 2008.

[167] Tom Darden, Darrin York, and Lee Pedersen. Particle mesh Ewald: An N·log (N) method for Ewald sums in large systems. *J. Chem. Phys.*, 98(12):10089–10092, 1993.

[168] Ulrich Essmann, Lalith Perera, Max L. Berkowitz, Tom Darden, Hsing Lee, and Lee G. Pedersen. A smooth particle mesh Ewald method. *J. Chem. Phys.*, 103(19):8577–8593, 1995.

[169] Volker Lesch, Hadrián Montes-Campos, Trinidad Méndez-Morales, Luis Javier Gallego, Andreas Heuer, Christian Schröder, and Luis M. Varela. Molecular dynamics analysis of the effect of electronic polarization on the structure and single-particle dynamics of mixtures of ionic liquids and lithium salts. *J. Chem. Phys.*, 145(20):204507, 2016.

[170] Tianying Yan, Christian J. Burnham, Mario G. Del Pópolo, and Gregory A. Voth. Molecular dynamics simulation of ionic liquids: The effect of electronic polarizability. *J. Phys. Chem. B*, 108(32):11877–11881, 2004.

[171] Eunsong Choi and Arun Yethiraj. Entropic mechanism for the lower critical solution temperature of poly (ethylene oxide) in a room temperature ionic liquid. *ACS Macro Lett.*, 4(7):799–803, 2015.

[172] Jacob Israelachvili. The different faces of poly (ethylene glycol). *Proc. Natl. Acad. Sci. U. S. A.*, 94(16):8378–8379, 1997.

[173] Mohammad Hadi Ghatee and Amin Reza Zolghadr. Local depolarization in hydrophobic and hydrophilic ionic liquids/water mixtures: car–parrinello and classical molecular dynamics simulation. *J. Phys. Chem. C*, 117(5):2066–2077, 2013.

[174] Víctor Gómez-González, J. Manuel Otero-Mato, Hadrián Montes-Campos, Xabier García-Andrade, Amador García-Fuente, Andrés Vega, Jesús Carrete, Oscar Cabeza, Luis J. Gallego, and Luis M. Varela. Borophene vs. graphene interfaces: Tuning the electric double layer in ionic liquids. *J. Mol. Liq.*, 303:112647, 2020.

[175] A. Maitra and A. Heuer. Cation transport in polymer electrolytes: A microscopic approach. *Phys. Rev. Lett.*, 98(22):227802, 2007.

[176] Trinidad Mendez-Morales, Jesus Carrete, Silvia Bouzon-Capelo, Martin Perez-Rodriguez, Oscar Cabeza, Luis J. Gallego, and Luis M. Varela. MD simulations of the formation of stable clusters in mixtures of alkaline salts and imidazolium-based ionic liquids. *J. Phys. Chem. B*, 117(11):3207–3220, 2013.

[177] Arindam Dutta, Shirsendu Mitra, Mitali Basak, and Tamal Banerjee. A comprehensive review on batteries and supercapacitors: development and challenges since their inception. *Energy Storage*, 5(1):e339, 2023.

[178] Arumugam Manthiram. An outlook on lithium ion battery technology. *ACS Cent. Sci.*, 3(10):1063–1069, 2017.

[179] Alvaro Masias, James Marcicki, and William A. Paxton. Opportunities and challenges of lithium ion batteries in automotive applications. *ACS Energy Lett.*, 6(2):621–630, 2021.

[180] Vinodkumar Etacheri, Rotem Marom, Ran Elazari, Gregory Salitra, and Doron Aurbach. Challenges in the development of advanced Li-ion batteries: a review. *Energy Environ. Sci.*, 4(9):3243–3262, 2011.

[181] Jie Xiao. How lithium dendrites form in liquid batteries. *Science*, 366(6464):426–427, 2019.

[182] DEa Fenton. Complexes of Alkali Metal Ions with Poly (etylene oxide). *Polymer*, 14:589, 1973.

[183] M. B. Armand, J. M. Chabagno, M. J. la Duclot, et al. Fast ion transport in solids: electrodes and electrolytes. In *Proceedings of the International Conference on Fast Ion Transport in Solids, Electrodes, and Electrolytes, Lake Geneva, Wisconsin, USA, May 21–25*, 1979.

[184] Michel Armand. Polymer solid electrolytes-an overview. *Solid State Ionics*, 9:745–754, 1983.

[185] C. Berthier, W. Gorecki, M. Minier, M. B. Armand, J. M. Chabagno, and Ph Rigaud. Microscopic investigation of ionic conductivity in alkali metal salts-poly (ethylene oxide) adducts. *Solid State Ionics*, 11(1):91–95, 1983.

[186] Yoichi Tominaga, Kenta Yamazaki, and Vannasa Nanthana. Effect of anions on lithium ion conduction in poly (ethylene carbonate)-based polymer electrolytes. *J. Electrochem Soc.*, 162(2):A3133, 2015.

[187] Changwoo Do, Peter Lunkenheimer, Diddo Diddens, Marion Götz, Matthias Weiß, Alois Loidl, Xiao-Guang Sun, Jürgen Allgaier, and Michael Ohl. Li+ transport in poly (ethylene oxide) based electrolytes: neutron scattering, dielectric spectroscopy, and molecular dynamics simulations. *Phys. Rev. Lett.*, 111(1):018301, 2013.

[188] Diddo Diddens, Andreas Heuer, and Oleg Borodin. Understanding the lithium transport within a rouse-based model for a PEO/LiTFSI polymer electrolyte. *Macromolecules*, 43(4):2028–2036, 2010.

[189] Guomin Mao, Marie-Louise Saboungi, David L. Price, Michel B. Armand, and W. S. Howells. Structure of liquid PEO-LiTFSI electrolyte. *Phys. Rev. Lett.*, 84(24):5536, 2000.

[190] Luciano T. Costa, Leonardo J. A. Siqueira, Bruno G. Nicolau, and Mauro C. C. Ribeiro. Raman spectra of polymer electrolytes based on poly (ethylene glycol) dimethyl ether, lithium perchlorate, and the ionic liquid 1-butyl-3-methylimidazolium hexafluorophosphate. *Vib. Spectrosc*, 54(2):155–158, 2010.

[191] F. Croce, G. B. Appetecchi, L. Persi, and B. Scrosati. Nanocomposite polymer electrolytes for lithium batteries. *Nature*, 394(6692):456–458, 1998.

[192] F. Croce, L. Persi, F. Ronci, and B. Scrosati. Nanocomposite polymer electrolytes and their impact on the lithium battery technology. *Solid State Ionics*, 135(1-4):47–52, 2000.

USC

[193] Shufeng Song, Yongmin Wu, Weiping Tang, Fan Deng, Jianyao Yao, Zongwen Liu, Rongjie Hu, Alamusi, Zhaoyin Wen, Li Lu, et al. Composite solid polymer electrolyte with garnet nanosheets in poly (ethylene oxide). *ACS Sustain. Chem. Eng.*, 7(7):7163–7170, 2019.

[194] A. Manuel Stephan. Review on gel polymer electrolytes for lithium batteries. *Eur. Polym. J.*, 42(1):21–42, 2006.

[195] Thomas Rüther, Anand I. Bhatt, Adam S. Best, Kenneth R. Harris, and Anthony F. Hollenkamp. Electrolytes for lithium (sodium) batteries based on ionic liquids: Highlighting the key role played by the anion. *Batter. Supercaps*, 3(9):793–827, 2020.

[196] Suojiang Zhang, Ning Sun, Xuezhong He, Xingmei Lu, and Xiangping Zhang. Physical properties of ionic liquids: database and evaluation. *J. Phys. Chem. Ref. Data*, 35(4):1475–1517, 2006.

[197] I. M. Marrucho, L. C. Branco, and L. P. N. Rebelo. Ionic liquids in pharmaceutical applications. *Annu. Rev. Chem. Biomol.*, 5:527–546, 2014.

[198] V. Borgel, E. Markevich, D. Aurbach, G. Semrau, and M. Schmidt. On the application of ionic liquids for rechargeable Li batteries: High voltage systems. *J. Power Sources*, 189(1):331–336, 2009.

[199] Pablo Vallet, Silvia Bouzón-Capelo, Trinidad Méndez-Morales, Víctor Gómez-González, Yago Arosa, Raúl de la Fuente, Elena López-Lago, Julio R. Rodríguez, Luis J. Gallego, Juan J. Parajó, et al. On the physical properties of mixtures of nitrate salts and protic ionic liquids. *J. Mol. Liq.*, 350:118483, 2022.

[200] Jakob Asenbauer, Nour Ben Hassen, Bryan D. McCloskey, and John M. Prausnitz. Solubilities and ionic conductivities of ionic liquids containing lithium salts. *Electrochim Acta*, 247:1038–1043, 2017.

[201] Mark P. Rosenwinkel and Monika Schönhoff. Polymer-Induced Inversion of the Li+ Drift Direction in Ionic Liquid-Based Ternary Polymer Electrolytes. *Macromol Chem. Physic.*, 223(8):2100320, 2022.

[202] S. K. Chaurasia, A. L. Saroj, Shalu Shalu, V. K. Singh, A. K. Tripathi, A. K. Gupta, Y. L. Verma, and R. K. Singh. Studies on structural, thermal and AC conductivity scaling of PEO-LiPF6 polymer electrolyte with added ionic liquid [BMIMPF6]. *AIP Adv.*, 5(7), 2015.

[203] Yeon Hwa Kim, Gouri Cheruvally, Jae Won Choi, Jou Hyeon Ahn, Ki Won Kim, Hyo Jun Ahn, Doo Seong Choi, and Choong Eui Song. Electrochemical Properties of PEO-Based Polymer Electrolytes Blended with Different Room Temperature Ionic Liquids. In *Macromolecular Symposia*, volume 249, pages 183–189. Wiley Online Library, 2007.

[204] Jae-Won Choi, Gouri Cheruvally, Yeon-Hwa Kim, Jae-Kwang Kim, James Manuel, Prasanth Raghavan, Jou-Hyeon Ahn, Ki-Won Kim, Hyo-Jun Ahn, Doo Seong Choi, et al. Poly (ethylene oxide)-based polymer electrolyte incorporating room-temperature ionic liquid for lithium batteries. *Solid State Ionics*, 178(19-20):1235–1241, 2007.

[205] Changbao Zhu, Hu Cheng, and Yong Yang. Electrochemical characterization of two types of PEO-based polymer electrolytes with room-temperature ionic liquids. *J. Electrochem Soc.*, 155(8):A569, 2008.

[206] Luciano T. Costa, Bing Sun, Fabian Jeschull, and Daniel Brandell. Polymer-ionic liquid ternary systems for Li-battery electrolytes: Molecular dynamics studies of LiTFSI in a EMIm-TFSI and PEO blend. *J. Chem. Phys.*, 143(2):024904, 2015.

[207] Jaschar Atik, Diddo Diddens, Johannes Helmut Thienenkamp, Gunther Brunklaus, Martin Winter, and Elie Paillard. Cation-assisted lithium-ion transport for high-performance peo-based ternary solid polymer electrolytes. *Angew. Chem. Int. Ed.*, 60(21):11919–11927, 2021.

[208] Jaschar Atik, Johannes Helmut Thienenkamp, Gunther Brunklaus, Martin Winter, and Elie Paillard. Ionic liquid plasticizers comprising solvating cations for lithium metal polymer batteries. *Electrochim Acta*, 398:139333, 2021.

[209] Matthew D. Widstrom, Kyle B. Ludwig, Jesse E. Matthews, Angelique Jarry, Metecan Erdi, Arthur V. Cresce, Gary Rubloff, and Peter Kofinas. Enabling high performance all-solid-state lithium metal batteries using solid polymer electrolytes plasticized with ionic liquid. *Electrochim Acta*, 345:136156, 2020.

[210] Furui Ma, Zengqi Zhang, Wenchao Yan, Xiaodi Ma, Deye Sun, Yongcheng Jin, Xiaochun Chen, and Kuang He. Solid polymer electrolyte based on polymerized ionic liquid for high performance all-solid-state lithium-ion batteries. *ACS Sustain. Chem. Eng.*, 7(5):4675–4683, 2019.

[211] Jan-Philipp Hoffknecht, Alina Wettstein, Jaschar Atik, Christian Krause, Johannes Thienenkamp, Gunther Brunklaus, Martin Winter, Diddo Diddens, Andreas Heuer, and Elie Paillard. Coordinating Anions "to the Rescue" of the Lithium Ion Mobility in Ternary Solid Polymer Electrolytes Plasticized With Ionic Liquids. *Adv. Energy Mater.*, 13(1):2202789, 2023.

[212] Henrik de Vries, Sangsik Jeong, and Stefano Passerini. Ternary polymer electrolytes incorporating pyrrolidinium-imide ionic liquids. *Rsc Adv.*, 5(18):13598–13606, 2015.

[213] Mario Joost, Miriam Kunze, Sangsik Jeong, Monika Schönhoff, Martin Winter, and Stefano Passerini. Ionic mobility in ternary polymer electrolytes for lithium-ion batteries. *Electrochim Acta*, 86:330–338, 2012.

[214] Patrik Johansson. Computational modelling of polymer electrolytes: What do 30 years of research efforts provide us today? *Electrochim Acta*, 175:42–46, 2015.

[215] Santosh Mogurampelly, Oleg Borodin, and Venkat Ganesan. Computer simulations of ion transport in polymer electrolyte membranes. *Annu. Rev. Chem. Biomol.*, 7:349–371, 2016.

[216] Mahsa Ebadi, Cleber Marchiori, Jonas Mindemark, Daniel Brandell, and C. Moyses Araujo. Assessing structure and stability of polymer/lithium-metal interfaces from first-principles calculations. *J. Mater. Chem. A*, 7(14):8394–8404, 2019.

USC UNIVERSIDADE DE SANTIAGO DE COMPOSTELA

[217] Amina Mirsakiyeva, Mahsa Ebadi, C. Moyses Araujo, Daniel Brandell, Peter Broqvist, and Jolla Kullgren. Initial steps in PEO decomposition on a Li metal electrode. *J. Phys. Chem. C*, 123(37):22851–22857, 2019.

[218] Mirko Fischer, Andreas Heuer, and Diddo Diddens. Structure and Transport Properties of Poly (ethylene oxide)-Based Cross-Linked Polymer Electrolytes- A Molecular Dynamics Simulations Study. *Macromolecules*, 55(22):10229–10242, 2022.

[219] José M. Otero-Mato, Alejandro Rivera-Pousa, Hadrián Montes-Campos, Oscar Cabeza, A. Heuer, D. Diddens, and Luis M. Varela. Computational study of the structure of ternary ionic liquid/salt/polymer electrolytes based on protic ionic liquids. *J. Mol. Liq.*, 333:115883, 2021.

[220] Joyjit Chattoraj, Diddo Diddens, and Andreas Heuer. Effects of ionic liquids on cation dynamics in amorphous polyethylene oxide electrolytes. *J. Chem. Phys.*, 140(2):024906, 2014.

[221] Chao Xu, Bing Sun, Torbjörn Gustafsson, Kristina Edström, Daniel Brandell, and Maria Hahlin. Interface layer formation in solid polymer electrolyte lithium batteries: an XPS study. *J. Mater. Chem. A*, 2(20):7256–7264, 2014.

[222] Andreas Thum, Diddo Diddens, and Andreas Heuer. Impact of Charged Surfaces on the Structure and Dynamics of Polymer Electrolytes: Insights from Atomistic Simulations. *J. Phys. Chem. C*, 125(46):25392–25403, 2021.

[223] William Humphrey, Andrew Dalke, and Klaus Schulten. VMD: visual molecular dynamics. *J. Mol. Graphics*, 14(1):33–38, 1996.

[224] Tom Darden, Darrin York, and Lee Pedersen. Particle mesh Ewald: An N log (N) method for Ewald sums in large systems. *J. Chem. Phys.*, 98(12):10089–10092, 1993.

[225] I. Yeh and M. L. Berkowitz. Ewald summation for systems with slab geometry. *J. Chem. Phys.*, 111(7):3155–3162, 1999.

[226] Céline Merlet, Clarisse Péan, Benjamin Rotenberg, Paul A. Madden, Patrice Simon, and Mathieu Salanne. Simulating supercapacitors: Can we model electrodes as constant charge surfaces? *J. Phys. Chem. Lett.*, 4(2):264–268, 2013.

[227] Jinyuan Yang, Zheng Bo, Huachao Yang, Hualei Qi, Jing Kong, Jianhua Yan, and Kefa Cen. Reliability of Constant Charge Method for Molecular Dynamics Simulations on EDLCs in Nanometer and Sub-Nanometer Spaces. *ChemElectroChem*, 4(10):2486–2493, 2017.

[228] Denis J. Evans and Brad Lee Holian. The nose–hoover thermostat. *J. Chem. Phys.*, 83(8):4069–4074, 1985.

[229] Jiahuan Tong, Shengli Wu, Nicolas Von Solms, Xiaodong Liang, Feng Huo, Qing Zhou, Hongyan He, and Suojiang Zhang. The effect of concentration of lithium salt on the structural and transport properties of ionic liquid-based electrolytes. *Front. Chem.*, 7:945, 2020.

[230] Amir Taghavi Nasrabadi and Venkat Ganesan. Structure and transport properties of lithium-doped aprotic and protic ionic liquid electrolytes: Insights from molecular dynamics simulations. *J. Phys. Chem. B*, 123(26):5588–5600, 2019.

[231] O. Leenaerts, B. Partoens, and F. M. Peeters. Water on graphene: Hydrophobicity and dipole moment using density functional theory. *Phys. Rev. B*, 79(23):235440, 2009.

[232] Xiaoqian Zhang, Shanhong Wan, Jibin Pu, Liping Wang, and Xueqin Liu. Highly hydrophobic and adhesive performance of graphene films. *J. Mater. Chem.*, 21(33):12251–12258, 2011.

[233] Susan Perkin, Tim Albrecht, and Jacob Klein. Layering and shear properties of an ionic liquid, 1-ethyl-3-methylimidazolium ethylsulfate, confined to nano-films between mica surfaces. *Phys. Chem. Chem. Phys.*, 12(6):1243–1247, 2010.

[234] Robert Hayes, Natalia Borisenko, Matthew K. Tam, Patrick C. Howlett, Frank Endres, and Rob Atkin. Double layer structure of ionic liquids at the Au (111) electrode interface: an atomic force microscopy investigation. *J. Phys. Chem. C*, 115(14):6855–6863, 2011.

[235] X. Yu and A. Manthiram. Electrode–electrolyte interfaces in lithium-based batteries. *Energy Environ. Sci.*, 11:527–543, 2018.

[236] L. Miao, Z. Song, D. Zhu, L. Li, L. Gan, and M. Liu. Recent advances in carbon-based supercapacitors. *Mater.Adv.*, 1:945–966, 2020.

[237] M. Gauthier, T. J. Carney, A. Grimaud, L. Giordano, N. Pour, H.-H. Chang, D. P. Fenning, S. F. Lux, O. Paschos, C. Bauer, F. Maglia, S. Lupart, P. Lamp, and Y. Shao-Horn. Electrode-electrolyte interface in Li-ion batteries: current understanding and new insights. *J. Phys. Chem. Lett.*, 6:4653–4672, 2015.

[238] J. Kasnatscheew, R. Wagner, M. Winter, and I. Cekic-Laskovic. Interfaces and Materials in Lithium Ion Batteries: Challenges for Theoretical Electrochemistry . *Top Curr. Chem. (Z)*, 16:376(1)–376(29), 2018.

[239] H. Matsumoto. Review: Ionic liquids as a potential electrolyte for energy devices. In *2014 IEEE International Nanoelectronics Conference (INEC)*, pages 1–4, 2014.

[240] Salvatore Marullo, Francesca D'Anna, Carla Rizzo, and Floriana Billeci. Ionic liquids: "normal" solvents or nanostructured fluids? *Org. Biomol. Chem.*, 19:2076–2095, 2021.

[241] Shanshan Pan, Meng Yao, Jiahe Zhang, Bosen Li, Chunxian Xing, Xianli Song, Peipei Su, and Haitao Zhang. Recognition of Ionic Liquids as High-Voltage Electrolytes for Supercapacitors. *Front. Chem.*, 8:261(1)–261(18), 2020.

[242] Masayoshi Watanabe, Morgan L. Thomas, Shiguo Zhang, Kazuhide Ueno, Tomohiro Yasuda, and Kaoru Dokko. Application of Ionic Liquids to Energy Storage and Conversion Materials and Devices. *Chem. Rev.*, 117:7190–7239, 2017.

[243] K. Karuppasamy, J. Theerthagiri, D. Vikraman, C.-J. Yim, S. Hussain, R. Sharma, T. Maiyalagan, J. Qin, and H.-S. Kim. Ionic Liquid-Based Electrolytes for Energy Storage Devices: A Brief Review on Their Limits and Applications. *Polymers-Basel*, 12:918(1)–918(37), 2020.

USC UNIVERSIDADE DE SANTIAGO DE COMPOSTELA

[244] X. Wang, M. Salari, D. Jiang, J. C. Varela, B. Anasori, D. J. Wesolowski, S. Dai, M. W. Grinstaff, and Y. Gogotsi. Electrode material–ionic liquid coupling for electrochemical energy storage. *Nat. Rev. Mater.*, 5:787–808, 2020.

[245] Nicolas Dupré, Philippe Moreau, Eric De Vito, Lucille Quazuguel, Maxime Boniface, Harald Kren, Pascale Bayle-Guillemaud, and Dominique Guyomard. Carbonate and Ionic Liquid Mixes as Electrolytes To Modify Interphases and Improve Cell Safety in Silicon-Based Li-Ion Batteries. *Chem. Mater.*, 29:8132–8146, 2017.

[246] T. Vogl, S. Menne, and A. Balducci. Mixtures of protic ionic liquids and propylene carbonate as advanced electrolytes for lithium-ion batteries. *Phys. Chem. Chem. Phys.*, 16:25014–25023, 2014.

[247] Linh T.M. Le, Thanh D. Vo, Khanh H.P. Ngo, S. Okada, F. Alloin, A. Garg, and Phung M.L. Le. Mixing ionic liquids and ethylene carbonate as safe electrolytes for lithium-ion batteries. *J. Mol. Liq.*, 271:769–777, 2018.

[248] Robert Hayes, Gregory G. Warr, and Rob Atkin. Structure and Nanostructure in Ionic Liquids. *Chem. Rev.*, 115:6357–6426, 2015.

[249] Kangsheng Huang, Sheng Bi, Barış Kurt, Chengyang Xu, Langyuan Wu, Zhiwei Li, Guang Feng, and Xiaogang Zhang. Regulation of SEI Formation by Anion Receptors to Achieve Ultra-Stable Lithium-Metal Batteries. *Angew.Chem. Int. Ed.*, 60:19232–19240, 2021.

[250] Z. Yu, H. Wang, X. Kong, W. Huang, Y. Tsao, D. G. Mackanic, K. Wang, X. Wang, W. Huang, S. Choudhury, Y. Zheng, C. V. Amanchukwu, S. T. Hung, Y. Ma, E. G. Lomeli, J. Qin, Y. Cui, and Z. Bao. Molecular design for electrolyte solvents enabling energy-dense and long-cycling lithium metal batteries. *Nat. Energy*, 5:526–533, 2020.

[251] Chong Yan, Hao-Ran Li, Xiang Chen, Xue-Qiang Zhang, Xin-Bing Cheng, Rui Xu, Jia-Qi Huang, and Qiang Zhang. Regulating the Inner Helmholtz Plane for Stable Solid Electrolyte Interphase on Lithium Metal Anodes. *J. Am. Chem. Soc.*, 141:9422–9429, 2019.

[252] A. A. Kornyshev and R. Qiao. Three-Dimensional Double Layers. *J. Phys. Chem. C*, 118:18285–18290, 2014.

[253] G.-B. Pan and W. Freyland. 2D phase transition of PF_6 adlayers at the electrified ionic liquid/Au(111) interface. *Chem. Phys. Lett.*, 427:96–100, 2006.

[254] D. Borissov, C. L. Aravinda, and W. Freyland. Comparative Investigation of Underpotential Deposition of Ag from Aqueous and Ionic Electrolytes: An Electrochemical and In Situ STM Study. *J. Phys. Chem. B*, 109:11606–11615, 2005.

[255] Y. Liu, Y. Zhang, G. Wu, and J. Hu. Coexistence of Liquid and Solid Phases of Bmim-PF_6 Ionic Liquid on Mica Surfaces at Room Temperature. *J. Am. Chem. Soc.*, 128:7456–7457, 2006.

[256] Y.-Z. Su, Y.-C. Fu, J.-W. Yan, Z.-B. Chen, and B.-W. Mao. Double Layer of Au(100)/Ionic Liquid Interface and Its Stability in Imidazolium-Based Ionic Liquids. *Angew. Chem. Int. Ed.*, 48:5148–5151, 2009.

[257] Y.-Z. Su, J.-W. Yan, M.-G. Li, Z.-X. Xie, B.-W. Mao, and Z.-Q. Tian. Adsorption of Solvent Cations on Au(111) and Au(100) in Alkylimidazolium-Based Ionic Liquids – Worm-Like versus Micelle-Like Structures. *Z. Phys. Chem.*, 226:979–994, 2012.

[258] Y. Su, J. Yan, M. Li, M. Zhang, and B. Mao. Electric Double Layer of Au(100)/Imidazolium-Based Ionic Liquids Interface: Effect of Cation Size. *J. Phys. Chem. C*, 117:205–212, 2013.

[259] F. Buchner, K. Forster-Tonigold, B. Uhl, D. Alwast, N. Wagner, H. Farkhondeh, A. Groß, and R. J. Behm. Toward the Microscopic Identification of Anions and Cations at the Ionic Liquid|Ag(111) Interface: A Combined Experimental and Theoretical Investigation. *ACS Nano*, 7:7773–7784, 2013.

[260] T. Cremer, M. Stark, A. Deyko, H.-P. Steinrück, and F. Maier. Liquid/Solid Interface of Ultrathin Ionic Liquid Films: $[C_1C_1Im][Tf_2N]$ and $[C_8C_1Im][Tf_2N]$ on Au(111). *Langmuir*, 27:3662–3671, 2011.

[261] R. Foulston, S. Gangopadhyay, C. Chiutu, P. Moriarty, and R. G. Jones. Mono- and multilayer adsorption of an ionic liquid on Au(110). *Phys. Chem. Chem. Phys.*, 14:6054–6066, 2012.

[262] L. Tamam, B. M. Ocko, H. Reichert, and M. Deutsch. Checkerboard Self-Patterning of an Ionic Liquid Film on Mercury. *Phys. Rev. Lett.*, 106:197801(1)–197801(4), 2011.

[263] W. Freyland. Interfacial phase transitions in conducting fluids. *Phys. Chem. Chem. Phys.*, 10:923–936, 2008.

[264] G.-B. Pan and W. Freyland. In situ STM investigation of spinodal decomposition and surface alloying during underpotential deposition of Cd on Au(111) from an ionic liquid. *Phys. Chem. Chem. Phys.*, 9:3286–3290, 2007.

[265] R. Wen, B. Rahn, and O. M. Magnussen. Potential-Dependent Adlayer Structure and Dynamics at the Ionic Liquid/Au(111) Interface: A Molecular-Scale In Situ Video-STM Study. *Angew. Chem. Int. Ed.*, 54:1–6, 2015.

[266] N. Borisenko, R. Atkin, A. Lahiri, S. Z. E. Abedin, and F. Endres. Effect of dissolved LiCl on the ionic liquid–Au(111) interface: an in situ STM study. *J. Phys.: Condens. Matter.*, 26:284111(1)–284111(9), 2014.

[267] F. Endres, N. Borisenko, S. Z. E. Abedin, R. Hayes, and R. Atkin. The interface ionic liquid(s)/electrode(s): In situ STM and AFM measurements. *Faraday Discuss.*, 154:221–233, 2012.

[268] A. Elbourne, S. McDonald, K. Voïchovsky, F. Endres, G. G. Warr, and R. Atkin. Nanostructure of the Ionic Liquid-Graphite Stern Layer. *ACS Nano*, 9:7608–7620, 2015.

[269] D. Ebeling, S. Bradler, B. Roling, and A. Schirmeisen. 3-Dimensional Structure of a Prototypical Ionic Liquid-Solid Interface: Ionic Crystal-Like Behavior Induced by Molecule-Substrate Interactions. *J. Phys. Chem. C*, 120:11947–11955, 2016.

[270] B. Rotenberg and M. Salanne. Structural Transitions at Ionic Liquid Interfaces. *J. Phys. Chem. Lett.*, 6:4978–4985, 2015.

USC

[271] M. Pounds, S. Tazi, M. Salanne, and P. A. Madden. Ion adsorption at a metallic electrode: an ab initio based simulation study. *J. Phys.: Condens. Matter.*, 21:424109(1)–424109(11), 2009.

[272] S. Tazi, M. Salanne, C. Simon, P. Turq, M. Pounds, and P. A. Madden. Potential-Induced Ordering Transition of the Adsorbed Layer at the Ionic Liquid/Electrified Metal Interface. *J. Phys. Chem. B*, 114:8453–8459, 2010.

[273] C. Merlet, D. T. Limmer, M. Salanne, R. van Roij, P. A. Madden, D. Chandler, and B. Rotenberg. The Electric Double Layer Has a Life of Its Own. *J. Phys. Chem. C*, 118:18291–18298, 2014.

[274] S. Begic, E. Jónsson, F. Chen, and M. Forsyth. Molecular dynamics simulations of pyrrolidinium and imidazolium ionic liquids at graphene interfaces. *Phys. Chem. Chem. Phys.*, 19:30010–30020, 2017.

[275] J. L. Ma, Q. Meng, and J. Fan. Charge driven lateral structural evolution of ions in electric double layer capacitors strongly correlates with differential capacitance. *Phys. Chem. Chem. Phys.*, 20:8054–8063, 2018.

[276] Borja Docampo-Álvarez, Victor Gómez-González, Hadrián Montes-Campos, José M. Otero-Mato, Trinidad Méndez-Morales, Oscar Cabeza, L. J. Gallego, Ruth M. Lynden-Bell, Vladislav B. Ivaništšev, Maxim V. Fedorov, et al. Molecular dynamics simulation of the behaviour of water in nano-confined ionic liquid–water mixtures. *J. Phys. Condens. Matter*, 28(46):464001, 2016.

[277] V. Gómez-González, B. Docampo-Álvarez, T. Méndez-Morales, O. Cabeza, V. B. Ivanistsev, M. V. Fedorov, L. J. Gallego, and L. M. Varela. Molecular dynamics simulation of the structure and interfacial free energy barriers of mixtures of ionic liquids and divalent salts near a graphene wall. *Phys. Chem. Chem. Phys.*, 19:846–853, 2017.

[278] H. Montes-Campos, J. M. Otero-Mato, T. Méndez-Morales, O. Cabeza, L. J. Gallego, A. Ciach, and L. M. Varela. Two-dimensional pattern formation in ionic liquids confined between graphene walls. *Phys. Chem. Chem. Phys.*, 19:24505–24512, 2017.

[279] José M. Otero-Mato, Hadrián Montes-Campos, Oscar Cabeza, Diddo Diddens, Alina Ciach, Luis J. Gallego, and Luis M. Varela. 3D structure of the electric double layer of ionic liquid–alcohol mixtures at the electrochemical interface. *Phys. Chem. Chem. Phys.*, 20(48):30412–30427, 2018.

[280] Hadrián Montes-Campos, Jose Manuel Otero-Mato, Roberto Carlos Longo, Oscar Cabeza, Luis Javier Gallego, and Luis Miguel Varela. Mixtures of Lithium Salts and Ionic Liquids at Defected Graphene Walls. *J. Mol. Liq.*, 289:111083, 2019.

[281] V. Ivanistsev, K. Kirchner, T. Kirchner, and M. V. Fedorov. Restructuring of the electrical double layer in ionic liquids upon charging. *J. Phys.: Condens. Matter.*, 27:102101(1)–102101(5), 2015.

[282] V. Ivanistsev and M. V. Fedorov. Interfaces between Charged Surfaces and Ionic Liquids: Insights from Molecular Simulations. *Electrochem. Soc. Interface*, 23:65–69, 2014.

[283] T. Abe, H. Fukuda, Y. Iriyama, and Z. Ogumi. Solvated Li-Ion Transfer at Interface Between Graphite and Electrolyte. *J. Electrochem. Soc.*, 151:A1120–A1123, 2004.

[284] Y. Yamada, Y. Iriyama, T. Abe, and Z. Ogumi. Kinetics of Lithium Ion Transfer at the Interface between Graphite and Liquid Electrolytes: Effects of Solvent and Surface Film. *Langmuir*, 25:12766–12770, 2009.

[285] A. W. Cresce and K. Xu. Preferential Solvation of Li^+ Directs Formation of Interphase on Graphitic Anode. *ECS Solid State Lett.*, 14:A154–A156, 2011.

[286] A. W. Cresce, O. Borodin, and K. Xu. Correlating Li^+ Solvation Sheath Structure with Interphasial Chemistry on Graphite. *J. Phys. Chem. C*, 116:26111–26117, 2012.

[287] K. Xu, A. W. Cresce, and U. Lee. Differentiating Contributions to "Ion Transfer" Barrier from Interphasial Resistance and Li^+ Desolvation at Electrolyte/Graphite Interface. *Langmuir*, 26:11538–11543, 2010.

[288] K. Xu and A. W. Cresce. Li^+-solvation/desolvation dictates interphasial processes on graphitic anode in Li ion cells. *J. Mater. Res.*, 27:2327–2341, 2012.

[289] M. Zhou, P. Bai, X. Ji, J. Yang, C. Wang, and Y. Xu. Electrolytes and Interphases in Potassium Ion Batteries. *Adv. Mat.*, 33:2003741(1)–2003741(22), 2021.

[290] M.-T. F. Rodrigues, X. Lin, H. Gullapalli, M. W. Grinstaff, and P. M. Ajayan. Rate limiting activity of charge transfer during lithiation from ionic liquids. *J. Power Sources*, 330:84–91, 2016.

[291] A. M. Smith and S. Perkin. Influence of Lithium Solutes on Double-Layer Structure of Ionic Liquids. *J. Phys. Chem. Lett.*, 6:4857–4861, 2015.

[292] Y. Ishihara, K. Miyazaki, T. Fukutsuka, and T. Abe. Lithium-Ion Transfer at the Interface between High Potential Negative Electrodes and Ionic Liquids. *J. Electrochem. Soc.*, 161:A1939–A1942, 2014.

[293] F. Sagane, T. Abe, and Z. Ogumi. Electrochemical Analysis of Lithium-Ion Transfer Reaction through the Interface between Ceramic Electrolyte and Ionic Liquids. *J. Electrochem. Soc.*, 159:A1766–A1769, 2012.

[294] V. Ivanistsev, T. Méndez-Morales, Ruth M. Lynden-Bell, O. Cabeza, L. J. Gallego, L. M. Varela, and M. V. Fedorov. Molecular origin of high free energy barriers for alkali metal ion transfer through ionic liquid–graphene electrode interfaces. *Phys. Chem. Chem. Phys.*, 18:1302–1310, 2016.

[295] S. W. Coles, M. Mishin, S. Perkin, M. V. Fedorov, and V. B. Ivanistsev. The nanostructure of a lithium glyme solvate ionic liquid at electrified interfaces. *Phys. Chem. Chem. Phys.*, 19:11004–11010, 2017.

[296] J. B. Haskins, J. J. Wu, and J. W. Lawson. Computational and Experimental Study of Li-Doped Ionic Liquids at Electrified Interfaces. *J. Phys. Chem. C*, 120:11993–12011, 2016.

USC UNIVERSIDADE DE SANTIAGO DE COMPOSTELA

[297] G. D. Smith, O. Borodin, S. P. Russo, R. J. Rees, and A. F. Hollenkamp. A molecular dynamics simulation study of $LiFePO_4$/electrolyte interfaces: structure and Li^+ transport in carbonate and ionic liquid electrolytes. *Phys. Chem. Chem. Phys.*, 11:9884–9897, 2009.

[298] J. Vatamanu, O. Borodin, and G. D. Smith. Molecular Dynamics Simulation Studies of the Structure of a Mixed Carbonate/$LiPF_6$ Electrolyte near Graphite Surface as a Function of Electrode Potential. *J. Phys. Chem. C*, 116:1114–1121, 2012.

[299] Kazem Zhour, José M. Otero-Mato, Fouad El Haj Hassan, Hussein Fahs, Majid Vaezzadeh, E. López-Lago, Luis J. Gallego, and Luis M. Varela. Tuning the hybrid borophene-/graphene-ionic liquid interface: Effect of metal cations on the electronic and photonic properties. *J. Mol. Liq.*, 321:114759, 2021.

[300] V. Gómez-González, Amador Garcìa-Fuente, A. Vega, J. Carrete, O. Cabeza, L. J. Gallego, and L. M. Varela. Density functional study of charge transfer at the graphene/ionic liquid interface. *J. Phys. Chem. C*, 122(27):15070–15077, 2018.

[301] L. E. Camacho-Forero, T. W. Smith, and P. B. Balbuena. Effects of High and Low Salt Concentration in Electrolytes at Lithium-Metal Anode Surfaces. *J. Phys. Chem. C*, 121:182–194, 2016.

[302] C. Wei, K. Jiang, T. Fang, and X. Liu. Insight into the adsorption of Imidazolium-based ionic liquids on graphene by first principles simulation. *J. Mol. Liq.*, 338:116641(1)–116641(9), 2021.

[303] A. Budi, A. Basile, G. Opletal, A. F. Hollenkamp, A. S. Best, R. J. Rees, A. I. Bhatt, A. P. O'Mullane, and S. P. Russo. Study of the Initial Stage of Solid Electrolyte Interphase Formation upon Chemical Reaction of Lithium Metal and N-Methyl-N-Propyl-Pyrrolidinium-Bis(Fluorosulfonyl)Imide. *J. Phys. Chem. C*, 116:19789–19797, 2012.

[304] H. Yildirim, J. B. Haskins, Jr. C. W. Bauschlicher, and J. W. Lawson. Decomposition of Ionic Liquids at Lithium Interfaces. 1. Ab Initio Molecular Dynamics Simulations. *J. Phys. Chem. C*, 121:28214–28234, 2017.

[305] B. V. Merinov, S. V. Zybin, S. Naserifar, S. Morozov, J. Oppenheim, W. A. Goddard, J. Lee, J. H. Lee, H. E. Han, Y. C. Choi, and S. H. Kim. Interface Structure in Li-Metal/[Pyr_{14}][TFSI]-Ionic Liquid System from ab Initio Molecular Dynamics Simulations. *J. Phys. Chem. Lett.*, 10:4577–4586, 2019.

[306] B. V. Merinov, S. Naserifar, S. V. Zybin, S. Morozov, W. A. Goddard, J. Lee, J. H. Lee, H. E. Han, Y. C. Choi, and S. H. Kim. Li-diffusion at the interface between Limetal and [Pyr_{14}][TFSI]-ionic liquid: Ab initio molecular dynamics simulations. *J. Chem. Phys.*, 152:031101(1)–031101(8), 2020.

[307] J. Clarke-Hannaford, M. Breedon, A. S. Best, and M. J. S. Spencer. The interaction of ethylammonium tetrafluoroborate [$EtNH_3^+$][BF_4] ionic liquid on the Li(001) surface: towards understanding early SEI formation on Li metal. *Phys. Chem. Chem. Phys.*, 21:10028–10037, 2019.

[308] G. Kresse and J. Furthmüller. Efficient iterative schemes for ab initio total-energy calculations using a plane-wave basis set. *Phys. Rev. B*, 54:11169–11186, 1996.

[309] G. Kresse and D. Joubert. From ultrasoft pseudopotentials to the projector augmented-wave method. *Phys. Rev. B*, 59:1758–1775, 1999.

[310] P.E. Blochl. Projector augmented-wave method. *Phys. Rev. B*, 50:17953–17979, 1994.

[311] S. Grimme. Semiempirical GGA-type density functional constructed with a long-range dispersion correction. *J. Comput. Chem.*, 27:1787–1799, 2006.

[312] Minho Kim, Tim Gould, Ekaterina I. Izgorodina, Dario Rocca, and Sébastien Lebègue. Establishing the accuracy of density functional approaches for the description of noncovalent interactions in ionic liquids. *Phys. Chem. Chem. Phys.*, 23:25558–25564, 2021.

[313] Anoopa Thomas, K. Rudharachari Maiyelvaganan, Shanmugasundaram Kamalakannan, and Muthuramalingam Prakash. Density Functional Theory Studies on Zeolitic Imidazolate Framework-8 and Ionic Liquid-Based Composite Materials. *ACS Omega*, 4(27):22655–22666, 2019. PMID: 31909350.

[314] Graeme Henkelman, Andri Arnaldsson, and Hannes Jónsson. A fast and robust algorithm for Bader decomposition of charge density. *Comput. Mater. Sci.*, 36:354–360, 2006.

[315] E. Sanville, S. D. Kenny, R. Smith, and G. Henkelman. Improved grid-based algorithm for Bader charge allocation. *J. Comput. Chem.*, 28:899–908, 2007.

[316] W. Tang, E. Sanville, and G. Henkelman. A grid-based Bader analysis algorithm without lattice bias. *J. Phys.: Condens. Matter.*, 21:084204–084210, 2009.

[317] M. Yu and D. R. Trinkle. Accurate and efficient algorithm for Bader charge integration. *J. Chem. Phys.*, 134:064111–064118, 2011.

[318] Kristin Persson, Yoyo Hinuma, Ying Shirley Meng, Anton Van der Ven, and Gerbrand Ceder. Thermodynamic and kinetic properties of the Li-graphite system from first-principles calculations. *Phys. Rev. B*, 82(12):125416, 2010.

[319] Eunseok Lee and Kristin A. Persson. Li absorption and intercalation in single layer graphene and few layer graphene by first principles. *Nano Lett.*, 12(9):4624–4628, 2012.

[320] Robert D. Shannon. Revised effective ionic radii and systematic studies of interatomic distances in halides and chalcogenides. *Acta crystallographica section A: crystal physics, diffraction, theoretical and general crystallography*, 32(5):751–767, 1976.

[321] Alexander Stoppa, Johannes Hunger, Richard Buchner, Glenn Hefter, Andreas Thoman, and Hanspeter Helm. Interactions and Dynamics in Ionic Liquids. *J. Phys. Chem. B*, 112(16):4854–4858, 2008. PMID: 18370433.

[322] Kazem Zhour, José M. Otero-Mato, Fouad El Haj Hassan, Hussein Fahs, Majid Vaezzadeh, E. López-Lago, Luis J. Gallego, and Luis M. Varela. Electronic and optical properties of borophene and graphene with an adsorbed ionic liquid: A density functional theory study. *J. Mol. Liq.*, 316:113803, 2020.

USC UNIVERSIDADE DE SANTIAGO DE COMPOSTELA

[323] T. Mendez-Morales, M. Burbano, M. Haefele, B. Rotenberg, and M. Salanne. Ion-ion correlations across and between electrified graphene layers. *J. Chem. Phys.*, 148:193812(1)–193812(7), 2018.

[324] T. Méndez-Morales, N. Ganfoud, Z. Li, M. Haefele, B. Rotenberg, and M. Salanne. Performance of microporous carbon electrodes for supercapacitors: Comparing graphene with disordered materials. *Energy Storage Mater.*, 17:88–92, 2019.

[325] J. Vatamanu, L. Cao, O. Borodin, D. Bedrov, and G. D. Smith. On the Influence of Surface Topography on the Electric Double Layer Structure and Differential Capacitance of Graphite/Ionic Liquid Interfaces. *J.Phys.Chem.Lett.*, 2:2267–2272, 2011.

[326] F. Chevallier, F. Poli, B. Montigny, and M. Letellier. In situ ^{7}Li nuclear magnetic resonance observation of the electrochemical intercalation of lithium in graphite: second cycle analysis. *Carbon*, 61:140–153, 2013.

[327] C. E. Banks, T. J. Davies, G. G. Wildgoose, and R. G. Compton. Electrocatalysis at graphite and carbon nanotube modified electrodes: edge-plane sites and tube ends are the reactive sites. *Chem. Commun.*, pages 829–841, 2005.

[328] L. Xiao, E. J. F. Dickinson, G. G. Wildgoose, and R. G. Compton. A Comparison of Electron Transfer Kinetics of Three Common Carbon Electrode Surfaces in Acetonitrile and in Room Temperature Ionic Liquid 1-Butyl-3-Methylimidiazonium Hexafluorophosphate: Correlation to Surface Structure and the Limit of the Diffusion Domain Approximation. *Electroanal*, 22:269–276, 2010.

[329] Zhongjian Xie, Bin Zhang, Yanqi Ge, Yao Zhu, Guohui Nie, YuFeng Song, Chang-Keun Lim, Han Zhang, and Paras N. Prasad. Chemistry, Functionalization, and Applications of Recent Monoelemental Two-Dimensional Materials and Their Heterostructures. *Chem. Rev.*, 122(1):1127–1207, 2022.

[330] Hui Qiao, Huating Liu, Zongyu Huang, Rong Hu, Qian Ma, Jianxin Zhong, and Xiang Qi. Tunable Electronic and Optical Properties of 2D Monoelemental Materials Beyond Graphene for Promising Applications. *Energy Environ. Mat.*, 4(4):522–543, 2021.

[331] L A. Falkovsky. Optical properties of graphene. *J. Phys. Conf. Ser.*, 129(1):012004, 2008.

[332] Dimitrios G. Papageorgiou, Ian A. Kinloch, and Robert J. Young. Mechanical properties of graphene and graphene-based nanocomposites. *Prog. Mater. Sci.*, 90:75–127, 2017.

[333] A. H. Castro Neto, F. Guinea, N. M. R. Peres, K. S. Novoselov, and A. K. Geim. The electronic properties of graphene. *Rev. Mod. Phys.*, 81:109–162, 2009.

[334] Nzar Rauf Abdullah, Botan Jawdat Abdullah, Chi-Shung Tang, and Vidar Gudmundsson. Properties of BC6N monolayer derived by first-principle computation: Influences of interactions between dopant atoms on thermoelectric and optical properties. *Mat. Sci. Semicon Proc.*, 135:106073, 2021.

[335] Muhammad Rafique, Yong Shuai, Irfan Ahmed, Rameez Shaikh, and Mohsin Ali Tunio. Tailoring electronic and optical parameters of bilayer graphene through boron and nitrogen atom co-substitution; an ab-initio study. *Appl. Surf. Sci.*, 480:463–471, 2019.

[336] Gina Ambrosio, Giovanni Drera, Giovanni Di Santo, Luca Petaccia, Lakshya Daukiya, Anton Brown, Brandon Hirsch, Steven De Feyter, Luigi Sangaletti, and Stefania Pagliara. Interface Chemistry of Graphene/Cu Grafted By 3,4,5-Tri-Methoxyphenyl. *Sci. Rep.*, 10:1–9, 2020.

[337] V. Kumar and R. Santosh. First-principle calculations of structural, electronic, optical and thermodynamical properties of fluorinated graphene. *Mater. Sci. Eng. B*, 246:127–135, 2019.

[338] Muh. Yusrul Hanna, Iman Santoso, and Moh. Adhib Ulil Absor. The Role of the Oxygen Impurity on the Electronic Properties of Monolayer Graphene: A Density-Functional Study. *J. Phys. Conf. Ser.*, 1011(1):012071, apr 2018.

[339] T Sruthi and Tarafder Kartick. Route to achieving enhanced quantum capacitance in functionalized graphene based supercapacitor electrodes. *J. Phys. Condens. Matter*, 31(47):475502, aug 2019.

[340] Rui You, Yu-Qing Liu, Yi-Long Hao, Dong-Dong Han, Yong-Lai Zhang, and Zheng You. Laser Fabrication of Graphene-Based Flexible Electronics. *Adv. Mater.*, 32(15):1901981, 2020.

[341] A.G. Olabi, Mohammad Ali Abdelkareem, Tabbi Wilberforce, and Enas Taha Sayed. Application of graphene in energy storage device – A review. *Renewable Sustainable Energy Rev.*, 135:110026, 2021.

[342] Subhashree Priyadarsini, Swaraj Mohanty, Sumit Mukherjee, Srirupa Basu, and Monalisa Mishra. Graphene and graphene oxide as nanomaterials for medicine and biology application. *J. Nanostruct. Chem.*, 8:123–137, 2018.

[343] Yancong Qiao, Xiaoshi Li, Thomas Hirtz, Ge Deng, Yuhong Wei, Mingrui Li, Shourui Ji, Qi Wu, Jinming Jian, Fan Wu, et al. Graphene-based wearable sensors. *Nanoscale*, 11(41):18923–18945, 2019.

[344] Farhad Larki, Yaser Abdi, Parviz Kameli, and Hadi Salamati. An effort towards full graphene photodetectors. *Photonic Sensors*, pages 1–37, 2022.

[345] Stevanus Alvin, Handi Setiadi Cahyadi, Jieun Hwang, Wonyoung Chang, Sang Kyu Kwak, and Jaehoon Kim. Revealing the Intercalation Mechanisms of Lithium, Sodium, and Potassium in Hard Carbon. *Adv. Energy Mater.*, 10(20):2000283, 2020.

[346] Yuqi Li, Yaxiang Lu, Philipp Adelhelm, Maria-Magdalena Titirici, and Yong-Sheng Hu. Intercalation chemistry of graphite: alkali metal ions and beyond. *Chem. Soc. Rev.*, 48:4655–4687, 2019.

[347] Xiaojie Liu, Yong Han, James W. Evans, Albert K. Engstfeld, R. Juergen Behm, Michael C. Tringides, Myron Hupalo, Hai-Qing Lin, Li Huang, Kai-Ming Ho, et al. Growth morphology and properties of metals on graphene. *Prog. Surf. Sci.*, 90(4):397–443, 2015.

[348] Sanjeev K. Gupta, Himadri R. Soni, and Prafulla K. Jha. Electronic and phonon bandstructures of pristine few layer and metal doped graphene using first principles calculations. *AIP Adv.*, 3(3):032117, 2013.

USC UNIVERSIDADE DE SANTIAGO DE COMPOSTELA

[349] Min Xu, Hongyan Wang, Songsong Sun, Hengtao Li, Xiumei Li, Yuanzheng Chen, and Yuxiang Ni. First-Principles Study of Metal Atoms Adsorption on 2D Dumbbell C4N. *Phys. Status Solidi B.*, 257(1):1900205, 2020.

[350] Muhammad Rafique, Yong Shuai, He-Ping Tan, and Muhammad Hassan. Manipulating intrinsic behaviors of graphene by substituting alkaline earth metal atoms in its structure. *RSC Adv.*, 7:16360–16370, 2017.

[351] Ace Christian F. Serraon, Julie Anne D. Del Rosario, Po-Ya Abel Chuang, Meng Nan Chong, Yoshitada Morikawa, Allan Abraham B. Padama, and Joey D. Ocon. Alkaline earth atom doping-induced changes in the electronic and magnetic properties of graphene: a density functional theory study. *RSC Adv.*, 11:6268–6283, 2021.

[352] Kevin T. Chan, J. B. Neaton, and Marvin L. Cohen. First-principles study of metal adatom adsorption on graphene. *Phys. Rev. B*, 77:235430, Jun 2008.

[353] Saif Ullah, Pablo A. Denis, and Fernando Sato. Adsorption and diffusion of alkali-atoms (Li, Na, and K) on BeN dual doped graphene. *Int. J. Quantum Chem.*, 119(11):e25900, 2019.

[354] Artur P. Durajski, Kamil M. Skoczylas, and Radosław Szczęśniak. Superconductivity in bilayer graphene intercalated with alkali and alkaline earth metals. *Phys. Chem. Chem. Phys.*, 21:5925–5931, 2019.

[355] C. S. Praveen, Simone Piccinin, and Stefano Fabris. Adsorption of alkali adatoms on graphene supported by the Au/Ni(111) surface. *Phys. Rev. B*, 92:075403, 2015.

[356] O. Farkad, R. Takassa, F. Elfatouaki, S. Hassine, Y. Ijdiyaou, E.A. Ibnouelghazi, and D. Abouelaoualim. Structural, electronic and optical properties of AB bilayer graphene intercalated by Sr atom: A first principles study. *Diam. Relat. Mater.*, 126:109082, 2022.

[357] Tomoaki Kaneko and Riichiro Saito. First-principles study on interlayer state in alkali and alkaline earth metal atoms intercalated bilayer graphene. *Surf. Sci.*, 665:1–9, 2017.

[358] Yong Shuai, Muhammad Rafique, M. Moazam Baloch, Mohsin Ali Tunio, and Irfan Ahmed. DFT study on tailoring the structural, electronic and optical properties of bilayer graphene through metalloids intercalation. *Chem. Phys.*, 536:110828, 2020.

[359] Zhaohui Wang, Sverre M. Selbach, and Tor Grande. Van der Waals density functional study of the energetics of alkali metal intercalation in graphite. *RSC Adv.*, 4:4069–4079, 2014.

[360] Emilia Olsson, Guoliang Chai, Martin Dove, and Qiong Cai. Adsorption and migration of alkali metals (Li, Na, and K) on pristine and defective graphene surfaces. *Nanoscale*, 11:5274–5284, 2019.

[361] Srimanta Pakhira, Kevin P. Lucht, and Jose L. Mendoza-Cortes. Dirac cone in two dimensional bilayer graphene by intercalation with V, Nb, and Ta transition metals. *J. Chem. Phys.*, 148(6):064707, 2018.

USC UNIVERSIDADE DE SANTIAGO DE COMPOSTELA

[362] Srimanta Pakhira and Jose L. Mendoza-Cortes. Tuning the Dirac Cone of Bilayer and Bulk Structure Graphene by Intercalating First Row Transition Metals Using First-Principles Calculations. *J. Phys. Chem. C*, 122(9):4768–4782, 2018.

[363] Ehsan Kianfar and Sajjad Mafi. Ionic liquids: properties, application, and synthesis. *Fine Chem. Eng.*, pages 22–31, 2021.

[364] Mark B. Shiflett. *Commercial applications of ionic liquids*, volume 605. Springer, 2020.

[365] Gagandeep Kaur, Harsh Kumar, and Meenu Singla. Diverse applications of ionic liquids: A comprehensive review. *J. Mol. Liq.*, page 118556, 2022.

[366] Adam J. Greer, Johan Jacquemin, and Christopher Hardacre. Industrial applications of ionic liquids. *Molecules*, 25(21):5207, 2020.

[367] Qingwei Gao, Yumeng Zhang, Shuting Xu, Aatto Laaksonen, Yudan Zhu, Xiaoyan Ji, and Xiaohua Lu. Physicochemical properties and structure of fluid at nano-/micro-interface: Progress in simulation and experimental study. *Green Energy Environ.*, 5(3):274–285, 2020. SI: Molecular Thermodynamics for Green Engineering.

[368] Soha Aldroubi, Nicolas Brun, Ibrahim Bou Malham, and Ahmad Mehdi. When graphene meets ionic liquids: a good match for the design of functional materials. *Nanoscale*, 13:2750–2779, 2021.

[369] Peter Snapp, Jin Myung Kim, Chullhee Cho, Juyoung Leem, Md Farhadul Haque, and SungWoo Nam. Interaction of 2D materials with liquids: wettability, electrochemical properties, friction, and emerging directions. *NPG Asia Mater.*, 12:1–16, 2020.

[370] Razieh Talaei, Behzad Khalili, and Masoud Mokhtary. Modulation of opto-electronic properties of the functionalized hexagonal boron nitride nanosheets with tunable aryl alkyl ionic liquids (TAAILs): Defect based analysis. *J. Mol. Liq.*, 304:112696, 2020.

[371] V. S. Anithaa, R. Shankar, and S. Vijayakumar. Structural and electronic properties of graphene and its derivatives physisorbed by ionic liquids. *Diam. Relat. Mater.*, 109:108005, 2020.

[372] Cesar Herrera, Rafael Alcalde, Mert Atilhan, and Santiago Aparicio. Theoretical study on amino acid-based ionic pairs and their interaction with carbon nanostructures. *J. Phys. Chem. C*, 118(18):9741–9757, 2014.

[373] Muraledharan Shyama and Senthilkumar Lakshmipathi. Adsorption properties of amino acid-based ionic liquids (AAILs) on edge fluorinated graphene surface–a DFT study. *Mol. Simulat*, 47(13):1066–1077, 2021.

[374] Yanjing He, Yandong Guo, Fang Yan, Tianhao Yu, Lei Liu, Xiaochun Zhang, and Tao Zheng. Density functional theory study of adsorption of ionic liquids on graphene oxide surface. *Chem. Eng. Sci.*, 245:116946, 2021.

[375] Anton Ruzanov, Meeri Lembinen, Heigo Ers, Jose M. Garcia de la Vega, Isabel Lage-Estebanez, Enn Lust, and Vladislav B. Ivanistsev. Density functional theory study of ionic liquid adsorption on circumcoronene shaped graphene. *J. Phys. Chem. C*, 122(5):2624–2631, 2018.

USC UNIVERSIDADE DE SANTIAGO DE COMPOSTELA

[376] Durgesh Wagle, Ganesh Kamath, and Gary A. Baker. Elucidating interactions between ionic liquids and polycyclic aromatic hydrocarbons by quantum chemical calculations. *J. Phys. Chem. C*, 117(9):4521–4532, 2013.

[377] T. P. C. Klaver, M. Luppi, M. H. F. Sluiter, M. C. Kroon, and B. J. Thijsse. DFT Study of 1,3-Dimethylimidazolium Tetrafluoroborate on Al and Cu(111) Surfaces. *J. Phys. Chem. C*, 115(30):14718–14730, 2011.

[378] H. Valencia, M. Kohyama, S. Tanaka, and H. Matsumoto. Ab initio study of EMIM-BF_4 crystal interaction with a Li (100) surface as a model for ionic liquid/Li interfaces in Li-ion batteries. *J. Chem. Phys.*, 131(24):244705(1)–244705(11), 2009.

[379] Chunlei Wei, Kun Jiang, Timing Fang, and Xiaomin Liu. Effects of anions and alkyl chain length of imidazolium-based ionic liquids at the Au (111) surface on interfacial structure: a first-principles study. *Green Chem. Eng.*, 2(4):402–411, 2021.

[380] Lin Zhu and Aiping Fu. The Influence of Ionic Liquids Adsorption on the Electronic and Optical Properties of Phosphorene and Arsenene with Different Phases: A Computational Study. *Molecules*, 27(8):2518, 2022.

[381] Mehdi Shakourian-Fard, Zahra Jamshidi, Ahmad Bayat, and Ganesh Kamath. Meta-hybrid density functional theory study of adsorption of imidazolium-and ammonium-based ionic liquids on graphene sheet. *J. Phys. Chem. C*, 119(13):7095–7108, 2015.

[382] Mehdi Shakourian-Fard and Ganesh Kamath. The effect of defect types on the electronic and optical properties of graphene nanoflakes physisorbed by ionic liquids. *Phys. Chem. Chem. Phys.*, 19(6):4383–4395, 2017.

[383] Mehdi Shakourian-Fard, S. Maryamdokht Taimoory, Volodymyr Semeniuchenko, Ganesh Kamath, and John F. Trant. The effect of ionic liquid adsorption on the electronic and optical properties of fluorographene nanosheets. *J. Mol. Liq.*, 268:206–214, 2018.

[384] Rozana Bari, George Tamas, Fahmida Irin, Adelia J.A. Aquino, Micah J. Green, and Edward L. Quitevis. Direct exfoliation of graphene in ionic liquids with aromatic groups. *Colloids Surf. A: Physicochem. Eng. Asp.*, 463:63–69, 2014.

[385] Gregorio García, Mert Atilhan, and Santiago Aparicio. In silico rational design of ionic liquids for the exfoliation and dispersion of boron nitride nanosheets. *Phys. Chem. Chem. Phys.*, 18(2):1212–1224, 2016.

[386] Mehdi Shakourian-Fard, Ganesh Kamath, and Zahra Jamshidi. Trends in physisorption of ionic liquids on boron-nitride sheets. *J. Phys. Chem. C*, 118(45):26003–26016, 2014.

[387] Gregorio García, Mert Atilhan, and Santiago Aparicio. Adsorption of choline benzoate ionic liquid on graphene, silicene, germanene and boron-nitride nanosheets: a DFT perspective. *Phys. Chem. Chem. Phys.*, 17(25):16315–16326, 2015.

[388] Murugan Lalitha and Senthilkumar Lakshmipathi. Interface energetics of $[Emim]^+[X]^-$ and $[Bmim]^+[X]^-$ ($X=BF_4ClPF_6TfOTf_2N$) based ionic liquids on graphene, defective graphene, and graphyne surfaces. *J. Mol. Liq.*, 236:124–134, 2017.

[389] Yunxiang Lu, Yumei Hong, Zhijian Xu, and Honglai Liu. Interfacial interactions and structures of imidazolium-based ionic liquids on black phosphorus surface from first-principles. *J. Mol. Liq.*, 335:116562, 2021.

[390] Yunxiang Lu, Yanmin Xu, Ling Lu, Zhijian Xu, and Honglai Liu. Interfacial interactions and structures of protic ionic liquids on a graphite surface: A first-principles study and comparison with aprotic ionic liquids. *Phys. Chem. Chem. Phys.*, 23(34):18338–18348, 2021.

[391] Mehdi Shakourian-Fard, Hamid Reza Ghenaatian, Ganesh Kamath, and S. Maryamdokht Taimoory. Unraveling the effect of nitrogen doping on graphene nanoflakes and the adsorption properties of ionic liquids: A DFT study. *J. Mol. Liq.*, 312:113400, 2020.

[392] Yingqi Tang, Wenbo Huai, Hao Li, Xiaotong Mao, Ju Xie, Jin Yong Lee, and Aiping Fu. Adsorption of [BF4]- anion-based ionic liquids on phosphorene, arsenene, and antimonene: A density functional theory study. *Int. J. Quantum Chem.*, 121(15):e26668, 2021.

[393] Biswajit Mandal, Shamik Chakrabarti, and Awalendra K. Thakur. DFT simulation of NaFeSnO4 structure, electronic and electrochemical properties validated by experimental results. *Nato. Sc. S. Ss. Iii. C. S.*, 192:110401, 2021.

[394] Helena Matabosch Coromina, Beatrice Adeniran, Robert Mokaya, and Darren A. Walsh. Bridging the performance gap between electric double-layer capacitors and batteries with high-energy/high-power carbon nanotube-based electrodes. *J. Mater. Chem. A*, 4(38):14586–14594, 2016.

[395] Mao-Cheng Liu, Chun Lu, Yan Xu, Yu-Xia Hu, Jun Li, Hui Zhang, Yu-Shan Zhang, Bing-Mei Zhang, Ling-Bin Kong, Wen-Wu Liu, et al. Three-dimensional interconnected reticular porous carbon from corn starch by a sample sol–gel method toward high-performance supercapacitors with aqueous and ionic liquid electrolytes. *ACS Sustain. Chem. Eng.*, 7(22):18690–18699, 2019.

[396] Paolo Giannozzi, Oscar Baseggio, Pietro Bonfà, Davide Brunato, Roberto Car, Ivan Carnimeo, Carlo Cavazzoni, Stefano De Gironcoli, Pietro Delugas, Fabrizio Ferrari Ruffino, et al. Quantum ESPRESSO toward the exascale. *J. Chem. Phys.*, 152(15):154105, 2020.

[397] M. P. A. T. Methfessel and A. T. Paxton. High-precision sampling for Brillouin-zone integration in metals. *Phys. Rev. B*, 40(6):3616, 1989.

[398] Richard F. W. Bader. Atoms in molecules. *Acc. Chem. Res.*, 18(1):9–15, 1985.

[399] David R. Lide. *CRC Handbook of Chemistry and Physics. 84th Edition*. CRC Press, 2003.

[400] Z. H. Zhu and G. Q. Lu. Comparative Study of Li, Na, and K Adsorptions on Graphite by Using ab Initio Method. *Langmuir*, 20(24):10751–10755, 2004.

[401] Bernard A. Boukamp. A linear Kronig-Kramers transform test for immittance data validation. *J. Electrochem Soc.*, 142(6):1885, 1995.

USC

[402] Palash Nath, Suman Chowdhury, D. Sanyal, and Debnarayan Jana. Ab-initio calculation of electronic and optical properties of nitrogen and boron doped graphene nanosheet. *Carbon*, 73:275–282, 2014.

[403] Frederick Wooten. *Optical properties of solids*. Citeseer, 1972.

[404] Suman Chowdhury, Arnab Majumdar, and Debnarayan Jana. Electronic and optical properties of the supercell of 8-Pmmn borophene modified on doping by H, Li, Be, and C: a DFT approach. *Appl. Phys. A*, 125(5):1–14, 2019.

USC
UNIVERSIDADE DE SANTIAGO DE COMPOSTELA





This thesis contains a comprehensive study of the properties of mixtures of ionic liquids with cosolvents of interest, with the focus on hybrid ionogels. The main objective of this work is to unveil the different relevant interactions that take place in these systems and their effects. For this purpose, computational simulations using molecular dynamics and density functional theory calculations are performed. Reported results analyze how the structure and dynamics of the systems are affected by the presence of interfaces or different computational models. Moreover, the electronic interactions at the electrode-electrolyte interface are considered.